ISSN 2313–5891 (Online)
ISSN 2304–974X (Print)

Ukrainian Food Journal

Volume 15, Issue 3
2026

Kyiv **Київ**

2026

Ukrainian Food Journal is an international scientific journal that publishes articles by specialists in food sciences, engineering and technology, biotechnology, and chemistry.

Ukrainian Food Journal – це міжнародне наукове видання, яке публікує статті фахівців у галузі харчових наук, інженерії та технологій, біотехнологій і хімії.

Ukrainian Food Journal is indexed and abstracted in international scientific databases

Ukrainian Food Journal індексується та реферується в міжнародних наукових базах даних

Index Copernicus (2012)
EBSCO (2013)
Google Scholar (2013)
UlrichsWeb (2013)
CABI full text (2014)
Online Library of University of Southern Denmark (2014)
Directory of Open Access scholarly Resources (ROAD) (2014)
European Reference Index for Humanities and Social Sciences (ERIH PLUS) (2014)
Directory of Open Access Journals (DOAJ) (2015)
InfoBase Index (2015)
Chemical Abstracts Service Source Index (CASSI) (2016)
FSTA (Food Science and Technology Abstracts) (2018)
Web of Science (Emerging Sourses Citaton Index) (2018)
Scopus (2022)

Ukrainian Food Journal включено у перелік наукових фахових видань України з технічних наук, категорія А (Наказ Міністерства освіти і науки України № 358 від 15.03.2019)

Editorial office address:

National University
of Food Technologies
68 Volodymyrska str.
Kyiv 01601, **Ukraine**

Адреса редакції:

Національний університет
харчових технологій
вул. Володимирська, 68
Київ 01601, **Україна**

e-mail: **ufj_nuft@meta.ua**

© NUFT, 2026

© НУХТ, 2026

Ukrainian Food Journal is an open-access, peer-reviewed scientific journal published by the National University of Food Technologies (Kyiv, Ukraine). The journal publishes original research articles, short communications, review articles, and news covering all areas of food science, including food technology, engineering, nutrition, food biotechnology, and chemistry.

Manuscripts must present novel findings, demonstrate a clear connection to food science, and be of broad interest to the international scientific community.

Please note that the journal's scope does not include the following types of submissions:

Manuscripts making medical claims or reporting studies involving human or animal subjects, as these topics are beyond the journal's scope.

Manuscripts that do not demonstrate sufficient scientific novelty or significance, including those addressing routine practical or engineering problems without a clear scientific contribution.

Ukrainian Food Journal is published quarterly, with four issues released each year in March, June, September, and December.

Manuscript Evaluation and Peer Review

Upon receipt, each manuscript is initially evaluated by the Editor-in-Chief to determine whether it falls within the journal's scope. The Editor-in-Chief also checks the manuscript's formatting, style, and illustrative materials and may suggest improvements. Based on this initial evaluation, the Editor-in-Chief decides whether the manuscript should be sent for peer review.

All manuscripts submitted to the *Ukrainian Food Journal* undergo double-blind peer review. Each manuscript is evaluated by at least two independent reviewers: one member of the Editorial Board and one external reviewer who is not affiliated with either the Editorial Board or the publisher. This process aims to ensure an objective and balanced assessment of the manuscript's scientific quality.

The full Guide for Authors is available on our website:
http://ufj.nuft.edu.ua

International Editorial Board

Editor-in-Chief:

Olena Stabnikova, Dr., *National University of Food Technologies, Ukraine*

Members of Editorial Board:

Sonia Amariei, PhD, Prof., *University "Ştefan cel Mare" of Suceava, Romania*
Eirin Marie Skjøndal Bar, PhD, Assoc. Prof., *Norwegian University of Science and Technology, Trondheim, Norway*
Yurii Bilan, PhD, Prof., *Tomas Bata University in Zlin, Czech Republic*
Kirsten Brandt, PhD, *Newcastle University, United Kingdom*
Moisés Burachik, PhD, *Institute of Agricultural Biotechnology of Rosario* (*INDEAR*), *Bioceres Group, Rosario, Argentina*
Stanka Damianova, PhD, Prof., *Ruse University "Angel Kanchev", branch Razgrad, Bulgaria*
Yuliya Dzyazko, PhD, Prof., *Institute of General and Inorganic Chemistry of the National Academy of Sciences of Ukraine*
Yun-Hwa Peggy Hsieh, PhD, Prof. Emerita, *Florida State University, USA*
Lelieveld Huub, PhD, *Global Harmonization Initiative Association, The Netherlands*
Sheila Kilonzi, PhD, *Karatina University, Kenya*
Jasmina Lukinac, PhD, Assoc. Prof., *University of Osijek, Croatia*
Dora Marinova, PhD, Prof., *Curtin University Sustainability Policy Institute, Curtin University, Australia*
Rana Mustafa, PhD, *Global Institute for Food Security, University of Saskatchewan, Canada*
Godwin D. Ndossi, PhD, Prof., *Hubert Kairuki Memorial University, Dar es Salaam, Tanzania*
Umezuruike Linus Opara, PhD, Prof., *Stellenbosch University, Cape Town, South Africa*
Semih Otles, PhD, Prof., *Ege University, Turkey*
Octavio Paredes-López, PhD, Prof., *The Center for Research and Advanced Studies of the National Polytechnic Institute, Guanajuato, Mexico*
Tetiana Pirog, PhD, Prof., *National University of Food Technologies, Ukraine*
Cristina Popovici, PhD, Assoc. Prof., *Technical University of Moldova*
Agota Giedrė Raišienė, PhD, *Lithuanian Institute of Agrarian Economics, Lithuania*
Egon Schnitzler, PhD, Prof., *State University of Ponta Grossa, Ponta Grossa, Brazil*
Oleksandr Shevchenko, PhD, Prof., *National University for Food Technologies, Ukraine*
Cristina Luisa Miranda Silva, PhD, Assoc. Prof., *Portuguese Catholic University – College of Biotechnology, Portugal*
Stefan Stefanov, PhD, Prof., *University of Food Technologies, Bulgaria*
Yordanka Stefanova, PhD, Assist. Prof., *University of Plovdiv "Paisii Hilendarski", Bulgaria*
María S. Tapia, PhD, Prof., *Central University of Venezuela, Caracas, Venezuela; COR MEM of the Academy of Physical, Mathematical and Natural Sciences of Venezuela*
Bảo Thy Vương, PhD, *Mekong University, Vietnam*

Managing Editor:

Oleksii Gubenia, PhD, Assoc. Prof., *National University of Food Technologies, Ukraine*

Contents

Editorial……. 607

Food Technology……..……..…….. 608

Paula Vieira Guedes, Egon Schnitzler
Effects of ultrasound treatment on different starches and their thermal properties... 608

Tatiana Cuşmenco, Irina Dianu, Natalia Netreba, Vladislav Reşitca, Artur Macari
Vegetable oil-based recovery of carotenoids from sea buckthorn pomace for butter fortification..... 645

Eunjeong Park, Ki Han Kwon
Plant-derived food processing by-products as functional protein and fiber enrichers……. 679

Hafize Fidan, Boryana Kavrakova, Ira Taneva, Ivayla Dincheva, Anton Lazarov, Stanka Damyanova, Albena Stoyanova
Essential oils rich in geraniol and citronellol……. 702

Ludmila Saleba, Maria Ratsuk, Tetiana Yurova, Eugen Kalinsky, Olha Semeshko
Technological role of psyllium-agar hydrocolloid system in improving the structure and sensory properties of gluten-free rice-corn cupcakes…….…….. 716

Esraa Shams, Mahmoud Gouda, Abd-Elbaset Salama, Galal Magdy
Bioactive compounds and antinutritional factors in olive pomace…… 732

Tamara Nosenko, Iryna Levchuk, Oleksandr Klymenko
Comparative evaluation of synthetic antioxidants for improving the oxidative stability of soybean oil……... 748

Aisha Noushad, Radhalakshmi Venugopal, Maya Raman, Nasreen Pathanayath Abdul Salam, Linu Mohammad Salim, Sajad Rehman, Jisha Manakulam Shaik Moideen, Anooja Thomas
Green synthesis of silver nanoparticles using *Piper betel* leaf extract for PLA-based active packaging films……. 762

Valeriy Demchenko, Olena Stabnikova, Andrii Marynin, Nataliia Rybalchenko
Active packaging films from PLA with *Rosmarinus officinalis* extract…… 786

Oleh Kuzmin, Oleksandra Niemirich, Olena Podobii, Yuliia Zaporozhets, Oleksandr Velikanov
Aroma characteristics and volatile composition of sterilized mushroom pâté…….. 802

Olena Tunik, Iryna Shevchenko
Physicochemical stability of cooked sausages during frozen storage under different cryostabilisation conditions…… 831

Microbiology, Biotechnology……..... 847

Hanna Bondar, Oleksandra Parkhomova, Viktoriia Krasinko, Olena Bilyk
Biotechnological potential of iron-adapted *Saccharomyces cerevisiae* for producing bakery products enriched with bioaccessible iron…… 847

Oksana Skrotska, Oleksandr Zholobko, Maria Protsenko, Iryna Kovshar
Current advances in biosynthesis of selenium nanoparticles using microorganisms 871

Processes and Equipment ……..... 921

Viktor Vytvytskyi, Oleksandr Sokolskyi, Ihor Mikulionok, Oleksandr Gavva, Vladyslav Vytvytskyi
Effect of viscoelastic properties on layer thickness distribution in coextruded packaging films…… 921

Economics and Management…….. 935

Mariana Dubravská, Elena Širá, Ladislav Mura
International business activities of food enterprises in the Slovak Republic considering current trends and business sustainability…….. 935

Andrii Dankevych, Meherun Nesa Mitu, Nurul Mohammad Zayed, Vitalii Nitsenko, Keisha LaRaine Ingram
Impact of retail food loss on undernourishment in developing countries…….. 949

Patrik Rovny, Lubos Smutka , Inna Cabelkova
Competitiveness of Visegrad Countries' sugar sectors after EU sugar quota abolition and under EU-Mercosur Agreement…….. 977

Instructions for authors……..... 998

Editorial

Russia continues to claim human lives, destroy Ukrainian cities and villages, damage industrial facilities, energy and transport networks, agricultural and logistics facilities, and healthcare institutions. Educational and research institutions are also among the targets of attacks, including schools, universities, and research institutes.

In September, a Russian drone attack on the Presidium of the National Academy of Sciences of Ukraine caused severe damage to its premises and resulted in loss of life.

The National University of Food Technologies, the founding institution of Ukrainian Food Journal, has also suffered significant damage. One of the university's buildings was severely affected, while more than 160 windows were shattered in another building. Classrooms, laboratories, and utility systems were damaged just as winter was approaching.



Presidium Building of the National Academy of Sciences of Ukraine
Source: Facebook page of Denys Kurbatov, Deputy Minister of Education and Science of Ukraine https://www.facebook.com/denys.kurbatov



Damaged Building of the National University of Food Technologies

Despite these extremely challenging circumstances, teachers, researchers, and students across Ukraine continue their educational and scientific activities. Ukrainian Food Journal also continues to publish, remaining free of charge for both authors and readers.

We thank the international community for its support of Ukraine, as well as the researchers whose valuable contributions help maintain the journal's scientific quality and ranking.

DOI: 10.24263/2304-974X-2026-15-3-3

Effects of ultrasound treatment on different starches and their thermal properties

Paula Vieira Guedes, Egon Schnitzler

State University of Ponta Grossa, Ponta Brazil

Keywords:

Modified starch
Ultrasound
Differential scanning calorimetry
Thermogravimetry

Article history:

Received 16.04.2026
Received in revised form 18.07.2026
Accepted 30.06.2026

Corresponding author:

Egon Schnitzler
E-mail: egons@uepg.br

DOI:
10.24263/2304-974X-2026-15-3-4

Abstract

Introduction. Starch is the most abundant natural biopolymer and the main energy reserve in plants. However, native starch often lacks the properties required for industrial applications. Starch can be modified by enzymatic, genetic, chemical, or physical methods, with physical modification being more environmentally friendly.

Materials and methods. In this review, the structures and properties of native starches and starches modified by ultrasonication, either alone or in combination with other modification methods, were examined based on the available literature. The reviewed studies indicate that the results obtained may differ even for starches derived from the same botanical source, depending on the treatment conditions and experimental parameters.

Results and discussion. The structures and main properties of native starches were discussed, as well as their changes after ultrasound treatment. The reported ultrasound power ranged from 60 to 600 W, frequency from 20 to 40 kHz, and amplitude from 40 to 70%, with starch-to-water ratios ranging from 3% to 90%. Starches modified by ultrasound in combination with other physical and chemical techniques were also considered. This review focused on the results obtained by thermogravimetry (TG) and differential scanning calorimetry (DSC). Under a nitrogen atmosphere, TG analysis generally shows two main stages of mass loss in starch: the first is associated with dehydration, followed by a region of relative thermal stability, while the second corresponds to thermal decomposition, resulting in a final carbonaceous residue of approximately 20%. Under an air atmosphere, starch generally exhibits three main stages of mass loss. The first is attributed to dehydration, followed by a region of relative stability, whereas the second and third stages correspond to consecutive processes associated with the decomposition of organic matter and subsequent oxidation, resulting in ash formation. DSC analysis can be performed under conditions similar to those used for TG analysis, and both endothermic and exothermic phenomena can be observed. However, DSC is mainly used to analyze the gelatinization behavior of starches. Gelatinization is a relatively weak thermal transition that occurs in the presence of water.

Conclusions. For both TG and DSC analyses, the experimental conditions are important, including the crucible type, heating rate, temperature range, sample mass, atmosphere (inert or oxidative, e.g., N_2, CO_2, or air), and gas flow rate. For DSC studies of starch gelatinization, the starch-to-water ratio and sample preparation conditions are also critical.

Introduction

One of the most abundant carbohydrates in nature is starch. It is the major reserve polysaccharide in green plants and an important source of energy. Starch is considered an essential source of energy for humans and animals (Bet et al., 2014; Dias et al., 2023; Ruths et al., 2024; Zhu et al., 2015). Starch is an important compound with a wide range of applications in numerous industrial sectors, including food, pharmaceutical, chemical, papermaking, textile, and medical industries. Therefore, starch and starch-based products play an important role in the global economy. Starch consists mainly of two polysaccharides: α-amylose and amylopectin. The main botanical sources of starch include cereals (corn, wheat, rice, barley, and rye), legumes (lentils, beans, soybean, and faba bean), roots and tubers (potato, cassava, yam, and sweet potato), and unripe fruits (banana and mango) (Bet et al., 2018; Borsato et al., 2022; Lindeboom et al., 2004).

In its native form, starch rarely possesses all the characteristics required for industrial applications. Starch can be modified by physical, chemical, enzymatic, or genetic processes (Kumari & Sit, 2023; Mainardes et al., 2024; Rubanka et al., 2025; Shulga & Shulga, 2026). These modification methods can provide starch with specific functional properties required for various technological applications. In recent years, the use of physical methods for starch modification has increased, mainly due to the need to reduce environmental pollution associated with chemical modification processes (Ashogbon & Akintayo, 2014; BeMiller & Huber, 2015; Carmona-Garcia et al., 2016; Sujka, 2017).

Ultrasound is a physical method that has been successfully applied to the treatment of various types of starch. Ultrasound refers to sound waves with frequencies above the upper limit of human hearing (generally above 20 kHz). Ultrasound waves propagate through a liquid medium and are generated by transducers, which can be piezoelectric or magnetostrictive. These transducers produce high-energy vibrations that are amplified and transferred to a sonotrode or probe in direct contact with the liquid medium containing starch (Carmona-Garcia et al., 2016; Herceg et al., 2010).

Thermal analysis is the study of the relationship between a property of a sample and its temperature while the sample is heated or cooled under controlled conditions. This definition encompasses several techniques, among which differential scanning calorimetry (DSC) and thermogravimetry or thermogravimetric analysis (TG or TGA) are commonly used in food science. DSC measures the difference in heat flow rate between a sample and a reference material, and the resulting curve is referred to as a DSC curve. TG or TGA measures the mass of a sample as a function of temperature, producing a TG or TGA curve. Derivative thermogravimetry (DTG) represents the first mathematical derivative of the TG or TGA curve. The DTG curve is useful for determining the main stages and temperatures of mass loss observed in TG curves.

In TG and DSC experiments, the experimental conditions are of great importance, including the type of crucible, heating rate, temperature range, sample mass, atmosphere (e.g., N_2, air, or CO_2), and gas flow rate. In DSC studies of starch gelatinization, the starch-to-water ratio and sample preparation conditions are also important factors (Bernal et al., 2002; Cavalheiro et al., 1995; Giolito & Ionashiro, 1988; Ionashiro & Giolito, 1986; Lever et al., 2014; Wendlandt, 1986).

This review aims to summarize the results reported in the literature for different native and ultrasound-modified starches, with particular emphasis on the main findings obtained using thermal analysis techniques, including thermogravimetry (TG), derivative thermogravimetry (DTG), and differential scanning calorimetry (DSC).

The literature search was conducted using the ScienceDirect database because of its extensive coverage of Food Science and Technology. The following keywords and combinations were used: “Ultrasound-modified starch”; “Ultrasound treatment AND starch structure”; “Ultrasound AND starch properties”; and “Ultrasound-assisted modification of starch”.

Structures and properties of native starches

Starch granules exhibit a hierarchical structure with dimensions ranging from more than 1 to 100 μm, growth rings of 100–400 nm, blocklets of 20–50 nm, crystalline and amorphous lamellae of 9–10 nm, and molecular structures of 0.1–1 nm (Wu et al., 2022). The growth rings are composed of blocklets formed by alternating amorphous and crystalline lamellae. Crystalline lamellae consist mainly of clusters of amylopectin lateral chains organized into double helices, whereas amorphous lamellae are primarily composed of amylopectin branching points (Wu et al., 2022; Zhu, 2015). These distinct structural arrangements have been classified into starch polymorphs, categorized as A, B, and C types, with the latter representing a combination of A- and B-type structures. The packing of double helices in type A polymorphs is relatively compact and associated with a lower water content, whereas type B starch exhibits a more open structure containing a hydrated helical core (Bonto et al., 2021; Hsein-Chih & Sarko, 1978).

Native starch typically contains 15–30% amylose, with the remaining 70–85% consisting of amylopectin. The molecular weight of amylopectin is significantly higher than that of amylose, and the overall structure of starch can be described as a complex semicrystalline matrix (He et al., 2023a). In addition to its main components, amylose and amylopectin, starch granules interact with other biomolecular constituents and contain minor amounts of non-carbohydrate components, such as lipids, proteins, and mineral salts (e.g., phosphorus). These components play important roles in determining starch functionality (Alcázar-Alay et al., 2015; Raghunathan et al., 2021) and influence the structural changes that occur during processing (Bonto et al., 2021).

Native starch exhibits low stability, is insoluble in water and iodine at room temperature, is prone to retrogradation, and is susceptible to viscosity loss under low pH and high-temperature conditions (Bonto et al., 2021; He et al., 2023). It also displays low shear resistance (Raghunathan et al., 2021). These characteristics limit it potential applications in food processing (He et al., 2023; Kaur & Gill, 2019).

When native starch is heated in an aqueous medium, the granules absorb water and progressively swell, accompanied by leaching and partial solubilization of their components. This process advances until the granular structure collapses and loses its organization, a phenomenon known as gelatinization. Subsequently, during system cooling, the amorphous regions of polysaccharide chains interact through hydrophobic forces, promoting molecular reassociation and reorganization, a process referred to as retrogradation (Zhu, 2015).

Ultrasonication in the modification of starch structures and properties

Ultrasonication is a technology that employs mechanical waves within different ultrasound frequency ranges, including diagnostic low-energy ultrasound (high frequency: 1–10 MHz), extended-range ultrasound (100 kHz–1 MHz), and power ultrasound (16–100 kHz) (Bonto et al., 2021). For food materials, ultrasound can be classified as either modifying (high-power ultrasound) or sensing (low-power ultrasound) (Awad et al., 2012; Bonto et al., 2021). High-power ultrasound (>5 W/cm²) at lower frequencies (around 40 kHz or within the

range of 20–100 kHz) has been used to modify the functional and physicochemical properties of food products, providing beneficial preservation effects while maintaining product quality and ensuring food safety (Bonto et al., 2021; Ding et al., 2019; Ogutu et al., 2015; Sango et al., 2014). Consequently, this technology has broad potential for industrial processing, particularly for the modification of biopolymers such as starch, which is an essential ingredient in a wide variety of food products.

Starch structural modification can be effectively promoted through high-intensity ultrasonication (HIU), and its effectiveness has been demonstrated in numerous studies. This treatment can alter several starch characteristics, including amylose content, granule aggregation and structure, solubility, and viscometric behavior. Ultrasonic treatment can induce physical depolymerization of starch and affect its double-helical structure, promoting changes toward less ordered or single-helical structures and thereby modifying its physicochemical properties (Li et al., 2018). A schematic overview of ultrasound-induced modifications in starch structure and physicochemical properties is presented in Figure 1.

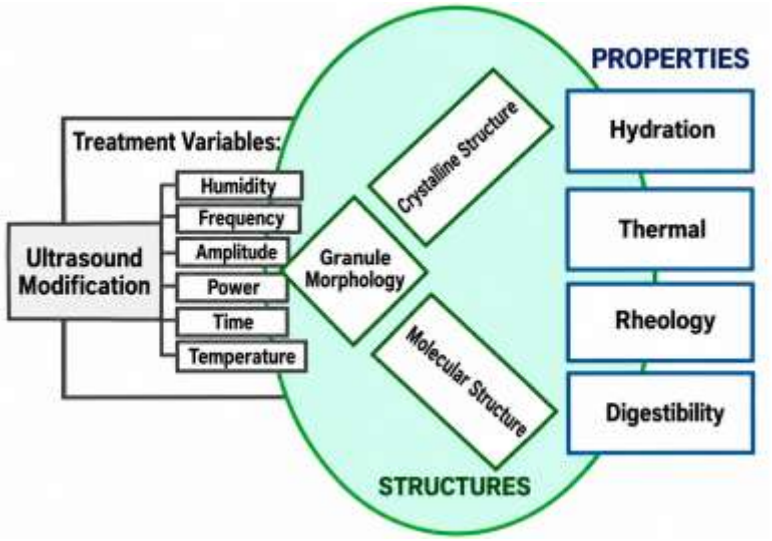

Figure 1. Schematic overview of ultrasound-induced modifications in starch structure and physicochemical properties

Specifically for starch, ultrasonication has been applied in various fields, including food preservation and processing, emulsification, starch inclusion complex formation, development of starch-based edible films, and the production of bioethanol from this polymer. Overall, starch modification by ultrasound stands out as a simple, efficient, high-yield, and environmentally friendly process, as it does not generate residual waste. However, key limitations include heat generation during processing, which may increase the system temperature, and insufficient standardization, reproducibility, and stability of the resulting modifications (Wu et al., 2022).

Ultrasonic treatment of starch is predominantly carried out using ultrasonic bath or probe systems. Baths generally operate at fixed frequencies, with variations only in acoustic energy density or output amplitude, whereas probe systems receive energy from a transducer resonating at a defined frequency, delivering ultrasonic energy directly to the sample.

Commercial probe sonicators are equipped with generators operating in a narrow frequency range (±500 Hz around 20 kHz) and allow precise amplitude control, enabling adjustments to fine-tune ultrasonic vibrations at the probe tip. The choice between systems depends on the characteristics of the sample. Probe systems are generally more suitable for samples dispersed in liquid media because they provide more consistent amplitude delivery despite changes in sample concentration, volume, viscosity, and temperature during processing (Bonto et al., 2021).

Starch modification by ultrasound occurs primarily through acoustic cavitation, which involves the rapid formation, growth, and violent collapse of microbubbles in the liquid medium (Li et al., 2018). The physical effects generated by cavitation, such as localized pressure, temperature fluctuations, and turbulence, together with its chemical effects, determine the extent and nature of ultrasonic modification (Wang et al., 2022). In starch-water systems, the energy generated by cavitation is transferred to starch granules, promoting intense shear forces and increasing temperature (Zhu, 2015). These effects result in degradation of macromolecular C–C bonds and formation of long-chain radicals (Kim et al., 2013; Manchun et al., 2012), suggesting molecular chain scission and the production of linear fragments (Chanet al., 2010), which in turn lead to structural and property changes in starch (Zhu, 2015).

In addition to cavitation, another mechanism associated with ultrasonication is radical attack, whereby partial decomposition of water produces hydroxyl (•OH) and hydrogen (•H) radicals that degrade starch polymers (Chan et al., 2010; Raghunathan et al., 2021). Recombination of these radicals may yield new molecular products, and their action likely induces chemical alterations in starch through molecular chain scission (Czechowska-Biskup et al., 2005).

Studies demonstrated that ultrasound treatment degrades starch polymers, generating amorphous starch with increased amylose content, reduced viscosity, and increased solubility (He et al., 2023). These findings are consistent with the results of Amini & Razavi (2015). However, starch granule corrosion was not observed when low-power ultrasound (2.5 and 4.1 W) was applied, suggesting that ultrasonic power magnitude is a critical parameter for mechanical distortion of starch granules (Bonto et al., 2021; Zuo et al., 2009).

Results from multiple studies confirm significant changes in starch treated with high intensity ultrasound. Ding et al. (2019), observed that treating retrograded starch with high intensity ultrasound (100–600 W for 30 min) increased apparent amylose content, rapidly digestible starch, and slowly digestible starch, while resistant starch and enzymatic resistance decreased. Wang et al. (2020) found that high intensity ultrasound treatment of sweet potato starch (300 W for 15–30 min) disrupted starch aggregation structure, increased swelling power and solubility, and reduced pasting temperature and viscosity (Table 1).

In a recent study, Wang et al. (2022), treated kiwi starch to investigate structure–function relationships under varying power levels (0, 200, 400, 600 W) and durations (0, 10, 20, 30 min). High-power ultrasound destroyed the granular morphology, forming pits and cracks and reducing particle size. Significant increases were observed in amylose content, swelling power, water solubility index, viscosity, and setback value. Regarding pasting and gel texture properties, ultrasound disrupted the ordered double-helical structure and decreased crystal number, thereby reducing gelatinization temperature. Overall, both storage modulus (G′) and loss modulus (G″) increased, demonstrating elastic characteristics. A significant increase in resistant starch was also observed, while rapidly and slowly digestible starch fractions decreased.

Table 1

Gelatinization temperature range of different starch sources (To –Tc)

Starch of plant	T_{Gel} (°C)
Rice (*Oryza sativa*)	68–78
Potato (*Solanum tuberosum*)	59–68
Cassava (*Manihot esculenta*)	60–76
Arracacha (*Arracacia xanthorrhiza*)	59–69
Maize (*Zea mays*)	62–72
Wheat (*Triticum aestivum*)	58–64
Common vetch (*Vicia sativa*)	65–72
Chickpea (*Cicer arietinum*)	60–75
Lentil (*Lens culinaris*)	62–74
Common bean (*Phaseolus vulgaris*)	65–80
Green banana (*Musa spp.*)	70–82
Loquat (*Eriobotrya japonica*)	60–71
Amaranth (*Amaranthus* spp.)	68–74
Brazilian pine seed (*Araucaria angustifolia*)	60–71

Source: adapted from Andrade et al. (2014); Cordoba et al. (2016); Li et al. (2022); Liu et al. (2021); Romko (2024); Santos et al. (2025); Wang et al. (2020); Zhang et al. (2023); Zhu (2015); Zuo et al. (2024)

Kong (2018) reported that ultrasound induces superficial damage to starch granules and increases swelling power and water solubility, while simultaneously reducing crystallinity, pasting viscosity, and the relative degree of polymerization. The effects of ultrasound on starch structure and properties, summarized in Table 2, can be outlined as follows: granule deformation; formation of surface pores and fissures; reduction in relative crystallinity (RC) without altering the crystalline type; degradation of molecular chains accompanied by a decrease in weight-average molecular weight (MW); increase in amylose content (AM); and increases in solubility (S) and swelling power (SP). Conversely, reductions are observed in peak viscosity (PV), final viscosity (FV), minimum viscosity (MV), breakdown viscosity (BV), and setback viscosity (SV), as well as in gelatinization temperatures: onset (To), peak (Tp), and conclusion (Tc). Furthermore, starch pastes tend to exhibit more elastic characteristics, and digestibility may increase or decrease depending on the treatment conditions (Wu, 2022). Table 2 show several studies with different starches treated by ultrasonication.

Thermal properties

Evidence indicates that ultrasonic treatment promotes a reduction in gelatinization temperatures (To, Tp, and Tc) as well as in pasting parameters (PV, FV, TV, SV, and BV) in chestnut starch (Wang et al., 2020) and conventional maize starch (Wu et al., 2022). In addition, a decrease in gelatinization enthalpy (ΔH) has been observed in several starches, including waxy and normal maize (Amini & Razavi, 2015; Jambrak et al., 2010; Wang et al., 2020; Yang et al., 2019), sweet potato and chestnut starches (Wang et al., 2020), cassava starch (Monroyet al., 2018), and retrograded high-amylose maize starch (Veelaert, 2014).

This reduction in enthalpy, is directly related to the length of amylopectin branched chains, has been attributed to amylopectin degradation, as well as to the disruption of crystalline structures and ordered double-helical regions (Falsafi et al., 2019; Raghunathan et al., 2021; Yang et al., 2019).

However, the thermal properties of a 5% (w/v) suspension of non-waxy rice starch were affected by ultrasonic power, treatment time, and amplitude (100–1000 W, 0–120 min, and amplitudes of Φ6 and Φ10). Within a short ultrasonication period (0–60 min), the onset temperature (To), peak gelatinization temperature (Tp), and gelatinization enthalpy (ΔH) decreased markedly, but increased when the treatment was extended to 120 min. In this regard, destruction of the granular structure caused by higher ultrasonic intensity may facilitate water penetration into starch granules and promote interactions with starch chains, thereby reducing To and Tp. Conversely, prolonged treatment increased the temperature of the rice starch suspension and caused partial gelatinization and chain cross-linking, which led to increases in To and Tp (Yu et al., 2013).

In another study involving normal, waxy, and high-amylose maize starches, ultrasonic treatment resulted in a slight increase in To values and a reduction in gelatinization enthalpy (Yu et al., 2013).

In the study by Zheng et al. (2013), the peak viscosity of starch subjected to dual-frequency ultrasonic treatment was lower than that of native starch. The solubility of treated starch, compared with native starch, increased with ultrasonic exposure time, and dual-frequency ultrasonic treatment reached peak viscosity after 60 min.

Ultrasonic treatment reduced starch crystallinity to varying extents, depending on processing conditions (Ding et al., 2020; Kaur & Gill, 2019; Li et al., 2018; Monroy et al., 2018; Wang et al., 2020; Zhu et al., 2012). For example, under probe-type sonication (0–155 W, 30 min), potato starch crystallinity slightly decreased from 24.2% to 21.0% (53), whereas probe-type sonication (300 W, 15–30 min) reduced the crystallinity of sweet potato starch from 31.6±1.3% to 26.1±1.5% (Wang et al., 2020).

Regarding ultrasonic power, To and Tp were not affected at low power levels (< 500 W), which may be due to the pressure generated by ultrasound being insufficient to induce changes in starch granules; however, both parameters decreased markedly when the power was increased to 1000 W. With respect to ultrasonic intensity, both To and Tp decreased when treated at amplitude Φ6 and power of 100–1000 W for 60 min but increased when the treatment time was extended from 60 to 120 min under the same conditions.

Herceg et al. (2010), investigated the impact of high-power ultrasound on the rheological and pasting properties of wheat starch, showing that mechanical damage to starch granules facilitated water penetration into the granules during heating, resulting in changes in starch rheology and pasting behavior. The treatment reduced the gelatinization temperature of treated starch compared with native starch, which accounted for greater granule swelling upon heating. These findings are consistent with those of Bel Haaj et al. (2013), who described the isolation and characterization of starch nanoparticles produced by high-intensity ultrasound and found that this treatment improved solubility, swelling power, and water absorption capacity, while decreasing the viscosity consistency index and gelatinization enthalpy.

In waxy maize starch, an increase in pasting temperature has been reported and attributed to greater resistance of starch granules to swelling. In contrast, peak viscosity and setback values decreased. This behavior is explained by the intense shear forces generated during the cavitation process, which promote the cleavage of long polymer chains into shorter segments, resulting in lower peak viscosity. Furthermore, ultrasonication tends to inhibit the retrogradation process, contributing to reduced setback values. On the other hand, in rice

starch, higher peak viscosity values have been reported, possibly related to the presence of a higher proportion of low-solubility components, which require greater energy. The higher setback values may be associated with the depolymerization of components leached during ultrasonic treatment (Yang et al., 2019).

Double modification of starches

The dual modification method is developed using a combination of two modification techniques which may be physical-physical, physical-chemical, physical-biological, chemical-chemical, chemical-biological, or biological-biological (He, 2023). In one study, dual physical modification proved more effective than single physical modification. The physicochemical properties of corn and potato starches modified solely by ultrasound and microwave treatments were compared against those modified via dual treatment (Zhou, 2023). The results demonstrated that dual modification significantly influenced the solubility, dehydration rate, and *in vitro* digestibility of potato starch, as evidenced by the data presented in Table 3.

Ultrasound, as a physical modification method, can also facilitate the chemical or enzymatic modification of starch (Zhang et al., 2020). As an aid to chemical modification, ultrasound offers advantages such as the use of smaller quantities of chemicals and reduced processing time (He et al., 2023).

Porous starch is a modified starch product that has recently attracted interest. It features abundant pores distributed across the granule surface and extending toward the central cavities, without compromising the integrity of its granular structure (Li et al., 2016; Veelaert, 2014).

Porous starch can generally be produced using three common modification methods: enzymatic treatment, chemical/physical treatment, or a combination of enzymatic and chemical/physical treatments (Latip et al., 2020). The formation of pore structures within the starch granule results in a large surface area and high pore volume, enabling the use of porous starch in numerous applications—such as a carrier for flavors, probiotics, antioxidants, vegetable oils, and drugs, as well as an adsorbent for heavy metals and a component in skincare fluids, among others (Latip et al., 2020; Li et al., 2016).

The unique characteristics and advantages of porous starch have driven further research in this field, focusing on understanding physicochemical properties, enhancing porous structure, developing porous starches from new sources, and exploring their applications. Although enzymatic hydrolysis alone can produce porous starch, its efficiency can be further improved when combined with physical treatments, such as ultrasonication (Li et al., 2016).

Table 2

Different starch sources subjected to ultrasound modification

	10% (w/v); Amplitude: 40, 50, 60 and 70%; Frequency: 20 kHz; Time: 30 min.	Crystallinity increased after US but remained below native starch; particle size increased up to 50% amplitude and decreased at higher intensities, without evidence of granule agglomeration.	–	40% US: lower ΔH; 50%: highest degradation temperature; 60%: widest thermal stability range.		DSC-Q200; 2.5 mg sample + 10 μL distilled water (1:4, w/v); hermetically sealed aluminium pans; 20–100 °C at 10 °C/min; air flow 50 mL/min.		
Arrowhead tubers (*Sagittaria sagittifolia* L.) - linoleic/stearic acid complexes	Dual-frequency power ultrasound (20/40 kHz; 20, 40 and 60 min)	Formation of V-type crystalline structures (V6-I, II); ↑ short-range molecular order (FTIR 1045/1022 cm^{-1}); CI >65%; sponge-like/flaky morphology depending on fatty acid complex; ↑ complexing index; flaky, irregular structure with rough surfaces.	–	DSC confirmed V-type crystalline structure	–	3–5 mg sample + 16 μL water in sealed pans and equilibrated for 24 h. Heated from 25 to 150 °C at 10 °C/min; To, Tp, Tc and ΔH determined.	↑ Digestion resistance; partial conversion ofRDSto RS; potential application in functional starch-based ingredients.	

	Starch in water: 5% (p/v); In a probe-type sonicator at 20 kHz, intensity 39, 48, 63 W/cm² or an ultrasound bath with an intensity of 5 W/cm²; Time: 10 and 20 min.; Temperature: 25 °C.	Presence of fissures and pores on the surface of the starch granules, reduction in size at the highest sonication (US) intensity, and increased amylose content. A decrease in the degree of crystallinity. It was shown that the crystalline structures of oat starch granules were destroyed to some extent after US, whereas the A-type crystalline pattern remained unchanged.	Decreased swelling power, solubility, transmittance, water- and lipid-retention capacity. The syneresis results revealed larger amounts of water expelled from US starch gels during 5 days of storage compared with native gels.	The onset, peak and final gelatinisation temperatures increased, whereas the gelatinisation temperature range decreased due to US. Decrease in ΔT and ΔH.	Decrease in paste viscosity with ultrasound treatment. Gel hardness decreased after US.	~1 mg starch (1:3, starch:water, w/w); 25–125 °C, 10 °C/min		
	Starch in water: 40% (p/v); Power: 200 W; Frequency: 24 kHz; Amplitude: 50 and 100%; Cycle: 0.50 and 0.75 (100%); Time: 20 and 60 min.; Temperature: 40 °C	Cracks, fissures, depressions and cavities were observed on the surface of the granules; damage to the granules increased with increasing US cycle, producing more visible erosion. It causes debranching of amylopectin (AP).	An increase in solubilized starch content and a decrease in the Mw of dissolved starch occurred with increasing cycle, amplitude and treatment time. However, increasing the cycle led to a slight increase in Mw.	Tg (glass transition temperature) decreased by up to 17% compared with native starch.	The US-treated starch showed pseudoplastic behaviour and significantly reduce paste viscosity (V), with greater US intensity producing greater reduction in V. It reduced the resistance of the system (gel).	–		

	Starch in water: 10% (p/v); Frequency: 20 kHz, Power: 60, 105, 155 W; Temperature: 16, 21 and 33 ºC; Time: 30 min.	US induced notches and grooves on the granule surface. The B-type crystalline structure was little affected. The surface fractal structure transformed into a mass fractal structure in starch granules with increasing power, indicating that compact starch granules swelled to a greater extent and became looser. The morphology and crystallinity of the crystals were little affected. Disordering of the crystalline lamellae reduced molecular order. The amylose (AM) structure was more a f f e c		–		–		
Potato, wheat, maize and rice (*Solanum tuberosum, Triticum aestivum, Zea mays* and *Oryza sativa*)	Starch in water/ethanol: 30% (p/v); Frequency: 20 KHz; Power: 170 W; Time: 30 min.; Temperature: 20 ºC.	Cracks and depressions appeared on the granule surface, especially for potato and wheat starches. Potato starch sonicated in ethanol showed no signs of erosion. US treatment was more effective in large granules than in small granules. Water was a good medium for the cavitation process compared with ethanol.	Increased solubility, WAC and swelling power (SP).	–	Decrease in paste viscosity with US treatment.	–	–	
Sweet potato (*Ipomoea batatas* L. Lam.)		Increased porosity and severe damage to the crystalline structure.		–			–	

Sweet potato (*Ipomoea batatas* L. Lam.)	Starch in water: 6% (w/w); Power: 300 W; 20 kHz, 30 °C for 15, 20, 25 and 30 min, using pulsed mode (3 s on/5 s off) with a 13 mm probe. Time: 15–30 min.	Pores, fissures and depressions appeared on the granule surface, with greater structural changes as treatment duration increased; the crystalline type remained unchanged, but RC decreased; AM increased, whereas the ordered double-helix content was reduced.		Tc and ΔH decreased. Decreased crystallinity and gelatinisation temperature; disruption of ordered structures.	SV increased; PV, FV and BV decreased. G′ > G″ and both increased with US time and frequency. Decreased pasting temperature, peak, final and breakdown viscosities; enhanced retrogradation and gel strength.	DSC Q2000; sample adjusted to 70% moisture and equilibrated at 30 °C for 12 h; heated from 30 to 100 °C at 5 °C/min; empty aluminium pan as reference. Gelatinisation parameters: To, Tp, Tc and ΔH. –	Development of starch-based ingredients with tailored functionality	
		Surface with depressions and pores, with change in size.	Increased hydrolysis rate and absorption.		Change in pasting behaviour.	Increase in hydrolysis rate.	Production of starches with modified properties.	
Mung bean (*Vigna radiata* L.)	α-Amylase(5 U/g), bathsingle-frequency bath ultrasound (25, 40 kHz) and dual frequency (25 - 40 kHz).	The pores on the granule surface gradually increased and became larger, and particle size decreased.	–	–	The reduction in sugar content increased, starch retrogradation accelerated, and PV decreased.	–	Enhanced starch hydrolysis; potential application in starch modification for the food and other processing industries.	

Chickpea andlentil (*Cicer arietinum* and *Lens culinaris*)	Starch in water: 5% (p/v); Power: 30%; Amplitude: 50%; Time: 15 min.	Decrease in mean granule diameter compared with native starches. Significant change in starch morphology.	SP increased and solubility decreased ($p < 0.05$).	Apparent viscosity decreased ($p < 0.05$). Gelatinisation temperatures (To, Tp, ΔT, ΔH) decreased with US treatment.	The starches showed typically non-Newtonian and shear thinningbehavior since the viscosities of both samples showed a decrease with increasing shear rate. Flow behavior index of the starchdid not show significant change with US ($p < 0.05$).	The starch suspension with a starch to water ratio of 1:2 (w/w) was prepared by mixing on magnetic stirrer. The suspension was loaded into the aluminum pans with a capacity of 30 μl. The samples were heated from 25 to 120 °C with a heating rate of 10 °C/min.	Its use is practical due to higher isolation efficiency and lower production costs. Increase stability, processability, and resistant starch content, and in-crease or decrease viscosity and gelatinization time. As thickening agents, stabilizers, and emulsifiers.	
	Time: 3–9 min.	Surface with roughness, fissures and slight damage. Birefringence and B-type crystalline pattern unchanged; RC reduced.	Tendency towards increased solubility with higher intensity.	Stable.	PV and FV decreasedwith increasing treatment time and amplitude.	–		
	Starch in water: 5% (p/v), were treated under 5 US conditions: Power: 200 W for 30 min.; 400 W for 30 min.; 600 W for 30 min., 20 and 10 min.	Destroyed the granular morpho-logy, formed holes and cracks on the surface, and reduced particle size and short-r a n g	Swelling power, water solubility index increased.	GT decreased ($p < 0.05$).V and SV *(setback)* increased ($p < 0.05$).	Elastic characteristics with increasing G′ and G″. In the pasting and gel texture properties, US destroyed the ordered double-helix structure of the starch and reduced the number of crystals, reducing GT.	To, Tp, Tc, and ΔH were determined using DSC.	Special food applications: ingredients in systems requiring gelatinisation at lower T, prebiotic formulations and high-RS functional foods. Potential for starch-based products with improved processing performance.	

	Starch in water: 45% (p/v); Power: 90, 180, 270, 360 and 450 W; Frequency: 25 kHz; Time: 30 min. Pulse: 5:5 s; Temperature: 25 ºC	Surface pores increased with US power; ordered aggregate structure loosened; short-range order and double-helix organisation increased; amorphous region expanded.	–	The gelatinisation temperature and thermal stability increased.	At 270 W, PV and FV were 2.23 and 2.64 times higher than those of native starch. Gelatinisation V decreased at powers of 360 and 450 W. Starch viscoelasticity increased, but decreased at powers of 360 and 450 W.	DSC 2500; 5 mg sample + 10 µL distilled water; equilibrated at 4 °C for 12 h; heated from 30 to 160 °C at 10 °C/min.	Production of starch-based products with tailored quality and functional Properties	
	Starch in water: 5% (p/v); Temperature: 20±1 ºC; Amplitude: 60 and 80%; Time: 40 min. (60%), 10 and 30 min. (80%).	Degradation of the starch polymer with the appearance of cracks, fissures and surface erosion. 80% for 30 min. caused the greatest structural damage.	Higher solubility. There was an increase ($p < 0.05$) in SP, mainly in the higher-intensity treatments.	Reduction in GT and ΔH, indicating lower crystalline organisation.	Change in PV; in some treatments there was a reduction in V. 80% for 30 min. showed the greatest rheological modification.		Thickener with faster hydration; ingredients for instant-preparation products.	
	Starch in water: 5% (p/v); Power: 750 W; Amplitude: 40% and 60%;	The granule surface became rough and showed fissures and channels; the C-type crystalline pattern was unaffected, but RC was reduced.		Under the most severe conditions, the thermal transition was undetectable;ΔH was reduced.	Newtonian behaviour. Changes at molecular level; improved paste stability under refrigeration		Tailor-made starch derivatives with controlled properties for specific food and industrial applications.	
Cassava and maize (*Manihot esculenta* and *Zea mays*)	Starch in water: 20 % (p/v); Amplitude: 40 kHz; Frequency: 99%; Time: 10 and 20 min.; Temperature: 26±2 ºC.	Grooves, cracks, notches and spots appeared on the surface. There was a slight decrease in the degree of crystallinity of maize starch and cassava starch compared with the n a t i		GT did not change with the treatments, but ΔH decreased for cassava and maize starch after 10 min of treatment and increased after 20 min of treatment.	–	Sample: 5 mg were placed in the aluminum pans and mixed with 20 µl of water; sealed a n d l	Systems requiring texture modification without altering the gelatinisation temperature.	Rahaman et al., 2021

			–	Higher degra-dation T and thermal stability at certain amplitudes.	Increase in PV and shear resistance.			
Cassava, maizenormal maize and yam (*Manihot esculenta, Colocasia esculenta* and *Zea mays* L.)	Starch in water: 10% (p/v); Amplitude: 20 kHz; Time: 30 min.	Cracks and corrosion appeared on the granule surface; small particles were generated; yam starch was more sensitive to US than cassava and maize; the crystalline structure was strongly affected; RC and short-range order were reduced. Crystallinity values decreased compared with native starches.	–	Reduction in thermal stability and crystallinity values compared with native starches.			Micro- and nanoparticles are useful in food packaging (composite materials) and drug delivery (carriers).	
Indian wheat (*Triticum aestivum* L.)	30 kHz probe; Power: 100 W, 100% amplitude, pulsed mode (80% duty cycle); Time: 15 or 30 min; 10% (w/v) starch suspension.	Surface scrapes and deformities; A-type crystalline pattern retained; ↑ relative crystallinity; ↓ FTIR 1022/995 cm^{-1} ratio; altered granule size distribution.	↑ Swelling power; ↑ oil absorption capacity; ↑ amylose content.				Improved hydration and oil absorption; potential for functional food applications.	
High-amylose maize (*Zea mays* L.)								

	Starch in water: 5% (p/v); Frequency: 25 kHz, 20 kHz and dual frequency 20 to 25 kHz; Power (max.) 400 W; Time 40 min.; Temperature: 30 ºC.	Native maize starch had a polygonal shape with a solid surface. Some pores and surface erosion were observed on the granule surface after a single US treatment. Dual-frequency treatment caused changes in granule size and produced greater surface erosion in maize starch granules compared with single-frequency treatment.				Hu et al., 2015
Normal maize, waxy maize and amylomaize (*Zea mays* L. *var. ceratina* and *Zea mays* L.)		Breakdown of starch chains in the amorphous region, allowing chain reorganisation. Porosity and rupture in amylose-rich starch.	Increase in swelling power and solubility, with reduced viscosity.	Slight shift of gelatinisation temperatures to higher values.		
	Starch in water: 10–20% (w/w); Temperature: 25-65 ºC; Frequency: 24 kHz; Time: 10-20 min.; Amplitude: 50-100%.	The granule surface was damaged by the treatment, with fissures and cavities. Crystallinity was maintained with an A-type pattern, with slight modifications in the amorphous regions.	Increase in solubility and SP.	Decrease in gelatinisation ΔH and reduction in the GT range, pseudoplasticity and consistency coefficient.	Decrease in apparent viscosity and consistency, with paste showing lower shear resistance.	

	Starch in water: 10% (p/v); Frequency: 24 kHz; Power: 100, 300 and 400 W; Amplitude: 100%; Intensities: 34, 55, 73 W/cm² (probe) and 2 W/cm² (bath); Time: 15 and 30 min.	Rupture and damage to the starch granule.Treatment of maize starch distorts the crystalline region of the starch granules before reversible hydration of the amorphous phase, resulting in destruction of the granular structure.	The increase in swelling power is associated with the water absorption capacity and solubility of maize starch granules, respectively.The easier entry of water into maize starch granules is due to granule rupture by US, which leads to greater water absorption and retention.		A decrease in the consistency coefficient (k) was also observed. k gradually decreased with increasing ultrasound power.	Starch suspensions were sealed in aluminium pans, equilibrated for 24 h, and heated from 25 to 95 °C at 10 °C/min. To, Tp, Tc, and ΔH	Improved hydration properties; potential for starch modification in food applications.	
Normal maize (*Zea mays* L.)	Starch in water: 30% (w/v); Frequency: 40 kHz; Power: 420–540 W; Temperature: 40–60 ºC; Time: 20–40 min.	Damaged granules with notches and cracks on the surface. Surface notches and grooves; ↓ relative crystallinity; A-type crystalline pattern retained; reduced birefringence.	–	ΔH decreased; To, Tp and Tc increased and decreased.	↓ Peak viscosity (PV), ↓ breakdown (BV), ↓ setback (SV)	3 mg starch (1:3, starch:water, w/w) equilibrated for 12 h; heated from 20 to 100 °C at 10 °C/min. To, Tp, Tc, ΔT, and ΔH were	↑ Enzymatic hydrolysis efficiency; reduced liquefaction time; ↑ dextrose equivalent (DE).	

Waxy maize (*Zea mays* L. var *ceratina*)	Starch in water: 3% (p/v); DBS in deionised water; Power: 25 kHz; Time: 4, 8 and 12 min.	US and recrystalization treatment resulted in a uniform size of starch nanoparticles and their distribution in the aqueous system.					Debranched starch nanoparticles are used as thickening agents, adsorbent materials and in functional foods.	
Waxy maize (*Zea mays* L. var *ceratina*)	30% (w/w) waxy corn starch dispersion; ultrasound treatment at 15 kHz and 100 or 400 W for 40 min at 25 °C using a 38 mm titanium probe; subsequent cooling at 5±0.5 °C.	Some notches and grooves appeared on the granule surface; the A-type crystalline structure was unchanged, but RC, double-helix content and Mw decreased.	–	To, Tp and Tc increased, whereas ΔH, PV, TV, BV, FV and SV decreased. Ultrasound increased gelatinisation temperatures (To, Tp and Tc) and decreased gelatinisation enthalpy (ΔH). At 400 W, To, Tp and Te increased by 5.28, 3.69, 5.32 °C, while ΔH decreased from 14.13 J/g (native) to 10.21 J/g, indicating disruption of weak crystalline structures and double-helical order.	Ultrasound increased pasting temperature (67.43–68.00 °C) and decreased peak viscosity and setback, indicating greater resistance to swelling and reduced short-term retrogradation. The effects were more pronounced at 400 W.	DSC Q2000; starch:water ratio of 1:2 (w/v); sealed in aluminium pans and equilibrated overnight at room temperature; heated from 20 to 120 °C at 10 °C/min under N_2; empty pan as reference.	Potential use in food applications requiring modified structural and functional properties	

	Starch in water: 10% (w/v); Powers: 100, 200, 300, 400, 500, and 600 W; 20kHz;1200 W; Probe: 6 mm. Pulse-mode ultrasonication: 2 s on/2 s off for 30 min in an ice bath; samples cooled to room temperature.	Ultrasound altered starch morphology, producing a more compact block-like structure; increased particle size, short-range molecular order and V-type crystallinity, while reducing long-range order.	Swelling power and solubility decreased at low temperature (65 °C) but increased at higher temperatures (80–95 °C), particularly after high-power ultrasonication.	Decreased ΔH associated with amylopectin double helices and increased ΔH associated with V-amylose single helices.	Increased slowly digestible starch (SDS) and resistant starch (RS) fractions, with a reduction in rapidly digestible starch (RDS).	DSC: 1 mg starch with 1.5 μL distilled water, equilibrated for 24 h; 30–180 °C at 10 °C/min.	Regulation of starch digestibility in starch-rich foods.	
Retrograded maize with high amylose (*Zea mays* L.)	Frequency: 20 kHz;Power: 100–600 W; Time: 30 min.3% (w/v) starch in water; 400 W, amplitudes of 50 and 100% for 10–30min.	At 100–300 W, the granules maintained their integritywith only slight disruption; at 400–600 W, irregular fragments were observed; RCdecreased; short-range order increased.		ΔH decreased.				
	Ultrasound treatment after alcalase hydrolysis; 20 kHz; 5 or 10% starch; 75 or 100% amplitude; 15 or 30 min.	Changes were associated with structural reorganisation and increased crystalline order.		Alcalase treatment reduced gelatinisation temperatures and increased ΔHgel. Subsequent ultrasound increased Tp in most treatments, with no significant changes in ΔHgel.		DSC Q200; starch:water ratio 1:4 (w/v); 2.5–3.0 mg sample; 30–100 °C at 10 °C/min; air flow 50 mL/min.	Thermally processed foods; slow-release encapsulation systems; textile, cosmetic and printing ink applications.	

	Concentration: 15%; Power: 400 W; Time: 5, 12.5 and 20 min.	Activation of polyphenol oxidase, improvement in bioactives and antioxidant activity.				Valuable addition to functional cereals and bakery products.	Mustač et
Quinoa and maiz (*Chenopodium quinoa* Willd. and *Zea mays* L.)	Starch in water: 7.5% (w/v); Amplitude: 50%, with a cycle of 3 s and a 1 s pause; Frequency: 20 kHz;Intensity: 27.3 W/cm²; Time: 2, 4, 8, 14 and 22 h.	A balance was observed between AM leaching and surface damage in large-granule starch (maize). As treatment progressed, more cracked and broken granules were found. Granules became more dispersed after US; however, when the treatment time increased to 14 h or more, the granules reaggregated. The morphology and particle size of small-granule starches were less influenced by US compared with large-granule starches.	In small-granule starch (quinoa), short-term US caused an increase in SP.	RC decreased with long-term treatment.	The increase in amylose after US resulted in increased gel hardness. The relative degree of crystallinity decreased for both starches after 22 h of treatment.		
Sorghum (*Sorghum bicolor* L. Moench)	Concentration: 10%, 15% and 20% (w/v) starch in water; Intensity: 80 W/cm²; Time: 3, 4 and 5 min.	Fermentation followed by US improved the phenolic content and functional and textural properties.				Sorghum extrudates are used in the production of gluten-free products.	
Tapioca gum (*Manihot esculenta* Crantz)	Starch in water: 3% (p/v); Power: 400 W; Amplitude: 50 and 100%; Time: 10–30 min.	Deformed and broken granules aggregated and formed a film-like structure; the crystalline structure was destroyed.	SP and solubility increased. Higher swelling power and solubility values were associated with water absorption capacity.				

Purple taro (*Colocasia esculenta* L.)	10% (w/v) starch in water; Amplitudes of 40–60% for 30 min.	Deformed granules with surface cracks; crystalline type unaffected; RC reduced.		Thermal stability, PV and FV increased; To, Tp, Tc and BV decreased.			
Wheat, barley, rice and normal maize *(Triticum aestivum, Hordeum vulgare* L., *Oryza sativa* and *Zea mays*)	20% (w/v) starch in water; 24 kHz; 100 W for 15 and 30 min.	Broken and damaged granules with depressions, pores and channels on the surface, mainly for maize starch; crystalline structure unaffected.	The SP and solubility contents increased ($p < 0.05$).		Shear-thinning behaviour with $G' > G''$; G' and G'' increased during the initial 15 min, but decreased at 30 min.		
	Starch in water: 10% (p/v); US bath at 690 W and probe-type sonicationprobe at 200 W (continuous) and 400 W (intermittent) power for 15 and 30 min.	With probe-type US at 400 W, the granules showed only fine fissures, whereas the granules largely disintegrated at 200 W; with US bath treatment for 15 min, irregularities and a deeply concave geometry appeared on the granule surface, whereas the granules disintegrated after 30 min.	Higher solubility oil absorption an low swelling capacity. Probe-type US at 200 W led to the lowest SP.			Improved oil absorption; potencial for applications requiring Enhanced absorption properties.	
		Damage to the granule structure, facilitating water penetration during heating.					

	Starch in water: 20% (p/v); Frequency: 35 kHz; Power: 240 W; Amplitude: 100%; Time: 20, 40 and 60 min.	Native wheat starch granules had a smooth surface. US treatment produced a rough surface, with some grooves and fissures in the starch granule. Cracks were observed in some granules after 60 min of treatment.					
	–140 kJ; Time: 20 min.	Granule roughness and rupture, greater H bonding.	Improved water retention and distribution.	Increase in gelatinisation ΔH.			

Abbreviations:
AM, amylose; AP, amylopectin; CAW, water absorption capacity; RC, relative crystallinity; G' storage modulus; G", loss modulus; H, hydrogen; Mw, average molar mass; swelling power; SP, solubility power; ($p < 0,05$), significant difference; k, consistency coefficient; RDS, rapidly digestible starch; RS, resistant starch; SDS, slowly digestible starch; T, temperature; TG, gelatinization temperature; Tc, final gelatinization temperature; To, onset gelatinization temperature; Tp, peak gelatinization temperature; TPC, total phenolic compound content; US, ultrasonication; V, viscosity; BV, breakdown viscosity; VF, final viscosity; VM, minimum viscosity; PV, peak viscosity; SV, Setback viscosity; ΔH, gelatinization enthalpy change.

Table 3

Different starch sources subjected to ultrasound-assisted dual modification and an additional modification method

					r		
		Significant improvement in gelling properties.	Starch suspension in water: 40% (w/v); Power: 200 W; Frequency: 24 kHz; Amplitude: 50 and 100%; Duty cycle: 0.50 and 0.75 (100%); Time: 20 and 60 min; Temperature: 40 °C; HCl (0.36 M) with a reaction time of 4 h.	–	US alone initially reduced gel strength, while acid-thinning (AT) increased it by ~90%. Combined US-AT further enhanced gel strength, with greater effects at higher US intensity.	Production of acid-thinned starch with tailored functional properties.	
		The physical and structural Properties of native starch were improved.	Potato starch solution (0.1 M) treated with ultrasound for 15 min at 220 V and 0.7 A. Acid hydrolysis was carried out using 50 mL of a 2% starch suspension with 2 mL of 98% sulphuric acid and distilled water for a total hydrolysis time of 45 min.			Modified starch nanoparticles can be loaded with antioxidants and applied in foods, food packaging, barrier coatings and encapsulation systems.	
e	Arrowhead-derived resistant (*Sagittaria trifólia* var. *sinensis*)	Increased RS3 yield (34.46%), enzymolysis rate and amylose content; improved solubility, swelling power, transparency and water absorption capacity.	Enzymolysis: starch suspension (4%, w/v) gelatinised at 100 °C for 20 min; cooled to 50 °C and adjusted to pH 5.0; pullulanase (27.24 NPUN/g starch) added and enzymolysis for 24 h at 50 °C under magnetic stirring. Enzyme inactivated at 100 °C for 10 min, retrogradation at 4 °C for 24 h., filtration and freeze-drying.Ultrasound-assisted	DSC: 2.5 mg sample + 7.5 µL water; equilibration (1 h); 30–300 °C; 10 °C min^{-1}; empty aluminium pan a s r e	DSC analysis indicated changes in the thermal behaviour of RS3, associated with increased crystallinity and a more ordered and stable double-helix structure.	Potential application in the efficient production of RS3 and functional starch ingredients.	

			enzymolysis: enzymolysis, with US for 10 min at 250 W, 60 kHz, 171.42 W/L, pulsed 20 s on/5 s off. Enzymolysis performed at 50 °C for 24 h, followed by enzyme inactivation, retrogradation (4 °C, 24 h), filtration and freeze-drying.				
	Normal corn (*Zea mays* L.)	Facilitates acid-thinning modification in a shorter processing time; and tunable functional properties.	Normal corn starch (15–40% w/w) in water or H_2SO_4 (3.16–4.5 M); ultrasound bath at 40 kHz, 350 W, 100% amplitude, 10, 20 or 40 °C for 15, 30 or 45 min.		Decreased gelatinisation activation energy. Decreased complex viscosity and breakdown; reduced gel elasticity, time-dependency and structural recovery; flow behaviour changed from pseudoplastic to Newtonian under acidic sonication.	Rapid production of granular acid-thinned starch (<1 h) without additional chemicals.	Razavi,
Ultrasound and freeze–thaw treatment	Highly lipophilic potato starch (*Solanum tuberosum* L.)	7US-FTS supports higher processing temperatures, encapsulated more oil, and showed greater resistance to digestion, enabling its use as RS in food processing.	Amplitude: 20–60%; Time: 2–12 min; Frequency: 20 kHz; Power: 750 W; Temperature: 25 °C. Freeze–thaw treatment: freezing at –20 °C for 3 h followed by thawing at 50 °C for 30 min. Freeze–thaw cycles (0, 3, 6, 9, 12 and 15) and combined ultrasound/freeze–thaw cycles (0, 1, 3, 5, 7, 9 and 11).		After treatment, the crystalline structure of the starch was destroyed and the paste viscosity decreased. The increase in gelatinisation temperature indicated that 7 US-FTS could withstand Higher processing temperatures and was expected to become a more heat-r e	Encapsulate of bioactive compounds, pharmaceuticals, MOOS, and preservatives with low hydrophilicity, unpleasant odour, poor pH resistance or low oxidative stability.	
Ultrasound and freeze–thaw treatment	High-amylose maize (*Zea mays* L.)	Increased SDS and RS contents, enabling the development of low-	RS3 suspension (3 g/70 mL); ultrasonication at 20 kHz using a Ø6 mm titanium probe; power: 100–600 W;	DSC: 1 mg starch with 1.5 µL distilled water in sealed	Gelatinisation enthalpy (ΔH); appearance of a new exothermic peak	Potential for the development of low-glycaemic foods.	

		glycaemic foods.	pulse mode (2 s on/2 s off) for 30 min in an ice bath. Following ultrasonication, samples were freeze-dried: frozen at −80 °C overnight, vacuum-dried (<100 Pa) from −30 to 10 °C for 24 h, then milled and stored at 4 °C.	aluminium pans; 30–180 °C at 10 °C/min.			
	Maize and potato (*Zea mays* L., *Solanum tuberosum*)	Dual modification was more effective than single modification	Temperature: 35 °C; Frequency: 20 kHz; Microwave treatment: 90 W for 3 min + ultrasound for 30 min; 180 W for 3 min + ultrasound for 40 min; 360 W for 3 min + ultrasound for 30 min; 600 W for 1 min + ultrasound for 40 min.		Increased peak viscosity; improved water and oil absorption capacities; improved freeze–thaw stability.		
		Ultrasound altered the starch structure, enhancing the subsequent action of ozone.	Starch concentration: 10% (w/w); Treatment time: 8 h; Temperature: 24–26 °C; Frequency: 25 kHz; Power: 72 W/L; Ozone concentration: 42 mg O_3/L for 15 min at 25 °C. Treatments included O_3, O_3–US and US–O_3.		WAI, WSI, pasting properties and gel strength were more affected by ozone than by ultrasound. Paste clarity was higher in the combined treatments, particularly when ultrasound preceded ozone treatment.		
					Changes in G′ and G″ depended on the treatment. Gelatinisation temperature increased.	Potential application as thickening and texturising agents.	
Ultrasound and heat–moisture treatment		May assist in selecting the most appropriate ultrasound and HMT	MT at 25% moisture content and 120 °C for 0, 1, 4, 8 and 12 h. Ultrasound treatment: 10% (w/w) starch suspension		All HMT–US combinations reduced crystallinity, molecular weight, pasting index and peak viscosity at		

(HMT)		conditions for starch modification.	for 20 min at 300 W and 20 kHz. Combined treatments: HMT1–US, HMT4–US, HMT8–US, HMT12–US and ultrasound pre-treatment.		70–90 °C, while increasing resistant starch content. Ultrasound-assisted HMT increased viscosity and high-temperature paste stability.		
Ultrasound-assisted treatment + octenyl succinic anhydride (OSA) modification.		Mechanochemical effect of ultrasound on starch granules, enhancing OSA modification.	35% (w/v) starch suspension; 500 W; 35 °C; 0, 5, 15, 30 and 60 min; intermittent sonication (5 min treatment/25 min pause), after modified with OSA (3%, dry basis).	DSC: 5 mg sample + 15 μL distilled water; equilibrated at 4 °C for 12 h; 20–100 °C at 10 °C/min under N_2 (60 mL/min). at 10 °C/min under N_2 (60	Gelatinisation and thermal degradation behaviour.	Potential applications in food products requiring modified thermal and functional properties	
	Mung bean (*Vigna radiata* L.)	Dual treatment produced superior starch Properties.	Starch concentration: ½ (w/v); Power: 300 W; Time: 10, 30 and 50 min; Temperature: 25 °C. Plasma treatment: 40 V and 1 A; Time: 1, 3 and 9 min; Moisture content: 25%.		Unlike ultrasound, plasma treatment alone significantly ($p < 0.05$) reduced paste viscosity and swelling power. All treatments increased gelatinisation temperatures and ΔH. Dual treatment also enhanced paste thermal stability owing to the synergistic effect of ultrasound and plasma.		
	Tapioca starch (*Manihot esculenta*	The sequence of modification influences starch properties.			Reduced swelling power; reduced paste viscosity; increased resistant starch and		

	Crantz)				slowly digestible starch contents.		
		Ultrasound facilitates the rearrangement of starch-amylose molecules.			Affected starch granule size. Molecular rearrangement occurred during enzymatic hydrolysis.		

Abbreviations:
AM, amylose; AP, amylopectin; WAC, water absorption capacity; RC, relative crystallinity; DS, degree of substitution; G′, storage modulus; G″, loss modulus; H, hydrogen; HMT, heat–moisture treatment; MW, microwave; MOOs, microorganisms; Mw, molecular weight; OSA, octenyl succinic anhydride; O_3, ozone; OAC, oil absorption capacity; SP, swelling power; SI, solubility index; ($p < 0.05$), significant difference; k, consistency coefficient; RS3, retrograded starch; RDS, rapidly digestible starch; SDS, sodium dodecyl sulphate; GT, gelatinization temperature; US, ultrasonication; PV, paste viscosity; WAI, water absorption index; WSI, water solubility index; ΔH, gelatinization enthalpy change; 7US-FTS, starch subjected to seven ultrasound-assisted freeze-thaw cycles.

Thermal analysis (TG and DSC) results

Valencia et al. (2012), employ thermogravimetric study (TG) in native starches from tubers: canna (humidity~12%), bore (humidity~11%) and cassava (humidity~14%). The TG curves were obtained in a thermogravimetric analyser (TGA-2920–TA Instr.), under a flow of dry N_2 (50 mL/min). The samples were weighed directly into aluminum crucible (2-5 mg) and then heated from 25–325 ºC, at heating rate of 10 ºC/min. Authors found that starches reveal three main weight loss regions. The first region between 25-225 ºC, due the evaporation of physically weakly and chemically strongly bound water. The total weight loss of the starches due to water evaporation is about 9-10% at 105 ºC. The second transition region, authors found between 105-275 ºC, and attributed to a strongly bound water fraction of the starch structure still exists and it is not evaporated. The third weight loss region was observed above 275 ºC, and the maximum degradation rate of the starches is about ~290 ºC. At the end of the heating process, authors observed the residual mass content (m_{res}) for each starch, calculated as a percentage of the original mass, i.e., canna ~30 wt%, bore ~75 wt% and cassava ~20 wt%.

Colman et al. (2014), made an investigation on the effects of microwave radiation in starches from cassava. The thermogravimetric curves (TG) were obtained with the thermal analysis system TGA- 50 (Shimadzu). The samples were heated from 35-600 ºC using open alumina crucible with mass around 7.0 mg under synthetic air flow of 150 mL/min in a heating rate of 10 ºC/min. In this work, the native cassava starch (7.26 mg) was analysed under the conditions previously cited. It was possible to observe three mass loss: the 1st from 35-146 ºC due the dehydration process (10.6%), followed by a stability step (146-174 ºC). After, the 2nd mass loss occurs between 276-425 ºC and was attributed to decomposition of organic matter (73.8%) and followed by the 3rd step of mass loss (15.5%), due to oxidation of organic matter with ash formation (0.1%) as final residue. The modified starches by microwaves at 5, 10 and 15 min show similar procedure with temperature reduction after dehydration as well as the after the oxidation process. The thermogravimetric behavior of all starches when performed in air atmosphere occurs in a similar way.

In agreement with Valencia et al. (2012), the DSC analysis were made using a modulated DSC model MDSC 2920 (TA Instr.), under a flow of N_2 (50 mL/min). The samples were weighed directly into an aluminum crucible (4 - 8 mg), which was hermetically sealed. An empty aluminum crucible was used as reference. Each crucible was heated from 0–250 ºC at a heating rate of 10 ºC/min. The values found to peak temperature of canna, bore and cassava starches were 92.13; 81.53 and 63.01 ºC, respectively. The enthalpy of each sample was 432.01; 381.40 and 338.01 J/g, respectively.

According Colman et al. (2014), the DSC curves were obtained using thermal analysis system model DSC-Q-200 (TA Instr.), in two different temperature program. The first was carried out to follow the thermogravimetric process: samples were heated from 35–600 ºC using aluminum crucible with perforated cover and mass of starch around 7.0 mg. It was performed in air atmosphere with flow of 150 mL/min at a heating rate of 10 ºC/min. The native cassava starch show the 1st endothermic peak that occurs at Tp = 101 ºC and is due to dehydration process; the calculated enthalpy ΔH = 302.3 J/g. The 2nd exotherm peak occurs at Tp = 370.3 ºC is due the decomposition of organic matter, ΔH = 544.6 J/g and the 3rd exothermic peak occurs at Tp = 571.7 ºC and attributed to oxidation of organic matter which ΔH = 518.7 J/g.

In the second temperature program, the DSC curves were carried out with the objective to study gelatinization process. Each analysis was performed under air atmosphere (50 mL/min), heating rate 5 ºC/min and sample weighing about 2.5 mg. A 4:1 (water:starch w/w)

mixture was prepared and maintained for 60 min to equilibrate the moisture content. The crucibles were hermetically sealed and heated from 35 - 100 °C.

The measurement of starch gelatinization is a weak transition that always occurs in presence of water and it is important that it be carried out in sealed crucible. In this study was used 3.19 mg of native cassava starch and 12.76 μL of distilled water (rate 1:4). The obtained parameters were: To = 58.77 °C, Tp = 64.57 °C and Tc = 69.56 °C. The calculated enthalpy ΔH = 10.88 J/g.

An investigation on ultrasound effects on the structure and chemical reactivity of cornstarch granules was performed by Huang et al. (2007). Cornstarch granules (200 g) were suspended in a sufficient volume of water to give a concentration of 30% (w/v). The US treatment: power 500 W, time 3-15 min, pulse mode continuous sonication for 15 s, and stop for 5 s. The DSC curves were performed with starch suspensions adjusted to 70%. Pans were sealed and equilibrated overnight at room temperature before heating in the DSC. The DSC instrument model Diamond-I (Perkin Elmer), measurements were carried out at a heating rate of 10 °C/min from 5 to 100 °C. The results of Tp were between 74.48 to 78.34 °C and ΔH between 10.1 to 11.8 J/g.

Jambrak et al. (2010) made ultrasound treatment of corn starch with 24 kHz probe and ultrasound treatment with 24 kHz bath. Suspensions of corn starch were prepared at 1%, 2% and 10% water and treated by ultrasound. The gelatinization properties were analyzed in a DSC 822e (Mettler Toledo).

Corn starch suspensions were weighed in standard aluminum crucibles (40 μL) which were sealed and equilibrated for 24 hours at room temperature. The starch slurry was gelatinized in DSC using heating rate of 10 °C/min from 25 to 95 °C.

In an investigation of starch from banana (*Musa cavendish* var."Nanica") (Izidoro et al., 2011), green banana starch (GBS) was dried: in conventional oven (GBS A), in spray dryer (GBS B), with ultrasound pretreatment and dried in conventional oven (GBS C), with ultrasound pretreatment and dried in spray dryer (GBS D). Authors apply ultrasound (24 W, 40% amplitude, 20 kHz frequency) by 1 hour with pulsations in the range of 1 min. The gelatinization parameters were determined by Micro DSC III (Setaram). Approximately 2 mg samples were weighed on aluminum pan and 10 μL of deionized water were added. Each sample was submitted to heating program 25-100 °C at 0.10 °C min^{-1}. Authors observe that the gelatinization temperature (Tp) was influenced by the type of drying: the spray dried banana starch (Tp of GBS B and GBS D show lower gelatinization temperature).

Amini et al. (2015) prepared dispersions of corn starch which were subjected to sonication 24kHz. The properties of starch samples were measured using DSC 822e (Mettler Toledo); 5 mg of starch accurately weighed and transferred to aluminum crucibles. Appropriate amounts of deionized water were added to prepare 15% w/w concentration. The crucibles were sealed and allowed to rest for 1 hour at room temperature before performing the experiments. The curves were done from 20 to 200 °C at a heating rate of 10 °C/min.

Luo et al. (2008), performed a study on the effects of ultrasonic treatment on the physicochemical properties of maize starches differing in amylose content. Normal maize, waxy maize and amylomaize V starches (100 g) were adjusted to 70% moisture. Ultrasonic treatment was carried out with stirring for 30 min at 30 °C and sonication energy input of 100 W. Gelatinization temperatures and enthalpy were measured on a DSC 2 (Perkin Elmer). Water (8.0 μL) was added with a microsyringe to starch (2.5 mg) in the DSC pans, which were sealed, reweighed and kept overnight at room temperature. The heating was from 20–180 °C and heating rate 10 °C/min. The DSC curve was recorded with water as reference.

Authors conclude that all studied starches show decrease in gelatinization (Tp) as well as decrease in the enthalpy (ΔH).

Barboza et al. (2024), in study of effect of ultrasound (20 kHz, amplitude 50 and 100% by 25 and 50 min) on thermal, structural and pasting and morphological properties of commercial *Maranta arundinacea* starch (arrowroot), apply the thermogravimetry (TG) in a TGA-50 thermobalance (Shimadzu). Each mass sample were around 7 mg weighed in open alumina crucible. The atmosphere was in air with flow of 150 ºC, heating rate 10 ºC/min, from 30-600 ºC. TG and DTG curves show mass loss in three steps, due to dehydration, decomposition of organic matter followed of oxidation of organic matter. The DSC curves to study the gelatinization of each sample were performed in the instrument DSC-Q200 (TA Instr.) in aluminum crucibles (2.0 mg of starch and 8 μL distilled water) and sealed; heating rate of 10 ºC/min, from 30-100 ºC in air atmosphere with flow of 50 mL/min. TG curves show some reduction in thermal stability and DSC curves show a decrease in the peak temperature with a slight increase in ΔH.

In a study on ultrasonic modification of purple taro starch (*Colocasia esculenta* B. Tini), Martins et al. (2020) treated native starch from purple taro suspensions (10% w/v) with ultrasound (Vibra-Cell 500–Sonic, 20 kHz) at 40, 50 and 60% amplitude for 30 min each sample. TG curves were obtained in TGA-50 thermobalance (Shimadzu). The instrument was calibrated with standard mass and verified with standard $CaC_2O_4{\cdot}H_2O$. Approximately 8.0 mg of each sample was placed in alumina crucible, heated from 30-650 ºC and a heating rate of 10 ºC/min, under 150 mL/min compressed dry air flow. The mass loss percentages and DTG curves were calculated using TA-60 WS data analysis software. All TG/DTG curves show similarities: the first mass loss is due to dehydration, followed by certain stability. Above 250 ºC occurs decomposition of organic matter followed of oxidation. Under higher US vibration amplitudes (50 and 60%), a decrease in thermal stability was observed. The gelatinization curves were obtained in the DSC Q-200 (TA Instr.) previously calibrated according to manufacturer and checked with Indium standard (99.99% purity, melting point 156.6 ºC, ΔH = 28.56 J/g. Approximately 2.7 mg (dry basis) of starch in distilled water (1:4 w/v) was added to perform each analysis, being homogenized in a aluminum crucible and resting for 1 hour at room temperature to stabilize the moisture content. The flow of compressed air was 50 mL/min, temperature range from 20-100 ºC and heating rate of 10 ºC/min. The lowest gelatinization temperature range (ΔT = 12.2 ºC) was found in US 60% amplitude; this may be related to the influence of higher vibration amplitude on the granule structure, as well as in the reduction of starch size and cracks formation visualized by morphological analysis (SEM).

Dias et al. (2023) investigated the effects of chemical and physical modifications on starch isolated from *Colocasia esculenta*. The US was applied 20 kHz at 60%. The time were 15 and 30 min. The acid hydrolysis was HCl 0.1 mol/L and 0.5 mol/L for 1 hour and after washed and dried. TG curves were obtained in TGA-50 thermobalance (Shimadzu). A mass around 8 mg was weighed in alumina crucible and subjected to controlled heating rate of 10 ºC/min from 30-650 ºC under air flow 150 mL/min. A starch water suspension (1:4 ratio, w/v) was prepared in aluminum crucible, which was sealed with lid and kept at room temperature by 60 min before analysis. To perform the gelatinization process was used the calorimeter DSC Q-200 (TA Instr.), calibrated previously with indium 99.99%. DSC curves were made from 30-100 ºC under air flow 50 mL/min and heating rate of 10 ºC/min. Results reveal that thermal stability increased after ultrasonication especially after the double modification.

Conclusions

This investigation aimed to review and analyze recent research on starch modification using ultrasound, both alone and in combination with other methods. The analyzed literature made it possible to identify consistent trends regarding the effects of ultrasound on different starch sources and to understand the relationships between processing parameters and the resulting structural and functional changes.

It was observed that ultrasound induces changes in granular structure, crystallinity, and thermal, rheological, and hydration properties, with the effects depending on the treatment conditions and starch source. Ultrasound treatment also demonstrates synergistic potential when combined with other modification techniques.

Ultrasound-assisted starch modification presents significant potential for scientific and technological development, particularly for the production of sustainable functional materials and the optimization of starch properties for specific applications. Therefore, this approach provides relevant opportunities for future research and industrial innovation.

Thermoanalytical techniques, particularly thermogravimetry or thermogravimetric analysis (TG or TGA) and differential scanning calorimetry (DSC), are widely used in starch studies. The TG technique plays an important role in evaluating the thermal stability and decomposition behavior of these materials. The first derivative of the TG curve, called derivative thermogravimetry (DTG), is an important mathematical tool that facilitates the identification of mass-loss events observed in TG curves.

However, when using these techniques, it is important to report all experimental conditions under which the analyses were performed, including the sample mass. When multiple samples are analyzed, their masses should be as similar as possible; for example, if the first sample has a mass of approximately 5 mg, the remaining samples should have comparable masses. Other important parameters include the type of crucible and whether it is used with or without a lid, the atmosphere or purge gas and its flow rate, the heating rate, and the temperature range.

It is also important to use the correct terminology, such as TG curve, DTG curve, and DSC curve, rather than the term “thermogram.” The latter term is generally associated with images obtained by thermography, particularly in medical applications.

Starch gelatinization is a process that occurs when intermolecular interactions within amylose (AM) and amylopectin (AP) structures are disrupted in the presence of water and heat. Water molecules interact with the available hydrophilic sites, resulting in granule swelling, loss of structural order, and the formation of a viscous paste. Starch gelatinization is commonly evaluated using differential scanning calorimetry (DSC), which provides DSC curves.

Starch gelatinization is an endothermic process. The onset temperature (To), peak temperature (Tp), and conclusion temperature (Tc) can be determined from the DSC curve, together with the enthalpy of gelatinization (ΔH). It should be emphasized that gelatinization is a relatively weak thermal transition. Therefore, the starch-to-water ratio must be carefully defined (e.g., 1:1, 1:2, or 1:3), and the measurements should be performed using hermetically sealed crucibles to prevent water loss during heating.

Acknowledgements. Authors would like to Brazilian organizations CAPES and CNPQ for financial support.

References

Alcázar-Alay, S. C., & Meireles, M. A. A. (2015). Physicochemical properties, modifications and applications of starches from different botanical sources. *Food Science & Technology, 35*(2), 215–236. https://doi.org/10.1590/1678-457X.6749

Amini, A. M., & Razavi, S. M. (2015). Ultrasound-assisted acid-thinning of corn starch: Morphological, physicochemical, and rheological properties. *Starch/Stärke, 67*, 640–653. https://doi.org/10.1002/star.201400228

Amini, A. M., Razavi, S. M. A., & Mortazavi, S. A. (2015). Morphological, physicochemical, and viscoelastic properties of sonicated corn starch. *Carbohydrate Polymers, 122*, 282–292. https://doi.org/10.1016/j.carbpol.2015.01.020

Andrade, M. M. P., Oliveira, C. S., Colman, T. A. D., Costa, F. J. O. G., & Schnitzler, E. (2014). Effects of heat-moisture treatment on organic cassava starch: Thermal, rheological and structural study. *Journal of Thermal Analysis and Calorimetry, 115*, 2115–2122. https://doi.org/10.1007/s10973-013-3159-3

Awad, T. S., Moharram, H. A., Shaltout, O. E., Asker, D., & Youssef, M. M. (2012). Applications of ultrasound in analysis, processing and quality control of food: A review. *Food Research International, 48*(2), 410–427. https://doi.org/10.1016/j.foodres.2012.05.004

Ashogbon, A. O., & Akintayo, E. T. (2014). Recent trend in the physical and chemical modification of starches from different botanical sources: A review. *Starch/Stärke, 66*, 41–57. https://doi.org/10.1002/star.201300106

Barboza, R. A., Bet, C. D., Beninca, C., Bisinella, R. Z. B., Romko, S. S., Schnitzler, E., & Giurciulescu, L. (2024). Effect of ultrasound on the thermal, structural, pasting and morphological properties of *Maranta arundinacea* starch. *Carpathian Journal of Food Science and Technology, 16*(1), 135–145. https://doi.org/10.34302/crpjfst/2024.16.1.11

Bel Haaj, S., Magnin, A., Pétrier, C., & Boufi, S. (2013). Starch nanoparticles formation via high power ultrasonication. *Carbohydrate Polymers, 92*(2), 1625–1632. https://doi.org/10.1016/j.carbpol.2012.11.022

BeMiller, J. N., & Huber, K. C. (2015). Physical modification of food starch functionalities. *Annual Review of Food Science and Technology, 6*, 19–69. https://doi.org/10.1146/annurev-food-022814-015552

Bernal, C., Couto, A. B. C., Breviglieri, S. T., & Cavalheiro, E. T. G. (2002). Influência de alguns parâmetros experimentais nos resultados de análises calorimétricas diferenciais. *Química Nova, 25*(5), 849–855.

Bernardo, C. O., Ascheri, J. L. R., Chávez, D. W. H., & Carvalho, C. W. P. (2018). Ultrasound-assisted extraction of yam (*Dioscorea bulbifera*) starch: Effect on morphology and functional properties. *Starch/Stärke, 70*, 1700185. https://doi.org/10.1002/star.201700185

Bet, C. D., Cordoba, L. P., Ribeiro, L. S., & Schnitzler, E. (2016). Common vetch (*Vicia sativa*) as a new starch source: Its thermal, rheological and structural properties after acid hydrolysis. *Food Biophysics, 11*, 275–282. https://doi.org/10.1007/s11483-016-9439-2

Bet, C. D., Oliveira, C. D., Colman, T. A. D., Marinho, M. T., Lacerda, L. G., Ramos, A. P., & Schnitzler, E. (2018). Organic amaranth starch: A study of its technological properties after heat-moisture treatment. *Food Chemistry, 264*, 435–442. https://doi.org/10.1016/j.foodchem.2018.05.021

Bisinella, R. Z. B., Beninca, C., Bet, C. D., de Oliveira, C. S., Demiate, I. M., & Schnitzler, E. (2022). Thermal, structural and morphological characterisation of organic rice starch after physical treatment. *Journal of Thermal Analysis and Calorimetry, 147*, 3615–3623. https://doi.org/10.1007/s10973-021-10712-7

Bitik, A., Sumnu, G. Ş., & Öztop, H. M. (2019). Physicochemical and structural characterization of microfluidized and sonicated legume starches. *Food and Bioprocess Technology, 12*(7), 1144–1156. https://doi.org/10.1007/s11947-019-02264-4

Bonto, A. P., Tiozon, R. N., Jr., Sreenivasulu, N., & Camacho, D. H. (2021). Impact of ultrasonic treatment on rice starch and grain functional properties: A review. *Ultrasonics Sonochemistry, 71*, 105383. https://doi.org/10.1016/j.ultsonch.2020.105383

Borsato, M. P., Bet, C. D., Bisinella, R. Z. B., Lacerda, L. G., & Schnitzler, E. (2022). Buckwheat starch (*Fagopyrum esculentum*): Aqueous extraction, modification by HMT and characterization. *Carpathian Journal of Food Science and Technology, 14*(2), 147–154. https://doi.org/10.34302/crpjfst/2022.14.2.12

Carmona-Garcia, R., Bello-Pérez, L. A., Aguirre-Cruz, A., Aparício-Sanguilan, A., Hernández-Torres, J., & Alvarez-Ramirez, J. (2016). Effect of ultrasonic treatment on the morphological, physico-chemical, functional and rheological properties of starches with different granule size. *Starch/Stärke, 68*, 972–979. https://doi.org/10.1002/star.201600019

Castanha, N., Lima, D. C., Júnior, M. D. M., Campanella, O. H., & Augusto, P. E. D. (2019). Combining ozone and ultrasound technologies to modify cornstarch. *International Journal of Biological Macromolecules, 139*, 63–74. https://doi.org/10.1016/j.ijbiomac.2019.07.161

Cavalheiro, E. T. G., Ionashiro, M., Breviglieri, S. T., Marino, G., & Chierice, G. O. (1995). Influência de fatores experimentais nos resultados de análises termogravimétricas. *Química Nova, 18*(3), 305–308.

Chan, H. T., Bhat, R., & Karim, A. A. (2010). Effects of sodium dodecyl sulphate and sonication treatment on physicochemical properties of starch. *Food Chemistry, 120*(3), 703–709. https://doi.org/10.1016/j.foodchem.2009.10.066

Chan, C. H., Wu, R. G., Yi, W., & Shao, Y. (2021). Effect of ultrasound and temperature on digestibility of high-amylose maize starch. *Food Hydrocolloids, 119*, 106831. https://doi.org/10.1016/j.foodhyd.2021.106831

Colman, T. A. D., Demiate, I. M., & Schnitzler, E. (2014). The effect of microwave radiation on some thermal, rheological and structural properties of cassava starch. *Journal of Thermal Analysis and Calorimetry, 115*, 2245–2252. https://doi.org/10.1007/s10973-012-2866-5

Cordoba, L. P., Ribeiro, L. S., Rosa, L. S., Lacerda, L. G., & Schnitzler, E. (2016). Effect of enzymatic treatments on thermal, rheological and structural properties of pinhão starch. *Thermochimica Acta, 642*, 45–51. https://doi.org/10.1016/j.tca.2016.08.020

Czechowska-Biskup, R., Rokita, B., Lotfy, S., Ulanski, P., & Rosiak, J. M. (2005). Degradation of chitosan and starch by 360-kHz ultrasound. *Carbohydrate Polymers, 60*, 175–184. https://doi.org/10.1016/j.carbpol.2004.12.001

Dias, T. D. L., Romko, S. S., Beninca, C., Lacerda, L. G., Bisinella, R. Z. B., Bet, C. D., & Schnitzler, E. (2023). Effects of controlled ultrasound and partial hydrolysis of micro starch granules from *Colocasia esculenta* L. Schott: Thermal, morphological and structural properties. *Journal of Thermal Analysis and Calorimetry, 148*, 7707–7716. https://doi.org/10.1007/s10973-023-12240-y

Ding, Y., Luo, F., & Lin, Q. (2019). Insights into the relations between the molecular structures and digestion properties of retrograded starch after ultrasonic treatment. *Food Chemistry, 294*, 248–259. https://doi.org/10.1016/j.foodchem.2019.05.050

Ding, Y., Liang, Y., Luo, F., Ouyang, Q., & Lin, Q. (2020). Understanding the mechanism of ultrasonication-regulated digestibility properties of retrograded starch following vacuum freeze drying. *Carbohydrate Polymers, 228*, 115350. https://doi.org/10.1016/j.carbpol.2019.115350

Giolito, I., & Ionashiro, M. (1988). Nomenclatura, padrões e apresentação dos resultados em análise térmica–Parte II. *Cerâmica, 34*, 225–227.

Falsafi, S. R., Maghsoudlou, Y., Aalami, M., Jafari, S. M., & Raeisi, M. (2019). Physicochemical and morphological properties of resistant starch type 4 prepared under ultrasound and conventional conditions and their in-vitro and in-vivo digestibilities. *Ultrasonics Sonochemistry, 53*, 110–119. https://doi.org/10.1016/j.ultsonch.2018.12.039

Han, L., Cao, S., Yu, Y., Xu, X., Cao, X., & Chen, W. (2021). Modification in physicochemical, structural and digestive properties of pea starch during heat-moisture process assisted by pre- and post-treatment of ultrasound. *Food Chemistry, 360*, 129929. https://doi.org/10.1016/j.foodchem.2021.129929

He, R., Li, S., Zhao, G., Zhai, L., Qin, P., & Yang, L. (2023). Starch modification with molecular transformation, physicochemical characteristics, and industrial usability: A state-of-the-art review. *Polymers, 15*(13), 2935. https://doi.org/10.3390/polym15132935

Herceg, I. L., Jambrak, A. R., Šubarić, D., Brnčić, M., Rimac Brnčić, S., Badanjak, M., Tripalo, B., Ježek, D., Novotni, D., & Herceg, Z. (2010). Texture and pasting properties of ultrasonically treated corn starch. *Czech Journal of Food Sciences, 28*(2), 83–93. https://doi.org/10.17221/50/2009-CJFS

Hsein-Chih, H. W., & Sarko, A. (1978). The double-helical molecular structure of crystalline A-amylose. *Carbohydrate Research, 54*(1), C3–C6. https://doi.org/10.1016/S0008-6215(00)80566-2

Hu, A., Lu, J., Zheng, J., Sun, J., Yang, L., Zhang, X., Zhang, Y., & Lin, Q. (2013). Ultrasonically aided enzymatical effects on the properties and structure of mung bean starch. *Innovative Food Science & Emerging Technologies, 20*, 146–151. https://doi.org/10.1016/j.ifset.2013.08.005

Hu, A., Jiao, S., Zheng, J., Fan, Y., Chen, L., & Zhang, Z. (2015). Ultrasonic frequency effect on corn starch and its cavitation. *LWT–Food Science and Technology*, *60*(2), 941–947. https://doi.org/10.1016/j.lwt.2014.10.048

Huang, Q., Li, L., & Fu, X. (2007). Ultrasound effects on the structure and chemical reactivity of cornstarch granules. *Starch/Stärke, 59*, 371–378. https://doi.org/10.1002/star.200700614

Ionashiro, M., & Giolito, I. (1980). Nomenclatura, padrões e apresentação dos resultados em análise térmica–Parte I. *Cerâmica, 26*, 26–32.

Izidoro, R. I., Sierakowski, M.-R., Haminiuk, C. W. I., Souza, C. F., & Scheer, A. P. (2011). Physical and chemical properties of ultrasonically spray-dried green banana (Musa cavendish) starch. *Journal of Food Engineering, 104*, 639–648. https://doi.org/10.1016/j.jfoodeng.2011.02.002

Jamalabadi, M., Saremnezhad, S., Bahrami, A., & Jafari, S. M. (2019). The influence of bath and probe sonication on the physicochemical and microstructural properties of wheat starch. *Food Science & Nutrition*, *7*(7), 2427–2435. https://doi.org/10.1002/fsn3.1111

Jambrak, A. R., Herceg, Z., Šubarić, D., Babić, J., Brnčić, M., Brnčić, S. R., Bosiljkov, T., Čvek, D., Tripalo, B., & Gelo, J. (2010). Ultrasound effect on physical properties of corn starch. *Carbohydrate Polymers*, *79*(1), 91–100. https://doi.org/10.1016/j.carbpol.2009.07.051

Karwasra, B. L., Kaur, M., & Gill, B. S. (2020). Impact of ultrasonication on functional and structural properties of Indian wheat (*Triticum aestivum* L.) cultivar starches. *International Journal of Biological Macromolecules, 164*, 1858–1866. https://doi.org/10.1016/j.ijbiomac.2020.08.013

Kaur, H., & Gill, B. S. (2019). Effects of high-intensity ultrasound treatment on structural and physicochemical properties of starches obtained from different cereals. *International Journal of Biological Macromolecules, 126*, 367–375. https://doi.org/10.1016/j.ijbiomac.2018.12.149

Khurshida, S., Das, M. J., Deka, S. C., & Sit, N. (2021). Effect of dual modification sequence on physicochemical, pasting, rheological and digestibility properties of cassava starch modified by acetic acid and ultrasound. *International Journal of Biological Macromolecules, 188*, 649–656. https://doi.org/10.1016/j.ijbiomac.2021.08.062

Kim, J., Ren, C., & Shin, M. (2013). Physicochemical properties of starch isolated from eight different varieties of Korean sweet potatoes. *Starch/Stärke, 65*(11–12), 923–930. https://doi.org/10.1002/star.201200217

Kong, X. (2019). Starches modified by nonconventional techniques and food applications. In M. T. P. S. Clerici, U. M. Sampaio, & M. Schmiele (Eds.), *Starches for food application: Chemical, technological and health properties* (pp. 271–295). Academic Press. https://doi.org/10.1016/B978-0-12-809440-2.00007-0

Kumari, B., & Sit, N. (2023). Comprehensive review on single and dual modification of starch: Methods, properties and applications. *International Journal of Biological Macromolecules, 253*(3), 126952. https://doi.org/10.1016/j.ijbiomac.2023.126952

Latip, D. N. H., Samsudin, H., Utra, U., & Alias, K. A. (2020). Modification methods toward the production of porous starch: A review. *Critical Reviews in Food Science and Nutrition, 61*(17), 2841–2862. https://doi.org/10.1080/10408398.2020.1789064

Lever, T., Haines, P., Rouquerol, J., Charsley, E. L., Van Eckeren, P., & Burlett, D. J. (2014). ICTAC nomenclature of thermal analysis (IUPAC Recommendations 2014). *Pure and Applied Chemistry*, *86*(4), 545–553. https://doi.org/10.1515/pac-2012-0609

Li, H., Thui Ho, V. T., Turner, M. S., & Dhital, S. (2016). Encapsulation of Lactobacillus plantarum in porous maize starch. *LWT–Food Science and Technology, 74*, 542–549. https://doi.org/10.1016/j.lwt.2016.08.019

Li, M., Li, J., & Zhu, C. (2018). Effect of ultrasound pretreatment on enzymolysis and physicochemical properties of corn starch. *International Journal of Biological Macromolecules, 111*, 848–856. https://doi.org/10.1016/j.ijbiomac.2017.12.156

Li, X., Ge, X., Guo, C., & Liu, B. G. (2023). Effect of ultrasound on structure and digestibility of pea starch. *Foods, 12*(13), 2620. https://doi.org/10.3390/foods12132620

Liang, Q., Chen, X., Ren, X., Yang, X., Raza, H., & Ma, H. (2021). Effects of ultrasound-assisted enzymolysis on the physicochemical properties and structure of arrowhead-derived resistant starch. *LWT–Food Science and Technology*, *147*, 111616. https://doi.org/10.1016/j.lwt.2021.111616

Liang, Y. C., Huang, P. H., & Chang, W. C. (2025). Effect of high-power ultrasonication and heat treatments on the physicochemical properties of wheat starch–caffeic acid complexes. *LWT–Food Science and Technology, 237*, 118806. https://doi.org/10.1016/j.lwt.2025.118806

Lin, X., Sun, S., Wang, B., Zheng, B., & Guo, Z. (2020). Structural and physicochemical properties of lotus seed starch nanoparticles prepared using ultrasonic-assisted enzymatic hydrolysis. *Ultrasonics Sonochemistry, 68*, 105199. https://doi.org/10.1016/j.ultsonch.2020.105199

Lindeboom, N., Chang, P. R., & Tyler, R. T. (2004). Analytical, biochemical and physicochemical aspects of starch granule size, with emphasis on small granule starches: A review. *Starch/Stärke, 50*, 89–99. https://doi.org/10.1002/star.200300218

Litvyak, V. (2018). Size and morphological features of native starch granules of different botanical origin. *Ukrainian Food Journal, 7*(4), 563–576. https://doi.org/10.24263/2304-974X-2018-7-4-3

Lohani, U. C., Muthukumarappan, K., & Meletharayil, G. H. (2016). Application of hydrodynamic cavitation to improve antioxidant activity in sorghum flour and apple pomace. *Food and Bioproducts Processing, 100*, 335–343. https://doi.org/10.1016/j.fbp.2016.08.005

Luo, Z., Fu, X., He, X., Luo, F., Gao, Q., & Yu, S. (2008). Effect of ultrasonic treatment on the physicochemical properties of maize starches differing in amylose content. *Starch/Stärke, 60*(11), 646–653. https://doi.org/10.1002/star.200800014

Mainardes, B., Mikota, L. M., Bet, C. D., Marinho, M. T., Bisinella, R. Z. B., Romko, S. S., & Schnitzler, E. (2024). Extraction and physical modification of Mango palmer kernel starch and its application in cookies. *Ukrainian Food Journal, 13*(2), 231–246. https://doi.org/10.24263/2304-974X-2024-13-2-3

Majzoobi, M., Hedayati, S., & Farahnaky, A. (2015). Functional properties of microporous wheat starch produced by α-amylase and sonication. *Food Bioscience, 11*, 79–84. https://doi.org/10.1016/j.fbio.2015.05.001

Mallakpour, S., & Khodadadzadeh, L. (2018). Ultrasonic-assisted fabrication of starch/MWCNT-glucose nanocomposites for drug delivery. *Ultrasonics Sonochemistry, 40*, 402–409. https://doi.org/10.1016/j.ultsonch.2017.07.033

Manchun, S., Nunthanid, J., Limmatvapirat, S., & Sriamornsak, P. (2012). Effect of ultrasonic treatment on physical properties of tapioca starch. *Advanced Materials Research, 506*, 294–297. https://doi.org/10.4028/www.scientific.net/AMR.506.294

Martins, A., Beninca, C., Bet, C. D., Bisinella, R. Z. B., Oliveira, C. S., Hornung, P. S., & Schnitzler, E. (2020). Ultrasonic modification of purple taro starch (*Colocasia esculenta* B. Tini): Structural, physicochemical and thermal properties. *Journal of Thermal Analysis and Calorimetry, 142*, 819–828. https://doi.org/10.1007/s10973-020-09298-3

Minakawa, A. F. K., Faria-Tischer, C. S. P., & Mali, S. (2019). Simple ultrasound method to obtain starch micro- and nanoparticles from cassava, corn and yam starches. *Food Chemistry, 283*, 11–18. https://doi.org/10.1016/j.foodchem.2019.01.015

Monroy, Y., Rivero, S., & García, M. A. (2018). Microstructural and techno-functional properties of cassava starch modified by ultrasound. *Ultrasonics Sonochemistry, 42*, 795–804. https://doi.org/10.1016/j.ultsonch.2017.12.048

Mustač, N. Č., Voučko, B., Novotni, D., Drakula, S., Gudelj, A., Dujmić, F., & Ćurić, D. (2019). Optimization of high intensity ultrasound treatment of proso millet bran to improve physical and nutritional quality. *Food Technology & Biotechnology, 57*(2), 183–190. https://doi.org/10.17113/ftb.57.02.19.6100

Ogutu, F. O., Mu, T., Elahi, R., Zhang, M., & Sun, H. (2015). Ultrasonic modification of selected polysaccharides: A review. *Journal of Food Processing and Technology, 6*, 446. https://doi.org/10.4172/2157-7110.1000446

Raghunathan, R., Pandiselvam, R., Kothakota, A., Khaneghah, A. M., & Gavahian, M. (2021). The application of emerging non-thermal technologies for the modification of cereal starches. *LWT–Food Science and Technology, 138*, 110795. https://doi.org/10.1016/j.lwt.2020.110795

Rahaman, A., Kumari, A., Zeng, X.-A., Adil Farooq, M., Siddique, R., Khlifa, I., Siddeeg, A., Ali, M., & Faisal Manzoor, M. (2021). Ultrasound-based modification and structural-functional analysis of corn and cassava starch. *Ultrasonics Sonochemistry, 80*, 105795. https://doi.org/10.1016/j.ultsonch.2021.105795

Raza, H., Liang, Q., Ameer, K., Ma, H., & Ren, X. (2022). Dual-frequency power ultrasound effects on the complexing index, physicochemical properties, and digestion mechanism of arrowhead starch-lipid complexes. *Ultrasonics Sonochemistry, 84*, 105978. https://doi.org/10.1016/j.ultsonch.2022.105978

Romko, S. S. (2024). *Avaliação das propriedades térmicas e estruturais de amido de semente de nêspera (Eriobotrya japonica Lindl.) modificado fisicamente* [Master's thesis, Universidade Estadual de Ponta Grossa].

Rubanka, K., Pysarets, O., Levkivska, T., Samoilik, O., & Shpak, V. (2025). Effect of pregelatinized corn starch on the technological and quality properties of pea dough and snacks. *Ukrainian Journal of Food Science, 13*(1), 55–66. https://doi.org/10.24263/2310-1008-2025-13-1-7

Ruths, L. C., Maior, L. O., Bach, D., Romko, S. S., Schnitzler, E., Demiate, I. M., & Lacerda, L. G. (2024). Effects of continuous and repeated dry heat treatment on the technological properties of green banana (*Musa paradisiaca*) starch. *Food Science & Technology, 44*, e00057, 1–8. https://doi.org/10.5327/fst.00057

Qin, Y., Qiu, C., Hu, Y., Ge, S., Wang, J., & Jin, Z. (2020). In situ self-assembly of nanoparticles into waxberry-like starch microspheres enhanced the mechanical strength, fatigue resistance, and adhesiveness of hydrogels. *ACS Applied Materials & Interfaces, 12*(41), 46609–46620. https://doi.org/10.1021/acsami.0c10327

Sango, D. M., Abela, D., McElhatton, A., & Valdramidis, V. P. (2014). Assisted ultrasound applications for the production of safe foods. *Journal of Applied Microbiology, 116*(5), 1067–1083. https://doi.org/10.1111/jam.12468

Santos, S. S. J., Bet, C. D., Bisinella, R. B. Z., Romko, S. S., & Schnitzler, E. (2025). Ultrasound-assisted modification and multianalytical characterization of organic *Arracacia xanthorrhiza* starch. *Ukrainian Food Journal, 14*(3), 406–419. https://doi.org/10.24263/2304-974X-2025-14-3-4

Satmalawati, E. M., Pranoto, Y., Marseno, D. W., & Marsono, Y. (2020). The physicochemical characteristics of cassava starch modified by ultrasonication. *IOP Conference Series: Materials Science and Engineering, 980*, 012030.

Shabana, S., Prasansha, R., Kalinina, I., Potoroko, I., Bagale, U., & Shirish, S. H. (2019). Ultrasound assisted acid hydrolyzed structure modification and loading of antioxidants on potato starch nanoparticles. *Ultrasonics Sonochemistry, 51*, 444–450. https://doi.org/10.1016/j.ultsonch.2018.07.023

Shen, H., Guo, Y., Zhao, J., Zhao, J., Ge, X., Zhang, Q., & Yan, W. (2021). The multiscale structure and physicochemical properties of mung bean starch modified by ultrasound combined with plasma treatment. *International Journal of Biological Macromolecules, 191*, 821–831. https://doi.org/10.1016/j.ijbiomac.2021.09.157

Shulga, S., & Shulga, O. (2026). Modification of potato starch by acylation with acetyllactic acid chloride for food and packaging applications. *Ukrainian Food Journal, 15*(2), 390–400. https://doi.org/10.24263/2304-974X-2026-15-2-8

Sujka, M. (2017). Ultrasonic modification of starch–Impact on granules porosity. *Ultrasonics Sonochemistry, 37*, 424–429. https://doi.org/10.1016/j.ultsonch.2017.02.001

Ulbrich, M., Bai, Y., & Flöter, E. (2020). The supporting effect of ultrasound on the acid hydrolysis of granular potato starch. *Carbohydrate Polymers, 230*, 115633. https://doi.org/10.1016/j.carbpol.2019.115633

Valencia, G. A., Henao, A. C. A., & Zapata, R. A. V. (2012). Comparative study and characterization of starches isolated from unconventional tuber sources. *Journal of Polymer Engineering, 32*, 531–537. https://doi.org/10.1515/polyeng-2012-0092

Veelaert, S. (2014). *Powdered acid-loaded carrier material* (U.S. Patent No. US20140017381A1). U.S. Patent and Trademark Office.

Wang, S., Hu, X., Wang, Z., Bao, Q., Zhou, B., Li, T., & Li, S. (2020). Preparation and characterization of highly lipophilic modified potato starch by ultrasound and freeze-thaw treatments. *Ultrasonics Sonochemistry, 64*, 105054. https://doi.org/10.1016/j.ultsonch.2020.105054

Wang, J., Lv, X., Lan, T., Lei, Y., Suo, J., Zhao, Q., Lei, J., Sun, X., & Ma, T. (2022). Modification in structural, physicochemical, functional, and in vitro digestive properties of kiwi starch by high-power ultrasound treatment. *Ultrasonics Sonochemistry, 86*, 106004. https://doi.org/10.1016/j.ultsonch.2022.106004

Wang, N., You, Y., Liao, X., Zhang, F., Kan, J., & Zheng, J. (2023). Ultrasonic modification of lotus starch based on multi-scale structure: Pasting, rheological, and thermal properties. *LWT–Food Science and Technology, 184*, 115030. https://doi.org/10.1016/j.lwt.2023.115030

Wei, Y., Li, G., & Zhu, F. (2023). Impact of long-term ultrasound treatment on structural and physicochemical properties of starches differing in granule size. *Carbohydrate Polymers, 320*, 121195. https://doi.org/10.1016/j.carbpol.2023.121195

Wendlandt, W. W. (1986). Thermal analysis (3rd ed.). John Wiley.

Wu, Z., Qiao, D., Zhao, S., Lin, Q., Zhang, B., & Xie, F. (2022). Nonthermal physical modification of starch: An overview of recent research into structure and property alterations. *International Journal of Biological Macromolecules, 203*, 153–175. https://doi.org/10.1016/j.ijbiomac.2022.01.103

Yang, Q. Y., Lu, X. X., Chen, Y. Z., Luo, Z. G., & Xiao, Z. G. (2019). Fine structure, crystalline and physicochemical properties of waxy corn starch treated by ultrasound irradiation. *Ultrasonics Sonochemistry, 51*, 350–358. https://doi.org/10.1016/j.ultsonch.2018.09.001

Yu, S., Zhang, Y., Ge, Y., Zhang, Y., Sun, T., Jiao, Y., & Zheng, X. Q. (2013). Effects of ultrasound processing on the thermal and retrogradation properties of nonwaxy rice starch. *Journal of Food Process Engineering, 36*(6), 793–802. https://doi.org/10.1111/jfpe.12048

Zhang, Y., Dai, Y., Hou, H., Li, X., Dong, H., Wang, W., & Zhang, H. (2020). Ultrasound-assisted preparation of octenyl succinic anhydride modified starch and its influence mechanism on the quality. *Food Chemistry: X, 5*, 100077. https://doi.org/10.1016/j.fochx.2020.100077

Zheng, J., Li, Q., Hu, A., Yang, L., Lü, J., Zhang, X., & Lin, Q. (2013). Dual-frequency ultrasound effect on structure and properties of sweet potato starch. *Starch/Stärke, 65*(7–8), 621–627. https://doi.org/10.1002/star.201200197

Zhou, Y., Wang, M., Wang, L., Liu, L., Wu, Y., & Ouyang, J. (2023). Comparison of the effect of ultrasound and microwave on the functional properties and in vitro digestibility of normal maize starch and potato starch. *Journal of Food Process Engineering, 46*, e14222. https://doi.org/10.1111/jfpe.14222

Zhu, F. (2015). Impact of ultrasound on structure, physicochemical properties, modifications and applications of starch. *Trends in Food Science & Technology, 43*, 1–17. https://doi.org/10.1016/j.tifs.2014.12.008

Zhu, J., Li, L., Chen, L., & Li, X. (2012). Study on supramolecular structural changes of ultrasonic-treated potato starch granules. *Food Hydrocolloids, 29*(1), 116–122. https://doi.org/10.1016/j.foodhyd.2012.02.004

Zuo, J. Y., Knoerzer, K., Mawson, R., Kentish, S., & Ashokkumar, M. (2009). The pasting properties of sonicated waxy rice starch suspensions. *Ultrasonics Sonochemistry, 16*, 462–468. https://doi.org/10.1016/j.ultsonch.2009.01.002

Zuo, R., Kong, X., Wang, Y., He, Y., Deng, S., Zhuang, X., & Qiu, D. (2024). Isolation and characterization of natural nano starch from amaranth starch. *International Journal of Biological Macromolecules, 260*, 129525.

Cite:

Guedes, P. V., & Schnitzler, E. (2026). Effects of ultrasound treatment on different starches and their thermal properties. *Ukrainian Food Journal, 15*(3), 608–644. https://doi.org/10.24263/2304-974X-2026-15-3-4

Vegetable oil-based recovery of carotenoids from sea buckthorn pomace for butter fortification

Tatiana Cușmenco, Irina Dianu, Natalia Netreba, Vladislav Rești ca, Artur Macari

Technical University of Moldova, Chisinau, Republic of Moldova

Keywords:

Sea buckthorn
Pomace
Carotenoid extraction
Vegetable oil
Antioxidant
Butter
Fortification

Article history:

Received 04.02.2026
Received in revised form 16.04.2026
Accepted 30.06.2026

Corresponding author:

Tatiana Cușmenco
E-mail: tatiana.cusmenco@sa.utm.md

DOI:
10.24263/2304-974X-2026-15-3-5

Abstract

Introduction. The aim of the research is to investigate the vegetable oil-based extraction of carotenoids from sea buckthorn pomace and their subsequent incorporation into butter as a functional food matrix with enhanced antioxidant properties.

Materials and methods. Vegetable oil-based extraction was used to recover carotenoids from sea buckthorn pomace. Lutein, zeaxanthin, zeaxanthin dipalmitate, and total carotenoids were analyzed by HPLC-DAD and spectrophotometry. Antioxidant capacity was determined using 2,2′-azino-bis(3-ethylbenzothiazoline-6-sulfonic acid) (ABTS) and 2,2-diphenyl-1-picrylhydrazyl (DPPH) assays. Butter samples were evaluated for sensory attributes, oxidative stability, microbiological quality, texture, color, and antioxidant capacity using standard analytical methods.

Results and discussion. Increasing the ethanol proportion in the biphasic sunflower-oil/ethanol system lowered the extraction yield (from 81.3% at 65/35 to 31.3% at 35/65) but increased the concentration of bioactive compounds in the extracts. The 35/65 system (SBLE 5) provided the highest levels of total carotenoids (74.2 mg/g), lutein (1.73 mg/g), zeaxanthin (4.44 mg/g), and total phenolics (1.30 mg GAE/g), as well as the highest antioxidant capacity (ABTS 1.48 and DPPH 0.85 mg TE/g). This demonstrated a clear trade-off between extraction yield and enrichment of the extract with bioactive compounds, with the lower ethanol proportion favoring overall recovery and the higher proportion favoring selective enrichment. Incorporation of the extract into butter at concentrations of 0.5–2.5% showed that 1.0% was the most suitable level, providing the highest sensory acceptability and the lowest peroxide value (0.52 mEq O_2/kg fat). Higher extract concentrations adversely affected aroma and taste and were associated with increased oxidation, suggesting that excessive enrichment may reduce product quality. Fortification progressively softened the butter, with hardness decreasing by 13–45%, and increased lightness, b* value, and the yellowness index. At the same time, the saponification index and microbiological safety parameters remained unchanged, indicating that extract incorporation did not adversely affect these quality characteristics. The melting temperature and thermal hysteresis also increased with increasing extract concentration. All treatment effects were statistically significant (one-way ANOVA, Tukey HSD, $p < 0.05$).

Conclusions. Sea buckthorn pomace-derived carotenoid extracts exhibited high antioxidant capacity and effective incorporation into butter as a functional food matrix. Hexane extracts showed higher activity compared to methanolic fractions, indicating a stronger contribution of lipophilic compounds.

Introduction

The European Farm to Fork Strategy promotes the transition towards sustainable food systems that support food security, nutrition, public health, and reduced environmental impact (European Commission, 2020). In this context, the valorisation of agro-industrial by-products represents a promising approach to improve the sustainability of food production while recovering valuable bioactive compounds for the development of functional foods (Stabnikova et al., 2023a, b). Plant pomaces generated during juice and oil processing are particularly promising because they retain carotenoids, phenolics, vitamins, and other functional constituents that can be recovered and incorporated into food products.

Plant-derived bioactive compounds, particularly antioxidants, are of growing interest because of their potential role in maintaining redox homeostasis and limiting oxidative stress associated with chronic diseases (Garcia-Llorens et al., 2025; Ilari et al., 2025; Onu et al., 2025; Tüğen & Buruleanu, 2026; Vasheka & Petrusha, 2022). By neutralizing reactive oxygen and nitrogen species, dietary antioxidants can reduce oxidative damage and contribute to the functional properties of foods (Ma et al., 2025; Mubeen et al., 2025). However, their effectiveness depends not only on their intrinsic activity but also on their stability and behavior within the food matrix, which can affect their bioavailability and functional performance.

Among plant-derived bioactive compounds, carotenoids are of particular interest because of their antioxidant activity and potential health benefits. These natural pigments possess an extended system of conjugated double bonds that provides antioxidant properties but also makes them susceptible to chemical and physical degradation (Kolašinac et al., 2025; Kurek et al., 2025). Carotenoids are predominantly lipophilic and readily soluble in lipid phases but have limited solubility in aqueous systems. Their physicochemical properties favor their incorporation into lipid-rich food matrices, while exposure to light and oxygen can promote autoxidation, isomerization, and photooxidation, resulting in loss of color, biological activity, and stability (Sereti et al., 2025; Zhao et al., 2025).



Figure 1. ***Hippophae rhamnoides***

Sea buckthorn (*Hippophae rhamnoides* L.) (Figure 1) is a valuable source of carotenoids, tocopherols, and unsaturated fatty acids with considerable antioxidant potential (Jiang et al., 2026; Li et al., 2026). During fruit processing, a proportion of these substances remains in the solid fractions, making sea buckthorn pomace a promising secondary source of lipophilic compounds (Zhang et al., 2023). Its composition depends on the relative proportions of pulp, seed, and peel, while processing operations such as pressing and drying can affect the distribution and retention of these constituents (Zhou et al., 2025; Zhu et al., 2025). Thus, sea buckthorn pomace can be valorised as a source of natural carotenoids for food applications while reducing agro-industrial waste.

The extraction of lipophilic compounds from sea buckthorn pomace can be enhanced by ultrasound through acoustic cavitation, which promotes disruption of the plant matrix and improves mass transfer (Kavindya et al., 2026; Zoglopiti et al., 2025). The combination of ultrasound with a lipid solvent can facilitate the solubilization and transfer of hydrophobic compounds into the lipid phase by increasing contact between the extraction medium and the plant matrix and reducing diffusion limitations (Lučić & Onjia, 2025; Maleki et al., 2024; Ordóñez-Santos et al., 2015; Tang et al.,

2024). This approach can therefore facilitate the recovery of carotenoid-rich extracts within relatively short processing times (Ferraz & Silva, 2025; Kagueyam et al., 2025; Tüğen & Özge, 2025).

Butter represents a lipid-rich food matrix suitable for the incorporation of lipophilic bioactive compounds such as carotenoids. As a water-in-oil emulsion with a continuous lipid phase structured by a fat crystal network, butter can facilitate the solubilization and retention of carotenoids within its fat phase (Bao & Pignitter, 2023; Bihola et al., 2026). The semi-solid structure of butter may also influence oxygen diffusion and molecular mobility, potentially affecting the stability of incorporated lipophilic compounds (Acevedo & Marangoni, 2015; Macias-Rodriguez & Marangoni, 2018).

In this context, the aim of the present study was to obtain a carotenoid-rich oil extract from sea buckthorn pomace and incorporate it into butter as a lipid-based functional food system. The effects of extract incorporation on carotenoid content and antioxidant capacity, as well as on the physicochemical, sensory, microbiological, textural, and color properties of butter, were investigated.

Materials and methods

Materials

Sea buckthorn (*Hippophae rhamnoides* L.) berries, obtained from a mixture of the Clara and Mara cultivars grown in commercial plantations in Călărași District, Republic of Moldova (47.2550° N, 28.3080° E), were used as the raw material. Juice extraction was carried out at a fruit processing facility in Clișova, Orhei District, Republic of Moldova (47.3920° N, 28.8320° E). The resulting pomace was dried at ≤40 °C to a residual moisture content of 9.8% and ground to a fine powder with an average particle size of ≤0.5 mm. A standardized sample mass of 2.0 g of dried, ground pomace was used for all extraction experiments.

Chemicals

All chemicals and reagents used throughout the study were of analytical or HPLC grade and were used without further purification. Folin–Ciocalteu reagent, gallic acid, sodium carbonate (Na_2CO_3), ABTS (2,2′-azinobis(3-ethylbenzothiazoline-6-sulfonic acid)), DPPH (2,2-diphenyl-1-picrylhydrazyl), potassium persulfate ($K_2S_2O_8$), and Trolox were obtained from Sigma-Aldrich (St. Louis, MO, USA). Methanol, ethanol, hexane, acetonitrile, ethyl acetate, hydrochloric acid (HCl), sodium hydroxide (NaOH), potassium hydroxide (KOH), phenolphthalein, and diethyl ether were purchased from Merck (Darmstadt, Germany). Carotenoid standards (lutein, zeaxanthin, and zeaxanthin dipalmitate) were also obtained from Sigma-Aldrich (USA). Standard buffer solutions (pH 4.00, 7.00, and 10.00) used for instrument calibration were supplied by Merck (Germany). Microbiological culture media, including Buffered Peptone Water (BPW), Plate Count Agar (PCA), Baird–Parker agar, Xylose Lysine Deoxycholate (XLD) agar, and Sabouraud Dextrose Agar (SDA), were purchased from Oxoid (Thermo Fisher Scientific, UK). Sterile saline solution (0.85% NaCl) and microbiological consumables were used for sample preparation and serial dilutions. Deionized water was used throughout the study.

Preparation of sea buckthorn lipophilic extracts (SBLE)

The extraction of lipophilic compounds was performed using a biphasic food-grade system consisting of sunflower oil (Floris, Republic of Moldova) and food-grade ethanol (96.6% v/v; Ecochimie). The oil/ethanol ratio was varied according to the experimental

design: 65/35, 60/40, 55/45, 50/50, and 35/65 (v/v). Ultrasound-assisted extraction was performed using an ISOLAB 621.06.006 ultrasonic device (Laborgeräte GmbH, Germany) at a frequency of 37 kHz and an ultrasonic power of 240 W. Extraction was conducted at 20 ± 1 °C for 372 s. Each experimental condition was performed in triplicate (n = 3).

After extraction, ethanol was removed by rotary evaporation (Hei-VAP Advantage, Heidolph Instruments GmbH & Co. KG, Germany) under reduced pressure (1 mbar). Evaporation was performed at a bath temperature of 45 ± 1 °C and a vapor temperature of 29 ± 1 °C until complete solvent removal, yielding a lipid-soluble extract concentrated in sunflower oil. The extracts were transferred to amber glass containers, hermetically sealed with minimal headspace, and stored at 4 ± 1 °C in the dark until further analysis to minimize oxidation and degradation of bioactive compounds.

Manufacture of butter with sea buckthorn lipophilic extracts (BSBLE).

BSBLE were manufactured according to the following technological procedure. Whole cow's milk (approximately 32 L), with a fat content of 4.1%, obtained from Simmental cows raised at the didactic-experimental farm of the Technical University of Moldova, was used for butter manufacture. Approximately 3.5 kg of sweet cream with a fat content of about 40% was separated from the whole milk. The cream was subjected to physical maturation at 8 ± 1 °C for 12–16 h to promote partial crystallization of milk fat and improve churning efficiency.

After maturation, the sweet cream was standardized to a fat content of approximately 38%. SBLE was incorporated at concentrations of 0.5, 1.0, 1.5, 2.0, and 2.5% (m/m) relative to the cream mass. A sample without extract addition was used as the control. The mixtures were homogenized to ensure uniform distribution of the extract within the lipid phase.

Butter was produced by churning at 500 rpm for 15 min at 8 ± 1 °C until complete separation of buttermilk. All experimental variants were produced under identical conditions in three independent replicates (n = 3). The resulting butter grains were washed twice with cold water (8 ± 2 °C) to remove residual buttermilk and then worked until a homogeneous structure and uniform distribution of the aqueous phase within the lipid matrix were obtained. The BSBLE samples were packaged in airtight containers, protected from light, and stored at 4 ± 1 °C until analysis.

Quality and stability

Quality and stability were evaluated in the following order: sensory characteristics, physicochemical properties, microbiological quality, texture, color, and antioxidant capacity.

Determination of bioactive profiling and antioxidant capacity of SBLE

The bioactive profile of SBLE was characterized by quantification of total phenolic content (TPC, mg GAE/g extract), antioxidant capacity (ABTS and DPPH assays, mg TE/g extract, and major carotenoid compounds (lutein, zeaxanthin, zeaxanthin dipalmitate, and total carotenoids, mg/g extract). All determinations were performed in triplicate (n=3), and results were expressed on an extract basis.

Determination of total phenolic content (TPC). The total phenolic content (TPC) was determined using the Folin-Ciocalteu (F.C.) spectrophotometric method. Briefly, aliquots of the extract were mixed with Folin–Ciocalteu reagent and sodium carbonate solution, followed by incubation at room temperature in the dark, according to the method described by Pérez et al. (2023). Absorbance was measured at 765 nm using a UV–Vis spectrophotometer (Shimadzu UV-1800, Japan). A calibration curve prepared using gallic acid was used for quantification ($R^2 = 0.9978$), and the results were expressed as mg gallic acid equivalents per gram of extract (mg GAE/g extract).

The TPC was calculated according to the following equation:

$$\mathrm{TPC} = \frac{\mathrm{C} \times \mathrm{V}}{\mathrm{m}}$$

where C is the concentration obtained from the calibration curve (mg/mL); V is the extract volume (mL); and m is the sample mass (g).

Determination of antioxidant capacity (AC) assays. Antioxidant capacity (AC) was evaluated using the ABTS radical cation decolorization assay. The $ABTS^{\bullet+}$ solution was generated by reacting a 7 mM ABTS stock solution with 2.45 mM potassium persulfate, followed by incubation in the dark for 12–16 h at room temperature. Prior to analysis, the solution was diluted with ethanol to an absorbance of 0.70 ± 0.02 at 734 nm. After addition of the extract, the reduction in absorbance was measured at 734 nm.

$$\%\ \mathrm{inhibition} = \frac{\mathrm{A_0} - \mathrm{A_s}}{\mathrm{A_0}} \times 100$$

where A_0 is the absorbance of the control and A_s is the absorbance of the sample (Munteanu and Apetrei, 2021).

AC_{ABTC} was expressed as expressed as mg Trolox equivalents per gram of extract (mg TE/g extract) using a Trolox calibration curve ($R^2 = 0.9987$).

DPPH (2.2-diphenyl-1-picrylhydrazyl) radical scavenging capacity was determined using a methanolic DPPH solution (0.1 mmol/L). The reaction mixture containing extract and DPPH solution was incubated in the dark at room temperature until stable absorbance was achieved. Absorbance was measured at 517 nm.

$$\%\ \mathrm{inhibition} = \frac{\mathrm{A_0} - \mathrm{A_s}}{\mathrm{A_0}} \times 100$$

AC_{DPPH} was expressed as mg Trolox equivalents per gram of extract (mg TE/g extract).

Determination of carotenoid compounds in sea buckthorn pomace extract. Carotenoids (lutein, zeaxanthin, and zeaxanthin dipalmitate) were quantified using high-performance liquid chromatography (HPLC, Agilent 1260 Infinity, USA) equipped with a diode array detector (DAD). Separation was performed on a reversed-phase C18 column (250 × 4.6 mm, 5 μm particle size) maintained at 25 °C. The mobile phase consisted of methanol (A) and acetonitrile–ethyl acetate (B) in gradient elution mode. The flow rate was set at 1.0 mL/min, and detection was performed at 450 nm.

Compounds were identified by comparing their retention times and UV–Vis spectra with those of authentic standards. Calibration curves for lutein, zeaxanthin, and zeaxanthin dipalmitate showed strong linearity between concentration and detector response (R^2 = 0.9997) (Xu et al., 2023).

$$\mathrm{Compound} = \frac{\mathrm{C} \times \mathrm{V}}{\mathrm{m}}$$

where C is the concentration obtained from the calibration curve (mg/mL); V is the extract volume (mL); and m is the sample mass (g).

Determination of total carotenoids (mg/g extract). The total carotenoids (mg/g) were determined by Xu et al. (2023), spectrophotometrically at 450 nm using appropriate solvent extraction. Absorbance was measured after complete clarification of the extract.

$$\mathrm{Total\ carotenoids} = \frac{\mathrm{A} \times \mathrm{V} \times 10^4}{\mathrm{E}^{1\%}_{1\mathrm{cm}} \times \mathrm{m}}$$

where A is the absorbance at 450 nm; V is the extract volume (mL); $E^{1\%}/_{1cm}$ is the extinction coefficient; and m is the sample mass (g).

Determination of antioxidant capacity of butter with sea buckthorn lipophilic extracts (BSBLE)

For the antioxidant characterization of the fortified butter, the lipophilic and polar fractions were recovered separately from each BSBLE sample. Portions of 2.0 g of butter were extracted with 10 mL of n-hexane and, in parallel, with 10 mL of methanol (1:5, m/v) under magnetic stirring for 30 min at 20 ± 1 °C, followed by centrifugation (4000 rpm, 10 min) and collection of the supernatant. The antioxidant capacity of both extracts was determined by the ABTS assay as described above and expressed as mg Trolox equivalents per 100 g of butter (mg TE/100 g).

BSBLE sensory evaluation

Sensory evaluation of BSBLE was performed using a 9-point hedonic scale (1 = dislike extremely; 9 = like extremely), in accordance with the methodology described in ISO 11136:2013. The sensory evaluation was carried out by a panel consisting of 9 participants, including 6 academic staff members and 3 students from the Faculty of Food Technology, Technical University of Moldova. The panel included 7 women and 2 men, aged between 21 and 53 years. BSBLE samples were presented in equal portions at a serving temperature of approximately 12 ± 1 °C, in identical white porcelain containers coded to minimize visual bias. The evaluation was conducted under controlled laboratory conditions (21 ± 1 °C, neutral lighting, and absence of interfering odors). The order of BSBLE presentation was randomized for each participant. Between samples, participants used unsweetened tea to rinse their palate to minimize carry-over effects on sensory perception. The following sensory attributes were evaluated: appearance, color, consistency, aroma, taste, and overall acceptability.

BSBLE physicochemical analysis

Determination of BSBLE titratable acidity. The titratable acidity **(**TA) of BSBLE was determined using an acid-base titration method (AOAC International, 2019). A weighed portion of fat BSBLE was dissolved in a neutralized mixture of ethanol and diethyl ether (1:1, v/v). The solution was titrated with standardized sodium hydroxide (NaOH) solution (0.1 N) using phenolphthalein as an indicator. The endpoint was considered the appearance of a persistent pale pink color lasting for at least 30 seconds. TA was calculated and expressed as mg NaOH per g of fat using the following equation:

$$\text{Titratable Acidity} = \frac{V \times N \times 40}{m}$$

where V is the volume of NaOH used for titration (mL); N is the normality of the NaOH solution; 40 is the equivalent molecular weight of NaOH (mg/mmol); and m is the mass of the fat sample (g).

Determination of **BSBLE saponification index (SI).** The saponification index (SI) (ISO 3657:2020) was determined using the alkaline reflux saponification method followed by back titration of excess alkali. Two grams of butter were placed in a conical flask and dissolved in 5 mL of distilled ethyl alcohol. Then, 25 mL of 0.5 N alcoholic potassium hydroxide (KOH) solution was added. The flask was attached to a reflux condenser and the mixture was heated under reflux until a clear solution was obtained, indicating complete saponification. In parallel, a blank determination was carried out under the same conditions without the addition of BSBLE. After refluxing, both solutions were cooled, phenolphthalein indicator was added, and the excess alkali was titrated with 0.5 N hydrochloric acid (HCl) until the pink color disappeared. The SI (mg NaOH/g fat) was calculated using the following equation:

$$SI = (V_B - V_S) \times 0.5 \times 56/m$$

where V_B is the volume of HCl used for the blank (mL); V_S is the volume of HCl used for the sample (mL); 56 is the equivalent mass of potassium hydroxide (mg/mmol), and m is the mass of the sample (g).

Determination of BSBLE peroxide value (PV). The method is based on the reaction between primary lipid oxidation products (peroxides and hydroperoxides) and potassium iodide in an acidic medium, with the release of free iodine, which is subsequently quantified by titration with sodium thiosulfate solution **(**ISO 3960:2017). The released iodine was titrated with sodium thiosulfate solution, and the amount consumed was used to determine the peroxide value of the sample. The PV (mEq O_2/kg fat) was calculated using the following equation:

$$PV = \frac{(V_1 - V_2) \times C \times K \times 1000}{m}$$

where V_1 is the volume of sodium thiosulfate solution used for the sample (mL); V_2 is the volume of sodium thiosulfate solution used for the blank (mL); C is the concentration of sodium thiosulfate solution (mol/mL); K is the correction factor of sodium thiosulfate solution titer; 1000 is the conversion factor to mmol/kg, and

m = mass of fat in the extract (g), calculated as:

$$m = m_1 - m_2$$

where m_1 is the mass of the flask after drying (g); m_2 is the mass of the flask before drying (g).

Determination of BSBLE Reichert-Meissl (RM) and Polenske indexes. The Reichert-Meissl (RM) and Polenske indexes **(**ISO 480:1972**)** were determined using the saponification, steam distillation, and alkalimetric titration method**.** The method is based on the separation of volatile fatty acids from milk fat by steam distillation, followed by the quantitative determination of the water-soluble and water-insoluble fractions by titration with a standardized sodium hydroxide (NaOH) solution. For the analysis, 5 g of BSBLE were saponified using glycerol and sulfuric acid (H_2SO_4). After saponification, the volatile fatty acids were separated by steam distillation using a glass distillation apparatus equipped with a condenser. The distillate was cooled and filtered. The water-soluble volatile fatty acids in the distillate were titrated with a standardized NaOH solution to determine the RM index. The water-insoluble volatile fatty acids retained on the filter paper were dissolved in ethanol and subsequently titrated with the same NaOH solution to determine the Polenske value. The RM index was calculated using the following equation:

$$RM = (A - B) \times N \times 11$$

where A is the volume of the standardized NaOH solution used for the sample (mL); B s the volume of the standardized NaOH solution used for the blank (mL); N is the normality of the standardized NaOH solution.

The Polenske index was calculated using the following equation:

$$Polenske = 10 \times V \times N$$

where **V**is the volume of the standardized NaOH solution used for the sample (mL); **N** is the normality of the standardized NaOH solution.

Determination of BSBLE water content. The water content (ISO 3727-1:2001) in BSBLE samples was determined using the oven-drying method in a drying oven (POL-ECO-APARATURA SP.J.SLW 115 SMART, Poland) at 105±2°C, until complete removal of water and attainment of constant weight. The samples were placed in pre-weighed weighing dishes and subjected to drying, followed by cooling in a desiccator and reweighing under ambient conditions. The determination was based on the mass difference between the initial and final weight of the

BSBLE samples, corresponding to the amount of water removed during the drying process. Water content was calculated using the following equation:

$$\text{Water content}(\%) = \frac{M_1 - M_2}{M_0} \times 100$$

where $M_1$is the mass of the dish with the sample before drying (g); $M_2$is the mass of the dish with the sample after drying (g); M_0 is the initial mass of the butter sample (g).

Determination of BSBLE thermostability (c.u.). The BSBLE thermostability was determined according to ISO 11036:2020, using the cylinder deformation method. Cylindrical samples measuring 20 mm in height and 20 mm in diameter were prepared from each BSBLE sample and placed in a thermostatic chamber (POL-ECO-APARATURA SP.J.SLW 115 SMART, Poland) at 30 ± 1 °C for 2 h. After thermostating, the diameter of the cylinder base was measured, and thermostability was calculated as the ratio between the initial and final diameters of the cylinder base. Thermostability was calculated using the following equation:

$$\text{Thermostability} = \frac{D_0}{D_1}$$

where D_0 is the initial diameter of the butter cylinder base (mm); D_1 is the diameter of the butter cylinder base after thermostating (mm).

Determination of BSBLE plasma pH. The pH of the plasma in BSBLE samples was determined in the aqueous phase separated from the lipid system. For phase separation, approximately 10 g of butter were gently melted at 40–45 °C using a thermostatic water bath (Memmert WNB, Germany). The melted samples were then centrifuged using a laboratory centrifuge MPW-380R (MPW Med. Instruments, Poland) at 4000 rpm for 10–15 min to achieve clear separation between the lipid phase and the aqueous phase (plasma). The resulting aqueous fraction was collected using a graduated glass pipette (Brand GmbH, Germany) and immediately used for pH determination. pH measurements were performed using a Testo digital pH meter (Testo SE & Co. KGaA, Germany) equipped with a combined glass electrode. Prior to analysis, the instrument was calibrated using standard buffer solutions at pH 4.00, 7.00, and 10.00 (Merck, Germany) at 25 ± 1 °C. The electrode was directly immersed in the aqueous phase, and the pH value was recorded after signal stabilization.

Determination of BSBLE thermal transition parameters. The thermal transition parameters of BSBLE were determined using a modified method by ISO 6321:2021. The BSBLE samples were gradually heated until complete melting, and the corresponding temperature was recorded as the melting temperature (Tm). Subsequently, the BSBLE samples were cooled under controlled conditions, and the temperature at which crystallization began was recorded as the solidification temperature (Ts). Temperature was monitored using a DT-882 infrared thermometer (CEM Instruments, China), allowing non-contact continuous measurement of thermal changes in the BSBLE sample. Thermal hysteresis (ΔT) was calculated as the difference between the melting and solidification temperatures according to the following equation:

$$\Delta T = T_m - T_s$$

where: T_m is the melting temperature (°C); T_s is the solidification temperature (°C).

BSBLE microbiological analysis

The microbiological quality and safety of BSBLE samples were evaluated by determining coliform bacteria, *Staphylococcus aureus*, and pathogenic microorganisms, including *Salmonella* spp. Yeast and mould counts were determined as indicators of product spoilage. Coliform bacteria were determined using selective plating techniques on appropriate chromogenic/differential media, followed by incubation under standardized conditions, and

results were expressed as absence in 0.001 g of sample, in accordance with ISO 4832:2006. *Staphylococcus aureus* was detected using selective and differential culture media, followed by incubation and confirmatory tests for coagulase-positive staphylococci, according to ISO 6888-1:2021, with results expressed as absence in 0.1 g of sample. Pathogenic microorganisms, including *Salmonella* spp., were detected using a pre-enrichment step in buffered peptone water, followed by selective enrichment, isolation on selective agar media, and biochemical/serological confirmation, according to (ISO 6579-1:2017). Results were expressed as absence in 25 g of sample. Yeasts and moulds were enumerated by surface plating on selective fungal media, followed by incubation at controlled temperature conditions, according to ISO 21527-1:2008. Results were expressed as colony-forming units per gram (CFU/g), with a detection limit of ≤ 50 CFU/g.

BSBLE texture profile analysis (TPA)

The textural properties of BSBLE samples enriched with SBLE were determined using a TA.HDplusC texture analyzer (Stable Micro Systems, Godalming, UK) equipped with a 5 kg load cell and a P/0.75S cylindrical probe (Lis et al., 2021). Texture profile analysis (TPA) was performed to evaluate hardness (g), adhesiveness (g·s), elasticity (%), cohesiveness (%), resilience (%), gumminess (g), and chewiness (g). Prior to analysis, butter samples were conditioned to a controlled temperature to ensure uniform consistency. Each sample was placed on the analyzer platform and subjected to a double compression cycle to a defined deformation level, simulating mastication conditions. The force–time curves obtained during compression were used to calculate the textural parameters.

Determination of BSBLE color attributes and yellowness index (YI)

Color attributes of BSBLE samples were determined in the CIELAB color space (L*, a*, b*) using a calibrated colorimetric system (ISO 11664-4:2019). The CIELAB system describes color through three coordinates: lightness (L*), red-green coordinate (a*), and yellow-blue coordinate (b*). Based on the primary CIELAB parameters, additional color indices were calculated, including total color difference (ΔE*), chroma (C*), hue angle (h°), and yellowness index (YI), according to the following equations:
The total color difference was calculated as:

$$\Delta E^* = \sqrt{(L_2^* - L_1^*)^2 + (a_2^* - a_1^*)^2 + (b_2^* - b_1^*)^2}$$

where L^*_1, a^*_1, b^*_1 is the control sample; L^*_2, a^*_2, b^*_2 is the analyzed sample.

Chroma (C*) was calculated as:

$$C^* = \sqrt{(a^*)^2 + (b^*)^2}$$

Hue angle (h°) was determined as:

$$h^\circ = \tan^{-1}\left(\frac{b^*}{a^*}\right)$$

The yellowness index (YI) was calculated to quantify the yellow coloration of the BSBLE samples, using the following relationship:

$$YI = \frac{142.86 \cdot b^*}{L^*}$$

Statistical analysis

All experiments were carried out in three independent replicates (n = 3), and results are expressed as mean ± standard deviation. Prior to parametric testing, normality of the data was verified using the Shapiro-Wilk test and homogeneity of variances using the Levene test.

Differences among treatments were evaluated by one-way analysis of variance (ANOVA); when the F-test was significant, means were separated using Tukey's honestly significant difference (HSD) test at $\alpha = 0.05$. Within each table, means not sharing a common superscript letter differ significantly ($p < 0.05$). Sensory scores are reported as the mean ± standard deviation of three independent panel sessions. Associations between paired physicochemical or antioxidant parameters were assessed by Pearson correlation and least-squares linear regression, reporting the coefficient of determination (R^2) and the significance of the correlation coefficient (t-test on r, n = 6 paired means). Calculations were performed in Microsoft Excel 365 (PHStat2 v3.11), and the ANOVA and Tukey HSD groupings were independently cross-checked using a dedicated statistical package.

Results and discussion

Effect of oil-ethanol ratio on extraction yield, antioxidant capacity and carotenoid profile of SBLE

The results presented in Table 1 demonstrate that variation in the oil/ethanol ratio significantly influenced both extraction efficiency and the bioactive composition of the obtained lipophilic extracts ($p < 0.05$). Although all samples were prepared from the same amount of raw material (2.0 g of dried pomace), changes in solvent composition led to marked differences in extraction yield and in the recovery of biologically active compounds.

Table 1

Influence of solvent ratio and ultrasonic time on extraction yield, carotenoid content and antioxidant capacity of SBLE

Parameter	C	SBLE 1	SBLE 2	SBLE 3	SBLE 4	SBLE 5
Oil/Ethanol (v/v)	100/0	65/35	60/40	55/45	50/50	35/65
Ultrasound time (s)	372					
Extraction yield (%)	49.77±0.02^{d}	81.28±0.06^{a}	68.70±0.05^{b}	56.28±0.04^{c}	43.75±0.03^{e}	1.30±0.01^{f}
TPC (mg GAE/g extract)	0.61±0.03^{c}	0.41±0.02^{d}	0.55±0.02^{c}	0.76±0.03^{b}	0.60±0.02^{c}	1.30±0.04^{a}
ACABTS (mg TE/g extract)	0.50±0.03^{e}	0.62±0.03^{d}	0.78±0.04^{c}	1.41±0.05^{a}	1.07±0.04^{b}	1.48±0.05^{a}
ACDPPH (mg TE/g extract)	0.42±0.02^{c}	0.34±0.02^{d}	0.43±0.03^{c}	0.65±0.03^{b}	0.62±0.03^{b}	0.85±0.04^{a}
Lutein (mg/g extract)	0.64±0.01^{d}	1.55±0.02^{c}	1.68±0.02^{a}	1.56±0.02^{c}	1.65±0.02^{b}	1.73±0.03^{a}
Zeaxanthin (mg/g extract)	1.60±0.03^{e}	3.99±0.04^{d}	4.32±0.04^{b}	4.13±0.04^{c}	4.23±0.04^{b}	4.44±0.05^{a}
Z-dipalmitate (mg/g extract)	13.03±0.05^{b}	11.76±0.06^{e}	12.90±0.06^{b}	12.82±0.06^{c}	12.01±0.05^{d}	14.01±0.06^{a}
Total carotenoids (mg/g extract)	67.29±0.10^{f}	71.05±0.12^{c}	72.37±0.12^{b}	69.25±0.11^{d}	68.46±0.11^{e}	74.17±0.13^{a}

Note: C – control sample obtained using pure oil (100/0, v/v); SBLE 1 – extract obtained using a 65/35 (v/v) oil/ethanol ratio; SBLE 2 – extract obtained using a 60/40 (v/v) oil/ethanol ratio; SBLE 3 – extract obtained using a 55/45 (v/v) oil/ethanol ratio; SBLE 4 – extract obtained using a 50/50 (v/v) oil/ethanol ratio; SBLE 5 – extract obtained using a 35/65 (v/v) oil/ethanol ratio; TPC – total phenolic content; GAE – gallic acid equivalents; AC – antioxidant capacity; TE – Trolox equivalents. Data are presented as mean ± SD (n = 3). Different superscript letters within the same row indicate significant differences ($p < 0.05$).

The highest extraction yield was obtained for sample SBLE 1 (65/35), reaching 81.28 %, which corresponds to an approximately 63% increase compared to the control sample (C- 49.77 %), $p < 0.05$. With increasing ethanol proportion, the extraction yield decreased progressively to 68.70 % (SBLE 2), 56.28 % (SBLE 3), 43.75 % (SBLE 4), and 31.30 % (SBLE 5). This behavior suggests that a higher proportion of oil promotes the recovery of a greater total mass of extracted compounds, including non-selective lipid fractions. However, a higher extraction yield was not directly associated with increased concentrations of bioactive compounds, highlighting the distinction between total extracted mass and the biological quality of the extract.

This observation is further confirmed by the total carotenoid content. Although SBLE 1 exhibited the highest extraction yield, its total carotenoid content (71.05 mg/g extract) was lower than the maximum value recorded for SBLE 5 (74.17 mg/g extract), ($p < 0.05$). Compared with the control sample (C- 67.29 mg/g extract), SBLE 5 showed an increase of approximately 10.2%, ($p < 0.05$), indicating a more selective extraction of carotenoid compounds. These findings suggest that the rate-limiting step of the process is not carotenoid solubilization in oil, but rather their release from the plant matrix, which is enhanced by increasing ethanol proportion.

Total phenolic content (TPC) showed one of the most pronounced variations among samples. The lowest value was observed in SBLE 1 (0.41 mg GAE/g extract), while SBLE 5 reached 1.30 mg GAE/g extract, corresponding to more than a threefold increase, ($p < 0.05$). This confirms the essential role of ethanol in extracting residual phenolic compounds from sea buckthorn pomace, due to its polarity and ability to interact with hydroxyl-containing structures.

A similar trend was observed for individual carotenoid compounds. Lutein content increased from 0.64 mg/g extract in the control sample to 1.73 mg/g extract in SBLE 5, corresponding to an increase of approximately 170%, ($p < 0.05$). Likewise, zeaxanthin increased from 1.60 mg/g extract in the control to 4.44 mg/g extract in SBLE 5, representing nearly a 2.8-fold increase ($p < 0.05$). These results indicate that xanthophylls are particularly sensitive to solvent composition and benefit from higher ethanol proportions, which facilitate the disruption of interactions between carotenoids and membrane structures.

In the case of Z-dipalmitate, a different behavior was observed. The lowest value was recorded in SBLE 1 (11.76 mg/g extract), whereas the highest value was found in SBLE 5 (14.01 mg/g extract), ($p < 0.05$). The relatively narrow variation across samples suggests that carotenoid esters are less affected by changes in solvent polarity compared to free xanthophylls, likely due to their strongly hydrophobic nature and higher affinity for the oil phase.

Antioxidant capacity (AC) followed a similar overall trend. AC_{ABTS} values increased from 0.50 mg TE/g extract in the control to 1.48 mg TE/g extract in SBLE 5, representing an almost threefold increase, ($p < 0.05$). Likewise, AC_{DPPH} increased from 0.42 mg TE/g extract to 0.85 mg TE/g extract, ($p < 0.05$). The positive correlation between TPC, carotenoid content, and AC suggests a cumulative contribution of these compounds to radical scavenging capacity.

When comparing the experimental samples, a clear trade-off is observed between overall extraction yield and enrichment in bioactive compounds. The 65/35 system maximizes total extracted mass, whereas the 35/65 system yields the highest values for TPC, ABTS, DPPH, lutein, zeaxanthin, Z-dipalmitate, and total carotenoids. This behavior demonstrates that extraction efficiency should not be evaluated solely in terms of yield, but also in terms of selective enrichment in high-value bioactive compounds. For subsequent applications involving butter fortification with bioactive compounds, sample S5 exhibits the most favorable compositional profile, providing simultaneously the highest carotenoid concentration and antioxidant capacity. It should be noted that, in the present design, the ultrasound time co-varied

with the oil/ethanol ratio (Table 1); the reported effects therefore reflect the combined influence of solvent composition and sonication time.

Although the extraction of bioactive compounds from plant sources such as sea buckthorn, tomato, carrot, red pepper, or marigold has been extensively studied, the current literature indicates that most investigations are focused on mono-solvent extraction systems (water, ethanol, hexane, or individual vegetable oils), which limits both the selectivity and stability of the obtained lipophilic fractions. For instance, carotenoid extraction from carrot (Viñas-Ospino et al., 2023) and tomato (Chaudhary et al., 2024) has predominantly been reported using hexane- or ethanol-based systems. However, these methods have drawbacks related to solvent toxicity, thermal degradation, and potential losses of oxidation-sensitive compounds. In the case of sea buckthorn, recent studies have shown that ultrasound-assisted extraction using 70–75% ethanol can yield total phenolic contents of up to 42.86 mg GAE/g extract, together with high antioxidant capacity; however, these approaches do not valorise the lipid fraction within an integrated extraction system (Wu et al., 2024).

Conventional and accelerated techniques for the extraction of sea buckthorn oil and carotenoids, including Soxhlet extraction, supercritical CO_2 extraction, and accelerated solvent extraction (ASE), have demonstrated relatively high β-carotene yields (1.2–1.7 mg/g oil), but remain limited by insufficient control over selectivity and potential degradation of oxidation-sensitive compounds during processing (Mihalcea et al., 2021; Vilas-Franquesa et al., 2022). In contrast, ultrasound-assisted extraction can reduce processing time and enhance the recovery of bioactive compounds through acoustic cavitation and intensified mass transfer, with reported carotenoid levels reaching up to 237 mg β-carotene equivalents/100 g oil in sea buckthorn oil (Sanwal et al., 2022).

However, a significant scientific gap remains regarding the use of biphasic vegetable oil-ethanol systems as an integrated food-grade extraction medium, particularly for sea buckthorn pomace, where the combination of a polar phase (ethanol) and a lipophilic phase (vegetable oil) could simultaneously enable the release of residual phenolic compounds and the solubilization of carotenoids within a single system (Gherasim et al., 2024; Pandey et al., 2025). Moreover, the literature provides limited data on the correlation between solvent-to-solvent ratio, ultrasound time, and the full profile of bioactive compounds (lutein, zeaxanthin, carotenoid esters) under conditions directly applicable to the food industry.

In this context, the present study proposes an integrated ultrasound-assisted extraction approach using sunflower oil-ethanol systems at different ratios, aiming to simultaneously optimize extraction yield and bioactive compound concentration. This strategy enables the production of stable and food-compatible lipophilic extracts with direct applicability in functional food formulation, including dairy products and fortified butter, thereby contributing to the valorisation of sea buckthorn processing by-products.

Sensory evaluation of BSBLE

Sensory evaluation of BSBLE revealed a clear dose-dependent response, characteristic of lipid-based food systems fortified with bioactive-rich lipophilic extracts, where improvements in visual quality are progressively counterbalanced by adverse modifications in the aromatic profile at higher incorporation levels ($p < 0.05$) (Table 2). The hedonic scores (9-point scale) ranged from 6.6 to 9.0, indicating substantial variability in sensory perception as a function of extract concentration. Color was the most positively affected attribute following extract addition, increasing progressively from 7.6 (Control) to 9.0 (BSBLE 1.00), while remaining high at higher concentrations (8.8-8.9) ($p < 0.05$).

Table 2

Impact of SBLE on sensory quality of butter

Sensory attribute	Control	BSBLE 0.50	BSBLE 1.00	BSBLE 1.50	BSBLE 2.00	BSBLE 2.50
	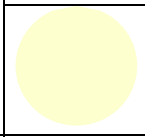					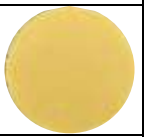
Appearance	7.9±0.2 ^{b}	8.3±0.2 ^{a}	**8.8±0.1** ^{a}	8.4±0.2 ^{a}	8.1±0.2 ^{b}	7.8±0.3 ^{b}
Color	7.6±0.3 ^{c}	8.5±0.2 ^{b}	**9.0±0.1** ^{a}	8.9±0.1 ^{a}	8.9±0.1 ^{a}	8.8±0.1 ^{a}
Consistency	8.4±0.2 ^{a}	8.6±0.2 ^{a}	**8.7±0.1** ^{a}	8.3±0.2 ^{a}	8.0±0.3 ^{b}	7.7±0.3 ^{b}
Aroma	8.2±0.2 ^{a}	8.6±0.2 ^{a}	**8.8±0.1** ^{a}	8.0±0.2 ^{b}	7.4±0.3 ^{b}	6.9±0.4 ^{c}
Taste	8.1±0.2 ^{b}	8.7±0.1 ^{a}	**8.9±0.1** ^{a}	8.0±0.2 ^{b}	7.2±0.3 ^{c}	6.6±0.4 ^{c}
Overall acceptability	8.0±0.2 ^{b}	8.7±0.1 ^{a}	**8.9±0.1** ^{a}	8.1±0.2 ^{b}	7.5±0.3 ^{c}	7.0±0.3 ^{c}

Note: Control- butter without extract addition; BSBLE 0.50-2.50- butter fortified with 0.50-2.50% SBLE. Values are expressed as mean ± standard deviation (SD). All samples were evaluated by a trained sensory panel, and measurements were performed in triplicate (n = 3). Different superscript letters within the same row indicate significant differences ($p < 0.05$).

This behavior is directly associated with the accumulation of lipophilic carotenoids (lutein, zeaxanthin, and carotenoid esters), which exhibit strong absorption in the blue region of the visible spectrum, thereby enhancing the yellow-orange coloration of the fat phase. From a physicochemical perspective, the high compatibility between these hydrophobic pigments and the triglyceride matrix of butter explains their efficient incorporation and the stability of color intensity even at elevated extract levels.

Regarding appearance and texture, only moderate variations were observed, with optimal scores recorded for BSBLE 1.00 (8.8 and 8.7, respectively) ($p < 0.05$). At low and intermediate incorporation levels, the extract did not significantly disrupt the crystalline fat network responsible for butter's characteristic structure. However, at higher concentrations (BSBLE 2.00 and 2.50), a gradual decrease in scores (down to 7.7-7.8) was observed ($p < 0.05$), likely due to the interference of the unsaturated lipid fraction of the extract with triglyceride crystallization processes, leading to partial destabilization of the fat crystal network and consequent textural changes perceived by the sensory panel.

Aroma and taste exhibited the highest sensitivity to extract concentration, with a distinct optimum at BSBLE 1.00 (8.81 and 8.9), followed by a marked decline at higher levels (down to 6.9 and 6.6 at BSBLE 2.50) ($p < 0.05$). This trend can be explained by the balance between the beneficial contribution of bioactive volatile compounds at low concentrations and their excessive accumulation at higher doses. Sea buckthorn-derived terpenes, aldehydes, and oxidizable lipid fractions contribute positively to aroma complexity at moderate levels; however, at elevated concentrations, they become dominant and induce vegetal, resinous, and slightly bitter notes, thereby reducing hedonic acceptance. Additionally, interactions between residual phenolic compounds and the lipid matrix may further intensify perceived astringency and aromatic intensity.

Overall acceptability confirmed a clear technological optimum at BSBLE 1.00 (8.9), followed by BSBLE 0.50 (8.7), both exceeding the control sample (8.0) ($p < 0.05$). This pattern indicates a synergistic effect at moderate fortification levels, where improved visual attributes and the presence of bioactive compounds positively influence overall perception without inducing sensory imbalance. Exceeding this optimal range leads to an "over-

fortification" phenomenon, characterized by sensory receptor saturation and an imbalance between the neutral lipid notes of butter and the active sensory profile of the extract.

The results obtained for butter fortified with SBLE are consistent with previous studies that have employed carotenoid-rich and lipophilic bioactive extracts in emulsion-based food systems and dairy products. Study by Ghendov-Moșanu et al. (2020) demonstrated that the incorporation of sea buckthorn lipophilic extract into cream cheese did not adversely affect the sensory characteristics of the product, while simultaneously enhancing its antioxidant capacity and oxidative stability. The authors highlighted that the lipophilic fraction of sea buckthorn exhibits high compatibility with dairy lipid matrices, promoting the uniform distribution of carotenoids and preserving sensory acceptability. The significant improvement in color observed in the BSBLE samples can be attributed to the high concentration of xanthophylls present in the extract. Tudor et al. (2020) reported that sea buckthorn oil represents one of the richest natural sources of lutein, zeaxanthin, and zeaxanthin dipalmitate, the latter accounting for approximately 38% of the total carotenoids identified. These pigments exhibit a strong affinity for lipid-based systems and enhanced bioaccessibility when dispersed within fat-rich emulsions. Consequently, the progressive increase in color scores observed in the fortified butter samples may be explained by the efficient incorporation of these carotenoids into the butter fat matrix, resulting in a more intense and attractive yellow-orange coloration.

The highest sensory scores obtained for BSBLE 1.00 suggest the existence of an optimal extract concentration at which functional and sensory benefits are simultaneously maximized. A similar trend was reported by Silyvridou et al. (2024), who investigated the incorporation of sea buckthorn extracts into yogurt and observed that formulations containing 0.5-1.0% extract achieved the highest consumer acceptability scores. In contrast, increasing the extract concentration to 2-3% resulted in a decline in sensory preference, mainly due to the intensification of aroma-related attributes and alterations in the overall sensory profile.

The reduction in aroma and taste scores observed for BSBLE 2.00 and BSBLE 2.50 may be explained by the accumulation of sea buckthorn-specific volatile compounds together with residual phenolic constituents co-extracted with carotenoids. In lipid-rich systems, terpenes, aldehydes, and oxygenated carotenoid derivatives possess relatively low sensory perception thresholds and may become dominant at elevated concentrations, generating vegetal, resinous, or slightly bitter notes. This phenomenon is commonly reported in the development of functional foods and is often described as "over-fortification," a condition in which increasing the concentration of a bioactive ingredient no longer enhances product quality but instead reduces consumer acceptance.

Furthermore, the use of lipophilic extracts offers important technological advantages compared with whole fruits or aqueous extracts, as carotenoids are already solubilized within a lipid phase that is fully compatible with the butter matrix. Such compatibility promotes homogeneous dispersion of bioactive compounds, minimizes phase separation, and contributes to improved color stability and antioxidant protection during storage. Therefore, the superior sensory performance of BSBLE 1.00 can be attributed not only to its optimal concentration of carotenoids and phenolic compounds but also to the favorable interactions established between the lipophilic extract and the triglyceride network characteristic of emulsions (Tereshchuk et al., 2022).

Physicochemical indices of BSBLE

The results presented in Table 3 demonstrate a concentration-dependent modulation of lipid stability and physicochemical indices in butter fortified with BSBLE, reflecting specific

interactions between lipophilic bioactive compounds and the triglyceride matrix of dairy fat ($p < 0.05$). The observed behavior is governed by the balance between the antioxidant capacity of carotenoids and residual phenolic compounds and the structural contribution of the additional lipid fraction introduced with the extract.

Table 3

Changes in lipid stability and physicochemical indices of butter enriched with BSBLE

Sample	TA (mg NaOH/g fat)	SI (mg NaOH/g fat)	PV (mEq O_2/kg fat)
Control	1.60±0.04 [c]	225.80±0.30 [a]	0.91±0.07 [a]
BSBLE 0.50	1.14±0.02 [e]	225.10±0.25 [b]	0.60±0.05 [b]
BSBLE 1.00	1.38±0.01 [d]	224.60±0.20 [b]	0.52±0.04 [c]
BSBLE 1.50	1.72±0.03 [b]	224.10±0.30 [c]	0.55±0.04 [b]
BSBLE 2.00	1.89±0.02 [a]	223.60±0.25 [c]	0.61±0.05 [b]
BSBLE 2.50	1.93±0.05 [a]	223.00±0.20 [d]	0.68±0.05 [b]

Note: Control- butter without extract addition; BSBLE 0.50-2.50 represent butter samples fortified with 0.50-2.50% BSBLE respectively; TA- titratable acidity; SI- saponification index; PV- peroxide value. All determinations are expressed as mean ± standard deviation (SD). Differences were considered significant at $p < 0.05$. The measurements were performed in triplicate (n = 3).

Titratable acidity (TA) increases progressively with BSBLE concentration (from 1.14 to 1.93 mg NaOH/g fat), ($p < 0.05$), indicating enhanced release of free fatty acids. This trend may be explained by two complementary mechanisms: structural modifications in the fat matrix induced by the presence of the extract, which may increase the accessibility of ester bonds to hydrolytic reactions and the potential influence of residual bioactive compounds on lipid stability, particularly at higher incorporation levels. In dairy lipid systems, titratable acidity is considered a sensitive indicator of hydrolytic and oxidative lipid degradation.

The saponification index (SI) shows only minor variation (from 225.80 to 223.00 mg NaOH/g fat), ($p < 0.05$), indicating that the fundamental triglyceride structure of butter remains essentially unchanged. This finding is particularly important, as the saponification value is directly related to the average molecular weight of fatty acids; its stability confirms that BSBLE does not induce chemical degradation or restructuring of the lipid fraction, but rather behaves as a physically dispersed phase within the fat matrix. This is consistent with previous reports on lipophilic plant extracts incorporated into dairy systems, where modifications are predominantly physical and related to dispersion phenomena rather than chemical transformation.

In contrast, the peroxide value (PV) exhibits a non-linear trend, characterized by a marked reduction at low and intermediate BSBLE concentrations, with a minimum observed at BSBLE 1.00 (0.52 mEq O_2/kg fat), ($p < 0.05$). The initial decrease compared to the control (0.91 mEq O_2/kg fat), ($p < 0.05$), can be attributed to the antioxidant capacity of carotenoids, particularly lutein and zeaxanthin, which act through singlet oxygen quenching and interruption of lipid radical propagation reactions in the fat phase. This effect is most pronounced at moderate concentrations, where the bioactive compounds are homogeneously distributed and effectively interact with lipid radicals at the oxidation interface. Such behavior is well documented in lipid systems, where carotenoids are recognized as efficient antioxidants due to their lipophilicity and preferential localization in oxidation-sensitive regions of the matrix.

The subsequent increase in peroxide values at higher BSBLE levels (1.50-2.50), ($p < 0.05$), suggests that the optimal antioxidant threshold is exceeded and that competing effects begin to emerge. From a chemical standpoint, this behavior may be explained by the incorporation of an additional lipid fraction introduced with the extract, potentially containing more oxidation-prone

unsaturated fatty acids than native milk fat; possible aggregation or over-saturation of carotenoids within the lipid phase, which reduces their radical-scavenging efficiency; increased matrix heterogeneity, facilitating oxygen diffusion and promoting lipid oxidation initiation. Such U-shaped or biphasic antioxidant responses are frequently reported in food lipid systems containing natural antioxidants, where activity is highly dependent on concentration, dispersion, and microstructural distribution.

The results confirm the existence of an optimal fortification level (BSBLE 1.00), ($p < 0.05$), at which antioxidant protection is maximized while maintaining lipid structural integrity. Beyond this threshold, a competition arises between the protective effects of carotenoids and the structural and compositional changes induced by higher extract loads, leading to a slight decline in oxidative stability. This concentration-dependent behavior is characteristic of functional lipid-enriched food systems and highlights the necessity of precise formulation optimization for dairy applications.

Correlation analysis of physicochemical indices of BSBLE

The correlation analysis of BSBLE reveals robust statistical associations between compositional indices and physicochemical parameters; however, their interpretation remains limited by the indirect nature of the employed markers and the absence of independent mechanistic validation. In its current form, the dataset supports covariation-type relationships rather than demonstrated causal links.

The extremely high correlation between the Reichert-Meissl (RM) index and the Polenske index ($R^2 = 0.986$, $p < 0.001$) (Figure 2) is consistent across all butter enriched with SBLE, ranging from the control (RM: 1.87, Polenske: 0.17) and increasing progressively up to butter enriched with SBLE 2.50 (RM: 4.72, Polenske: 1.57), indicating an almost proportional variation of volatile acidic and semi-volatile fractions. This overlap suggests that BSBLE -induced compositional changes simultaneously affect both compound classes, most likely through a common mechanism of lipid degradation or release of short- and medium-chain fatty acids. However, the very high correlation raises concerns regarding the lack of analytical orthogonality between the two indices, indicating that RM and Polenske do not discriminate between distinct processes but rather reflect the same global transformation of volatile fractions. Consequently, the variation observed across samples (from control to BSBLE 2.50) may be interpreted more as a gradient of processing intensity than as independent mechanistic changes.

Thermostability (Figure 3) exhibits a negative correlation with water content (R^2=0.805, $p < 0.05$), observed over the range from the control (12.20 %) to butter enriched with BSBLE 2.50 (15.81 %), where increasing water content is associated with relatively minor variations in thermostability (Control - 0.76 %, SBLE 0.50 - 0.96 %, BSBLE 1.00 - 1.00 %, SBLE 2.50 - 0.98 %). This behavior is consistent with the plasticizing effect of water, which reduces intermolecular interactions and lowers the energy required for phase transitions. Nevertheless, the relatively high data dispersion indicates significant unexplained variability, suggesting that water is not the sole governing factor. Structural modifications induced by SBLE are likely to further contribute to stability, accounting for deviations from the linear model.

The strong negative correlation between pH and the RM index (Figure 4) (R^2=0.924, $p < 0.05$), observed across the entire BSBLE, from pH 5.91 (Control) to 4.62 (BSBLE 0.50) and subsequently stabilizing between 4.59 and 4.54 (BSBLE 1.00-2.50), indicates progressive acidification associated with increasing RM values (from 1.87 to 4.72). From a chemical perspective, this trend is consistent with the accumulation of volatile fatty acids and the associated shift in acid-base equilibrium.

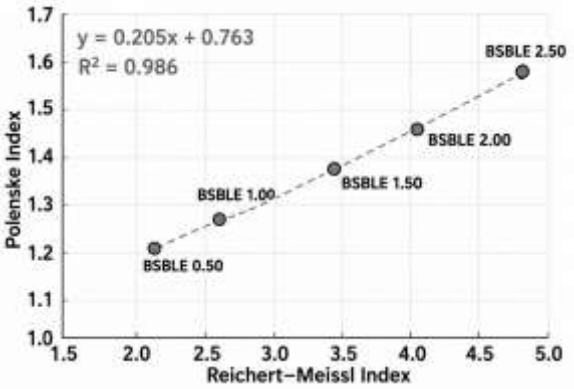

Figure 2. Variability of the Polenske index in relation to the Reichert-Meissl index at different BSBLE concentrations

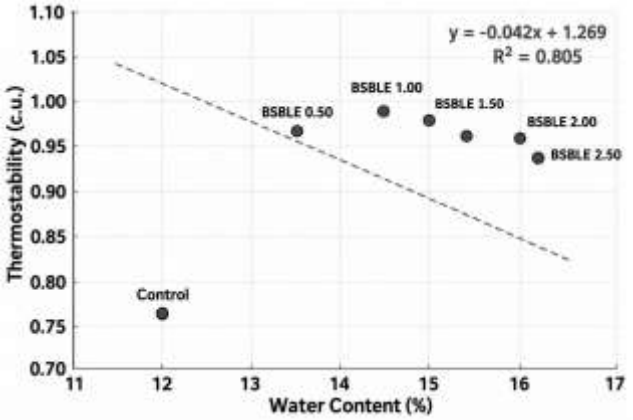

Figure 3. Relationship between thermostability and water content at different BSBLE concentrations

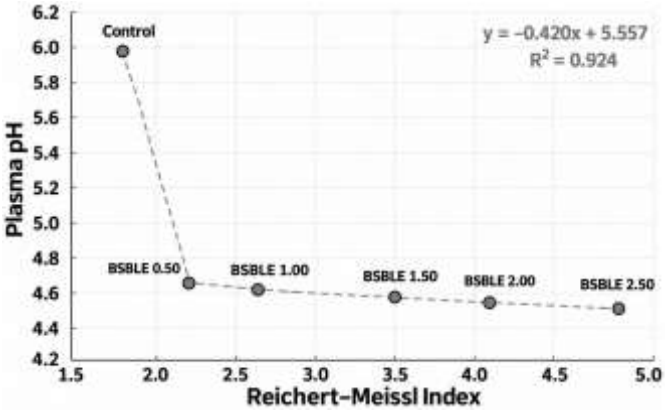

Figure 4. Correlation between plasma pH and the Reichert-Meissl index at different BSBLE concentrations

However, the deviation from linearity at higher RM values (BSBLE 2.50), where pH remains stable within the narrow range of 4.55-4.54, suggests the establishment of a buffered equilibrium regime or the emergence of buffering effects. This may be attributed to the presence of buffering constituents (residual proteins, phosphate systems, or multiprotic weak organic acids), while RM continues to increase (from 3.69 to 4.72), indicating a partial decoupling between acid accumulation and pH response.

The correlation patterns observed in BSBLE are consistent with recent literature on lipid oxidation and hydrolysis mechanisms in complex food systems, where degradation processes do not occur independently but are instead tightly interconnected through shared chemical pathways. Contemporary studies indicate that lipid oxidation and triglyceride hydrolysis proceed simultaneously in food matrices, generating a wide range of volatile and non-volatile compounds with correlated evolution (Oh et al., 2023). In particular, in dispersed lipid systems, it has been demonstrated that oxidation mechanisms are strongly influenced by interfacial organization and the presence of the aqueous phase, leading to interdependent responses between chemical and physical parameters (Bao & Pignitter, 2023). This observation is relevant to the BSBLE system, where the increase in water content is correlated with changes in thermal stability, suggesting a combined effect of plasticization and structural reorganization of the matrix. The very high correlation between indices associated with volatile fractions (RM and Polenske) can be explained by the fact that lipid degradation products originate from the same oxidation and hydrolysis pathways, resulting in a simultaneous distribution of volatile fatty acids. Recent literature further emphasizes that such global indices exhibit limited orthogonality, as they respond to the same pool of compounds derived from triglyceride degradation, thereby producing strong correlations among variables originating from overlapping chemical fractions (Kang & Yeo, 2024). Regarding the relationship between pH and lipid degradation, recent studies have shown that the accumulation of secondary lipid oxidation products, including aldehydes and volatile fatty acids, induces changes in acid-base equilibrium as well as protein-lipid interactions within food matrices (Huang et al., 2024). These processes lead to an initial decrease in pH, followed by stabilization once the system reaches a limited buffering capacity. This behavior is consistent with the pH stabilization observed in BSBLE samples at approximately 4.5-4.6, despite the continued increase in RM index values.

Furthermore, the literature indicates that interactions between lipid oxidation products and structural components of food matrices can induce changes in physical and thermal stability without proportionally affecting global chemical indicators (Geng et al., 2023). This phenomenon explains the observed decoupling between the continuous increase in the RM index and the relatively stable behavior of pH and thermal stability at higher BSBLE intensities.

Thermal transition parameters of BSBLE

The data presented in Figure 5 demonstrate a systematic dependence of phase transition parameters on BSBLE concentration in butter lipid systems. In the control, the melting temperature (Tm) is 30.21 °C, while the solidification temperature (Ts) is 12.54 °C, corresponding to a thermal hysteresis (ΔT) of 17.67°C, characteristic of a polymorphic lipid system in which heating and cooling transitions are not thermodynamically congruent. With increasing SBLE concentration up to 2.50, the Tm increases progressively to 33.94 °C, corresponding to an absolute change of +3.73 °C relative to the control. The magnitude of this variation exceeds the associated experimental uncertainty and is supported by the

monotonic trend across all concentrations (from 30.21 to 33.94°C), indicating a systematic effect ($p < 0.05$).

From a thermodynamic perspective, this increase reflects a progressive stabilization of the crystalline phase, associated with a reduction in its Gibbs free energy and enhanced intermolecular cohesion within the lipid matrix. In parallel, the Ts decreases from 12.54 °C to 11.31 °C (-1.23°C), showing a lower amplitude variation but a consistent overall downward trend ($p < 0.05$).

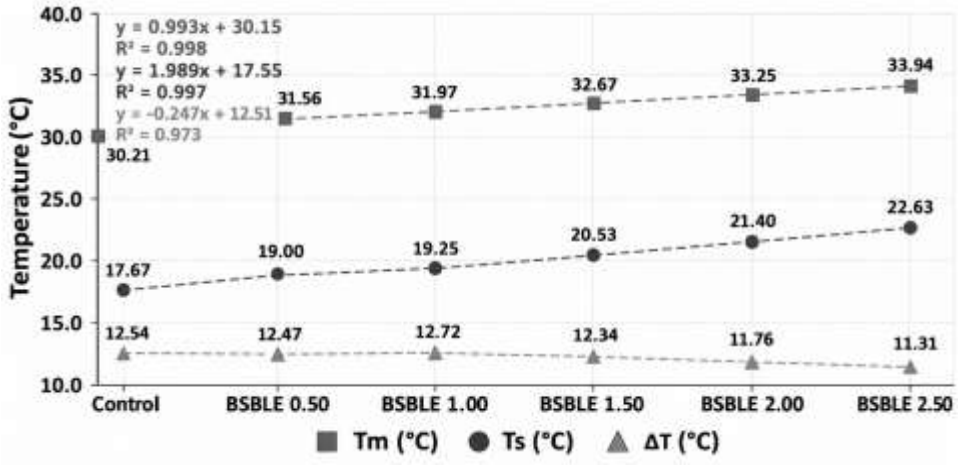

Figure 5. Thermal transition parameters of BSBLE

Although a local fluctuation is observed at BSBLE 1.00 (12.72 °C), the general tendency at higher concentrations indicates that crystallization is predominantly governed by kinetic effects. In this context, the decrease in Ts is consistent with an increased degree of supercooling required for nucleation, implying a reduced probability of stable crystal nucleus formation.

Within this framework, ΔT, increases from 17.67 °C to 22.63 °C (+4.96 °C), reflecting a progressively enhanced separation between heating and cooling transitions. The simultaneous increase in Tm and decrease in Ts leads to an expansion of the transition interval, indicating a decoupling between the thermodynamic stability of the solid phase and the kinetic control of crystallization. The consistency of these variations, both in terms of directional trends and their magnitude relative to experimental uncertainties, supports their systematic nature ($p < 0.05$).

An important finding of the present study is the progressive increase in melting temperature accompanied by a decrease in solidification temperature, suggesting that the incorporation of SBLE into butter simultaneously influences both the thermodynamic stability and crystallization kinetics of the lipid system. This behavior is consistent with findings reported for complex lipid matrices, in which modifications in lipid composition promote crystalline reorganization and alter the thermal phase transition profile. In the study conducted by Declerck et al. (2021) on cocoa butter, differential scanning calorimetry (DSC) revealed that the different polymorphic forms exhibited melting temperatures ranging from 28.1 °C for the metastable α-form to 39.9 °C for the thermodynamically stable β-form. The authors demonstrated that the shift toward higher melting temperatures resulted from the transformation of metastable crystals into more ordered crystalline structures, characterized

by improved molecular packing and lower Gibbs free energy (Declerck et al., 2021). Comparable findings were reported by Gerlei et al. (2024), who investigated the crystallization behavior of lipid blends intended for spreadable fat applications. DSC analysis demonstrated that changes in the ratio of lipid fractions significantly affected both melting and crystallization temperatures, as well as the polymorphic transitions of triacylglycerols. The authors showed that the incorporation of additional lipid components promoted the reorganization of the crystalline network and the formation of more stable crystal structures, which was reflected by a shift of melting temperatures toward higher values and by modifications in the crystallization profile. Furthermore, the study demonstrated that compositional changes influenced nucleation processes and crystal growth kinetics, resulting in marked differences between melting and solidification behavior (Gerlei et al., 2024). Regarding the crystallization process, the present results revealed a decrease in solidification temperature from 12.54 °C to 11.31 °C, suggesting that a greater degree of supercooling was required to initiate nucleation. A similar behavior was described by Gouveia et al. (2019), who demonstrated that crystallization temperature is governed predominantly by nucleation processes and crystal growth kinetics, making it considerably more sensitive to compositional changes than the melting temperature. The authors concluded that the reorganization of lipid fractions delays nucleation and shifts the crystallization temperature toward lower values without substantially affecting the stability of the already-formed crystalline phase (Gouveia et al., 2019).

Microbiological quality and safety of BSBLE

The microbiological analysis (Table 4) demonstrated that all experimental BSBLE, including the control sample and those supplemented with 0.50-2.50% SBLE, fully complied with the established microbiological safety criteria, with no differences observed among the tested samples. Coliform bacteria were not detected in 0.001 g, *Staphylococcus aureus* was not detected in 0.1 g, and pathogenic microorganisms, including *Salmonella*, were absent in 25 g of BSBLE. Likewise, yeast and mold counts remained ≤50 CFU/g, complying with the maximum permissible microbiological limits.

The consistency of these results across all treatments indicates that SBLE incorporation, regardless of concentration, does not adversely affect the microbiological quality of the product or compromise the microbiological stability of the lipid matrix.

The absence of coliform bacteria in all samples represents an important indicator of the hygienic quality of the manufacturing process, as this microbial group is widely recognized as an indicator of secondary contamination and sanitation efficiency during food processing. The presence of coliforms would suggest contamination originating from raw materials, inadequate hygienic practices, or post-processing contamination.

Their absence in both the control and BSBLE samples confirms that the functional ingredient does not constitute a source of microbial contamination and that the manufacturing process was conducted under appropriately controlled hygienic conditions.

A similar pattern was observed for *Staphylococcus aureus*, a microorganism commonly regarded as an indicator of human-associated contamination and one of the principal causative agents of foodborne intoxication. The absence of *S. aureus* in all formulations demonstrates that raw material handling and product processing were carried out under appropriate hygienic conditions. Furthermore, these findings confirm that the incorporation of SBLE, even at the highest concentration tested (2.50%), neither alters the microbiological profile of the product nor promotes the proliferation of this microorganism.

Table 4

Microbiological quality and safety parameters of BSBLE

Sample	Coliform bacteria	*Staphylococcus aureus*	Pathogenic microorganisms (including *Salmonella*)	Yeasts (CFU/g)	Molds (CFU/g)	Permissible limit
Control	Not detected in 0.001 g	Not detected in 0.1 g	Not detected in 25 g	≤ 50	≤ 50	Absent in 0.001 g / 0.1 g / 25 g
BSBLE 0.50	Not detected in 0.001 g	Not detected in 0.1 g	Not detected in 25 g	≤ 50	≤ 50	Absent in 0.001 g / 0.1 g / 25 g
BSBLE 1.00	Not detected in 0.001 g	Not detected in 0.1 g	Not detected in 25 g	≤ 50	≤ 50	Absent in 0.001 g / 0.1 g / 25 g
BSBLE 1.50	Not detected in 0.001 g	Not detected in 0.1 g	Not detected in 25 g	≤ 50	≤ 50	Absent in 0.001 g / 0.1 g / 25 g
BSBLE 2.00	Not detected in 0.001 g	Not detected in 0.1 g	Not detected in 25 g	≤ 50	≤ 50	Absent in 0.001 g / 0.1 g / 25 g
BSBLE 2.50	Not detected in 0.001 g	Not detected in 0.1 g	Not detected in 25 g	≤ 50	≤ 50	Absent in 0.001 g / 0.1 g / 25 g

Note: Control- butter without extract addition; BSBLE 0.50-2.50 represent butter samples fortified with 0.50-2.50% BSBLE respectively. All determinations are expressed as mean ± standard deviation (SD). The measurements were performed in triplicate (n = 3).

Equally important is the absence of pathogenic microorganisms, including *Salmonella*, in 25 g of product across all experimental formulations. This finding confirms the microbiological safety of the developed products and indicates that both the raw materials and the incorporated functional ingredient possessed satisfactory microbiological quality. Moreover, the absence of pathogenic bacteria can also be attributed to the intrinsic characteristics of the lipid matrix. High-fat food systems generally exhibit low water activity, thereby limiting the availability of free water required for microbial metabolism and proliferation. Under these conditions, the growth of most pathogenic bacteria is effectively restricted, contributing to the microbiological stability of the product throughout processing and storage.

Regarding fungal contamination, all samples exhibited yeast and mold counts of ≤50 CFU/g, with no differences observed between the control and BSBLE. The maintenance of these values indicates that SBLE incorporation did not alter the physicochemical environment of the product in a manner that would favor fungal growth. This observation is particularly significant because yeasts and molds are among the primary microorganisms responsible for the spoilage of high-fat foods during storage, owing to their greater tolerance to reduced water activity compared with most bacteria. Therefore, the absence of differences among formulations demonstrates that BSBLE does not compromise the microbiological stability of the product or increase its susceptibility to fungal spoilage.

Comparative evaluation of all experimental formulations revealed that increasing the SBLE concentration from 0.50% to 2.50% did not induce measurable changes in any of the microbiological parameters compared with the control. These findings confirm the

microbiological compatibility of SBLE with the lipid matrix and demonstrate that its incorporation at concentrations up to 2.50% does not affect the microbiological quality or safety of the final product. Furthermore, the physicochemical and thermostability modifications observed in the present study, including the increase in melting temperature, the decrease in solidification temperature, and the expansion of thermal hysteresis, were not accompanied by alterations in the microbiological profile. This agreement indicates that the structural reorganization of the lipid matrix induced by SBLE occurs without compromising the microbiological stability of the product.

These results are consistent with the general principles of food safety, according to which microbiological risks are primarily determined by initial contamination and the effectiveness of implemented control measures during processing. Rathi et al. (2026) emphasize that pathogenic microorganisms such as *Salmonella* spp., *Staphylococcus aureus*, *Escherichia coli*, and *Listeria monocytogenes* remain among the main agents responsible for foodborne diseases, and their control critically depends on the correct application of food safety systems, including good hygiene practices and HACCP-based procedures. In this context, the complete absence of these pathogens in all analyzed samples reflects the effectiveness of the hygienic and sanitary control applied throughout processing.

Regarding the effect of bioactive ingredients, recent literature shows that the addition of plant extracts may influence the microbial load of butter. Study by Sadri-Saeen et al. (2024) demonstrated that the use of ethanolic extract of chia seeds in pasteurized butter led to a significant reduction in microbial load during refrigerated storage, with decreases of 1.5-2.6 log CFU/g for yeasts and molds, as well as non-detectable levels of *E. coli* and *S. aureus*.

The absence of coliforms in all samples is an important indicator of the hygienic quality of the technological process. Coliforms are considered indicators of secondary contamination and are widely used to assess hygiene efficiency in the food industry. In the scientific literature, their presence is associated with poor hygiene practices or post-processing contamination, whereas properly processed products frequently show levels below detection limits or complete absence (Rathi et al., 2026).

A similar trend was observed for *S.aureus*, a microorganism associated with human-origin contamination. The literature highlights that this pathogen may be present in food products under improper handling conditions; however, it is effectively controlled through the application of good hygiene practices and adequate thermal processing (Rathi et al., 2026).

Furthermore, the absence of *Salmonella* in 25 g of product is consistent with the known behavior of lipid matrices, in which the multiplication of pathogenic bacteria is severely limited by low water activity and the lack of a suitable environment for growth. Recent studies confirm that the effective implementation of food safety systems significantly reduces the risk of contamination with such pathogens in dairy products (Rathi et al., 2026).

Yeasts and molds, being more tolerant to low water activity conditions, have their development nevertheless restricted in lipid matrices due to limited nutrient availability and the compact structure of the fat phase. In comparison, studies on similar products have reported greater variations in fungal load, particularly under fluctuating hygienic conditions (Sadri-Saeen et al., 2024).

Texture profile analysis of BSBLE

The results presented in Table 5 highlight a clear dependence on SBLE concentration; however, the comparative analysis between samples indicates that the observed changes are not strictly linear, but rather reflect successive stages of lipid matrix reorganization, characterized by distinct structural thresholds ($p < 0.05$). Compared with the control, the

incorporation of 0.5% SBLE leads to a reduction in hardness from 85.42 g to 74.10 g (-13.2%), accompanied by a decrease in adhesiveness from 117.88 to 102.30 g·s ($p < 0.05$).

These changes suggest an initial disruption of the triacylglycerol crystalline network, without a significant alteration of the internal cohesiveness. From a structural perspective, this range corresponds to a phase of adjustment in lipid nucleation and crystal growth. Increasing SBLE concentration to 1.0% amplifies the mechanical weakening effect, with hardness decreasing to 62.80 g (-26.4% compared to control) and adhesiveness to 88.40 g·s ($p < 0.05$).

Table 5

Changes in textural properties of BSBLE

Textural parameters	Control	BSBLE 0.5	BSBLE 1.0	BSBLE 1.5	BSBLE 2.0	BSBLE 2.5
Hardness (g)	85.42±2.05^{a}	74.10±2.10^{b}	62.80±2.25^{c}	55.60±2.15^{d}	51.40±2.15^{d}	47.20±2.00^{e}
Adhesiveness (g·s)	117.88±3.10^{a}	102.30±2.90^{b}	88.40±2.80^{c}	80.30±2.70^{d}	75.10±2.60^{d}	69.80±2.55^{e}
Elasticity (%)	1.00±0.01^{b}	1.01±0.02^{b}	1.03±0.01^{a}	1.06±0.02^{a}	1.05±0.01^{a}	1.02±0.01^{b}
Cohesiveness (%)	0.33±0.01^{b}	0.39±0.02^{a}	0.43±0.04^{a}	0.46±0.05^{a}	0.42±0.04^{a}	0.47±0.05^{a}
Resilience (%)	0.06±0.01^{c}	0.08±0.01^{b}	0.09±0.02^{b}	0.11±0.01^{b}	0.13±0.02^{a}	0.15± 0.01^{a}
Gumminess (g)	28.61±1.10^{a}	27.80±1.07^{a}	25.60±1.10^{b}	24.90±1.08^{b}	23.70±1.05^{b}	21.50±1.03^{c}
Chewiness (g)	28.60±1.12^{a}	28.10±1.08^{a}	26.00±1.10^{a}	25.40±1.10^{b}	24.20±1.06^{b}	22.00±1.052^{c}

Note: Control- butter without extract addition; BSBLE 0.50–2.50 represent butter samples fortified with 0.50-2.50% BSBLE respectively. All determinations are expressed as mean ± standard deviation (SD). The measurements were performed in triplicate (n = 3). Differences were considered significant at $p < 0.05$.

The difference relative to 0.5% indicates the surpassing of a structural reorganization threshold, where BSBLE interference with triglyceride packing becomes more pronounced. Elasticity increases slightly to 1.03, suggesting an incipient modification of the balance between crystalline and liquid phases. At 1.5% BSBLE, hardness decreases further to 55.60 g (-34.9% compared to control), while adhesiveness reaches 80.30 g·s ($p < 0.05$). At this stage, the reduced rate of change compared to the previous interval suggests a tendency toward a partially stabilized reorganization regime.

In parallel, the increase in cohesiveness to 0.46 indicates an internal structural consolidation, suggesting that the reduction in rigidity is not associated with network disintegration, but rather with a redistribution of crystalline phases. At 2.0% BSBLE, the decreasing trend continues, with hardness reaching 51.40 g (-39.8% compared to control) and adhesiveness 75.10 g·s ($p < 0.05$). However, the variations between 1.5% and 2.0% are relatively small, suggesting the system enters a pseudo-plateau region, where crystal reorganization becomes less intense. Cohesiveness shows a minor fluctuation (0.42), remaining within the same statistical group as the other fortified samples. At 2.5% SBLE, hardness reaches its minimum value of 47.20 g (-44.7% compared to control), while adhesiveness decreases to 69.80 g·s ($p < 0.05$). At this stage, cohesiveness reaches 0.47,

statistically comparable to the intermediate concentrations (shared superscript letter), indicating that the residual crystalline network is retained without significant destabilization even at the highest extract load.

Derived parameters, gumminess and chewiness, follow an overall decreasing trend from the control sample (28.61 and 28.60 g, respectively) to 2.5% SBLE (21.50 and 22.00 g), confirming a reduced mechanical energy required for deformation and structural fragmentation ($p < 0.05$). This evolution is directly correlated with the decrease in hardness and reflects a reduction in the overall structural resistance of the system. These modifications suggest that SBLE influences the microstructural organization of the lipid phase, leading to reduced density and continuity of the crystalline network, together with a redistribution of internal interactions that supports material cohesiveness. The observed transition is characteristic of lipid systems in which compositional changes induce adjustments in the balance between crystalline and amorphous phases, without compromising the overall structural integrity of the product.

The textural modifications observed in the BSBLE are consistent with recent findings reported in the literature for lipid-based matrices such as butter, where structural variations are primarily governed by the reorganization of the triacylglycerol network and changes in solid fat content. Recent studies have confirmed that reductions in hardness and adhesiveness are closely associated with decreased crystalline lipid density and alterations in fundamental rheological parameters. In a study investigating commercially available butters subjected to temperature variations, Yang et al. (2024) reported a decrease in hardness with increasing liquid fat fraction, accompanied by reductions in storage modulus (G′) and resistance to deformation, confirming that texture is largely controlled by the solid-liquid fat balance within the lipid network.

Similarly, Rosa et al. (2023), in a study demonstrated that the incorporation of bioactive compounds encapsulated in butter significantly modifies textural parameters, including reductions in firmness and changes in cohesiveness, without causing structural destabilization of the lipid system. The authors attributed these effects to fat phase redistribution and interference with crystallization processes, resulting in a more flexible yet structurally stable matrix.

Furthermore, comparative studies on butter and fat analog systems have shown that reductions in hardness are strongly correlated with decreases in adhesiveness and deformation energy, parameters directly linked to crystalline network density and lipid crystal size distribution (Teng et al., 2024).

In addition, recent literature highlights that butter structure is highly sensitive to compositional modifications, emulsifiers, or bioactive extracts, which can induce polymorphic transitions between β′ and β forms, directly affecting hardness and cohesiveness (Timlin et al., 2024). Complementarily, recent multiscale simulation models have demonstrated that macroscopic textural properties directly emerge from microstructural lipid rearrangements at the level of crystalline aggregation and solid phase distribution (Nozawa, 2026). This relationship explains why moderate changes in cohesiveness can coexist with significant reductions in hardness without structural collapse of the system.

Color parameters of BSBLE

The comparative analysis of the samples in Table 6 reveals a clear concentration-dependent effect of BSBLE on color parameters, with changes that are consistent from a physicochemical and optical perspective ($p < 0.05$). First, lightness (L*) increases significantly across all levels ($p < 0.05$). Compared to the control (83.59), each addition of

SBLE results in a gradual increase: 85.36 (BSBLE 0.50), 86.56 (BSBLE 1.00), 87.42 (BSBLE 1.50), 89.45 (BSBLE 2.00), and 91.21 (BSBLE 2.50). The total difference of approximately +7.6 units suggests a progressive modification of the optical properties of the matrix, most likely due to increased light scattering and reduced selective absorption in the visible region. From a physical standpoint, this behavior is typical of systems in which added compounds alter the refractive index and internal microstructure, thereby enhancing diffuse reflectance.

Table 6

Color attributes and YI of BSBLE

Sample	L*	a*	b*	ΔE	C*	h°	YI
Control	83.59 ±1.49 [b]	-5.65 ±0.24 [a]	30.54 ±0.52 [f]	13.68 ±0.64 [a]	31.06 ±0.48 [e]	100.5 ±0.7 [c]	52.09 ±1.12 [b]
BSBLE 0.50	85.36 ±1.46 [b]	-6.31 ±0.22 [b]	33.12 ±0.56 [e]	13.27 ±0.62 [a]	33.74 ±0.52 [d]	101.0 ±0.8 [b]	55.23 ±1.15 [b]
BSBLE 1.00	86.56 ±1.43 [b]	-6.36 ±0.25 [b]	35.19 ±0.59 [d]	12.56 ±0.67 [a]	35.75 ±0.55 [c]	102.2 ±0.9 [b]	58.10 ±1.18 [a]
BSBLE 1.50	87.42 ±1.45 [a]	-6.43 ±0.24 [b]	37.09 ±0.51 [c]	12.13 ±0.66 [a]	37.65 ±0.57 [b]	103.0 ±0.9 [b]	60.71 ±1.20 [a]
BSBLE 2.00	89.45 ±1.42 [a]	-6.47 ±0.21 [b]	39.05 ±0.54 [b]	11.87 ±0.64 [b]	38.59 ±0.60 [a]	105.7 ±1.0 [a]	60.90 ±1.22 [a]
BSBLE 2.50	91.21 ±1.49 [a]	-6.53 ±0.20 [b]	41.00 ±0.51 [a]	11.69 ±0.68 [b]	39.54 ±0.62 [a]	106.5 ±1.0 [a]	61.18 ±1.25 [a]

Note: Control – butter without extract addition; BSBLE 0.50 –2.50 represent butter samples fortified with 0.50 –2.50% BSBLE respectively; L* – lightness; a* – red-green coordinate; b* – yellow-blue coordinate; ΔE* – total color difference; C* – chroma; h° – hue angle; YI – yellowness index. ΔE* values represent the total colour difference calculated against a fixed reference standard used for instrument calibration; consequently, the control sample also presents a non-zero ΔE*, and the values are intended for comparison across samples rather than as self –differences. All determinations are expressed as mean ± standard deviation (SD). Differences were considered significant at $p < 0.05$. The measurements were performed in triplicate (n = 3).

The a* component remains negative across all samples (ranging from -5.65 to -6.53), indicating a persistent greenish tendency ($p < 0.05$). Although the variation is relatively small, it is consistent across treatments, particularly between the control and the 2.50 BSBLE sample (difference of approximately 0.88 units). This shift suggests a slight increase in absorption in the red region of the spectrum, potentially attributable to phenolic compounds in BSBLE, which are known to exhibit selective absorption in the 480-600 nm range.

In contrast, the b* parameter shows the most pronounced change among all color coordinates, increasing from 30.54 (Control) to 33.12 (BSBLE 0.50), 35.19 (BSBLE 1.00), 37.09 (BSBLE 1.50), 39.05 (BSBLE 2.00), and 41.00 (BSBLE 2.50) ($p < 0.05$). The overall increase of approximately 10.5 units indicates a strong enhancement of the yellow component. Spectrophotometrically, this suggests increased absorption in the blue region (400-500 nm), resulting in a more pronounced yellow appearance. Such behavior is commonly associated with flavonoids, oxidized polyphenols, or pigments formed through oxidative reactions.

The C* follows the same trend as b*, increasing steadily from 31.06 (Control) to 33.74 (BSBLE 0.50), 35.75 (BSBLE 1.00), 37.65 (BSBLE 1.50), 38.59 (BSBLE 2.00), and 39.54 (BSBLE 2.50) ($p < 0.05$). This increase is mathematically consistent with the relationship C*

= $\sqrt{(a^2 + b^2)}$, indicating that changes in b* are the dominant contributor to chromatic enhancement. Accordingly, the increase in C* reflects not only a shift in hue but also a higher color saturation.

The h° increases gradually from 100.5 (Control) to 101.0 (BSBLE 0.50), 102.2 (BSBLE 1.00), 103.0 (BSBLE 1.50), 105.7 (BSBLE 2.00), and 106.5 (BSBLE 2.50) ($p < 0.05$). This trend indicates a rotation in the CIELAB color space toward more yellow-green regions. Theoretically, variations in h° are governed by the ratio between a* and b*, and the more pronounced increase in b* explains the observed directional shift.

The YI increases almost linearly across samples: 52.09 (Control), 55.23 (BSBLE 0.50), 58.10 (BSBLE 1.00), 60.71 (BSBLE 1.50), 60.90 (BSBLE 2.00), and 61.18 (BSBLE 2.50) ($p < 0.05$). The total increase of approximately 9 units confirms an enhanced yellow perception, directly correlated with the increase in b*. From a materials science perspective, YI is highly sensitive to spectral changes in the blue region, supporting the hypothesis that SBLE introduces or activates chromophores that preferentially absorb in this wavelength range.

The ΔE remains high across all samples but shows a slight decreasing trend from 13.68 (Control vs. 0.50) to 11.69 (BSBLE 2.50). Comparison across levels suggests that the most pronounced changes occur at lower concentrations, after which the system approaches a saturation regime where further increases in BSBLE produce more moderate perceptual effects. Importantly, all ΔE values above 10 indicate clearly perceptible color differences, confirming the strong visual impact of BSBLE incorporation ($p < 0.05$).

The results obtained in this study are consistent with the recent literature regarding variations in color parameters in butter, where L*, b*, and YI have been shown to be strongly influenced by lipid composition, carotenoid content, and the structure of fat globules. For instance, study by Cheng and Wu (2024) reported that in β-carotene-enriched butter, b* values increased significantly within the range of 28.4-42.7, accompanied by an increase in the YI, which was linearly correlated with the content of lipophilic pigments, demonstrating the direct role of carotenoids in enhancing the yellow color of butter (Cheng & Wu, 2024). Similarly, study by O'Callaghan et al. (2016) showed that butter derived from pasture-fed cows exhibits significantly higher b* values (approximately 24-30) compared to Total Mixed Ration feeding systems, due to the increased transfer of β-carotene from forage into the lipid fraction of milk, confirming the direct relationship between diet and yellow color intensity.

Moreover, recent studies on commercial butter have highlighted that variations in L* (84.0-92.5) are influenced not only by chemical composition but also by fat globule size and the degree of triglyceride crystallization, which significantly affects light scattering and consequently leads to changes in perceived lightness (Cais-Sokolińska et al., 2024). It has also been demonstrated that the YI is a more sensitive indicator than b* for differentiating butter samples with different lipid profiles, being strongly correlated with carotenoid levels and fatty acid composition ($R^2 > 0.95$) (Cheng & Wu, 2024).

Antioxidant capacity of BSBLE

The antioxidant capacity (AC) (Figure 6) of the BSBLE in the methanolic extract, increased from 0.88 mg TE/100 g in the control to 4.87 mg TE/100 g at the highest tested concentration (BSBLE 2.50), representing a 5.5-fold increase relative to the initial value ($p < 0.05$). Similarly, the hexane extract exhibited an increase from 1.64 mg TE/100 g to 5.91 mg TE/100 g, representing a 3.6-fold increase over the investigated concentration range ($p < 0.05$). Although both extracts displayed a concentration-dependent response, the hexane extract consistently exhibited higher AC than the methanolic extract throughout the entire experimental range ($p < 0.05$).

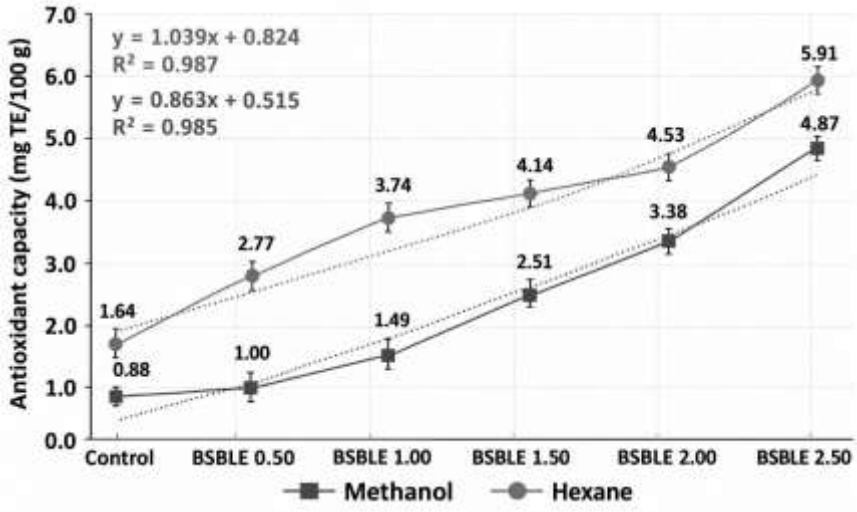

Figure 6. Antioxidant capacity of BSBLE methanolic and hexane extracts

Specifically, at a concentration of 0.50 BSBLE, the AC of the hexane extract (2.77 mg TE/100 g) was 2.8-fold higher than that of the methanolic extract (1.00 mg TE/100 g) ($p < 0.05$). At 1.00 BSBLE, the difference remained substantial, with values of 3.74 and 1.49 mg TE/100 g, respectively, indicating that the AC of the hexane extract was 2.5-fold higher than that of the methanolic extract ($p < 0.05$). As the concentration increased further, the difference gradually decreased, with the hexane extract exhibiting 1.6-fold, 1.3-fold, and 1.2-fold higher AC than the methanolic extract at concentrations of 1.50, 2.00, and 2.50, respectively ($p < 0.05$). This progressive reduction in the difference suggests that the antioxidant efficiencies of the two extracts become increasingly similar at higher concentrations.

Regression analysis demonstrated an almost linear relationship between extract concentration and antioxidant capacity for both extraction systems. The estimated coefficients of determination ($R^2 = 0.987$ for the methanolic extract ($p < 0.001$) and $R^2 = 0.985$ for the hexane extract, $p < 0.001$) indicate that more than 95% of the variability in antioxidant capacity can be explained by extract concentration alone. These findings suggest that, within the investigated concentration range, the ABTS assay did not reach a saturation point and that the availability of radical-scavenging compounds remained the primary factor governing the antioxidant response.

The consistently higher AC observed in the hexane extract suggests that the non-polar fraction of BSBLE contains compounds with a greater ability to reduce the ABTS•+ radical. As a non-polar solvent, hexane preferentially extracts lipophilic constituents such as carotenoids, tocopherols, terpenoids and other hydrophobic secondary metabolites, all of which are recognized for their high radical-scavenging efficiency through electron donation and stabilization of reactive radical species. In contrast, methanol primarily extracts polar antioxidants, including phenolic acids and flavonoids. Although these compounds are widely acknowledged as potent antioxidants, their effectiveness in the AC_{ABTS} assay may vary depending on their chemical structure, degree of hydroxylation, molecular weight, and possible synergistic or antagonistic interactions within the extract matrix.

Furthermore, the progressive reduction in the difference between the two extraction systems with increasing concentration suggests that the contribution of the polar antioxidant

fraction becomes more pronounced at higher extract concentrations. This behavior may indicate the existence of synergistic interactions among different classes of antioxidant compounds present in BSBLE, a phenomenon frequently reported for complex natural extracts in which the overall antioxidant capacity results from the combined activity of multiple bioactive constituents rather than from a single dominant compound.

Recent literature confirms a clear trend regarding the use of plant extracts as natural agents for oxidative stabilization in lipid matrices such as butter and other dairy fat-based products. A recent 2025 study demonstrated that the addition of *Curcuma longa* extract and rosemary essential oil to fermented butter significantly improved oxidative stability, reducing the formation of primary lipid oxidation products and increasing the overall antioxidant capacity of the system, with ABTS values increasing from approximately 1.2 to 4.8 mg TE/100g depending on the added concentration. The authors reported that systems enriched with plant extracts exhibited antioxidant capacity comparable to synthetic antioxidants, confirming the effectiveness of phenolic and terpenoid compounds in protecting the lipid fraction (Gomes et al., 2025). In another recent study, the use of rosemary extract in structured lipid systems demonstrated a significant improvement in the oxidative stability of omega-3-rich margarine, by reducing peroxide formation from approximately 12.5 to 3.1 meq O_2/kg fat and increasing total antioxidant capacity up to approximately 6.0 mg TE/g. This effect was attributed to the high content of phenolic compounds in rosemary (*Rosmarinus officinalis* L.*)*, particularly carnosic acid and carnosol, which act as efficient electron donors in radical reactions (Dhiman & Chopra, 2025). Similarly, recent studies on butter enriched with aromatic plant extracts from the *Lamiaceae* family reported a significant reduction in secondary lipid oxidation products, with thiobarbituric acid reactive substances (TBARS) values decreasing from approximately 0.35 to 0.12 mg MDA (malondialdehyde)/kg, alongside an increase in total antioxidant capacity to approximately 5-7 mg TE/g. These results were strongly correlated with the concentration of added phenolic compounds, indicating a direct relationship between bioactive content and oxidative stability of dairy fat products (Kalinowska et al., 2014). Furthermore, comparative studies on butter enriched with green tea powder demonstrated a significant improvement in antioxidant capacity measured by ABTS and CUPRAC assays, with values increasing from approximately 2.0 to 6.5 mg TE/g, as well as a reduction in lipid oxidation indices during storage of up to 50-70% compared to the control. In these systems, the antioxidant capacity of plant extracts was comparable to or even higher than synthetic antioxidants such as butylated hydroxytoluene BHT, confirming the effectiveness of polyphenolic compounds in stabilizing dairy fats (Çakmakçı et al., 2023).

Across all analyzed parameters, the assumptions of normality and homogeneity of variance were satisfied, validating the use of one-way ANOVA. The Tukey HSD groupings showed consistent and well-separated superscript patterns with low within-group variability, indicating that the observed differences between extraction systems and BSBLE fortification levels reflect genuine treatment effects rather than experimental noise. This statistical robustness supports the reliability of the quality and functional trends discussed above and reinforces the case for the extraction system and dosage level identified as most favorable

Conclusions

The biphasic sunflower-oil/ethanol ultrasound-assisted system efficiently recovered carotenoids from sea buckthorn pomace. Increasing the ethanol proportion lowered the total extraction yield but selectively enriched the extract in bioactive compounds, with the 35/65 ratio (SBLE 5) providing the highest carotenoid, phenolic, and antioxidant values ($p < 0.05$).

Thus, a clear trade-off was observed between extraction yield, which was maximal at the 65/35 ratio, and bioactive enrichment, which was maximal at the 35/65 ratio. In butter, a 1.0% incorporation level was optimal, providing the highest sensory acceptability and the lowest peroxide value (0.52 mEq O_2/kg fat); above this level, aroma, taste, and oxidative stability declined, indicating that higher extract concentrations were less favorable. Fortification progressively softened the matrix, with hardness decreasing by 13–45%, and increased lightness, b*, and the yellowness index, while the saponification index and microbiological safety parameters remained unaffected. The melting temperature and thermal hysteresis increased with increasing extract concentration, indicating changes in the crystalline organization of the fat phase. In fortified butter, the hexane (lipophilic) fraction showed higher antioxidant capacity than the methanolic fraction, although this difference decreased at higher extract concentrations. Overall, sea buckthorn lipophilic extract represents a promising natural functional ingredient for butter, although further studies are needed to identify the individual bioactive compounds contributing to its effects and to validate the storage stability of the fortified product.

Acknowledgment. The research was supported by the Institutional Project, subprogram 020405 "Optimizing food processing technologies in the context of the circular bioeconomy and climate change", Bio-OpTehPAS, being implemented at the Technical University of Moldova.

References

Acevedo, N. C., & Marangoni, A. G. (2015). Nanostructured fat crystal systems. *Annual Review of Food Science and Technology, 6*, 71-96. https://doi.org/10.1146/annurev-food-030713-092400

AOAC International. (2019). *Official methods of analysis of AOAC International* (21st ed.). AOAC International.

Bao, Y. & Pignitter, M. (2023). Mechanisms of lipid oxidation in water-in-oil emulsions and oxidomics-guided discovery of targeted protective approaches. *Comprehensive Reviews in Food Science and Food Safety*, *22*(4), 2678-2705. https://doi.org/10.1111/1541-4337.13158

Bihola, A., Suvera, P., Jana, A. H., Pratiksha P. P., Chaudhary, M. B., & Adil, S. (2026), Microstructural characterization of dairy products: structure-function relationships, processing effects, and industrial significance. *Discover Food, 6*, 124. https://doi.org/10.1007/s44187-026-00828-w

Cais-Sokolińska, D., Bielska, P., & Pawlak, T. (2024). *Color measurement of butter available on the Polish market, Mendeley Data*. https://doi.org/10.17632/2ktsr76452.1

Çakmakçı, S., Gülçin, İ., Gündoğdu, E., Öztekin, H. E., & Taslimi P. (2023). The comparison with commercial antioxidants, effects on colour, and sensory properties of green tea powder in butter, *Antioxidants*, *12*(8), 1522. https://doi.org/10.3390/antiox12081522

Chaudhary, K., Khalid, S., Zahid, M., Ansar, S., Zaffar, M., Hassan S. A., Naeem, M., Maan, A. A., Aadil, R. M. (2024). Emerging ways to extract lycopene from waste of tomato and other fruits, a comprehensive review. *Journal of Food Process Engineering*, *47*(9), e14720. https://doi.org/10.1111/jfpe.14720

Cheng, S. & Wu, S. (2024). A shelf life prediction method for butter based on the effects of β-carotene on colour and oxidative stability. *International Journal of Dairy Technology*, *77*, 961-972. https://doi.org/10.1111/1471-0307.13078

Declerck, A., Nelis, V., Danthine, S., Dewettinck, K., & Van der Meeren, P. (2021). Characterisation of fat crystal polymorphism in cocoa butter by time-domain nmr and dsc deconvolution. *Foods*, *10*(3), 520. https://doi.org/10.3390/foods10030520

Dhiman, A., & Chopra, R. (2025). Rosemary extract as a natural antioxidant in structured lipid systems: a sustainable approach to enhance stability of perilla seed oil based omega-3 fatty acid rich margarine. *Frontiers in Sustainable Food Systems*, *9*, 1654058. https://doi.org/10.3389/fsufs.2025.1654058

European Commission. (2020). *A Farm to Fork Strategy for a Fair, Healthy and Environmentally-Friendly Food System*, Brussels. *https://eur-lex.europa.eu/legal-content/en/txt/?uri=celex:52020dc0381*

Ferraz, L.P., & Silva, E.K. (2025). Pulsed electric fields and ultrasound for enhanced mass transfer in extraction and drying in food processing. *ACS Food Science & Technology*, *5*(9), 3229-3253. https://doi.org/10.1021/acsfoodscitech.5c00567

Garcia-Llorens, G., El Ouardi, M., & Valls-Belles, V. (2025). Oxidative stress fundamentals: unraveling the pathophysiological role of redox imbalance in non-communicable diseases. *Applied Sciences*, *15*(18), 10191. https://doi.org/10.3390/app151810191

Gerlei, M., Pierson, H., Ponçot, M., Kahn, C. J. F., & Linder, M. (2024). Chemical composition and crystallization behavior of oil and fat blends for spreadable fat applications. *Foods*, *13*(20), 3305. https://doi.org/10.3390/foods13203305

Geng, L, Liu, K., & Zhang, H. (2023). Lipid oxidation in foods and its implications on proteins, *Frontiers in Nutrition*. *10*, 1192199. https://doi.org/10.3389/fnut.2023.1192199

Ghendov-Moșanu, A., Sturza, R., Opriș, O., Lung, I., Popescu, L., Popovici, V., Soran, M. L., & Patraș, A. (2020). Effect of lipophilic sea buckthorn extract on cream cheese properties. *Journal of Food Science and Technology*, *57*, 628-637. https://doi.org/10.1007/s13197-019-04094-w

Gherasim, C. E., Focşan, M., Ciont, C., Bunea, A., Rugină, D., & Pintea, A. (2024). Stability and bioaccessibility of carotenoids from sea buckthorn pomace encapsulated in alginate hydrogel beads. *Nutrients*, *16*(16), 2726. https://doi.org/10.3390/nu16162726

Gomes, M. M., Vianna, N. S., Romani, L. C., Longo, V. D., Mossi, A. J., Treiche, H., Bertan, L.C., & Tormen, L. (2025). Obtaining extracts of *Curcuma longa* and rosemary essential oil and evaluation of antioxidant capacity: application in preventing oxidation of fermented butter. *Food and Humanity*, *4*, 100561. https://doi.org/10.1016/j.foohum.2025.100561

Gouveia, J. R., Lixandrão, K. C. L., Tavares, L. B., Lixandrão F. P. H., Garcia G. E. S., & dos Santos, D. J. (2019). Thermal transitions of cocoa butter: a novel characterization method by temperature modulation, *Foods*, *8*(10), 449. https://doi.org/10.3390/foods8100449

Huang, Y., Sarkhel, S., Roy, A., & Mohan, A. (2024). Interrelationship of lipid aldehydes mediated protein oxidation in muscle foods. *Critical Reviews in Food Science and Nutrition*, *64*(32), 1180911825. https://doi.org/10.1080/10408398.2023.2245029

Ilari, S., Proietti, S., Milani, F., Vitiello, L., Muscoli, C., Russo, P., & Bonassi, S. (2025). Dietary patterns, oxidative stress, and early inflammation: A systematic review and meta-analysis comparing mediterranean, vegan, and vegetarian diets. *Nutrients*, *17*(3), 548. https://doi.org/10.3390/nu17030548

ISO 11136: 2013. *Sensory analysis - Methodology - General guidance for conducting hedonic tests with consumers*. Geneva, Switzerland: ISO.

ISO 3657:2020. *Animal and vegetable fats and oils - Determination of saponification value*. Geneva, Switzerland: ISO.

ISO 3960:2017. *Animal and vegetable fats and oils - Determination of peroxide value - Iodometric (visual) endpoint determination*. International Organization for Standardization, Geneva, Switzerland.

ISO 480:1972. *Milk Fat - Determination of Reichert-Meissl Value and Polenske Value (Reference Method).* International Organization for Standardization, Geneva, Switzerland.

ISO 3727-1:2001. *Butter - Determination of moisture, non-fat solids and fat contents - Part 1: Determination of moisture content (Reference method).* International Organization for Standardization (ISO), Geneva, Switzerland.

ISO 11036:2020. *Sensory analysis - Methodology - Texture profile*. Geneva, Switzerland: ISO.

ISO 660:2020. *Animal and vegetable fats and oils - Determination of acid value and acidity*. Geneva, Switzerland: ISO.

ISO 6321:2021. *Animal and vegetable fats and oils - Determination of melting point in open capillary tubes - Slip point*. Geneva, Switzerland: ISO.

ISO 4832:2006. *Microbiology of food and animal feeding stuffs - Horizontal method for the enumeration of coliforms - Colony-count technique*. ISO.

ISO 6888-1:2021. *Microbiology of the food chain - Horizontal method for the enumeration of coagulase-positive staphylococci (Staphylococcus aureus and other species) - Part 1: Method using Baird-Parker agar medium.* ISO.

ISO 6579-1:2017. *Microbiology of the food chain - Hrizontal method for the detection, enumeration and serotyping of Salmonella - Part 1: Detection of Salmonella spp.* ISO.

ISO 21527-1:2008. *Microbiology of food and animal feeding stuffs - Horizontal method for the enumeration of yeasts and moulds - Part 1: Colony count technique in products with water activity greater than 0.95*. ISO.

ISO 11664-4:2019. *Colorimetry - Part 4: CIE 1976 L*a*b* colour space*. Geneva, Switzerland: ISO.

Jiang, X., Sun, M., Deng, W., Zhu, M., Wang, L., Zheng, L., Xing, J., & Hong, J. (2026). From nutritional profile to circular bioeconomy: a review of sea buckthorn oil and by-product valorization. *Foods*, *15*(11), 1873. https://doi.org/10.3390/foods15111873

Kagueyam, S. S., dos Santos Filho J.R., Contato, A.G., de Souza, C.G.M., Castoldi, R., Corrêa, R. C. G., Conte Junior, C. A., Yamaguchi N. U., Bracht A., Peralta R. M. (2025). Green extraction of bioactive compounds from plant-based agri-food residues: Advances toward sustainable valorization. *Plants*, *14*(23), 3597. https://doi.org/10.3390/plants14233597

Kalinowska, M., Ziarno, M., & Sigida, E. (2014). Oxidative stability of butter with added phenolics from Lamiaceae herbs. *International Journal of Food Science + Technology*, *49*(3), 768-775. https://doi.org/10.1111/ijfs.12364

Kang, J., & Yeo, J. (2024). Critical overview of lipid oxidation in food systems using lipidomics. *Food Science and Biotechnology*, *34*, 837-849. https://doi.org/10.1007/s10068-024-01726-6

Kavindya, G., Alahakoon, P., Herath, A., Ekanayake, P., Karunarathna, O., Thilakarathna, N., Abeysinghe, D., & Bandara, P. (2026). Hybrid ultrasound-based extraction techniques in food industry: A state-of-the-art review. *Food Physics*, *3*, 100092. https://doi.org/10.1016/j.foodp.2026.100092

Kolašinac, S. M., Pećinar, I., Gajić, R., Mutavdžić, D., & Dajić Stevanović, Z. P. (2025), Raman spectroscopy in the characterization of food carotenoids: challenges and prospects, *Foods*, *14*(6), 953. https://doi.org/10.3390/foods14060953

Kurek, M. A., Aktaş, H., Pokorski, P., Pogorzelska-Nowicka, E., Custodio-Mendoza, J.A. (2025). A comprehensive review of analytical approaches for carotenoids assessment in plant-based foods: Advances, applications, and future directions. *Applied Sciences*, *15*(7), 3506. https://doi.org/10.3390/app15073506

Li, N., Fan, P., Wang, L., Feng, L., Long, H., Yang, W., Wang, J., Zhao, Y., Liu, H., Guo, Y., & Gong, P. (2026). Sea buckthorn for future foods: Bioactive mechanisms, synthetic biology, and precision delivery systems. *Food Research International*, *229*, 118364. https://doi.org/10.1016/j.foodres.2026.118364

Lis, A., Staniewski, B., & Ziajka, J. (2021). *A comparison of butter texture measurements with the AP 4/2 penetrometer and TA.XT Plus texture analyzer*. *International Journal of Food Properties, 24*(1), 1744-1757. https://doi.org/10.1080/10942912.2021.19992d62

Lučić, M., & Onjia, A. (2025). Ultrasoun-assisted microextraction for food chemical contaminant analysis: A review. *Processes, 13*(11), 3677. https://doi.org/10.3390/pr13113677

Ma, Z. F., Fu, C., & Lee, Y. Y. (2025). The modulatory role of bioactive compounds in functional foods on inflammation and metabolic pathways in chronic diseases. *Foods, 14*(5), 821. https://doi.org/10.3390/foods14050821

Macias-Rodriguez, B. A., & Marangoni, A. G. (2018). Linear and nonlinear rheological behavior of fat crystal networks. *Critical Reviews in Food Science and Nutrition*, *58*(14), 2398-2415. https://doi.org/10.1080/10408398.2017.1325835

Maleki, S., Abedi, E., Hashemi, & S. M. B. (2024). Ultrasound mode- and amplitude-dependent carotenoid behavior in sunflower oil systems. *Ultrasonics Sonochemistry*, *111*, 107130. https://doi.org/10.1016/j.ultsonch.2024.107130

Mihalcea, L., Turturică, M., Cucolea, E. I. Dănilă, G. M., Dumitrașcu, L., Coman, G., Constantin, O. E., Grigore-Gurgu, L., & Stănciuc, N. (2021). CO_2 supercritical fluid extraction of oleoresins from sea buckthorn pomace: evidence of advanced bioactive profile and selected functionality. *Antioxidants*, *10*(11), 1681. https://doi.org/10.3390/antiox10111681

Mubeen, B., Hasnain, A., Naqvi, S. A. H., Hakim, F., & Naqvi, S. S. H. (2025). Phytochemicals as multi-target therapeutic agents for oxidative stress-driven pathologies: mechanisms, synergies, and clinical prospects. *Phyton-International Journal of Experimental Botany*, *94*(7), 1941-1971. https://doi.org/10.32604/phyton.2025.064056

Munteanu, I. G., & Apetrei, C. (2021). Analytical methods used in determining antioxidant activity: A Review. *International Journal of Molecular Sciences*, *22*(7), 3380. https://doi.org/10.3390/ijms22073380

Nozawa, E. (2026). Theoretical relationship between macro-texture and micro-structure in dairy processing revealed by multi-scale simulation. *Journal of Chemical Physics*, *164*(12), 124903. https://arxiv.org/abs/2601.15051

O'Callaghan, T. F., Faulkner, H., McAuliffe, S., O'Sullivan, M. G., Hennessy, D., Dillon, P., Kilcawley, K. N., Stanton, C., & Ross R. P. (2016). Quality characteristics, chemical composition, and sensory properties of butter from cows on pasture versus indoor feeding systems. *Journal of Dairy Science, 99*(12), 9441–9460. https://doi.org/10.3168/jds.2016-11271

Oh, W. Y., Kim, M. J., & Lee, J. H. (2023). Approaches of lipid oxidation mechanisms in oil matrices using association colloids. *Food Science and Biotechnology, 32*, 1805-1819. https://doi.org/10.1007/s10068-023-01359-1

Onu, A., Trofin, D. M., Tutu, A., Onu, I., Galaction, A. I., Sardaru, D. P., Trofin, D., Onita, C. A., Iordan, D. A., & Matei, D. V. (2025). Integrative strategies for preventing and managing metabolic syndrome: the impact of exercise and diet on oxidative stress reduction - A review. *Life*, *15*(5), 757. https://doi.org/10.3390/life15050757

Ordóñez-Santos, L. E., Pinzón-Zarate, L. X., & González-Salcedo, L. O. (2015). Optimization of ultrasonic-assisted extraction of total carotenoids from peach palm fruit by-products with sunflower oil using response surface methodology. *Ultrasonics Sonochemistry, 27*, 560-566. https://doi.org/10.1016/j.ultsonch.2015.04.010

Pandey, S., Gupta, A., Mahato, D. K., Paul, V., Tripathi, A. D., Rasane, P., Kumar, P., Kamle, M., & Haque, S. (2025). Lutein and zeaxanthin: source, extraction, stability, bioactivity, and functional food applications. *Current Pharmaceutical Biotechnology*, *27*(3), 261-276. https://doi.org/10.2174/0113892010334209241206113640

Pérez, M., Domínguez-López, I., & Lamuela-Raventós, R.M. (2023). The chemistry behind the Folin-Ciocalteu method for the estimation of (poly)phenol content in food: Total phenolic intake in

a Mediterranean dietary pattern. *Journal of Agricultural and Food Chemistry, 71*(46), 17543-17553. https://doi.org/10.1021/acs.jafc.3c04022

Rathi, K., Devi, N., Singh, B., Ayyagari, A., Kumar, V., Chaudhari, D. N., Ahire, J. J. (2026). Microbial risks in food: evaluation of implementation of food safety measures. *Hygiene, 6*(1), 12. https://doi.org/10.3390/hygiene6010012

Rosa, M. C., Mahieu, B., Filho, E. R. T., Cavalcanti, R. N., Martinsm M., Sobral, L. A., Sant'Anna, C., Esmerino, E. A., Goldbeck, R., Pimentel, T. C., Silva, M. C., & Cruz, A. G. (2023). Impact of adding xylooligosaccharides encapsulated in butter: Microstructural, optical, rheological and sensory aspects. *Food Research International, 170*, 113003. https://doi.org/10.1016/j.foodres.2023.113003

Sadri-Saeen, Z., Khani, M., & Fadaei, V. (2024). Improving the microbial quality and sensory properties of pasteurized sweet cream butter during refrigerated storage using chia seed ethanolic extract. *Food Science and Nutrition, 12(1),* 564-573. https://doi.org/10.1002/fsn3.3802

Sanwal, N., Mishra, S., Sahu, J. K., & Naik, S. N. (2022). Effect of ultrasound-assisted extraction on sea buckthorn seed oil quality and carotenoids. *LWT - Food Science and Technology, 153*, 112386. https://doi.org/10.1016/j.lwt.2021.112386

Sereti, F., Alexandri, M., Papapostolou, H., Papadaki, A., & Kopsahelis, N. (2025). Recent progress in carotenoid encapsulation: Effects on storage stability, bioaccessibility and bioavailability for advanced innovative food applications. *Food Research International, 14*(203), 115861. https://doi.org/10.1016/j.foodres.2025.115861

Silyvridou, A., Bari, A., Georgopoulou, T., Baxevanou, C., & Giannouli, P. (2024). Aqua extracts of lyophilized sea buckthorn modify fermentation and quality properties of set-type yogurt. *Applied Sciences, 14*(17), 7634. https://doi.org/10.3390/app14177634

Stabnikova, O., Shevchenko, O., Stabnikov, V., & Paredes-López, O. (Eds.) (2023a). *Bioconversion of waste to value-added products*, CRC Press, Boca Raton. https://doi.org/10.1201/9781003329671

Stabnikova, O., Shevchenko, A., Stabnikov, V., & Paredes-López, O. (2023b). Utilization of plant processing wastes for enrichment of bakery and confectionery products. *Ukrainian Food Journal, 12*(2), 299-308. https://doi.org/10.24263/2304-974X-2023-12-2-11

Tang, J., Zhu, X., Jambrak, A. R., Sun, D. W., & Tiwari, B. K. (2024). Mechanistic and synergistic aspects of ultrasonics and hydrodynamic cavitation for food processing. *Critical Reviews in Food Science and Nutrition, 64*, 8587-8608. https://doi.org/10.1080/10408398.2023.2201834

Teng, C., Chen, D., & Campanella, O. H. (2024). Structural and textural properties of a novel animal fat-trimming analog based on salted butter and alginate. *LWT- Food Science and Technology, 192*, 115538. https://doi.org/10.1016/j.lwt.2023.115538

Tereshchuk, L. V., Starovoitova, K. V., Vyushinsky, P. A., & Zagorodnikov, K. A. (2022). The use of sea buckthorn processing products in the creation of a functional biologically active food emulsion. *Foods, 11*(15), 2226. https://doi.org/10.3390/foods11152226

Timlin, M., Brodkorb, A., O'Callaghan, T. F., Harbourne, N., Drouin, G., Pacheco-Pappenheim, S., Murphy, J. P., O'Donovan, M., Hennessy, D., Pierce, K. M., Fitzpatrick, E., McCarthy, K., Hogan, S. A., Corrigan, B. M., & Sheehan, J. J. (2024). Pasture feeding improves the nutritional, textural, and techno-functional characteristics of butter. *Journal of Dairy Science, 107*(8), 5376-5392. https://doi.org/10.3168/jds.2023-24092

Tudor, C., Bohn, T., Iddir, M., Dulf, F. V., Focşan, M., Rugină, D. O., & Pintea, A. (2020). Sea buckthorn oil as a valuable source of bioaccessible xanthophylls, *Nutrients, 12*(1), 76. https://doi.org/10.3390/nu12010076

Tüğen, A. & Buruleanu, C. L. (2026), The role of plant-derived bioactive compounds in mitigating oxidative stress. *Foods, 15*(1), 108. https://doi.org/10.3390/foods15010108

Tüğen, A., & Özge T. Ü. (2025), Recent innovations and novel technologies for the upcycling of bioactive compounds from food wastes. *Czech Journal of Food Sciences, 43*(6), 377-397. https://doi.org/10.17221/122/2025-cjfs2

Vasheka, O., & Petrusha, O. (2022). Use of plant additives for enrichment of butter mixtures. In O. Paredes-López, O. Shevchenko, V. Stabnikov, & V. Ivanov (Eds.), *Bioenhancement and fortification of foods for a healthy diet* (pp. 203–218). CRC Press. https://doi.org/10.1201/9781003225287-13

Viñas-Ospino, A., López-Malo, D., Esteve, M. J., Frígola, A., & Blesa, J. (2023). Green solvents: emerging alternatives for carotenoid extraction from fruit and vegetable by-products, *Foods, 12*(4), 863. https://doi.org/10.3390/foods12040863

Vilas-Franquesa, A., Juan, B., & Saldo, J. (2022), Targeted analysis of sea buckthorn oil extracted by accelerated solvent extraction technique using green and conventional solvents. *LWT - Food Science and Technology, 164,* 113643. https://doi.org/10.1016/j.lwt.2022.113643

Xu, J., Lin, J., Peng, S., Zhao, H., Wang, Y., Rao, L., Liao, X., & Zhao, L. (2023). Development of an HPLC-PDA method for the determination of capsanthin, zeaxanthin, lutein, β-cryptoxanthin and β-carotene simultaneously in chili peppers and products. *Molecules, 28*(5), 2362. https://doi.org/10.3390/molecules28052362

Yang, X., Saunders, A., & Mohan, M. S. (2024). Effect of temperature on the rheological, textural, and sensory properties of butters from New Zealand market. *Journal of Texture Studies, 55*(4), e12859. https://doi.org/10.1111/jtxs.12859

Wu, D., Yang, Z., Li, J., Huang, H., Xia, Q., Ye, X., & Liu, D. (2024). Optimizing the solvent selection of the ultrasound-assisted extraction of sea buckthorn (*Hippophae rhamnoides* L.) pomace: phenolic profiles and antioxidant activity. *Foods*, *13*(3), 482. https://doi.org/10.3390/foods13030482

Zhang, X., Li, M., Zhu, L., Geng, Z., Liu, X., Cheng, Z., Zhao, M., Zhang, Q., & Yang, X. (2023). Sea buckthorn pretreatment, drying, and processing of high-quality products: Current status and trends. *Foods, 12*(23), 4255. https://doi.org/10.3390/foods12234255

Zhao, D., Li, C., Zeng, N., Wang, D., Zhang, N., Li, B. X. (2025). Current advances in the biosynthesis and sustainable production strategies of carotenoids and their multifaceted applications in the food industry. *Food Bioscience, 64*, 105864. https://doi.org/10.1016/j.fbio.2025.105864

Zhou, Z., He, Z., He, Y., & Peng Q. (2025), From desert greening to human health: a systematic review of the extraction, unique structure, and bioactivity of sea buckthorn proanthocyanidins, *Foods*, *14*(18), 3203. https://doi.org/10.3390/foods14183203

Zhu, P., Ren, Y., Wei, C., Luo, J., Wu, D., Ye, X., Donlao, N., & Tian, J. (2025). Compounds from sea buckthorn and their application in food: A review. *Food Chemistry, 476*, 143428. https://doi.org/10.1016/j.foodchem.2025.143428

Zoglopiti, E., Roufou, S., Psakis, G., Okafor, E. T., Dasenaki, M., Gatt, R., & Valdramidis, V. P. (2025). Unravelling the hydrodynamic cavitation potential in food processing: Underlying mechanisms, crucial parameters, and antimicrobial efficacy. *Food Engineering Reviews, 17,* 994-1035. https://doi.org/10.1007/s12393-025-09419-4

Cite:

Cușmenco, T., Dianu, I., Netreba, N., Reșitca, V., & Macari, A. (2026). Vegetable oil-based recovery of carotenoids from sea buckthorn pomace for butter fortification. *Ukrainian Food Journal, 15*(3), 645–678. https://doi.org/10.24263/2304-974X-2026-15-3-5

Plant-derived food processing by-products as functional protein and fiber enrichers

Eunjeong Park[1], Ki Han Kwon[2]

1 - Dongguk University, Seoul, Republic of Korea
2 - Kookmin University, Seoul, Republic of Korea

Keywords:

Plant by-products
Protein
Enrichment
Dietary fiber
Functional food
Sustainability

Article history:

Received
29.09.2025
Received in
revised form
20.08.2026
Accepted
30.09.2026

Corresponding author:

Ki Han Kwon
E-mail:
kihan.kwon@
kookmin.ac.kr

DOI:
10.24263/2304-974X-2026-15-3-6

Abstract

Introduction. This review aims to comprehensively examine recent research trends and potential applications of plant-based by-products as functional ingredients for protein and dietary fiber fortification.

Materials and methods. A systematic literature search was conducted in Scopus, Web of Science, PubMed, and Google Scholar for studies published between 2001 and 2025 using keywords related to plant by-products, protein enrichment, dietary fiber, and functional foods. Study selection followed PRISMA guidelines, focusing on nutritional composition, processing technologies, food applications, safety, and regulatory aspects.

Results and discussion. Grain, fruit, and vegetable by-products contain 10–35% protein and 20–60% dietary fiber, along with polyphenols and minerals. Their composition and functional properties vary depending on the plant source, processing conditions, and extraction methods.

Enzymatic processing, fermentation, and micronization can improve protein solubility and digestibility, fiber functionality, and technological properties, including water-holding, oil-holding, and emulsifying capacities. Ingredients derived from these by-products can enhance the nutritional value of baked goods, convenience foods, plant-based meat alternatives, snacks, and beverages. However, excessive addition may affect texture, color, flavor, and consumer acceptance, making it necessary to optimize inclusion levels for each food product. Differences in protein digestibility, fiber fermentability, and bioactive compound availability should also be considered when assessing potential health benefits, which require further confirmation through human studies. Although many by-products contain relatively low levels of contaminants, safety management is needed to address microbial contamination and allergenicity risks. Raw material variability and the lack of standardized processing methods may affect ingredient quality, while differences in regulations across the European Union, the United States, and Asian countries may hinder large-scale commercialization and international trade.

Conclusions. Plant-based food processing by-products are promising sustainable sources of protein and dietary fiber for functional food development. Future research should address nutrient bioavailability, allergen safety, quality standardization, and industrial feasibility. This review offers practical guidance for researchers, industry, and policymakers to support sustainable food systems.

Introduction

The global food industry generates millions of tons of plant-based by-products annually, including fruit peels, seeds, juice pulp, grain bran, and vegetable by-products (Plakantonaki et al., 2023). Traditionally discarded or used as low-value animal feed, these by-products are actually rich in high-quality nutrients such as protein, dietary fiber, polyphenols, vitamins, and minerals (Difonzo et al., 2022; Stabnikova et al., 2023a, b). Recently, growing concerns about food security, environmental sustainability, and the circular economy have spurred active efforts to reintroduce these by-products into the human food system (Rațu et al., 2023). Protein and dietary fiber play a crucial role in reducing the risk of chronic diseases such as obesity, diabetes, and cardiovascular disease (Jaouhari et al., 2023). Utilizing plant-based by-products as sources of protein and dietary fiber for food fortification can achieve two benefits simultaneously: enhancing the nutritional value of foods and reducing their environmental footprint (Liu et al., 2023).

The nutritional composition and functional properties of plant-based by-products vary considerably depending on the plant species, processing methods, and conditions used during food production. Advances in food engineering, such as enzymatic hydrolysis, fermentation, extrusion, and micronization, enable the effective recovery and utilization of proteins, dietary fibers, and bioactive compounds from these materials. These techniques can also improve solubility, digestibility, water-holding capacity, and sensory characteristics, making by-product-derived ingredients more suitable for incorporation into diverse food products (Nemli et al., 2025). Recent studies have demonstrated the benefits of incorporating fruit and vegetable residues, grain bran, and oilseed hulls into bread, plant-based meat alternatives, snacks, and beverages (Chau, 2026; Mironeasa et al., 2024; Tlais et al., 2020; Tsykhanovska et al., 2024). These applications can enhance protein and dietary fiber content, increase antioxidant activity, and modify desirable technological properties such as texture and water retention. However, challenges remain, including the stability of bioactive components during processing and storage, potential allergenicity, microbial safety, variability in raw material composition, and insufficient international regulations for large-scale commercialization (Vilas-Franquesa et al., 2024).

This paper comprehensively reviews the latest research trends and application cases for utilizing plant-based food processing by-products as protein and dietary fiber fortification materials. It summarizes their nutritional composition, pretreatment and processing technologies, functional characteristics in various food groups, safety aspects, and the current status of international regulations. Particular attention is given to the factors affecting the nutritional and functional quality of by-product-derived ingredients and their practical application in food products. By identifying the limitations of current research and future research needs, this review aims to contribute to the development of sustainable, nutrient-rich foods and the establishment of a circular, low-waste food system (Hussain et al., 2020).

Materials and methods

Literature search and data collection

To comprehensively review research trends on utilizing plant-based food processing by-products as protein and dietary fiber enrichment materials, relevant literature was collected. Literature published from 2001 to 2025 was searched across the Scopus, Web of Science, PubMed, and Google Scholar databases. The search employed keywords such as plant by products, food processing waste, protein enrichment, dietary fiber, functional foods,

and sustainability, combined with Boolean operators like "AND" and "OR" to maximize breadth. Additionally, the bibliographies of key papers and relevant reviews were directly examined to secure further related materials.

Inclusion and exclusion criteria

Inclusion criteria were set as (i) studies reporting the nutritional composition, processing technology, and functional characteristics of plant-based food processing by-products, (ii) studies applying these by-products to human food for protein or dietary fiber fortification purposes, and (iii) papers published in English. Conversely, studies dealing solely with animal feed, patents, conference abstracts, and other sources with insufficient data, as well as sources not peer-reviewed, were excluded.

Literature selection and data extraction

During the initial search phase, 150 papers were identified from Scopus, Web of Science, PubMed, and Google Scholar, with an additional 85 papers found through grey literature and citation tracing, resulting in a total of 235 papers. After removing 54 duplicate articles, two reviewers independently conducted an initial screening of the titles and abstracts of 181 articles. Of these, 158 articles deemed relevant were re-evaluated in full text. Ultimately, 131 articles meeting the study objectives and inclusion criteria were included in this review. From each final selected document, the following information was systematically extracted: plant raw materials, by-product types, pretreatment and processing methods, protein and dietary fiber content, functional and sensory characteristics, safety assessment, and regulatory information. The literature search and selection process is summarized in the PRISMA flow diagram Figure 1.

Data analysis and synthesis

The results of the selected literature were synthesized using descriptive and comparative methods. Nutritional data were summarized as means or ranges, and changes in protein solubility, digestibility, and dietary fiber functionality following processing were categorized. Results concerning microbiological safety, allergenic potential, and consumer acceptability were also collected and compared. Regulatory statuses across regions including the European Union (EU), North America, and Asia were compiled to identify international trends and research gaps.

Utilization of cereal processing by-products

The grain processing industry generates large quantities of various by-products, including wheat bran, rice bran, oat hulls, and corn germ meal (Salazar-López et al., 2020). These by-products have long been treated as animal feed or waste, but they are now recognized as important resources for nutritional fortification and achieving a circular economy in the food industry due to their rich content of protein (15–25%), total dietary fiber (40–55%), β-glucan, phenolic acids, and minerals such as iron, zinc, and magnesium (Fărcaș et al., 2021). Various technological processing methods have been developed to utilize these by-products as food ingredients. Micronization and ultrafine milling reduce particle size, improving dough viscoelasticity and water retention capacity (Helkar et al., 2016).

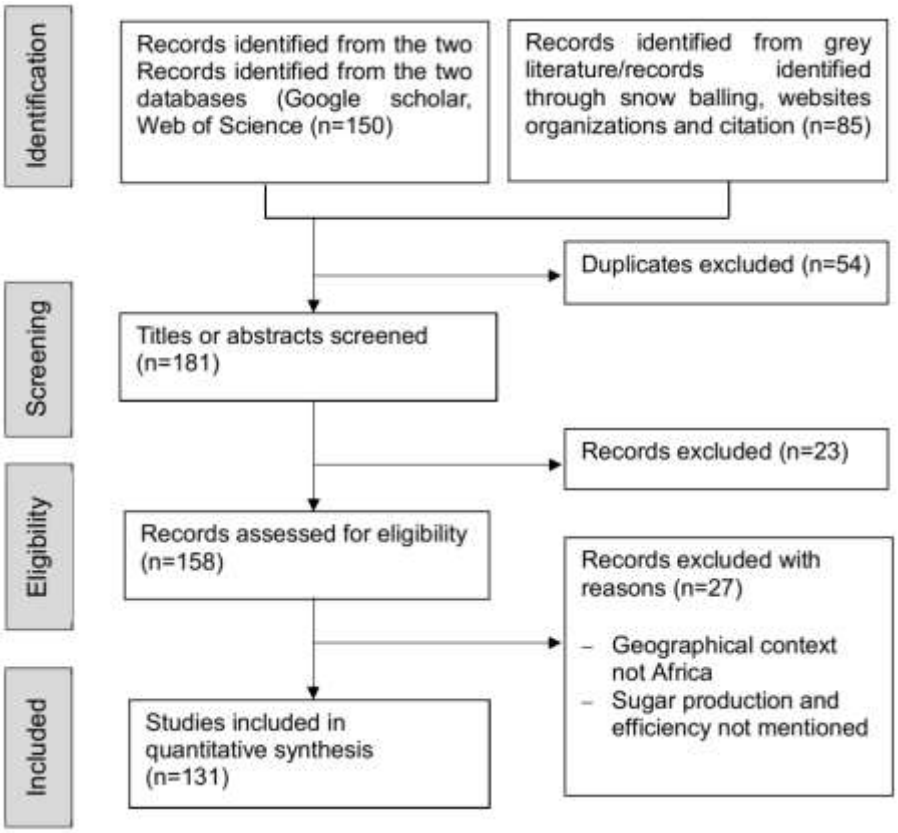

Figure 1. Records retrieval process using the PRISMA flow diagram

Enzymatic hydrolysis and lactic acid bacteria fermentation convert insoluble fiber into soluble fiber, enhancing fiber functionality and decomposing phytate to improve protein digestibility (Sharma et al., 2016). Furthermore, extrusion and steam treatment processes inactivate inherent lipases and lipoxygenases, enhancing storage stability while preserving key nutrients (Schieber et al., 2001). The most extensively researched area is baking and grain-based foods. Reports indicate that replacing 10-30% of wheat flour with finely ground wheat bran or rice bran significantly increases protein and dietary fiber content, while lowering the bread's glycemic index (GI) from approximately 70 to around 60 (Esa et al., 2013). Adding 15% oat bran improved bread volume and soft texture, while corn germ meal increased mineral content and imparted a nutty flavor (Rajagopal et al., 2024). For pasta and noodles, numerous reports indicate that adding up to 20% wheat bran can increase total dietary fiber content by 2-3 times while maintaining cooking characteristics (Cheng et al., 2022). Beyond baked goods, cereal by-products are applied to breakfast cereals, snack bars, gluten-free products, and plant-based meat alternatives. For instance, adding rice bran to gluten-free muffins increased protein content by about 25% and inhibited fat oxidation during storage (Paz et al., 2020). Extruded barley husk powder enhanced antioxidant activity and extended shelf life in instant cereals. Safety and quality control are also critical considerations. While generally safe, grain by-products carry the potential for detecting mycotoxins (such as deoxynivalenol and ochratoxin A) in wheat bran or rice bran (Cruz et

al., 2007). To mitigate these risks, proper storage management and process treatments like fermentation or extrusion are necessary. The main pretreatment and processing steps of cereal by-products and their effects on protein digestibility and fiber solubility are summarized in Figure 2.

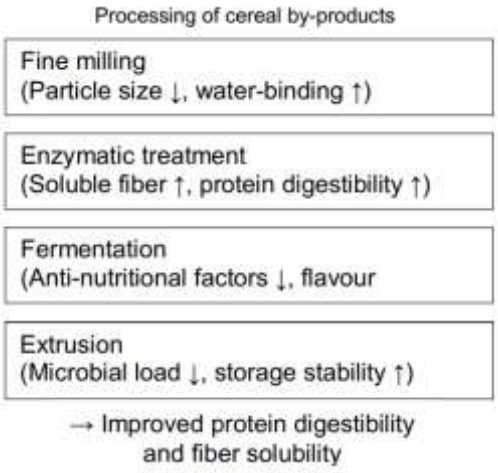

Figure 2. Processing of cereal by-products and their effects on protein digestibility and fiber solubility

In actual studies, products undergoing these treatments showed significantly lower microbial contamination. In sensory evaluation, finely ground and enzymatically treated wheat bran showed similar acceptability to control products (Błaszczyk et al., 2025). Representative applications of cereal processing by-products in bread, pasta, snacks, and other foods are summarized in Table 1.

Table 1

Representative applications of cereal processing by-products in human foods

Food category	By-products applied	Incorporation level (%)	Protein and dietary fiber enrichment	Sensory effects
Bread	Wheat bran, rice bran, oat bran	10–30	Protein 1.5–2×higher; total dietary fiber ~2 × higher; glycemic index lowered by 10–15 units	Maintains loaf volume and crumb structure; enhanced nutty flavour
Pasta	Wheat bran, barley bran	10–20	Protein and dietary fiber increased by 2–3	Maintains cooking quality; firmer bite
Snacks	Corn germ meal, oat bran	5–15	Protein increased 20–30%; fiber enrichment and antioxidant activity enhanced	Retains crispness; pleasant roasted flavour

Utilization of fruit processing by-products

Fruit peels, seeds, and pulp residues generated during juicing and processing account for 20–50% of the total raw material (Kandemir et al., 2022). They contain 35–60% total dietary fiber, 8–15% protein, and 2–5 g/100 g (dry basis) of polyphenols. Long discarded or used as animal feed after juice and wine production, these by-products are now being reconsidered as valuable functional food ingredients (Fidelis et al., 2019). Their key nutrients and the main food application routes are illustrated in Figure 3.

Representative materials are apple and grape by-products. Apple pomace is rich in soluble and insoluble dietary fiber and polyphenols, contributing to antioxidant effects and improved gut health. Multiple studies show that adding 10–20% apple peel and pulp residue to bread dough increases total dietary fiber by 1.5–2 times, boosts antioxidant activity by 20–40%, and significantly lowers the glycemic index (Wadhwa et al., 2016).

Grape skins and seeds are rich in resveratrol and proanthocyanidins, offering excellent antioxidant and anti-inflammatory effects. Reports indicate that adding 5-10% to cookies and biscuits deepens color and significantly boosts antioxidant capacity (Arvanitoyannis & Varzakas, 2008).

Citrus peels, berry pomace, and pomegranate peels are also emerging as important resources. Citrus peels are rich in soluble pectin and flavonoids, enhancing the viscosity and antioxidant capacity of jellies and beverages (Chavan et al., 2018).

Blueberry and raspberry pomace provide anthocyanins, strengthening color and antioxidant functions (Jara-Palacios et al., 2019). Recent studies have also reported cases where mango and pineapple by-products were powdered and applied to smoothies and ice cream to boost vitamin C and carotenoid content (Kumar et al., 2020).

Representative nutritional composition, addition levels, and sensory or nutritional effects of major fruit by-products are summarized in Table 2. Various pretreatment technologies enzymatic processing, fermentation, freeze-drying, and high-pressure processing are applied to maximize the functionality of fruit by-products (Teshome et al., 2023). Enzymatic processing increases the extraction rate of polyphenols and pectin, while fermentation promotes the proliferation of beneficial bacteria and the production of bioactive peptides. Furthermore, ultrafine grinding aids in improving water-binding capacity and texture (Estrada-Gil et al., 2024). Safety and storage stability are key conditions for practical application (Pujapanda et al., 2025). While most fruit by-products have reported heavy metal and pesticide residues below permissible limits, their high moisture content poses risks of mold growth and mycotoxin production (Pushparaj et al., 2023). To address this, post-processing technologies like drying/freeze-drying, sterilization, and vacuum packaging are essential, with confirmed efficacy in reducing microbial counts by up to 2-3 log (Raveendran et al., 2025). Consumer acceptance is also positive.

Numerous studies report that bread, cookies, and beverages using apple and grape by-products enhance health and eco-friendly images, improving purchase intent (Miolla et al., 2023; Stabnikova et al., 2023b). However, exceeding a 20% addition rate can intensify color and flavor, potentially reducing palatability in some products, necessitating the establishment of optimal addition ratios for each product (Subhash et al., 2024). From environmental and economic perspectives, recycling fruit by-products offers significant advantages (Campos et al., 2020). For example, utilizing grape pomace as a food ingredient after winemaking can reduce greenhouse gas emissions by 30-40% compared to landfill or incineration, while also substantially lowering by-product collection and processing costs (Lucarini et al., 2021). These environmental and economic advantages are illustrated in Figure 4.

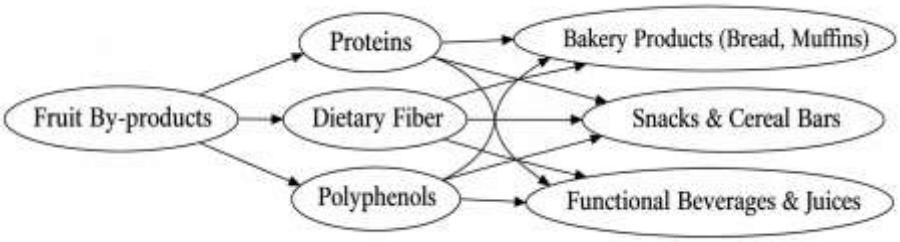

Figure 3. Fruit by-products – key components and food applications

Table 2

Fruit by-product composition and applications

Fruit by-product	Key nutrients	Typical addition (%)	Applied foods	Sensory/Nutritional effects
Apple pomace	Dietary fiber, polyphenols	5–15	Bakery (bread, muffins), cereal bars	Enhanced fiber content, improved antioxidant capacity, mild fruity flavor
Grape pomace	Anthocyanins, tannins, fiber	3–10	Beverages, snacks, bakery	Increased antioxidant activity and color, slight tartness
Citrus peel	Vitamin C, flavonoids, fiber	5–12	Marmalade, bakery, beverages	May improve viscosity and antioxidant capacity due to pectin and flavonoid content.

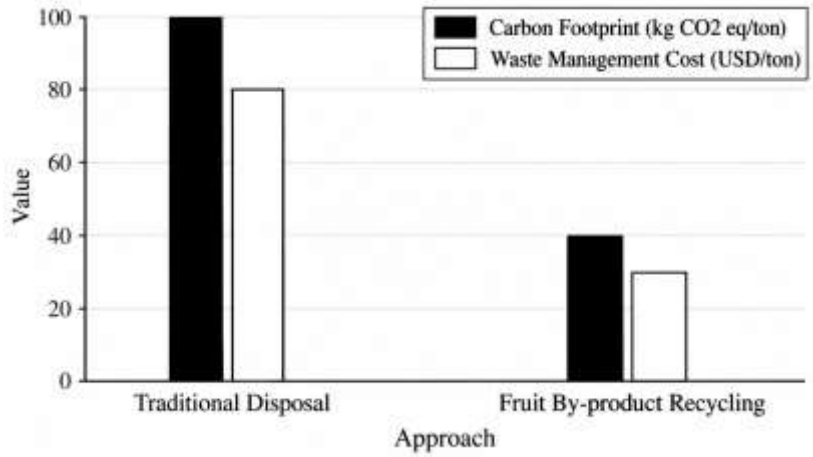

Figure 4. Carbon footprint and waste cost reduction from fruit by-product recycling

3. Utilization of vegetable and oilseed processing by-products

The husks, seeds, juice residues, and meal generated during vegetable and oilseed processing contain 20–35% protein, 30–50% dietary fiber, vitamins, carotenoids, and unsaturated fatty acids, making them highly nutritious (Akanbi et al., 2019). Historically, most were used as feed or fertilizer, but recently, their utilization as high-protein, high-fiber functional food ingredients has become widespread (Oreopoulou & Tzia, 2007). Representative vegetable by-products include tomato skins and seeds, carrot pomace, and broccoli stems (Lau et al., 2021). Tomato by-products are rich in lycopene and beta-carotene, with reported antioxidant and anti-cancer effects (Laranjeira et al., 2022). When powdered and added to bread, pasta, or sauces, they enhance both color and nutrition (Gheribi and Khwaldia, 2021). Carrot pulp provides beta-carotene and soluble fiber, enhancing the antioxidant activity and palatability of muffins and snack bars (Redondo-Cuenca et al., 2016). Broccoli stem and leaf by-products contain functional components like sulforaphane and other glucosinolates, contributing to anti-inflammatory and immune-boosting effects (Li et al., 2024). Oilseed by-products are also important protein sources (Sá et al., 2021; Tsykhanovska et al., 2024). Sunflower, pumpkin, flax, and sesame seed meal are high-protein cakes remaining after oil extraction, containing 30-45% protein, essential amino acids, unsaturated fatty acids, and lignans (Kotecka-Majchrzak et al., 2020). These by-products are utilized in developing protein supplement powders, plant-based meat alternatives, high-protein snacks, and energy bars. For example, adding up to 15% sunflower seed meal to bread dough has been reported to increase protein content by over 25% while maintaining a soft texture after baking (Drăghici et al., 2023). Representative protein and dietary fiber contents, functional components, food applications, and sensory or nutritional effects of key vegetable and oilseed by-products are summarized in Table 3. Processes such as enzymatic treatment, fermentation, freeze-drying, and ultrafine grinding are employed to enhance the stability and sensory characteristics of functional ingredients (Oyinloye & Yoon, 2020). Enzymatic treatment converts insoluble fiber into soluble fiber, increasing water-binding capacity and viscosity, while fermentation effectively breaks down proteins and improves flavor. Ultrafine grinding aids in texture and color homogenization, while freeze-drying minimizes the loss of vitamins and carotenoids (Zhao, 2024). Regarding safety, trace amounts of residual pesticides or heavy metals may be detected in vegetable by-products, making raw material selection, washing, and storage management essential (Bajwa & Sandhu, 2014). For oilseed by-products, potential risks like aflatoxin and other mycotoxins have been reported; however, high-temperature pressing, fermentation, and sterilization processes can reduce most to levels below regulatory standards (Bhat & Reddy, 2017). Actual studies show that combining sterilization and drying processes reduces microbial counts by up to 3 log or more (Bordin et al., 2014). Consumer acceptance studies revealed that high protein and dietary fiber fortification, along with a plant-based and eco-friendly image, are key factors increasing purchase intent. Products like pasta with added tomato peel or snacks incorporating broccoli by-products were positively perceived by consumers for their color and flavor (de Castro Carvalho et al., 2025). Plant-based meat alternatives using oilseed hulls also demonstrated high market potential as meat substitutes (Eliopoulos et al., 2022). The environmental and economic benefits are also significant. Converting vegetable and oilseed by-products into food ingredients can reduce greenhouse gas emissions by 25–40% compared to landfilling or incineration, while also cutting by-product disposal costs and creating new revenue streams through the production of high-value-added products (Ebner et al., 2014). Thus, vegetable and oilseed processing by-products possess multi-layered value through nutritional fortification, functional enhancement, and sustainability improvement (Wang, 2013). They offer extensive potential applications across diverse food industries, including baking, plant-based meat alternatives, snacks, and beverages. Key challenges for commercialization going forward will be ensuring nutritional stability during long-term storage, addressing potential specific allergen risks, and establishing international quality and regulatory standards (Englert et al., 2021).

Table 3

Vegetable and oilseed by-product composition and applications

Vegetable/ Oilseed by-product	Protein (%)	Dietary fiber (%)	Key functional compounds	Applied foods	Nutritional/ Sensory effects
Tomato pomace	15–20	40–50	Lycopene, β-carotene, polyphenols	Bakery products, sauces, functional snacks	Enhanced antioxidant activity and color stability
Carrot pomace	8–12	45–55	β-carotene, phenolics	Bakery products, baby foods, beverages	Natural colorant, improved vitamin A content
Soybean okara	25–30	50–55	Isoflavones, oligosaccharides	Meat analogues, bakery, smoothies	High-quality plant protein, improved texture
Rapeseed meal	35–40	25–35	Glucosinolates, phytosterols	Plant protein powders, meat substitutes	High protein enrichment, distinct nutty flavor

Technological and sensory implications

When applying plant-based processing by-products to food, the manufacturing process and the physical and sensory qualities of the final product are key considerations (Amoah et al., 2020). By-products typically possess high fiber content and distinctive color and aroma, directly impacting multiple stages of the manufacturing process, such as dough viscoelasticity, water retention capacity, and pore structure (Zarzycki et al., 2024). For example, in baking, replacing part of the wheat flour with wheat bran, rice bran, or fruit/vegetable peel powder increases the dough's water absorption rate, necessitating adjustments to hydration levels and fermentation time (Gómez & Martinez, 2018).

Reducing particle size through micro-milling or enzyme treatment, or increasing the soluble fiber ratio, improves gluten network formation and creates a more uniform pore structure, maintaining bread volume and softness (Brouns et al., 2012). In snack foods, while grain bran and fruit peel powders can lower expansion rates, reports indicate that combining fermentation and extrusion processes enhances texture (Dey et al., 2021).

From a sensory perspective, the color, aroma, and taste of by-products determine a product's palatability and market acceptance. Grape skins and blueberry pulp, for instance, can impart a deep purple hue to enhance visual appeal, but high addition ratios may cause bitterness or astringency (Li et al., 2015). Conversely, apple peel and tomato peel powder can complement sweetness and umami, yielding positive effects (Bhardwaj et al., 2022). Recent research actively explores reducing off-flavours and enhancing flavor through combinations with spices, herbs, and natural flavourings, or via enzymatic fermentation (McDonald, 2017). Water activity and storage stability are also critical. By-products with high moisture content can promote microbial growth and lipid oxidation (Das et al., 2021). Therefore, regulating moisture through techniques like freeze-drying, vacuum drying, or vacuum packaging, combined with antioxidants, is recommended. This also helps maintain the product's color, aroma, and texture during storage (Athira et al., 2023).

Key technological changes and sensory quality improvement strategies associated with cereal, fruit, vegetable, and oilseed by-products are summarized in Table 4. From an economic

and industrial perspective, process suitability is also crucial. When adding a by-product incorporation process to existing production lines, additional equipment and production costs must be minimized, and standardized pretreatment guidelines are needed to maintain optimal particle size and moisture content (Koutinas et al., 2014). In summary, this demonstrates that successfully commercializing protein and dietary fiber fortification using plant-based by-products requires integrated management encompassing process technology, sensory quality, and economic viability—going beyond simple nutritional supplementation (Lee, 2012).

Table 4

Processing changes and sensory improvement strategies by by-product type

By-product type	Processing challenges	Sensory issues	Mitigation strategies	Recommended addition (%)
Cereal bran	Increased water absorption, dough densification	Reduced loaf volume, harder crumb	Optimize fermentation time and mixing, add gluten enhancers	5–15
Fruit pomace	High moisture and acidity affecting dough stability	Sour or fruity taste, darker crumb color	Control moisture, add natural sweeteners or flavor balancing agents	3–10
Vegetable pomace	Fiber-rich particles causing texture roughness	Vegetable odour, coarse mouthfeel	Use fine milling, blanching, or fermentation to reduce odors	5–12
Oilseed meal	Protein bitterness and potential off-flavours	Bitterness, beany flavor	Combine with sweet or umami ingredients, apply deodorization techniques	5–20

Safety and regulatory aspects

Ensuring safety and regulatory compliance are key conditions for commercializing plant-based processed by-products in food applications. By-products are rich in moisture and nutrients, making them prone to becoming environments conducive to mold and bacterial growth (Minervini et al., 2022). Residual pesticides, heavy metals, and mycotoxins, including aflatoxins, ochratoxin A, and deoxynivalenol (DON), may be present in raw materials (Pinotti et al., 2016). Research indicates that certain by-products, such as wheat bran, rice bran, and fruit juice residues, risk exceeding permissible mold toxin levels if harvested or stored under poor conditions. Therefore, pre- and post-harvest management, washing, low-temperature/low-humidity storage, drying, and sterilization processes are essential, along with regular microbial and toxin testing (Samaddar et al., 2017). Processing steps such as enzymatic treatment, fermentation, high-pressure processing, freeze-drying, and heat treatment have been shown to be effective in reducing microbial loads and, in some cases, decreasing toxin levels (Alp & Bulantekin, 2021). Lactic acid bacteria fermentation can lower pH and inhibit the growth of pathogenic microorganisms, while high-pressure processing and steam sterilization can reduce mold and bacterial counts by 3–5 log units, depending on the processing conditions (Shi & Maktabdar, 2022). Key hazards detected in cereal, fruit, vegetable, and oilseed by-products, along with mitigation or removal techniques and international safety limits, are summarized in Table 5.

Table 5

Key hazards, mitigation techniques, and international safety limits for food by products

By-product type	Key hazards	Mitigation/removal techniques	International safety limits
Cereal bran	Mycotoxins (aflatoxins, DON), heavy metals	Sorting, cleaning, mycotoxin-binding agents, controlled storage	Aflatoxin B1 ≤2 mg/kg (EU), DON ≤750 mg/kg (EU)
Fruit pomace	Pesticide residues, patulin, mycotoxins	Washing, UV treatment, fermentation, ozone treatment	Patulin ≤50 mg/kg (EU), pesticide MRLs vary by fruit
Vegetable pomace	Nitrate accumulation, pesticide residues	Blanching, high-pressure processing, good agricultural practices	Nitrate ≤2000 mg/kg (EU), pesticide MRLs vary by vegetable
Oilseed meal	Mycotoxins (aflatoxin), heavy metals, residual solvents	Cold pressing, solvent-free extraction, microbial detoxification	Aflatoxin B1 ≤2 mg/kg (EU), lead ≤0.1 mg/kg (Codex)

Additionally, high-fat by-products carry a risk of rancidity during storage, so oxygen-barrier packaging and the addition of natural antioxidants are recommended (Singh et al., 2018). From a regulatory perspective, the use of plant-based by-products as food ingredients follows different approval systems depending on the country or region (Shah et al., 2024). In the European Union (EU), most new foods derived from by-products fall under the Novel Food Regulation, requiring scientific substantiation of raw material safety, production processes, and final product characteristics (Precup et al., 2024). While certain by-products are already listed on the positive list, changes to the raw material or production process necessitate separate review (Koutinas et al., 2014). The U.S. Food and Drug Administration (FDA) permits the use of by-products deemed safe through its Generally Recognized as Safe (GRAS) system, requiring prior notification procedures when necessary (Nollet & Ali, 2024). In Asia, Japan applies its 'New Food and Additives' management guidelines, while South Korea enforces the Food Sanitation Act and Health Functional Food regulations (Kim et al., 2006). China and Southeast Asian countries have established similar safety review procedures, though standardization remains insufficient (Van de Kaa & Greeven, 2017). Labelling is also a critical challenge. The EU and North America recommend clearly stating ingredient names, potential allergens, nutritional information, and sustainability-related details like 'upcycled' on product labels (Rao et al., 2021). Asian countries are also trending toward mandatory labelling for allergens and genetically modified ingredients. Such labelling directly impacts consumer trust and purchasing decisions (Gendel, 2012). Recent research highlights the allergenic potential of by-products as a new concern. For instance, certain oilseed hulls may contain protein allergens, and gluten-related proteins can exist in grain by-products (Socas-Rodríguez et al., 2021). While enzyme treatment and fermentation have shown some effectiveness in breaking down allergens, more sophisticated protein denaturation/removal technologies and long-term clinical studies are needed for commercial application (Ferrer-Gallego & Silva, 2022).

Regulations also hold significant importance from environmental and economic perspectives. Countries emphasizing sustainability are promoting market entry for by-product-recycled foods through systems like Upcycled Food Certification, positively impacting corporate eco-friendly image enhancement and market expansion (Ko et al., 2013). In conclusion, utilizing plant-based processing by-products as functional protein and dietary fiber fortification materials

necessitates rigorous safety management at the raw material stage, reduction of hazards during processing, and compliance with international regulatory and labelling standards (Darko et al., 2024). Going forward, standardization through harmonization of regulations across nations will be a key challenge for commercial expansion (Minervini et al., 2022).

Environmental and economic benefits

The utilization of food processing by-products as food ingredients is evaluated as a sustainability strategy that goes beyond simple nutritional fortification (Augustin et al., 2016). By products constitute a significant portion of food industry waste, and their landfill or incineration emits large quantities of greenhouse gases like methane and carbon dioxide (RedCorn et al., 2018). Recent Life Cycle Assessment (LCA) studies report that recycling fruit, grain, vegetable, and oilseed by-products into food ingredients can reduce the carbon footprint by 25 to 50% (Nutrizio et al., 2024). Converting grape skins and seeds generated after wine production into food materials could yield annual CO_2-equivalent reductions of thousands of tons compared to landfill or incineration (Spigno et al., 2017).

Directly applying by-products to food or extracting high-value components (proteins, dietary fiber, antioxidants, etc.) maximizes resource efficiency and reduces food resource waste (Fu & Zhang, 2025). This also contributes to reducing land occupation and water usage by decreasing the land and water resources required for cultivating grain proteins (Wu et al., 2014). Furthermore, recycling by-products reduces agricultural by-product management costs and can support achieving carbon neutrality goals in the long term (Chen et al., 2025).

The economic benefits are also significant. Utilizing by-products reduces raw material costs and enables the creation of additional revenue through high value added products like functional foods, high-protein snacks, and prebiotic beverages (Yu et al., 2025). Applying wheat bran at a 20% level in the baking industry reduces flour usage, cutting raw material costs by 10-15% while maintaining product price competitiveness (Cappelli & Cini, 2021). In juice production processes, utilizing apple or citrus peels for pectin and polyphenol extraction offsets existing disposal costs and generates additional sales (Nadar et al., 2022). Expected reductions in carbon emissions, water usage, and raw material costs, as well as representative value-creation cases from plant-based by-products, are summarized in Table 6.

The economic utilization of by-products positively contributes to income diversification for local communities and farms (Delgado and Siamwalla, 2018). When small and medium-sized farms and food processing companies develop new product lines using by-products as raw materials, employment creation can be expected throughout the purchasing, processing, and distribution of agricultural by-products (Topleva & Prokopov, 2020). Furthermore, through by-product upcycling, companies can enhance their environmental and social responsibility (ESG) values and secure market competitiveness by obtaining sustainability certifications (Ghisellini et al., 2024). These benefits are also significant from a policy perspective. The European Union and some North American countries provide incentives such as eco-labels for recycled by-product products, tax benefits, and R&D support (Rubik et al., 2008). This serves as a driving force for companies to expand sustainable production processes and product development, and acts as a factor highlighting a positive image in international trade (De Medeiros et al., 2014). In conclusion, the systematic utilization of plant-based food processing by-products is a strategy that can simultaneously achieve greenhouse gas reduction, resource conservation, cost savings, and new revenue generation (Boukid, 2024). These environmental and economic benefits position by-products not as mere waste but as a core resource for the sustainable food industry, and they are expected to play an increasingly important role in future food policies and corporate strategies (Otles et al., 2015).

Table 6

Environmental and economic benefits of using plant-based by-products

By-product type	Estimated carbon emission reduction (%)	Estimated water use reduction (%)	Raw material cost saving (%)	Typical value-added applications
Cereal bran	25–40	20–30	15–25	High-fiber bread and pasta; bio-packaging films
Fruit pomace	30–45	25–35	20–30	Functional bakery and beverage products; antioxidant extracts
Vegetable pomace	20–35	15–25	10–20	Vegetable-based snacks and sauces; natural colorants
Oilseed meal	25–40	20–30	15–25	Plant protein powders; nutraceutical and feed supplements

Consumer perception and market prospects

Consumer perception and acceptance are key success factors for utilizing plant-based food processing by-products as food ingredients (Nitzko, 2023). Recent surveys indicate that consumers' heightened interest in health, eco-friendliness, and ethical consumption leads to positive purchasing intentions when terms like “upcycling” and “zero waste” are used (Hossen et al., 2024). Notably, when scientific evidence is presented such as enhanced protein and dietary fiber content, antioxidant properties, and improved gut health consumers tend to show willingness to purchase even at premium prices (Markosyan et al., 2009). Sensory characteristics directly influence consumer acceptance.

Research indicates that when by-product addition rates in bread, snacks, and beverages range from 10 to 20%, changes in color, taste, and texture either positively impact or show minimal difference (Eche et al., 2025). However, at rates exceeding 30%, some products exhibited astringency, dark coloration, and coarse texture, which reduced palatability. Consequently, establishing optimal addition ratios and developing flavor improvement technologies are considered key to market success (Nehir El & Simsek, 2012). Recent efforts to enhance sensory quality by utilizing herbs and natural flavours or reducing off-flavors through fermentation and enzyme treatment are gaining attention (Latha Ravi et al., 2025). From a market outlook perspective, plant-based by-product foods are also showing steep growth. According to global market research, the food upcycling industry is projected to grow at an average annual rate of 6-8% through 2030 (Bhatia et al., 2024). Demand is expected to surge particularly in functional bakery products, high-protein snacks, plant-based meat alternatives, and health beverages (Boukid et al., 2024). Rising prices of plant-based protein sources and the spread of sustainable management (ESG) will further accelerate this trend (Prasad et al., 2025). Policy and certification support also aids market expansion. Europe and North America encourage differentiation and consumer trust in by-product-based foods through certifications like Upcycled Food Certification and Sustainable Food Label (Swaraj et al., 2025).

Some Asian countries have also introduced eco-friendly and low-carbon labels to support the expansion of distribution networks (Sarkar, 2012). These systems positively impact product

promotion and entry into premium markets (Lee, 2025). E-commerce and digital marketing are also key growth drivers for foods utilizing by-products (Wang et al., 2021).

Consumer reactions to health and eco-friendly content can spread rapidly via social media and online shopping platforms, enabling even small brands to rapidly expand their market reach (Nabivi, 2025). Cases have been reported where products such as wheat bran-enriched bread and grape skin snacks saw a sharp increase in consumer awareness through online reviews and social media sharing (Kowalska et al., 2023). In conclusion, plant-based by-product foods can achieve large-scale market entry when consumer awareness, sensory quality management, eco-friendly certification, and digital marketing strategies are combined (Sharma et al., 2024). Strengthening scientific evidence for long-term health benefits, standardized labelling, and expanding international certifications are projected to be key drivers of future market growth (Bennett, 2022).

Research gaps and future perspectives

This review confirms that plant-based food processing by-products hold high potential as sustainable sources of protein and dietary fiber (Khan et al., 2023). However, challenges remain to be addressed for commercial and academic advancement. Sufficient data from human studies on the nutritional value and bioactivity of by-product proteins, intestinal fermentation characteristics of fibers, and the metabolic pathways of polyphenols in the body are still lacking (Yang et al., 2023). Most research remains confined to in vitro digestion models or animal studies, necessitating long-term clinical trials to strengthen the scientific evidence. Furthermore, systematic research on the stability of functional components during storage and processing is lacking (Saeidnia et al., 2015).

The effects of various processing methods such as drying, fermentation, extrusion, and freezing on the long-term quality retention of protein, dietary fiber, and antioxidant components must be quantitatively evaluated (Sui et al., 2025). Data on allergies and potential toxicity is also limited (Madsen et al., 2009). Protein allergens in certain oilseed hulls or gluten in grain by-products could pose risks to sensitive consumers, necessitating research to verify the effectiveness of reduction techniques like fermentation or enzymatic treatment at the human level (Gouda & Bekhit, 2022).

The lack of international regulations and quality standards is also cited as a major barrier to commercialization. Differences in permitted raw materials, processing methods, and labelling requirements between countries create barriers to import/export and large-scale commercialization (Janasik et al., 2023). Therefore, establishing global guidelines linked to bodies like the Codex Alimentarius and a standardized labelling system is required (Fortin, 2023). Furthermore, developing an integrated model that evaluates economic viability and supply chain analysis reflecting the costs of collecting, storing, transporting, and processing by-products alongside carbon footprint and water usage could provide substantial grounds for corporate investment decisions and policy formulation (Van Der Vorst et al., 2009).

Future research necessitates a multidisciplinary approach combining food science, nutrition, environmental engineering, and economics (Van Raan & Van Leeuwen, 2002). Efforts to enhance the stability of functional components and improve sensory quality by applying advanced processing technologies such as nanotechnology, precision fermentation, and 3D food printing are also expected to proliferate (Sohel et al., 2025). Simultaneously, if standardized indicators for comprehensive sustainability assessment are developed and regulatory harmonization is achieved through international cooperation systems, plant-based food processing by-products could establish themselves as a key strategy supporting both global food security and carbon neutrality goals (Newman & Styring, 2023).

Conclusions

This review comprehensively examined the nutritional and functional potential of plant-based by-products generated during the processing of grains, fruits, vegetables, and oilseeds as a sustainable source of protein and dietary fiber. Recent studies have demonstrated that various pretreatment and processing technologies can enhance the protein digestibility, fiber solubility, and antioxidant activity of these by-products, while also improving quality across a wide range of food categories including baked goods, snacks, plant-based meat alternatives, and beverages. Such utilization offers not only nutritional fortification but also simultaneous environmental and economic benefits such as waste reduction, greenhouse gas mitigation, and raw material cost savings. However, several challenges remain for commercial diffusion. There is a lack of clinical data supporting the nutritional effects and bioavailability of by-product proteins and functional components at the human level. Standardized research on quality stability and allergen safety during long-term storage and processing is also insufficient. Furthermore, the absence of internationally unified regulatory and labelling standards creates barriers to import/export and large-scale commercialization. Future research and policy should evolve toward establishing an integrated evaluation system encompassing nutrition, technology, environment, and economics through a multidisciplinary approach, while developing advanced processing technologies and global quality and regulatory standards. If these efforts proceed in parallel, plant-based food processing by-products will establish themselves as a key food resource contributing to strengthening global food security, realizing a circular economy, and achieving carbon neutrality.

References

Akanbi, T. O., Dare, K. O., & Aryee, A. N. (2019). High-value products from cereal, nuts, fruits, and vegetables wastes. In *By-products from agriculture and fisheries: Adding value for food, feed, pharma, and fuels* (pp. 347–368). Academic Press. https://doi.org/10.1016/B978-0-12-817189-5.00013-0

Alp, D., & Bulantekin, Ö. (2021). The microbiological quality of various foods dried by applying different drying methods: A review. *European Food Research and Technology, 247*(6), 1333–1343. https://doi.org/10.1007/s00217-021-03707-9

Amoah, I., Taarji, N., Johnson, P. N. T., Barrett, J., Cairncross, C., & Rush, E. (2020). Plant-based food by-products: Prospects for valorisation in functional bread development. *Sustainability, 12*(18), 7785. https://doi.org/10.3390/su12187785

Arvanitoyannis, I. S., & Varzakas, T. H. (2008). Fruit/fruit juice waste management: Treatment methods and potential uses of treated waste. In *Waste management for the food industries* (Vol. 2, pp. 569–628). Academic Press. https://doi.org/10.1016/B978-012373654-3.50019-4

Athira, V. A., Gokulvel, E., Nandhu Lal, A. M., Venugopalan, V. V., Rajkumar, V., & Venkatesh, T. (2023). Advances in drying techniques for retention of antioxidants in agro produces. *Critical Reviews in Food Science and Nutrition, 63*(31), 10849–10865. https://doi.org/10.1080/10408398.2022.2075081

Augustin, M. A., Riley, M., Stockmann, R., Bennett, L., Kahl, A., Lockett, T., & Cobiac, L. (2016). Role of food processing in food and nutrition security. *Trends in Food Science & Technology, 56*, 115–125. https://doi.org/10.1016/j.tifs.2016.08.005

Bajwa, U., & Sandhu, K. S. (2014). Effect of handling and processing on pesticide residues in food: A review. *Journal of Food Science and Technology, 51*(2), 201–220. https://doi.org/10.1007/s13197-011-0499-5

Bennett, E. A. (2022). The efficacy of voluntary standards, sustainability certifications, and ethical labels. In *Research handbook on global governance, business and human rights* (pp. 177–204). Edward Elgar Publishing. https://doi.org/10.4337/9781788114807.00020

Bhardwaj, K., Najda, A., Sharma, R., Nurzyńska-Wierdak, R., Dhanjal, D. S., Sharma, R., & Bhardwaj, P. (2022). Fruit and vegetable peel-enriched functional foods: Potential avenues and health perspectives. *Evidence-Based Complementary and Alternative Medicine, 2022*, 8543881. https://doi.org/10.1155/2022/8543881

Bhat, R., & Reddy, K. R. N. (2017). Challenges and issues concerning mycotoxins contamination in oil seeds and their edible oils: Updates from last decade. *Food Chemistry, 215*, 425–437. https://doi.org/10.1016/j.foodchem.2016.07.144

Bhatia, S. K., Patel, A. K., & Yang, Y. H. (2024). The green revolution of food waste upcycling to produce polyhydroxyalkanoates. *Trends in Biotechnology, 42*(10), 1273–1287. https://doi.org/10.1016/j.tibtech.2024.04.005

Błaszczyk, K., Szczepanek, M., Nowak, R., Szablewska, K. S., Alexa, E. C., & Pop, G. (2025). Black barley grain and its processing by-product as a potential raw material for functional food. *Food and Bioprocess Technology, 18*(5), 4859–4874. https://doi.org/10.1007/s11947-025-03546-7

Bordin, K., Sawada, M. M., Rodrigues, C. E. D. C., da Fonseca, C. R., & Oliveira, C. A. F. (2014). Incidence of aflatoxins in oil seeds and possible transfer to oil: A review. *Food Engineering Reviews, 6*(1), 20–28. https://doi.org/10.1007/s12393-013-9078-3

Boukid, F. (2024). Holistic benefits of plant-based foods for sustainable agrifood systems. *Current Opinion in Food Science, 58*, 101184. https://doi.org/10.1016/j.cofs.2024.101184

Boukid, F., Mefleh, M., Mameri, H., & Rosell, C. M. (2024). Plant protein innovations in snacks and bakery: Synergy of market trends and scientific advances. *Food Bioscience, 57*, 105580. https://doi.org/10.1016/j.fbio.2024.105580

Brouns, F., Hemery, Y., Price, R., & Anson, N. M. (2012). Wheat aleurone: Separation, composition, health aspects, and potential food use. *Critical Reviews in Food Science and Nutrition, 52*(6), 553–568. https://doi.org/10.1080/10408398.2010.500245

Campos, D. A., Gómez-García, R., Vilas-Boas, A. A., Madureira, A. R., & Pintado, M. M. (2020). Management of fruit industrial by-products: A case study on circular economy approach. *Molecules, 25*(2), 320. https://doi.org/10.3390/molecules25020320

Cappelli, A., & Cini, E. (2021). Challenges and opportunities in wheat flour, pasta, bread, and bakery product production chains: A systematic review of innovations and improvement strategies to increase sustainability, productivity, and product quality. *Sustainability, 13*(5), 2608. https://doi.org/10.3390/su13052608

Chavan, P., Singh, A. K., & Kaur, G. (2018). Recent progress in the utilization of industrial waste and by-products of citrus fruits: A review. *Journal of Food Process Engineering, 41*(8), e12895. https://doi.org/10.1111/jfpe.12895

Chau, N. B. (2026). Physicochemical, rheological and sensory properties of cottage cheese beverage enriched with fresh and freeze-dried guava puree. *Ukrainian Food Journal, 15*(1), 35–48. https://doi.org/10.24263/2304-974X2026-15-1-5

Chen, S. C. I., Dang, X., Xu, Q. Q., & Own, C. M. (2025). Transforming waste into value: Sustainable recycling of agricultural resources under the "carbon peak and carbon neutrality" vision. *Sustainability, 17*(1), 55. https://doi.org/10.3390/su17010055

Cheng, W., Sun, Y., Fan, M., Li, Y., Wang, L., & Qian, H. (2022). Wheat bran, as the resource of dietary fiber: A review. *Critical Reviews in Food Science and Nutrition, 62*(26), 7269–7281. https://doi.org/10.1080/10408398.2021.1916747

Cruz, J. M., Moldes, A. B., Bustos, G., Torrado, A., & Domínguez, J. M. (2007). Integral utilisation of barley husk for the production of food additives. *Journal of the Science of Food and Agriculture, 87*(6), 1000–1008. https://doi.org/10.1002/jsfa.2812

Darko, H. S. O., Ismaiel, L., Fanesi, B., Pacetti, D., & Lucci, P. (2024). Current trends in food processing by-products as sources of high value-added compounds in food fortification. *Foods, 13*(17), 2658. https://doi.org/10.3390/foods13172658

Das, A. K., Nanda, P. K., Chowdhury, N. R., Dandapat, P., Gagaoua, M., Chauhan, P., & Lorenzo, J. M. (2021). Application of pomegranate by-products in muscle foods: Oxidative indices, colour stability, shelf life and health benefits. *Molecules, 26*(2), 467. https://doi.org/10.3390/molecules26020467

de Castro Carvalho, G., Carneiro, J. D. D. S., Rocha, R. A. R., & Pereira, E. (2025). Plant-based trends: Consumer's perception and factors that influence the purchase of plant-based products. *British Food Journal*, *127*(9), 3396-3426. https://doi.org/10.1108/BFJ-09-2024-0861

De Medeiros, J. F., Ribeiro, J. L. D., & Cortimiglia, M. N. (2014). Success factors for environmentally sustainable product innovation: A systematic literature review. *Journal of Cleaner Production, 65*, 76–86. https://doi.org/10.1016/j.jclepro.2013.08.035

Delgado, C. L., & Siamwalla, A. (2018). Rural economy and farm income diversification in developing countries. In *Food security, diversification and resource management: Refocusing the role of agriculture?* (pp. 126–143). Routledge. https://doi.org/10.4324/9781351061328-9

Dey, D., Richter, J. K., Ek, P., Gu, B. J., & Ganjyal, G. M. (2021). Utilization of food processing by-products in extrusion processing: A review. *Frontiers in Sustainable Food Systems, 4*, 603751. https://doi.org/10.3389/fsufs.2020.603751

Difonzo, G., de Gennaro, G., Pasqualone, A., & Caponio, F. (2022). Potential use of plant-based by-products and waste to improve the quality of gluten-free foods. *Journal of the Science of Food and Agriculture, 102*(6), 2199–2211. https://doi.org/10.1002/jsfa.11641

Drăghici, M. C., Geicu-Cristea, M., Popa, E. E., Popescu, P. A., Miteluț, A. C., & Popa, M. E. (2023). A review of plant-based, high protein snack bars: Composition, nutritional value and health benefits. *Scientific Papers. Series B. Horticulture, 67*(1), 579-584.

Ebner, J., Babbitt, C., Winer, M., Hilton, B., & Williamson, A. (2014). Life cycle greenhouse gas (GHG) impacts of a novel process for converting food waste to ethanol and co-products. *Applied Energy, 130*, 86–93. https://doi.org/10.1016/j.apenergy.2014.05.018

Eche, V., Emenike, C. U., & Rupasinghe, H. V. (2025). Nutritional value of brewer's spent grain and consumer acceptance of its value-added food products. *Foods, 14*(16), 2900. https://doi.org/10.3390/foods14162900

Eliopoulos, C., Markou, G., Langousi, I., & Arapoglou, D. (2022). Reintegration of food industry by-products: Potential applications. *Foods, 11*(22), 3743. https://doi.org/10.3390/foods11223743

Englert, L., Mahler, V., & Bonertz, A. (2021). Regulatory requirements for the quality of allergen products for allergen immunotherapy of food allergy. *Current Allergy and Asthma Reports, 21*(5), 32. https://doi.org/10.1007/s11882-021-01004-8

Esa, N. M., Ling, T. B., & Peng, L. S. (2013). By-products of rice processing: An overview of health benefits and applications. *Journal of Rice Research, 1*(1), 2. https://doi.org/10.4172/jrr.1000107

Estrada-Gil, L. E., Cerda-Cejudo, N. D., Chávez-González, M. L., Flores-Gallegos, A. C., Govea-Salas, M., Contreras-Esquivel, J. C., & Ascacio-Valdés, J. A. (2024). Food waste revalorization as a functional food or ingredient. In *Engineering principles for food processing technology and product realization* (pp. 321–336). Apple Academic Press. https://doi.org/10.1201/9781003330024-20

Fărcaș, A., Drețcanu, G., Pop, T. D., Enaru, B., Socaci, S., & Diaconeasa, Z. (2021). Cereal processing by-products as rich sources of phenolic compounds and their potential bioactivities. *Nutrients, 13*(11), 3934. https://doi.org/10.3390/nu13113934

Ferrer-Gallego, R., & Silva, P. (2022). The wine industry by-products: Applications for food industry and health benefits. *Antioxidants, 11*(10), 2025. https://doi.org/10.3390/antiox11102025

Fidelis, M., de Moura, C., Kabbas Junior, T., Pap, N., Mattila, P., Mäkinen, S., & Granato, D. (2019). Fruit seeds as sources of bioactive compounds: Sustainable production of high value-added ingredients from by-products within circular economy. *Molecules, 24*(21), 3854. https://doi.org/10.3390/molecules24213854

Fortin, N. D. (2023). Global governance of food safety: The role of the FAO, WHO, and Codex Alimentarius in regulatory harmonization. In *Research handbook on international food law* (pp. 227–242). Edward Elgar Publishing. https://doi.org/10.4337/9781802201110.00022

Fu, P., & Zhang, Y. (2025). Enhancing resource efficiency and value addition in food and agricultural by-product processing: A green recycling approach. *Frontiers in Sustainable Food Systems, 9*, 1589807. https://doi.org/10.3389/fsufs.2025.1589807

Gendel, S. M. (2012). Comparison of international food allergen labelling regulations. *Regulatory Toxicology and Pharmacology, 63*(2), 279–285. https://doi.org/10.1016/j.yrtph.2012.04.001

Gheribi, R., & Khwaldia, K. (2021). Tomato (lycopene and β-carotene) and cancer. In *Nutraceuticals and cancer signaling: Clinical aspects and mode of action* (pp. 39–60). Springer International Publishing. https://doi.org/10.1007/978-3-030-79408-8_3

Ghisellini, P., Quinto, I., Passaro, R., & Ulgiati, S. (2024). Exploring environmental and social performances of circular start-ups: An orientation and certification assessment. *Business Strategy and the Environment, 33*(4), 3222–3241. https://doi.org/10.1002/bse.3618

Gómez, M., & Martinez, M. M. (2018). Fruit and vegetable by-products as novel ingredients to improve the nutritional quality of baked goods. *Critical Reviews in Food Science and Nutrition, 58*(13), 2119–2135. https://doi.org/10.1080/10408398.2017.1305946

Gouda, M., & Bekhit, A. E. D. A. (2022). Allergenicity risks associated with novel proteins and rapid methods of detection. In *Alternative proteins* (pp. 379–406). CRC Press. https://doi.org/10.1201/9781003221800-18

Helkar, P. B., Sahoo, A. K., & Patil, N. J. (2016). Review: Food industry by-products used as a functional food ingredients. *International Journal of Waste Resources, 6*(3), 1–6. https://doi.org/10.4172/2252-5211.1000248

Hossen, S., Mridha, Y., Rahman, A., Ouboucetta, R., & Amin, M. R. (2024). Consumer perceptions and purchasing trends of eco-friendly textile products in the US market. *International Journal of Business and Economics, 1*(2), 20–32. https://doi.org/10.62304/ijbm.v1i2.145

Hussain, S., Jõudu, I., & Bhat, R. (2020). Dietary fiber from underutilized plant resources: A positive approach for valorization of fruit and vegetable wastes. *Sustainability, 12*(13), 5401. https://doi.org/10.3390/su12135401

Janasik, M., Jagusiak-Kocik, M., & Ulewicz, R. (2023). Barriers to technology transfer and commercialization of research findings: Case study. *Organization and Management Series, 179*(1), 164–180. http://dx.doi.org/10.29119/1641-3466.2023.179.9

Jaouhari, Y., Travaglia, F., Giovannelli, L., Picco, A., Oz, E., Oz, F., & Bordiga, M. (2023). From industrial food waste to bioactive ingredients: A review on the sustainable management and transformation of plant-derived food waste. *Foods, 12*(11), 2183. https://doi.org/10.3390/foods12112183

Jara-Palacios, M. J., Santisteban, A., Gordillo, B., Hernanz, D., Heredia, F. J., & Escudero-Gilete, M. L. (2019). Comparative study of red berry pomaces (blueberry, red raspberry, red currant and blackberry) as source of antioxidants and pigments. *European Food Research and Technology, 245*(1), 1–9. https://doi.org/10.1007/s00217-018-3148-9

Kandemir, K., Piskin, E., Xiao, J., Tomas, M., & Capanoglu, E. (2022). Fruit juice industry wastes as a source of bioactives. *Journal of Agricultural and Food Chemistry, 70*(23), 6805–6832. https://doi.org/10.1021/acs.jafc.1c08254

Khan, Z. S., Amir, S., Sokač Cvetnić, T., Jurinjak Tušek, A., Benković, M., Jurina, T., & Gajdoš Kljusurić, J. (2023). Sustainable isolation of bioactive compounds and proteins from plant-based food (and by-products). *Plants, 12*(16), 2904. https://doi.org/10.3390/plants12162904

Kim, J. Y., Kim, D. B., & Lee, H. J. (2006). Regulations on health/functional foods in Korea. *Toxicology, 221*(1), 112–118. https://doi.org/10.1016/j.tox.2006.01.015

Ko, E., Hwang, Y. K., & Kim, E. Y. (2013). Green marketing' functions in building corporate image in the retail setting. *Journal of Business Research, 66*(10), 1709–1715. https://doi.org/10.1016/j.jbusres.2012.11.007

Kotecka-Majchrzak, K., Sumara, A., Fornal, E., & Montowska, M. (2020). Oilseed proteins: Properties and application as a food ingredient. *Trends in Food Science & Technology, 106*, 160–170. https://doi.org/10.1016/j.tifs.2020.09.015

Koutinas, A. A., Vlysidis, A., Pleissner, D., Kopsahelis, N., Garcia, I. L., Kookos, I. K., & Lin, C. S. K. (2014). Valorization of industrial waste and by-product streams via fermentation for the production of chemicals and biopolymers. *Chemical Society Reviews, 43*(8), 2587–2627. https://doi.org/10.1039/C3CS60366K

Kowalska, H., Masiarz, E., Ignaczak, A., Marzec, A., Hać-Szymańczuk, E., Salamon, A., & Galus, S. (2023). Advances in multigrain snack bar technology and consumer expectations: A review. *Food Reviews International, 39*(1), 93–118. https://doi.org/10.1080/87559129.2021.1989137

Kumar, C. S., Ali, A., & Manickavasagan, A. (2020). Health benefits of substituting added sugars with fruits in developing value-added food products: A review. *International Journal of Nutrition, Pharmacology, Neurological Diseases, 10*(3), 75–90. https://doi.org/10.4103/ijnpnd.ijnpnd_7_20

Laranjeira, T., Costa, A., Faria-Silva, C., Ribeiro, D., de Oliveira, J. M. P. F., Simoes, S., & Ascenso, A. (2022). Sustainable valorization of tomato by-products to obtain bioactive compounds: Their potential in inflammation and cancer management. *Molecules, 27*(5), 1701. https://doi.org/10.3390/molecules27051701

Latha Ravi, J., Ghosh, P., Ahmad, F., Haque, S., Barciela, P., Chamorro, F., & Rana, S. S. (2025). Microbial conversion of vegetable waste for flavor additives via solid-state fermentation: A comprehensive review. *Frontiers in Nutrition, 12*, 1445189. https://doi.org/10.3389/fnut.2025.1445189

Lau, K. Q., Sabran, M. R., & Shafie, S. R. (2021). Utilization of vegetable and fruit by-products as functional ingredient and food. *Frontiers in Nutrition, 8*, 661693. https://doi.org/10.3389/fnut.2021.661693

Lee, D. (2012). Turning waste into by-product. *Manufacturing & Service Operations Management, 14*(1), 115–127. https://doi.org/10.1287/msom.1110.0357

Lee, S. W. (2025). Green logistics innovations: Sustainable supply chain strategies in emerging markets. *SSRN Electronic Journal*, 5166641. https://doi.org/10.2139/ssrn.5166641

Li, L., Ma, P., Nirasawa, S., & Liu, H. (2024). Formation, immunomodulatory activities, and enhancement of glucosinolates and sulforaphane in broccoli sprouts: A review for maximizing the health benefits to human. *Critical Reviews in Food Science and Nutrition, 64*(20), 7118–7148. https://doi.org/10.1080/10408398.2022.2151736

Li, X. E., Jervis, S. M., & Drake, M. A. (2015). Examining extrinsic factors that influence product acceptance: A review. *Journal of Food Science, 80*(5), R901–R909. https://doi.org/10.1111/1750-3841.12836

Liu, Z., de Souza, T. S., Holland, B., Dunshea, F., Barrow, C., & Suleria, H. A. (2023). Valorization of food waste to produce value-added products based on its bioactive compounds. *Processes, 11*(3), 840. https://doi.org/10.3390/pr11030840

Lucarini, M., Durazzo, A., Bernini, R., Campo, M., Vita, C., Souto, E. B., & Romani, A. (2021). Fruit wastes as a valuable source of value-added compounds: A collaborative perspective. *Molecules, 26*(21), 6338. https://doi.org/10.3390/molecules26216338

Madsen, C. B., Hattersley, S., Buck, J., Gendel, S. M., Houben, G. F., Hourihane, J. B., & Crevel, R. W. R. (2009). Approaches to risk assessment in food allergy: Report from a workshop "Developing a framework for assessing the risk from allergenic foods." *Food and Chemical Toxicology, 47*(2), 480–489. https://doi.org/10.1016/j.fct.2008.12.001

Markosyan, A., McCluskey, J. J., & Wahl, T. I. (2009). Consumer response to information about a functional food product: Apples enriched with antioxidants. *Canadian Journal of Agricultural Economics/Revue canadienne d'agroeconomie, 57*(3), 325–341. https://doi.org/10.1111/j.1744-7976.2009.01153.x

McDonald, S. T. (2017). Concepts of flavor creation in novel nutraceuticals and functional food formulations. In *Developing new functional food and nutraceutical products* (pp. 231–247). Academic Press. https://doi.org/10.1016/B978-0-12-802780-6.00013-0

Minervini, F., Comitini, F., De Boni, A., Fiorino, G. M., Rodrigues, F., Tlais, A. Z. A., & De Angelis, M. (2022). Sustainable and health-protecting food ingredients from bioprocessed food by-products and wastes. *Sustainability, 14*(22), 15283. https://doi.org/10.3390/su142215283

Miolla, R., Ottomano Palmisano, G., Roma, R., Caponio, F., Difonzo, G., & De Boni, A. (2023). Functional foods acceptability: A consumers' survey on bread enriched with oenological by-products. *Foods, 12*(10), 2014. https://doi.org/10.3390/foods12102014

Mironeasa, S., Ungureanu-Iuga, M., Ursachi, V.F., & Mironeasa, C. (2024). Seedless grape pomace to increase fiber content in extruded corn snacks. *Ukrainian Food Journal, 13*(4), 657–674. https://doi.org/10.24263/2304-974X-2024-13-4-3

Nabivi, E. (2025). The role of social media in green marketing: How eco-friendly content influences brand attitude and consumer engagement. *Sustainability, 17*(5), 1965. https://doi.org/10.3390/su17051965

Nadar, C. G., Arora, A., & Shastri, Y. (2022). Sustainability challenges and opportunities in pectin extraction from fruit waste. *ACS Engineering Au, 2*(2), 61–74. https://doi.org/10.1021/acsengineeringau.1c00033

Nehir El, S., & Simsek, S. (2012). Food technological applications for optimal nutrition: An overview of opportunities for the food industry. *Comprehensive Reviews in Food Science and Food Safety, 11*(1), 2–12. https://doi.org/10.1111/j.1541-4337.2011.00169.x

Nemli, E., Günal-Köroğlu, D., Apak, R., & Capanoglu, E. (2025). Potential of plant-based oil processing wastes/by-products as an alternative source of bioactive compounds in the food industry. *Foods, 14*(15), 2718. https://doi.org/10.3390/foods14152718

Newman, A. J., & Styring, P. (2023). The pursuit of methodological harmonization within the holistic sustainability assessment of CCU projects: A history and critical review. *Frontiers in Sustainability, 3,* 1057476. https://doi.org/10.3389/frsus.2022.1057476

Nitzko, S. (2023). Consumer acceptance of the use of plant and animal by-products of food manufacturing for human nutrition. *Food and Humanity, 1,* 1238–1249. https://doi.org/10.1016/j.foohum.2023.09.019

Nollet, L. M., & Ali, F. (2024). Food products regulations in the United States. In *Global regulations of medicinal, pharmaceutical, and food products* (pp. 310–321). CRC Press. https://doi.org/10.1201/9781003330215-24

Nutrizio, M., Dukić, J., Sabljak, I., Samardžija, A., Fučkar, V. B., Djekić, I., & Jambrak, A. R. (2024). Upcycling of food by-products and waste: Nonthermal green extractions and life cycle assessment approach. *Sustainability, 16*(21), 9143. https://doi.org/10.3390/su16219143

Oreopoulou, V., & Tzia, C. (2007). Utilization of plant by-products for the recovery of proteins, dietary fibers, antioxidants, and colorants. In *Utilization of by-products and treatment of waste in the food industry* (pp. 209–232). Springer US. https://doi.org/10.1007/978-0-387-35766-9_10

Otles, S., Despoudi, S., Bucatariu, C., & Kartal, C. (2015). Food waste management, valorization, and sustainability in the food industry. In *Food waste recovery* (pp. 3–23). Academic Press. https://doi.org/10.1016/B978-0-12-800351-0.00001-7

Oyinloye, T. M., & Yoon, W. B. (2020). Effect of freeze-drying on quality and grinding process of food produce: A review. *Processes, 8*(3), 354. https://doi.org/10.3390/pr8030354

Paz, G. M., King, J. M., Prinyawiwatkul, W., Tyus, C. M., & Aleman, R. J. (2020). High-protein rice flour in the development of gluten-free muffins. *Journal of Food Science, 85*(5), 1397–1402. https://doi.org/10.1111/1750-3841.15114

Pinotti, L., Ottoboni, M., Giromini, C., Dell'Orto, V., & Cheli, F. (2016). Mycotoxin contamination in the EU feed supply chain: A focus on cereal by-products. *Toxins, 8*(2), 45. https://doi.org/10.3390/toxins8020045

Plakantonaki, S., Roussis, I., Bilalis, D., & Priniotakis, G. (2023). Dietary fiber from plant-based food wastes: A comprehensive approach to cereal, fruit, and vegetable waste valorization. *Processes, 11*(5), 1580. https://doi.org/10.3390/pr11051580

Prasad, S., Gupta, E., Yadav, S., Babulal, K. S., & Mishra, S. (2025). Plant-based food industry: Overview and trends. In K. Younis & O. Yousuf (Eds.), *The future of plant protein: Innovations, challenges, and opportunities* (pp. 73–97). Singapore: Springer. https://doi.org/10.1007/978-981-96-4190-1_4

Precup, G., Marini, E., Zakidou, P., Beneventi, E., Consuelo, C., Fernández-Fraguas, C., Garcia Ruiz, E., Laganaro, M., Magani, M., Mech, A., Noriega Fernandez, E., Nuin Garciarena, I., Rodriguez Fernandez, P., Roldan Torres, R., Rossi, A., Ruggeri, L., Suriano, F., Ververis, E., Liu, Y., Smeraldi, C., & Germini, A. (2024). Novel foods, food enzymes, and food additives derived from food by-products of plant or animal origin: Principles and overview of the EFSA safety assessment. *Frontiers in Nutrition, 11,* 1390734. https://doi.org/10.3389/fnut.2024.1390734

Pujapanda, R., Hamid, Bashir, O., Shams, R., Dash, K. K., Goksen, G., Shaikh, A. M., & Kovács, B. (2025). Influence of carrier agents on nutritional, chemical, and antioxidant profiles of fruit

juices during drying processes: A comprehensive review. *Discover Food, 5*, Article 228. https://doi.org/10.1007/s44187-025-00504-5

Pushparaj, K., Meyyazhagan, A., Pappuswamy, M., Mousavi Khaneghah, A., Liu, W. C., & Balasubramanian, B. (2023). Occurrence, identification, and decontamination of potential mycotoxins in fruits and fruit by-products. *Food Frontiers, 4*(1), 32–46. https://doi.org/10.1002/fft2.188

Rajagopal, V., Vincent, H., Anand, T., & Dekka, S. (2024). Value addition of grains. In C. K. Sunil, K. A. Athmaselvi, N. Venkatachalapathy, C. Anandharamakrishnan, & V. M. Balasubramaniam (Eds.), *Unit operations in food grain processing* (pp. 453–472). Academic Press. https://doi.org/10.1016/B978-0-443-19529-5.00017-6

Rao, M., Bast, A., & De Boer, A. (2021). Valorized food processing by-products in the EU: Finding the balance between safety, nutrition, and sustainability. *Sustainability, 13*, 4428. https://doi.org/10.3390/su13084428

Rațu, R. N., Veleșcu, I. D., Stoica, F., Usturoi, A., Arsenoaia, V. N., Crivei, I. C., & Brumă, I. S. (2023). Application of agri-food by-products in the food industry. *Agriculture, 13*, 1559. https://doi.org/10.3390/agriculture13081559

Raveendran, A., Ezhil Vendan, S., Vivek Babu, C. S., & Singh, S. A. (2025). Mitigation of contaminants in foods: Pesticide residues, heavy metals, mycotoxins in various food commodities and strategies for their mitigation to ensure food safety. In D. Mondal, & M. M. Rahman (Eds.), *Food toxicity and safety* (pp. 3–36). Springer Nature Singapore. https://doi.org/10.1007/978-981-97-7030-5_1

RedCorn, R., Fatemi, S., & Engelberth, A. S. (2018). Comparing end-use potential for industrial food-waste sources. *Engineering, 4*, 371–380. https://doi.org/10.1016/j.eng.2018.05.010

Redondo-Cuenca, A., Villanueva-Suárez, M. J., & Goñi, I. (2016). Healthy dietary fibers from plant food by-products. In Y. H. Hui, & E. Özgül Evranuz (Eds.), *Handbook of vegetable preservation and processing* (pp. 25–56). CRC Press. https://doi.org/10.1201/b19227-4

Rubik, F., Scheer, D., & Iraldo, F. (2008). Eco-labelling and product development: Potentials and experiences. *International Journal of Product Development, 6*(3/4), 393–419.

Sá, A. G. A., da Silva, D. C., Pacheco, M. T. B., Moreno, Y. M. F., & Carciofi, B. A. M. (2021). Oilseed by-products as plant-based protein sources: Amino acid profile and digestibility. *Future Foods, 3*, 100023. https://doi.org/10.1016/j.fufo.2021.100023

Saeidnia, S., Manayi, A., & Abdollahi, M. (2015). From in vitro experiments to in vivo and clinical studies: Pros and cons. *Current Drug Discovery Technologies, 12*(4), 218–224. https://doi.org/10.2174/1570163813666160114093140

Salazar-López, N. J., Ovando-Martínez, M., & Domínguez-Avila, J. A. (2020). Cereal/grain by-products. In R. Campos-Vega, B. D. Oomah, & H. A. Vergara-Castañeda (Eds.), *Food wastes and by-products: Nutraceutical and health potential* (pp. 1–34). Academic Press. https://doi.org/10.1016/B978-0-12-818189-4.00001-1

Samaddar, A., Azam, M. M., Singaravadivel, K., Venkatachalapathy, N., Swain, B. B., & Mishra, P. (2017). Postharvest management and value addition of rice and its by-products. In S. Mohanty, P. G. Chengappa, M. Hedge, J. K. Ladha, S. Baruah, E. Kannan, A. V. Manjunatha (Eds.), *The future rice strategy for India* (pp. 301–334). Academic Press. https://doi.org/10.1016/B978-0-12-805374-4.00014-0

Sarkar, A. N. (2012). Green branding and eco-innovations for evolving a sustainable green marketing strategy. *Asia-Pacific Journal of Management Research and Innovation, 8*, 39–58. https://doi.org/10.1177/097324701100800104

Schieber, A., Stintzing, F. C., & Carle, R. (2001). By-products of plant food processing as a source of functional compounds: Recent developments. *Trends in Food Science & Technology, 12*, 401–413. https://doi.org/10.1016/S0924-2244(02)00012-2

Shah, H., Ahmed, L., & Barry-Ryan, C. (2024). Ensuring compliance: A review of EU regulations and standards for incorporating legume and legume by-product proteins in food formulations. *Heliyon, 10*, e29624. https://doi.org/10.1016/j.heliyon.2024.e29624

Sharma, N., Yeasmen, N., Dube, L., & Orsat, V. (2024). Rise of plant-based beverages: A consumer-driven perspective. *Food Reviews International, 40*, 3315–3341. https://doi.org/10.1080/87559129.2022.2072624

Sharma, S. K., Bansal, S., Mangal, M., Dixit, A. K., Gupta, R. K., & Mangal, A. K. (2016). Utilization of food processing by-products as dietary, functional, and novel fiber: A review. *Critical Reviews in Food Science and Nutrition, 56*, 1647–1661. https://doi.org/10.1080/10408398.2013.794327

Shi, C., & Maktabdar, M. (2022). Lactic acid bacteria as biopreservation against spoilage molds in dairy products: A review. *Frontiers in Microbiology, 12*, 819684. https://doi.org/10.3389/fmicb.2021.819684

Singh, P., Singh, T. P., & Gandhi, N. (2018). Prevention of lipid oxidation in muscle foods by milk proteins and peptides: A review. *Food Reviews International, 34*, 226–247. https://doi.org/10.1080/87559129.2016.1261293

Socas-Rodríguez, B., Álvarez-Rivera, G., Valdés, A., Ibáñez, E., & Cifuentes, A. (2021). Food by-products and food wastes: Are they safe enough for their valorization? *Trends in Food Science & Technology, 114*, 133–147. https://doi.org/10.1016/j.tifs.2021.05.010

Sohel, A., Sahu, S., Mitchell, G. R., & Patel, M. K. (2025). 3D food printing: A comprehensive review and critical analysis on technologies, food materials, applications, challenges, and future prospects. *Food Engineering Reviews*, 1–29. https://doi.org/10.1007/s12393-025-09435-9

Spigno, G., Marinoni, L., & Garrido, G. D. (2017). State of the art in grape processing by-products. In C. M. Galanakis (Ed.), *Handbook of grape processing by-products* (pp. 1–27). Academic Press. https://doi.org/10.1016/B978-0-12-809870-7.00001-3

Stabnikova, O., Shevchenko, O., Stabnikov, V., & Paredes-López, O. (Eds.). (2023a). *Bioconversion of waste to value-added products*. Boca Raton, FL: CRC Press. https://doi.org/10.1201/9781003329671

Stabnikova, O., Shevchenko, A., Stabnikov, V., & Paredes-López, O. (2023b). Utilization of plant processing wastes for enrichment of bakery and confectionery products. *Ukrainian Food Journal, 12*(2), 299–308. https://doi.org/10.24263/2304-974X-2023-12-2-11

Subhash, A. J., Bamigbade, G. B., & Ayyash, M. (2024). Current insights into date by-product valorization for sustainable food industries and technology. *Sustainable Food Technology, 2*, 331–361. https://doi.org/10.1039/D3FB00058A

Sui, W., Wang, S., Chen, Y., Li, X., Zhuang, X., Yan, X., & Song, Y. (2025). Insights into the structural and nutritional variations in soluble dietary fibers in fruits and vegetables influenced by food processing techniques. *Foods, 14*, 1861. https://doi.org/10.3390/foods14111861

Swaraj, A. N., Moses, J. A., & Manickam, L. (2025). Sustainable food upcycling: Perspectives on manufacturing challenges and certification requirements for large-scale commercialization. *Sustainable Food Technology, 3*, 648–664. https://doi.org/10.1039/SFT-2025-00321

Teshome, E., Teka, T. A., Nandasiri, R., Rout, J. R., Harouna, D. V., Astatkie, T., & Urugo, M. M. (2023). Fruit by-products and their industrial applications for nutritional benefits and health promotion: A comprehensive review. *Sustainability, 15*, 7840. https://doi.org/10.3390/su15107840

Tsykhanovska, I., Stabnikova, O., Riabchykov, M., Lazarieva, T., & Korolyova, N. (2024). Effect of partial replacement of wheat flour by flour from extruded sunflower seed kernels on muffins quality. *Plant Foods for Human Nutrition, 79*(4), 769–778. https://doi.org/10.1007/s11130-024-01232-4

Tlais, A. Z. A., Fiorino, G. M., Polo, A., Filannino, P., & Di Cagno, R. (2020). High-value compounds in fruit, vegetable and cereal by-products: An overview of potential sustainable reuse and exploitation. *Molecules, 25*, 2987. https://doi.org/10.3390/molecules25132987

Topleva, S. A., & Prokopov, T. V. (2020). Integrated business model for sustainability of small and medium-sized enterprises in the food industry: Creating value added through ecodesign. *British Food Journal, 122*, 1463–1483. https://doi.org/10.1108/BFJ-07-2019-0509

Tsykhanovska, I., Stabnikova, O., Riabchykov, M., Lazarieva, T., & Korolyova, N. (2024). Effect of partial replacement of wheat flour by flour from extruded sunflower seed kernels on muffins

quality. *Plant Foods for Human Nutrition, 79*(4), 769–778. https://doi.org/10.1007/s11130-024-01232-4

Van de Kaa, G., & Greeven, M. (2017). LED standardization in China and South East Asia: Stakeholders, infrastructure and institutional regimes. *Renewable and Sustainable Energy Reviews, 72*, 863–870. https://doi.org/10.1016/j.rser.2017.01.100

Van Der Vorst, J. G., Tromp, S. O., & Zee, D. J. V. D. (2009). Simulation modelling for food supply chain redesign: Integrated decision making on product quality, sustainability and logistics. *International Journal of Production Research, 47*, 6611–6631. https://doi.org/10.1080/00207540802461879

Van Raan, A. F., & Van Leeuwen, T. N. (2002). Assessment of the scientific basis of interdisciplinary, applied research: Application of bibliometric methods in nutrition and food research. *Research Policy, 31*, 611–632. https://doi.org/10.1016/S0048-7333(01)00130-9

Vilas-Franquesa, A., Casertano, M., Tresserra-Rimbau, A., Vallverdú-Queralt, A., & Torres-León, C. (2024). Recent advances in bio-based extraction processes for the recovery of bound phenolics from agro-industrial by-products and their biological activity. *Critical Reviews in Food Science and Nutrition, 64*, 10643–10667. https://doi.org/10.1080/10408398.2023.2186292

Wadhwa, M., Bakshi, M. P. S., & Makkar, H. P. S. (2016). Wastes to worth: Value added products from fruit and vegetable wastes. *CABI Reviews, 2015*, 1–25. https://doi.org/10.1079/pavsnnr201510057

Wang, L. J. (2013). Production of bioenergy and bioproducts from food processing wastes: A review. *Transactions of the ASABE, 56*, 217–230. https://doi.org/10.13031/2013.42505

Wang, X., Xie, J., & Fan, Z. P. (2021). B2C cross-border e-commerce logistics mode selection considering product returns. *International Journal of Production Research, 59*, 3841–3860. https://doi.org/10.1080/00207543.2020.1759847

Wu, G., Bazer, F. W., & Cross, H. R. (2014). Land-based production of animal protein: Impacts, efficiency, and sustainability. *Annals of the New York Academy of Sciences, 1328*, 18–28. https://doi.org/10.1111/nyas.12566

Yang, F., Chen, C., Ni, D., Yang, Y., Tian, J., Li, Y., & Wang, L. (2023). Effects of fermentation on bioactivity and the composition of polyphenols contained in polyphenol-rich foods: A review. *Foods, 12*, 3315. https://doi.org/10.3390/foods12173315

Yu, J. C., Wu, Y. J. Z., & Shin, W. S. (2025). From waste to value: Integrating legume by-products into sustainable industrialization. *Comprehensive Reviews in Food Science and Food Safety, 24*, e70174. https://doi.org/10.1111/1541-4337.70174

Zarzycki, P., Wirkijowska, A., Teterycz, D., & Łysakowska, P. (2024). Innovations in wheat bread: Using food industry by-products for better quality and nutrition. *Applied Sciences, 14*, 3976. https://doi.org/10.3390/app14103976

Zhao, D. (2024). Plant-based protein processing and texture properties. In *Flavor-associated applications in health and wellness food products* (pp. 295–319). Springer International Publishing. https://doi.org/10.1007/978-3-031-59094-8_15

Cite:

Park, E., & Kwon, K. H. (2026). Plant-derived food processing by-products as functional protein and fiber enrichers. *Ukrainian Food Journal, 15*(3), 679–701. https://doi.org/10.24263/2304-974X-2026-15-3-6

Essential oils rich in geraniol and citronellol

Hafize Fidan[1], Boryana Kavrakova[2], Ira Taneva[2], Ivayla Dincheva[3], Anton Lazarov[4], Stanka Damyanova[5], Albena Stoyanova[1]

1 – University of Food Technologies, Plovdiv, Bulgaria
2 – Trakia University, Yambol, Bulgaria
3 – AgroBioInstitute, Agricultural Academy, Sofia, Bulgaria,
4 – Laant Ltd., Cheshnegirovo, Bulgaria
5 – University of Ruse "Angel Kanchev", Branch-Razgrad, Bulgaria

Keywords:

Essential oil
Geranium
Palmarosa
Citronella
Composition
Antimicrobial
Antioxidant

Article history:

Received 22.03.2026
Received in revised form 23.04.2026
Accepted 30.06.2026

Corresponding author:

Stanka Damyanova
E-mail: sdamianova@uni-ruse.bg

DOI:
10.24263/2304-974X-2026-15-3-7

Abstract

Introduction. The chemical composition, antimicrobial activity, and antioxidant activity of geranium, palmarosa, and citronella essential oils containing the monoterpene alcohols geraniol and citronellol were comparatively evaluated.

Materials and methods. The chemical composition of the essential oils was determined by gas chromatography–mass spectrometry (GC–MS). Antioxidant activity was assessed using 2,2-diphenyl-1-picrylhydrazyl (DPPH) radical scavenging, 2,2′-azinobis-(3-ethylbenzothiazoline-6-sulfonic acid) (ABTS) radical cation decolorization, and ferric reducing antioxidant power (FRAP) assays. Antibacterial activity was evaluated by a modified agar diffusion method against *Escherichia coli*, *Salmonella enterica*, *Listeria monocytogenes*, *Staphylococcus aureus*, and *Bacillus subtilis*.

Results and discussion. The three essential oils showed distinct chemical profiles, particularly in the contents of the monoterpene alcohols geraniol and citronellol. Palmarosa essential oil contained the highest concentration of geraniol (81.20%), whereas geranium essential oil had the highest citronellol content (19.90%). Geranium and citronella essential oils contained 7.15% and 12.30% geraniol, respectively, while citronellol accounted for 1.28% in citronella essential oil. Both the individual monoterpene alcohols and the essential oils showed greater antibacterial activity against Gram-positive than Gram-negative bacteria. Geraniol was active against *S. aureus* and *B. subtilis*, whereas citronellol inhibited *S. enterica*, *S. aureus*, and *B. subtilis*. Among the essential oils, geranium inhibited *B. subtilis*, palmarosa inhibited *S. aureus* and *B. subtilis*, and citronella inhibited *S. aureus*. None of the essential oils inhibited the tested Gram-negative bacteria, indicating selective antibacterial activity. The antioxidant activity of both the monoterpene alcohols and essential oils was relatively low across the DPPH, ABTS, and FRAP assays, with no pronounced antioxidant effects observed under the experimental conditions.

Conclusions. Essential oils from geranium, palmarosa, and citronella, containing the monoterpene alcohols geraniol and citronellol, exhibited pronounced inhibitory activity against the tested Gram-positive bacteria. In contrast, their antioxidant activity was low, as demonstrated by the DPPH, ABTS, and FRAP assays.

Introduction

Essential oils are complex mixtures of volatile plant-derived compounds that have attracted considerable interest because of their diverse biological properties, including antimicrobial, antioxidant, anti-inflammatory, and insect-repellent activities (Ivanova et al., 2016; Stabnikova et al., 2026a, b). These properties are largely associated with the presence of terpenes and terpenoids, whose type and relative abundance contribute to the chemical profile and biological activity of individual essential oils (Guimarães et al., 2019; Siddiqui et al., 2024). Among these compounds, the monoterpene alcohols geraniol and citronellol are of particular interest because of their widespread occurrence in aromatic plants and their reported antimicrobial and antioxidant properties.

Geraniol and citronellol are acyclic monoterpene alcohols that occur as major or important constituents of numerous plant essential oils, including those obtained from rose (*Rosa damascena* Mill.) (Atanasova et al., 2017), rose geranium (*Pelargonium* spp.) (Bergman et al., 2021), palmarosa (*Cymbopogon martinii* (Roxb.) W. Watson) (Cebi, 2021a), and citronella (*Cymbopogon nardus* (L.) Rendle) (Wany et al., 2014), among others. In addition to contributing to the characteristic floral and rose-like aromas of these oils, geraniol and citronellol have attracted attention because of their antimicrobial properties and potential contribution to the biological activity of essential oils. However, their relative concentrations can vary considerably among plant species and oils, resulting in differences in chemical composition and biological activity (Bauer et al., 2001; Başer & Buchbauer, 2010; Stoyanova, 2022).

Rose geranium is a perennial subshrub belonging to the family Geraniaceae and is cultivated in many countries worldwide. Its essential oil is obtained by steam distillation and is typically characterized by relatively high concentrations of citronellol (22–55%) and geraniol (18–25%), together with linalool (7–13%), nerol, and other minor volatile compounds. Owing to its pleasant floral fragrance and biological properties, rose geranium essential oil is widely used in the perfume, cosmetic, aromatherapy, and food industries (Boukhatem et al., 2013; Can et al., 2018; Cocos et al., 2023; Seo et al., 2009; Singh et al., 2013; Stoyanova, 2022).

Palmarosa is a perennial grass belonging to the family Poaceae and is cultivated in many tropical and subtropical regions. Its essential oil is obtained by steam distillation and is distinguished by a particularly high geraniol content (68–92%), with lower amounts of linalool, geranyl acetate, and other volatile constituents. This high geraniol content makes palmarosa essential oil an important natural source of this monoterpene alcohol. Its pleasant rose-like aroma and biological properties have contributed to its use in the perfume, cosmetic, aromatherapy, and food industries (Stoyanova, 2022).

Citronella is a perennial grass belonging to the family Poaceae and is cultivated extensively in tropical and subtropical regions. Citronella essential oil is obtained mainly from *Cymbopogon nardus* and *Cymbopogon winterianus*. The oil of *C. nardus* contains geraniol (15–23%) and citronellol (3.0–8.5%) together with citronellal, methyl isoeugenol, geranyl acetate, and other volatile constituents. In *C. winterianus*, geraniol (20–25%), citronellol (8.5–14%), and citronellal (21–40%) are among the predominant compounds. The presence of geraniol and citronellol, together with other characteristic constituents, contributes to the biological properties and characteristic aroma of citronella essential oils (Stoyanova, 2022).

Thus, rose geranium, palmarosa, and citronella essential oils represent three different compositional patterns of geraniol and citronellol: rose geranium is characterized by the simultaneous presence of relatively high amounts of both alcohols, palmarosa is particularly rich in geraniol, whereas citronella contains both compounds together with other characteristic monoterpenes. This makes these oils suitable for comparative evaluation of their chemical composition and biological properties.

Therefore, the aim of this study was to comparatively evaluate the chemical composition, antimicrobial activity, and antioxidant activity of three commercial essential oils rich in the monoterpene alcohols geraniol and citronellol: rose geranium, palmarosa, and citronella essential oils.

Materials and methods

Materials

Three commercial essential oils were used in this study, all purchased from Armina Bio OOD (Bulgaria): geranium (*Pelargonium roseum* Willd.), originating from Madagascar; palmarosa (*Cymbopogon martini* (Roxburgh.) W. Watson (Stapf.), originating from Nepal; citronella (*Cympogon nardus* (L.) Rend.), originating from India.

The monoterpene alcohols geraniol and citronellol were purchased from Sigma-Aldrich Chemistry GmbH (Darmstadt, Germany). All chemicals used for the analyses were of analytical grade.

Methods

Chemical composition of the essential oils. The chemical composition of the essential oils was determined by GC–MS analysis. GC analysis was performed using an Agilent 7890A gas chromatograph (Agilent Technologies Inc., Santa Clara, CA, USA) equipped with an HP-5MS column (30 m × 250 μm × 0.25 μm). The temperature program was as follows: 35 °C for 3 min, increased at 5 °C/min to 250 °C, and held for 3 min, with a total run time of 49 min. Helium was used as the carrier gas at a constant flow rate of 1 mL/min, and the split ratio was 30:1. GC–MS analysis was performed using an Agilent 5975C mass selective detector under the same chromatographic conditions. Component identification was based on comparison of retention indices and mass spectra with spectral databases and literature data (Adams, 2007).

Microbiological study. Bacterial strains relevant to foodborne infections and intoxications were used as test microorganisms. The strains were supplied by the National Bank for Industrial Microorganisms and Cell Cultures. The following Gram-negative bacteria, *Escherichia coli* ATCC 8739 and *Salmonella enterica* subsp. *enterica* serovar Abony NCTC 6017, and Gram-positive bacteria, *Listeria monocytogenes* NCTC 11994, *Staphylococcus aureus* ATCC 25093, and *Bacillus subtilis* ATCC 6633, were used in this study.

Selective media were used for the microbiological tests: Listeria Oxford Agar Base supplemented with cycloheximide (Biolife), Endo Agar (Merck), Leifson Agar (Merck), Baird Parker Agar Base supplemented with a yolk-tellurite supplement (Biolife), and Plate Count Agar (Merck).

Colony counting. Serial ten-fold dilutions of the saline suspensions were prepared, and two consecutive dilutions were inoculated onto the appropriate selective media using the spread plate technique. For each dilution, 1 mL of the suspension was evenly distributed over four pre-prepared and dried agar plates. Dilutions yielding 25–250 colonies were used for enumeration. The number of viable microorganisms was calculated according to Equation:

$$N=\Sigma C/[(n_1+0.1n_2)d] \quad (1)$$

where N is the number of colony-forming units per milliliter or gram (CFU/mL or CFU/g); ΣC is the sum of the colonies counted on all plates; n_1 is the number of plates counted at the lower dilution; n_2 is the number of plates counted at the higher dilution; and d is the dilution factor corresponding to the first dilution used for counting.

Determination of antibacterial activity of the essential oils. Antibacterial activity was determined using a modified agar diffusion method by measuring the inhibition zones around metal rings containing the tested essential oils. Selective media were inoculated with suspensions of the test microorganisms prepared from 24-h cultures grown on PCA slants. A suitable ten-fold dilution of each suspension was inoculated into melted and cooled selective medium at 45–50 °C. The cell concentration in the agar was considered equivalent to that of the dilution suspension because 1 mL of the suspension was inoculated into 99 mL of the medium. After solidification, sterile metal rings with a diameter of 6 mm were placed on the agar surface, and 150 µL of the tested essential oil was added to each ring. A solution of phosphate-buffered saline (PBS; Sigma, São Paulo, Brazil) containing 0.5% (v/v) Polysorbate 80 (Tween® 80) was used as a negative control. The plates were incubated at 37 °C, and the diameters of the growth inhibition zones were measured after 24 and 48 h. The antibacterial activities of the tested essential oils were then compared (Zaika, 1988).

Antioxidant activity of the essential oils

2,2-diphenyl-1-picrylhydrazyl (DPPH) radical scavenging. The DPPH radical scavenging activity was evaluated by adding 0.15 mL of the tested essential oil to 2.85 mL of freshly prepared 0.1 mM DPPH solution in methanol. The samples were incubated for 15 min at 37 °C in the dark. The decrease in absorbance at 517 nm was measured spectrophotometrically against a methanol blank (Misharina, 2016). The radical scavenging activity of the essential oils was expressed as mM Trolox® equivalents (TE) per gram of dry weight (dw).

2,2′-Azino-bis(3-ethylbenzothiazoline-6-sulfonic acid) (ABTS) assay. The ABTS•+ radical cation was generated by mixing an aliquot of 7.0 mM ABTS solution in distilled water with 2.45 mM potassium persulfate in distilled water. The reaction was carried out for 16 h at ambient temperature in the dark. Before analysis, 2.0 mL of the generated ABTS•+ solution was diluted with methanol at a ratio of 1:30 (v/v) to obtain a working solution with a final absorbance of approximately 1.0–1.1 at 734 nm. Then, 2.85 mL of the ABTS•+ solution was added to 0.15 mL of the essential oil. After incubation for 15 min at 37 °C in the dark, the absorbance was measured at 734 nm against methanol as a blank (Re et al., 1999). The results were expressed as mM Trolox equivalents (TE) per mL.

Ferric reducing antioxidant power assay (FRAP). FRAP assay. The FRAP method was performed as previously described (Benzie & Strain, 1996). Three mL of freshly prepared FRAP reagent (consisting of 10 parts 0.3 M acetate buffer (pH 3.6), 1 part 10 mM 2,4,6-tripyridyl-s-triazine (TPTZ) in 40 mM HCl, and 1 part 20 mM $FeCl_3 \cdot 6H_2O$ in distilled water) were mixed with 0.1 mL of the essential oil. After 10 min at 37 °C in the dark, the absorbance was measured at 593 nm against a blank prepared with the solvent used for extraction. The results were expressed as mM TE per gram dw.

Statistical analysis

All experiments were performed in triplicate, and the values presented in the tables are expressed as means±standard deviations (SD). The experimental data were statistically evaluated using analysis of variance (ANOVA) with Statgraphics Centurion XVI Version 16.2.04 software (StatPoint Technologies, Inc., USA). Duncan's multiple range test was used to determine differences among the means, and statistical significance was defined at $p < 0.05$.

Results and discussion

Chemical composition of essential oils rich in geraniol and citronellol

Essential oils are volatile, aromatic mixtures of secondary plant metabolites composed mainly of terpenes and their oxygenated derivatives. The chemical compositions of the investigated essential oils are presented in Table 1 and Figures 1–3. GC–MS analysis showed that:

Geranium essential oil contained 37 identified compounds, accounting for 99.98% of the total oil composition. Of these, 16 compounds were present at concentrations above 1%, whereas the remaining 21 compounds were detected at levels below 1%. The major constituents (≥3%) were citronellol (19.90%), citronellyl formate (19.58%), guaia-6,9-diene (13.80%), geraniol (7.15%), geranyl formate (6.69%), linalool (5.55%), and isomenthone (4.83%).

Palmarosa essential oil contained 10 identified compounds, representing 99.67% of the total composition. Four compounds were present at concentrations above 1%, while the remaining six compounds occurred at levels below 1%. The predominant constituents (≥3%) were geraniol (81.20%) and geranyl acetate (12.69%).

Citronella essential oil contained 44 identified compounds, accounting for 99.84% of the total composition. Nineteen compounds were detected at concentrations above 1%, whereas 25 compounds were present at concentrations below 1%. The principal constituents (≥3%) were (E)-methyl isoeugenol (19.15%), geraniol (12.53%), camphene (9.97%), borneol (8.43%), geranyl acetate (7.23%), limonene (6.98%), and citronellal (3.20%).

Table 1

Chemical composition of essential oils rich of geraniol and citronellol, TIC[1], %

Peak No	RT[2], min	RI[3]	Compound	Essential oils from		
				geranium	palmarosa	citronella
1	8.77	920	Tricyclene	-[4]	-	1.24±0.01
2	9.14	933	α-Pinene	0.46[a]±0.01	-	2.48[b]±0.02
3	9.67	945	Camphene	-	-	9.97±0.09
4	11.29	1001	δ-2-Carene	-	-	0.09±0.01
5	12.28	1024	Limonene	-	-	6.98±0.06
6	12.54	1033	(Z)-β-Ocimene	-	0.10[a]±0.01	0.55[b]±0.01
7	12.86	1045	(E)-β-Ocimene	-	0.59[a]±0.01	0.21[b]±0.01
8	14.07	1086	p-Mentha-2,4(8)-diene	-	-	0.30±0.01
9	14.57	1094	β-Linalool	5.55[a]±0.50	2.51[b]±0.22	0.33[c]±0.01
10	14.83	1108	(Z)-Rose oxide	1.39 0.10	-	-
11	15.32	1120	(E)-Rose oxide	0.50±0.01	-	-
12.	16.02	1140	neo-allo-Ocimene	-	-	0.18±0.1
13	16.23	1147	Menthone	2.84±0.22	-	-
14	16.13	1148	Citronellal	-	-	3.20±0.03
15	16.50	1156	iso-Menthone	4.83±0.44	-	-
16	16.74	1161	Borneol	-	-	8.43±0.08
17	16.99	1173	Terpinen-4-ol	-	-	0.61±0.01
18	17.45	1185	α-Terpineol	0.21[a]±0.01	-	1.43[b]±0.01
19	18.43	1222	Citronellol	19.90[a]±1.80	-	1.48[b]±0.01
20	18.68	1239	Neral	0.64±0.01	-	-
21	19.25	1250	Geraniol	7.15[a]±0.70	81.20[b]±8.00	12.53[c]±0.10
22	19.54	1266	Geranial	0.16[a]±0.01	0.28[b]±0.01	0.11[c]±0.01
23	19.66	1276	Citronellyl formate	19.58±0.80	-	-
24	19.73	1266	Neryl formate	0.26±0.01	-	-

Peak No	RT[2], min	RI[3]	Compound	Essential oils from		
				geranium	palmarosa	citronella
25	19.92	1281	Bornyl acetate	-	-	0.88±0.01
26	20.32	1298	Geranyl formate	6.69[a]±0.60	0.24[b]±0.01	0.34[c]±0.01
27	21.62	1345	α-Terpinyl acetate	0.23[a]±0.01	-	0.77[b]±0.01
28	21.69	1351	Citronellyl acetate	0.48[a]±0.01	-	1.18[b]±0.01
29	22.48	1380	Geranyl acetate	0.46[a]±0.01	12.69[b]±10.00	7.2[c]±0.07
30	22.61	1386	β-Bourbonene	1.77[a]±0.01	-	0.17[b]±0.01
31	22.76	1391	β-Elemene	-	-	1.29±0.01
32.	23.08	1405	(Z)-Isoeugenol	-	-	0.57±0.01
33	23.54	1417	β-Caryophyllene	1.88[a]±0.01	1.41[b]±0.01	2.23[c]±0.02
34	23.86	1440	(Z)-β-Farnesene	0.93[a]±0.01	-	0.58[b]±0.01
35	24.02	1446	Citronellyl propionate	0.69±0.01	-	-
36	24.10	1450	Guaia-6,9-diene	13.8 ±1.22	-	-
37	24.44	1452	(E)-Isoeugenol	-	-	0.70±0.01
38	24.92	1475	Geranyl propanoate	1.18[a]±0.01	-	0.12[b]±0.01
39	25.09	1483	Germacrene D	0.64[a]±0.01	-	0.77[a]±0.01
40	25.20	1489	(3Z,6E)- α-Farnesene	-	-	3.15±0.03
41	25.27	1494	(E)-Methyl isoeugenol	-	-	19.15±0.17
42	25.30	1505	(E,E)-α-Farnesene	0.27±0.01	-	-
43	25.58	1511	Germacrene A	-	-	0.50±0.01
44	25.47	1521	Eugenol acetate	0.15±0.01	-	-
45	25,87	1525	δ-Cadinene	-	-	0.62±0.01
46	25.61	1536	α-Cadinene	0.34±0.01	-	1.88±0.01
47	26.12	1547	Citronellyl butyrate	-	-	0.44±0.01
48	25.87	1550	(Z)-Cadinene ether	0.16±0.01	-	-
49	26.73	1553	Elemol	-	-	1.95±0.01
50	25.99	1557	(E)-Cadinene ether	1.04±0.01	-	-
51	26.12	1563	(E)-Isoelemicin	1.32±0.01	-	-
52	26.87	1566	Geranyl butanoate	-	-	2.39±0.02
53	26.73	1592	6-methoxy-Isoelemicin	0.11±0.01	-	-
54	26.87	1601	Geranyl 2-methyl butanoate	1.23[a]±0.01	0.10[b]±0.01	-
55	28.70	1627	10-epi-γ-Eudesmol	0.38[a]±0.01	-	0.30[a]±0.01
56	28.92	1632	Citronellyl pentanoate	0.30[a]±0.01	-	0.28[a]±0.01
57	28.96	1635	γ-Eudesmol	0.16[a]±0.01	-	0.22[b]±0.01
58	29.05	1640	epi-α-Muurolol	0.42[a]±0.01	-	0.52[b]±0.01
59	29.23	1653	α-Cadinol	-	-	1.34±0.01
60	30.08	1686	Geranyl angelate	1.88[a]±0.01	-	0.15[b]±0.01
61	31.22	1755	Geranyl caproate	-	0.65±0.01	-
Aliphatic hydrocarbons, %				-	-	1.24
Monoterpene hydrocarbons, %				0.46	0.59	20.79
Oxygenated monoterpenes, %				74.27	98.00	41.97
Sesquiterpene hydrocarbons, %				19.64	1.41	11.21
Oxygenated sesquiterpenes, %				2.16	-	4.34
Phenylpropanoids, %				1.58	-	20.45
Others, %				1.89	-	-

Note: [1]total ion current; [2] retention time, min; [3] retention (Kovat's) index; [4] below 0.05% of TIC or not detected.

[a, b, c] - indices showing significant differences ($p < 0.05$) between the mean values in the rows

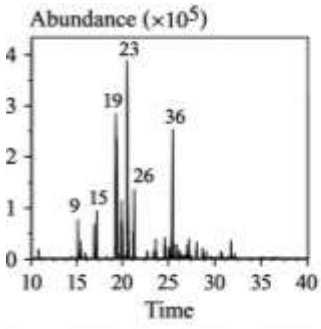

Figure 1.
GC–MS chromatogram of commercial geranium essential oil

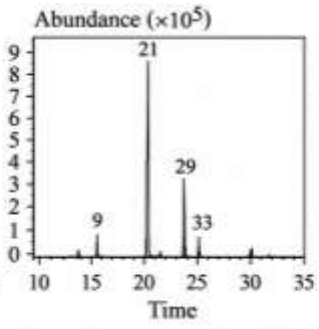

Figure 2.
GC–MS chromatogram of commercial palmarosa essential oil

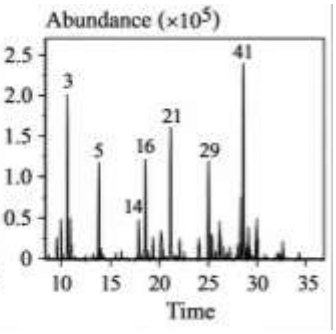

Figure 3.
GC–MS chromatogram of commercial citronella essential oil

Note. Peak numbers correspond to the compounds listed in Table 1

Comparative analysis indicated that the chemical compositions of the analyzed essential oils are generally consistent with those reported in the literature, although quantitative differences in the relative abundance of individual constituents were observed.

Geranium essential oil. In an Egyptian sample, the major constituents were citronellol (27.67%), cis-menthone (10.23%), linalool (10.05%), eudesmol (9.40%), geranyl formate (6.87%), and rose oxide (5.77%) (Abd El-Kareem et al., 2020). Another study on Egyptian geranium essential oil reported citronellol (30.68%), geraniol (9.68%), and citronellyl formate (9.90%) as the principal constituents (Cebi, 2021b). An Iraqi oil was characterized by citronellyl isovalerate (10.41%), menthol (9.61%), linalool (8.63%), p-menthone (6.31%), and geranyl tiglate (4.99%) (Ahamad & Uthirapathy, 2021). Tunisian geranium essential oil contained citronellol (21.9%), citronellyl formate (13.2%), geraniol (11.1%), eudesmol (7.9%), geranyl formate (6.2%), and linalool (5.6%) (Boukhris et al., 2013). In Serbia, the major constituents were citronellol (24.54%), geraniol (15.33%), citronellyl formate (10.66%), and linalool (9.80%) (Džamić et al., 2014). Geranium essential oil from Algeria contained geraniol (23.5%) and citronellol (19.4%) as the predominant components (Medjdoub et al., 2024). Indian geranium oil was rich in citronellol (33.6%), geraniol (26.8%), linalool (10.5%), citronellyl formate (9.7%), and menthone (6.0%) (Rana et al., 2002). Iranian geranium essential oil contained citronellol (44.63%), citronellyl formate (14.22%), isomenthone (6.34%), geraniol (5.30%), and caryophyllene (3.55%) (Azhdarzadeh et al., 2018). Polish geranium oil was characterized by citronellol (22.28%), geraniol (15.50%), geranyl acetate (13.13%), limonene (9.27%), 2-phenylethanol (5.93%), and linalool (5.59%) (Szutt et al., 2019).

Palmarosa essential oil. Essential oil from Nepal was characterized by high concentrations of neral (36.1%) and geranial (53.1%) (Dangol et al., 2023). Indian palmarosa essential oil contained geraniol (67.6–83.6%), geranyl acetate (2.3–15.9%), geranial (1.0–8.8%), linalool (1.6–3.4%), and citronellol plus nerol (0–2.1%) (Raina et al., 2003). Brazilian palmarosa oil was dominated by geraniol (57.49%) and geranyl acetate (13.56%) (Andrade et al., 2014). A more recent study from India reported a different chemical profile, with carveol (11.32–20.87%), trans-p-mentha-1(7),8-dien-2-ol (12.90–19.58%), and cis-piperitol (15.27%) as the major constituents (Sonigra & Meena, 2025).

Citronella essential oil. Thai citronella essential oil was reported to contain citronellal (27.5%), geraniol (20.4%), and citronellol (13.4%) as its principal constituents (Jantamas et al., 2016).

The observed differences in the chemical compositions of the essential oils can be attributed to the influence of various biological, geographical, soil and climatic, and technological factors, including plant genotype, environmental conditions, cultivation practices, harvesting stage, and extraction method, as has also been reported for other essential oil-bearing plants (Bauer et al., 2001; Başer & Buchbauer, 2010; Stoyanova, 2022).

The observed differences in the chemical composition of the essential oils can be attributed to the influence of various biological, environmental, and technological factors, including plant genotype, geographical origin, soil and climatic conditions, cultivation practices, harvest stage, and extraction method. Similar variability has been reported for other essential oil-bearing plants (Bauer et al., 2001; Başer & Buchbauer, 2010; Stoyanova, 2022).

The distribution of the major classes of compounds identified in the investigated essential oils is presented in Table 1. The results revealed distinct differences in the chemical profiles of the three essential oils. Geranium essential oil was dominated by oxygenated monoterpenes (74.27%), followed by sesquiterpene hydrocarbons (19.64%), oxygenated sesquiterpenes (2.16%), other compounds (1.89%), phenylpropanoids (1.58%), and monoterpene hydrocarbons (0.46%). Palmarosa essential oil consisted predominantly of oxygenated monoterpenes (97.67%), with considerably lower proportions of sesquiterpene hydrocarbons (1.41%) and monoterpene hydrocarbons (0.59%). In contrast, citronella essential oil exhibited a more complex chemical profile, comprising oxygenated monoterpenes (41.97%), monoterpene hydrocarbons (20.79%), phenylpropanoids (20.45%), sesquiterpene hydrocarbons (11.21%), oxygenated sesquiterpenes (4.34%), and aliphatic hydrocarbons (1.24%).

The biological activity of essential oils is known to depend largely on the functional groups of their constituent compounds. According to Griffin et al., the relative order of biological activity is: phenols > alcohols > aldehydes > ketones > esters > hydrocarbons (Griffin et al., 1999). The distribution of oxygenated constituents according to their functional groups (expressed as a percentage of the total oxygenated compounds) is also presented in Table 1 and revealed marked differences among the investigated essential oils. Geranium essential oil was characterized by a predominance of esters (43.26%), mainly represented by citronellyl formate and geranyl formate, followed by alcohols (42.27%), represented primarily by citronellol, geraniol, and linalool. Lower proportions of ketones (9.60%), oxides (2.37%), ethers (1.50%), and aldehydes (1.00%) were also identified. Palmarosa essential oil was dominated by alcohols (85.71%), almost entirely represented by geraniol, followed by esters (14.00%), mainly geranyl acetate, while aldehydes accounted for only 0.29%. In contrast, citronella essential oil contained alcohols (43.72%) as the predominant oxygenated constituents, represented mainly by geraniol and borneol. These were followed by phenols (30.64%), represented primarily by methyl isoeugenol, esters (20.68%), mainly geranyl acetate, and aldehydes (4.96%).

Antimicrobial activity

The antimicrobial activities of the investigated essential oils and the monoterpene alcohols are presented in Table 2.

Table 2

Inhibition zone of aromatic components and essential oils from, mm

Test-microorganisms	Filtrat, μL	Geraniol	Citronellol	Geranium	Palmarosa	Citronella
E. coli ATCC 8739	150	-*	-	-	-	-
	100			-	-	-
		12.0±0.1	-			
	50	-	-	-	-	
S. enterica NCTC 6017	150	-	-	-	-	
	100			-	-	-
		9.0±0.2[a]	7.5±0.1[b]			
	50	-	-	-	-	-
S. aureus SATCC 25093	150	-	-	-	7.3±0.1	8.1±0.2
	100					
		6.8±0.1[a]	9.9±0.2[b]	-	7.0±0.2[a]	7.4±0.1[c]
	50	-	-		6.9±0.1[a]	7.1±0.1[b]
L.monocytogenes NCTC 11994	150	-	-	-	-	-
	100	-	-	-	-	-
	50	-	-		-	-
B. subtilis ATCC 6633	150	-	-	9.2±0.2[a]	9.0±0.2[a]	-
	100					-
		10.0±0.1[a]	8.7±0.1[b]	8.2±0.1[c]	8.6±0.1[b]	-
	50	-	-	7.5±0.1[a]	8.2±0.2[b]	-

* No inhibitory activity was observed

[a, b, c] - indices showing significant differences ($p < 0.05$) between the mean values in the rows

The results showed that geraniol exhibited inhibitory activity against the Gram-negative bacteria *E. coli* and *S. enterica* as well as against the Gram-positive bacteria *S. aureus* and *B. subtilis*. Citronellol was active against the Gram-negative bacterium *S. enterica* and the Gram-positive bacteria *S. aureus* and *B. subtilis*. Neither monoterpene alcohol exhibited inhibitory activity against the Gram-positive bacterium *L. monocytogenes*.

The pronounced antimicrobial activity of geraniol and citronellol against the Gram-positive bacteria *S. aureus* and *B. subtilis* is consistent with previous reports (Dangol et al., 2023; de Lira et al., 2020; Jirovetz et al., 2007; Santamarta et al., 2023). The three essential oils also exhibited selective activity against Gram-positive bacteria. Specifically, geranium essential oil inhibited the growth of *B. subtilis*, palmarosa essential oil was active against both *S. aureus* and *B. subtilis*, whereas citronella essential oil inhibited only *S. aureus*. Similar findings have been reported by other authors, who demonstrated strong inhibitory effects of geranium essential oil against Gram-positive bacterial strains, particularly *B. cereus*, *B. subtilis*, and *S. aureus* (Carmen & Hancu, 2014; Choi et al., 2022; Džamić et al., 2014; Rosato et al., 2007). Likewise, pronounced antibacterial activity of palmarosa essential oil against Gram-positive bacteria has been documented in several studies (Dangol et al., 2023; Jantamas et al., 2016; Santamarta et al., 2023).

The greater susceptibility of Gram-positive bacteria is generally attributed to the absence of an outer membrane, allowing hydrophobic constituents of essential oils, particularly oxygenated monoterpenes such as geraniol and citronellol, to penetrate the cell wall more readily. In contrast, the lipopolysaccharide-rich outer membrane of Gram-negative bacteria acts as an effective permeability barrier, reducing the antimicrobial efficacy of essential oil constituents.

Antioxidant activity

The antioxidant activities of the three essential oils and their major monoterpene alcohols are presented in Table 3. The differences observed among the obtained values can be attributed to the distinct reaction mechanisms underlying the DPPH, ABTS, and FRAP assays. Comparable antioxidant activities of geraniol and citronellol were observed in the DPPH and FRAP assays, whereas more pronounced differences were found using the ABTS assay. The three essential oils also exhibited different levels of antioxidant activity, which can be explained by differences in their chemical composition and the relative abundance of antioxidant constituents.

Previous studies have reported relatively low antioxidant activity for geranium and palmarosa essential oils. For geranium essential oil, Džamić et al. (2014) reported a DPPH radical scavenging activity of approximately 50% at an EC_{50} value of 0.802 mg/mL, while Medjdoub et al. (2024) determined antioxidant activities of 19.66 mg/mL and 10.79 μg/mL using the DPPH and ABTS assays, respectively. For palmarosa essential oil, Lawrence et al. (2012) reported an IC_{50} value of 0.125 mg/mL in the DPPH assay. Overall, these findings are in agreement with the present results, indicating that the investigated essential oils possess relatively low antioxidant activity.

Table 3

Antioxidant activity of aromatic components and essential oils

Compounds	DPPH, % inhibition	ABTS, % inhibition	FRAP, mM TE/mL
Geraniol	21.98±0.20^{a}	57.47±0.55^{a}	0.221± 0.02^{a}
Citronellol	19.53±0.17^{b}	43.54±0.40^{b}	0.215± 0.02^{b}
Geranium essential oil	16.92±0.15^{c}	75.34±0.71^{c}	0.221± 0.02^{a}
Palmarosa essential oil	15.91±0.14^{c}	65.29±0.62^{d}	0.268± 0.02^{c}
Citronella essential oil	21.14±0.20^{a}	72.85±0.70^{e}	0.252± 0.02^{d}

$^{a\text{-}e}$ - indices showing significant differences ($p < 0.05$) between the mean values in the columns

Conclusions

Among the three essential oils investigated, palmarosa essential oil contained the highest concentration of the monoterpene alcohol geraniol, whereas its content was considerably lower in geranium and citronella essential oils. Geraniol exhibited antimicrobial activity against the Gram-positive bacteria *Staphylococcus aureus* and *Bacillus subtilis*, whereas citronellol was active against the Gram-negative bacterium *Salmonella enterica* and the Gram-positive bacteria *S. aureus* and *B. subtilis*. The essential oils displayed selective antibacterial activity against Gram-positive bacteria. Geranium essential oil inhibited the growth of *B. subtilis*, palmarosa essential oil was active against both *S. aureus* and *B. subtilis*, and citronella essential oil inhibited *S. aureus*. None of the essential oils exhibited antibacterial activity against the tested Gram-negative bacteria. Both monoterpene alcohols and the three essential oils exhibited relatively low antioxidant activity, as demonstrated by the DPPH, ABTS, and FRAP assays.

References

Abd El-Kareem, M., Rabbih, M., Elansary, H., & Al-Mana, F. (2020). Mass spectral fragmentation of *Pelargonium graveolens* essential oil using GC MS semi-empirical calculations and biological potential. *Process*, *8*(2), 128. https://doi.org/10.3390/pr8020128

Adams, R. (2007). Identification of essential oil components by Gas Chromatography/Mass Spectroscopy; Allured Publishing Corporation: Carol Stream, IL, USA.

Ahamad, J., & Uthirapathy, S. (2021). Chemical characterization and antidiabetic activity of essential oils from *Pelargonium graveolens* leaves. *The Scientific Journal of Koya University*, *9*(1), 101-113. https://doi.org/10.14500/aro.10791

Andrade, B., Conti, B., Santiago, K., Fernandes, A., & Sforcin, J. (2014). *Cymbopogon martinii* essential oil and geraniol at non-cytotoxic concentrations exerted immunomodulatory/anti-inflammatory effects in human monocytes. *Journal of Pharmacy and Pharmacology*, *66*(10), 1491-1496. https://doi.org/10.1111/jphp.12278

Atanasova, T., Kakalova M., Stefanof L., Petkova M., Stoyanova A., Damyanova S., & Desyk, M. (2016). Chemical composition of essential oil from *Rosa damascena* Mill., growing in new region of Bulgaria. *Ukrainian Food Journal*, 5(3), 492-498.

Azhdarzadeh, F., Hojjat, M., & Didehban, S. (2018). Chemical composition and antimicrobial activity of *Pelargonium roseum* essential oil from Southwest of Iran. *Journal of Food and Bioprocess Engineering*, *1*(1), 33-38.

Başer, H., & Buchbauer, G. (2010). *Handbook of essential oils: Science, technology, and applications*. Taylor and Francis Group.

Bauer, K., Garbe, D., & Surburg, H. (2001). *Common fragrance and flavor materials: Preparation, properties and uses* (4th completely revised ed.). Wiley-VCH.

Benzie, I., & Strain, J. (1996) Ferric reducing ability of plasma (frap) as a measure of antioxidant power: The FRAP assay. *Analytical Biochemistry*, *239*(1), 70-76. https://doi.org/10.1006/abio.1996.0292

Bergman, M. E, Bhardwaj, M., & Phillips, M. A. (2021). Cytosolic geraniol and citronellol biosynthesis require a Nudix hydrolase in rose-scented geranium (*Pelargonium graveolens*). *Plant Journal*, *107*(2), 493-510. https://doi.org/10.1111/tpj.15304

Boukhatem, M., Kameli, A., & Saidi, F. (2013). Essential oil of Algerian rose-scented geranium (*Pelargonium graveolens*): Chemical composition and antimicrobial activity against food

spoilage pathogens. *Food Control*, *34*(1), 208-213. https://doi.org/10.1016/j.foodcont.2013.03.045

Boukhris, M., Simmonds, M., Sayadi, S., & Bouaziz, M. (2013). Chemical composition and biological activities of polar extracts and essential oil of rose-scented geranium, *Pelargonium graveolens*. *Phytotherapy Research*, *27*(8), 1206-1213. https://doi.org/10.1002/ptr.4853

Can, E., Kizak, V., Can, S., & Özçiçek, E. (2018). Anesthetic potential of geranium (*Pelargonium graveolens*) oil for two cichlid species, *Sciaenochromis fryeri* and *Labidochromis caeruleus*. *Aquaculture*, *491*, 59-64. https://doi.org/10.1016/j.aquaculture.2018.03.013

Carmen, G., & Hancu, G. (2014). Antimicrobial and antifungal activity of *Pelargonium roseum* essential oils. *Advanced Pharmaceutical Bulletin*, *4*(2), 511-514. https://doi.org/10.5681/apb.2014.075

Cebi, N. (2021a). Quantification of the geranium essential oil, palmarosa essential oil and phenylethyl alcohol in rosa damascena essential oil using atr-ftir spectroscopy combined with chemometrics. *Foods*, *10*(8), 1848. https://doi.org/10.3390/foods10081848

Cebi, N. (2021). Chemical fingerprinting of the geranium (*Pelargonium graveolens*) essential oil by using FTIR, Raman and GC-MS techniques. *Avrupa Bilim Ve Teknoloji Dergisi*, *25*, 810-814. https://doi.org/10.31590/ejosat.969661

Choi, J., Jang, T., & Kim, J. (2022). Antibacterial effect of essential oil on *Staphylococcus aureus*-resistant strain (MRSA), the causative agent of dermatitis. *Journal of the Korean Society of Cosmetology*, *28*(5), 956-961.

Cocoș, D., Earar, K., Dinu, M., Lungu, I., Bazbanela, C., & Galea, C. (2023). Perspectives on the use of geranium essential oil: *Pelargonium graveolens* and *Pelargonium roseum*, in dental medicine. *Romanian Journal of Medical and Dental Education*, *12*(2), 23-34.

Dangol, S., Poudel, D., Ojha, P., Maharjan, S., Poudel, A., Satyal, R., Rokaya, A., Timsina, S., Dosoky, N., Satyal, P., & Setzer, W. (2023). Essential oil composition analysis of *Cymbopogon* species from eastern Nepal by GC-MS and chiral GC-MS, and antimicrobial activity of some major compounds. *Molecules*, *28*(2), 543. https://doi.org/10.3390/molecules28020543

Džamić, A., Soković, M., Ristić, M., Grujić, S., Mileski, K., & Marin P. (2014). Chemical composition, antifungal and antioxidant activity of *Pelargonium graveolens* essential oil. *Journal of Applied Pharmaceutical Science*, *4*(3), 1-5. https://doi.org/10.7324/JAPS.2014.40301

Griffin, S., Wyllie, G., Markham, J., & Leach, D. (1999). The role of structure and molecular properties of terpenoids in determining their antimicrobial activity, *Flavour and Fragrance Journal*, *14*(5), 322-332. https://doi.org/10.1002/(SICI)1099-1026(199909/10)14:5<322::AID-FFJ837>3.0.CO;2-4

Guimarães, A. C., Meireles, L. M., Lemos, M. F., Guimarães, M. C. C., Endringer, D. C., Fronza, M., & Scherer, R. (2019). Antibacterial activity of terpenes and terpenoids present in essential oils. *Molecules, 24*(13), 2471. https://doi.org/10.3390/molecules24132471

Ivanova, M., Teneva, O., Dushkova, M., Vlaseva, R., Stoyanova. A. (2020). Effect of canola oil and natural antioxidant of basil on chemical and sensory properties of fresh cheese. *Ukrainian Food Journal*, *9*(2), 373-382, https://doi.org: 10.24263/2304-974X-2020-9-2-9

Jantamas, S., Matan, N.**,** Matan, N., & Aewsiri T. (2016). Improvement of antifungal activity of citronella oil against *Aspergillus flavus* on rubberwood (*Hevea brasiliensis*) using heat curing. *Journal of Tropical Forest Science***,** *28*(1), 39-47. https://www.jstor.org/stable/43748077

Jirovetz, L., Buchbauer, G., Schmidt, E., Stoyanova, A., Denkova, Z., Nicolova, R., & Geissler, M. (2007). Purity, antimicrobial activities and olfactoric evaluations of geraniol/nerol and

various of their derivatives. *Journal of Essential Oil Research*, *19*(3), 288-291. https://doi.org/10.1080/10412905.2007.9699283

Lawrence, K., Lawrence, R., Parihar, D., Srivastava, R., & Charan, A. (2012). Antioxidant activity of palmarosa essential oil (*Cymbopogon martini*) grown in north Indian Plains. *Asian Pacific Journal of Tropical Biomedicine*, *2*(2), S888-S891. https://doi.org/10.1016/S2221-1691(12)60330-X

Lira, M. H. P. de, Andrade Júnior, F. P. de., Moraes, G. F.Q., da Silva Macena, G. da. S., Pereira, F. de. O., & Lima. I. O. (2020). Antimicrobial activity of geraniol: An integrative review. *Journal of Essential Oil Research*, *32*(2), 187-197. https://doi.org/10.1080/10412905.2020.1745697

Medjdoub, H., Bouali, W., Semaoui, M., Benaissa, A., Chaib, F., & Azzi, A. (2024). Chemical composition, antioxidant and antibacterial activities of the essential oil of *Pelargonium graveolens* L'Hér. *Chemical Papers*, *79*(4), 1-9. https://doi.org/10.1007/s11696-024-03859-8

Misharina, T. (2016). Antiradical properties of essential oils and extracts from coriander, cardamom, white red, and black peppers. *Applied of Biochemistry and Microbiology*, *52*, 79-86. https://doi.org/10.1134/S0003683816010087

Raina, V., Srivastava, S., Aggarwal, K., Syamasundar, K., & Khanuja, S. (2003). Essential oil composition of *Cymbopogon martinii* from different places in India. *Flavour and Fragrance Journal*, *18*(4), 312-315. https://doi.org/10.1002/ffj.1222

Rana, V., Juyal, J., & Blazquez, M. A. (2002). Chemical constituents of essential oil of *Pelargonium graveolens* leaves. *International Journal of Aromatherapy*, *12*(4), 216-218. https://doi.org/10.1016/S0962-4562(03)00003-1

Re, R., Pellegrini, N., Proteggente, A., Pannala, A., Yang, M., & Rice-Evans, C. (1999). Antioxidant activity applying an improved ABTS radical cation decolorization assay. *Free Radic Biology and Medicine*, *26*(9-10), 1231. https://doi.org/10.1016/S0891-5849(98)00315-3

Rosato, A., Vitali, C., Laurentis, N., Armenise, D., & Milillo, M. (2007). Antibacterial effect of some essential oils administered alone or in combination with norfloxacin. *Phytomedicine*, *14*(11), 727-732. https://doi.org/10.1016/j.phymed.2007.01.005

Santamarta, S., Aldavero, A., & Rojo, M. (2023). Essential oil of *Cymbopogon martini*, source of geraniol, as a potential antibacterial agent against *Bacillus subtilis*, a pathogen of the bakery industry. *F1000Research*, *10*, 1027. https://doi.org/10.12688/f1000research.54196.2

Seo, S. M., Kim, J., Lee, S., Shin, C., Shin, S., & Park, I. (2009). Fumigant antitermitic activity of plant essential oils and components from ajowan (*Trachyspermum ammi*), allspice (*Pimenta dioica*), caraway (*Carum carvi*), dill (*Anethum graveolens*), geranium (*Pelargonium graveolens*), and litsea (*Litsea cubeba*) oils against Japanese termite (*Reticulitermes speratus* Kolbe). *Journal of Agricultural and Food Chemistry*, *57*(15), 6596-6602. https://doi.org/10.1021/jf9015416

Siddiqui, T., Sharma, V., Khan, M.U., & Gupta, K. (2024). Terpenoids in essential oils: Chemistry, classification, and potential impact on human health and industry. *Phytomedicine Plus*, *4*(2), 100549. https://doi.org/10.1016/j.phyplu.2024.100549

Singh, M., Singh, U., Ram, M., Yadav, A., & Chanotiya, C. (2013). Biomass yield, essential oil yield and quality of geranium (*Pelargonium graveolens* L. Her.) as influenced by intercropping with garlic (*Allium sativum* L.) under subtropical and temperate climate of India. *Industrial Crops and Products*, *46*, 234-237. http://dx.doi.org/10.1016/j.indcrop.2013.01.032

Sonigra, P., & Meenap, M. (2025). Influence of growth stage on the chemical composition, antimicrobial, and antioxidant potential of *Cymbopogon martinii* (Roxb.) Wats. essential oil. *Frontiers in Plant Science*, *16*, 1660363. https://doi.org/10.3389/fpls.2025.1660363

Stabnikova, O., Stabnikov, V., & Paredes-López, O. (2026a). Spices and essential oils in food preservation: From natural additives to active packaging systems. *Plant Food for Human Nutrition*, *81*, 69. https://doi.org/10.1007/s11130-026-01519-8

Stabnikova, O., Marynin, A., Stabnikov, V., Svyatnenko, R., & Demchenko, V. (2026). Plant essential oils for food shelf-life extension and active packaging systems. *Ukrainian Food Journal*, *15*(2), 323–360. https://doi.org/10.24263/2304-974X-2026-15-2-6

Stoyanova, A. (2022). *A guide for the specialist in the aromatic industry*. Bulgarian National Association of Essential Oils, Perfumery and Cosmetics, Plovdiv.

Szutt, A., Dołhańczuk-Śródka, A., & Sporek, M. (2019). Evaluation of chemical composition of essential oils derived from different *Pelargonium* species leaves. *Ecological Chemistry and Engineering S*, *26*(4), 807-816. https://doi.org/10.1515/eces-2019-0057

Wany, A., Kumar, A., Nallapeta, S., Jha, S., Nigam, V. K., & Pandey, D. (2014). Extraction and characterization of essential oil components based on geraniol and citronellol from Java citronella (*Cymbopogon winterianus* Jowitt). *Plant Growth Regulation*, *73*(2), 133-145. 10.1007/s10725-013-9875-7

Zaika, L. (1988). Spices and herbs: Their antimicrobial activity and its determination. *Journal of Food Safety*, *2*, 97-118. https://doi.org/10.1111/j.1745-4565.1988.tb00511.x

Cite:

Fidan, H., Kavrakova, B., Taneva, I., Dincheva, I., Lazarov, A., Damyanova, S., & Stoyanova, A. (2026). Essential oils rich in geraniol and citronellol. *Ukrainian Food Journal*, *15*(3), 702–715. https://doi.org/10.24263/2304-974X-2026-15-3-7

Technological role of psyllium-agar hydrocolloid system in improving the structure and sensory properties of gluten-free rice-corn cupcakes

Ludmila Saleba[1], Maria Ratsuk[1], Tetiana Yurova[1], Eugen Kalinsky[1], Olha Semeshko[1,2]

1 – Kherson National Technical University, Khmelnytskyi, Ukraine
2 – Slovak Academy of Sciences, Košice, Slovakia

Keywords:

Gluten-free
Cupcake
Rice-corn flour
Psyllium
Agar
Texture
Dough

Article history:

Received 22.02.2026
Received in revised form 14.07.2026
Accepted 30.06.2026

Corresponding author:

Olha Semeshko
E-mail:
solgaya@gmail.com

DOI: 10.24263/2304-974X-2026-15-3-8

Abstract

Introduction. This study investigated the effect of psyllium and agar on the physicochemical and sensory properties of rice–corn gluten-free cupcakes.

Materials and methods. Cupcakes were prepared using rice (R) and corn (C) flour blends at ratios from 90:10 to 50:50. The R60:C40 formulation was further modified with psyllium (1–5%), agar (0.1%), and their combination. Baking loss, dough expansion ratio, moisture content, specific volume, and alkalinity were determined using standard physicochemical methods. Sensory evaluation was performed by 25 untrained panellists using a 9-point hedonic scale.

Results and discussion. The rice-to-corn flour ratio significantly affected cupcake structure and quality. Increasing corn flour content from 10% to 40% reduced baking loss from 8.93% to 7.70% and increased dough expansion ratio from 0.61 to 0.69. The R60 formulation demonstrated the most balanced physicochemical and sensory characteristics, including a moisture content of 13.38% and a specific volume of 167.33 mL/100 g. Sensory scores for shape, texture, and crumb consistency reached 7.2–7.8 points, approaching those of the wheat-based control. The addition of psyllium increased the specific volume to 169.67 mL/100 g at a concentration of 5%, while moisture content decreased from 12.52% to 11.60%, indicating strong water-binding properties and improved gas retention. Agar used individually reduced specific volume to 146.00 mL/100 g and decreased dough expansion ratio to 0.62, likely due to increased matrix rigidity. The combined incorporation of 5% psyllium and 0.1% agar further improved the properties of the gluten-free formulation, increasing moisture content to 13.86% and dough expansion ratio to 0.72, comparable to that of the wheat-based control (0.71). The combined hydrocolloid system produced a homogeneous, fine-porous crumb structure and improved sensory scores for texture and crumb consistency to 8.1–8.2 points. These results suggest that psyllium contributed to gas-cell stabilisation and moisture retention, whereas agar reinforced the structural network and limited excessive expansion.

Conclusions. The optimal gluten-free cupcake formulation was obtained using a rice-to-corn flour ratio of 60:40 combined with 5% psyllium and 0.1% agar. The psyllium–agar system effectively compensated for the absence of gluten and improved structural stability, moisture retention, and sensory quality of gluten-free cupcakes.

Introduction

The prevalence of celiac disease continues to increase worldwide (Celiac Disease Foundation, 2020). As a strict gluten-free diet is currently the only medically recognized treatment, the development of gluten-free foods, including bakery products, is of increasing importance (Mark & Watson, 2024; Stabnikova et al., 2021). However, developing gluten-free bakery products with acceptable structural and sensory quality remains a significant technological challenge due to the absence of gluten, which plays a critical role in gas retention and crumb formation in wheat-based systems (Demirkesen & Ozkaya, 2022; Jukić et al., 2024; Ungureanu-Iuga & Cobuz, 2025).

Different gluten-free cereal flours, such as buckwheat, oat flake, sorghum, and pearl millet, have been investigated for the development of gluten-free bakery products owing to their nutritional and functional properties (Banu & Aprodu, 2024; Coronel et al., 2025; Costa et al., 2024; Ojo et al., 2026; Shevchenko, 2022). Nevertheless, gluten-free baked goods are more commonly formulated using rice and corn flours because of their availability, neutral flavour (rice), and contribution to colour and flavour development (corn) (Šmídová & Rysová, 2022; Woomer & Adedeji, 2021). Rice flour is rich in starch and exhibits high water absorption capacity, whereas corn flour contains higher levels of proteins, lipids, and sugars, contributing to flavour and colour development (Culetu et al., 2021; Hu et al., 2024; Jalali et al., 2020). However, these flours exhibit complementary technological limitations: rice flour tends to produce sticky structures, while corn flour produces firmer, less cohesive crumbs. Therefore, combining rice and corn flours is considered a rational strategy to improve the structural and sensory properties of gluten-free formulations.

Despite this, rice–corn systems still lack a continuous viscoelastic network, which is essential for stabilising gas cells during baking. In gluten-free systems, structure development relies primarily on starch–hydrocolloid interactions. Hydrocolloids are therefore widely used to mimic gluten functionality by modifying water distribution, increasing batter viscosity, and improving gas retention and crumb stability (Capriles et al., 2023; Xu et al., 2020).

Among hydrocolloids, agar is known for its strong thermoreversible gel-forming properties, which contribute to structural reinforcement during thermal processing (Stoican et al., 2021). In contrast, psyllium husk, a fibre-rich ingredient composed mainly of arabinoxylans, exhibits high water-binding capacity and forms viscous networks upon hydration (Franco et al., 2020; Fratelli et al., 2018). Psyllium has been widely used in gluten-free systems for its ability to improve dough structure, enhance moisture retention, and reduce staling (Thakur & Thakur, 2014).

In addition to its technological functionality, psyllium is a valuable dietary fibre source that can improve the nutritional profile of gluten-free products (Ishaq et al. 2024; Slashcheva et al., 2022). This is particularly important given that many hydrocolloids used in gluten-free formulations provide limited nutritional benefits. Therefore, the use of fibre-rich structuring agents offers a promising strategy for developing multifunctional gluten-free products.

Although hydrocolloids such as psyllium and agar have been individually studied in gluten-free bakery products, including bread, cookies, and cakes (Costa et al., 2024; Franco & Gómez, 2022; Franco et al., 2024; Gruppi et al., 2024; Khan et al., 2021; Manik & Nur, 2021; Mohtarami et al., 2022; Yeganeh et al., 2024), their combined application in cupcake formulations remains insufficiently explored. In particular, the potential synergistic interaction between viscosity-enhancing and gel-forming hydrocolloids in stabilising gluten-free batter systems has not been fully elucidated.

This study investigates the technological role of a psyllium–agar hydrocolloid system in gluten-free cupcakes based on rice–corn flour blends. The objective was to evaluate the effects of individual and combined hydrocolloids on physicochemical properties, structure formation, and sensory characteristics. Special attention was given to structure–function relationships, including moisture distribution, gas retention, and crumb architecture, in order to identify an optimal formulation and provide practical insights into gluten-free bakery design.

Materials and methods

Materials

All raw materials and ingredients were commercially available products produced in Ukraine. Wheat flour (10.3% protein, 1.1% fat, and 70.0% carbohydrates), rice flour (8.8% protein, 0.5% fat, and 77.1% carbohydrates), and corn flour (7.2% protein, 1.5% fat, and 72.1% carbohydrates) were used as the main raw materials.

The cupcake formulations also included butter (82.5% fat), white crystalline sugar, mélange, food-grade salt, powdered sugar, ammonium carbonate, and vanilla essence. Psyllium husk powder and agar were used as hydrocolloids.

For alkalinity determination, hydrochloric acid (HCl, 35%, p.a.) and bromothymol blue (≥97.0%) were used.

Preparation of cupcakes

The control and gluten-free cupcake formulations were based on the same basic recipe, with flour composition being the primary variable. The control formulation contained wheat flour (288.8 g), sugar (216.6 g), butter (216.6 g), eggs (173.2 g), salt (0.86 g), vanilla essence (0.86 g), and ammonium carbonate (0.86 g) per batch. Butter was whipped for 7 min using a planetary mixer (Kenwood Chef XL KVL4170S, UK), followed by the addition of sugar and whipping for an additional 5 min, with eggs gradually incorporated. Vanilla essence, ammonium carbonate, and salt were then added and mixed thoroughly. Wheat flour was incorporated, and the batter was mixed until homogeneous. Portions (50 g) of batter were deposited into paper-lined moulds and baked at 180 °C for 25 min in an electric oven (Bosch HBF114BR0K, Germany).

In the gluten-free formulations, wheat flour was completely replaced by rice and corn flour at different ratios, while the amounts of the other basic ingredients were kept constant. Psyllium and agar were subsequently incorporated into the selected rice–corn flour formulation at the specified concentrations. The formulations of the control and gluten-free cupcakes are presented in Table 1.

Table 1

Composition of control and gluten-free cupcake formulations (g per batch)

Sample	WF	RF	CF	SUG	B	E	S	VE	AC	P	A
Control	288.8	–	–	216.6	216.6	173.2	0.86	0.86	0.86	–	–
R90:C10	–	259.9	28.9							–	–
R80:C20	–	231.0	57.8							–	–
R70:C30	–	202.2	86.6							–	–
R60:C40	–	173.3	115.5							–	–
R50:C50	–	144.4	144.4							–	–
R60:C40 +1%P	–	173.3	115.5							2.89	–
R60:C40 +3%P	–	173.3	115.5							8.66	–
R60:C40 +5%P	–	173.3	115.5							14.44	–
R60:C40 +0.1%A	–	173.3	115.5							–	0.29
R60:C40 +5%P+0.1%A	–	173.3	115.5							14.44	0.29

Abbreviations: WF – wheat flour; RF – rice flour; CF – corn flour; SUG – sugar; B – butter; E – eggs; S – salt; VE – vanilla essence; AC – ammonium carbonate; P – psyllium; A – agar.

For gluten-free cupcakes, wheat flour was completely replaced with mixtures of rice and corn flour at different ratios (R90:C10, R80:C20, R70:C30, R60:C40, and R50:C50). Based on preliminary experiments, the R60:C40 formulation was selected for further modification. Hydrocolloids were incorporated as follows: 1%, 3%, and 5% psyllium (samples R60:C40+1% P, R60:C40+3% P, R60:C40+5% P), 0.1% agar (R60:C40+0.1% A), and a combination of 5% psyllium and 0.1% agar (R60:C40+5% P+0.1% A). All percentages were calculated relative to total flour weight.

Physicochemical properties of cupcakes

Physicochemical properties were determined using standard methods. Dough and cupcake mass were measured using an analytical balance (Kern ABT 220-5DM, Kern & Sohn GmbH, Balingen, Germany). Cupcake height was measured using a digital calliper. Volume was determined by the rapeseed displacement method (Thakur et al., 2024).

Baking loss (%) was calculated as the mass difference between dough and baked product relative to the mass of the baked cupcake. Dough expansion ratio was calculated as the ratio of cupcake height after baking to that before baking. Moisture content (%) was determined gravimetrically after drying at 130 °C for 45 min in a laboratory oven (Memmert UF55, Memmert GmbH, Germany). Specific volume (mL/100 g) was calculated as the ratio of volume to mass. Alkalinity was determined by titration with hydrochloric acid, using bromothymol blue as an indicator, until a yellow endpoint was reached, and was expressed on a dry matter basis (Khutsidze et al., 2024).

Sensory evaluation

Sensory evaluation was conducted to provide an initial assessment of consumer perception of the developed gluten-free cupcake formulations and to complement instrumental measurements of structural and physicochemical properties. The sensory study was therefore designed as a preliminary consumer-oriented assessment for formulation screening rather than a full consumer acceptance test.

A panel of 25 untrained participants (40% male, 60% female; age range: 20–50 years) was recruited from students and staff of the Department of Chemical Technologies, Expertise, and Food Safety at Kherson National Technical University. All participants were regular consumers of bakery products and evaluated all samples in a single session. The study protocol was approved by the institutional ethics committee, and informed consent was obtained from all participants prior to evaluation.

Before testing, panellists received a brief standardised orientation on the evaluation procedure, assessed attributes, and the use of the 9-point hedonic scale, without formal descriptive sensory training.

Samples were prepared on the day of evaluation and served at room temperature (22 ± 2 °C). Each sample was coded with a random three-digit number and presented in randomised order to minimise order bias. Distilled water was provided for palate cleansing between samples.

Panellists evaluated appearance (shape), colour, texture (mouthfeel), taste, and odour using a 9-point hedonic scale (1 = dislike extremely; 5 = neither like nor dislike; 9 = like extremely), which is commonly applied in preliminary consumer perception studies of food products (Chiș et al., 2020; Drabińska et al., 2018; Jabeen et al., 2022).

Because the same participants evaluated all samples, sensory data were treated as related ordinal variables. Differences among samples were assessed using the Friedman test, followed by the Nemenyi post hoc test when significant differences were detected ($p < 0.05$) (Norton et al., 2022). Results are expressed as mean ± standard deviation (SD), and sensory profiles were visualised using radar plots based on mean hedonic scores.

Due to the relatively small panel size (n = 25), the results should be interpreted as preliminary indications of consumer perception and are primarily intended to support formulation screening. Further studies with larger consumer panels are required to confirm product acceptance.

Statistical analysis

All physicochemical parameters (baking loss, dough expansion ratio, moisture content, and specific volume) were determined in triplicate (n = 3). Data are presented as mean ± standard deviation (SD). One-way analysis of variance (ANOVA) was used to evaluate the effect of flour composition on the measured parameters. Differences were considered statistically significant at $p < 0.05$, and Tukey's post hoc test was applied for multiple comparisons. Regression analysis was used to describe the relationships between flour composition and selected physicochemical properties.

Results and discussion

Selection of the optimal rice–corn flour ratio

At the initial stage, the optimal composition of the gluten-free flour mixture was determined to establish a rational basis for further formulation development. Cupcakes were prepared using rice and corn flour blends at different ratios (Table 1), while a wheat-based formulation served as the control. The external appearance and crumb structure are presented in Figure 1.



Figure 1. External appearance (top) and cross-sections (bottom) of cupcakes prepared with different rice–corn flour ratios:
(a) control; (b) R90:C10; (c) R80:C20; (d) R70:C30; (e) R60:C40; (f) R50:C50.

The control sample exhibited a typical domed shape, smooth surface, and a dense, homogeneous crumb structure with fine porosity. In contrast, sample R90 showed limited expansion, a flat surface, and cavities along the side walls, indicating insufficient gas retention. Its crumb was heterogeneous, with an irregular pore distribution. Increasing the proportion of corn flour to 20–40% resulted in a marked improvement in product morphology. Samples R80, R70, and R60 exhibited slight doming, smooth surfaces without structural defects, and a more uniform crumb structure. At a 1:1 ratio (R50), the surface characteristics were comparable to those of the control, while the crumb remained compact and homogeneous. Overall, the incorporation of corn flour was associated with improved morphological characteristics and greater structural uniformity of the gluten-free cupcakes.

To quantify these effects, physicochemical properties were evaluated (Figure 2), while reference values for the control sample were as follows: mass loss 6.41 ± 0.04 %; dough expansion ratio 0.71 ± 0.01; moisture content 13.47 ± 0.06 %; specific volume 112.30 ± 1.50 mL/100 g.

One-way ANOVA confirmed that the flour ratio significantly affected all measured parameters ($p < 0.05$) (Table 2).

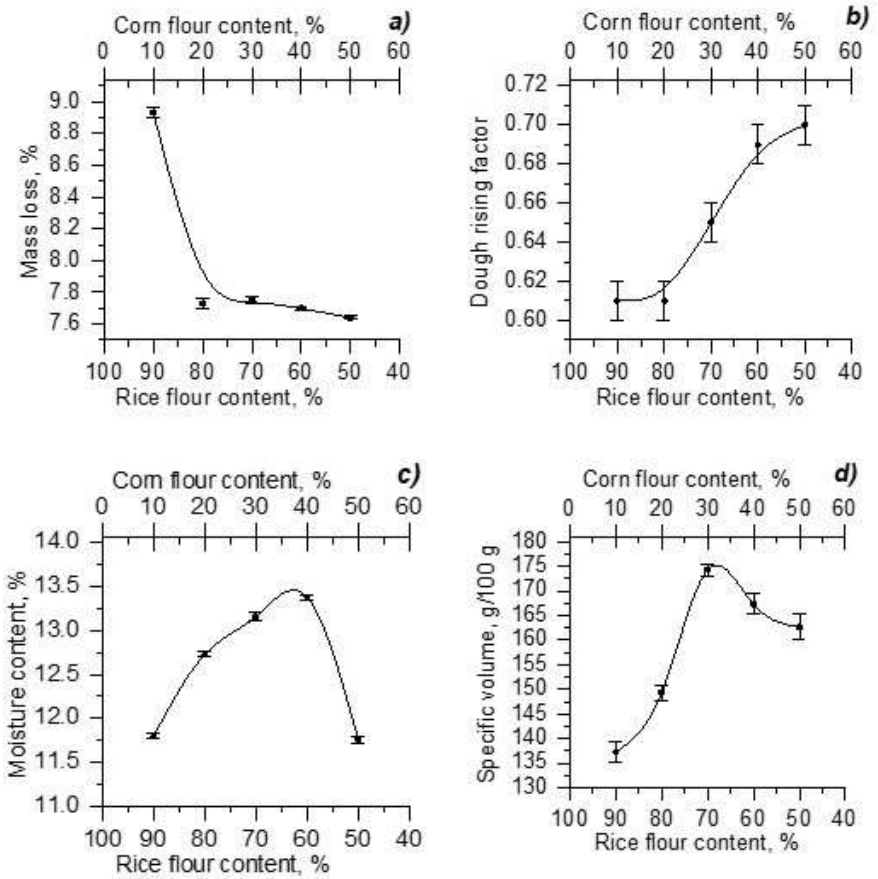

Figure 2. Effect of rice-to-corn flour ratio on physicochemical properties of gluten-free cupcakes: (a) baking loss; (b) dough expansion ratio; (c) moisture content; (d) specific volume

Table 2

Effect of rice-to-corn flour ratio on physicochemical properties of gluten-free cupcakes

Sample	Baking loss, %	Dough expansion ratio	Moisture content, %	Specific volume, mL/100 g
R90:C10	8.93±0.03[a]	0.61±0.01[a]	11.80±0.03[a]	137.33±2.08[a]
R80:C20	7.75±0.02[b]	0.61±0.01[a]	12.73±0.03[b]	149.33±1.53[b]
R70:C30	7.73±0.03[b]	0.65±0.01[b]	13.16±0.04[c]	162.67±2.52[c]
R60:C40	7.70±0.01[c]	0.69±0.01[c]	13.38±0.03[c]	167.33±2.08[d]
R50:C50	7.64±0.01[d]	0.70±0.01[c]	11.76±0.04[a]	174.33±1.15[e]

Note: means within the same column with different superscripts are significantly different at $p \leq 0.05$.

Tukey's HSD test revealed non-linear relationships, suggesting an optimal formulation rather than a monotonic trend. Baking loss decreased from 8.93% to 7.70% as the corn flour content increased from 10% to 40%, with a slight further reduction at 50% (Figure 2a). This reduction may be associated with the formation of a denser crust, limiting moisture diffusion during baking. The dough expansion ratio increased with increasing corn flour content, reaching 0.69 for samples R60:C40 and R50:C50, values close to the control (0.71) (Figure 2b). This behaviour is consistent with the improved morphology observed in Figure 1 and suggests enhanced gas retention within the batter matrix. Moisture content ranged from 11.83% to 13.38% in gluten-free samples, compared to 13.47% in the control (Figure 2c). These results indicate that appropriate rice–corn combinations can maintain moisture levels comparable to wheat-based formulations. The dependence of specific volume on flour ratio exhibited a non-linear trend (Figure 2d), with a maximum value observed for sample R70:C30 (175 mL/100 g). Notably, all gluten-free samples showed higher specific volume than the control (112 mL/100 g), indicating that rice–corn blends can form aerated structures despite the absence of gluten.

Sensory evaluation further supported these findings (Table 3, Figure 3).

Table 3

Sensory evaluation of cupcakes prepared with different rice–corn flour ratios

Sample	Attribute				
	Shape	Colour	Texture	Taste and odour	Crumb consistency
Control	8.3±0.48[a]	8.5±0.53[a]	8.4±0.52[a]	8.1±0.79[a]	8.2±0.63[a]
R90:C10	5.1±0.57[d]	7.5±0.53[c]	6.5±0.53[c]	5.4±0.52[d]	4.8±0.42[d]
R80:C20	5.4±0.52[d]	7.8±0.42[bc]	7.3±0.48[bc]	5.9±0.57[c]	5.7±0.48[c]
R70:C30	6.1±0.74[c]	7.8±0.42[bc]	7.4±0.52[b]	7.2±0.42[b]	6.9±0.57[b]
R60:C40	7.2±0.63[b]	8.4±0.52[a]	7.7±0.48[ab]	7.8±0.42[a]	7.4±0.52[ab]
R50:C50	7.7±0.48[ab]	8.3±0.42[a]	7.5±0.53[ab]	7.2±0.63[b]	7.2±0.63[b]

Note: means within the same column with different superscripts are significantly different at $p \leq 0.05$.

Significant differences among samples were confirmed by the Friedman–Nemenyi test ($p < 0.05$) (Table 4, Table 5).

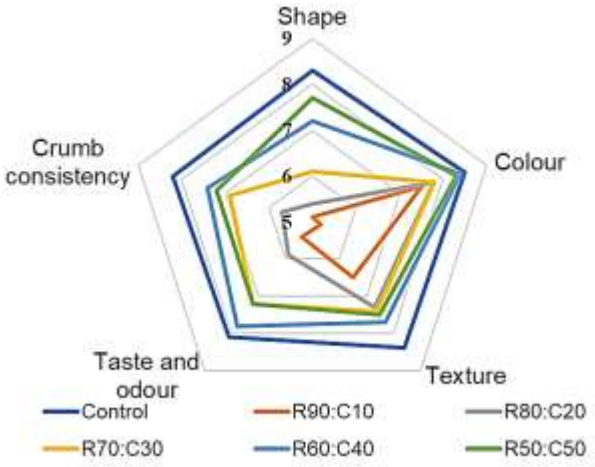

Figure 3. Sensory profiles of gluten-free cupcakes with different rice–corn flour ratios based on mean hedonic scores

Table 4

Sensory evaluation of cupcakes prepared with different rice–corn flour ratios

Sample	Attribute				
	Shape	Colour	Texture	Taste and odour	Crumb consistency
Control	8.3±0.48^{a}	8.5±0.53^{a}	8.4±0.52^{a}	8.1±0.79^{a}	8.2±0.63^{a}
R90:C10	5.1±0.57^{d}	7.5±0.53^{c}	6.5±0.53^{c}	5.4±0.52^{d}	4.8±0.42^{d}
R80:C20	5.4±0.52^{d}	7.8±0.42^{bc}	7.3±0.48^{bc}	5.9±0.57^{c}	5.7±0.48^{c}
R70:C30	6.1±0.74^{c}	7.8±0.42^{bc}	7.4±0.52^{b}	7.2±0.42^{b}	6.9±0.57^{b}
R60:C40	7.2±0.63^{b}	8.4±0.52^{a}	7.7±0.48^{ab}	7.8±0.42^{a}	7.4±0.52^{ab}
R50:C50	7.7±0.48^{ab}	8.3±0.42^{a}	7.5±0.53^{ab}	7.2±0.63^{b}	7.2±0.63^{b}

Note: means within the same column with different superscripts are significantly different at $p \leq 0.05$.

Table 5

Friedman test for sensory evaluation of gluten-free cupcakes with different rice and corn flour contents

Attribute	χ^2	p-value
Shape	47.48	< 0.001
Colour	20.89	< 0.001
Texture	36.38	< 0.001
Taste and odour	43.84	< 0.001
Crumb consistency	43.91	< 0.001

Different superscript letters within the same column indicate significant differences according to the Friedman-Nemenyi test ($p < 0.05$). The control sample achieved the highest scores across all attributes. Among gluten-free formulations, R90:C10 received the lowest scores, particularly for texture and taste, which is consistent with its poor structural characteristics. Increasing corn flour content led to progressive improvements in sensory

attributes related to structure and mouthfeel. Sample R60:C40 exhibited the most balanced sensory profile among gluten-free formulations, achieving high scores for colour, texture, and taste. These results agree with instrumental measurements, which indicated improved expansion and crumb uniformity at this ratio. In contrast, sample R50:C50 showed slightly lower taste scores, possibly due to a more pronounced corn flavour.

The results demonstrate that optimisation of the rice-to-corn flour ratio is critical for achieving desirable structural and sensory properties. Based on the combined physicochemical and sensory evaluation, the R60:C40 formulation was identified as the optimal composition. To further improve the texture of gluten-free cupcakes and approximate that of the wheat-based control, the incorporation of hydrocolloids was investigated in the subsequent stage.

Effect of individual hydrocolloids on the quality of gluten-free cupcakes

Hydrocolloids are widely used in gluten-free systems due to their ability to modify water distribution and stabilise structure-forming matrices. In the present study, the individual effects of psyllium and agar were evaluated using the previously selected R60:C40 flour formulation.

Psyllium was incorporated at 1, 3, and 5% (R60:C40+1% P, R60:C40+3% P, and R60:C40+5% P), while agar was added at 0.1% (R60:C40+0.1% A), as higher concentrations are known to induce excessive gel rigidity and negatively affect product quality (Bertasa et al., 2020; Mamat et al., 2014; Salehi, 2020). The physicochemical properties of the samples are summarised in Table 6.

Table 6

Physicochemical properties of gluten-free cupcakes containing individual hydrocolloids

Sample	Baking loss, %	Dough expansion ratio	Moisture content, %	Specific volume, mL/100 g
R60:C40	7.70±0.01^{a}	0.69±0.01^{a}	13.38±0.03^{a}	166.00±1.00^{a}
R60:C40 + 1% P	7.91±0.02^{b}	0.66±0.01^{b}	12.52±0.02^{b}	167.33±2.08^{ab}
R60:C40 + 3% P	8.02±0.02^{c}	0.65±0.02^{bc}	12.01±0.02^{c}	169.33±0.58^{b}
R60:C40 + 5% P	8.10±0.01^{d}	0.63±0.01^{c}	11.60±0.03^{d}	169.67±1.15^{b}
R60:C40 + 0.1% A	8.25±0.02^{e}	0.62±0.01^{c}	11.83±0.03^{c}	146.00±1.00^{c}

Note: means within the same column with different superscripts are significantly different at $p \leqslant 0.05$.

One-way ANOVA confirmed that hydrocolloid type and concentration significantly affected all measured parameters ($p < 0.05$). Tukey's HSD test indicated that psyllium concentration had a pronounced effect on baking loss and moisture content, whereas dough expansion ratio and specific volume exhibited non-linear responses. Increasing psyllium concentration from 1% to 5% resulted in a gradual increase in baking loss (7.91–8.10%) and a corresponding decrease in moisture content (12.52–11.60%). This behaviour can be attributed to the high water-binding capacity of psyllium, which promotes water immobilisation within the fibre network and reduces the amount of free water available during baking. The dough expansion ratio decreased from 0.66 to 0.63 as psyllium concentration increased, suggesting partial restriction of gas expansion due to matrix densification. However, specific volume increased at higher psyllium levels (3–5%), reaching approximately 169 mL/100 g. This indicates that, despite reduced expansion, the stabilised structure effectively retains gas within the crumb matrix. In contrast, agar addition

resulted in the highest baking loss (8.25%), the lowest expansion ratio (0.62), and a substantial decrease in specific volume (146 mL/100 g). These results suggest the formation of a rigid gel network that limits gas cell growth and reduces crumb aeration.

Sensory evaluation results are presented in Table 7, Table 8, and Figure 4. Significant differences among samples were confirmed by the Friedman–Nemenyi test ($p < 0.05$), primarily for structure-related attributes.

Table 7

Sensory evaluation of gluten-free cupcakes containing individual hydrocolloids

Sample	Shape	Colour	Texture	Taste and odour	Crumb consistency
R60:C40	7.2±0.63^{c}	8.3±0.48	7.5±0.53	7.8±0.42	7.4±0.52^{b}
R60:C40 + 1% P	7.3±0.48^{c}	8.2±0.42	7.5±0.53	7.8±0.42	7.4±0.52 ^{b}
R60:C40 + 3% P	7.8±0.63^{b}	8.2±0.42	7.6±0.52	7.9±0.32	7.6±0.52 ^{ab}
R60:C40 + 5% P	8.1±0.57^{a}	8.1±0.32	7.6±0.70	7.9±0.32	7.8±0.42^{a}
R60:C40 + 0.1% A	7.8±0.42^{b}	8.3±0.48	7.8±0.63	7.8±0.42	7.9±0.57^{a}

Note: means within the same column with different superscripts are significantly different at $p \leq 0.05$.

Table 8

Friedman test for sensory evaluation of gluten-free cupcakes with different rice and corn flour contents

Attribute	χ^2	p-value
Shape	47.48	< 0.001
Colour	20.89	< 0.001
Texture	36.38	< 0.001
Taste and odour	43.84	< 0.001
Crumb consistency	43.91	< 0.001

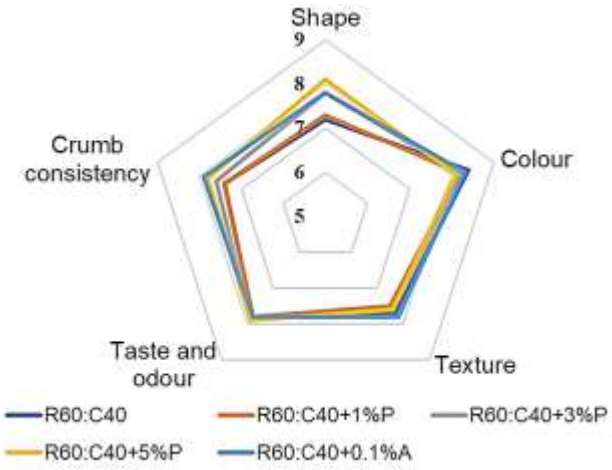

Figure 4. Sensory profiles of gluten-free cupcakes containing individual hydrocolloids based on mean hedonic scores

Psyllium incorporation led to progressive improvements in shape and crumb consistency. The sample containing 5% psyllium achieved the highest scores for these attributes, while colour and flavour were not significantly affected ($p > 0.05$). In contrast, agar-containing samples exhibited comparable structural scores but tended to produce a firmer crumb. Visual assessment (Figure 5) supported these findings. Samples R60:C40+5%P and R60:C40+0.1%A exhibited regular shape, smooth surfaces, and a uniform crumb structure. However, the psyllium-enriched sample showed a slightly drier and more crumbly texture, consistent with its lower moisture content.



Figure 5. External appearance (top) and cross-sections (bottom) of gluten-free cupcakes containing individual hydrocolloids:
(a) wheat-based control; (b) gluten-free R60:C40; (c) R60:C40 + 5% psyllium;
(d) R60:C40 + 0.1% agar; (e) gluten-free R60:C40 containing 5% psyllium and 0.1% agar

Overall, the results demonstrate distinct functional roles for the hydrocolloids investigated. Psyllium enhances gas retention and contributes to the formation of a stable, aerated structure, whereas agar promotes matrix rigidity and limits expansion. Based on the combined physicochemical and sensory evaluation, 5% psyllium was identified as the most effective individual hydrocolloid level. Given these complementary effects, the combined application of psyllium and agar was further investigated to evaluate potential synergistic interactions.

Effect of hydrocolloid combination on the quality of gluten-free cupcakes

All results should be presented, discussed and compared with previously published data. Do not repeat parts of the introduction and description of materials and methods in this section. To evaluate the combined effect of hydrocolloids, a composite system consisting of 5% psyllium and 0.1% agar was incorporated into the optimised R60:C40 formulation (R60:C40+5% P+0.1% A), based on the results obtained for individual hydrocolloids.

The external appearance and crumb structure of the optimised gluten-free cupcake were compared with those of the wheat-based control and the hydrocolloid-free sample (Figure 5). The hydrocolloid-containing cupcake exhibited a regular domed shape, smooth surfaces without structural defects, and a homogeneous crumb with fine pores, indicating effective stabilisation of the gluten-free matrix. Physicochemical properties are summarised in Table 9 and Table 10.

Table 9

Physicochemical properties of control and gluten-free cupcakes with a hydrocolloid combination

Sample	Baking loss, %	Dough expansion ratio	Moisture content, %	Specific volume, mL/100 g	Alkalinity, °
Control	6.41±0.04	0.71±0.01	13.47±0.06	112.30±1.50	1.80±0.01
R60:C40	7.70±0.01	0.69±0.01	13.38±0.03	166.00±1.00	1.80±0.01
R60:C40 + 5%P + 0.1%A	8.88±0.02	0.72±0.02	13.86±0.02	149.70±0.60	1.80±0.01

P – psyllium; A – agar. Values are expressed as mean±SD (n = 3).

Table 10

Results of one-way ANOVA for the effect of psyllium concentration on quality parameters of cakes

Parameter	F-value (df = 3, 8)	p-value
Weight loss, %	425.9	< 0.001
Moisture, %	2406	< 0.001
Dough rise coefficient	23.56	< 0.001
Specific volume, cm^3/100 g	5.13	0.028

Replacing wheat flour with a rice-corn mixture increased the specific volume from 112.3 to 166.0 mL/100 g. The addition of the hydrocolloid combination reduced this value to 149.7 mL/100 g, reflecting the formation of a more compact and uniform crumb structure. Despite this decrease, the specific volume remained substantially higher than that of the control. The dough expansion ratio (0.72) was comparable to that of the control (0.71), indicating efficient gas retention during baking. Moisture content increased to 13.86%, which can be attributed to the high water-binding capacity of both hydrocolloids. Alkalinity remained unchanged, confirming that hydrocolloid incorporation did not interfere with the leavening system. Comparison with formulations containing individual hydrocolloids revealed that the combined system provided improved moisture retention and a more balanced structure than either psyllium or agar alone. This behaviour indicates a synergistic interaction, in which psyllium contributes to water retention and gas stabilisation, while agar reinforces the structural network and limits excessive expansion.

Sensory evaluation results are presented in Table 11, Table 12, and Figure 6.

Table 11

Sensory evaluation of control and gluten-free cupcakes containing a hydrocolloid combination

Sample	Shape	Colour	Texture	Taste and odour	Crumb consistency
Control	8.3±0.48	8.5±0.53	8.4±0.52	8.1±0.74	8.2±0.63
R60:C40	7.2±0.63	8.3±0.48	7.5±0.53	7.8±0.42	7.4±0.52
R60:C40+5%P+0.1%A	8.2±0.42	8.1±0.32	8.2±0.63	8.0±0.67	8.1±0.57

P – psyllium; A – agar. Values are expressed as mean±SD.

Friedman test revealed significant differences for shape, texture, and crumb consistency ($p < 0.05$), while colour, taste and odour did not differ significantly ($p > 0.05$)

Table 12

Friedman test for sensory evaluation of gluten-free cupcakes based on rice and corn flour with the different contents

Attribute	χ^2	p-value	
Shape	17.43	< 0.001	significant
Surface	4.80	0.091	not significant
Colour	12.50	0.002	significant
Crumb appearance	1.04	0.595	not significant
Taste & odour	8.72	0.013	significant

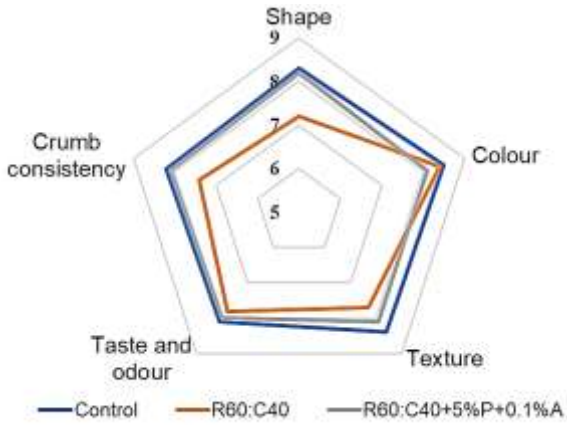

Figure 6. Sensory profiles of gluten-free cupcakes containing a psyllium-agar hydrocolloid combination based on mean hedonic scores

Significant differences among samples were observed for shape, texture, and crumb consistency ($p < 0.05$), whereas colour and flavour were not significantly affected ($p > 0.05$). The composite formulation achieved sensory scores comparable to those of the wheat-based control and higher than those of the hydrocolloid-free gluten-free sample. Improvement was primarily associated with texture-related attributes, reflecting enhanced crumb uniformity and structural stability. Although the optimised sample exhibited a slightly lower specific volume than the hydrocolloid-free formulation, panellists preferred its more homogeneous and cohesive crumb structure. This suggests that perceived textural quality is more strongly influenced by crumb uniformity than by maximum volume alone. The combined use of psyllium and agar effectively compensated for the structural limitations of the gluten-free system. The synergistic action of these hydrocolloids resulted in physicochemical and sensory properties approaching those of the wheat-based control, demonstrating the potential of this approach for improving gluten-free bakery products.

Conclusions

The results of this study demonstrate that the rice-to-corn flour ratio is a key factor influencing the structural and quality characteristics of gluten-free cupcakes. Among the investigated formulations, a rice-to-corn flour ratio of 60:40 provided the most favourable

balance between physicochemical properties and sensory acceptability and was therefore selected as the optimal base formulation. Psyllium was identified as an effective structure-forming agent in the gluten-free formulations. At concentrations of 3–5% (flour basis), it enhanced crumb aeration and increased specific volume, whereas agar used individually promoted matrix densification and restricted gas expansion, highlighting the distinct functional roles of the investigated hydrocolloids. The combined application of psyllium (5%) and agar (0.1%) resulted in improved moisture retention, dough expansion comparable to that of the wheat-based control, and the formation of a homogeneous, fine-porous crumb structure. Sensory evaluation confirmed that this hydrocolloid combination significantly improved structure-related attributes, including shape, texture, and crumb consistency, while maintaining flavour acceptability comparable to that of the control. Overall, the psyllium–agar combination improved the structural characteristics of the rice–corn gluten-free formulation and represents a promising approach for developing gluten-free cupcakes with enhanced structural stability and sensory quality.

References

Banu, I., & Aprodu, I. (2024). Assessment of the performance of oat flakes and pumpkin seed powders in gluten-free dough and bread based on rice flour. *Applied Sciences, 14*(8), 3479. https://doi.org/10.3390/app14083479

Bertasa, M., Dodero, A., Alloisio, M., Vicini, S., Riedo, C., Sansonetti, A., Scalarone, D., & Castellano, M. (2020). Agar gel strength: A correlation study between chemical composition and rheological properties. *European Polymer Journal, 123*, 109442. https://doi.org/10.1016/j.eurpolymj.2019.109442

Capriles, V. D., de Aguiar, E. V., Dos Santos, F. G., Aguilar Fernández, M. E., de Melo, B. G., Tagliapietra, B. L., Scarton, M., Silva Clerici, M. T. P., & Conti, A. C. (2023). Current status and future prospects of sensory and consumer research approaches to gluten-free bakery and pasta products. *Food Research International, 173*, 113389. https://doi.org/10.1016/j.foodres.2023.113389

Celiac Disease Foundation. (2020). *Incidence of celiac disease steadily increasing.* https://celiac.org/about-the-foundation/featured-news/2020/02/incidence-of-celiac-disease-steadily-increasing/

Chiș, M. S., Pop, A., Păucean, A., Socaci, S. A., Alexa, E., Man, S. M., Bota, M., & Muste, S. (2020). Fatty acids, volatile and sensory profile of multigrain biscuits enriched with spent malt rootlets. *Molecules, 25*, 442. https://doi.org/10.3390/molecules25030442

Coronel, E. B., Ixtaina, V. Y., & Capitani, M. I. (2025). Nutritional and functional characterization of chia expeller and gluten-free flours as ingredients for premixes. *Plant Foods for Human Nutrition, 80*(1), 43. https://doi.org/10.1007/s11130-025-01297-9

Costa, I. M., Pêgo e Silva, L. M., de Souza Cardoso, A., Abreu Silva, A. N., Araújo da Silva, N. H., da Veiga Correia, V. T., dos Santos, A. N., Barbosa, C. D., da Silva, W. A., de Carvalho, C. W. P., Trombete, F. M., & Fante, C. A. (2024). Impact of fiber addition on quality and consumer perception of whole-grain cakes produced with extruded pearl millet (*Pennisetum glaucum*) flour. *Journal of Cereal Science, 120*, 104039. https://doi.org/10.1016/j.jcs.2024.104039

Culetu, A., Susman, I. E., Duta, D. E., & Belc, N. (2021). Nutritional and functional properties of gluten-free flours. *Applied Sciences, 11*, 6283. https://doi.org/10.3390/app11146283

Demirkesen, I., & Ozkaya, B. (2022). Recent strategies for tackling the problems in gluten-free diet and products. *Critical Reviews in Food Science and Nutrition, 62*(3), 571–597. https://doi.org/10.1080/10408398.2020.1823814

Drabińska, N., Ciska, E., Szmatowicz, B., & Krupa-Kozak, U. (2018). Broccoli by-products improve the nutraceutical potential of gluten-free mini sponge cakes. *Food Chemistry, 267*, 170–177. https://doi.org/10.1016/j.foodchem.2017.08.119

Franco, M., & Gómez, M. (2022). Effect of psyllium on physical properties, composition and acceptability of whole grain breads. *Foods, 11*, 1685. https://doi.org/10.3390/foods11121685

Franco, M., Spotti, M. J., Gómez, M., & Martinez, M. M. (2024). Understanding the influence of the arabinoxylan-rich psyllium (*Plantago ovata*) husk on dough elasticity and bread staling. *Food Hydrocolloids, 154*, 110099. https://doi.org/10.1016/j.foodhyd.2024.110099

Fratelli, C., Muniz, D. G., Santos, F. G., & Capriles, V. D. (2018). Modelling the effects of psyllium and water in gluten-free bread. *Journal of Functional Foods, 42*, 339–345. https://doi.org/10.1016/j.jff.2018.01.015

Gruppi, A., Giuberti, G., Duserm Garrido, G., & Spigno, G. (2024). Effect of different fibre addition on cookie dough and texture. *Food Science and Technology International, 30*(7), 614–622. https://doi.org/10.1177/10820132231162475

Hu, X., Wang, Y., Qiu, D., & He, L. (2024). Comparison of prolamins from different cereals based on structure and functionality. *Journal of Cereal Science, 120*, 104052. https://doi.org/10.1016/j.jcs.2024.104052

Ishaq, A., Nadeem, M., Ahmad, R., Ahmed, Z., & Khalid, N. (2024). Recent advances in applications of marine hydrocolloids for improving bread quality. *Food Hydrocolloids, 148*, 109424. https://doi.org/10.1016/j.foodhyd.2023.109424

Jabeen, S., Khan, A. U., Ahmad, W., Ahmed, M.-ud-D., Ali, M. A., Rashid, S., Rashid, A., & Sharifi-Rad, J. (2022). Development of gluten-free cupcakes enriched with almond, flaxseed, and chickpea flours. *Journal of Food Quality*, 2022, 4049905. https://doi.org/10.1155/2022/4049905

Jalali, M., Sheikholeslami, Z., Elhamirad, A. H., Haddad, M. H., Khodaparast, M. H. H. & Karimi, M. (2020). The effect of ultrasound process and pre-gelatinization of corn flour on gluten-free pan bread. *Journal of Food Science and Technology, 57*(3), 993–1002. https://doi.org/10.1007/s13197-019-04132-7

Jukić, M., Koceva Komlenić, D., Nakov, G., Begić, M., Keresturi, S., & Lukinac, J. (2024). Effects of the addition of xanthan gum and rice flour to maize starch on quality of gluten-free biscuit. *Ukrainian Food Journal, 13*(1), 124–142. https://doi.org/10.24263/2304-974X-2024-13-1-9

Khan, R., Shehzadi, K., Bacha, U., Afzal, M. N., Tanweer, A., Nasim, M., Khan, S., Mohtarami, F., Rashidi, Z., & Pirsa, S. (2021). Physico-functional, nutritional and sensorial features of psyllium husk enriched gluten-free oat cookies. *Nurture, 15*(1), 1–8. https://doi.org/10.55951/nurture.v15i1.1

Khutsidze, T., Pruidze, E., Silagadze, M., Dzneladze, E., Pkhakadze, G., & Berulava, I. (2024). A flour composite mixture for gluten-free confectionery. *Potravinarstvo Slovak Journal of Food Sciences, 18*, 453–467. https://doi.org/10.5219/1958

Mamat, H., Matanjun, P., Ibrahim, S., Amin, S. F. M., Hamid, M. A., & Rameli, A. S. (2014). The effect of seaweed composite flour on the textural properties of dough and bread. *Journal of Applied Phycology, 26*(2), 1057–1062. https://doi.org/10.1007/S10811-013-0082-8

Manik, L. C. M., & Nur, M. (2021). The recent development of gluten-free bread quality using hydrocolloids. *IOP Conference Series: Earth and Environmental Science, 733*, 012101. https://doi.org/10.1088/1755-1315/733/1/012101

Mark, Y., & Watson, S. (2024). Market overview of health and wellness food products. In X. Du & J. Yang (Eds.), *Flavor-associated applications in health and wellness food products* (pp. 3–19). Springer. https://doi.org/10.1007/978-3-031-51808-9

Mohtarami, F., Rashidi, Z., & Pirsa, S. (2022). Extraction of flaxseed and *Plantago psyllium* mucilage. *Journal of Food Processing and Preservation, 46*(11), e16964. https://doi.org/10.1111/jfpp.16964

Franco, E. A. N., Sanches-Silva, A., Ribeiro-Santos, R., & de Melo, N. R. (2020). Psyllium (*Plantago ovata* Forsk). *Trends in Food Science & Technology, 96*, 166–175. https://doi.org/10.1016/j.tifs.2019.12.006

Norton, V., Lignou, S., & Methven, L. (2022). Promoting protein intake in an ageing population. *Nutrients, 14*, 5083. https://doi.org/10.3390/nu14235083

Ojo, O. A., Ewetola, D. O., Oke, E. K., Oluwayemisi, O. E., Onipede, A. J., & Obadina, A. O. (2026). Properties of extruded breakfast cereals made from fermented sorghum flour and tigernut pomace

blends. *Ukrainian Food Journal, 15*(1), 115–130. https://doi.org/10.24263/2304-974X-2026-15-1-10

Salehi, F. (2020). Effect of common and new gums on bakery products. *Journal of Texture Studies, 51*(2), 361–370. https://doi.org/10.1111/jtxs.12482

Shevchenko, A. (2022). Artichoke powder and buckwheat bran in diabetic bakery products. In O. Paredes-López, O. Shevchenko, V. Stabnikov, & V. Ivanov (Eds.), *Bioenhancement and fortification of foods for a healthy diet* (pp. 115–134). CRC Press. https://doi.org/10.1201/9781003225287-8

Slashcheva, A., Fedorova, D., & Lanska, V. (2022). Problems and prospects of gluten-free bakery products in Ukraine. *SWorldJournal*, 15-01, 8–13. https://doi.org/10.30888/2663-5712.2022-15-01-018

Stabnikova, O., Marinin, A., & Stabnikov, V. (2021). Main trends in application of novel natural additives for food production. *Ukrainian Food Journal, 10*(3), 524–551. https://doi.org/10.24263/2304-974X-2021-10-3-8

Stoican, E. C., Moșoiu, C. E., & Israel-Roming, F. (2021). Gluten-free products and possibilities of new formulation. *Scientific Bulletin, Series F, Biotechnologies, 25*(1), 76–86.

Šmídová, Z., & Rysová, J. (2022). Gluten-free bread and bakery products technology. *Foods, 11*, 480. https://doi.org/10.3390/foods11030480

Thakur, V. K., & Thakur, M. K. (2014). Recent trends in hydrogels based on psyllium polysaccharide. *Journal of Cleaner Production, 82*, 1–15. https://doi.org/10.1016/j.jclepro.2014.06.066

Thakur, K., Kapoor, S., Gupta, M., Khatkar, S. K., Bala, M., & Mahajan, B. V. C. (2024). Tomato seed fractions enriched muffins. *International Journal of Food Science and Technology, 59*(10), 7240–7249. https://doi.org/10.1111/ijfs.17449

Ungureanu-Iuga, M., & Cobuz, C. (2025). Effects of whey and grape peels on pasta physical and sensory properties. *Ukrainian Journal of Food Science, 13*(1), 5–16. https://doi.org/10.24263/2310-1008-2025-13-1-3

Woomer, J. S., & Adedeji, A. A. (2021). Current applications of gluten-free grains: A review. *Critical Reviews in Food Science and Nutrition, 61*(1), 14–24. https://doi.org/10.1080/10408398.2020.1713724

Xu, J., Zhang, Y., Wang, W., & Li, Y. (2020). Advanced properties of gluten-free cookies, cakes, and crackers. *Trends in Food Science & Technology, 103*, 200–213. https://doi.org/10.1016/j.tifs.2020.07.017

Yeganeh, P., Emamifar, A., Karami, M., & Salehi, F. (2024). Investigation on replacing egg with soy flour and psyllium seed gum. *Journal of Food Science and Technology (Iran), 20*(143), 62–77. https://doi.org/10.22034/FSCT.20.143.62

Cite:

Saleba, L., Ratsuk, M., Yurova, T., Kalinsky, E., & Semeshko, O. (2026). Technological role of psyllium-agar hydrocolloid system in improving the structure and sensory properties of gluten-free rice-corn cupcakes. *Ukrainian Food Journal, 15*(3), 716–731. https://doi.org/10.24263/2304-974X-2026-15-3-8

Bioactive compounds and antinutritional factors in olive pomace

Esraa Shams[1], Mahmoud Gouda[1], Abd-Elbaset Salama[1], Galal Magdy[1,2]

1 – Kafrelsheikh University, Kafrelsheikh, Egypt
2 – Mansoura National University, Gamasa, Egypt

Keywords:

Olive pomace
Selenium
Fortification
Bioactive
Synergistic effect
Antioxidant
HPLC

Article history:

Received 19.03.2026
Received in revised form 10.06.2026
Accepted 30.06.2026

Corresponding author:

Esraa Shams
E-mail: esraa.s.shams@gmail.com

DOI:
10.24263/2304-974X-2026-15-3-9

Abstract

Introduction. This study aimed to evaluate the nutritional composition, phenolic profile, antioxidant activity, and the potential synergistic effect of sodium selenite (SS) fortification with phenolic compounds in Manzanillo olive pomace (OP).

Materials and methods. Total phenolic content and total flavonoid content were determined spectrophotometrically before and after fortification with SS. Individual phenolic and flavonoid compounds were identified and quantified by HPLC. Antioxidant activity was evaluated using a radical scavenging activity (RSA) assay.

Results and discussion. Crude Manzanillo OP had a low moisture content (10.17%), which may contribute to improved storage stability by limiting microbial growth and enzymatic degradation. It also had a high crude fiber content (35.71%) and was rich in essential minerals, particularly potassium (1302.27 mg/100 g), as well as calcium, phosphorus, sodium, magnesium, iron, copper, zinc, and manganese. Extraction yield and phenolic content did not show the same trend.

Sequential solvent extraction (SSE) and methanol extraction provided the highest yields (85.6% and 81.20%, respectively), whereas methanol and ethanol extracts had the highest phenolic contents (49.93 and 47.92 mg GAE/g, respectively) and flavonoid contents (30.42 and 27.15 mg QE/g, respectively). Phytic acid content also varied depending on the extraction method, with the highest values observed for green extraction (0.53%) and methanol extraction (0.49%). The 70% methanol extract showed the strongest antioxidant activity (RSA = 55.37%; IC_{50} = 0.13 mg/mL). Sodium selenite fortification (0–55 μg) significantly increased phenolic and flavonoid contents and antioxidant activity in a concentration-dependent manner across the extracts. In the methanol extract, phenolic content increased to 70.48 mg GAE/g, flavonoid content to 41.22 mg QE/g, and antioxidant activity to RSA = 78.15% and IC_{50} = 0.09 mg/mL. These results suggest a potential synergistic effect between phenolic compounds and selenium.

HPLC-UV analysis at 280 and 330 nm confirmed that quinic acid, oleuropein, and related secoiridoids were among the predominant phenolic compounds, consistent with the observed antioxidant activity. Overall, the findings support the potential use of Manzanillo olive pomace as a low-cost source of natural phenolic antioxidants, while selenium fortification may further enhance its functional and nutraceutical value.

Conclusions. The combined effects of phenolic compounds and sodium selenite fortification indicate that olive pomace extracts have potential for use in the development of functional foods and dietary supplements.

Introduction

The olive tree, *Olea europaea* L., is an evergreen member of the Oleaceae family that has been cultivated for its fruit and ornamental value in the Mediterranean region since at least 3000 BCE (Leouifoudi et al., 2015). The Manzanillo cultivar (*Olea europaea* L. cv. Manzanillo) is well established and widely cultivated in Egypt (Taha & Khalifa, 2024).

Despite the economic and nutritional benefits of olive oil, vast quantities of waste are generated during olive oil production (Selim et al., 2022). The utilization of olive wastes and by-products has received increasing attention because they are rich in bioactive compounds that can improve packaging properties and enhance the functionality and shelf life of foods (Stempfle et al., 2021). Moreover, their valorisation is consistent with current efforts to convert food processing waste into value-added products within the framework of a circular bioeconomy (Stabnikova et al., 2023a, b). Among these by-products, olive pomace (OP) consists of olive skin, stones, pulp, and kernels. This residue accounts for 78–83% w/w of the total olive weight processed in the mill (Akay et al., 2015). It consists of a lignocellulosic matrix, phenolic compounds, uronic acids, fatty residues, and antioxidant components such as polyphenols and carotenoids (Selim et al., 2022).

The total phenolic content (TPC) in olive pomace can vary widely, but it often represents 2% to 4% of the pomace's dry weight (Cioffi et al., 2010). Approximately 98% of the phenolic compounds present in olive fruits are retained in OP, with hydroxytyrosol and comselogoside reported as the two major polyphenols (Munekata et al., 2020).

The total flavonoid content (TFC) of olive pomace extracts (OPEs) was 48.32 ± 0.50 and 82.68 ± 0.71 mg/g in autumn and spring, respectively (Moustafa et al., 2022). Ethanol extracts of olive pomace exhibited antioxidant activity of 93.4%, compared with 80.4% for the reference antioxidant α-tocopherol (Halwaz et al., 2018).

Selenium is an essential mineral naturally present in foods and also available through fortified foods and dietary supplements. It is a component of 25 selenoproteins (Gladyshev et al., 2016). The Recommended Dietary Allowance (RDA) for selenium is 30 μg/day for children aged 4–8 years, 40 μg/day for those aged 9–13 years, and 55 μg/day for individuals aged 14 years and older (Institute of Medicine (US) Panel on Dietary Antioxidants and Related Compounds, 2000).

Although selenium nanoparticles (SeNPs) produced using bacteria and yeasts have generally shown lower toxicity than inorganic selenium forms (Skrotska et al., 2025; Stabnikova et al., 2023c), their use in food applications remains challenging because of the lack of standardized production methods and insufficient characterization of their physicochemical properties. Moreover, studies in laboratory rodents have reported adverse effects of SeNPs, including disturbances in lipid, fatty acid, protein, and carbohydrate metabolism, as well as intestinal and blood alterations (Benko et al., 2012; Hadrup et al., 2016, 2019; He et al., 2014; Urbankova et al., 2021). SeNPs may also cross the blood-brain barrier (Lesnichaya et al., 2020). These findings highlight the need for further safety assessment before SeNPs can be considered for food and nutraceutical applications.

Therefore, sodium selenite (SS), a well-characterized inorganic selenium source, was selected for selenium fortification in the present study. Its addition requires careful control because excessive selenium intake may cause adverse effects (Bai et al., 2024). Moreover, sodium selenite differs from some organic selenium forms in terms of absorption, metabolism, and retention, which should be considered when developing selenium-fortified foods (Thomson, 2003). The amount added should be adjusted to provide an adequate selenium intake while minimizing the risk of excessive exposure.

Accordingly, the present study aimed to fortify olive pomace extract (OPE) with sodium selenite (SS) and evaluate the effects of SS addition on the phenolic content, flavonoid content, and antioxidant activity of the extract. This approach combines the bioactive compounds of olive pomace with an inorganic selenium source and explores the potential of selenium-fortified OPE as a functional ingredient for value-added food products.

Materials and methods

Materials

Olive pomace (OP) was transported directly in paper bags to the Food Technology Laboratory, Department of Food Sciences, Faculty of Agriculture, Kafrelsheikh University. The samples were dried in an electric air oven at 50 °C for 24 h and then ground to pass through a 60-mesh sieve. The resulting OP powder was stored in airtight glass jars at 4 °C until further use.

All chemicals and reagents used in this study were of analytical grade. Ethanol, methanol, n-hexane, chloroform, ethyl acetate, sodium selenite, Folin–Ciocalteu reagent, aluminum chloride, and ABTS, as well as acetonitrile, acetic acid, and all HPLC standards, were purchased from Al Ghomhorya for Chemicals (Tanta, Egypt).

Methods

Proximate chemical composition of crude Manzanillo olive pomace

The proximate composition of OP was analyzed according to AOAC (2022). Moisture content was measured by oven drying at 105 °C, crude protein by the Micro-Kjeldahl method using a nitrogen conversion factor of 6.25, lipids by Soxhlet extraction with petroleum ether (40–60 °C), ash by incineration in a muffle furnace at 550 °C, and crude fiber by acid–alkali digestion.

Carbohydrate content was calculated by difference, and available carbohydrates were calculated as total carbohydrates minus crude fiber.

Minerals content in crude Manzanillo olive pomace

The ash obtained from OP was dissolved in hydrochloric acid (1 mL concentrated HCl diluted to 100 mL with distilled water). Sodium and potassium were determined by flame photometry according to Hesse (1971), while magnesium, calcium, copper, zinc, manganese, and iron were analysed by atomic absorption spectrometry (AAS) according to Cottenie et al. (1982).

Extraction of bioactive compounds from Manzanillo olive pomace

Extraction by soaking. OP was extracted separately with 70% methanol, 70% ethanol, and 70% chloroform at a solid-to-liquid ratio of 1:10 (w/v) for 24 h at room temperature with occasional shaking (Tibaoui et al., 2023).

Green extraction (GE). Microwave-assisted extraction was performed using distilled water as a green solvent at a solid-to-liquid ratio of 1:10 (w/v) (Louis et al., 2025).

Sequential solvent extraction (SSE). Dried OP powder was subjected to sequential maceration extraction at a solid-to-liquid ratio of 1:15 (w/v) for 24 h per cycle at 25 °C and 150 rpm. Extraction was performed over five cycles using solvents of increasing polarity in the following order: n-hexane, chloroform, ethyl acetate, ethanol, and methanol. The filtrates obtained with each solvent were combined after re-extraction of the residue (Tibaoui et al., 2023). The extracts were filtered, concentrated under reduced pressure using a rotary evaporator, and stored until analysis (Nakra et al., 2025; Radzi et al., 2022).

Preparation of sodium selenite-enriched olive pomace extracts

The selenium fortification levels were selected based on the recommended dietary allowance (RDA) for selenium. SS-enriched OPE was prepared at three concentrations, designated OPE+SS1, OPE+SS2, and OPE+SS3, providing approximately 30, 40, and 55 μg of selenium, respectively. Three replicates were prepared for each treatment.

Consumption of 100 g of a product fortified with OPE+SS1, OPE+SS2, or OPE+SS3 may contribute substantially to meeting the daily selenium requirement, which ranges from 30 to 55 μg/day depending on age. Selenium is also obtained from other dietary sources and should therefore be considered as part of the total daily intake. The tolerable upper intake level for selenium is 400 μg/day for adults (Turck et al., 2023).

Phytic acid as an antinutritional factor in olive pomace extracts

Phytic acid was determined according to Haug and Lantzsch (1983). One gram of dried OPE was extracted with 50 mL of 0.2 N HCl. An aliquot (0.5 mL) was mixed with 1 mL of ferric ammonium sulfate and boiled for 30 min. After cooling, 2 mL of 2,2′-bipyridine–thioglycolic acid reagent was added. Absorbance was measured at 519 nm, and phytic acid content was calculated using a standard curve prepared over the range of 1–50 mg.

Total phenolic content, total flavonoid content, and antioxidant activity in olive pomace extracts

The total phenolic content (TPC) and total flavonoid content (TFC) of OPE were determined colorimetrically using the Folin–Ciocalteu method (Lamuela-Raventós, 2017) and aluminium chloride method (AOAC, 2022), respectively.

Antioxidant activity was assessed using the 2,2′-azino-bis(3-ethylbenzothiazoline-6-sulfonic acid) (ABTS) radical scavenging assay (Re et al., 1999) with a UV–Vis spectrophotometer (Shimadzu UV-1800, Shimadzu, Kyoto, Japan). The results were expressed as radical scavenging activity (RSA) and IC_{50}, defined as the concentration required to scavenge 50% of free radicals.

Identification and quantification of phenolic and flavonoid compounds in olive pomace extracts using HPLC

Phenolic compounds in OPE were identified and quantified by HPLC-DAD. Analyses were performed using an Agilent 1200 series HPLC system equipped with a quaternary pump, vacuum degasser, and UV-VIS detector. An aliquot of 5 μL of OPE was injected onto a C18 column (250 mm × 4.6 mm i.d.). Separation was performed using a gradient of solvent A (8% acetic acid) and solvent B (acetonitrile) at a flow rate of 1 mL/min and a column temperature of 35 °C. Detection was performed at 280 and 330 nm. Identification was based on comparison with reference standards, and the identified compounds were quantified using calibration curves generated from the corresponding standards (Brown et al., 2011).

Statistical analysis

Data are presented as mean ± standard deviation (SD), except for IC50 values, which are presented as mean ± standard error of the mean (SEM). One-way ANOVA was used for comparisons involving a single factor, while two-way ANOVA was used to evaluate the effects of two factors and their interaction. Tukey's honestly significant difference (HSD) test was used for post hoc comparisons. Differences among means were considered statistically significant at $p \leq 0.05$. All statistical analyses were performed using SPSS version 29.0.1.0 (IBM Corp., Armonk, NY, USA).

Results and discussion

Chemical composition of crude Manzanillo olive pomace

Table 1 shows the proximate chemical composition and mineral content of crude Manzanillo olive pomace.

Table 1

Chemical composition of crude olive pomace

Components, %		Minerals, mg/100 g DW	
Moisture	10.17±0.05	Sodium (Na)	222.81±0.07
Fat	16.32±0.06	Calcium (Ca)	132.78±0.15
Crude protein	7.57±0.03	Potassium (K)	1302.27±0.35
Ash	1.86±0.04	Phosphorus (P)	89.36±0.09
Total carbohydrates	74.25±0.13	Magnesium (Mg)	76.68±0.17
Crude fiber	35.71±0.03	Iron (Fe)	17.91±0.05
Available carbohydrates	38.55±0.16	Copper (Cu)	0.53±0.34
		Zinc (Zn)	0.97±0.11
		Manganese (Mn)	0.49±0.16

Note: Mean ± SD (n = 3) is shown

The moisture content was 10.17%, which was slightly higher than the value of 10.07% reported by Trindade et al. (2023). The fat content was 16.32%, which falls within the range of 15.61–21.34% reported by Ribeiro et al. (2020). The crude protein content was 7.57%, which falls within the range of 4.25–17% reported by Aissaoui et al. (2023) and Lammi et al. (2018). The ash content was 1.86%, within the range of 0.5–6% reported by Tawarah (2014). The total carbohydrate content was 74.25%, which was lower than the value of 77.91% reported by Meguid et al. (2025). The crude fiber content was 35.71%, within the range of 33–40.72% reported by Ramachandran et al. (2007), while the available carbohydrate content was 38.55%.

The results indicate that crude OP has a relatively low moisture content, which may contribute to its storage stability. Its high crude fiber and total carbohydrate contents indicate that OP can serve as a source of dietary fiber, while its fat and crude protein contents contribute to its nutritional value.

Table 1 also presents the mineral composition of crude Manzanillo olive pomace on a dry weight (DW) basis. Potassium was the predominant mineral, with a content of 1302.27 mg/100 g, followed by sodium (222.81 mg/100 g), calcium (132.78 mg/100 g), phosphorus (89.36 mg/100 g), magnesium (76.68 mg/100 g), iron (17.91 mg/100 g), zinc (0.97 mg/100 g), copper (0.53 mg/100 g), and manganese (0.49 mg/100 g).

The sodium content (222.81 mg/100 g) was lower than the 580 mg/100 g reported by Alcazar-Ruiz et al. (2021). The calcium content (132.78 mg/100 g) was within the range of 132–165 mg/100 g reported by Ribeiro et al. (2021), while the potassium content (1302.27 mg/100 g) was within the range of 264–1532 mg/100 g reported by Miranda et al. (2014).

The phosphorus content (89.36 mg/100 g) also fell within the reported range of 69.10–104 mg/100 g (Černe et al., 2023). Similarly, the magnesium content (76.68 mg/100 g) was within the range of 20–100 mg/100 g reported by Alcazar-Ruiz et al. (2023).

The contents of iron, zinc, and copper were 17.91, 0.97, and 0.53 mg/100 g, respectively, following the order Fe > Zn > Cu, which was consistent with the pattern

reported by Mekersi et al. (2024). The manganese content was 0.49 mg/100 g, slightly lower than the 0.5 mg/100 g reported by Ameziane et al. (2018).

The mineral composition of crude OP indicates the presence of several essential minerals that contribute to its nutritional value (Sica et al., 2002). The relatively high potassium content is of nutritional interest because adequate potassium intake is associated with cardiovascular and metabolic health (Aburto et al., 2013; D'Elia et al., 2011, 2014; Shin et al., 2013). The presence of other essential minerals, including iron and zinc, further supports the potential use of OP as a functional food ingredient (Tsoupras et al., 2024) and as a source of compounds of interest for nutraceutical applications (Monteiro et al., 2024).

Extraction yields and antinutritional factors in olive pomace using different solvents

Table 2 shows that the highest extraction yield for Manzanillo cultivar OP was achieved by sequential solvent extraction (SSE) at 85.6%, followed by methanol extraction at 81.2%, ethanol extraction at 75.2%, and green extraction (GE) at 71.74%, while the lowest yield was observed with chloroform extraction (68.8%).

The extraction yields for OP ranged from 68.8% to 85.6%, which were generally within the range of 51.2% (0.512 g/g) reported by Martins et al. (2024) to 85% reported by Yanik (2017), with the SSE yield being slightly higher than the upper value reported by Yanik (2017).

Table 2

Extraction yields (%) and anti-nutritional factors (%) in olive pomace using different solvents (dry extract)

Parameters	Soaking extraction by 70%			GE	SSE
	methanol	ethanol	chloroform		
Extraction yield	81.20±0.17^{d}	75.20±0.11^{c}	68.80±0.24^{a}	71.74±0.27^{b}	85.60±0.09^{e}
Phytic acid	0.49±0.10^{c}	0.31±0.02^{b}	0.08±0.02^{a}	0.53±0.16^{d}	0.47±0.06^{c}

Mean ± SD. GE - Green extraction; SSE - Sequential solvent extraction. Different letters indicate significant differences between rows ($p \leq 0.05$; one-way ANOVA, Tukey post hoc).

The extraction yields obtained for Manzanillo OP showed that SSE provided the highest yield, followed by methanol, ethanol, GE, and chloroform extraction. The higher yield obtained with SSE may be related to the sequential use of solvents with different polarities, which can facilitate the extraction of a wider range of compounds from the OP matrix. Methanol and ethanol also produced relatively high yields, supporting their common use for the extraction of phenolic and other bioactive compounds. The lowest yield was observed with chloroform, indicating its lower extraction efficiency for the compounds present in OP.

Table 2 also showed variability in phytic acid content depending on the extraction method. The highest phytic acid content was observed in the GE extract, followed by the methanol, SSE, ethanol, and chloroform extracts. These values were within or close to the range of 0.26–0.48% reported by Paié-Ribeiro et al. (2024). The differences in phytic acid content among the extracts indicate that the extraction method and solvent type influenced the recovery of this antinutritional factor from Manzanillo OP.

Total phenolic and total flavonoid contents in olive pomace extracts with and without sodium selenite fortification using three extraction methods

The results (Table 3) showed that the highest total phenolic content (TPC) was obtained with the 70% methanol extract (49.93 mg GAE/g), followed by the 70% ethanol extract (47.92 mg GAE/g), SSE extract (35.62 mg GAE/g), and 70% chloroform extract (32.33 mg GAE/g), whereas the GE extract had the lowest TPC (21.78 mg GAE/g).

The TPC values obtained in the present study were within the range of 21.99 mg GAE/g (21,989.22 mg GAE/kg) reported by Cravotto et al. (2022) to 57.96 mg GAE/g reported by Stramarkou et al. (2023).

The TFC in Manzanillo OPE showed that the highest flavonoid levels were found in the 70% methanol extract at 30.42 mg QE/g, followed by 70% ethanol extracts 27.15 mg QE/g, the GE extract at 23.28 mg QE/g, while the lowest levels were in the 70% chloroform and SSE extracts at 19.77 and 19.32 mg QE/g, respectively; this falls within the (1.96:3.17 g QE/100g) 19.6:31.7 mg QE/g range reported by (Nunes et al., 2021).

Table 3

Total phenolic and total flavonoid contents in olive pomace extract and selenium-fortified olive pomace extracts using different solvents (dry extract)

	Soaking extraction by 70%			GE	SSE
Extracts	**Methanol**	**Ethanol**	**Chloroform**		
TPC					
OPE	49.93 ± 0.94^{Ee}	47.92 ± 1.15^{Ed}	32.33 ± 1.08^{Db}	21.78 ± 1.02^{Aa}	35.62 ± 0.51^{Cc}
OPE+SS1	56.20 ± 0.42^{Fe}	50.67 ± 0.32^{Fd}	39.61 ± 0.83^{Ec}	26.93 ± 0.24^{Ca}	37.79 ± 0.02^{Db}
OPE+SS2	62.27 ± 0.61^{Ge}	55.70 ± 0.7^{Fd}	46.92 ± 0.09^{Fc}	36.05 ± 1.2^{Fa}	43.86 ± 0.82^{Fb}
OPE+SS3	70.48 ± 0.24^{He}	64.99 ± 0.41^{Gd}	60.31 ± 0.51^{Gc}	48.75 ± 0.36^{Ha}	55.26 ± 0.91^{Gb}
TFC					
OPE	30.42 ± 0.44^{Ae}	27.15 ± 0.59^{Ad}	19.77 ± 0.56^{Ab}	23.28 ± 0.53^{Bc}	19.32 ± 0.26^{Aa}
OPE+SS1	33.20 ± 0.30^{Be}	31.60 ± 0.43^{Bd}	23.19 ± 0.69^{Ba}	28.42 ± 0.33^{Dc}	24.09 ± 0.25^{Ab}
OPE+SS2	39.06 ± 0.05^{Ce}	37.58 ± 0.45^{Cd}	29.32 ± 0.40^{Ca}	32.14 ± 0.41^{Ec}	29.41 ± 0.14^{Bb}
OPE+SS3	41.22 ± 0.38^{Dd}	46.44 ± 0.27^{De}	39.47 ± 0.30^{Eb}	39.96 ± 0.18^{Gc}	38.58 ± 0.14^{Ea}

Note: Mean ± SD (n = 3). Different lowercase superscript letters within the same row indicate significant differences among extraction methods at the same selenium supplementation level, whereas different uppercase superscript letters within the same column indicate significant differences among selenium supplementation levels for the same extract ($p \leq 0.05$; two-way ANOVA followed by Tukey's post hoc test). GE - green extraction, SSE -sequential solvent extraction, OPE - olive pomace extract, TPC- total phenolic content, TFC - total flavonoid content, OPE+SS1 - OPE with supplemented with 30 μg of sodium selenite, OPE+SS2 - OPE with supplemented with 40 μg of sodium selenite, and OPE+SS3 - OPE with supplemented with 55 μg of sodium selenite.

SS fortification significantly increased TPC in Manzanillo OPE. Following SS3 fortification, the TPC increased from 49.93 to 70.48 mg GAE/g in the 70% methanol extract, from 47.92 to 64.99 mg GAE/g in the 70% ethanol extract, from 32.33 to 60.31 mg GAE/g in the 70% chloroform extract, from 21.78 to 48.75 mg GAE/g in the GE extract, and from 35.62 to 55.26 mg GAE/g in the SSE extract. SS fortification also significantly increased TFC in Manzanillo OPE. Following SS3 fortification, the TFC increased from 30.42 to 41.22 mg QE/g in the 70% methanol extract, from 27.15 to 46.44 mg QE/g in the 70% ethanol extract, from 19.77 to 39.47 mg QE/g in the 70% chloroform extract, from 23.28 to 39.96

mg QE/g in the GE extract, and from 19.32 to 38.58 mg QE/g in the SSE extract. These results are consistent with previous reports that selenium treatment can affect phenolic and flavonoid contents (Gąsecka et al., 2015).

Antioxidant activity of olive pomace extracts based on radical scavenging activity and IC_{50} values

The results showed that the 70% methanol extract had the highest antioxidant activity among the non-fortified extracts, with the highest RSA (55.37%) and the lowest IC_{50} value (0.13 mg/mL), followed by the 70% ethanol extract (RSA = 53.14%, IC_{50} = 0.13 mg/mL) (Table 4).

Table 4

Antioxidant activity (AA) of olive pomace extracts measured by RSA (%) and IC_{50} values (mg/mL) (dry extract)

EST	AA	Soaking extraction by 70%			GE	SSE
		Methanol	Ethanol	Chloroform		
OPE	RSA	55.37 ±0.38^{Ce}	53.14 ±0.77^{Cd}	35.85 ±0.89^{Eb}	24.15 ±0.80^{Ea}	39.50 ±0.42^{Dc}
	IC_{50}	0.13 ±0.07^{Ba}	0.13 ±0.03^{Ba}	0.20 ±0.11^{Db}	0.30 ±0.16^{Dc}	0.19 ±0.06^{Cb}
OPE+SS1	RSA	62.32 ±0.11^{De}	56.19 ±0.09^{Dd}	43.92 ±0.07^{Fc}	29.86 ±0.05^{Fa}	41.90 ±0.11^{Eb}
	IC_{50}	0.12 ±0.05^{Ba}	0.13 ±0.08^{Ba}	0.17 ±0.10^{Cb}	0.24 ±0.06^{Cc}	0.18 ±0.10^{Cb}
OPE+SS2	RSA	69.05 ±0.10^{Ee}	61.77 ±0.03^{Ed}	52.03 ±0.09^{Gc}	39.98 ±0.02^{Ga}	48.64 ±0.02^{Fb}
	IC_{50}	0.11 ±0.02^{ABa}	0.12 ±0.06^{ABab}	0.14 ±0.04^{Bbc}	0.18 ±0.05^{Bd}	0.15 ±0.07^{Bc}
OPE+SS3	RSA	78.15 ±0.24^{Fe}	72.07 ±0.03^{Fd}	66.88 ±0.01^{Hc}	54.06 ±0.11^{Ha}	61.28 ±0.02^{Gb}
	IC_{50}	0.09 ±0.02^{Aa}	0.10 ±0.04^{Aab}	0.11 ±0.07^{Aab}	0.13 ±0.09^{Ac}	0.12 ±0.08^{Abc}

Note: RSA (mean ± SD) and IC_{50} (Mean ± SEM) (n = 3). Different lowercase superscript letters within the same row indicate significant differences among extraction methods at the same selenium supplementation level, whereas different uppercase superscript letters within the same column indicate significant differences among selenium supplementation levels for the same extract ($p \leq 0.05$; two-way ANOVA followed by Tukey's post hoc test). EST – extracts, AA - antioxidant activity, GE - green extraction, SSE - sequential solvent extraction, OPE - olive pomace extract, RSA - radical scavenging activity, IC_{50} - the concentration required to scavenge 50% of free radicals, OPE+SS1 - OPE with supplemented with 30 μg of sodium selenite, OPE+SS2 - OPE with supplemented with 40 μg of sodium selenite, and OPE+SS3 - OPE with supplemented with 55 μg of sodium selenite.

The GE extract showed the lowest antioxidant activity, with an RSA of 24.15% and an IC_{50} value of 0.30 mg/mL. The RSA values obtained in the present study were within the range of 17.2% reported by Wong et al. (2026) to 78.02% reported by Guerboub et al. (2025). The IC_{50} values were also within the range of 0.10 mg/mL (100.19 μg/mL) reported by Sylla et al. (2021) to 0.74 mg/mL reported by Stramarkou et al. (2023).

The addition of SS significantly increased antioxidant activity across all extracts. The increase in RSA and decrease in IC_{50} values depended on the OPE extraction method and SS concentration. The 70% methanol extract fortified with SS3 showed the highest antioxidant activity, with an RSA of 78.15% and an IC_{50} value of 0.09 mg/mL. The 70% ethanol extract fortified with the same SS concentration also showed high antioxidant activity, with an RSA of 72.07% and an IC_{50} value of 0.10 mg/mL. The alcoholic extracts (methanol and ethanol) showed a greater response to SS supplementation than the GE and chloroform extracts.

These findings indicate that SS supplementation enhanced the antioxidant activity of OPE in a concentration-dependent manner. This is consistent with the findings of Zhou et al. (2026), who reported that selenium biofortification enhanced the antioxidant capacity of a plant extract in vitro. The fortified alcoholic extracts, particularly the 70% methanol extract with SS3, showed the highest antioxidant activity and may be considered as potential sources for the development of antioxidant-rich products.

Identification and quantification of phenolic and flavonoid compounds in olive pomace extracts using HPLC at 280 nm and 330 nm

A wide range of phenolic compounds was identified in the OPE samples. Detection at 280 nm was generally suitable for phenolic acids and simple phenolic compounds, whereas detection at 330 nm improved the detection of certain flavonoids and phenolic acid derivatives.

HPLC analysis at 280 and 330 nm showed differences in the phenolic profiles of the extracts. The 70% ethanol extract had the highest summed content of identified compounds, reaching 2301.06 mg/100 g at 280 nm and 243.17 mg/100 g at 330 nm (Table 5). At 280 nm, the 70% chloroform extract had the second-highest total content (1127.21 mg/100 g), followed by SSE (799.32 mg/100 g) and 70% methanol (257.86 mg/100 g). At 330 nm, the corresponding values for SSE and 70% methanol were 274.30 and 121.59 mg/100 g, respectively, while GE showed the lowest total contents at both wavelengths (63.98 and 137.68 mg/100 g).

The compound-level data showed that several phenolic compounds were present at higher concentrations in the 70% ethanol extract. Quinic acid reached 650.06 mg/100 g at 280 nm, consistent with the findings of Dauber et al. (2026), who reported quinic acid as a major compound in OPE. Oleuropein diglucoside isomer b, oleuropein aglycone, and oleuropein reached 467.56, 285.50, and 233.32 mg/100 g, respectively, in the 70% ethanol extract. Protocatechuic acid and vanillic acid also showed their highest concentrations in the ethanol extract, at 152.17 and 138.63 mg/100 g, respectively. In contrast, hydroxytyrosol reached its highest concentration in the SSE extract (143.15 mg/100 g at 280 nm), compared with 86.53 mg/100 g in the ethanol extract.

These findings are consistent with previous reports describing hydroxytyrosol, tyrosol and their derivatives, oleuropein, oleuropein aglycone and their derivatives, flavonoids such as luteolin, apigenin, and rutin, and phenolic acids such as gallic, caffeic, cinnamic, p-coumaric, ferulic, and vanillic acids among the phenolic compounds present in olive pomace (Katsinas et al., 2021; Leo et al., 2025; Pavez et al., 2019).

The results demonstrate the potential of OP as a source of phenolic compounds that can be recovered using different extraction methods. In particular, the 70% ethanol extract showed a high content and diversity of identified phenolic compounds, indicating that ethanol extraction can be an effective approach for recovering phenolic compounds from OP. The valorization of OP as a source of bioactive compounds may also contribute to the utilization of olive-processing by-products and their potential application in functional food ingredients (Grigoletto et al., 2024; Tsoupras et al., 2024).

Table 5

Identification of phenolic compounds (mg/100 g) in olive pomace by HPLC (dry extract)

Phenolic compounds	Soaking extraction by 70%						GE		SSE	
	methanol		ethanol		chloroform					
	Wavelength, nm									
	280	330	280	330	280	330	280	330	280	330
Gallic acid	ND	ND	0.39	1.20	3.97	ND	0.39	0.59	0.01	1.85
Hydroxytyrosol	47.41	24.51	86.53	36.58	4.88	4.03	5.14	10.76	143.15	40.16
Coumaric acid	45.04	8.32	ND	10.97	2.95	2.17	3.11	7.37	29.15	14.09
p-hydro-xybenzoic acid	2.38	18.74	56.35	12.98	0.81	0.27	2.59	36.41	168.87	13.66
Tyrosol	4.79	0.61	19.24	16.83	ND	0.02	0.05	0.03	98.41	33.57
Hydroxytyrosol acetate	7.73	0.30	9.01	0.12	ND	ND	0.01	1.19	147.28	0.15
Chlorogenic acid	4.37	2.13	87.41	0.74	ND	6.51	ND	1.52	ND	ND
protocatechuic acid	6.90	ND	152.17	1.05	ND	ND	ND	0.70	37.99	11.85
Syringic acid	3.65	ND	ND	ND	ND	ND	ND	ND	ND	0.19
p-hydroxy-cinnamic acid	2.49	ND	ND	ND	ND	ND	ND	ND	6.57	ND
Epicatechin	1.69	0.95	ND	18.79	ND	ND	ND	ND	4.47	ND
Oleuropein	1.86	2.81	233.32	5.76	166.84	1.03	ND	ND	6.27	9.76
Vanillic acid	22.73	3.98	138.63	33.46	85.62	3.09	ND	ND	15.82	ND
Cinnamic acid	ND	ND	ND	ND	ND	ND	ND	ND	ND	5.51
oleoside	43.42	20.20	ND	ND	ND	2.58	ND	ND	ND	ND
Oleuropein isomer a	28.82	13.31	ND	ND	ND	ND	ND	ND	ND	ND
Quercetin	10.94	4.96	ND	14.43	ND	1.63	12.08	18.28	ND	ND
Caffeic acid	ND	3.31	ND	14.41	ND	ND	ND	ND	52.35	26.95
Ferulic acid	ND	1.59	27.35	3.59	ND	ND	0.55	4.65	3.45	ND
Quinic acid	ND	ND	650.06	ND	373.95	ND	ND	ND	7.66	ND
Luteolin-7-O-rutinoside	ND	ND	ND	38.51	ND	ND	ND	26.68	ND	ND
Oleuropein diglucoside isomer b	ND	ND	467.56	ND	267.84	ND	ND	ND	ND	ND
Comselogoside	ND	ND	ND	32.59	ND	3.80	18.96	29.50	ND	ND
Oleuropein aglycone	ND	ND	285.50	ND	189.57	ND	ND	ND	ND	ND
Luteolin	ND	ND	87.54	ND	ND	ND	ND	ND	ND	ND
Kaempferol	ND	ND	ND	1.16	ND	ND	ND	ND	ND	ND
Apigenin	ND	ND	ND	ND	30.78	ND	ND	ND	ND	ND
Verbascoside	ND	ND	ND	ND	ND	ND	0.49	ND	ND	ND
Syringol	ND	ND	ND	ND	ND	ND	0.89	ND	ND	ND
4-chloro-cinnamic acid	23.64	15.87	ND	ND	ND	ND	2.98	ND	2.52	7.26
Rutin	ND	ND	ND	ND	ND	ND	16.74	ND	ND	ND
Pinoresinol	ND	ND	ND	ND	ND	ND	ND	ND	75.35	ND
4-Methoxy-cinnamic acid	ND	ND	ND	ND	ND	ND	ND	ND	ND	109.30
Total (∑)	257.86	121.59	2301.06	243.17	1127.21	25.13	63.98	137.68	799.32	274.30

Note: ND - not detected. GE - green extraction; SSE - sequential solvent extraction.

Conclusions

Manzanillo olive pomace is characterized by a favorable nutritional composition, including high crude fiber and total carbohydrate contents and low moisture content, supporting its potential for functional food applications. It also contains several essential minerals, particularly potassium. The 70% methanol and 70% ethanol extracts showed the highest total phenolic content (TPC) and total flavonoid content (TFC), respectively, whereas sequential solvent extraction provided the highest extraction yield. Sodium selenite fortification significantly increased TPC, TFC, and antioxidant activity in a concentration-dependent manner. HPLC analysis showed that Manzanillo olive pomace contains diverse phenolic compounds, including oleuropein and hydroxytyrosol. Overall, Manzanillo olive pomace extract, either alone or fortified with selenium, represents a potential source of natural antioxidants and may have applications in the development of functional food ingredients and the valorisation of olive oil industry by-products.

Acknowledgment. The authors thank Dr. Abd-Elmoneim Refai for providing the samples used in this study.

References

Aburto, N. J., Hanson, S., Gutierrez, H., Hooper, L., Elliott, P., & Cappuccio, F. P. (2013). Effect of increased potassium intake on cardiovascular risk factors and disease: Systematic review and meta-analyses. *BMJ, 346*(3), f1378. https://doi.org/10.1136/bmj.f1378

Aburto, N. J., Hanson, S., Gutierrez, H., Hooper, L., Elliott, P., & Cappuccio, F. P. (2013). Effect of increased potassium intake on cardiovascular risk factors and disease: Systematic review and meta-analyses. *BMJ, 346*(3), f1378. https://doi.org/10.1136/bmj.f1378

Aissaoui, M. H., Trabelsi, A. B. H., Bensidhom, G., Ceylan, S., Leahy, J. J., & Kwapinski, W. (2023). Insights into olive pomace pyrolysis conversion to biofuels and biochars: Characterization and techno-economic evaluation. *Sustainable Chemistry and Pharmacy, 32*, 101022. https://doi.org/10.1016/j.scp.2023.101022

Akay, F., Kazan, A., Celiktas, M. S., & Yesil-Celiktas, O. (2015). A holistic engineering approach for utilization of olive pomace. *Journal of Supercritical Fluids, 99*, 1–7. https://doi.org/10.1016/j.supflu.2015.01.025

Alcazar-Ruiz, A., Dorado, F., & Sanchez-Silva, L. (2023). Bio-phenolic compounds production through fast pyrolysis: Demineralizing olive pomace pretreatments. *Food and Bioproducts Processing, 137*, 200–213. https://doi.org/10.1016/j.fbp.2022.12.002

Alcazar-Ruiz, A., Garcia-Carpintero, R., Dorado, F., & Sanchez-Silva, L. (2021). Valorization of olive oil industry subproducts: Ash and olive pomace fast pyrolysis. *Food and Bioproducts Processing, 125*, 37–45. https://doi.org/10.1016/j.fbp.2020.10.011

Ameziane, H., Nounah, A., Khamar, M., Cherkaoui, E., & Kabbour, M. R. (2018). Agrochemical characterization of olive pomace obtained by different systems of extraction. *Der Pharma Chemica, 10*(12), 33–40. https://www.derpharmachemica.com/pharma-chemica/agrochemical-characterization-of-olive-pomace-obtained-by-different-systems-of-extraction-15484.html

AOAC International. (2022). *Official methods of analysis of AOAC International* (22nd ed.). Arlington, VA, USA: AOAC International.

Bai, S., Zhang, M., Tang, H., Li, M., Wu, R., Wan, S., Chen, L., Wei, X., & Feng, S. (2024). Effects and impact of selenium on human health: A review. *Molecules, 30*(1), 50. https://doi.org/10.3390/molecules30010050

Benko, I., Nagy, G., Tanczos, B., Ungvari, E., Sztrik, A., Eszenyi, P., Prokisch, J., & Banfalvi, G. (2012). Subacute toxicity of nano-selenium compared to other selenium species in mice.

Environmental Toxicology and Chemistry, 31(12), 2812–2820. https://doi.org/10.1002/etc.1995

Brown, P., Chan, M., Paley, L., & Betz, J. (2011). Determination of major phenolic compounds in *Echinacea* spp. raw materials and finished products by high-performance liquid chromatography with ultraviolet detection: Single-laboratory validation matrix extension. *Journal of AOAC International, 94*(5), 1400–1410. https://doi.org/10.5740/jaoacint.11-142

Černe, M., Palčić, I., Major, N., Pasković, I., Perković, J., Užila, Z., Lukić, M., Romić, M., Ferri, T. Z., Ban, S. G., Lapanje, A., Hreščak, J., Heath, D. J., & Ban, D. (2023). Effect of olive-processing technology on the utilization of olive mill pomace as a soil amendment. *Journal of Environmental Quality, 52*(3), 610–629. https://doi.org/10.1002/jeq2.20464

Cioffi, G., Pesca, M., Caprariis, P., Braca, A., Severino, L., & Tommasi, N. (2010). Phenolic compounds in olive oil and olive pomace from Cilento (Campania, Italy) and their antioxidant activity. *Food Chemistry, 121*(1), 105–111. https://doi.org/10.1016/j.foodchem.2009.12.013

Cottenie, A., Verloo, M., Kickens, L., Velghe, G., & Camerlynck, R. (1982). *Chemical analysis for plant and soils*. Laboratory of Analytical and Agrochemistry, State University of Gent.

Cravotto, C., Fabiano-Tixier, A. S., Claux, O., Rapinel, V., Tomao, V., Stathopoulos, P., Skaltsounis, A. L., Tabasso, S., Jacques, L., & Chemat, F. (2022). Higher yield and polyphenol content in olive pomace extracts using 2-methyloxolane as bio-based solvent. *Foods, 11*(9), 1357. https://doi.org/10.3390/foods11091357

D'Elia, L., Barba, G., Cappuccio, F. P., & Strazzullo, P. (2011). Potassium intake, stroke, and cardiovascular disease a meta-analysis of prospective studies. *Journal of the American College of Cardiology, 57*(10), 1210-1219. https://doi.org/10.1016/j.jacc.2010.09.070

D'Elia, L., Iannotta, C., Sabino, P., & Ippolito, R. (2014). Potassium-rich diet and risk of stroke: updated meta-analysis. *Nutrition, Metabolism, and Cardiovascular Diseases, 24*(6), 585-587. https://doi.org/10.1016/j.numecd.2014.03.001

Dauber, C., Olt, V., Valdés, A., Alborés, S., Gámbaro, A., Ibáñez, E., & Vieitez, I. (2026). Green valorization of two-phase olive pomace via pressurized liquid extraction: process optimization, comprehensive metabolite analysis and functional applications. *Molecules, 31*(10), 1569. https://doi.org/10.3390/molecules31101569

Fitó, M., Torre, R. d. L., & Covas, M. I. (2007). Olive oil and oxidative stress. *Molecular Nutrition & Food Research, 51*(10), 1215–1224. https://doi.org/10.1002/mnfr.200600308

García-Morales, S., León-Morales, J. M., García-Gaytán, V., & Terreros-Rosales, L. G. (2023). Plant-based foods biofortified with selenium and their potential benefits for human health. In V. Gelen, A. Kara, & A. Kükürt (Eds.), *Plant-based foods biofortified with selenium and their potential benefits for human health*. London, UK: IntechOpen.

Gąsecka, M., Mleczek, M., Siwulski, M., Niedzielski, P., & Kozak, L. (2015). The effect of selenium on phenolics and flavonoids in selected edible white rot fungi. *LWT - Food Science and Technology, 63*(1), 726–731. https://doi.org/10.1016/j.lwt.2015.03.046

Gladyshev, V. N., Arnér, E. S. J., Berry, M. J., Brigelius-Flohé, R., Bruford, E. A., & et al. (2016). Selenoprotein gene nomenclature. *The Journal of Biological Chemistry, 291*(46), 24036–24040. https://doi.org/10.1074/jbc.M116.756155

Grigoletto, I., Salas, P. G., Valli, E., Bendini, A., Ferioli, F., Pasini, F., Villasclaras, S. S., García-Ruiz, R., & Toschi, T. G. (2024). HPLC-MS/MS phenolic characterization of olive pomace extracts obtained using an innovative mechanical approach. *Foods, 13*(2), 285. https://doi.org/10.3390/foods13020285

Guerboub, L., Soufi-Maddi, O., Ouldsaadi, L., Bey, M. B., Medouni-Haroune, L., Madani, K., & Boulekbache-Makhlouf, L. (2025). Ultra-turrax homogenization-assisted extraction of bioactive compounds from olive pomace using response surface methodology. *Food Analytical Methods, 18*, 2198–2207. https://doi.org/10.1007/s12161-025-02861-4

Hadrup, N., Loeschner, K., Mandrup, K., Ravn-Haren, G., Frandsen, H. L., Larsen, E. H., Lam, H. R., & Mortensen, A. (2019). Subacute oral toxicity investigation of selenium nanoparticles and selenite in rats. *Drug and Chemical Toxicology, 42*(1), 76–83. https://doi.org/10.1080/01480545.2018.1491589

Hadrup, N., Loeschner, K., Skov, K., Ravn-Haren, G., Larsen, E. H., Mortensen, A., Lam, H. R., & Frandsen, H. L. (2016). Effects of 14-day oral low dose selenium nanoparticles and selenite in rat—as determined by metabolite pattern determination. *PeerJ, 4*, e2601. https://doi.org/10.7717/peerj.2601

Halwaz, R., Hassan, A., Mansour, E., Osheba, A., & El-Bedawey, A. (2018). Antioxidant activity of olive leaf, pomace and virgin oil extracts from Picual cultivar and their heat and pH stability. *Menoufia Journal of Food Science, 11*(1), 89–106. https://fjard.journals.ekb.eg/article_175705_5272b9be0807aeb1339d8792f551e96b.pdf

Haug, W., & Lantzsch, H. J. (1983). Sensitive method of rapid determination of phytate in cereals and cereal products. *Journal of the Science of Food and Agriculture, 34*(12), 1423–1426. https://doi.org/10.1002/jsfa.2740341217

He, Y., Chen, S., Liu, Z., Cheng, C., Li, H., & Wang, M. (2014). Toxicity of selenium nanoparticles in male Sprague-Dawley rats at supranutritional and nonlethal levels. *Life Sciences, 115*(1–2), 44–51. https://doi.org/10.1016/j.lfs.2014.08.023

Hesse, P. R. (1971). *Soil chemical analysis*. London, UK: John Murray.

Institute of Medicine (US) Panel on Dietary Antioxidants and Related Compounds. (2000). *Dietary reference intakes for vitamin C, vitamin E, selenium, and carotenoids*. Washington, DC: National Academies Press.

Katsinas, N., Silva, A. B. D., Enríquez-de-Salamanca, A., Fernández, N., Bronze, M. R., & Rodríguez-Rojo, S. (2021). Pressurized liquid extraction optimization from supercritical defatted olive pomace: A green and selective phenolic extraction process. *ACS Sustainable Chemistry & Engineering, 9*(16), 5590–5602. https://doi.org/10.1021/acssuschemeng.0c09426

Khubulava, S., Chichiveishvili, N., Shavshishvili, N., Mulkijanyan, K., Khodeli, N., Jangavadze, M., Tsagareli, Z., Dgebuadze, M., & Phichkhaia, G. (2019). Effect of high dose of selenium nanoparticles on alimentary tract in rodents. *Journal of Nanomedicine & Nanotechnology, 10*(2), 531. https://doi.org/10.35248/2157-7439.19.10.531

Lammi, S., Barakat, A., Mayer-Laigle, C., Djenane, D., Gontard, N., & Angellier-Coussy, H. (2018). Dry fractionation of olive pomace as a sustainable process to produce fillers for biocomposites. *Powder Technology, 326*, 44–53. https://doi.org/10.1016/j.powtec.2017.11.060

Lamuela-Raventós, R. M. (2017). Folin-Ciocalteu method for the measurement of total phenolic content and antioxidant capacity: Recent trends and applications. In R. Apak, E. Capanoglu, & F. Shahidi (Eds.), *Measurement of antioxidant activity and capacity: Recent trends and applications* (pp. 107–115). Hoboken, NJ: John Wiley & Sons. https://doi.org/10.1002/9781119135388.ch6

Leo, E. G. D., Stranieri, C., Zoccatelli, G., Bellumori, M., Zonfrillo, B., Cominacini, L., & Pasini, A. M. F. (2025). Olive pomace extract acts as a new potent ferroptosis inhibitor in human cells. *Molecules, 30*(15), 3095. https://doi.org/10.3390/molecules30153095

Leouifoudi, I., Harnafi, H., & Abdelmajid, Z. (2015). Olive mill waste extracts: Polyphenols content, antioxidant, and antimicrobial activities. *Advances in Pharmacological and Pharmaceutical Sciences*, 714138, 1–11. https://doi.org/10.1155/2015/714138

Lesnichaya, M., Shendrik, R., Titov, E., & Sukhov, B. (2020). Synthesis and comparative assessment of antiradical activity, toxicity and biodistribution of κ-carrageenan-capped selenium nanoparticles of different size: In vivo and in vitro study. *IET Nanobiotechnology, 14*(6), 519–526. https://doi.org/10.1049/iet-nbt.2020.0023

Louis, A., Chich, J. F., Chepca, H., Schmitz, I., Hugueney, P., & Maia-Grondard, A. (2025). Green extraction method: Microwave-assisted water extraction followed by HILIC-HRMS analysis to quantify hydrophilic compounds in plants. *Metabolites, 15*(4), 223. https://doi.org/10.3390/metabo15040223

Martins, V. F. R., Ribeiro, T. B., Lopes, A. I., Pintado, M. E., Morais, R. M. S. C., & Morais, A. M. M. B. (2024). Comparison among different green extraction methods of polyphenolic compounds from exhausted olive oil pomace and the bioactivity of the extracts. *Molecules, 29*(9), 1935. https://doi.org/10.3390/molecules29091935

Meguid, G. G. A., Abouel-Yazeed, A. M., Abu-Tor, E. S. M., Nassar, M. A. A., & Aboufarrag, H. T. (2025). Chemical studies on olive pomace and seeds as a by-product from olive oil extraction.

Alexandria Science Exchange Journal, 46(3), 581–588. https://journals.ekb.eg/article_444178_564973c587d0e8c43fa7b4d1b56556bf.pdf

Mekersi, N., Kadi, K., Hackenberger, D. K., Casini, S., Addad, D., Thangaraj, R., Chen, Z., Zhang, C., & Yuvaraj, A. (2024). Accumulation of heavy metals from single and combined olive mill wastewater and pomace in soil and bioaccumulation in tissues of two earthworm species: Endogeic (*Aporrectodea trapezoides*) and epigeic (*Eisenia fetida*). *Environmental Science and Pollution Research, 31*, 45280–45294. https://doi.org/10.1007/s11356-024-34087-y

Miranda, T., Nogales, S., Román, S., Montero, I., Arranz, J. I., & Sepúlveda, F. J. (2014). Control of several emissions during olive pomace thermal degradation. *International Journal of Molecular Sciences, 15*(10), 18349–18361. https://doi.org/10.3390/ijms151018349

Monteiro, C. S. A., Adedara, I. A., Farombi, E. O., & Emanuelli, T. (2024). Nutraceutical potential of olive pomace: Insights from cell-based and clinical studies. *Journal of the Science of Food and Agriculture, 104*(7), 3807–3815. https://doi.org/10.1002/jsfa.13281

Moustafa, S., El-Ghany, N. A., & Elawady, M. (2022). A phytochemical study on *Olea europaea* L. olive leaf extract (cv. Koroneiki): Total flavonoids, phenolic content, and antioxidant activity. *Alexandria Pharmaceutical Sciences Journal, 56*(2), 123–134. https://aps.journals.ekb.eg/article_45119_b5e924be02716e7e7a2c169abc69bf83.pdf

Munekata, P. E. S., Nieto, G., Pateiro, M., & Lorenzo, J. M. (2020). Phenolic compounds obtained from *Olea europaea* by-products and their use to improve the quality and shelf life of meat and meat products—A review. *Antioxidants, 9*(11), 1061. https://doi.org/10.3390/antiox9111061

Nakra, S., Tripathy, S., & Srivastav, P. (2025). Drying as a preservation strategy for medicinal plants: Physicochemical and functional outcomes for food and human health. *Phytomedicine Plus, 5*, 100762. https://doi.org/10.1016/j.phyplu.2025.100762

Nunes, M. A., Palmeira, J. D., Melo, D., Machado, S., Lobo, J. C., Costa, A. S. G., Alves, R. C., Ferreira, H., & Oliveira, M. B. P. P. (2021). Chemical composition and antimicrobial activity of a new olive pomace functional ingredient. *Pharmaceuticals, 14*(9), 913. https://doi.org/10.3390/ph14090913

Nunes, M. A., Pimentel, F. B., Costa, A. S. G., Alves, R. C., & Oliveira, M. B. P. P. (2016). Olive by-products for functional and food applications: Challenging opportunities to face environmental constraints. *Innovative Food Science & Emerging Technologies, 35*, 139–148. https://doi.org/10.1016/j.ifset.2016.04.016

Paié-Ribeiro, J., Baptista, F., Teixeira, J., Guedes, C., Gomes, M. J., Teixeira, A., Barros, A. N., Pinheiro, V., & Outor-Monteiro, D. (2024). From waste to resource: Compositional analysis of olive cake's fatty acids, nutrients and antinutrients. *Applied Sciences, 14*(13), 5586. https://doi.org/10.3390/app14135586

Pavez, I. C., Lozano-Sánchez, J., Borrás-Linares, I., Nuñez, H., Robert, P., & Segura-Carretero, A. (2019). Obtaining an extract rich in phenolic compounds from olive pomace by pressurized liquid extraction. *Molecules, 24*(17), 3108. https://doi.org/10.3390/molecules24173108

Radzi, N. C., Bacho, S., & Mustapa, A. N. (2022). Review on drying methods for herbal plants. *Materials Today: Proceedings, 63*(4). https://doi.org/10.1016/j.matpr.2022.02.052

Ramachandran, S., Singh, S., Larroche, C., Soccol, C., & Pandey, A. (2007). Oil cakes and their biotechnological applications—A review. *Bioresource Technology, 98*(10), 2000–2009. https://doi.org/10.1016/j.biortech.2006.08.002

Re, R., Pellegrini, N., Proteggente, A., Pannala, A., Yang, M., & Rice-Evans, C. (1999). Antioxidant activity applying an improved ABTS radical cation decolorization assay. *Free Radical Biology and Medicine, 26*(9–10), 1231–1237. https://doi.org/10.1016/S0891-5849(98)00315-3

Ribeiro, T., Oliveira, A., Coelho, M., Veiga, M., Costa, E., Silva, S., Nunes, J., Vicente, A., & Pintado, M. (2021). Are olive pomace powders a safe source of bioactives and nutrients? *Journal of the Science of Food and Agriculture, 101*, 1963–1978. https://doi.org/10.1002/jsfa.10812

Ribeiro, T. B., Oliveira, A. L., Costa, C., Nunes, J., Vicente, A. A., & Pintado, M. (2020). Total and sustainable valorisation of olive pomace using a fractionation approach. *Applied Sciences, 10*(19), 6785. https://doi.org/10.3390/app10196785

Selim, S., Albqmi, M., Al-Sanea, M. M., Alnusaire, T. S., Almuhayawi, M. S., AbdElgawad, H., Jaouni, S. K. A., Elkelish, A., Hussein, S., Warrad, M., & El-Saadony, M. T. (2022). Valorizing the

usage of olive leaves, bioactive compounds, biological activities, and food applications: A comprehensive review. *Frontiers in Nutrition, 9*, 1008349. https://doi.org/10.3389/fnut.2022.1008349

Shin, D., Joh, H. K., Kim, K. H., & Park, S. M. (2013). Benefits of potassium intake on metabolic syndrome: The fourth Korean National Health and Nutrition Examination Survey. *Atherosclerosis, 230*(1), 80–85. https://www.sciencedirect.com/science/article/pii/S0021915013003912

Sica, D. A., Struthers, A. D., Cushman, W. C., Wood, M., Banas, J. S., & Epstein, M. (2002). Importance of potassium in cardiovascular disease. *Journal of Clinical Hypertension, 4*(3), 198–206. https://doi.org/10.1111/j.1524-6175.2002.01728.x

Skrotska, O., Protsenko, M., Zholobko, M., & Marynin, M. (2025). Biosynthesis and characterization of selenium nanoparticles by *Saccharomyces cerevisiae* M437. *Ukrainian Journal of Food Science, 13*(1), 91–110. https://doi.org/10.24263/2310-1008-2025-13-1-10

Stabnikova, O., Shevchenko, O., Stabnikov, V., & Paredes-López, O. (Eds.). (2023a). Bioconversion of waste to value-added products. Boca Raton, FL: CRC Press. https://doi.org/10.1201/9781003329671

Stabnikova, O., Shevchenko, A., Stabnikov, V., & Paredes-López, O. (2023b). Utilization of plant processing wastes for enrichment of bakery and confectionery products. *Ukrainian Food Journal, 12*(2), 299–308. https://doi.org/10.24263/2304-974X-2023-12-2-11

Stabnikova, O., Khonkiv, M., Kovshar, I., & Stabnikov, V. (2023c). Biosynthesis of selenium nanoparticles by lactic acid bacteria and areas of their possible applications. *World Journal of Microbiology and Biotechnology, 39*, 230. https://doi.org/10.1007/s11274-023-03673-6

Stempfle, S., Carlucci, D., Gennaro, B. C. d., Roselli, L., & Giannoccaro, G. (2021). Available pathways for operationalizing circular economy into the olive oil supply chain: Mapping evidence from a scoping literature review. *Sustainability, 13*(17), 9789. https://doi.org/10.3390/su13179789

Stramarkou, M., Missirli, T. V., Kyriakopoulou, K., Papadaki, S., Angelis-Dimakis, A., & Krokida, M. (2023). The recovery of bioactive compounds from olive pomace using green extraction processes. *Resources, 12*(7), 77. https://doi.org/10.3390/resources12070077

Sylla, N. N., Bouyahya, A., Taha, D., Dakka, N., & Elhajji, H. (2021). Study of the antioxidant and antidiabetic activity in vitro of free and encapsulated phenolic compounds of olive pomace. *Biocatalysis and Agricultural Biotechnology, 36*, 102126. https://www.sciencedirect.com/science/article/pii/S187881812100222X

Taha, A., & Khalifa, H. (2024). Olive in Egypt: Cultural practices for sustainable production. In V. S. Lagouri (Ed.), *Olive in Egypt: Cultural practices for sustainable production* (pp. 1–33). London, UK: IntechOpen.

Tawarah, K. (2014). Thermochemical assessment of solid and liquid fuels used for domestic space heating in Jordan. *Green and Sustainable Chemistry, 4*, 202–219. https://doi.org/10.4236/GSC.2014.44026

Thomson, C. D. (2003). Selenium | Physiology. In B. Caballero (Ed.), *Encyclopedia of food sciences and nutrition* (2nd ed., pp. 5117–5124). Oxford, UK: Academic Press.

Tibaoui, S., Essid, I., Smeti, S., & Atti, N. (2023). Effect of myrtle leaves integration in sheep diet and its addition as powder on leg meat's oxidative stability, physicochemical, microbiological and sensory properties during storage. *Food Science & Nutrition, 11*(4), 1860-1871. https://doi.org/10.1002/fsn3.3219

Trindade, P., Dalfolo, A. D. C., Monteiro, C. S. A., Wagner, R., Santos, B. A. D., Nora, F. M. D., Verruck, S., & Rosa, C. S. D. (2023). Development and characterization of biscuits with olive pomace. *Food Science and Technology, 43*, e99922. https://doi.org/10.1590/fst.99922

Tsoupras, A., Panagopoulou, E., & Kyzas, G. (2024). Olive pomace bioactives for functional foods and cosmetics. *AIMS Agriculture and Food, 9*(3), 743–766. https://doi.org/10.3934/agrfood.2024040

Turck, D., Bohn, T., Castenmiller, J., de Henauw, S., Hirsch-Ernst, K.-I., Knutsen, H. K., Maciuk, A., Mangelsdorf, I., McArdle, H. J., Peláez, C., Pentieva, K., Siani, A., Thies, F., Tsabouri, S., Vinceti, M., Aggett, P., Bouyrie, M., Cubadda, F., Ciccolallo, L., ... Naska, A. (2023). Scientific

opinion on the tolerable upper intake level for selenium. *EFSA Journal*, *21*(1), e07704. https://doi.org/10.2903/j.efsa.2023.7704

Urbankova, L., Skalickova, S., Pribilova, M., Ridoskova, A., Pelcova, P., Skladanka, J., & Horky, P. (2021). Effects of sub-lethal doses of selenium nanoparticles on the health status of rats. *Toxics*, *9*(2), 28. https://doi.org/10.3390/toxics9020028

Wong, Y. L., Boulos, S., Popp, M., Bongartz, A., & Nyström, L. (2026). Sensory aspects of olive pomace polyphenols - Linking phenolic composition to bitterness. *Journal of Agriculture and Food Research*, *29*, 103118. https://doi.org/10.1016/j.jafr.2026.103118

Yanik, D. K. (2017). Alternative to traditional olive pomace oil extraction systems: Microwave-assisted solvent extraction of oil from wet olive pomace. *LWT*, *77*, 45–51. https://doi.org/10.1016/j.lwt.2016.11.020

Zhou, F., Lin, Q., Chen, Y., & Gao, F. (2026). Antioxidant properties and correlation with chemical components in selenium-enriched *Ampelopsis grossedentata* extract. *Chinese Journal of Analytical Chemistry*, *54*(4), 100715.

Cite:

Shams, E., Gouda, M., Salama, A. E., & Magdy, G. (2026). Bioactive compounds and antinutritional factors in olive pomace. *Ukrainian Food Journal*, *15*(3), 732–747. https://doi.org/10.24263/2304-974X-2026-15-3-9

Comparative evaluation of synthetic antioxidants for improving the oxidative stability of soybean oil

Tamara Nosenko[1], Iryna Levchuk[2], Oleksandr Klymenko[1]

1 – National University of Food Technologies, Kyiv, Ukraine
2 – State Enterprise "Ukrmetrteststandard", Kyiv, Ukraine

Keywords:

Soybean
Oil
Oxidative stability
Synthetic antioxidant
Butylated hydroxytoluene
Butylated hydroxyanisole
Peroxide value

Article history:

Received 11.08.2025
Received in revised form 18.04.2026
Accepted 30.06.2026

Corresponding author:

Tamara Nosenko
E-mail: tamara_nosenko@ukr.net

DOI:
10.24263/2304-974X-2026-15-3-10

Abstract

Introduction. The objective of this study was to determine the concentrations of two synthetic antioxidants, butylated hydroxytoluene (BHT) and butylated hydroxyanisole (BHA), required to ensure the oxidative stability of soybean oil.

Materials and methods. The oxidative stability of soybean oil was evaluated using an accelerated oxidation method based on the Schaal Oven Test. The progress of oil oxidation was monitored by measuring the peroxide value at 2 h intervals during heating at 100 °C. Acid and peroxide values were determined using standard methods. The antioxidant activity of the oil was evaluated based on its 2,2-diphenyl-1-picrylhydrazyl (DPPH) radical-scavenging capacity. The fatty acid composition of soybean oil samples was determined by gas–liquid chromatography.

Results and discussion. BHT at concentrations of 0.01–0.03% sufficiently prolonged the induction period of soybean oil oxidation. The duration of the oil oxidation induction period increased to 6, 7, and 10 h at BHT concentrations of 0.01, 0.02, and 0.03%, respectively. BHA was less effective in prolonging the induction period of soybean oil oxidation. The induction period was 3 h at 0.01% BHA, 1 h longer at 0.02%, and 10 h at 0.03%. After the induction period, the peroxide value increased very slowly at 0.01 and 0.02% BHA and finally reached only 4.4 and 4.0 meq/kg, respectively. At the highest BHA concentration (0.03%), the induction period was followed by a sharp increase in peroxide value during the subsequent 5 h of heating. The final peroxide value was higher than those observed in the samples with lower BHA concentrations. A similar sharp increase in peroxide value after the induction period was observed at 0.03% BHT. After 11 h of heating, the peroxide values of soybean oil samples containing 0.01 and 0.02% BHT were higher than those of the corresponding samples containing BHA. The antioxidant activity of soybean oil samples containing synthetic antioxidants remained thermally stable only during the first 4 h of heating; thereafter, it decreased in almost all samples. After 8 h of accelerated oxidation, the antioxidant activity of soybean oil was higher in the presence of BHA and was comparable to that observed with BHT at all tested concentrations.

Conclusions. Butylated hydroxytoluene was more effective than butylated hydroxyanisole in prolonging the induction period of peroxide accumulation in soybean oil during accelerated oxidation at 100 °C. However, BHT showed lower thermal stability of antioxidant activity, and higher peroxide values were observed after the induction period, indicating less effective protection of soybean oil during the later stages of oxidation.

Introduction

Oils and fats, as well as oil-containing products, are susceptible to oxidation during processing and storage. As a result of fat oxidation, peroxide and other oxidation products are created, which negatively impact the sensory quality of foods (Gharby et al., 2025). The unpleasant taste and smell of edible oils is a result of the breakdown of polyunsaturated fatty acids, resulting in the formation of volatile aldehydes, ketones, and alcohols. These compounds, even at low concentrations, significantly reduce consumer acceptability and market value of the oils. The oxidation also reduces the nutritional quality of foods, decreasing the content of polyunsaturated fatty acids (Tao, 2015), fat-soluble vitamins (such as vitamins A, D, E, and K), and natural antioxidants, as well as produces potentially toxic compounds (Machado et al., 2023). These compounds may increase health risks, including cancer, atherosclerosis, heart disease, allergic reactions, and inflammation (Tao, 2015). Furthermore, oxidative deterioration imposes a substantial financial losses to the food producers. Therefore, regular monitoring and antioxidant strategies are crucial for maintaining the sensory and nutritional quality of vegetable oils.

Thus, oxidation stability of oils and fats is a significant problem for producers and consumers of fat-containing food and feed products (Indiarto & Qonit, 2020). A lot of factors influence this property of oil and fat (Choe & Min, 2006; Gharby et al., 2025). First of all, the rate of fat oxidation depends on the fatty acid composition (Redondo-Cuevas et al., 2018; Sabolová et al., 2020); the higher the content of polyunsaturated acids, the higher the oxidation rate. Oxidation stability of oils and fats also depends on the content of antioxidants (Pokorny, 2007; Reishe et al., 2008). The vegetable oils contain natural antioxidants – bioactive minor lipid components, such as well-known tocotrienols and tocopherols, and some other phenolic compounds (Hassanien et al., 2014; Tabee et al., 2008). Oxidation rate also depends on external influences – temperature and insolation. In order to prevent the fat deterioration and increase their shelf life, antioxidants are added to the fat-containing food and feed products (Choe & Min, 2009; Machado et al., 2023).

A trend toward the use of "natural" food additives in the food industry has been apparent for some time as a result of consumer demand. Plants are important sources of natural antioxidants, including ascorbic acid and tocopherols. Other natural antioxidants include carotenoids (Viljanen et al., 2002), flavonoids (Zahra et al., 2024), antioxidant proteins (Zhai et al., 2020), protein hydrolysates (Li et al., 2008a, 2008b; Pan et al., 2011), Maillard reaction products (Lohinova & Petrusha, 2023), and lignan compounds (Lee et al., 2007). Numerous naturally occurring phenolic antioxidants have been identified in plant sources and plant extracts (Avila-Sosa et al., 2010; Stabnikov et al., 2025; Stabnikova et al., 2024; Vollmannova et al., 2009). Recent research has focused on the isolation and identification of effective antioxidants of natural origin (Demidova et al., 2021; Fadda et al., 2022).

However, in spite of growing consumer preference for natural food additives, the synthetic antioxidants are widely used in food and feed processing to inhibit lipid oxidation (Mohanan, 2018). The most common synthetic antioxidants used in food are phenolic compounds, including butylated hydroxyanisole (BHA), butylated hydroxytoluene (BHT), propyl gallate (PG), ethoxyquin, ascorbylpalmitate, and tertiary butylhydroquinone (TBHQ). Phenols in which the aromatic ring contains alkyl groups (BHA and BHT) are highly effective antioxidants, which also have antimicrobial properties. BHA and BHT are heat-stable and could be used in heat processes, whereas PG decomposes at 148 ºC and TBHQ is heat-stable and used in heat-frying applications (Reishe et al., 2008). BHA and BHT are strongly lipophilic and are used extensively in oil-in-water emulsions. BHA and BHT are also typically used together in mixtures, acting synergistically. However, concerns have been

raised regarding the potential adverse health effects of excessive use of synthetic antioxidants, including cytotoxicity and carcinogenicity (Gharby et al., 2025). Phenolic antioxidants are effective at low concentrations and are often used at levels less than 0.01% (Machado et al., 2023). Allowable limits vary sufficiently depending on the food product and the antioxidant. Regulations concerning synthetic antioxidants also vary greatly from country to country. Usually, the maximal level of these antioxidants is 0.02%. At the same time, at high levels, phenolic compounds become prooxidants because of their high reactivity and participation in the initiation reactions. The reasonable concentration of every antioxidant for different fats has not been effectively investigated.

The objective of this study was to determine the optimal concentrations of the phenolic antioxidants butylated hydroxyanisole and butylated hydroxytoluene for inhibiting soybean oil oxidation and extending its shelf life.

Material and methods

Materials

Cold-pressed unrefined soybean oil produced by Tandem-2002 LLC (Ukraine), as well as butylated hydroxytoluene and butylated hydroxyanisole supplied by Himlaborreaktyv LLC (Ukraine), were used in this study.

Potassium iodide (pharmaceutical grade), sodium thiosulfate standard titers (Alfarus), potassium hydroxide standard titers (Alfarus), pharmaceutical-grade chloroform, and glacial acetic acid, all purchased from Himlaborreaktyv LLC (Ukraine), were used to determine the acid and peroxide values. For the determination of the antioxidant activity of soybean oil, 2,2-diphenyl-1-picrylhydrazyl (DPPH) from Sigma-Aldrich and pharmaceutical-grade ethyl acetate (Carlo Erba) were used. Fatty acids were identified by comparing their retention times with those of a standard mixture of fatty acid methyl esters (37-component FAME Mix, Supelco).

Methods

Accelerated oxidation test. The Schaal Oven Test, conducted under controlled conditions (Botosoa et al., 2022; Flores et al., 2021), was used to assess the oxidative stability of soybean oil. The method was modified by heating the oil at 100 °C in an oven. 100 mL of each oil sample was placed in open flasks and heated at 100 °C for 11–15 h. The peroxide value and antioxidant activity were determined at 2 h intervals by taking 2 g and 100 mg of oil from each sample, respectively. The induction period of accelerated oxidation was determined graphically from a plot of peroxide value against heating time.

Quality parameters. The acid and peroxide values were determined according to ISO 660:2020 and ISO 3960:2007, respectively.

Fatty acid composition analysis. The fatty acid composition of soybean oil was determined by gas–liquid chromatography of fatty acid methyl esters (Nosenko et al., 2014). For the preparation of fatty acid methyl esters, 100 mg of each oil sample was dissolved in 2 mL of BHT solution (0.5 g/L) in heptane. Then, 100 μL of sodium solution in methanol (46 mg/mL) was added, and the solution was mixed for 2 min and kept for 15 min. Subsequently,

1–2 g of sodium hydrmlosulfate was added. The samples were filtered through anhydrous sodium sulfate, after which 2 mL of BHT solution in heptane was added. The resulting solution was filtered again through a 0.45 μm cellulose membrane filter, and the filter was washed with 1 mL of the same solvent. The two filtrates were combined, and the resulting solution was used for analysis.

The fatty acid methyl esters were analyzed using a Hewlett Packard HP 6890 gas chromatograph equipped with an HP-88 capillary column (88% cyanopropyl aryl-polysiloxane; 100 m × 0.25 mm; film thickness, 0.25 μm; Agilent Technologies). The injector temperature was 280 °C, and the detector temperature was 290 °C. The temperature program was as follows: 60 °C for 4 min; heating to 150 °C at 4 °C/min and holding for 10 min; heating to 180 °C at 3 °C/min and holding for 5 min; heating to 190 °C at 3 °C/min and holding for 2 min; heating to 230 °C at 3 °C/min and holding for 2 min; and heating to 260 °C at 4 °C/min and holding for 2 min.

The carrier gas flow rate was 1.2 mL/min, and the injection volume was 1.0 μL. Fatty acids were identified by comparing their retention times with those of a standard mixture of fatty acid methyl esters (37-Component FAME Mix, Supelco). The results are presented as mean values±standard deviation of three analytical replicates.

DPPH˙ radical scavenging activity and kinetic analysis. Determination of the antioxidant activity of the oil was carried out by the method of 2,2-diphenyl-1-picrylhydrazyl (DPPH˙) radical scavenging activity (Broznic et al., 2016). The solution of 2,2-diphenyl-1-picrylhydrazyl at a concentration of 3 mg/100 mL in ethyl acetate, which had an optical density in the range of 0.7–0.9 at a wavelength of 520 nm, was used. To prepare the reaction mixture, 15 mL of DPPH˙ solution was added to 100 mg of oil, mixed thoroughly, and the initial optical density of the reaction mixture was determined at 520 nm (A_0). The reaction mixture was kept dark, and the optical density was measured at 520 nm after 30 min incubation (A_{30}) when the reaction reached a steady state. DPPH˙ radical scavenging activity (%) of the oil solutions calculated according to equation:

$$DPPH^{\cdot}scavenging = \frac{A_0 - A_{30}}{A_0} \cdot 100$$

Antioxidant activity was calculated as the total DPPH˙ scavenging effect for 30 min. The experiment at each time interval was performed in triplicate, and the mean values and standard deviations were calculated.

Statistical analysis

Each sample was analyzed in triplicate, and the results were reported as mean±standard deviation.

Results and discussion

Quality parameters of soybean oil

The chemical parameters and antioxidant activity of soybean oil are presented in Table 1.

Table 1

Chemical parameters of soybean oil

Sample	Acid value, mg KOH/g oil	Peroxide value, meq O_2/kg oil	Total DPPH˙ scavenging effect (after 30 min), %
Soybean oil	0.47±0.13	1.68±0.04	43.3±2.5

The low acid value of the pressed soybean oil indicates a low free fatty acid content, while the peroxide value of 1.68 meq/kg indicates a low level of primary oxidation products. Similar values for soybean oil were reported by Kozłowska and Gruczyńska (2018). Other cold-pressed oils have also demonstrated comparable quality parameters, with acid values ranging from 0.08 to 0.69 mg KOH/g and peroxide values between 0.60 and 9.55 meq O_2/kg (Prescha et al., 2014).

A wide range of methods is available for assessing antioxidant activity, and these methods differ considerably in their underlying mechanisms and measurement units (Prior et al., 2005). Using the DPPH radical-scavenging method described by Lee et al. (2015), the antioxidant capacity of soybean oil was relatively high. It was comparable to that of olive oil and higher than the values reported for corn oil (Lee et al., 2015).

Fatty acid composition analysis

The fatty acid composition of soybean oil is summarized in Table 2.

Table 2

Fatty acid composition of soybean oil

Fatty acid	Fatty acid content, % of total fatty acids
Palmitic acid (C16:0)	10.48±0.15
Palmitooleic acid (cis-9-C16:1)	0.09±0.05
Stearic acid (C18:0)	4.40±0.10
Oleic acid (cis-9-C18:1)	22.78±0.20
Vaccenic acid (cis-11-C18:1)	1.41±0.15
Linoleic acid (cis, cis-9,12-C18:2)	51.06±0.20
α-Linolenic acid (cis,cis,cis-9,12,15-C18:3)	7.92±0.20
Arachidic acid (C20:0)	0.46±0.05
Behenic acid (C22:0)	0.48±0.05
Lignocerinic acid (C24:0)	0.12
Saturated fatty acids (SFA)	15.94
Monounsaturated fatty acids (MUFA)	24.28
Polyunsaturated fatty acids (PUFA)	59.88
ω3 : ω6 ratio	1:6.5

Linoleic and oleic acids were identified as the major fatty acids in soybean oil (Table 2). The total polyunsaturated fatty acid (PUFA) content was approximately 60%, with an ω-3:ω-6 ratio of 1:6.5, which is close to the ratio of approximately 1:7 reported for soybean oil

(Reische et al., 2008; Stabnikova & Paredes-López, 2024). The high PUFA content of soybean oil contributes to its susceptibility to oxidation (Sarkar et al., 2015). Fatty acids containing two double bonds are 10–40 times more susceptible to oxidation than those containing a single double bond (Szterk et al., 2010). In particular, linoleic and linolenic acids in soybean oil are highly susceptible to oxidation (Casarotti & Jorge, 2014; Kim et al., 2010).

Oxidative stability of soybean oil during accelerated oxidation

The accelerated oxidation of soybean oil during 11 h resulted in an increase of peroxide value from 2.3 to 9.8 meq O_2/kg (Figure 1). The dependence of oil oxidation on heating duration was well described by an exponential equation with approximation reliability R^2 = 0.975.

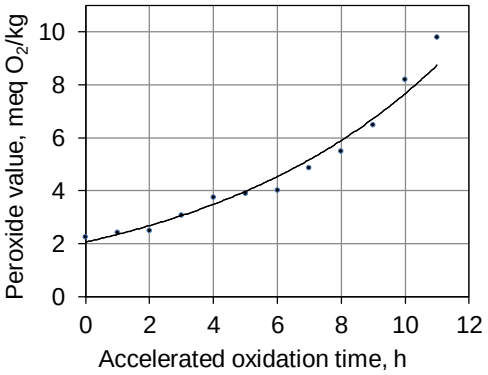

Figure 1. Peroxide values of soybean oil during accelerated oxidation at 100 °C

Numerous studies have determined the induction period of oils using the Rancimat method. The induction period is highly dependent on the temperature used in the Rancimat test. At 110 °C, the induction periods reported for several vegetable oils ranged from 5.1 to 27.6 h (Tabee et al., 2008), whereas those reported for rice bran, corn, peanut, and rapeseed oils ranged from 4.77 to 5.02 h. The shortest induction period, 2.4 h, was reported for grapeseed oil (Maszewska et al., 2018).

An increase in temperature significantly decreases oil stability. According to Farhoosh (2007), the induction period of refined soybean oil measured by the Rancimat method at 110 °C was approximately 6.3–6.8 h, whereas Rauen-Miguel et al. (1992) reported an induction period of 3.6 h at 120 °C. Previous studies have also reported induction periods at 120 °C of 4.10 h for refined rapeseed oil (Anwar et al., 2003) and 5.9 h (Kowalski et al., 2004); 1.89 h (Anwar et al., 2003), 3.05 h (Ayyildiz et al., 2015), and 3.5 h (Kowalski et al., 2004) for refined sunflower oil; 6.42 h for olive oil (Läubli & Bruttel, 1985); and 3.7–48.3 h for virgin olive oils (Mateos et al., 2006). Redondo-Cuevas et al. (2018) reported induction periods at 120 °C of 0.84, 2.16, 4.74, and 6.7 h for corn, sunflower, rapeseed, and olive oils, respectively.

In the present study, the induction period of soybean oil was approximately 2 h. After this period, the rate of peroxide formation increased, likely due to depletion of endogenous antioxidants and acceleration of autoxidation. The short induction period may be attributed to the high content of polyunsaturated fatty acids in soybean oil. The highly reactive double bonds of unsaturated fatty acids make them primary targets for free-radical reactions during autoxidation. Despite the short induction period, the rate of peroxide accumulation after this period remained relatively low.

Effect of butylated hydroxytoluene on the oxidative stability of soybean oil

In foods containing lipids, antioxidants delay the onset of oxidation or slow the rate at which it proceeds. These substances can occur as natural constituents of foods, but they can also be intentionally added to food products. Their role is not to enhance or improve food quality, but rather to maintain quality and extend shelf life. Antioxidants used in food processing should be inexpensive, nontoxic, effective at low concentrations, stable, and capable of surviving processing, while having minimal effects on color, flavor, and odor. The choice of antioxidant depends on the nature of the product and regulatory requirements (Giese, 1996).

Synthetic antioxidants offer high efficacy, low cost, and good stability in foods and are intentionally added to inhibit lipid oxidation. Synthetic antioxidants approved for use in foods include butylated hydroxyanisole (BHA), butylated hydroxytoluene (BHT), and others. BHT is a widely used monophenolic antioxidant. It is suitable for high-temperature processing but is less stable than BHA (Reische et al., 2008). BHT is also used extensively in the food industry, including in low-fat foods, fish products, packaging materials, and mineral oils.

The addition of BHT to soybean oil at concentrations of 0.01–0.03% increased the induction period of oxidation (Figure 2).

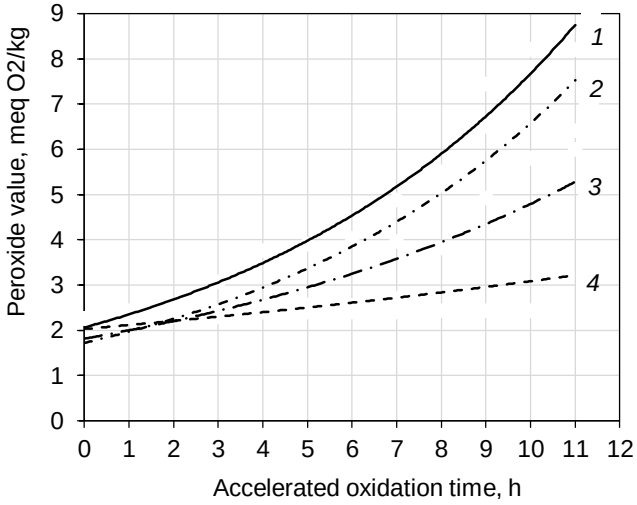

Figure 2. Peroxide values of soybean oil during accelerated oxidation at 100 °C in the presence of butylated hydroxytoluene:
1 – control; 2 – 0.01% BHT; 3 – 0.02% BHT; 4 – 0.03% BHT.

.

At 0.01% BHT, peroxide formation started after 6 h of oil heating, followed by intensive accumulation of peroxides. The final peroxide value was very close to that of the sample without BHT. At a BHT concentration of 0.02%, the induction period was prolonged to 7 h, after which rapid peroxide accumulation occurred. At 0.03% BHT, the induction period increased to 10 h, followed by a sharp increase in peroxide value.

Effect of butylated hydroxyanisole on the oxidative stability of soybean oil

Butylated hydroxyanisole (BHA) is one of the widely used antioxidants in the food industry. It is used in fats and oils, fat-containing foods, confectionery products, essential oils, food-coating materials, and waxes. According to Reische et al. (2008), BHA is effective in preventing oxidation of animal fats but is less effective in vegetable fats.

In the present study, butylated hydroxyanisole was less effective in prolonging the induction period of accelerated oxidation of soybean oil. The induction period was 3 h at a BHA concentration of 0.01% and increased by only 1 h at 0.02% BHA (Figure 3).

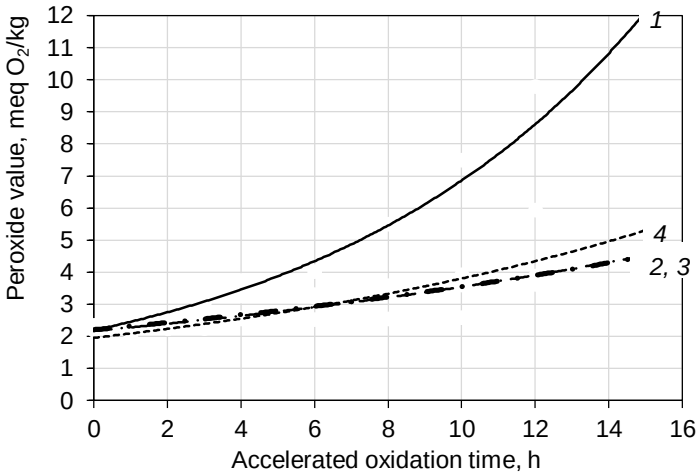

Figure 3. Peroxide values of soybean oil during accelerated oxidation at 100 °C in the presence of butylated hydroxyanisole:
1 – control, 2 – 0.01% BHA, 3 – 0.02% BHA, 4 – 0.03% BHA.

After the induction period, the peroxide value increased very slowly at these concentrations and reached final values of 4.0 and 4.4 meq O_2/kg at 0.02 and 0.01% BHA, respectively. In contrast, the higher BHA concentration of 0.03% increased the induction period to 10 h, followed by a sharp increase in peroxide value during the subsequent 5 h. The final peroxide value was higher than those observed at the lower BHA concentrations. A similar sharp increase in peroxide value after the induction period was observed for soybean oil containing 0.03% BHT.

The sharp increase in peroxide value at the highest concentrations of BHA and BHT may be related to the prooxidant behavior that phenolic antioxidants can exhibit under certain conditions. At elevated concentrations, phenolic compounds may participate in reactions involved in oxidation initiation because of their high reactivity (Reische et al., 2008). This mechanism may partly explain the accelerated accumulation of peroxides observed after the induction period at the highest concentrations of BHA and BHT.

Comparative effects of BHT and BHA on the oxidative stability of soybean oil

A comparative analysis of the effects of butylated hydroxytoluene (BHT) and butylated hydroxyanisole (BHA) on the accelerated oxidation of soybean oil at 100 °C showed that BHT

was more effective in prolonging the induction period at concentrations of 0.01 and 0.02% (Figure 4).

These results are consistent with the findings of Thbayh and Fiser (2022), who calculated the bond dissociation enthalpy, ionization potential, proton dissociation enthalpy, proton affinity, and electron transfer enthalpy of several antioxidants, including BHT and BHA. Their results indicated that BHT had the highest antioxidant potential among the studied antioxidants. Reische et al. (2008) reported that BHA was effective in preventing oxidation of animal fats but less effective in vegetable fats. At a concentration of 0.03%, however, the induction periods of soybean oil containing BHT and BHA were much closer.

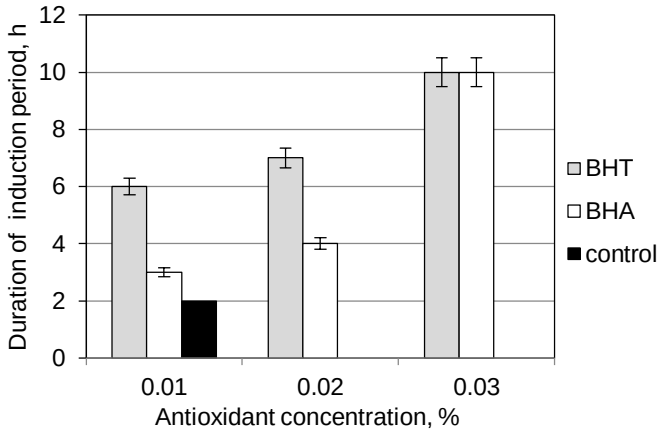

Figure 4. The comparable effect of butylated hydroxytoluene and butylated hydroxyanisole on the induction period during accelerated oxidation of soybean oil at 100 °C

Surprisingly, after 11 h of heating, the peroxide values of soybean oil containing BHT at concentrations of 0.01 and 0.02% were higher than those of the corresponding samples containing BHA (Figure 5).

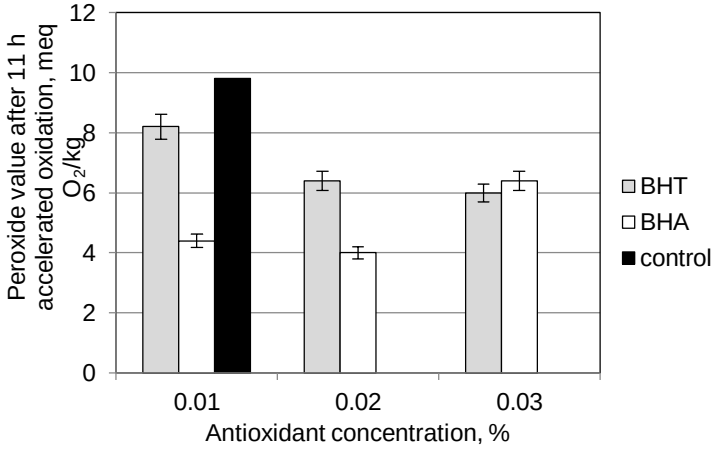

Figure 5. The comparable effect of butylated hydroxytoluene and butylated hydroxyanisole on the peroxide value of soybean oil after 11 h accelerated oxidation at 100 °C

Thus, BHT at low concentrations was more effective in prolonging the induction period but provided less effective protection against peroxide accumulation after this period. At the higher antioxidant concentration of 0.03%, the final peroxide values of soybean oil after 11 h of heating were similar for BHT and BHA.

The initial antioxidant capacity of soybean oil was approximately 43% DPPH• scavenging activity and remained stable during the first 4 h of heating at 100 °C (Figure 6).

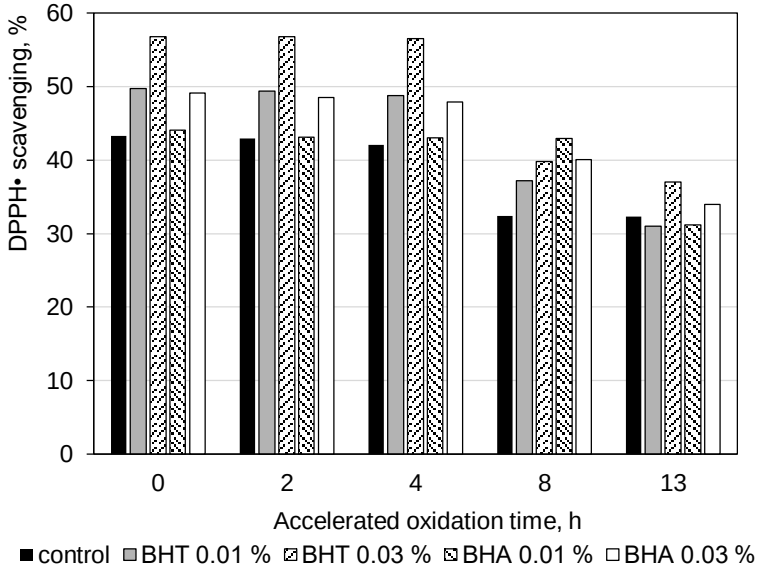

Figure 6. Influence of BHT and BHA on the antioxidant activity of soybean oil during accelerated oxidation at 100 °C

This period was longer than the induction period of soybean oil oxidation but corresponded to the period of relatively low oxidation rate. The highest initial antioxidant activity, approximately 57%, was observed in soybean oil containing 0.03% BHT, whereas the addition of 0.01% BHT increased the activity to approximately 50%. In contrast, the addition of 0.01% BHA did not change the initial antioxidant activity of soybean oil but maintained this activity at a relatively stable level for up to 8 h of accelerated oxidation. An increase in initial antioxidant activity based on DPPH• radical scavenging was observed only at higher BHA concentrations.

Overall, the results showed that the antioxidant capacity of soybean oil, as well as the antioxidant activity of BHT and BHA, remained relatively stable during the first 4 h of heating and decreased thereafter in almost all samples. However, BHA showed greater thermal stability than BHT, as indicated by its higher antioxidant activity after 8 h of accelerated oxidation at all tested concentrations. These results are consistent with the previously reported higher thermal stability of BHA (Reische et al., 2008).

Conclusions

Butylated hydroxytoluene (BHT) at concentrations of 0.01–0.03% prolonged the induction period of soybean oil accelerated oxidation at 100 °C, with higher BHT

concentrations resulting in longer induction periods. In contrast, extending the induction period of soybean oil oxidation with butylated hydroxyanisole (BHA) required a higher concentration, with the longest induction period observed at 0.03% BHA. However, BHT showed relatively lower thermal stability, as indicated by the increased oxidation rate and rapid rise in peroxide value after the induction period. BHA demonstrated higher thermal stability, particularly at concentrations of 0.01 and 0.02%, at which the post-induction oxidation rate remained relatively low and peroxide values increased gradually during prolonged heating. The antioxidant capacity of soybean oil, both without antioxidants and in the presence of BHT or BHA, remained relatively stable at 100 °C during the first 4 h and declined thereafter. No strong correlation was observed between the induction period of peroxide formation and antioxidant capacity, indicating that the oxidative stability of soybean oil is influenced by multiple factors.

Acknowledgment. The authors gratefully acknowledge the financial support provided by YEDNIST' GROUP (Ukraine) under a contract with the National University of Food Technologies (No. 02/25, dated 19 February 2025).

References

Anwar, F., Bhanger, M. I., & Kazi, T. G. (2003). Relationship between Rancimat and active oxygen method values at varying temperatures for several oils and fats. *Journal of the American Oil Chemists' Society*, *80*(2), 151–155. https://doi.org/10.1007/s11746-003-0668-2

Avila-Sosa, R., Gastelum-Franco, M. G., Camacho-Davila, A., Torres-Munoz, V. J., & Nevarez-Moorillon, G. V. (2010). Extracts of Mexican oregano (*Lippia berlandieri* Schauer) with antioxidant and antimicrobial activity. *Food and Bioprocess Technology*, *3*(3), 434–440. https://doi.org/10.1007/s11947-008-0085-7

Ayyildiz, H. F., Topkafa, M., Kara, H., & Sherazi, S. T. H. (2015). Evaluation of fatty acid composition, tocols profile, and oxidative stability of some fully refined edible oils. *International Journal of Food Properties*, *18*(9), 2064–2076. https://doi.org/10.1080/10942912.2014.962657

Botosoa, E. P., & Karoui, R. (2022). 3D front face fluorescence spectroscopy as a tool for monitoring the oxidation level of edible vegetable oil during storage at 60 °C. *LWT – Food Science and Technology*, *154*, 112659. https://doi.org/10.1016/j.lwt.2021.112659

Broznic, D., Juresic, G. C., & Milin, C. (2016). Involvement of α-, γ- and δ-tocopherol isomers from pumpkin (*Cucurbita pepo* L.) seed oil or oil mixtures in the biphasic DPPH• disappearance kinetics. *Food Technology and Biotechnology*, *54*(2), 200–210. https://doi.org/10.17113/ftb.54.02.16.4063

Casarotti, S. N., & Jorge, N. (2014). Antioxidant activity of rosemary extract in soybean oil under thermoxidation. *Journal of Food Processing and Preservation*, *38*(1), 136–145. https://doi.org/10.1111/j.1745-4549.2012.00755.x

Choe, E., & Min, D. B. (2006). Mechanisms and factors for edible oil oxidation. *Comprehensive Reviews in Food Science and Food Safety*, *5*(4), 169–186. https://doi.org/10.1111/j.1541-4337.2006.00009.x

Choe, E., & Min, D. B. (2009). Mechanisms of antioxidants in the oxidation of foods. *Comprehensive Reviews in Food Science and Food Safety*, *8*(4), 345–358. https://doi.org/10.1111/j.1541-4337.2009.00085.x

Demidova, A., Nosenko, T., Bahmach, V., Shemanska, E., & Molchenko, S. (2021). Study on antioxidants extraction from oak bark and their use for oxidation stability of sunflower oil. *Ukrainian Food Journal*, *10*(3), 552–563. https://doi.org/10.24263/2304-974X-2021-10-3-9

Fadda, A., Sanna, D., Sakar, E. H., Gharby, S., Mulas, M., Medda, S., Yesilbuk, N. S., Karasa, A. C., Gozukirmizi, C. K., Lucarini, M., Lombardi-Boccia, G., Diaconeasa, Z., & Durazzo, A. (2022). Innovative and sustainable technologies to enhance the oxidative stability of vegetable oils. *Sustainability, 14*(2), 849. https://doi.org/10.3390/su14020849

Farhoosh, R. (2007). The effect of operational parameters of the Rancimat method on the determination of the oxidative stability measures and shelf-life prediction of soybean oil. *Journal of the American Oil Chemists' Society, 84*(3), 205–209. https://doi.org/10.1007/s11746-006-1030-4

Flores, M., Avendano, V., Bravo, J., Valdés, C., Forero-Doria, O., Quitral, V., Vilcanqui, Y., & Viedma, J. O. (2021). Edible oil parameters during deterioration processes. *International Journal of Food Science, 2021*, 7105170. https://doi.org/10.1155/2021/7105170

Gharby, S., Asbbane, A., Ahmed, M. N., Gagour, J., Hallouch, O., Oubannin, S., Bijla, L., Goh, K. W., Bouyahya, A., & Ibourki, M. (2025). Vegetable oil oxidation: Mechanisms, impacts on quality, and approaches to enhance shelf life. *Food Chemistry: X, 28*(5), 102541. https://doi.org/10.1016/j.fochx.2025.102541

Giese, J. (1996). Antioxidants: Tools for preventing lipid oxidation. *Food Technology, 50*(11), 72–81. https://www.cabidigitallibrary.org/doi/full/10.5555/19971401790

Hassanien, M. M. M., Abdel-Razek, A. G., Rudzinska, M., Siger, A., Ratusz, K., & Przybylski, R. (2014). Phytochemical contents and oxidative stability of oils from non-traditional sources. *European Journal of Lipid Science and Technology, 116*(11), 1563–1571. https://doi.org/10.1002/ejlt.201300475

Indiarto, R., & Qonit, M. (2020). A review of soybean oil lipid oxidation and its prevention techniques. *International Journal of Advanced Science and Technology, 29*(6), 5030–5037.

Kim, J., Kim, D. N., Lee, S. H., Yoo, S. H., & Lee, S. (2010). Correlation of fatty acid composition of vegetable oils with rheological behaviour and oil uptake. *Food Chemistry, 118*, 398–402. https://doi.org/10.1016/j.foodchem.2009.05.011

Kowalski, B., Ratusz, K., Kowalska, D., & Bekas, W. (2004). Determination of the oxidative stability of vegetable oils by differential scanning calorimetry and Rancimat measurements. *European Journal of Lipid Science and Technology, 106*(3), 165–169. https://doi.org/10.1002/ejlt.200300915

Kozłowska, M., & Gruczyńska, E. (2018). Comparison of the oxidative stability of soybean and sunflower oils enriched with herbal plant extracts. *Chemical Papers, 72*, 2607–2615. https://doi.org/10.1007/s11696-018-0516-5

Läubli, M. W., & Bruttel, P. A. (1986). Determination of the oxidative stability of fats and oils: Comparison between the active oxygen method (AOCS Cd 12-57) and the Rancimat method. *Journal of the American Oil Chemists' Society, 63*(6), 792–795. https://doi.org/10.1007/BF02541966

Lee, A. Y., Lee, M. H., Lee, S., & Cho, E. J. (2015). Comparative study on antioxidant activity of vegetable oils under in vitro and cellular system. *Journal of Agricultural Science, 7*(3), 58–65. https://doi.org/10.5539/jas.v7n3p58

Lee, J., Kim, M., & Choe, E. (2007). Antioxidant activity of lignan compounds extracted from roasted sesame oil on the oxidation of sunflower oil. *Food Science and Biotechnology, 16*(6), 981–987. https://koreascience.kr/article/JAKO200709905797633.pdf

Li, X. X., Han, L. J., & Chen, L. J. (2008a). In vitro antioxidant activity of protein hydrolysates prepared from corn gluten meal. *Journal of the Science of Food and Agriculture, 88*(9), 1660–1666. https://doi.org/10.1002/jsfa.3264

Li, Y., Jiang, B., Zhang, T., Mu, W., & Liu, J. (2008b). Antioxidant and free radical-scavenging activities of chickpea protein hydrolysate (CPH). *Food Chemistry, 106*(2), 444–450. https://doi.org/10.1016/j.foodchem.2007.04.067

Lohinova, A., & Petrusha, O. (2023). Maillard reaction in food technologies. *Ukrainian Journal of Food Science, 11*(2), 81-109. https://doi.org/10.24263/2310-1008-2023-11-2-4

Machado, M., Rodriguez-Alcalá, L. M., Gomes, A. M., & Pintado, M. (2023). Vegetable oils oxidation: Mechanisms, consequences and protective strategies. *Food Reviews International, 39*(7), 4180–4197. https://doi.org/10.1080/87559129.2022.2026378

Maszewska, M., Florowska, A., Dłużewska, E., Wroniak, M., & Marciniak-Lukasiak, K. (2018). Oxidative stability of selected edible oils. *Molecules*, *23*(7), 1746. https://doi.org/10.3390/molecules23071746

Mateos, R., Uceda, M., Aguilera, M. P., Escuderos, M. E., & Maza, G. B. (2006). Relationship of Rancimat method values at varying temperatures for virgin olive oils. *European Food Research and Technology*, *223*(2), 246–252. https://doi.org/10.1007/s00217-005-0185-9

Mohanan, A., Nickerson, M. T., & Ghosh, S. (2018). Oxidative stability of flaxseed oil: Effect of hydrophilic, hydrophobic and intermediate polarity antioxidants. *Food Chemistry*, *266*, 524–533. https://doi.org/10.1016/j.foodchem.2018.05.117

Nosenko, T., Kot, T., & Kichshenko, V. (2014). Rapeseeds as a source of feed and food proteins. *Polish Journal of Food and Nutrition Sciences*, *64*(2), 109–114. https://doi.org/10.2478/pjfns-2013-0007

Pan, M., Jiang, T. S., & Pan, J. L. (2011). Antioxidant activities of rapeseed protein hydrolysates. *Food and Bioprocess Technology*, *4*(7), 1144–1152. https://doi.org/10.1007/s11947-009-0206-y

Pokorny, J. (2007). Antioxidants in food preservation. In M. S. Rahman (Ed.), *Handbook of food preservation* (pp. 260–286). CRC Press. https://doi.org/10.1201/9781420017373-18

Prescha, A., Grajzer, M., Dedyk, M., & Grajeta, H. (2014). The antioxidant activity and oxidative stability of cold-pressed oils. *Journal of the American Oil Chemists' Society*, *91*(8), 1291–1301. https://doi.org/10.1007/s11746-014-2479-1

Prior, R. L., Wu, X., & Schaich, K. (2005). Standardized methods for antioxidant capacity determination. *Journal of Agricultural and Food Chemistry*, *53*(10), 4290–4302. https://doi.org/10.1021/jf0502698

Redondo-Cuevas, L., Castellano, G., Torrens, F., & Raikos, V. (2018). Revealing the relationship between vegetable oil composition and oxidative stability: A multifactorial approach. *Journal of Food Composition and Analysis*, *66*, 221–229. https://doi.org/10.1016/j.jfca.2017.12.027

Reische, D. A., Lillard, D. W., & Eitemiller, R. R. (2008). Antioxidants. In D. B. Min (Ed.), *Food lipids: Chemistry, nutrition, and biotechnology* (pp. 409–434). CRC Press.

Sabolová, M., Zeman, V., Lebedová, G., Doležal, M., Soukup, J., & Réblová, Z. (2020). Relationship between the fat and oil composition and their initial oxidation rate during storage. *Czech Journal of Food Sciences*, *38*(6), 404–409. https://doi.org/10.17221/207/2020-CJFS

Sarkar, A., Golay, P. A., Acquistapace, S., & Craft, B. D. (2015). Increasing the oxidative stability of soybean oil through fortification with antioxidants. *International Journal of Food Science & Technology*, *50*(3), 666–673. https://doi.org/10.1111/ijfs.12671

Stabnikov, V., Stabnikova, O., & Paredes-López, O. (2025). Antioxidant compounds in wild edible berries. In S. Gubsky, O. Stabnikova, V. Stabnikov, & O. Paredes-López (Eds.), *Wild edible plants: Improving foods nutritional value and human health through biotechnology* (pp. 143–184). CRC Press. https://doi.org/10.1201/9781003486794-5

Stabnikova, O., & Paredes-López, O. (2024b). Plant materials for the production of functional foods for weight management and obesity prevention. *Current Nutrition & Food Science*, *20*(4), 401–422. https://doi.org/10.2174/1573401319666230705110854

Stabnikova, O., Stabnikov, V., & Paredes-López, O. (2024). Fruits of wild-grown shrubs for health nutrition. *Plant Foods for Human Nutrition*, *79*(1), 20-37. https://doi.org/10.1007/s11130-024-01144-3

Szterk, A., Roszko, M., Sosińska, E., Derewiaka, D., & Lewicki, P. P. (2010). Chemical composition and oxidative stability of selected plant oils. *Journal of the American Oil Chemists' Society*, *87*(6), 637–645. https://doi.org/10.1007/s11746-009-1539-4

Tabee, E., Azadmard-Damirchi, S., Jägerstad, M., & Dutta, P. C. (2008). Effects of α-tocopherol on oxidative stability and phytosterol oxidation during heating in some regular and high-oleic vegetable oils. *Journal of the American Oil Chemists' Society*, *85*(9), 857–867. https://doi.org/10.1007/s11746-008-1274-2

Tao, L. (2015). Oxidation of polyunsaturated fatty acids and its impact on food quality and human health. *Advances in Food Technology and Nutritional Sciences*, *1*(6), 135–142. https://doi.org/10.17140/AFTNSOJ-1-123

Thbayh, D. K., & Fiser, B. (2022). Computational study of synthetic and natural polymer additives—Antioxidant potential of BHA, TBHQ, BHT, and curcumin. *Polymer Degradation and Stability, 201*, 109979. https://doi.org/10.1016/j.polymdegradstab.2022.109979

Viljanen, K., Sunberg, S., Ohshima, T., & Heinonen, M. (2002). Carotenoids as antioxidants to prevent photooxidation. *European Journal of Lipid Science and Technology, 104*(6), 353–359. https://doi.org/10.1002/1438-9312(200206)104:6<353::aid-ejlt353>3.0.co;2-5

Vollmannova, A., Tomas, J., Urminska, D., Polakova, Z., Melichacova, S., & Krizova, L. (2009). Content of bioactive components in chosen cultivars of cranberries (*Vaccinium vitis-idaea* L.). *Czech Journal of Food Sciences, 27*(10), 248–251. https://doi.org/10.17221/940-CJFS

Zahra, M., Abrahamse, H., George, B. P. (2024). Flavonoids: Antioxidant powerhouses and their role in nanomedicine. *Antioxidants, 13*(8), 922. https://doi.org/10.3390/antiox13080922

Zhai, Y., Chen, Y., Teng, Z., & Zhao, Y. (2020). Identifying antioxidant proteins by using amino acid composition and protein-protein interactions. *Frontiers in Cell and Developmental Biology, 8*, 591487. https://doi.org/10.3389/fcell.2020.591487

Cite:

Nosenko, T., Levchuk, I., & Klymenko, O. (2026). Comparative evaluation of synthetic antioxidants for improving the oxidative stability of soybean oil. *Ukrainian Food Journal, 15*(3), 748–761. https://doi.org/10.24263/2304-974X-2026-15-3-10

Green synthesis of silver nanoparticles using *Piper betel* leaf extract for PLA-based active packaging films

Aisha Noushad[1], Radhalakshmi Venugopal[2], Maya Raman[3], Nasreen Pathanayath Abdul Salam[1], Linu Mohammad Salim[2], Sajad Rehman[2], Jisha Manakulam Shaik Moideen[2], Anooja Thomas[2]

1 – Mar Athanasios College for Advanced Studies, Tiruvalla, Kerala, India
2 – Mahatma Gandhi University, Kottayam, Kerala, India
3 - Kerala University of Fisheries and Ocean Studies, Panangad, Kochi, Kerala, India

Keywords:

Piper betel
Green synthesis
Silver
Nanoparticle
Zinc oxide
Polylactic acid
Packaging

Article history:

Received 23.04.2026
Received in revised form 16.08.2026
Accepted 30.09.2026

Corresponding author:

Radhalakshmi Venugopal
E-mail: radhalakshmivgn@gmail.com

DOI:
10.24263/2304-974X-2026-15-3-11

Abstract

Introduction. This study aimed to synthesise silver (Ag) and zinc oxide (ZnO) nanoparticles using *Piper betel* leaf extract, evaluate their antioxidant and antibacterial activities, and incorporate the more active nanoparticles into polylactic acid (PLA) to develop active packaging films.

Materials and methods. *Piper betel* leaf extract was used for the green synthesis of Ag and ZnO nanoparticles, which were characterised and evaluated for antioxidant activity using the 2,2-diphenyl-1-picrylhydrazyl (DPPH) and 2,2′-azino-bis(3-ethylbenzothiazoline-6-sulfonic acid) (ABTS) assays and for antibacterial activity against *Escherichia coli*, *Pseudomonas aeruginosa*, and *Staphylococcus aureus*. The selected nanoparticles were incorporated into PLA films, and their physical, barrier, mechanical, and biodegradation properties were evaluated. The films were also assessed for their effectiveness during grape storage.

Results and discussion. Ag nanoparticles exhibited higher antioxidant activity than ZnO nanoparticles, reaching 40.4% and 42.3% in the DPPH and ABTS assays, respectively, and showed stronger antibacterial activity against the tested microorganisms. The higher total phenolic and flavonoid contents detected in the Ag nanoparticles may be attributed to phytochemicals derived from the *Piper betel* leaf extract used during their green synthesis. Based on their high biological activity, Ag nanoparticles were selected for incorporation into PLA-based active packaging films. Addition of the nanoparticles improved the barrier and mechanical properties of the films. The water vapour transmission rate decreased to 74.2 $g/m^2/day$, while the gas transmission rate decreased to 290 $cm^3/m^2/day/atm$. Tensile strength increased to 261 kg/cm^2, whereas elongation at break reached 3.75%. During storage, grapes packaged in the active film with silver nanoparticles exhibited lower weight loss (12.8%) than those packaged in the control film (18.0%), indicating improved moisture retention and storage performance.

Conclusions. Incorporation of green-synthesised Ag nanoparticles produced using *Piper betel* leaf extract improved selected barrier and mechanical properties of PLA-based films and reduced grape weight loss during storage. These findings indicate the potential of the developed films for active food packaging applications and for improving the storage quality of fresh fruits.

Introduction

Increasing attention has been paid to the environmental pollution caused by the production and disposal of conventional synthetic plastics (Vaseashta et al., 2025). Although plastic packaging effectively protects food from contamination and spoilage during transportation and storage, its resistance to biodegradation contributes to environmental pollution and poses a serious threat to aquatic and terrestrial ecosystems. This has stimulated the development of biodegradable and more environmentally sustainable alternatives for food packaging (Wang et al., 2022).

Active packaging systems are particularly promising because they can provide additional functionalities, such as antimicrobial and antioxidant activity and improved oxygen barrier properties, which can help extend food shelf life, reduce the need for chemical additives and preservatives, and maintain food quality (Jamshidian et al., 2013; Sani et al., 2021; Stabnikova et al., 2026a, b). Among biodegradable polymers, polylactic acid (PLA) is one of the most widely studied materials for food packaging. PLA is a biodegradable and compostable aliphatic polyester produced from renewable resources, such as starch-rich crops, through fermentation and subsequent polymerisation of lactic acid. Its biodegradability, renewability, and suitable mechanical properties make PLA a promising alternative to conventional petrochemical-based polymers for food packaging applications (Jamshidian et al., 2013; Stabnikov et al., 2025).

Despite these advantages, PLA films have some limitations, including relatively low hydrophilicity, limited flexibility, and insufficient barrier and functional properties for certain food packaging applications. Therefore, various approaches have been investigated to modify the PLA matrix and improve its performance. The incorporation of nanoparticles (NPs) into PLA has been reported as an effective strategy for enhancing the functional, barrier, and mechanical properties of PLA-based packaging materials (Demchenko et al., 2025; Zhang et al., 2017).

Nanoparticles, typically ranging in size from 1 to 100 nm, possess unique physicochemical properties that differ from those of bulk materials, making them attractive for various technological applications. Green synthesis using plant extracts has gained increasing attention as a simple and environmentally friendly approach to nanoparticle production (Ealias & Saravanakumar, 2017). In particular, *Piper betel* leaf extract contains bioactive compounds that can act as reducing and stabilising agents in the synthesis of nanoparticles, including silver and zinc oxide nanoparticles (Gayadang et al., 2023; Harikrishnan et al., 2024).



Figure 1. *Piper betel* leaf (Koottakkodi nadan cultivar)

Betel leaf (*Piper betle* L.), a member of the family Piperaceae, is widely cultivated in tropical and subtropical regions of Asia and is valued for its diverse bioactive compounds. Its leaves contain phenolic compounds, flavonoids, tannins, and other phytochemicals that contribute to their antioxidant and antimicrobial properties (Barak & Mudgil, 2022; Kaur et al., 2019; Nayaka et al., 2021). These bioactive compounds can also act as reducing and stabilising agents in the green synthesis of nanoparticles, making *Piper betle* leaf extract a promising plant-based resource for nanoparticle production (Gayadang et al., 2023; Harikrishnan et al., 2024).

The present study aimed to develop biodegradable PLA-based active packaging films incorporating nanoparticles synthesised using *Piper betle* leaf extract and to evaluate their physicochemical properties and potential for improving the storage quality of grapes.

Materials and methods

Materials

Fresh *Piper betle* (Koottakkodi Nadan cultivar) leaves (Figure 1) were purchased from Malappuram District, Kerala, India. The leaves were washed, dried in a tray dryer (Duex, India) at 45 °C for 24 h, packed in low-density polyethylene pouches, and stored in a desiccator at 37 °C until use. Poly(lactic acid) (PLA) pellets (Ingeo 2003D; specific gravity, 1.24; melting temperature, 210 °C) were obtained from Natur Tec India Private Limited, Chennai, India.

Zinc acetate, sodium hydroxide, silver nitrate, Folin–Ciocalteu reagent, gallic acid, sodium carbonate, tannic acid, quercetin, chloroform, and other reagents of analytical grade were purchased from Associated Chemicals (Kochi, India). Distilled water was used for solution preparation.

Determination of proximate composition of betel leaves

The proximate composition of betel leaves, including moisture, ash, lipid, protein, and carbohydrate contents, was determined according to the official AOAC methods (AOAC International, 2023).

Preparation of betel leaf extract

Betel leaf extract was prepared according to Varadavenkatesan et al. (2019), with modifications. Briefly, 20 g of powdered betel leaves was mixed with 200 mL of distilled water and heated at 90 °C for 60 min in a flask (Equitron, India). After cooling, the mixture was filtered through Whatman No. 1 filter paper. The resulting pale-yellow extract was stored under refrigeration until use.

Green synthesis of BL-based nanoparticles

ZnO and Ag nanoparticles were synthesised using betel leaf extract according to previously reported methods (Joseph et al., 2021; Varadavenkatesan et al., 2019), with modifications. For ZnO nanoparticle synthesis, 20 mL of betel leaf extract was mixed with 50 mL of 50 mM zinc acetate using a magnetic stirrer (DAN logitec, India). Subsequently, 10 mL of 2 N NaOH was added dropwise at 80 °C, and the mixture was stirred for 60 min. The resulting white precipitate was collected by centrifugation (Tempstar, Mexico) at 6000 rpm for 30 min and lyophilised using a freeze dryer (AVM Industries, India). The dried ZnO nanoparticles were stored at −18 °C until further analysis.

For Ag nanoparticle synthesis, 10 mL of betel leaf extract was mixed with 100 mL of 20 mM silver nitrate and stirred at 70 °C until a colour change was observed. The resulting suspension was centrifuged at 6000 rpm for 30 min, and the collected pellet was lyophilised using a freeze dryer (AVM Industries, India). The dried Ag nanoparticles were stored at −18 °C until further analysis.

Characterisation of nanoparticles

The optical properties of the ZnO and Ag nanoparticles were analysed by UV–Vis spectroscopy over the wavelength range of 200–800 nm using a UV–Vis spectrophotometer (Amaze Instruments, India). The formation of the nanoparticles was confirmed based on their characteristic absorption peaks (Varadavenkatesan et al., 2019).

The functional groups associated with the nanoparticles were identified using Fourier-transform infrared spectroscopy with attenuated total reflectance (FTIR-ATR; Shimadzu IRPrestige-21, Japan) over the range of 550–4000 cm^{-1} at a resolution of 0.2 cm^{-1}.

The crystalline phases of the nanoparticles were determined by X-ray diffraction (XRD). Dried nanoparticle samples were analysed using a MiniFlex benchtop X-ray

diffractometer (Rigaku, Japan) equipped with a D/teX Ultra 250 1D detector and SmartLab SE II software. Measurements were performed over a 2θ range of 5–90° at a scan rate of 10°/min.

The hydrodynamic particle size and zeta potential were determined using a Litesizer DLS 500 particle analyser (Anton Paar, Austria). Nanoparticle suspensions were dispersed in water using a bath sonicator (Analab, India), and 2.5 mL of the suspension was transferred to an Omega cuvette for analysis (Nguyen et al., 2021).

The morphology of the Ag and ZnO nanoparticles was examined by transmission electron microscopy (TEM; JEOL, Japan). Nanoparticle suspensions were sonicated for 10 min, and a drop was placed onto carbon-coated copper grids and dried before analysis. TEM images were obtained at an accelerating voltage of 200 kV with a resolution of 0.22 nm (Kharat & Mendhulkar, 2016).

Determination of total phenolic, flavonoid, and tannin contents

The total phenolic content (TPC) was determined using a modified Folin–Ciocalteu method. Briefly, 0.5 mL of the sample was mixed with 0.5 mL of Folin–Ciocalteu reagent and 5 mL of distilled water and incubated for 10 min at 22 °C. Subsequently, 1.5 mL of 20% sodium carbonate was added, and the volume was adjusted to 10 mL with distilled water. The mixture was heated at 40 °C for 20 min in a water bath (Equitron, India), followed by cooling in an ice bath. Absorbance was measured at 755 nm using a UV–Vis spectrophotometer (Amaze Instruments, India). Gallic acid (0.1 mg/mL) was used as the standard.

The total flavonoid content (TFC) was determined using the aluminium chloride colorimetric method (Verawati et al., 2016). Briefly, 0.5 mL of the sample was mixed with 1.5 mL of methanol, 0.1 mL of 10% aluminium chloride, and 0.1 mL of 1 M sodium acetate. The volume was adjusted to 5 mL with distilled water, and the mixture was incubated for 30 min. Absorbance was measured at 415 nm using a UV–Vis spectrophotometer (Amaze Instruments, India). Quercetin (0.125 mg/mL) was used as the standard.

The total tannin content (TTC) was determined using the Folin–Ciocalteu method (Ci & Indira, 2016). Briefly, 0.1 mL of the sample was mixed with 0.5 mL of Folin–Ciocalteu reagent, 5 mL of distilled water, and 1 mL of 35% sodium carbonate. The volume was adjusted to 10 mL with distilled water. After incubation for 30 min, absorbance was measured at 700 nm using a UV–Vis spectrophotometer (Amaze Instruments, India). Tannic acid (0.1 mg/mL) was used as the standard.

Functional properties of nanoparticles

Antioxidant activity by DPPH radical scavenging assay. The antioxidant activity of the nanoparticles was evaluated using the DPPH (2,2-diphenyl-1-picrylhydrazyl) radical scavenging assay according to Hussen and Endalew (2023), with modifications. Briefly, nanoparticle suspensions were prepared in distilled water and diluted with methanol to obtain concentrations of 0.1, 0.2, 0.3, 0.4, and 0.5 μg/mL. For the assay, 2 mL of each nanoparticle suspension was mixed with 3 mL of DPPH solution and incubated in the dark at 22 °C for 30 min. The absorbance was measured at 517 nm using a UV–Vis spectrophotometer (Amaze Instruments, India). The decrease in absorbance relative to the DPPH control was used to determine the radical-scavenging activity.

The percentage of DPPH radical inhibition was calculated as:

$$\text{DPPH inhibition (\%)} = [(A_0 - A_1) / A_0] \times 100,$$

where A_0 is the absorbance of the DPPH control and A_1 is the absorbance of the nanoparticle–DPPH mixture.

Antioxidant activity by ABTS radical scavenging assay. 7 mM ABTS (2,2′-azino-bis(3-ethylbenzothiazoline-6-sulfonic acid)) and 2.4 mM potassium persulfate solutions were mixed in equal proportions and incubated for 12 h at room temperature in the dark to generate the $ABTS^{\bullet+}$ radical solution. The resulting solution was diluted with ethanol to obtain an absorbance of 0.70±0.01 at 734 nm.

For the assay, 40 μL of the nanoparticle suspension was mixed with 6 mL of the $ABTS^{\bullet+}$ solution and incubated under the same conditions. The absorbance was measured at 734 nm using a UV–Vis spectrophotometer (Amaze Instruments, India). The $ABTS^{\bullet+}$ solution without the sample was used as the control. The percentage of $ABTS^{\bullet+}$ radical inhibition was calculated as:

$$\text{ABTS inhibition (\%)} = [(A_0 - A_1) / A_0] \times 100,$$

where A_0 is the absorbance of the control and A_1 is the absorbance of the sample–$ABTS^{\bullet+}$ mixture.

Antimicrobial activity by the well diffusion method. The antibacterial activity of the ZnO and Ag nanoparticles was evaluated against the Gram-positive *Staphylococcus aureus* and the Gram-negative *Escherichia coli* and *Pseudomonas aeruginosa* using the agar well diffusion method (Logeswari et al., 2015). Briefly, bacterial inocula were uniformly spread over the surface of sterile Mueller–Hinton agar (MHA) plates using sterile cotton swabs. Wells were prepared using a sterile cork borer, and 50, 75, or 100 μL of nanoparticle suspension (40 mg/mL) was added to each well. Distilled water was used as the control. The plates were incubated at 35 °C for 18 h, after which the inhibition zones were measured in millimetres.

Preparation of PLA-based active packaging films incorporated with silver nanoparticles

PLA-based active packaging films were prepared by the solution casting method. For the control film, 4 g of PLA pellets were dissolved in 80 mL of chloroform under magnetic stirring (DAN logitec, India) for 5 h (Radhalakshmi et al., 2023). For the active films, 0.25 g of Ag nanoparticles (5 wt.% relative to the PLA mass) was added to the PLA-chloroform solution and mixed thoroughly. The resulting suspension was poured into glass Petri plates (20 cm in diameter) and dried at ambient temperature for 48 h. The dried films were carefully peeled from the Petri plates and used for further analyses.

Characterisation of the film

Thickness. Film thickness was measured at six different locations using a digital screw gauge (Insize, China) with an accuracy of 0.01 mm. The mean value was calculated and reported (Radhalakshmi et al., 2023).

pH, moisture content, and swelling degree. The pH of the films was measured using a digital pH meter (Eutech, Singapore) according to Radhalakshmi et al. (2023).

Moisture content was determined according to Kanatt et al. (2020). Film samples were dried in a hot-air oven (Equitron, India) at 105 °C for 24 h until a constant weight was reached. The analysis was performed in triplicate.

The swelling degree of the films was determined according to Ediyilyam et al. (2021). Briefly, film samples were weighed before and after immersion in distilled water. The samples were immersed in distilled water for 24 h at 37 °C, removed, and gently blotted with tissue paper to remove surface water. The swelling degree was calculated as:

$$\text{Swelling degree (\%)} = [(W_s - W_d) / Wd] \times 100,$$

where W_d is the weight of the dry film (g) and W_s is the weight of the film after immersion in water (g).

Phenolic compound migration from the films was evaluated using 95% ethanol and distilled water as food simulants for fatty and aqueous foods, respectively (Gebrechristos et al., 2020). Film samples (2 cm^2) were immersed in 5 mL of each food simulant and shaken at 125 rpm and 25 °C for 7 days.

After the exposure period, the concentration of migrated phenolic compounds was determined using the Folin-Ciocalteu method. 0.5 mL of the food simulant was mixed with 2.5 mL of 10% Folin-Ciocalteu reagent and 7.5% sodium bicarbonate solution. The mixture was incubated at 45 °C for 45 min, and the absorbance was measured at 760 nm using a UV–Vis spectrophotometer (Amaze Instruments, India).

Colour evaluation. The colour of the films was evaluated using a ColourFlex EZ colorimeter (HunterLab, USA). The CIELAB colour parameters L* (lightness), a* (red-green coordinate), and b* (yellow–blue coordinate) were measured. Chroma (C*) and colour difference (ΔE) were calculated from the measured parameters according to Kanatt et al. (2020).

The ΔE (the difference in colour) was calculated by,

$$\Delta E^* = [(\Delta L^*)^2 + (\Delta a^*)^2 + (\Delta b^*)^2]^{0.5}$$

Determination of water vapour transmission and gas transmission rate. The water vapour transmission rate (WVTR) of the films was determined using a gravimetric method according to Ediyilyam et al. (2021). Briefly, 10 mL of deionised water was placed in dishes with a mouth diameter of 2 cm and covered with the control or active films. The dishes were weighed initially and then placed in a hot-air oven (Equitron, India) at 40 °C for 24 h. After incubation, the dishes were reweighed, and the WVTR was calculated as:

$$WVTR = (W_i - W_t) / (A \times T),$$

where W_i is the initial weight of the dish (g), W_t is the final weight of the dish (g), A is the exposed area of the film (m^2), and T is the test duration (h).

The gas transmission rate (GTR) of the films was determined using a VAC-VBS gas permeability tester (Labthink Inc., USA) based on the differential-pressure method in accordance with GB/T 1038-2000. A gas diffusion cell was used to separate the two chambers with the film sample, which had been pre-conditioned for 24 h. Measurements were performed at 23±2 °C and 60% relative humidity. The GTR was determined by monitoring the pressure change in the lower chamber (Radhalakshmi et al., 2023).

Mechanical properties. The mechanical properties of the films, including tensile strength (TS) and elongation at break (E), were evaluated using a texture analyser (Sun2500, Italy) according to the relevant ASTM standard. Film specimens were cut into rectangular strips measuring 10 mm in width and 100 mm in length. A 1.5 kN load cell was used, and the crosshead speed was set at 25 mm/min.

Tensile strength was calculated by dividing the peak load (N) by the cross-sectional area of the film specimen (mm^2):

$$TS = F / A,$$

where *F* is the peak load (N) and A is the cross-sectional area of the specimen (mm^2).

Elongation at break was calculated by dividing the elongation at break by the initial specimen length and multiplying by 100 (Nouri & Nafchi, 2014):

$$E\ (\%) = [(L_b - L_0 / L_0] \times 100,$$

where L_0 is the initial specimen length (mm) and L_b is the specimen length at break (mm).

Biodegradability. The biodegradability of the films was evaluated using an indoor soil burial method (Plaeyao et al., 2025). Film specimens were cut into 1 × 1 cm² pieces and buried in 50 mL graduated cylinders containing 50 g of moist soil. The specimens were placed at a depth of 5 cm below the soil surface, with the soil filled to a total depth of 10 cm. To maintain soil moisture, 1 mL of water was added to the soil surface daily.

At predetermined intervals, the film samples were removed from the soil, rinsed with water to remove adhering soil particles, and air-dried at room temperature for 24 h. The degree of film biodegradation was calculated using the following equation:

$$\text{Biodegradation (\%)} = [(m_i - m_t) / m_i] \times 100,$$

where m_i is the initial weight of the film sample (g) and m_t is the weight of the film sample after the burial period (g).

Application of biodegradable packaging film on the shelf-life evaluation of grapes. Grapes of uniform size, shape, and firmness were initially washed with chlorinated water and subsequently rinsed with fresh water. Equal amounts of grapes were placed in three beakers. Two beakers were covered with the control and active films, while the third was covered with a glass plate and used as the open control. The samples were stored at room temperature for 7 days, and physical changes in the grapes were monitored throughout the storage period (Batool et al., 2022).

Statistical analysis

The experiments were carried out twice, and the mean±standard deviation was used to describe the results. Using R Studio, the one-way ANOVA was conducted using Tukey's significant difference test ($p<0.05$).

Results and discussions

Proximate composition of betel leaves

The proximate composition of betel leaves was as follows: moisture, 85.2%; carbohydrates, 9.3%; protein, 3.4%; crude fibre, 1.9%; ash, 1.9%; and lipids, 0.14%.

Characterisation of ZnO and Ag nanoparticles synthesised using betel leaf extract

UV–Visible spectroscopy

The UV–Vis absorption spectra of the nanoparticles were analysed in the wavelength range of 200–800 nm. The Ag and ZnO nanoparticles exhibited characteristic absorption bands within this range, indicating the formation of the respective nanoparticles. The absorption maxima were observed at 260, 358, and 574 nm for the Ag nanoparticles and at 302 and 356 nm for the ZnO nanoparticles. These absorption characteristics were generally consistent with previously reported results (Krishana et al., 2024; Theresih et al., 2021). The formation of Ag nanoparticles was also accompanied by a visible colour change of the reaction mixture from light yellow to reddish-brown, which is consistent with the formation of silver nanoparticles through a plant-mediated synthesis process (Kharat & Mendhulkar, 2016).

FTIR Spectroscopy

FTIR spectroscopy was used to identify the functional groups of phytochemicals associated with the formation and stabilisation of the ZnO and Ag nanoparticles synthesised using betel leaf extract. The FTIR spectra are presented in Figure 2.

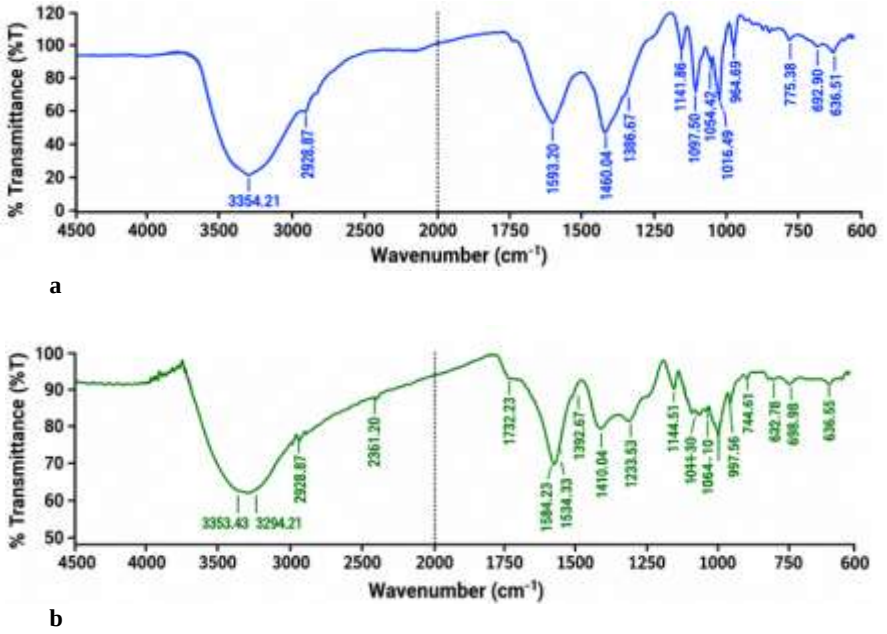

Figure 2. FTIR spectra of the synthesised (a) ZnO and (b) Ag nanoparticles

The FTIR spectrum of ZnO NPs showed a band at 2929 cm^{-1}, which was assigned to C–H stretching vibrations of alkanes. The band at 1593 cm^{-1} was attributed to C=O stretching vibrations characteristic of carboxylic acids. The bands observed in the 1408–1336 cm^{-1} region were associated with O–H vibrations of phenolic compounds. Additional bands at 1141 and 1016 cm^{-1} were assigned to C–O stretching vibrations of alkyl aryl ethers and primary alcohols, respectively. These functional groups indicate the presence of plant-derived compounds associated with the ZnO nanoparticles and may contribute to their formation and surface stabilisation.

The characteristic absorption bands in the 400–600 cm^{-1} region were attributed to Zn–O vibrations, confirming the formation of ZnO nanoparticles. Overall, the FTIR profile indicates the association of phytochemical constituents from the betel leaf extract with the ZnO nanoparticle surface. Phenolic compounds, carboxylic acids, alcohols and other oxygen-containing constituents may participate in the formation and stabilisation of the nanoparticles. These findings are consistent with previously reported FTIR characteristics of plant-mediated ZnO nanoparticles (Krishana et al., 2024; Mai et al., 2021; Nagarajaiah et al., 2023; Sharmila et al., 2018).

The observed FTIR bands for both ZnO and AgNPs suggest that several phytochemical constituents of the betel leaf extract were associated with the nanoparticle surface and may have contributed to nanoparticle formation and stabilisation. Thus, the FTIR results support the involvement of plant-derived functional groups in the green synthesis of ZnO and AgNPs. The obtained spectral characteristics are in agreement with previously reported studies on plant-mediated synthesis of metal and metal oxide nanoparticles (Jacob et al., 2012; Khan et al., 2020; Ramachandran et al., 2016; Rani & Rajasekharreddy, 2011).

Table 1

FTIR spectral bands and their assignments for the synthesised ZnO and Ag nanoparticles

Wave number (cm^{-1})	Functional group / vibration	Predicted compound
ZnO NPs		
2929	C–H stretching	Alkane
1593	C=O stretching	Carboxylic acid
1408–1336	O–H vibrations	Phenol
1141	C–O stretching	Alkyl aryl ether
1016	C–O stretching	Primary alcohol
400–600	Zn–O vibrations	Zinc oxide
AgNPs		
2902	C–H stretching	Alkane
2351	C≡N stretching	Nitrile
1235	C–N stretching	Aromatic amine
1138	C–O stretching	Alkyl aryl ether
1068	C–O stretching	Primary alcohol

X-ray diffraction studies (XRD)

The crystalline structure of the synthesised ZnO and Ag nanoparticles was investigated by X-ray diffraction (XRD), and the obtained diffraction patterns are presented in Figure 3.

The XRD pattern of the ZnO NPs (Figure 3a) exhibited distinct diffraction peaks at 2θ = 31.68°, 34.37°, 36.17°, 47.58°, 56.50°, 62.04°, and 66.60°. These characteristic reflections confirm the formation of a crystalline ZnO phase and are consistent with previously reported XRD patterns of plant-mediated ZnO nanoparticles (Harikrishnan et al., 2024; Krishana et al., 2024; Sharmila et al., 2018). The observed reflections are characteristic of the hexagonal wurtzite structure of ZnO. The relatively intense and well-defined diffraction peaks indicate a pronounced crystalline character of the synthesised ZnO NPs. The presence of minor additional reflections may be associated with residual phytochemical constituents originating from the betel leaf extract (Lagashetty et al., 2022). These results demonstrate the suitability of betel leaf extract as a plant-derived medium for the green synthesis of ZnO nanoparticles.

The XRD pattern of the AgNPs (Figure 3b) showed distinct diffraction peaks at 2θ = 32.13°, 38.07°, 43.64°, 64.46°, and 77.39°. The reflections observed in the region of approximately 38° and 44° are consistent with the characteristic diffraction pattern of crystalline metallic Ag and are generally assigned to the (111) and (200) planes, respectively. The presence of these reflections confirms the formation of crystalline Ag nanoparticles and agrees with previously reported results for plant-mediated synthesis of AgNPs (Khan et al., 2020; Ramachandran et al., 2016; Rani & Rajasekharreddy, 2011). The additional low-intensity reflections may be related to organic constituents of the betel leaf extract associated with the nanoparticle surface or to minor crystalline phases.

The broadening of diffraction peaks is generally associated with the nanoscale size of the crystallites, whereas sharp and intense reflections indicate a higher degree of crystallinity. Overall, the XRD results confirm the crystalline nature of both ZnO and AgNPs synthesised using betel leaf extract. The ZnO NPs exhibit the characteristic hexagonal wurtzite structure, while the crystalline Ag phase is associated with the face-centred cubic (fcc) structure of metallic silver. Similar crystalline characteristics have been reported for ZnO and Ag nanoparticles synthesised using plant-derived extracts (Theresih et al., 2021).

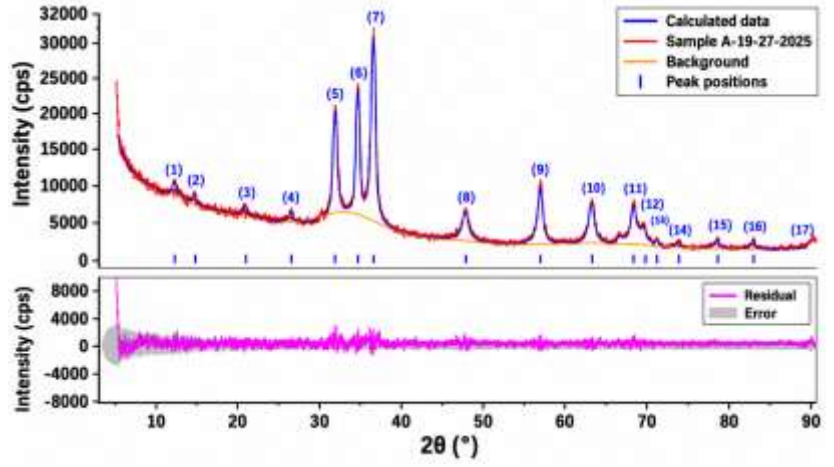

a

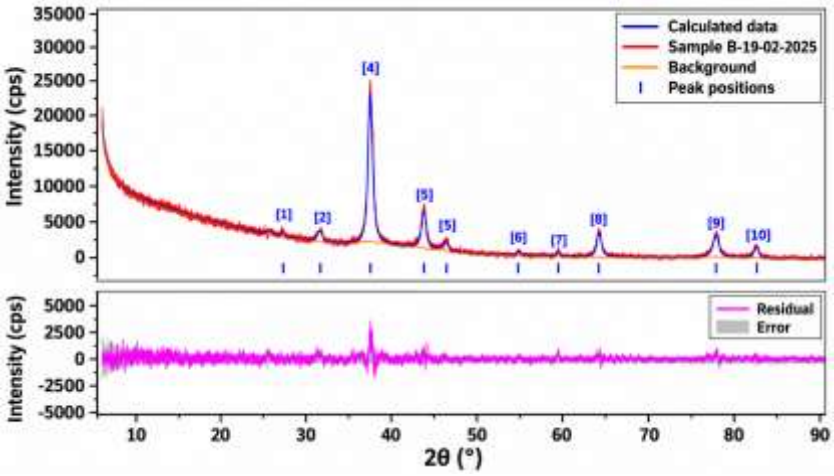

b

Figure 3. X-ray diffraction patterns of ZnO NPs (a) and AgNPs (b) synthesised using betel leaf extract

Particle size and zeta potential

The surface charge and colloidal stability of the synthesised nanoparticles using betel leaf extract were evaluated by zeta potential measurements. Figures 4a and b show the zeta potential distributions of the ZnO and AgNPs, respectively. The average zeta potential values were −7.0 mV for ZnO NPs and −10.5 mV for AgNPs. The negative zeta potential values indicate that the nanoparticle surfaces were associated with negatively charged molecules derived from the betel leaf extract. These surface-bound phytochemicals may contribute to electrostatic repulsion between particles and thus reduce their tendency to aggregate (Barzinjy & Azeez, 2020).

The more negative zeta potential observed for the AgNPs (−10.5 mV) compared with the ZnO NPs (−7.0 mV) suggests a somewhat greater electrostatic contribution to colloidal

stability. However, the relatively low absolute values of the zeta potential indicate that electrostatic repulsion alone is unlikely to provide strong colloidal stabilisation. The overall stability of the biosynthesised NPs may therefore also depend on steric effects and interactions of phytochemicals adsorbed onto the nanoparticle surfaces. Similar negative zeta potential values have been reported for plant-mediated ZnO and Ag nanoparticles (Harikrishnan et al., 2024; Nguyen et al., 2021).

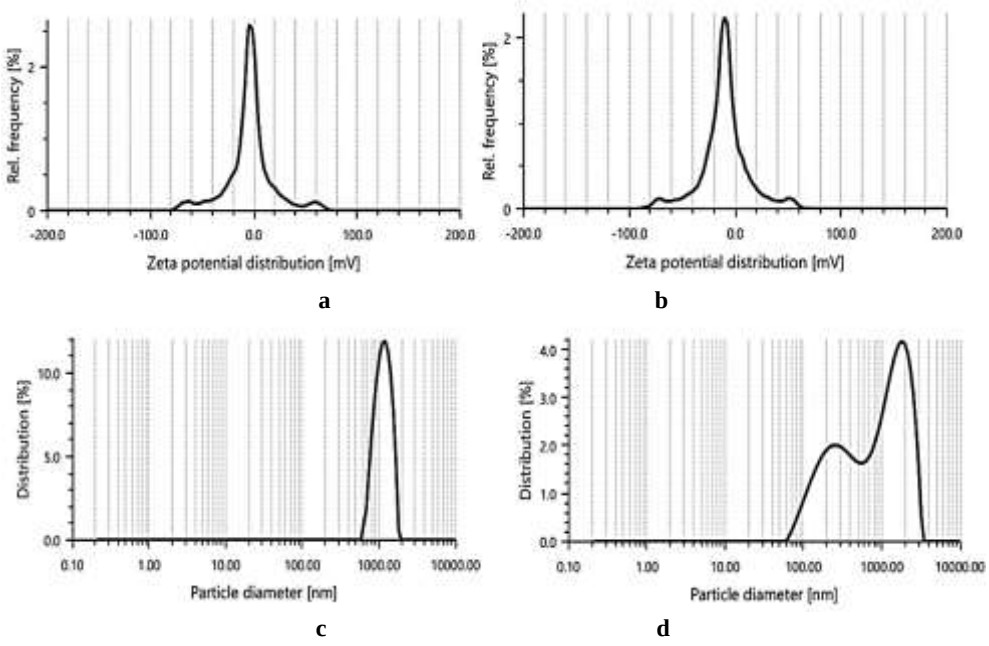

Figure 4. Zeta potential of ZnO (a) and Ag (b) nanoparticles; DLS size distribution of ZnO (c) and Ag (d) nanoparticles

Figures 4c and 4d show the dynamic light scattering (DLS) size distributions of the ZnO and Ag nanoparticles, respectively. Figure 4d shows two peaks, which may indicate the presence of nanoparticles of different sizes in the sample and could be related to the formation of aggregates (Yeap et al., 2018). The ZnONPs exhibited an average particle size of 2259 nm, while the AgNPs showed an average particle size of 1243 nm. DLS is based on the relationship between the Brownian motion of particles and the fluctuations in light scattering in a colloidal suspension (Rasmussen et al., 2020). The polydispersity index (PDI) was 29.1% for the ZnO NPs and 29.9% for the AgNPs. The relatively large particle sizes may be attributed to nanoparticle agglomeration (Berg et al., 2009; Tullo et al., 2005).

Transmission electron microscopy

Figure 5 shows the spherical morphology of the ZnO and Ag nanoparticles, as observed by transmission electron microscopy (TEM). The ZnO NPs had particle diameters ranging from 25 to 60 nm, while the AgNPs ranged from 20 to 70 nm (Bharathi et al., 2024; Nagarajaiah et al., 2023; Rashid et al., 2016). Aggregation of both types of nanoparticles was

observed in the TEM images. A thin organic layer surrounding the small particle aggregates was also observed, which may act as a capping layer derived from the betel leaf extract. This may contribute to the dispersion of the nanoparticles in the bio-reduced aqueous solution (Raj et al., 2018).

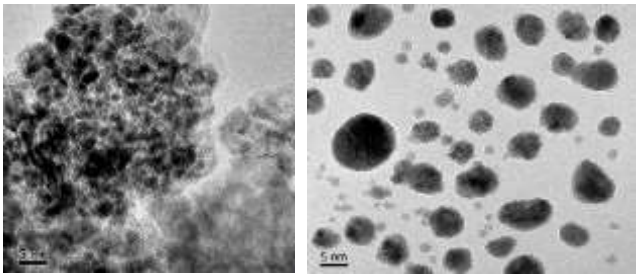

a **b**

Figure 5. TEM images of ZnONPs (a) and AgNPs(b) synthesised using betel leaf extract

The particle sizes observed by TEM were substantially smaller than the average sizes determined by DLS, which were 2259 nm for the ZnO NPs and 1243 nm for the AgNPs. This difference is consistent with the aggregation observed in the TEM images and the size distributions obtained by DLS. The negative zeta potential values observed for both ZnO and Ag nanoparticles may be attributed to the capping activity of biomolecules present in the betel leaf extract. These results are consistent with previous studies (Nagarajaiah et al., 2023; Rani & Rajasekharreddy, 2011).

Total phenolic, flavonoid, and tannin contents and antioxidant activities of ZnO and Ag nanoparticles synthesised using betel leaf extract

Phenols are effective scavengers of oxygen radicals due to their low electron reduction potential and relatively low reactivity. Table 2 presents the total phenolic content of the ZnO and AgNPs.

Table 2

Total phenolic, flavonoid, and tannin contents and antioxidant activities of ZnO and AgNPs synthesised using betel leaf extract

Properties	ZnO NPs	AgNPs
Total phenolic content, mg GAE/g	$17.34^{a\pm}0.9$	$22.61^{b\pm}0.3$
Total flavonoid content, mg QE/g	$1.8^{a\pm}0.2$	$7.35^{b}\pm0.3$
Total tannin content, mg TAE/g	$1.93^{a\pm}0.2$	$0.49^{b\pm}0.4$
DPPH radical scavenging assay (%)	$26.95^{a}\pm0.1$	$40.35^{b}\pm0.2$
ABTS radical scavenging assay (%)	$26.24^{a\pm}0.2$	$42.33^{b}\pm0.3$

Values represented as mean±standard deviation. Different superscripts in the same row indicate a significant difference ($p < 0.05$). GAE: Gallic acid equivalent, QE: Quercetin equivalent, TAE: Tannic acid equivalent, DPPH: 2,2-diphenyl-1-picrylhydrazyl, ABTS: 2,2-azino-bis (3-ethylbenzothiazoline-6-sulfonic acid)

The total phenolic content, expressed as mg gallic acid equivalents per gram (mg GAE/g), was lower in the ZnO NPs (17.34±0.9 mg GAE/g) than in the AgNPs (22.61±0.3 mg GAE/g), and the difference was statistically significant ($p < 0.05$). Compared with NPs synthesised using *Chenopodium murale*, *Persicaria hydropiper*, *Rubus discolor*, and *Lallemantia royleana*, the NPs synthesised using betel leaf extract showed a high total phenolic content (Mankad et al., 2016).

The quantity and position of free hydroxyl (OH) groups influence the antioxidant activity of flavonoids, a class of secondary metabolites with well-established antioxidant properties. As shown in Table 3, the total flavonoid content (TFC), expressed as milligrams of quercetin equivalents per gram (mg QE/g), was higher in the AgNPs (7.35±0.3 mg QE/g) than in the ZnO NPs (1.80±0.2 mg QE/g). Compared with ZnO and Ag nanoparticles synthesised using other plant extracts, the nanoparticles produced using betel leaf extract exhibited relatively high total flavonoid contents (Dangana et al., 2023; Geremew et al., 2023; Ghasemi et al., 2024; Hussain et al., 2021; Jain & Mehata, 2017). The difference in TFC between the ZnO NPs and AgNPs was statistically significant ($p < 0.05$).

Tannins are secondary plant metabolites that contribute to the biological properties of plant extracts. Although tannins are considered protective compounds that help plants respond to environmental stress and herbivory, excessive concentrations may be undesirable for human consumption (du Toit et al., 2020). Table 3 shows the total tannin content of the ZnO and AgNPs. The tannin content was 1.93±0.2 mg TAE/g in the ZnO NPs and 0.49±0.4 mg TAE/g in the AgNPs, with a statistically significant difference between the samples ($p < 0.05$). Compared with ZnO and AgNPs synthesised using other plant leaves, including *Ipomoea pes-caprae*, *Lallemantia royleana*, and *Rubus discolor*, the ZnO and AgNPs synthesised using betel leaf extract showed higher tannin contents (Ghasemi et al., 2024; Sharifi-Rad et al., 2024; Venkateasan et al., 2017). In the present study, the tannin content was relatively low compared with the phenolic and flavonoid contents.

Antioxidant activity

Table 3 shows the antioxidant activity of the studied nanoparticles synthesised using betel leaf extract. According to the DPPH radical-scavenging assay, AgNPs exhibited higher antioxidant activity (40.35±0.2%) than ZnO NPs (26.95±0.1%). These results are consistent with previous studies (Kharat & Mendhulkar, 2016). The higher phenolic content of AgNP may contribute to its greater antioxidant activity.

AgNPs also exhibited higher ABTS radical-scavenging activity (42.33±0.3%) than ZnO NPs (26.24±0.2%), possibly due to the presence of phenolic and flavonoid compounds (Ragavendran et al., 2024; Thanh et al., 2022). The values indicate significant differences among the treatments compared with the control ($p < 0.05$).

Antimicrobial activity

Antibacterial activity of AgNPs and ZnO NPs was assessed against both Gram-positive and Gram-negative bacteria (Table 3 and Figure 6). The results showed that AgNPs exhibited a greater inhibitory effect than ZnO NPs. The highest antimicrobial activity was observed against the Gram-positive bacterium *Staphylococcus aureus* compared with the Gram-negative bacteria *Escherichia coli* and *Pseudomonas aeruginosa*.

Table 3

Inhibition zones of Ag and ZnO nanoparticles against the tested microorganisms

Tested microorganisms	AgNPs, µL			ZnO NPs, µL		
	25	50	100	25	50	100
	Inhibition zone, mm					
Escherichia coli	17	19	21	16	17	19
Pseudomonas aeruginosa	17	19	20	17	18	20
Staphylococcus aureus	20	22	23	17	19	21

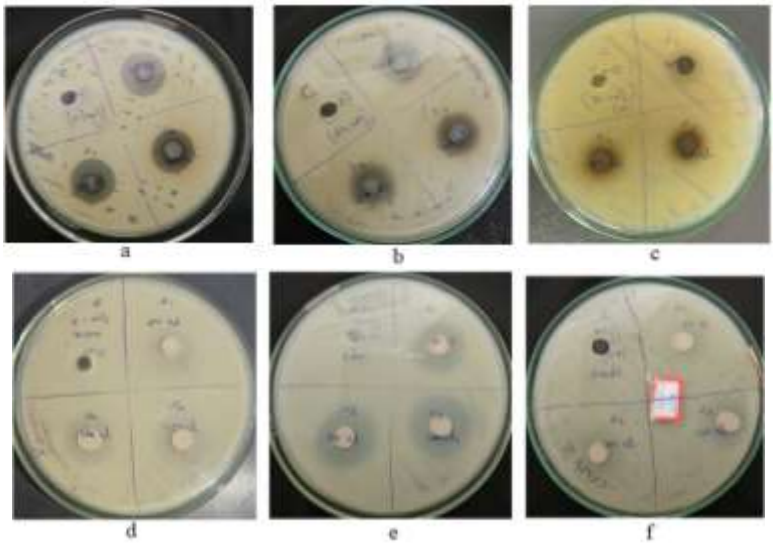

Figure 6. Inhibition zone of:
AgNPs against *Staphylococcus aureus* (a); *Pseudomonas aeruginosa* (b); *Escherichia coli* (c), and ZnO NPs against *S. aureus* (d); *P. aeruginosa* (e); *E. coli* (f)

A zone of inhibition measuring 18.66 mm for AgNPs and 18.33 mm for ZnO NPs was observed against *P. aeruginosa.* For *S. aureus*, the zones of inhibition measured 21.66±0.64 mm for AgNPs and 19.00±0.42 mm for ZnO NPs. Similarly, the zones of inhibition against *E. coli* measured 19.00±0.45 mm for AgNPs and 17.33±0.21 mm for ZnO NPs. The zone of inhibition increased with increasing NP concentration.

The lipopolysaccharide-rich outer membrane of Gram-negative bacteria may contribute to their greater resistance to antibacterial treatments. In contrast, Gram-positive bacteria have a relatively porous peptidoglycan layer, which may facilitate the penetration of bioactive compounds and their interference with cellular metabolism. Overall, AgNPs exhibited stronger antibacterial activity than ZnO NPs, which may be associated with its higher phenolic content and antioxidant activity. Since AgNPs showed better results than ZnO NPs in these analyses, it was selected for further application.

Characterisation of PLA-based biodegradable active packaging films incorporated with Ag nanoparticles

Physical and physicochemical properties of the films

Silver nanoparticles were further used to develop PLA-based biodegradable active packaging films. The obtained films were smooth and uniform, with no visible ridges**.** The thickness of the control and active films is presented in Table 4.

The average thickness of the control film was 123.5±0.1 μm, whereas that of the active film was 136.9±0.2 μm ($p < 0.05$). The incorporation of AgNPs increased the thickness of the PLA film. This increase may be attributed to the additional solid content provided by the AgNPs or to changes in the film structure and surface morphology. A similar increase in film thickness following the incorporation of nanoparticles has been reported in previous studies (Dai et al., 2022; Radhalakshmi et al., 2023; Shankar et al., 2018).

Table 4

Characteristics of packaging films

Parameters	Control film	Active film with AgNPs
Thickness (μm)	123.5^{a}±0.1	136.9^{b}±0.2
pH	5.0^{a}±0.3	4.3^{b}±0.2
Moisture content (%)	10.8^{a}±0.4	10.5^{a}±0.2
Swelling capacity (%)	1.4^{a}±0.1	0.9^{b}±0.3
WVTR (g/m²/day)	111.5^{a}±0.2	74.2^{b}±0.4
GTR (cm³/m²/day/atm)	346.9^{a}±0.1	290.0^{b}±0.3
Tensile strength (kg/cm²)	168.6^{a}±0.5	261^{b}±0.6
Elongation at break (%)	3.10^{a}±0.03	3.75^{a}±0.01

Note: Values represented as mean±standard deviation. Different superscripts in the same row indicate a significant difference ($p < 0.05$).

The pH of the control and active film-forming solutions is presented in Table 4. The pH decreased from 5.0±0.3 for the control film to 4.3±0.2 for the active film ($p < 0.05$). This result is consistent with previous findings (Radhalakshmi et al., 2023). The decrease in pH following the addition of AgNPs may be associated with acidic constituents originating from the plant extract, particularly polyphenolic compounds (Kapilraj et al., 2019; Manach et al., 2004).

The moisture content of food packaging films can affect the quality and shelf life of packaged products. In the present study, the moisture content was slightly reduced from 10.8±0.4% in the control film to 10.5±0.2% in the active film (Table 4). However, according to the superscript notation in Table 5, this difference was not statistically significant. Similar results have been reported for films containing nanoparticles (Radhalakshmi et al., 2023). Negahdari et al. (2021) also reported a decrease in the moisture content of chitosan films following the incorporation of silica nanoparticles.

The swelling capacity is an important characteristic that can affect the barrier properties and biodegradability of polymer films. The control film exhibited a higher swelling capacity (1.4±0.1%) than the active film (0.9±0.3%) ($p < 0.05$). The incorporation of AgNPs therefore reduced the swelling capacity of the PLA film. This reduction may be related to interactions between AgNPs and PLA molecules, which can reduce the free volume within the polymer matrix and limit the penetration of water molecules (Lu et al., 2020; Radhalakshmi et al., 2023).

Barrier properties of the films

For packaging films, the water vapour transmission rate (WVTR), which reflects the film's resistance to water vapour penetration, is an important parameter, particularly for food packaging applications (Gitari et al., 2019). The incorporation of AgNPs significantly reduced both WVTR and GTR ($p < 0.05$). The WVTR decreased from 111.5±0.2 g/m²/day for the control film to 74.2±0.4 g/m²/day for the active film (Table 5). Similarly, the GTR decreased from 346.9±0.1 to 290.0±0.3 cm³/m²/day/atm. These results are consistent with previous studies (Medina-Jaramillo et al., 2017; Radhalakshmi et al., 2023).

The improved gas barrier properties of the active film may be associated with the reinforcing effect of AgNPs and the reduced availability of pathways for oxygen diffusion through the polymer matrix (Kasai et al., 2020). Improved gas barrier properties are important for limiting oxygen exposure and thereby reducing oxidative deterioration of packaged foods (Radhalakshmi et al., 2023). Similarly, low WVTR is desirable for packaging foods with high moisture content because it can help maintain product stability and quality (Nouri & Nafchi, 2014).

Phenolic migration of the films

The migration of phenolic compounds from active packaging films is an important parameter for evaluating their potential application as active food packaging materials. It provides information on the release of bioactive compounds from the polymer matrix into food simulants and, consequently, on their potential availability during food packaging. Phenolic compound migration from the active PLA film was evaluated using two food simulants: distilled water, representing aqueous foods, and 95% ethanol, representing fatty foods. The film samples were exposed separately to each food simulant for 7 days. No migration of phenolic compounds was detected in distilled water. This may be related to the low content of phenolic compounds in the film and their strong interactions with the PLA matrix (Radhalakshmi et al., 2023). The migration of polyphenolic compounds can also be influenced by their concentration, interactions with the polymer matrix, and the properties of the surrounding medium (Gebrechristos et al., 2020). Figure 7 shows the migration of phenolic compounds from the active PLA film into 95% ethanol over 7 days.

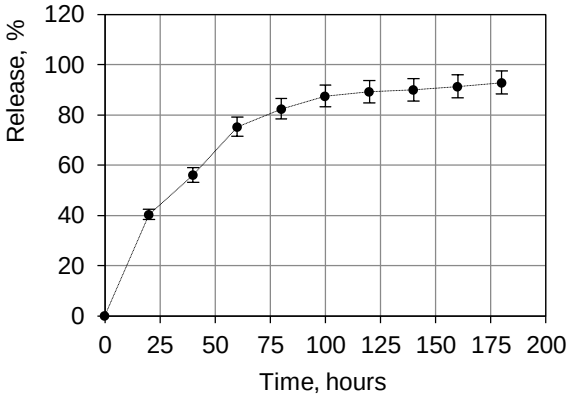

Figure 7. Phenolic compound migration from the active PLA film into 95% ethanol

The percentage of phenolic compound release increased with time. Initially, the release was 40.38±0.1%, reaching 89.21±0.2% after 100 h (approximately 5 days) and 92.9±0.1% on the 7th day. A rapid increase in phenolic compound migration was observed during the initial period, followed by a gradual stabilisation. This pattern may be attributed to the rapid release of phenolic compounds located at or near the film surface, followed by slower diffusion of compounds more strongly associated with the PLA matrix. The results are consistent with those reported by Radhalakshmi et al. (2023).

Mechanical properties of the films

Table 5 presents the tensile strength and elongation at break of the control and active films. Tensile strength represents the maximum stress that a film can withstand before breaking, whereas elongation at break reflects its ability to deform under tensile stress. The tensile strength increased from 168.6±0.5 kg/cm² for the control film to 261±0.6 kg/cm² for the active film ($p < 0.05$). This increase may be attributed to the reinforcing effect of the incorporated AgNPs, which can increase the rigidity of the polymer matrix and consequently affect its mechanical behaviour (Fathima et al., 2018).

The elongation at break was 3.10±0.03% for the control film and 3.75±0.01% for the active film; however, the difference was not statistically significant. The slight increase in elongation may be associated with interactions between PLA and components of the plant extract, which can influence polymer-chain mobility and the ability of the matrix to withstand external stress (Cheng

et al., 2021; Meng et al., 2018). Packaging films should possess sufficient mechanical strength and flexibility to maintain their integrity during storage and transportation (Benavides et al., 2012). The obtained results are consistent with previous studies (Martínez-Abad et al., 2014; Radhalakshmi et al., 2023; Vasile et al., 2017).

Biodegradability of the films

The biodegradability of the films was evaluated under soil burial conditions. After one day of burial, only minor visual changes, such as increased brittleness and turbidity, were observed. The biodegradability of the active film was 0.15±0.5%, compared with 0.12±0.3% for the control film. According to the statistical analysis, the difference between the films was not significant.

The film structure may be affected by temperature fluctuations during biodegradation, while other factors, such as burial time and moisture content, may also influence the degradation process (Chaubey et al., 2021). PLA biodegradation in a composting environment generally occurs in two stages. In the first stage, high-molecular-weight PLA chains undergo hydrolysis, producing lower-molecular-weight oligomers; this process is influenced by temperature and moisture. In the second stage, the resulting oligomers are further converted by microorganisms into CO_2, water, and humic substances (Yang et al., 2010). PLA chains with lower molecular weights contain a higher proportion of accessible chain-end groups and may therefore undergo hydrolysis more readily. In addition, the amorphous phase generally degrades more readily than the crystalline phase (Tanio et al., 1982).

The slightly higher biodegradability observed for the active film may be associated with structural changes induced by the incorporation of AgNPs, including an increase in the effective surface area available for interaction with the surrounding environment (Norozi et al., 2025). Overall, the results confirm that the developed PLA-based active films retain their biodegradable character.

Colour of the films

The colour characteristics of the films, including L*, a*, b*, h°, C*, and ΔE*, are presented in Table 5.

Table 5

Colour characteristics of the packaging films

Parameters	Control film	Active film with AgNPs
L*	$91.2^{a\pm}0.2$	$80.15^{b\pm}0.3$
a*	$-1.1^{a\pm}0.3$	$1.03^{b\pm}0.2$
b*	$-1.7^{a\pm}0.01$	$8.29^{b\pm}0.1$
h◦	$237.09^{a\pm}0.01$	$174.8^{b}\pm0.1$
c*	$2.02^{a\pm}0.01$	$2.3^{a\pm}0.2$
ΔE*	$91.1^{a\pm}0.1$	$80.5^{b}\pm0.1$

Note: Values represented as mean±standard deviation. Different superscripts in the same row indicate a significant difference ($p < 0.05$)

The L* value was 91.2±0.2 for the control film and 80.15±0.3 for the active film, indicating a decrease in lightness following the incorporation of AgNPs. The ΔE* values were 91.1±0.1 for the control film and 80.5±0.1 for the active film, indicating a difference in the overall colour characteristics of the films.

The a* value changed from −1.1±0.3 for the control film to 1.03±0.2 for the active film, indicating a shift from a greenish to a reddish hue. Similarly, the b* value increased from

−1.7±0.01 to 8.29±0.1, indicating a shift from a bluish to a yellowish hue. The C* values were 2.02±0.01 and 2.3±0.2 for the control and active films, respectively, with no significant difference between the samples. The hue angle (h°) decreased from 237.09±0.01 for the control film to 174.8±0.1 for the active film, further indicating a change in colour tone following the incorporation of AgNPs. Similar changes in the colour characteristics of active packaging films containing nanoparticles have been reported previously (Martínez-Abad et al., 2014; Radhalakshmi et al., 2023).

Shelf-life studies of grapes packed in active film

The weight loss of grapes during storage was used as an indicator of their preservation quality. All packed samples exhibited some weight loss during storage, most likely due to moisture loss from the grapes to the surrounding environment. After 7 days of storage, grapes packed in the active film showed significantly lower weight loss than those packed in the control film ($p < 0.05$). The weight loss was 12.82±0.2% for grapes packed in the active film, compared with 18.0±0.16% for grapes packed in the control film.

The lower weight loss observed for grapes packed in the active film may be associated with the improved barrier properties of the PLA film following the incorporation of AgNPs. The antimicrobial activity of AgNPs may also contribute to maintaining grape quality during storage by limiting microbial development. Grapes are highly perishable due to their rapid metabolism, susceptibility to physical damage, and vulnerability to various bacterial and fungal diseases (Do et al., 2025). In the present study, grape samples packed in the control film showed visible deterioration by the seventh day of storage, which was associated with microbial development.

The results indicate that incorporation of AgNPs into PLA films can improve the preservation of grapes during storage. Radhalakshmi et al. (2023) reported an extension of the shelf life of tuna meat using PLA films containing betel leaf extract. Other studies have also demonstrated the potential of betel-leaf-derived MgO and chitosan nanoparticles to extend the shelf life of various food products, including tilapia slices, chilli, and strawberries (Dam et al., 2024; Do et al., 2025). Overall, the active PLA film demonstrated promising potential for maintaining grape quality during storage.

Conclusions

The green synthesis of Ag and ZnO nanoparticles using betel leaf extract was successfully achieved, and the obtained nanoparticles were evaluated for their potential application in PLA-based active packaging films. The results demonstrated that AgNPs exhibited higher total phenolic and flavonoid contents, greater antioxidant activity, and stronger antibacterial activity against the tested microorganisms than ZnO NPs. Therefore, AgNPs were selected for incorporation into PLA films.

The incorporation of AgNPs into PLA resulted in several improvements in the functional properties of the films. The active film exhibited higher tensile strength (261±0.6 kg/cm²) than the control film (168.6±0.5 kg/cm²), while the difference in elongation at break was not statistically significant. The incorporation of AgNPs also reduced the swelling capacity and improved the barrier properties, with WVTR and GTR decreasing to 74.2±0.4 g/m²/day and 290.03±0.3 cm³/m²/day/atm, respectively. The moisture content showed no significant difference between the control and active films.

Phenolic compounds were released from the active film into 95% ethanol, whereas no detectable migration was observed in water. The films also retained their biodegradable character, with no significant difference in biodegradability between the control and active films under the conditions tested. In the shelf-life study, grapes packed with the active film showed significantly

lower weight loss after 7 days of storage (12.82±0.2%) than those packed with the control film (18.0±0.16%), indicating improved preservation during storage.

Overall, the developed PLA-based film containing AgNPs demonstrated favourable functional properties, including enhanced mechanical strength, improved barrier properties, antioxidant and antibacterial activity, and the ability to reduce grape weight loss during storage. These findings indicate the potential of AgNPs produced using betel leaf extract as an active component in biodegradable food packaging. Further studies are needed to evaluate nanoparticle safety and migration, potential interactions with food components, sensory properties, and the long-term performance of the films in different food-packaging applications.

References

AOAC International. (2023). Official methods of analysis of AOAC International (22nd ed.). AOAC International.

Barak, S., & Mudgil, D. (2022). Application of bioactives from herbs and spices for improving the functionality and shelf life of dairy products: A review. *Biointerface Research in Applied Chemistry, 13*(2), 1–12. https://doi.org/10.33263/briac132.141

Barzinjy, A. A., & Azeez, H. H. (2020). Green synthesis and characterization of zinc oxide nanoparticles using *Eucalyptus globulus* Labill. leaf extract and zinc nitrate hexahydrate salt. *SN Applied Sciences, 2*(5), 1–14. https://doi.org/10.1007/s42452-020-2813-1

Batool, M., Abid, A., Khurshid, S., Bashir, T., Ismail, M. A., Razaq, M. A., & Jamil, M. (2022). Quality control of nano-food packing material for grapes (*Vitis vinifera*) based on ZnO and polylactic acid (PLA) biofilm. *Arabian Journal for Science and Engineering, 47*(1), 319–331. https://doi.org/10.1007/s13369-021-05361-9

Benavides, S., Villalobos-Carvajal, R., & Reyes, J. E. (2012). Physical, mechanical and antibacterial properties of alginate film: Effect of the crosslinking degree and oregano essential oil concentration. *Journal of Food Engineering, 110*(2), 232–239. https://doi.org/10.1016/j.jfoodeng.2011.05.023

Berg, J. M., Romoser, A., Banerjee, N., Zebda, R., & Sayes, C. M. (2009). The relationship between pH and zeta potential of ∼30 nm metal oxide nanoparticle suspensions relevant to *in vitro* toxicological evaluations. *Nanotoxicology, 3*(4), 276–283. https://doi.org/10.3109/17435390903276941

Bharathi, A., Meena, R., Ravichandran, D., Natarajan, D., Gatasheh, M. K., Ahamed, A., Kawuri, R., & Murugesan, S. (2024). Green route to synthesize zinc oxide nanoparticles (ZnO-NPs) using leaf extracts of *Merremia quinquefolia* (L.) Hallier f. and their potential applications. *Journal of Molecular Structure, 1317,* 139110. https://doi.org/10.1016/j.molstruc.2024.139110

Chaubey, A., Aadil, K. R., & Jha, H. (2021). Synthesis and characterization of lignin–polylactic acid film as active food packaging material. *Materials Technology, 36*(10), 585–593. https://doi.org/10.1080/10667857.2020.1782060

Cheng, J., Lin, X., Wu, X., Liu, Q., Wan, S., & Zhang, Y. (2021). Preparation of a multifunctional silver nanoparticles–polylactic acid food packaging film using mango peel extract. *International Journal of Biological Macromolecules, 188*, 678–688. https://doi.org/10.1016/j.ijbiomac.2021.07.161

Ci, K.C., & Indira, G. (2016). Quantitative estimation of total phenolic, flavonoids, tannin and chlorophyll content of leaves of *Strobilanthes kunthiana* (Neelakurinji). *Journal of Medicinal Plants Studies, 4*, 282-286.

Dai, L., Li, R., Liang, Y., Liu, Y., Zhang, W., & Shi, S. (2022). Development of pomegranate peel extract and nano-ZnO co-reinforced polylactic acid film for active food packaging. *Membranes, 12*(11), Article 1108. https://doi.org/10.3390/membranes12111108

Dam, X. T., Duong, T. M., Mai, D. H., Thai, H., Vu, V. A., Vu, Q. T., Ngo, T. C. Q., Nguyen, T. A., & Nguyen, T. C. (2024). Preparation of novel bio-nanocomposites based on chitosan, *Piper betle* leaf extract and MgO nanoparticles for chili preservation. *Polymer Engineering and Science,*

64(6), 2795–2811. https://doi.org/10.1002/pen.26726

Dangana, R. S., George, R. C., & Agboola, F. K. (2023). The biosynthesis of zinc oxide nanoparticles using aqueous leaf extracts of *Cnidoscolus aconitifolius* and their biological activities. *Green Chemistry Letters and Reviews, 16*(1). https://doi.org/10.1080/17518253.2023.2169591

Demchenko, V., Mamunya, Y., Sytnyk, I., Iurzhenko, M., Krivtsun, I., Rybalchenko, N., Naumenko, K., Artiukh, L., Kowalczuk, M., Demchenko, O., & Marynin, A. (2025). Fabrication of polylactide composites with silver nanoparticles by sputtering deposition and their antimicrobial and antiviral applications. *Polymer International, 74*(3), 207–216. https://doi.org/10.1002/pi.6707

Do, N. H. N., Tran, V. T., Cao, H. M., Nguyen, H. C., Le, K. A., & Le, P. K. (2025). Novel *Piper betle* (L.) leaf extract-encapsulated chitosan nanoparticles as bioactive coatings for strawberry preservation. *Journal of Food Science and Technolog, 63*, 451–461. https://doi.org/10.1007/s13197-025-06248-5

du Toit, E. S., Sithole, J., & Vorster, J. (2020). Leaf harvesting severity affects total phenolic and tannin content of fresh and dry leaves of *Moringa oleifera* Lam. trees growing in Gauteng, South Africa. *South African Journal of Botany, 129*, 336–340. https://doi.org/10.1016/j.sajb.2019.08.035

Ealias, A. M., & Saravanakumar, M. P. (2017). A review on the classification, characterisation, synthesis of nanoparticles and their application. *IOP Conference Series: Materials Science and Engineering, 263*(3), 032019. https://doi.org/10.1088/1757-899X/263/3/032019

Ediyilyam, S., George, B., Shankar, S. S., Dennise, T. T., Wacławek, S., Cerník, M., & Padil, V. V. T. (2021). Chitosan/gelatin/silver nanoparticles composites films for biodegradable food packaging applications. *Polymers*, *13*(11), 1680. https://doi.org/10.3390/polym13111680

Fathima, P. E., Panda, S. K., Ashraf, P. M., Varghese, T. O., & Bindu, J. (2018). Polylactic acid/chitosan films for packaging of Indian white prawn (*Fenneropenaeus indicus*). *International Journal of Biological Macromolecules, 117*, 1002–1010. https://doi.org/10.1016/j.ijbiomac.2018.05.214

Gayadang, D., Mission, N. L. T., & Cajucom, E. L. (2023). Bioformulation of silver nanoparticles from betel leaf (*Piper betel*) extract and its antioxidant, cytotoxic and antibacterial properties. I*nternational Journal of Engineering Technologies and Management Research, 10*(8). https://doi.org/10.29121/ijetmr.v10.i8.2023.1354

Gebrechristos, H. Y., Ma, X., Xiao, F., He, Y., Zheng, S., Oyungerel, G., & Chen, W. (2020). Potato peel extracts as an antimicrobial and potential antioxidant in active edible film. *Food Science & Nutrition, 8*(12), 6338–6345. https://doi.org/10.1002/fsn3.1119

Geremew, A., Carson, L., Woldesenbet, S., Wang, H., Reeves, S., Brooks, N., Saganti, P., Weerasooriya, A., & Peace, E. (2023). Effect of zinc oxide nanoparticles synthesized from Carya illinoinensis leaf extract on growth and antioxidant properties of mustard (*Brassica juncea*). *Frontiers in Plant Science, 14*, 1108186. https://doi.org/10.3389/fpls.2023.1108186

Ghasemi, S., Dabirian, S., Kariminejad, F., Koohi, D. E., Nemattalab, M., Majidimoghadam, S., Zamani, E., & Yousefbeyk, F. (2024). Process optimization for green synthesis of silver nanoparticles using *Rubus discolor* leaves extract and its biological activities against multi-drug resistant bacteria and cancer cells. *Scientific Reports, 14*(1), 54702. https://doi.org/10.1038/s41598-024-54702-9

Gitari, B., Chang, B. P., Misra, M., Navabi, A., & Mohanty, A. K. (2019). A comparative study on the mechanical, thermal, and water barrier properties of PLA nanocomposite films prepared with bacterial nanocellulose and cellulose nanofibrils. *BioResource, 14*(1), 1867-1889.

Harikrishnan, A., Ramalingam, B., Nadeem, A., Veena, V. K., & Muthupandian, S. (2024). Eco-friendly synthesis of zinc oxide nanoparticles (ZnO NPs) from Piper betel leaf extract: Spectral characterization and its application on plant growth parameters in maize, fenugreek and red gram. *Materials Technology, 39*(1), 2298547. https://doi.org/10.1080/10667857.2023.2298547

Hussain, F., Hadi, F., & Rongliang, Q. (2021). Effects of zinc oxide nanoparticles on antioxidants, chlorophyll contents, and proline in *Persicaria hydropiper* L. and its potential for Pb phytoremediation. *Environmental Science and Pollution Research, 28*(26), 34697–34713. https://doi.org/10.1007/s11356-021-13132-0

Hussen, E. M., & Endalew, S. A. (2023). In vitro antioxidant and free-radical scavenging activities of polar leaf extracts of *Vernonia amygdalina*. *BMC Complementary Medicine and Therapies,*

23(1), 1–12. https://doi.org/10.1186/s12906-023-03923-y

Jacob, S. J. P., Finub, J. S., & Narayanan, A. (2012). Synthesis of silver nanoparticles using *Piper longum* leaf extracts and its cytotoxic activity against Hep-2 cell line. *Colloids and Surfaces B: Biointerfaces, 91*, 212–214. https://doi.org/10.1016/j.colsurfb.2011.11.001

Jain, S., & Mehata, M. S. (2017). Medicinal plant leaf extract and pure flavonoid mediated green synthesis of silver nanoparticles and their enhanced antibacterial property. *Scientific Reports, 7*, 15867. https://doi.org/10.1038/s41598-017-15724-8

Jamshidian, M., Tehrany, E. A., & Desobry, S. (2013). Antioxidants release from solvent-cast PLA film: Investigation of PLA antioxidant-active packaging. *Food and Bioprocess Technology, 6*(6), 1450–1463. https://doi.org/10.1007/s11947-012-0830-9

Joseph, J., Khor, K. Z., Moses, E. J., Lim, V., Aziz, M. Y., & Samad, N. A. (2021). In vitro anticancer effects of *Vernonia amygdalina* leaf extract and green-synthesised silver nanoparticles. *International Journal of Nanomedicine, 16*, 3599–3612. https://doi.org/10.2147/IJN.S303921

Kanatt, S. R. (2020). Development of active/intelligent food packaging film containing *Amaranthus* leaf extract for shelf life extension of chicken/fish during chilled storage. *Food Packaging and Shelf Life, 24*, 100506. https://doi.org/10.1016/j.fpsl.2020.100506

Kapilraj, N., Keerthanan, S., & Sithambaresan, M. (2019). Natural plant extracts as acid-base indicator and determination of their pKa value. *Journal of Chemistry, 2019*, 2031342. https://doi.org/10.1155/2019/2031342

Kasai, D., Chougale, R., Masti, S., Gouripur, G., Malabadi, R., Chalannavar, R., Raghu, A. V., Radhika, D., Shanavaz, H., & Dhanavant, S. (2020). Preparation, characterization and antimicrobial activity of betel-leaf-extract-doped polysaccharide blend films. *Green Materials, 9*(2), 49–68. https://doi.org/10.1680/jgrma.20.00014

Kaur, K., Rai, R., Trivedi, R. V., & Umekar, M. J. (2019). Review on betel leaf used in various ailments. *International Journal of Pharmacognosy, 6*(8), 259–267. https://doi.org/10.13040/ijpsr.0975-8232.ijp.6(8).259-67

Khan, S., Singh, S., Gaikwad, S., Nawani, N., Junnarkar, M., & Pawar, S. V. (2020). Optimization of process parameters for the synthesis of silver nanoparticles from *Piper betle* leaf aqueous extract, and evaluation of their antiphytofungal activity. *Environmental Science and Pollution Research International, 27*(22), 27221–27233. https://doi.org/ 10.1007/s11356-019-05239-2

Kharat, S. N., & Mendhulkar, V. D. (2016). Synthesis, characterization and studies on antioxidant activity of silver nanoparticles using *Elephantopus scaber* leaf extract. *Materials Science and Engineering: C, 62*, 719–724. https://doi.org/10.1016/j.msec.2016.02.024

Krishana, G. K. M., Shivaramakrishna, S., Sridhar, S., Ahmed, M., Ramanna, J., Chakith, M. R. S., Pradeep, S., Kavana, C. P., Shreevatsa, B., Shati, A. A., Alfaifi, M. Y., Eldin, S., Elbehairi, I., Shivamallu, C., Guru, D., & Prasad, S. (2024). Sustainable synthesis of zinc oxide nanoparticles using *Piper betle* petiole leaf extract: Antibacterial, antioxidant, and cytotoxic potential. *Results in Chemistry, 9*, 101646. https://doi.org/10.1016/j.rechem.2024.101646

Lagashetty, A. (2022). Synthesis and characterization of silver doped zinc oxide nanoparticle from beetle leaf extract: Evaluation of antimicrobial activity against human pathogenic bacteria and fungi. *International Journal for Research in Applied Science and Engineering Technology, 10*(5), 2703–2716. https://doi.org/10.22214/ijraset.2022.42914

Li, W., Zhang, C., Chi, H., Li, L., Lan, T., Han, P., Chen, H., & Qin, Y. (2017). Development of antimicrobial packaging film made from poly(lactic acid) incorporating titanium dioxide and silver nanoparticles. *Molecules, 22*(7), 1170. https://doi.org/10.3390/molecules22071170

Logeswari, P., Silambarasan, S., & Abraham, J. (2015). Synthesis of silver nanoparticles using plant extracts and analysis of their antimicrobial property. *Journal of Saudi Chemical Society, 19*(3), 311–317. https://doi.org/10.1016/j.jscs.2012.04.007

Lu, R., Sameen, D. E., Qin, W., Wu, D., Dai, J., Li, S., & Liu, Y. (2020). Development of polylactic acid films with selenium microparticles and their application for food packaging. *Coatings, 10*(3), 280. https://doi.org/10.3390/coatings10030280

Mai, Q., Tran, T., Anh, H., Nguyen, T., Doan, V., & Tran, Q. (2021). Biosynthesis of zinc oxide nanoparticles using aqueous *Piper betle* leaf extract and its application in surgical sutures. *Journal of Chemistry, 2021*, 8833864. https://doi.org/10.1155/2021/8833864

Maitra, M., Adari, R., & Radha, P. (2026). Sustainable packaging films: Polylactic acid-surface-modified nanocellulose-pectin biocomposite to extend shelf life of strawberry fruit. *Journal of Food Science and Technology, 63*, 333–347. https://doi.org/10.1007/s13197-024-06195-7

Manach, C., Scalbert, A., Morand, C., Rémésy, C., & Jiménez, L. (2004). Polyphenols: Food sources and bioavailability. T*he American Journal of Clinical Nutrition, 79*(5), 727–747. https://doi.org/10.1093/ajcn/79.5.727

Mankad, M., Patil, G., Patel, S., Patel, D., & Patel, A. (2016). Green synthesis of zinc oxide nanoparticles using *Azadirachta indica* A. Juss. leaves extract and its antibacterial activity against *Xanthomonas oryzae* pv. *oryzae*. *Annals of Phytomedicine, 5*(2), 76–86. https://doi.org/10.21276/ap.2016.5.2.9

Martínez-Abad, A., Ocio, M. J., & Lagaron, J. M. (2014). Morphology, physical properties, silver release, and antimicrobial capacity of ionic silver-loaded poly(L-lactide) films of interest in food-coating applications. *Journal of Applied Polymer Science, 131*(21), 41001. https://doi.org/10.1002/app.41001

Medina-Jaramillo, C., Ochoa-Yepes, O., Bernal, C., & Famá, L. (2017). Active and smart biodegradable packaging based on starch and natural extracts. *Carbohydrate Polymers, 176*, 187–194. https://doi.org/10.1016/j.carbpol.2017.08.079

Meng, F., Zhang, Y., Xiong, Z., Wang, G., Li, F., & Zhang, L. (2018). Mechanical, hydrophobic and thermal properties of an organic-inorganic hybrid carrageenan-polyvinyl alcohol composite film. *Composites Part B: Engineering, 143*, 1–8. https://doi.org/10.1016/j.compositesb.2017.12.009

Nagarajaiah, S., Nanda, N., Manjappa, P., Mutta, B., & Manoj, N. (2023). Evaluation of apoptosis in human breast cancer cell (MDA-MB-231) induced by ZnO nanoparticles synthesized using *Piper betle* leaf extract as bio-fuel. *Applied Physics A, 129*, 461. https://doi.org/10.1007/s00339-023-06731-w

Nayaka, N. M. D. M. W., Sasadara, M. M. V., Sanjaya, D. A., Yuda, P. E. S. K., Dewi, N. L. K. A. A., Cahyaningsih, E., & Hartati, R. (2021). *Piper betle* (L): Recent review of antibacterial and antifungal properties, safety profiles, and commercial applications. *Molecules, 26*(8), 2321. https://doi.org/10.3390/molecules26082321

Negahdari, M., Partovi, R., Talebi, F., Babaei, A., & Abdulkhani, A. (2021). Preparation, characterization, and preservation performance of active polylactic acid film containing *Origanum majorana* essential oil and zinc oxide nanoparticles for ground meat packaging. *Journal of Food Processing and Preservation, 45*(1), e15013. https://doi.org/10.1111/jfpp.15013

Nguyen, N. H., Nhi, T. T. Y., Van Nhi, N. T., Cuc, T. T. T., Tuan, P. M., & Nguyen, D. H. (2021). Comparative study of the silver nanoparticle synthesis ability and antibacterial activity of the *Piper betle* L. and *Piper sarmentosum* Roxb. extracts. *Journal of Nanomaterials, 2021*, 5518389. https://doi.org/10.1155/2021/5518389

Norozi, M., Peighambardoust, S. H., Khorram, S., & Hamishehkar, H. (2025). Cold plasma-enhanced polylactic acid/chitosan films incorporating zein nanoparticles: A promising strategy for developing food packaging materials. *Carbohydrate Polymer Technologies and Applications, 10*, 100852. https://doi.org/10.1016/j.carpta.2025.100852

Nouri, L., & Nafchi, A. M. (2014). Antibacterial, mechanical, and barrier properties of sago starch film incorporated with betel leaves extract. *International Journal of Biological Macromolecules, 66*, 254–259. https://doi.org/10.1016/j.ijbiomac.2014.02.044

Plaeyao, K., Talodthaisong, C., Yingyuen, W., Kaewbundit, R., Tun, W. S. T., Saenchoopa, A., Kayunkid, N., Wiwattananukul, R., Sakulsombat, M., & Kulchat, S. (2025). Biodegradable antibacterial food packaging based on carboxymethyl cellulose from sugarcane bagasse/cassava starch/chitosan/gingerol extract stabilized silver nanoparticles (Gin-AgNPs) and vanillin as cross-linking agent. *Food Chemistry, 466*, 142102. https://doi.org/10.1016/j.foodchem.2024.142102

Radhalakshmi, V., Raman, M., & Joy, M. R. (2023). Development of active packaging film based on poly(lactic acid) incorporated with *Piper betle* leaf ethanolic extract and its application in the shelf-life extension of tuna meat. *International Journal of Biological Macromolecules, 246*, 125751. https://doi.org/10.1016/j.ijbiomac.2023.125751

Ragavendran, C., Imath, M., Kamaraj, C., Nakouti, I., & Manoharadas, S. (2024). Eco-friendly

synthesis of betanin-conjugated zinc oxide nanoparticles: Antimicrobial efficacy and apoptotic pathway activation in oral cancer cells. *Molecular Biology Reports, 51*(1), 1–19. https://doi.org/10.1007/s11033-024-10039-0

Raj, S., Chand Mali, S., & Trivedi, R. (2018). Green synthesis and characterization of silver nanoparticles using *Enicostemma axillare* (Lam.) leaf extract. *Biochemical and Biophysical Research Communications, 503*(4), 2814–2819. https://doi.org/10.1016/j.bbrc.2018.08.045

Rajesh, S., Yadav Reddy, & Thayagrajan, L. S. (2016). Structural, optical, thermal and photocatalytic properties of ZnO nanoparticles of betel leaf by using green synthesis method. *Journal of Nanostructure, 6*(3), 250-255. https://doi.org/10.7508/JNS.2016.03.010

Ramachandran, K., Kalpana, D., Sathishkumar, Y., Lee, Y. S., Ravichandran, K., & Kumar, G. G. (2016). A facile green synthesis of silver nanoparticles using *Piper betle* biomass and its catalytic activity toward sensitive and selective nitrite detection. *Journal of Industrial and Engineering Chemistry, 35*, 29–35. https://doi.org/10.1016/j.jiec.2015.10.033

Rani, P. U., & Rajasekharreddy, P. (2011). Green synthesis of silver-protein (core–shell) nanoparticles using *Piper betle* L. leaf extract and its ecotoxicological studies on *Daphnia magna*. *Colloids and Surfaces A: Physicochemical and Engineering Aspects, 389*(1–3), 188–194. https://doi.org/10.1016/j.colsurfa.2011.08.028

Rasmussen, M. K., Pedersen, J. N., & Marie, R. (2020). Size and surface charge characterization of nanoparticles with a salt gradient. *Nature Communications, 11*(1), 1–8. https://doi.org/10.1038/s41467-020-15889-3

Rohaeti, E., Kasmudjiastuti, E., Murti, R. S., & Irwanto, D. (2020). Enhancement of antibacterial activity of suede leather through coating silver nanoparticles synthesized using *Piper betle*. *Rasayan Journal of Chemistry, 13*(1), 628–635. https://doi.org/10.31788/RJC.2020.1315516

Sani, M. A., Azizi-Lalabadi, M., Tavassoli, M., Mohammadi, K., & McClements, D. J. (2021). Recent advances in the development of smart and active biodegradable packaging materials. *Nanomaterials, 11*(5), 1331. https://doi.org/10.3390/nano11051331

Shankar, S., Wang, L. F., & Rhim, J. W. (2018). Incorporation of zinc oxide nanoparticles improved the mechanical, water vapor barrier, UV-light barrier, and antibacterial properties of PLA-based nanocomposite films. *Materials Science and Engineering: C, 93*, 289–298. https://doi.org/10.1016/j.msec.2018.08.002

Sharifi-Rad, M., Elshafie, H. S., & Pohl, P. (2024). Green synthesis of silver nanoparticles (AgNPs) by *Lallemantia royleana* leaf extract: Their bio-pharmaceutical and catalytic properties. *Journal of Photochemistry and Photobiology A: Chemistry, 448*, 115318. https://doi.org/10.1016/j.jphotochem.2023.115318

Sharmila, G., Muthukumaran, C., Sandiya, K., Santhiya, S., Pradeep, R. S., Kumar, N. M., Suriyanarayanan, N., & Thirumarimurugan, M. (2018). Biosynthesis, characterization, and antibacterial activity of zinc oxide nanoparticles derived from *Bauhinia tomentosa* leaf extract. *Journal of Nanostructure in Chemistry, 8*(3), 293–299. https://doi.org/10.1007/s40097-018-0271-8

Stabnikov, V., Kovshar, I., & Stabnikova, O. (2025). Recent advances in the study of the properties and applications of lactic acid bacteria. *World Journal of Microbiology and Biotechnology, 41*, 287. https://doi.org/10.1007/s11274-025-04499-0

Stabnikova, O., Khonkiv, M., Kovshar, I., & Stabnikov, V. (2023). Biosynthesis of selenium nanoparticles by lactic acid bacteria and areas of their possible applications. *World Journal of Microbiology and Biotechnology, 39*, 230. https://doi.org/10.1007/s11274-023-03673-6

Stabnikova, O., Stabnikov, V., & Paredes-López, O. (2026a). Spices and essential oils in food preservation: From natural additives to active packaging systems. *Plant Food for Human Nutrition, 81*, 69. https://doi.org/10.1007/s11130-026-01519-8

Stabnikova, O., Marynin, A., Stabnikov, V., Svyatnenko, R., & Demchenko, V. (2026b). Plant essential oils for food shelf-life extension and active packaging systems. *Ukrainian Food Journal, 15*(2), 323–360. https://doi.org/10.24263/2304-974X-2026-15-2-6

Tanio, T., Fukui, T., Shirakura, Y., Saito, T., Tomita, K., Kaiho, T., & Masamune, S. (1982). An extracellular poly(3-hydroxybutyrate) depolymerase from *Alcaligenes faecalis*. *European Journal of Biochemistry, 124*(1), 71–77. https://doi.org/10.1111/j.1432-1033.1982.tb05907.x

Thanh, N. C., Pugazhendhi, A., Chinnathambi, A., Alharbi, S. A., Subramani, B., Brindhadevi, K., Whangchai, N., & Pikulkaew, S. (2022). Silver nanoparticles (AgNPs) fabricating potential of aqueous shoot extract of *Aristolochia bracteolata* and assessed their antioxidant efficiency. *Environmental Research, 208*, 112683. https://doi.org/10.1016/j.envres.2022.112683

Theresih, K., Budimarwanti, C., Arty, I. S., Handayani, S., Ramadhani, N. P., & Kurniasih, R. (2021). Synthesis of ZnO nanoparticles from zinc acetate using red betel and bay leaves extract and its application as sunscreen. *Indonesian Journal of Chemistry and Environment, 4*(1), 31–38. https://doi.org/10.21831/ijoce.v4i1.45299

Tullo, A. (2005). An industry siesta. *Chemical & Engineering News, 83*(47), 36. https://doi.org/10.1021/cen-v083n047.p036

Varadavenkatesan, T., Lyubchik, E., Pai, S., Pugazhendhi, A., Vinayagam, R., & Selvaraj, R. (2019). Photocatalytic degradation of Rhodamine B by zinc oxide nanoparticles synthesized using the leaf extract of *Cyanometra ramiflora*. *Journal of Photochemistry and Photobiology B: Biology, 199*, 111621. https://doi.org/10.1016/j.jphotobiol.2019.111621

Vaseashta, A., Klavins, M., & Stabnikova, O. (Eds.). (2025). *Micro and nanoplastics in the aquatic environment*. CRC Press. https://doi.org/10.1201/9781003389460

Vasile, C., Academy, R., & Stan, M. (2017). New PLA/ZnO/Ag bionanocomposites for food packaging. *Express Polymer Letters, 11*, 531–544.

Venkateasan, A., Prabakaran, R., & Sujatha, V. (2017). Phytoextract-mediated synthesis of zinc oxide nanoparticles using aqueous leaves extract of *Ipomoea pes-caprae* (L.) R. Br. revealing its biological properties and photocatalytic activity. *Nanotechnology for Environmental Engineering, 2*(1), 1–15. https://doi.org/10.1007/s41204-017-0018-7

Verawati, Aria, M., Arel, A., & Ryanto, E. (2016). Antioxidant activity and total flavonoid content of fractions of piladang (*Solenostemon scutellarioides* (L.) Codd) leaf extract. *Der Pharmacia Lettre, 8*(18), 67–71.

Wang, Q., Chen, W., Zhu, W., McClements, D. J., Liu, X., & Liu, F. (2022). A review of multilayer and composite films and coatings for active biodegradable packaging. *Npj Science of Food, 6*(1). https://doi.org/10.1038/s41538-022-00132-8

Yang, Z., Peng, H., Wang, W., & Liu, T. (2010). Crystallization behavior of poly(ε-caprolactone)/layered double hydroxide nanocomposites. *Journal of Applied Polymer Science, 116*(5), 2658–2667. https://doi.org/10.1002/app

Yeap, S. P., Lim, J., Ngang, H. P., Ooi, B. S., & Ahmad, A. L. (2018). Role of particle–particle interaction towards effective interpretation of Z-average and particle size distributions from dynamic light scattering (DLS) analysis. *Journal of Nanoscience and Nanotechnology, 18*(10), 6957–6964. https://doi.org/10.1166/jnn.2018.15458

Cite:

Noushad, A., Venugopal, R., Raman, M., Abdul Salam, N. P., Salim, L. M., Rehman, S., Shaik Moideen, J. M., & Thomas, A. (2026). Green synthesis of silver nanoparticles using *Piper betel* leaf extract for PLA-based active packaging films. *Ukrainian Food Journal, 15*(3), 762–785. https://doi.org/10.24263/2304-974X-2026-15-3-11

Active packaging films from PLA with *Rosmarinus officinalis* extract

Valeriy Demchenko[1], Olena Stabnikova[2], Andrii Marynin[2], Nataliia Rybalchenko[3]

1 – E.O. Paton Electric Welding Institute, the NAS of Ukraine, Ukraine
2 – National University of Food Technologies, Kyiv, Ukraine
3 – D.K. Zabolotny Institute of Microbiology and Virology, the NAS of Ukraine, Ukraine

Keywords:

Active packaging
Polylactic acid
Rosemary extract
Silver nitrate
Nanoparticles
Antimicrobial activity

Article history:

Received 26.05.2026
Received in revised form 12.07.2026
Accepted 30.08.2026

Corresponding author:

Valeriy Demchenko
E-mail: dvaleriyl@ukr.net

DOI:
10.24263/2304-974X-2026-15-3-12

Abstract

Introduction. The aim was to develop a biodegradable polylactic acid (PLA)-based active packaging film containing commercial rosemary (*Rosmarinus officinalis* L.) extract (RE) to help maintain the quality and safety of perishable foods.

Materials and methods. PLA-based films containing RE, silver nitrate ($AgNO_3$), or silver nanoparticles (AgNPs) were prepared. Structural, thermal, and mechanical properties were analyzed by wide-angle X-ray scattering, thermogravimetric analysis, differential scanning calorimetry, and tensile testing. Antimicrobial activity against four bacterial species was assessed by the agar disk diffusion method.

Results and discussion. Biodegradable active packaging films based on PLA containing commercial rosemary extract, $AgNO_3$, and AgNPs were developed. X-ray diffraction analysis showed that the PLA granules had a semi-crystalline structure with a crystallinity of approximately 60%, whereas the PLA film exhibited a predominantly amorphous structure. The incorporation of RE did not cause significant changes in the structure of PLA, whereas the incorporation of AgNPs resulted in a shift of the amorphous halo and the appearance of reflections characteristic of crystalline metallic silver. The incorporation of RE, $AgNO_3$, and AgNPs at the studied concentrations did not significantly affect the main thermal degradation range of PLA, which occurred predominantly between 300 and 400 °C. However, these additives substantially affected cold crystallization and the degree of crystallinity of PLA, whereas the glass transition temperature remained within 56–60 °C and the melting temperature within 159–163 °C. The incorporation of RE reduced the elongation at break of the films. Films containing $AgNO_3$ exhibited antimicrobial activity against *Staphylococcus aureus*, *Escherichia coli*, and *Pseudomonas aeruginosa*.

Conclusions. Rosemary extract improved the tensile strength of PLA films while maintaining their structural and thermal stability. Its combination with $AgNO_3$ provided antimicrobial activity, highlighting the potential of these films for active food packaging.

Introduction

Food loss and waste (FLW) remains a major challenge to global food security and environmental sustainability. Approximately 13% of food produced worldwide (1.25 billion tonnes) is lost between harvest and retail, while an additional 19% (1.05 billion tonnes) is wasted at the consumer stage, with households accounting for nearly 60% of global food waste (FAO, 2025). Meanwhile, in 2023 alone, food insecurity affected 2.33 billion people worldwide, of whom one in eleven suffered from hunger. Furthermore, food loss and waste account approximately 8–10% of global greenhouse gas emissions, highlighting the urgent need to develop effective strategies for preserving food quality and extending its shelf life.

Prolongation of the shelf life of food products by preventing spoilage during storage is an effective way to reduce food loss. Among the available preservation technologies, active packaging has emerged as one of the most promising approaches because it can interact with food or its surrounding environment to maintain quality, improve safety, and delay deterioration (Maffioli et al., 2026; Pasichnyi et al., 2022).

Plant-based materials, including essential oils, oleoresins, and extracts, are widely investigated as natural active agents for food packaging owing to their antimicrobial and antioxidant properties (Stabnikova et al., 2026a, b). They suppress the growth of foodborne pathogens and spoilage microorganisms, retard oxidative deterioration, and provide an environmentally friendly alternative to synthetic preservatives. Among these materials, plant extracts have attracted increasing attention because of their broad spectrum of bioactive compounds, availability, and compatibility with polymeric and biodegradable packaging materials. Their effectiveness largely depends on the compatibility with the packaging matrix and controlled release of bioactive compounds, while encapsulation technologies have been extensively explored to improve stability and ensure prolonged activity.

Rosemary (*Rosmarinus officinalis* L., currently classified as *Salvia rosmarinus* Spenn.) is an evergreen perennial herb with small blue–white flowers belonging to the family Lamiaceae (Figure 1). It is characterized by woody stems and narrow, leathery leaves with a dark green upper surface and whitish underside, with a characteristic strong aroma. Rosemary extract is rich in phenolic diterpenes, particularly carnosic acid and carnosol, which exhibit strong antioxidant and antimicrobial activities. In addition, other compounds, such as rosmarinic acid, camphor, caffeic acid, ursolic acid, and betulinic acid, are also found (Andrade et al., 2018).



Figure 1. *Rosmarinus officinalis*

Rosemary extract is authorized as a food additive (E392) in the European Union (Regulation (EC) No 1333/2008, 2008) and is generally recognized as safe (GRAS) by the U.S. Food and Drug Administration (FDA) (Essential Oils, Oleoresins, and Natural Extractives, 2026). It is also approved for use as a natural antioxidant in several other countries, including China, Japan, Australia, and New Zealand. In 2016, the Joint FAO/WHO Expert Committee on Food Additives (JECFA) evaluated rosemary extract and established a temporary ADI of 0–0.3 mg/kg body weight, expressed as carnosic acid plus carnosol (EFSA (European Food Safety Authority), 2018).

Thus, rosemary extract is a promising component of active packaging owing to its

antioxidant and antimicrobial properties, as well as its established safety for use in the food industry. One approach to developing rosemary extract-based active packaging is to coat conventional low-density polyethylene (LDPE) films with the extract (Barbosa-Pereira et al., 2014; Emir Çoban & Pelin Can., 2013). However, petroleum-based packaging materials are associated with serious environmental issues, including dependence on non-renewable fossil resources, greenhouse gas emissions during polymer production, and their persistence in the environment after disposal, leading to pollution of aquatic and soil ecosystems (Stabnikova et al., 2025; Yacoub & Han, 2026). Therefore, a more sustainable strategy is the incorporation of rosemary extract directly into the film matrix, particularly when biodegradable polymers are used. For example, rosemary extract has been incorporated into chitosan-based films (de Lima et al., 2024; Ghasemian et al., 2024), furcellaran/gelatin hydrolysate films (Jancikova et al., 2024), and poly(butylene adipate-co-terephthalate)/polylactic acid composites at a ratio of 70:30 (He et al., 2020).

The aim of this study was to develop a biodegradable active food packaging film based on polylactic acid (PLA) and a commercial rosemary extract and to evaluate its structure, physicochemical properties, antimicrobial activity, and potential for use in the storage of meat and meat products.

Materials and methods

Materials

The following materials were used to produce the polylactide films (PLA) for packaging: polylactic acid granules (PLA-G) (manufacturer Ukraine), rosemary extract (RE) on an ethanol-glycerol basis with a dry matter content of 8.2% (PLO "FITOPHARM", Ukraine); chloroform with a molecular weight of 119.38 g/mol (Zhejiang Juhua Group Corporation, China); ethanol 97% v/v and silver nitrate with an exact molecular weight of 169.87 g/mol. All chemicals used in the study were of analytical grade.

Preparation of polymer systems

PLA granules (1 g) were dissolved in 20 mL of chloroform at 20 °C for 1 h with constant stirring to obtain a polymer solution.

For the first series of samples, commercial rosemary extract (RE) was added to the PLA solution at concentrations of 0.5, 1.0, and 2.0 wt.% and stirred for 30 min. For the second series, a previously prepared silver nitrate solution (0.15 M $AgNO_3$ in 97% ethanol) was added to the PLA solution containing RE at concentrations of 0.5, 1.0, and 2.0 wt.%. For the third series, silver nanoparticles (AgNPs) were synthesized by reducing aqueous silver nitrate ($AgNO_3$) with rosemary extract at 80 °C for 5 h. The resulting AgNPs were then incorporated into the PLA matrix at concentrations of 0.5, 1.0, and 2.0 wt.%. The resulting solutions from all three series were poured onto glass surfaces and dried at room temperature for 24 h.

Methods

X-ray diffraction. The structure of the film materials was investigated by wide-angle X-ray scattering (WAXS) using an XRD-7000 diffractometer (Shimadzu, Japan). Measurements were performed in Debye–Scherrer geometry in transmission mode, with the primary X-ray beam passing through the samples. CuK_α radiation ($\lambda = 1.54$ Å) was used as the X-ray source with a graphite monochromator. Diffraction patterns were recorded automatically in step-scanning mode at a tube voltage of 30 kV and a current of 30 mA. The

scattering angle (2θ) was varied from 3° to 50°, with an exposure time of 5 s per step. All measurements were performed at 293 ± 2 K.

The relative degree of crystallinity ($X_{cr(waxs)}$) of PLA was calculated according to the following equation:

$$X_{cr(waxs)} = Q_{cr} \cdot (Q_{cr} + Q_{am})^{-1} \cdot 100, \quad (1)$$

where Q_{cr} is the area of the diffraction maxima characterizing the crystalline structure of the polymer, and ($Q_{cr} + Q_{am}$) is the total integrated area of the diffractogram within the selected 2θ range ($2\theta_1$ - $2\theta_2$), corresponding to the semi-crystalline structure of the polymer (Demchenko et al., 2025a).

The mean short-range order period (d), characterizing the spatial arrangement of segments of the PLA macromolecular chains, was determined using the Bragg equation:

$$d = l \cdot (2\sin\theta_m)^{-1}, \quad (2)$$

where λ is the wavelength of the characteristic X-ray radiation (λ = 1.54 Å for CuKα radiation), and θ_m is the angular position of the diffraction maximum (Demchenko et al., 2025c; Vashchuk et al., 2023).

TGA analysis. The thermal degradation of the film materials was investigated by thermogravimetric analysis (TGA) using a TGA55 thermogravimetric analyzer (TA Instruments, USA). Measurements were performed in an air atmosphere from room temperature to 600 °C at a heating rate of 20 °C/min. The thermogravimetric curves were processed and analyzed using TRIOS Software.

DSC analysis. The thermal properties of the film materials were determined by differential scanning calorimetry (DSC) using a DSC 25 calorimeter (TA Instruments, USA). Measurements were performed in an air atmosphere at a heating rate of 20 °C/min over the temperature range of 20–200 °C. After the first heating cycle, the samples were rapidly cooled, followed by a second heating cycle under the same conditions. The data obtained during the second heating cycle were used to determine the thermal characteristics of the film materials.

Mechanical properties. The mechanical properties of the film materials were evaluated by uniaxial tensile testing using an AGS-10kNX universal testing machine (Shimadzu, Japan). The tensile strength was determined at a temperature of 20 ± 2 °C.

Antimicrobial activity. The antimicrobial activity of the film samples was evaluated against reference strains of opportunistic microorganisms. The Gram-positive bacteria *Staphylococcus aureus* (*S. aureus*) ATCC 25923 and *Bacillus subtilis* (*B. subtilis*) ATCC 6633, and the Gram-negative bacteria *Escherichia coli* (*E. coli*) ATCC 25922 and *Pseudomonas aeruginosa* (*P. aeruginosa*) ATCC 27853 were used as model microorganisms. Antimicrobial activity was determined by the agar disk diffusion method on Mueller–Hinton agar (MHA). MHA plates were inoculated with 10 μL of microbial suspension at a concentration of 2×10^5 CFU/mL, after which 10-mm-diameter film disks were placed on the agar surface. Following incubation at 37 °C for 24 h, antimicrobial activity was assessed by measuring the diameter of the growth inhibition zone around each film disk. Films without Ag nanoparticles were used as controls. The experiment was performed in triplicate, and the results are expressed as means ± the standard errors of the means. A Student's t-test was used to compare these results. P values lower than 0.05 were considered significant.

Results and discussion

Structural characterization by X-ray diffraction of PLA-based films

Analysis of the wide-angle X-ray diffraction patterns showed that the PLA granules (PLA-G) exhibited a semi-crystalline structure (Figure 2a, curve 1), as indicated by the presence of characteristic diffraction peaks at $2\theta \approx 16.3°$, 18.9°, and 22.5°.

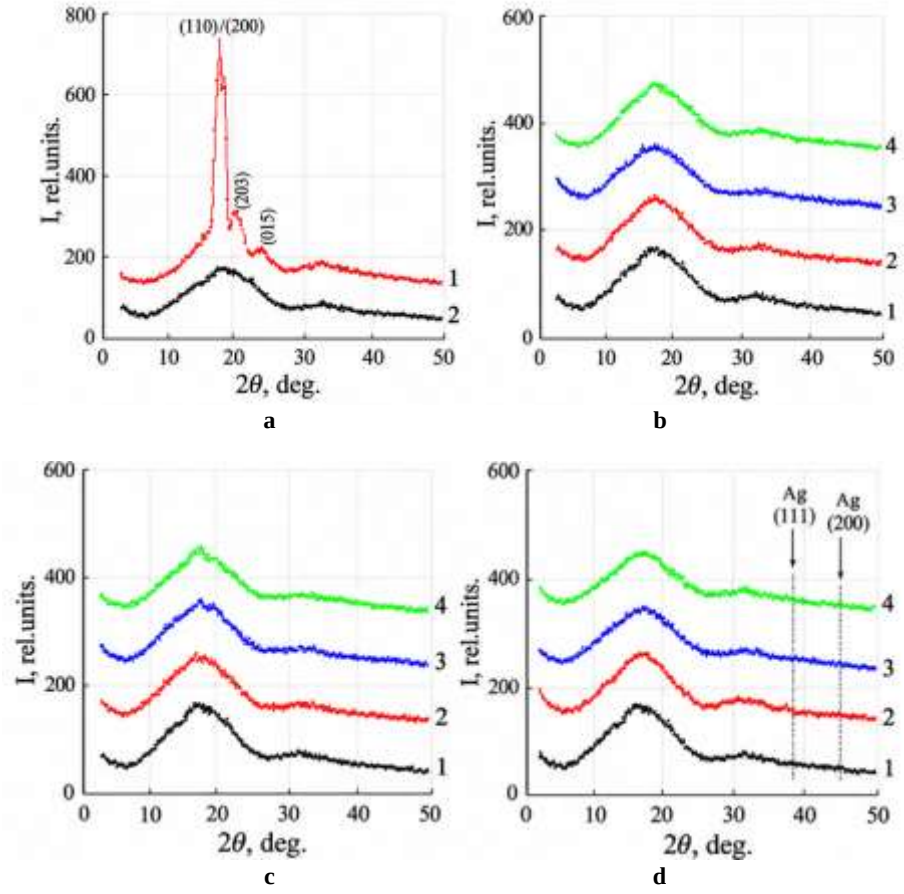

Figure 2. Wide-angle X-ray diffraction patterns:
(a) PLA-G (1) and PLA (2);
(b) PLA (1) containing different concentrations of rosemary extract: 0.5 wt.% (2), 1.0 wt.% (3), and 2.0 wt.% (4);
(c) PLA (1) containing different concentrations of rosemary extract and silver salt: 0.5 wt.% RE+0.5 wt.% $AgNO_3$ (2), 1.0 wt.% RE+1.0 wt.% $AgNO_3$ (3), 2.0 wt.% RE+2.0 wt.% $AgNO_3$ (4);
(d) PLA (1) containing different concentrations of rosemary extract and silver nanoparticles: 0.5 wt.% RE+0.5 wt.% AgNPs (2), 1.0 wt.% RE+1.0 wt.% AgNPs (3), 2.0 wt.% RE+2.0 wt.% AgNPs (4)

These peaks correspond to the crystallographic planes with Miller indices (110)/(200), (203), and (015), respectively, which are characteristic of the crystalline α-form of PLA (Demchenko et al., 2022, 2025b). The relative degree of crystallinity of the PLA-G, calculated using Equation (1), was approximately 60%.

The polylactide film (PLA) obtained by dissolving the PLA granules in chloroform followed by film formation exhibited a predominantly amorphous structure (Figure 2a, curve 2), as evidenced by the absence of distinct crystalline diffraction peaks and the presence of a broad diffuse amorphous halo. For the PLA film, a diffuse maximum was observed at $2\theta_m \approx 17.4°$, corresponding to a characteristic interplanar distance of $d \approx 5.10$ Å, as calculated using Equation (2). This d-spacing is associated with short-range structural correlations within the amorphous PLA phase.

The incorporation of rosemary extract into PLA at concentrations of 0.5, 1.0, and 2.0 wt.% does not cause significant changes in the diffraction patterns or result in the formation of new crystalline phases (Figure 2b). Similar diffraction patterns are observed for the PLA composites containing rosemary extract and silver nitrate at 0.5 wt.% RE + 0.5 wt.% $AgNO_3$, 1.0 wt.% RE + 1.0 wt.% $AgNO_3$, and 2.0 wt.% RE + 2.0 wt.% $AgNO_3$ (Figure 2c).

When silver nanoparticles, previously reduced from silver nitrate using rosemary extract, are incorporated, a somewhat different diffraction pattern is observed (Figure 2d, curves 1–4). The incorporation of silver nanoparticles into PLA is accompanied by a shift in the position of the diffraction maximum characteristic of the crystalline structure of polylactide and the corresponding Bragg spacing. For unmodified PLA, this maximum is observed at $2\theta_m \approx 17.4°$ ($d \approx 5.10$ Å), whereas for the sample containing 0.5 wt.% RE + 0.5 wt.% AgNPs, it shifts to $2\theta_m \approx 17.8°$ ($d \approx 4.97$ Å). For the sample containing 1.0 wt.% RE + 1.0 wt.% AgNPs, the maximum is observed at $2\theta_m \approx 17.6°$ ($d \approx 5.03$ Å), whereas for the sample containing 2.0 wt.% RE + 2.0 wt.% AgNPs, its position returns to $2\theta_m \approx 17.4°$ ($d \approx 5.10$ Å).

Alongside the diffuse amorphous halo, the diffraction patterns of the PLA+AgNPs film exhibit two additional low-intensity diffraction peaks at $2\theta \approx 38.4°$ and $2\theta \approx 44.4°$. These peaks correspond to the crystallographic planes with Miller indices (111) and (200), respectively, which are characteristic of the face-centered cubic (fcc) crystal lattice of metallic silver (Figure 2d, curves 2–3) (Demchenko et al., 2025b).

Thermal stability by thermogravimetric analysis (TGA) of PLA-based films

The thermogravimetric curves of the PLA samples in the form of granules (PLA-G) and films (PLA) exhibit similar overall thermal behavior (Figure 3a). For the PLA-G sample, practically no mass loss is observed up to approximately 300 °C, followed by a sharp decrease in mass in the temperature range of approximately 300–400 °C, corresponding to the main stage of PLA thermal degradation. For PLA, a more pronounced mass loss is observed during the initial heating stage, reaching approximately 12% in the temperature range of 60–140 °C. This mass loss may be attributed to the evaporation of residual chloroform. The main stage of thermal degradation of PLA also occurs within the temperature range of approximately 300–400 °C. Above 400 °C, the mass of both samples approaches zero, indicating nearly complete decomposition of the polymer matrix.

Overall, PLA-G exhibits slightly higher thermal stability during the initial heating stage, whereas the temperature range of the main degradation stage is similar for both samples.

The thermogravimetric curves of the PLA film and PLA films containing rosemary extract exhibit generally similar thermal behavior (Figure 3b). At the initial heating stage, up to approximately 150 °C, all samples show a slight mass loss, which may be associated with the removal of residual chloroform from the film materials.

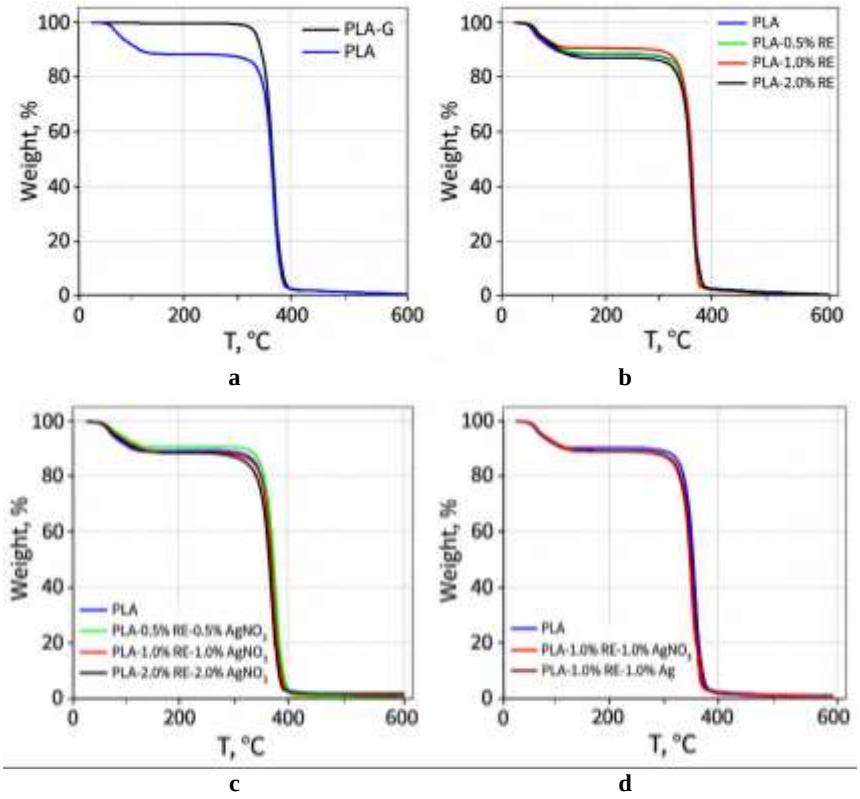

Figure 3. TGA curves:
(a) PLA-G and PLA;
(b) PLA containing different concentrations of rosemary extract;
(c) PLA containing different concentrations of rosemary extract and silver salt;
(d) PLA containing rosemary extract and rosemary extract and silver nanoparticles

For PLA films containing 0.5–2.0 wt.% rosemary extract, the mass loss at this stage is slightly lower than that observed for neat PLA. In the temperature range of approximately 300–400 °C, all investigated samples exhibit a sharp decrease in mass, corresponding to the main stage of thermal degradation of the PLA matrix. Above 400 °C, the mass of the samples approaches zero, indicating nearly complete thermal decomposition of the polymer matrix.

The TGA curves of PLA films containing rosemary extract and silver nitrate (Figure 3c) show generally similar mass-loss behavior to that of the PLA films containing rosemary extract alone (Figure 3b). At the initial stage, up to approximately 150 °C, all samples exhibit a slight mass loss, which may be associated with the removal of residual chloroform. The main mass loss occurs in the temperature range of approximately 300–400 °C and corresponds to the thermal degradation of the PLA matrix. The curves of the films containing 0.5, 1.0, and 2.0 wt.% RE + $AgNO_3$ remain close to that of neat PLA, although slight differences in the degradation behavior are observed. Above 400 °C, the mass of all samples approaches zero. The PLA films containing 1.0 wt.% RE, $AgNO_3$, or AgNPs exhibit similar thermal degradation behavior (Figure 3d).

Overall, the incorporation of rosemary extract, silver nitrate in combination with rosemary extract, and silver nanoparticles in combination with rosemary extract at concentrations of 0.5–2.0 wt.% does not result in a significant shift in the main thermal degradation region of PLA. This indicates that modification of the PLA polymer matrix with these components within the investigated concentration range does not substantially impair its thermal stability.

Differential scanning calorimetry (DSC) of PLA-based films

The differential scanning calorimetry (DSC) results reveal significant differences in the thermal and structural characteristics of polylactide depending on its physical form (granules or film) and the composition of the incorporated components (Figure 4, Table 1).

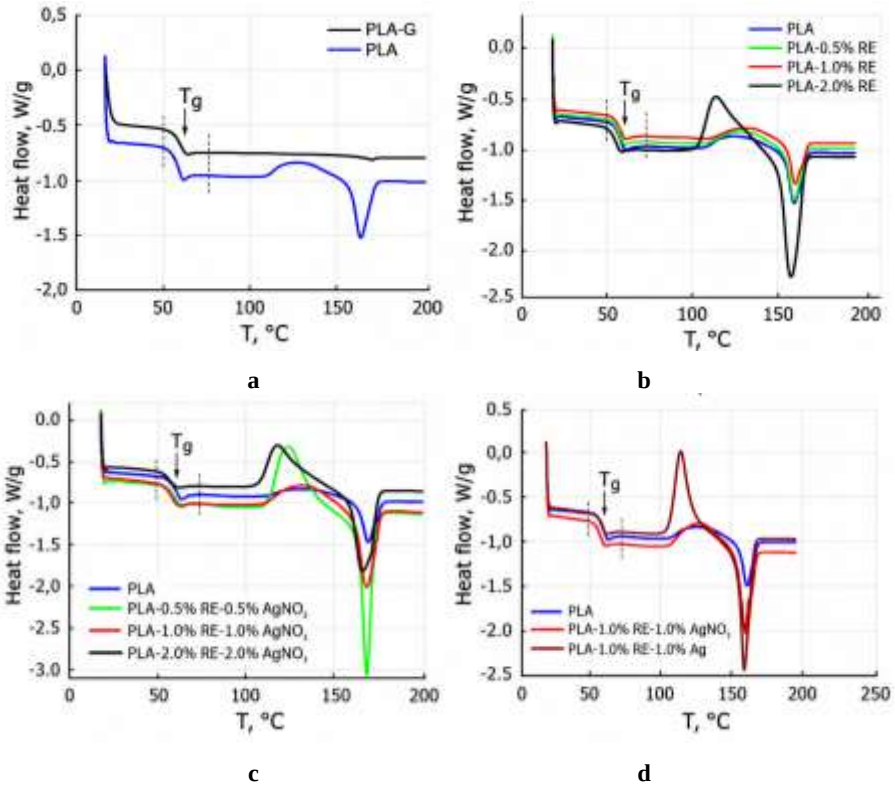

Figure 4. DSC curves:
(a) PLA-G and PLA;
(b) PLA containing different concentrations of rosemary extract;
(c) PLA containing different concentrations of rosemary extract and silver salt;
(d) PLA containing rosemary extract and rosemary extract and silver nanoparticles

Table 1

DSC parameters of PLA granules and PLA-based films

Sample	Glass transition, T_g, °C	Cold crystallization		Melting		Degree of crystallinity, $X_{cr(DSC)}$, %
		T_{cc}, °C	ΔH_{cc}, J/g	T_m, °C	ΔH_m, J/g	
PLA (granules)	57	–	–	168.2	0.71	0.76
PLA (film)	60	129.9	11.93	162.6	11.63	12.5
PLA (film) containing						
0.5 wt.% RE	58	134.2	12.41	162.2	12.2	13.18
1.0 wt.% RE	59	136.5	12.8	162.8	7.95	8.63
2.0 wt.% RE	56	116.6	34.71	160.4	35.42	38.86
0.5 wt.% RE + 0.5 wt.% $AgNO_3$	59	120.9	45.57	161.5	36.54	39.69
1.0 wt.% RE + 1.0 wt.% $AgNO_3$	57	139.9	24.11	161.7	23.77	26.00
2.0 wt.% RE + 2.0 wt.% $AgNO_3$	56	115.5	31.71	159.4	30.67	34.35
1.0 wt.% RE + 1.0 wt.% AgNPs	57	115.9	36.73	160.3	34.64	38.00

For granular PLA, the glass transition temperature (T_g) is 57 °C, the melting temperature (T_m) is 168.2 °C, and the degree of crystallinity ($X_{cr(DSC)}$) is only 0.76% (Table 1). It should be noted that the degree of crystallinity of the PLA sample in granules, determined by X-ray diffraction analysis, differs from the value obtained by DSC, since the latter was calculated based on the data of the second heating cycle, which corresponds to the maximum achievable degree of crystallinity of the polymer under the given analysis conditions. After PLA was formed into a film, the glass transition temperature slightly increased to 60 °C, whereas the melting temperature decreased to 162.6 °C. At the same time, a pronounced cold crystallization peak appeared on the DSC curve at 129.9 °C, with an enthalpy of 11.93 J/g (Figure 4a). The melting enthalpy was 11.63 J/g, and the calculated degree of crystallinity was 12.5%. The appearance of a cold crystallization peak after dissolution and film formation indicates that the polymer matrix retains a considerable potential for further crystallization upon heating after processing.

The incorporation of rosemary extract into PLA at a concentration of 0.5 wt.% results in a slight decrease in T_g to 58 °C, while the cold crystallization temperature increases to 134.2 °C, and the melting temperature remains virtually unchanged (162.2 °C) (Figure 4b). The degree of crystallinity of this sample increases to 13.18%. For the PLA sample containing 1.0 wt.% rosemary extract, T_g is 59 °C, T_{cc} is 136.5 °C, and Tm is 162.8 °C. At the same time, the degree of crystallinity decreases to 8.63%.

For PLA containing RE and $AgNO_3$, an even more pronounced effect of the modifiers on the crystallization behavior of the PLA matrix is observed (Figure 4c). For the PLA + 0.5 wt.% RE + 0.5 wt.% $AgNO_3$ sample, the cold crystallization temperature is 120.9 °C, while the cold crystallization enthalpy reaches 45.57 J/g. The melting temperature is 161.5 °C, and the degree of crystallinity is 39.69%, which is substantially higher than that of unmodified PLA. When the contents of rosemary extract and $AgNO_3$ are increased to 1.0 wt.%, the cold crystallization temperature increases to 139.9 °C, while the cold crystallization enthalpy decreases to 24.11 J/g. The melting temperature is 161.7 °C, and the degree of crystallinity is 26.0%. For the PLA + 2.0

wt.% RE + 2.0 wt.% $AgNO_3$ sample, Tcc decreases to 115.5 °C, whereas ΔHcc increases to 31.71 J/g. The melting temperature is 159.4 °C, and $X_{cr(DSC)}$ is 34.35%.

For the PLA with 1.0 wt.% RE and 1.0 wt.% $AgNO_3$ composite, T_g is 57 °C, T_{cc} is 115.9 °C, and T_m is 160.3 °C (Figure 4d). The cold crystallization enthalpy is 36.73 J/g, the melting enthalpy is 34.64 J/g, and the degree of crystallinity reaches 38%. Compared with the PLA with 1.0 wt.% RE and 1.0 wt.% $AgNO_3$ composite, the incorporation of pre-synthesized silver nanoparticles decreases the cold crystallization temperature from 139.9 to 115.9 °C and increases the degree of crystallinity from 26 to 38%.

Overall, the results demonstrate that rosemary extract, $AgNO_3$, and pre-synthesized silver nanoparticles have a substantial effect on the crystallization behavior of PLA films, whereas the glass transition temperature remains within a relatively narrow range of 56–60 °C, and the melting temperature ranges from 159 to 163 °C. The most significant changes are observed in the cold crystallization enthalpy and degree of crystallinity, the values of which vary considerably depending on the composite composition. These findings indicate that modification of PLA with rosemary extract, $AgNO_3$, and silver nanoparticles affects the ability of the polymer matrix to undergo structural rearrangement and crystallization upon heating.

Mechanical tests of PLA-based films

Figure 5 shows the stress–strain curves of PLA samples containing different concentrations of rosemary extract.

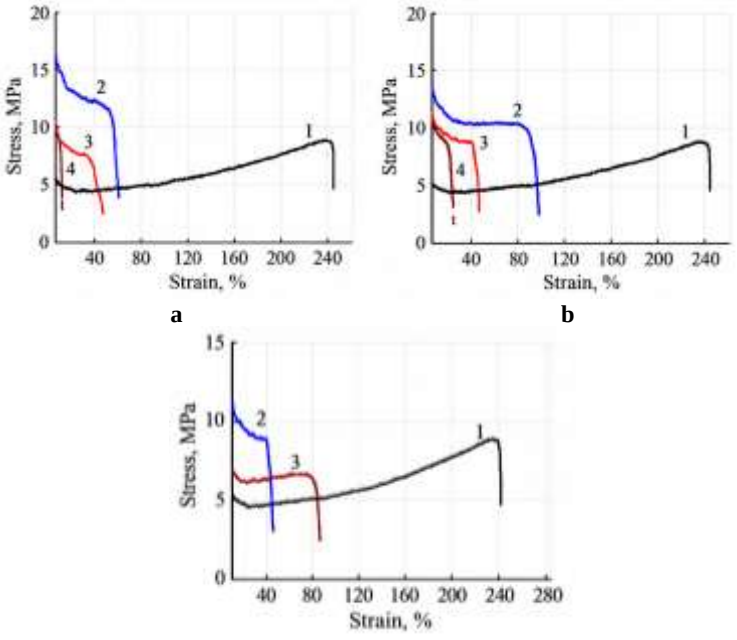

Figure 5. Mechanical strength of the samples:
(a) PLA (1) containing different concentrations of rosemary extract: 0.5 wt.% RE (2), 1.0 wt.% RE (3), 2.0 wt.% RE (4);
(b) PLA (1) containing different concentrations of rosemary extract and silver salt: 0.5 wt.% RE+0.5 wt.% $AgNO_3$ (2), 1.0 wt.% RE+1.0 wt.% $AgNO_3$ (3), 2.0 wt.% RE+2.0 wt.% $AgNO_3$ (4);
(c) PLA containing 1.0 wt.% rosemary extract (1), 1.0 wt.% $AgNO_3$ (2), 1.0 wt.% AgNPs (3)

For neat PLA (curve 1), the highest elongation at break, approximately 240%, is observed at a maximum stress of about 8–9 MPa, indicating the high deformability of the polylactide film. The incorporation of rosemary extract substantially alters the mechanical behavior of PLA. For the sample containing 0.5 wt.% rosemary extract (curve 2), the maximum stress increases to approximately 12–13 MPa, whereas the elongation at break decreases to about 60%. Increasing the rosemary extract concentration to 1.0 wt.% (curve 3) results in a further decrease in elongation at break to approximately 47%, while the maximum stress decreases to about 7.5–8.5 MPa. At 2.0 wt.% rosemary extract (curve 4), the elongation at break decreases markedly to approximately 11.5%, whereas the maximum stress remains at about 9–10 MPa. Overall, the incorporation of rosemary extract substantially reduces the elongation at break of PLA, indicating a pronounced decrease in ductility. At the same time, 0.5 wt.% rosemary extract increases the maximum stress compared with neat PLA, whereas further increases in the extract concentration to 1.0–2.0 wt.% result in lower strength characteristics.

Figure 5b shows the stress–strain curves of PLA samples containing rosemary extract and $AgNO_3$ at different concentrations. The incorporation of rosemary extract and $AgNO_3$ into PLA substantially altered the mechanical behavior of the polylactide matrix. For the PLA sample containing 0.5 wt.% rosemary extract and 0.5 wt.% $AgNO_3$ (curve 2), the maximum stress was approximately 10 MPa, while the elongation at break was about 100%. Increasing the concentrations of both components to 1.0 wt.% rosemary extract + 1.0 wt.% $AgNO_3$ (curve 3) resulted in a decrease in the maximum stress to approximately 9 MPa, whereas the elongation at break was about 48%. For the PLA sample containing 2.0 wt.% rosemary extract + 2.0 wt.% $AgNO_3$ (curve 4), a further decrease in both strength and deformability was observed: the maximum stress was approximately 9 MPa, while the elongation at break decreased to about 26%. Thus, the incorporation of rosemary extract in combination with $AgNO_3$ at a concentration of 0.5 wt.% provided the most pronounced improvement in the strength characteristics of PLA while maintaining sufficient deformability. Further increases in the concentrations of both components were accompanied by a decrease in elongation at break and a gradual deterioration of the strength characteristics.

Figure 5c shows the stress–strain curves of PLA containing 1.0 wt.% rosemary extract, AgNPs, or $AgNO_3$. For PLA containing 1.0 wt.% AgNPs (curve 3), the maximum stress is approximately 6.5 MPa, while the elongation at break is about 90%. PLA containing 1.0 wt.% $AgNO_3$ (curve 2) exhibits lower mechanical performance than PLA containing AgNPs (curve 3), whereas neat PLA (curve 1) exhibits the highest overall mechanical performance among the investigated samples.

Antimicrobial activity of PLA-based films

The antimicrobial activity of the PLA-based films was evaluated based on the diameter of the growth inhibition zones of the tested opportunistic microorganisms (Table 2, Figure 6).

For neat PLA (curve 1), the highest elongation at break, approximately 240%, is observed at a maximum stress of about 8–9 MPa, indicating the high deformability of the polylactide film. The incorporation of rosemary extract substantially alters the mechanical behavior of PLA. For the sample containing 0.5 wt.% rosemary extract (curve 2), the maximum stress increases to approximately 12–13 MPa, whereas the elongation at break decreases to about 60%. Increasing the rosemary extract concentration to 1.0 wt.% (curve 3) results in a further decrease in elongation at break to approximately 47%, while the maximum stress decreases to about 7.5–8.5 MPa. At 2.0 wt.% rosemary extract (curve 4), the elongation at break decreases markedly to approximately 11.5%, whereas the maximum stress remains at about 9–10 MPa. Overall, the incorporation of

rosemary extract substantially reduces the elongation at break of PLA, indicating a pronounced decrease in ductility. At the same time, 0.5 wt.% rosemary extract increases the maximum stress compared with neat PLA, whereas further increases in the extract concentration to 1.0–2.0 wt.% result in lower strength characteristics.

Table 2

Antimicrobial activity of PLA-based films

Sample No	Composition of film	Diameter of the growth inhibition zone, mm			
		S. aureus	***B. subtilis***	***E. coli***	***P. aeruginosa***
1	PLA	0	0	0	0
	PLA containing				
2	0.5 wt.% RE	0	0	0	0
3	1.0 wt.% RE	0	0	0	0
4	2.0 wt.% RE	0	0	0	0
5	0.5 wt.% RE+0.5 wt.% $AgNO_3$	0	0	13.35±0.29	12.20±0.26
6	1.0 wt.% RE+1.0 wt.% $AgNO_3$	24.08±0.55	0	21.81±0.50	16.85±0.39
7	2.0 wt.% RE+2.0 wt.% $AgNO_3$	19.15±0.42	0	20.40±0.52	19.46±0.42
8	1.0 wt.% RE+1.0 wt.% AgNPs	14.34±0.34	0	15.19±0.35	13.23±0.32

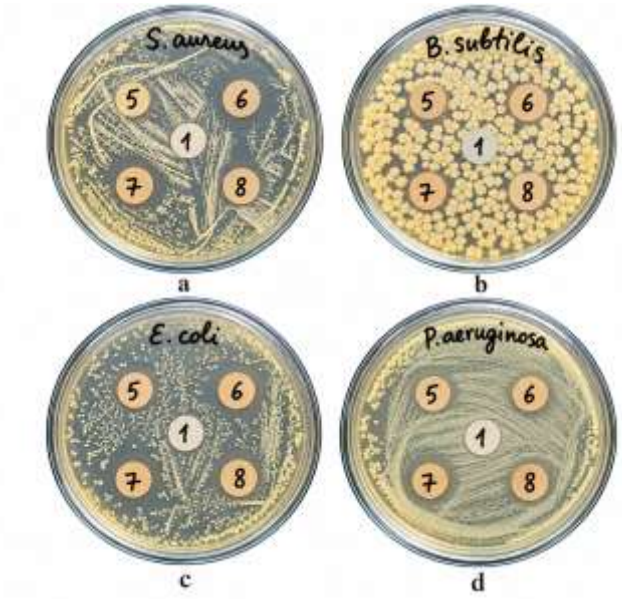

Figure 6. Antimicrobial activity of PLA-based films against *Staphylococcus aureus* (a), *Bacillus subtilis* (b), *Escherichia coli* (c), and *Pseudomonas aeruginosa* (d).
Film compositions are given in Table 2.

The absence of antimicrobial activity observed for PLA films containing rosemary extract is consistent with the recent findings of He et al. (2026), who reported that the antimicrobial effect of RE in PLA- and poly(butylene adipate-co-terephthalate) containing films was limited, although its incorporation improved the antioxidant properties and UV-shielding performance of the films.

Importantly, He et al. (2026) also reported that rosemary extract concentrations exceeding 1% caused film stickiness, making the films difficult to process. This observation suggests that increasing the extract content is not necessarily an appropriate strategy for enhancing the functional performance of plant-extract-based films, as excessive extract loading may adversely affect their technological properties.

In contrast, the incorporation of $AgNO_3$ together with rosemary extract substantially altered the antimicrobial properties of the PLA films. When 0.5 wt.% $AgNO_3$ was added to PLA containing 0.5 wt.% rosemary extract (sample 5), growth inhibition was observed only for the Gram-negative bacteria. The growth inhibition zone diameters were 13.35 ± 0.29 mm for *E. coli* and 12.20 ± 0.26 mm for *P. aeruginosa*, whereas no antimicrobial activity was detected against the Gram-positive bacteria *S. aureus* and *B. subtilis*. Increasing the concentrations of both rosemary extract and $AgNO_3$ from 0.5 to 1.0 wt.% (sample 6) resulted in larger inhibition zones against *S. aureus*, *E. coli*, and *P. aeruginosa*. The inhibition zones reached 24.08 ± 0.55 mm for *S. aureus*, 21.81 ± 0.50 mm for *E. coli*, and 16.85 ± 0.39 mm for *P. aeruginosa*, whereas no inhibition of *B. subtilis* was observed. Further increasing the concentrations of both components to 2.0 wt.% (sample 7) did not produce a further increase in inhibition for all tested strains. The inhibition zones decreased for *S. aureus* and *E. coli* to 19.15 ± 0.42 and 20.40 ± 0.52 mm, respectively, while increasing slightly for *P. aeruginosa* to 19.46 ± 0.42 mm.

The film containing 1.0 wt.% rosemary extract and 1.0 wt.% AgNPs (sample 8) also inhibited the growth of *S. aureus* (14.34 ± 0.34 mm), *E. coli* (15.19 ± 0.35 mm), and *P. aeruginosa* (13.23 ± 0.32 mm), although the inhibition zones were smaller than those observed for the corresponding film containing 1.0 wt.% $AgNO_3$ (sample 6). At the same nominal concentrations of the components, the $AgNO_3$-containing film exhibited larger inhibition zones than the AgNP-containing material. This difference may be related to the form and availability of silver, as well as the diffusion of antimicrobial silver-containing species from the polymer matrix into the agar medium.

According to the agar diffusion test, the broadest antimicrobial spectrum was observed for the PLA films containing 1.0 or 2.0 wt.% of both rosemary extract and $AgNO_3$, with each composition inhibiting three of the four tested strains (samples 6 and 7). None of the tested films inhibited the growth of *B. subtilis*, including the composition containing the highest concentration of $AgNO_3$, indicating that the antimicrobial activity of the developed materials was strongly strain-dependent. Overall, the antimicrobial activity of the PLA composites was associated with the presence of $AgNO_3$ or AgNPs, whereas rosemary extract alone did not exhibit detectable antimicrobial activity under the conditions of this study.

Conclusions

Biodegradable films based on PLA containing rosemary extract, $AgNO_3$, and silver nanoparticles were obtained. X-ray diffraction analysis showed that the initial PLA granules had a crystallinity of approximately 60%, whereas the resulting PLA film exhibited a predominantly amorphous structure. The incorporation of rosemary extract at concentrations of 0.5–2.0 wt.% did not cause significant structural changes in PLA, whereas the

incorporation of AgNPs was accompanied by a shift in the broad amorphous diffraction maximum characteristic of the PLA structure and the appearance of reflections characteristic of the crystal lattice of metallic silver. It was established that the incorporation of rosemary extract, $AgNO_3$, or AgNPs within the studied concentration range did not significantly affect the thermal stability of PLA-based films. The main stage of thermal degradation of all investigated films occurred predominantly within the range of 300–400 °C. DSC analysis showed that the studied components substantially affected the crystallization behavior of PLA. The degree of crystallinity varied depending on the film composition, whereas the glass transition temperature remained within 56–60 °C and the melting temperature within 159–163 °C. The incorporation of rosemary extract substantially altered the mechanical behavior of the PLA films, primarily by reducing their elongation at break. At a rosemary extract content of 0.5 wt.%, the tensile strength of PLA increased to approximately 10–11 MPa compared with 8–9 MPa for unmodified PLA; however, further increases in extract concentration were accompanied by a decrease in tensile strength. The PLA film without additives and films containing 0.5–2.0 wt.% rosemary extract showed no antimicrobial activity against the tested strains. Films containing both rosemary extract and $AgNO_3$ inhibited *S. aureus*, *E. coli*, and *P. aeruginosa*, with the widest antimicrobial spectrum observed at 1.0 and 2.0 wt.% of both components. At 1.0 wt.%, $AgNO_3$ provided larger inhibition zones than AgNPs. None of the films inhibited *B. subtilis*, indicating a strain-dependent antimicrobial effect. Overall, silver-containing additives show potential for developing PLA films with antimicrobial properties.

Further studies should focus on the comparative evaluation and selection of the most effective plant extract for incorporation into PLA films intended for meat packaging. The selected extract and film composition should then be optimized to achieve a balance between antimicrobial activity and physicomechanical properties. Finally, the most promising films should be evaluated with meat products during refrigerated storage to determine their effectiveness in maintaining product quality and extending shelf life.

Acknowledgments. The work was carried out with the financial support of a grant from the National Research Foundation of Ukraine "Development of packaging materials based on biopolymers with antimicrobial components of natural origin for long-term storage of food products" (Application ID 2025.07/0333).

References

Abd-Elhalim, B. T., Mohamed, E. S., Gamar, G. M., & Moawad, H. (2025). Biological activities and application of Rosmarinus officinalis extract to improve the preservation and microbial qualities of some local meat products. *Scientific Reports, 15*, 30806. https://doi.org/10.1038/s41598-025-14247-x

Al-Tayaw, T. S., Ade E. M., & Omer F. H. (2014). Phytochemical screening and antioxidant properties of alcoholic extract and antibacterial activity of *Rosmarinus officinalis* L. leaves. *Plant Science Today, 11*(3), 383-391. https://doi.org/10.14719/pst.3897

Andrade, J. M., Faustino, C., Garcia, C., Ladeiras, D., Reis, C. P., & Rijo, P. (2018). *Rosmarinus officinalis* L.: An update review of its phytochemistry and biological activity. *Future Science OA, 4*(4), FSO283. https://doi.org/10.4155/fsoa-2017-0124

Barbosa-Pereira, L., Aurrekoetxea, G. P., Angulo, I., Paseiro-Losada, P., & Cruz, J. M. (2014). Development of new active packaging films coated with natural phenolic compounds to improve the oxidative stability of beef. *Meat Science, 97*(2), 249–254. https://doi.org/10.1016/j.meatsci.2014.02.006

Bessi, A., Rais, C., Slimani, C., Elhanafi, L., Zeouk, I., Louafi, B., Ghadraoui, L.E., Bouchamma, E.O. (2025). Phytochemical screening, antioxidant and antibacterial activity of six medicinal and aromatic plants in Morocco: A comparative study. *Plant Breeding and Biotechnology, 13*, 15-32. https://doi.org/10.9787/PBB.2025.13.15

de Lima, A. F., Leite, R. H. d. L., Pereira, M. W. F., Silva, M. R. L., de Araújo, T. L. A. C., de Lima Júnior, D. M., Gomes, M. d. N. B., & Lima, P. d. O. (2024). Chitosan coating with rosemary extract increases shelf life and reduces water losses from beef. *Foods*, *13*(9), 1353. https://doi.org/10.3390/foods13091353

Demchenko, V., Mamunya, Y., Kobylinskyi, S., Riabov, S., Naumenko, K., Zahorodnia, S., Povnitsa, O., Rybalchenko, N., Iurzhenko, M., Adamus, G., & Kowalczuk, M. (2022). Structure-morphology-antimicrobial and antiviral activity relationship in silver-containing nanocomposites based on polylactide. *Molecules*, *27*(12), 3769. https://doi.org/10.3390/molecules27123769

Demchenko, V., Zaremba, P., Rybalchenko, N., Zahorodnia, S., Artiukh, L., Rybalchenko, T., Demchenko, O., Sytnyk, I., Zeng, D., Kobylinskyi, S., Goncharenko, L., & Iurzhenko, M. (2025a). Structural peculiarities of the silver-containing nanocomposites based on carboxymethyl cellulose-chitosan polyelectrolyte complexes and their antimicrobial and antiviral applications. *Scientific Reports*, *15*, 35087. https://doi.org/10.1038/s41598-025-18932-9

Demchenko V., Mamunya Y., Sytnyk I., Iurzhenko M., Krivtsun I., Rybalchenko N., Naumenko K., Artiukh L., Kowalczuk M., Demchenko O., & Marynin A. (2025b). Fabrication of polylactide composites with silver nanoparticles by sputtering deposition and their antimicrobial and antiviral applications. *Polymer International*, *74*(3), 207–216. https://doi.org/10.1002/pi.6707

Demchenko, V., Mamunya, Y., Sytnyk, I., Iurzhenko, M., Rybalchenko, N., Zahorodnia, S., Demchenko, O., Rushkovsky, S., Kunytskyi, D., Zeng, D., Talaniuk, V., & Musioł, M. (2025c). Wound dressing cryogel materials based on poly(vinyl alcohol), hyaluronic acid, and Ag_2O nanoparticles. *ACS Applied Materials & Interfaces*, *17*(38), 53312–53326. https://doi.org/10.1021/acsami.5c14960

EFSA Panel on Food Additives and Nutrient Sources added to Food (ANS). (2018). Refined exposure assessment of extracts of rosemary (E 392) from its use as food additive. *EFSA Journal*, *16*(8), e05373. https://doi.org/10.2903/j.efsa.2018.5373

Emir Çoban, Ö., & Pelin Can, Ö. (2013). The effect of active packaging film containing rosemary extract on the quality of smoked rainbow trout (*Oncorhynchus mykiss*). *Journal of Aquatic Food Product Technology*, *22*(4), 361–370. https://doi.org/10.1080/10498850.2011.652766

Essential oils, oleoresins (solvent-free), and natural extractives (including distillates), 21 C.F.R. § 182.20. (2026). https://www.ecfr.gov/current/title-21/chapter-I/subchapter-B/part-182/subpart-A/section-182.20

FaO. (2025). Food and Agricultural Organisation of the United Nations. The International Day of Awareness of Food Loss and Waste – 2025. Available online at 06.08.2026: https://www.fao.org/neareast/events/details/the-fao-regional-office-for-the-near-east-and-north-africa/en

Ghasemian, S.O., Ahmadi-Dastgerdi, A., Abdollahi, A., Tirtashi, F. E., Zokaei, M., Fallah, N., Izadi-NajafAbadi, P., & Dolatyari, F. (2024). The effect of active packaging film based on chitosan containing rosemary (*Rosmarinus officinalis* L.) Extract on cheese shelf life. *Journal of Food Biochemistry*, *2024*, 2108707. https://doi.org/10.1155/2024/2108707

He, X., Tang, L., & Huang, R. (2026). Active packaging films from PBAT/PLA with *Rosmarinus officinalis* L. extract: Antioxidant, UV-shielding, and compostable properties. *Molecules*, *31*(2), 217. https://doi.org/10.3390/molecules31020217

Jancikova, S., Jamróz, E., Kulawik, P., Tkaczewska, J., & Dordevic, D. (2019). Furcellaran/gelatin hydrolysate/rosemary extract composite films as active and intelligent packaging materials. *International Journal of Biological Macromolecules*, *131*, 19-28. https://doi.org/10.1016/j.ijbiomac.2019.03.050

Macedo, L. M. D., Santos, É. M. D., Ataide, J. A., Silva, G. T. D. S. E., Guarnieri, J. P. D. O., Lancellotti, M., Jozala, A. F., Rosa, P. C. P., & Mazzola, P. G. (2022). Development and evaluation of an antimicrobial formulation containing *Rosmarinus officinalis*. *Molecules*, *27*(16), 5049. https://doi.org/10.3390/molecules27165049

Maffioli, E, Ruggeri, M., Tommasino, C., Vigani, B., Rossi, S., & Sandri, G. (2026). Beyond barriers: Active packaging strategies for sustainable food protection. *Polymers, 18*(11), 1399. https://doi.org/10.3390/polym18111399

Pasichnyi, V., Marynin, A., Khrapachov, O., & Shvediuk, D. (2022). Modern packaging systems application to extend meat products shelf life. In O. Paredes-López, O. Shevchenko, V. Stabnikov, & V. Ivanov (Eds.), *Bioenhancement and fortification of foods for a healthy diet* (pp. 295–323). CRC Press. https://doi.org/10.1201/9781003225287-19

Regulation (EC) No 1333/2008 of the European Parliament and of the Council of 16 December 2008 on food additives. *Official Journal of the European Union*, L 354, 16–33. http://data.europa.eu/eli/reg/2008/1333/oj

Rožman, T., & Jeršek, B. (2009). Antimicrobial activity of rosemary extracts (*Rosmarinus officinalis* L.) against different species of *Listeria*. *Acta Agriculturae Slovenica, 93*(1), 51-58. https://doi.org/10.2478/v10014-009-0007-z

Stabnikova, O., Stabnikov, V., Marynin, A., Klavins, M., & Vaseashta, A. (2025). Microplastic pollution mitigation from fresh and marine water bodies. In A. Vaseashta, M. Klavins, & O. Stabnikova (Eds.), *Micro and nanoplastics in aquatic environment* (pp. 59–100). CRC Press. https://doi.org/10.1201/9781003389460-2

Stabnikova, O., Stabnikov, V., & Paredes-López, O. (2026a). Spices and essential oils in food preservation: From natural additives to active packaging systems. *Plant Food for Human Nutrition, 81*, 69. https://doi.org/10.1007/s11130-026-01519-8

Stabnikova, O., Marynin, A., Stabnikov, V., Svyatnenko, R., & Demchenko, V. (2026b). Plant essential oils for food shelf-life extension and active packaging systems. *Ukrainian Food Journal, 15*(2), 323–360. https://doi.org/10.24263/2304-974X-2026-15-2-6

Vashchuk, A., Motrunich, S., Lishchuk, P., Demchenko, V., Isaiev, M., & Iurzhenko, M. (2023).Thermal conductivity and mechanical properties of epoxy vitrimer nanocomposites reinforced with graphene oxide. *Applied Nanoscience, 13*(7), 4675–4683. https://doi.org/10.1007/s13204-022-02587-3

Yacoub, M., & Han, B. (2026). Terrestrial microplastic pollution: Occurrence, fate, and ecological effects on soil systems. *Microplastics, 5*(2), 67. https://doi.org/10.3390/microplastics5020067

Cite:

Demchenko, V., Stabnikova, O., Marynin, A., & Rybalchenko, N. (2026). Active packaging films from PLA with *Rosmarinus officinalis* extract. *Ukrainian Food Journal, 15*(3), 786–801. https://doi.org/10.24263/2304-974X-2026-15-3-12

Aroma characteristics and volatile composition of sterilized mushroom pâté

Oleh Kuzmin, Oleksandra Niemirich, Olena Podobii, Yuliia Zaporozhets, Oleksandr Velikanov

National University of Food Technologies, Kyiv, Ukraine

Keywords:

Mushroom pâté
Pleurotus ostreatus
Phaseolus vulgaris
Aroma profile
Volatile compound
GC-FID

Article history:

Received 27.02.2026
Received in revised form 11.07.2026
Accepted 30.06.2026

Corresponding author:

Oleh Kuzmin
E-mail: kuzmin_ovl@ukr.net

DOI:
10.24263/2304-974X-2026-15-3-13

Abstract

Introduction. The aim of the study was to characterize the aroma profile of sterilized mushroom pâté based on oyster mushroom and beans and to relate its sensory characteristics to the composition of volatile compounds.

Materials and methods. Mushroom pâté based on oyster mushroom (*Pleurotus ostreatus*) and beans (*Phaseolus vulgaris*) was studied using sensory profiling with 13 descriptors rated on a 5-point intensity scale and gas chromatography with flame ionization detection (GC-FID), with preliminary identification of volatile compounds based on experimental and literature retention indices.

Results and discussion. The sterilized pâté was characterized by a homogeneous, plastic, spreadable consistency, uniform deep brown color, pleasant, harmonious and balanced taste, and a complex aroma. The highest intensity (5 points) was recorded for the descriptors "pleasant," "harmonious," "balanced," and "sun-dried tomatoes"; "umami," "liver-like," and "beef-like" received 4 points; "delicate," "nutty," "mushroom-like," and "fatty" received 3 points; while "slightly sweet" and "typical of the ingredients" received 2 points. GC-FID analysis revealed 33 chromatographic peaks. Ketones (87.77%), esters (4.41%), aldehydes (1.74%), alcohols (1.53%), phenolic compounds (1.41%), and terpenes (1.39%) predominated in the volatile fraction based on relative peak area. The proportions of fatty acids, furans, sulfur-containing compounds, and alkanes were 0.70%, 0.49%, 0.36%, and 0.21%, respectively. Mushroom-like aroma notes may be associated with (E,Z)-3,6-nonadien-1-ol, dehydro-ar-ionene, and methylene bis(methyl sulfide); creamy, apple-like, rose-like, and honey-like notes with acetoin, β-damascenone, and (E)-β-damascone; spicy-woody notes with α-copaene, β-caryophyllene, eugenol, and methyleugenol; and fatty and oily notes with aldehydes, alcohols, and decanoic acid. The detected compounds were considered probable contributors to the formation of the corresponding aroma notes of the product. The combination of sensory profiling and GC-FID revealed probable relationships between the composition of the volatile fraction and the sensory characteristics of the product, particularly mushroom-like, meat-like, spicy, and fatty aroma notes.

Conclusions. The sterilized mushroom pâté showed a complex and balanced aroma profile, with pronounced pleasant, harmonious, sun-dried tomato, umami, meat-like, and mushroom-like notes. Ketones predominated in the volatile fraction (87.77%), while several detected compounds were probable contributors to mushroom-like, spicy, fatty, and other characteristic aroma notes. The results demonstrate relationships between the volatile composition and sensory characteristics of the pâté.

Introduction

Thermal processing can substantially alter the composition of the volatile fraction of a food matrix through transformation of compounds initially present in raw materials and formation of new volatile components (Selli et al., 2021). This is particularly relevant to mushroom pâté, whose aroma results from the combined contribution of volatile compounds originating from oyster mushroom (*Pleurotus ostreatus*) (Dubova et al., 2021; Yin et al., 2019; Zhao et al., 2024), beans (*Phaseolus vulgaris*) (Khrisanapant et al., 2022), onion (*Allium cepa*) (Tokitomo, 1995), carrot (*Daucus carota*) (Tian et al., 2024), black pepper (*Piper nigrum*) (Dosoky et al., 2019), paprika (*Capsicum annuum*) (Dippong et al., 2023), butter (Peterson & Reineccius, 2003), and sunflower oil (Liu et al., 2019).

Mushrooms are widely studied as food raw materials because of their nutritional value and diverse bioactive compounds, as summarized in recent reviews of wild and cultivated mushrooms (Stabnikova et al., 2024, 2025). However, the formation of the volatile and sensory profile of a sterilized mushroom pâté based on *Pleurotus ostreatus* remains insufficiently characterized.

Processing conditions substantially affect the volatile profile of *Pleurotus ostreatus*. Politowicz et al. (2018) reported a decrease in total volatile concentration from 4506 to a maximum of 245 μg/100 g dry matter after dehydration, while Timaná et al. (2024) demonstrated substantial changes in the composition of individual volatiles following drying. Thermal cooking also substantially modifies the volatile profile. Selli et al. (2021) reported a marked decrease in total volatile concentration after boiling and oven-cooking, with the lowest level after oven-cooking, while 1-octen-3-ol and methional showed the highest flavor dilution factor (FD = 2048) in raw and boiled samples. Roasting caused partial elimination of initial volatiles and formation of new aroma-active compounds; 17 pyrazines were detected in roasted *Pleurotus ostreatus*, with 3-ethyl-2,5-dimethylpyrazine reaching 21.22 μg/g fresh weight, together with Strecker aldehydes and sulfur-containing compounds (Tagkouli et al., 2021).

These findings demonstrate that processing can substantially modify the volatile fraction of *Pleurotus ostreatus*. However, volatile profile formation during high-temperature sterilization of an already formulated mushroom product in hermetically sealed containers represents a distinct technological issue. The multicomponent pâté matrix may promote additional thermal and oxidative transformations, particularly in its lipid and carbohydrate–protein components. Lipid oxidation and thermal treatment of sunflower oil can generate aldehydes, ketones, alcohols, furans, and other volatiles (Gómez-Cortés et al., 2015; Park et al., 2022). Accordingly, 2-undecenal (Huang et al., 2021), (E)-2-undecenal (Liu et al., 2019), and 4,5-epoxy-2-decenal (Goicoechea et al., 2008; Guillén & Goicoechea, 2008) may be relevant to the volatile profile of sterilized pâté because of their association with lipid oxidation and thermal degradation.

Vegetable and spice components may provide additional volatile compounds. Eugenol, characterized by sweet, spicy, and clove-like odor, has been identified in paprika (Izcara et al., 2022), carrot (Buttery & Takeoka, 2013), allspice (Götz et al., 2023), and onion (Arena et al., 2024). β-Caryophyllene has been reported in paprika (Serio et al., 2024), carrot (Tian et al., 2024), and black pepper (Dosoky et al., 2019), while α-copaene has been identified in paprika (Serio et al., 2024). Individual compounds may also originate from several ingredients: acetoin (3-hydroxy-2-butanone), with a buttery and creamy odor, has been reported in butter (Demirkol et al., 2016; Roosta et al., 2014), oyster mushroom (Kim et al., 2026), carrot (Tian et al., 2024), paprika (Mateo et al., 1997), and beans (Khrisanapant et al., 2022), whereas β-damascenone, associated with apple-, rose-, and honey-like notes, has been identified in cooked carrot and may also form during thermal degradation of carotenoids (Buttery & Takeoka, 2013; Zepka et al., 2014).

Thus, interpretation of the volatile profile of sterilized mushroom pâté requires consideration of both the probable origin and odor characteristics of individual compounds and their possible formation during thermal or oxidative processing. Despite extensive data on volatiles in mushrooms, legumes, vegetables, spices, and lipid systems, the volatile and sensory profile of sterilized pâté based on *Pleurotus ostreatus* and *Phaseolus vulgaris* remains insufficiently characterized. Clarifying the relationship between detected volatile compounds, their potential sources, odor properties, and sensory characteristics is therefore necessary for objective assessment of aroma quality and understanding the technological factors shaping the sensory profile of the finished product.

The aim of the study was to evaluate the aroma profile and quality of sterilized mushroom pâté based on oyster mushroom (*Pleurotus ostreatus*) and beans (*Phaseolus vulgaris*), determine the composition of volatile aroma compounds, and establish their probable relationship with the organoleptic properties of the product.

Materials and methods

Materials

The main raw material used for the production of mushroom pâté was oyster mushroom (*Pleurotus ostreatus*) – fresh cultivated mushrooms artificially enriched with the trace elements chromium (Cr) and selenium (Se) (Kuzmin et al., 2025). To increase the nutritional value and regulate the consistency of the pâté mass, cooked beans (*Phaseolus vulgaris*) were incorporated into the formulation.

The taste and aroma characteristics and formulation profile of the product were complemented by sautéed vegetables – onion (*Allium cepa*) and carrot (*Daucus carota*). Butter and refined sunflower oil were used as fat components. The spicy and taste characteristics were provided by table salt, ground black pepper (*Piper nigrum*), and paprika (*Capsicum annuum*).

Mushroom pâté technology

The technological process for the production of sterilized mushroom pâté with oyster mushroom and beans was carried out in accordance with the technical specifications (Bakhlukova et al., 2025) and followed the basic technological flow diagram presented in Figure 1.

The production technology included the preparation and thermal processing of plant-based raw materials, mixing of the formulation components, homogenization of the pâté mass, filling, hermetic sealing, sterilization, cooling, and storage. Fresh oyster mushroom, beans, onion, and carrot were sorted, foreign matter and unsuitable parts were removed, and the raw materials were washed. Fresh oyster mushroom was cut into pieces with a diameter of 10–20 mm and fried separately at 120–140 °C for 6–8 min. The beans were soaked in drinking water for 8–12 h at 18–20 °C and subsequently cooked at 98–100 °C for 60–90 min until culinary readiness. After peeling and washing, the onion and carrot were chopped and sautéed in a mixture of butter and refined sunflower oil at 100–110 °C for 8–12 min until softened and the characteristic color, taste, and aroma had developed. The prepared fried oyster mushroom, cooked beans, and sautéed vegetables were then mixed with the remaining formulation components, including the fat phase, table salt, and spices, and homogenized to obtain a uniform paste-like pâté mass. The temperature of the mass before filling was 70–80 °C.

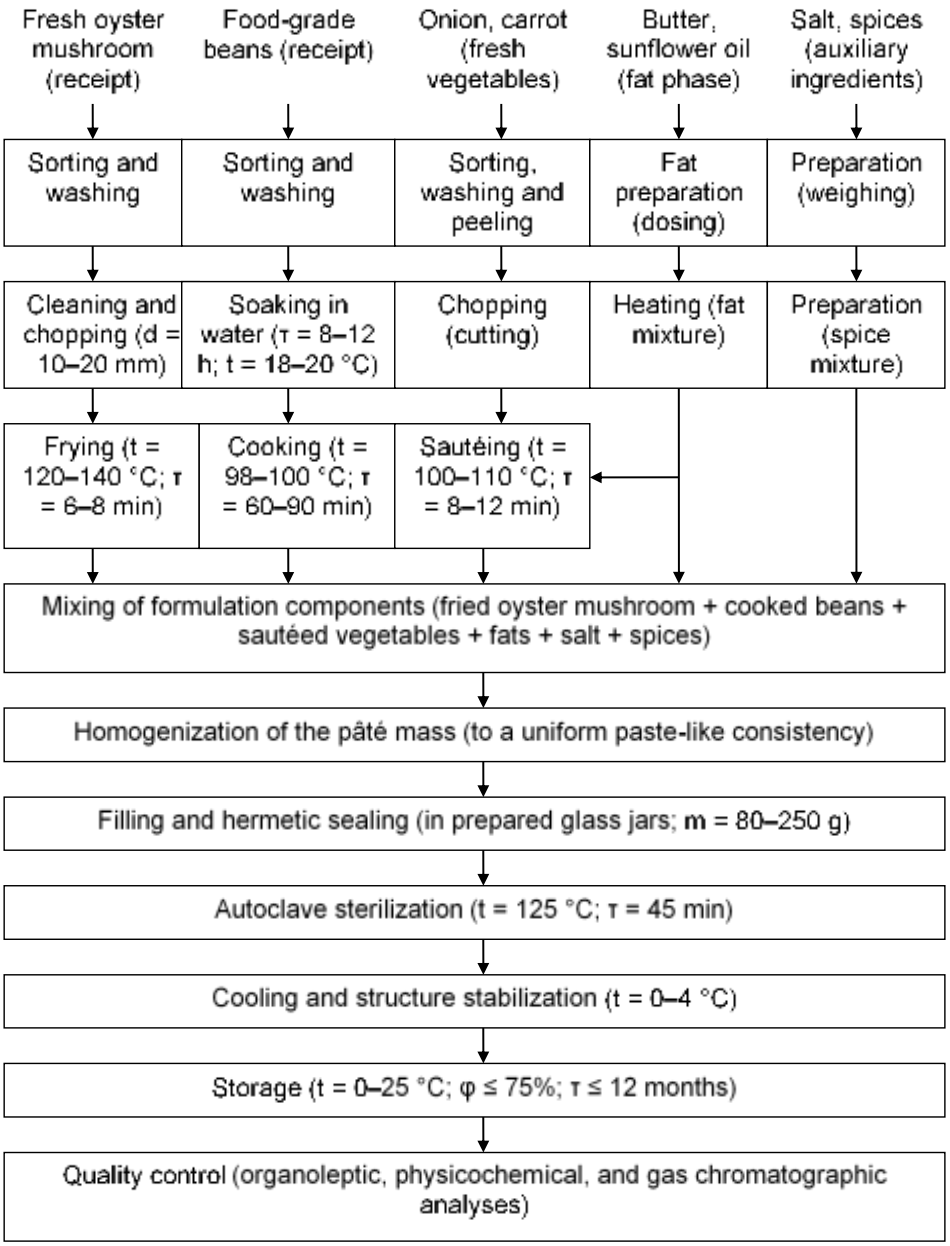

Figure 1. Basic technological flow diagram for the production of sterilized mushroom pâté with oyster mushroom and beans

The prepared pâté mass was filled into pre-prepared glass jars with a net weight of 80–250 g, after which the jars were hermetically sealed. Sterilization was performed in an autoclave at 125 °C for 45 min in accordance with the established technological regime. After

sterilization, the jars were cooled to 0–4 °C and held to stabilize the consistency and structure of the pâté mass. The finished product was stored at 0–25 °C and a relative humidity of ≤75% for up to 12 months. Quality control included organoleptic evaluation (Koretska et al., 2021), determination of physicochemical parameters, and analysis of volatile organic compounds by gas chromatography.

Gas chromatography

The qualitative composition of volatile aroma compounds in the mushroom pâté was investigated by gas chromatography (GC) using a Kristallux-4000M gas chromatograph equipped with a flame ionization detector (FID) (Tovstonoh et al., 2026). Chromatographic data acquisition and processing were performed using NetChrom v2.1 software. Volatile compounds were separated using an HP-5 capillary non-polar column manufactured by Agilent, with a length of 30 m, an internal diameter of 0.32 mm, and a stationary-phase film thickness of 0.25 μm (Tovstonoh et al., 2026). The HP-5 column belongs to the low-polarity column group based on 5% phenyl–95% dimethylpolysiloxane and, in terms of its chromatographic characteristics, is analogous to DB-5-type columns, allowing experimental retention indices to be compared with literature data obtained using columns of this type.

Nitrogen was used as the carrier gas, and the pressure at the capillary column was 0.5 atm. Nitrogen was also used as the auxiliary gas in the detection system at a flow rate of 30 cm^3/min, together with an additional nitrogen flow of 5 cm^3/min, in accordance with the established configuration of the flame ionization detector gas flows. The air flow rate was 250 cm^3/min, and the hydrogen flow rate was 30 cm^3/min. The injector temperature was 150 °C, and the detector temperature was 300 °C.

The column temperature was programmed from an initial temperature of 35 °C to a final temperature of 250 °C at a heating rate of 3 °C/min. According to the NetChrom v2.1 protocol, the initial and final temperatures were specified as stages of the temperature program; no separate hold time at the final temperature of 250 °C was specified in the protocol. Prior to chromatographic analysis, volatile compounds were extracted from the mushroom pâté sample and introduced into the chromatograph. The injected sample volume was 1 μL. The analysis provided the retention time (RT), height, area, and width of the chromatographic peaks.

Determination of retention indices

Retention indices (RI), determined on the non-polar HP-5 capillary column, were used for the preliminary identification of volatile compounds. n-Alkanes were used as reference compounds: hexane (RI = 600), heptane (RI = 700), and decane (RI = 1000). Experimental retention indices (RI_{exp}) were calculated based on the experimental retention times of the reference n-alkanes and their tabulated RI values for non-polar columns. The obtained RI_{exp} values were used for comparison with literature retention indices (RI_{lit}) reported for HP-5/DB-5-type columns.

Since the study was performed under temperature-programmed column conditions, the calculated RI values were considered experimental retention indices determined under temperature-programmed gas chromatography conditions. They were used primarily as a comparative parameter for the preliminary identification of volatile compounds.

Method for preliminary identification of volatile compounds

Since the Kristallux-4000M gas chromatograph used in the study was equipped with a flame ionization detector (FID), while a mass spectrometric detector was not employed, the identification of volatile compounds was performed as preliminary (tentative identification). It was based on comparison of the experimental retention indices (RI_{exp}) with literature values (RI_{lit}) reported for non-polar HP-5/DB-5-type columns, using the specialized FlavorNet database (Acree & Arn, 2026).

The initial selection of candidate compounds was performed according to the criterion of agreement between the experimental and literature retention indices, with the absolute deviation not exceeding 5 RI units:

$$|RI_{exp} - RI_{lit}| \leq 5.$$

This criterion was used as a working threshold for selecting candidate compounds and was not considered sufficient confirmation of their chemical structures. Definitive identification by mass spectrometry or authentic individual standards was not performed within the scope of this study.

To select the most probable candidate, the correspondence of the literature-reported aroma characteristics, chemical nature of the compound, and its possible source in the mushroom pâté formulation was additionally considered. The possible origin of volatile compounds from oyster mushroom (*Pleurotus ostreatus*), beans (*Phaseolus vulgaris*), onion (*Allium cepa*), carrot (*Daucus carota*), butter, sunflower oil, and spices was assessed, as well as the possibility of their formation as a result of technological processing.

When interpreting the chromatographic data, the main pathways involved in the formation of the volatile profile of food products were considered, including lipid oxidation, Maillard reactions (Ahn et al., 2025; Chen et al., 2018; Lohinova & Petrusha, 2023), thermal transformations of carbohydrates and amino acids, and the transformation of terpenoid and carotenoid compounds. Comprehensive comparison of the chromatographic characteristics with sensory profiling data was used to determine the most probable volatile compounds that may be associated with the formation of the characteristic organoleptic properties of the mushroom pâté.

Organoleptic evaluation

The organoleptic properties of the sterilized mushroom pâté based on oyster mushroom and beans were evaluated by sensory analysis in terms of appearance, color, consistency, taste, aftertaste, and odor (Kuzmin et al., 2025).

Sensory profile

The sensory profile of the mushroom pâté was determined using descriptive analysis (Dudarev & Kuzmin, 2023). Thirteen descriptors were used to characterize its taste and aroma properties (Kuzmin et al., 2023, 2025): «pleasant», «sweetish», «harmonious», «balanced», «tender», «ingredient-characteristic», «nutty», «umami», «mushroom», «liver-like», «beef-like», «sun-dried tomato», and «fatty». The intensity of each descriptor was evaluated using a 5-point scale: 1 – not perceptible; 2 – barely perceptible; 3 – moderately perceptible; 4 – clearly perceptible; 5 – highly perceptible. The results obtained were used to construct the sensory profile and subsequently compare it with the results of chromatographic analysis of volatile aroma compounds.

Results and discussions

Gas chromatographic analysis of volatile compounds

Gas chromatography enabled the determination of a complex multicomponent profile of the mushroom pâté (Figure 2).

The chromatogram of the sterilized mushroom pâté contained 33 chromatographic peaks, for which the retention time (RT, min), peak height (H, mV), peak width (W, s), peak area (A, mV·min), relative peak area (A, %), and experimental linear retention indices (RI_{exp}) were determined (Table 1). The results indicate a complex multicomponent profile of the volatile compounds in the studied product, formed through the combination of components originating from the raw materials and physicochemical transformations occurring during thermal processing and sterilization.

Peaks No 1, 2, and 4 corresponded to the reference n-alkanes – hexane (RI_{exp} = 600.000), heptane (RI_{exp} = 700.000), and decane (RI_{exp} = 1000.000), respectively, which were used to calibrate the linear retention index scale. These compounds served as reference standards for calculating the experimental retention indices of the other detected components.

As shown in Table 1, the distribution of chromatographic peak areas was highly uneven. The largest relative area was recorded for peak No 3 (RT = 2.04 min; RI_{exp} = 722.954), which accounted for 86.4568% of the total area of the detected peaks. This indicates a pronounced dominance of a single volatile component or compound contributing to the major part of the volatile profile of the sterilized mushroom pâté.

Among the other components, peak No 11 (RI_{exp} = 1357.102) had the largest relative area, accounting for 2.2671%. Peaks No 14 (0.9647%), 13 (0.9623%), 20 (0.9334%), 21 (0.8685%), 17 (0.8253%), 22 (0.7421%), 16 (0.6964%), and 19 (0.6220%) also made notable contributions to the chromatographic profile. Collectively, these components formed the second most prominent group of volatile compounds in the studied sample.

The other detected peaks were characterized by an individual relative area of less than 0.6%; however, their low abundance does not imply an absence of influence on the aroma profile of the product. Individual volatile compounds may have low sensory detection thresholds; therefore, even components represented by small chromatographic peak areas may substantially influence the overall aroma of the mushroom pâté. Thus, the intensity or area of a chromatographic peak does not always directly correlate with the sensory significance of the corresponding compound.

The vast majority of non-reference peaks were located within the RI_{exp} range of 1311.645–1415.980. The highest concentration of peaks was observed in the approximate RI_{exp} range of 1350–1400, indicating the presence of a considerable number of components with similar chromatographic characteristics. This distribution of experimental retention indices confirms the complex multicomponent composition of the volatile profile of the sterilized mushroom pâté.

Thus, chromatographic analysis showed that the volatile profile of the sterilized mushroom pâté was characterized by a pronounced dominance of peak No 3 (RI_{exp} = 722.954), against the background of a considerable number of components with relatively small peak areas. Further identification of the detected volatile compounds should be performed by comparing the obtained RI_{exp} values with literature retention indices for a column of similar polarity, using the criterion of agreement $|RI_{exp} - RI_{lit}| \leq 5$.

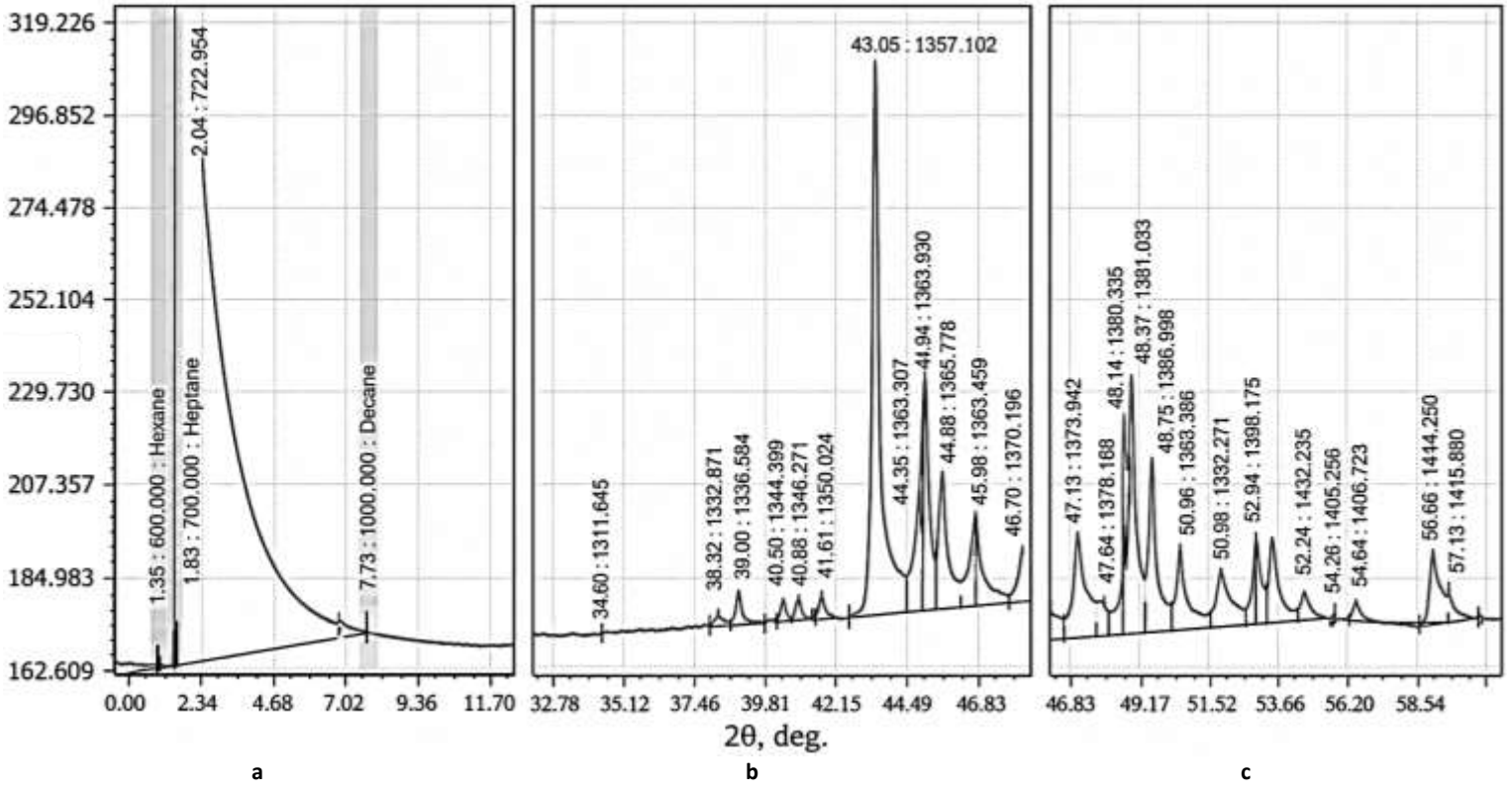

Figure 2. Chromatogram of volatile aroma compounds of the sterilized mushroom pâté:
a – region with low retention time (RT) values (00.00–11.70 min)
b – region with intermediate RT values (32.78–46.83 min)
c – region with high RT values (46.83–58.54 min)

Table 1

Chromatographic characteristics of volatile aroma compounds of the mushroom pâté

Peak No	RT, min	H, mV	H, %	W, s	A, mV·min	A, %	RI_{exp}
1	1.35	0.042	0.0115	0.80	0.0117	0.0008	600.000
2	1.83	46.432	1.7253	3.32	0.3856	0.0252	700.000
3	2.04	1802.416	66.9745	12.76	1324.7727	86.4568	722.954
4	7.73	0.028	0.0011	0.36	0.0079	0.0005	1000.000
5	34.60	1.052	0.0391	11.60	0.2322	0.0152	1311.645
6	38.32	2.629	0.0977	18.28	1.1023	0.0719	1332.871
7	39.01	11.282	0.4192	13.60	2.3886	0.1559	1336.584
8	40.50	5.575	0.2072	12.32	0.8287	0.0541	1344.399
9	40.86	4.808	0.1786	7.40	0.8059	0.0526	1346.271
10	41.61	5.673	0.2108	11.08	1.0340	0.0675	1350.024
11	43.05	136.349	5.0665	33.48	34.7385	2.2671	1357.102
12	44.35	41.850	1.5551	16.96	6.6996	0.4372	1363.307
13	44.49	74.784	2.7788	6.24	14.7459	0.9623	1363.950
14	44.88	53.388	1.9838	7.80	14.7815	0.9647	1365.778
15	45.68	43.031	1.5990	14.92	8.6271	0.5630	1369.459
16	45.85	26.189	0.9731	3.00	10.6716	0.6964	1370.199
17	47.13	40.310	1.4979	22.32	12.6463	0.8253	1375.942
18	47.64	10.620	0.3946	6.96	3.6938	0.2411	1378.189
19	48.14	62.226	2.3122	12.28	9.5316	0.6220	1380.335
20	48.31	69.929	2.5984	4.76	14.3027	0.9334	1381.083
21	48.76	43.878	1.6304	7.24	13.3078	0.8685	1382.998
22	49.56	33.444	1.2427	9.20	11.3716	0.7421	1386.386
23	50.54	5.181	0.1925	8.12	0.9329	0.0609	1390.479
24	50.69	6.833	0.2539	5.44	1.3291	0.0867	1391.085
25	50.98	26.053	0.9681	8.76	8.1265	0.5303	1392.271
26	51.76	36.256	1.3472	12.40	7.4834	0.4884	1395.454
27	52.00	28.447	1.0571	4.92	6.7759	0.4422	1396.409
28	52.45	17.881	0.6644	5.92	5.4373	0.3549	1398.175
29	53.27	10.711	0.3980	8.12	2.7933	0.1823	1401.425
30	54.26	0.829	0.0308	9.92	0.1092	0.0071	1405.256
31	54.65	5.876	0.2183	11.20	1.4337	0.0936	1406.723
32	56.66	29.532	1.0974	11.68	8.7666	0.5721	1414.250
33	57.13	7.664	0.2848	2.76	2.4186	0.1578	1415.980
Σ		**2691.196**	**100.0000**		**1532.2939**	**100.0000**	

Preliminary identification of the volatile aroma compounds of the mushroom pâté was performed by comparing the experimental retention index (RI_{exp}) with the literature retention index (RI_{lit}) for non-polar DB-5-type columns based on data from the FlavorNet database (Acree & Arn, 2026). The agreement between the experimental and literature values was assessed according to the criterion $|RI_{exp} - RI_{lit}| \leq 5$. For each chromatographic peak, its number, RI_{exp}, RI_{lit}, and compliance with the established criterion are presented, along with

the probable chemical group, probable volatile compound, and characteristic odor according to Acree and Arn (2026). The probable source of each component was determined taking into account the formulation raw materials and possible chemical transformations during technological processing of the product. The results of the preliminary identification are presented in Table 2.

Peak No 1 (RI_{exp} = 600.000) corresponded to the reference standard used to determine the linear retention index (RI) – hexane (RI_{lit} = 600). The compound belongs to the alkanes and is characterized by a typical hydrocarbon odor. Hexane was used as a reference standard for calibration of the linear retention index scale.

Peak No 2 (RI_{exp} = 700.000) corresponded to the reference standard used to determine the linear retention index (RI) – heptane (RI_{lit} = 700). The compound belongs to the alkanes and is characterized by a typical hydrocarbon odor. Heptane was used as a reference standard for calibration of the linear retention index scale.

Peak No 3 (RI_{exp} = 722.954). Within the search criterion of ±5 RI units, the most probable compound was acetoin (3-hydroxy-2-butanone) (RIlit = 718). The compound belongs to the ketones and is characterized by a buttery, creamy aroma (Acree & Arn, 2026). Its presence in the studied mushroom pâté may be associated with the use of butter (Demirkol et al., 2016; Roosta et al., 2014), as well as with the presence of acetoin in oyster mushroom (*Pleurotus ostreatus*) (Kim et al., 2026). Additional potential sources of this compound include carrot (*Daucus carota*) (Tian et al., 2024), paprika (*Capsicum annuum*) (Mateo et al., 1997), and beans (*Phaseolus vulgaris*) (Khrisanapant et al., 2022). Thus, acetoin is likely one of the dominant components contributing to the buttery and creamy notes of the aroma profile of the sterilized mushroom pâté.

Peak No 4 (RI_{exp} = 1000.000) corresponded to the reference standard used to determine the linear retention index (RI) – decane (RI_{lit} = 1000). The compound belongs to the alkanes and is characterized by a typical hydrocarbon odor. Decane was used as a reference standard for calibration of the linear retention index scale.

Peak No 5 (RIexp = 1311.645) was most probably assigned to decadienal (RI_{lit} = 1317) within the search criterion of ±5 RI units (1307–1317). The compound belongs to the aldehydes and is characterized by fried, waxy, and fatty odor notes (Acree & Arn, 2026). Its occurrence may be associated with thermal lipid oxidation, particularly the formation of 2,4-decadienal during heating (Sun et al., 2020). However, the presence of 2,4-decadienal was not confirmed in thermally processed oyster mushroom (*Pleurotus ostreatus*) (Tagkouli et al., 2021). Therefore, additional sources may include thermal transformations of the lipid fraction of the formulation components and volatile compounds formed during onion (*Allium cepa*) frying (Wang et al., 2023). This compound may contribute to the fried, fatty, and waxy odor notes of the mushroom pâté.

Peak No 6 (RI_{exp} = 1332.871) was most probably assigned to oxodecanal (RI_{lit} = 1333) within the preliminary identification criterion of ±5 RI units. The difference between the experimental and literature retention indices was only 0.129 RI units. The compound belongs to the aldehydes and is characterized by a fatty odor (Acree & Arn, 2026). Its occurrence in the mushroom pâté may be associated with thermal lipid oxidation, particularly involving sunflower oil, during which the formation of 4-oxodecanal has been reported (Takeoka et al., 1995). Thus, oxodecanal may result from thermal transformations of the lipid fraction of the formulation and contribute to the fatty odor notes of the studied product.

Table 2

Preliminary characterization of volatile components of mushroom pâté based on experimental retention indices for an equivalent DB-5-type column

Peak No	RI_{exp}	RI_{lit}	Chemical group	Volatile compound	Characteristic odor	Source
1	600.000	600	Alkanes	hexane	alkane	reference standard
2	700.000	700	Alkanes	heptane	alkane	reference standard
3	722.954	718	Ketones	acetoin (3-hydroxy-2-butanone)	butter, cream	butter (Demirkol et al., 2016; Roosta et al., 2014), oyster mushroom (Kim et al., 2026), carrot (Tian et al., 2024), paprika (Mateo et al., 1997), beans (Khrisanapant et al., 2022)
4	1000.000	1000	Alkanes	decane	alkane	reference standard
5	1311.645	1317	Aldehydes	decadienal	fried, wax, fat	thermal oxidation of lipids (2,4-decadienal) (Sun et al., 2020); oyster mushroom (2,4-decadienal) (Tagkouli et al., 2021); fried onion (Wang et al., 2023)
6	1332.871	1333	Aldehydes	oxodecanal	fat	products of thermal lipid oxidation (sunflower oil): 4-oxodecanal (Takeoka et al., 1995)
7	1336.584	1336	Terpenes	δ-muurolene	oil	pepper, leaves (*Piper sarmentosum*) (Rameshkumar et al., 2017)
8	1344.399	1345	Terpenes	α-cubebene	herb, wax	carrot (Tian et al., 2024), black pepper (Dosoky et al., 2019; Feitosa et al., 2024; Izcara et al., 2022; Nurjanah et al., 2025)
9	1346.271	1345	Terpenes	α-cubebene (coelution)	herb, wax	
10	1350.024	1350	Aldehydes	2-undecenal	sweet	products of thermal lipid oxidation (sunflower oil) (Huang et al., 2021; Liu et al., 2019), onion (Arena et al., 2024), beans (Khrisanapant et al., 2022)
11	1357.102	1357	Esters	citronellyl acetate	rose, dust	pepper (*Piper sarmentosum*) (Nugroho et al., 2020)
12	1363.307	1364	Phenolic compounds	eugenol	clove, honey	paprika (Izcara et al., 2022; Mateo et al., 1997), carrot (Buttery & Takeoka, 2013; Tian et al., 2024), green pepper (Nurjanah et al., 2025), allspice (Götz et al., 2023), onion (Arena et al., 2024)
13	1363.950	1364	Phenolic compounds	eugenol (coelution)	clove, honey	
14	1365.778	1366	Aldehydes	(E)-2-undecenal	soap, fat, green	products of thermal lipid oxidation (sunflower oil) (Liu et al., 2019)
15	1369.459	1371	Alcohols	undecanol	mandarin	products of thermal lipid oxidation (sunflower oil) (Liu et al., 2019)
16	1370.199	1373	Fatty acids	decanoic acid	rancid, fat	butter (Demirkol et al., 2016), products of fat oxidation

17	1375.942	1377	Terpenes	α-copaene	wood, spice	paprika (Serio et al., 2024), carrot (Tian et al., 2024), black pepper (Feitosa et al., 2024; Nurjanah et al., 2025)
18	1378.189	1379	Esters	hexyl hexanoate	apple peel, peach	legumes (Karolkowski et al., 2021)
19	1380.335	1380	Aldehydes	epoxy-2-decenal	metal, green	products of thermal lipid oxidation (sunflower oil): 4,5-epoxy-2-decenal (Goicoechea et al., 2008; Guillén and Goicoechea, 2008)
20	1381.083	1382	Esters	geranyl acetate	rose	carrot (Alves-Silva et al., 2016; Tian et al., 2024)
21	1382.998	1383	Alcohols	(E,Z)-3,6-nonadien-1-ol	fish	mushrooms (Liu et al., 2024)
22	1386.386	1386	Ketones	β-damascenone	apple, rose, honey	carrot (Buttery & Takeoka, 2013), thermal degradation of carotenoids
23	1390.479	1389	Terpenes	dehydro-ar-ionene	licorice	dried mushrooms (Zhang et al., 2024)
24	1391.085	1393	Terpenes	β-elemene	herb, wax, fresh	paprika (Serio et al., 2024), carrot (Muchlinski et al., 2020; Tian et al., 2024), black pepper (Dosoky et al., 2019; Jirovetz et al., 2002)
25	1392.271	1393	Esters	isobornyl propionate	fruit, turpentine	fungal mycelium (Wang et al., 2020)
26	1395.454	1397	Furans	ethylfuranone	spice	products of thermal lipid oxidation (vegetable oils): 5-ethyl-2(5H)-furanone (Gómez-Cortés et al., 2015)
27	1396.409	1398	Esters	ethyl decanoate	grape	products of thermal lipid oxidation (vegetable oils) (Park et al., 2022)
28	1398.175	1400	Sulfur-containing compounds	methylene bis(methyl sulfide)	garlic, sulfur	mushrooms (Splivallo et al., 2011)
29	1401.425	1400	Alkanes	tetradecane	alkane	butter (ghee) (Lee et al., 1991), oyster mushroom (Sarıyer et al., 2024), onion (Arena et al., 2024; Villière et al., 2015)
30	1405.256	1407	Phenolic compounds	methyleugenol	clove, spice	carrot leaves (Yahyaa et al., 2019), allspice (Götz et al., 2023)
31	1406.723	1408	Alcohols	decyl alcohol (1-decanol)	orange, oil	oyster mushroom (Jung et al., 2019)
32	1414.250	1415	Ketones	(E)-β-damascone	apple	thermal degradation of β-carotene (Zepka et al., 2014)
33	1415.980	1417	Terpenes	β-caryophyllene	spice, clove	paprika (Serio et al., 2024), carrot (Alasalvar et al., 1999; Kjeldsen et al., 2003; Tian et al., 2024), black pepper (Dosoky et al., 2019)

Peak No 7 (RI_{exp} = 1336.584) was most probably assigned to δ-muurolene (RI_{lit} = 1336) within the search criterion of ±5 RI units. The compound belongs to the terpenes, specifically sesquiterpene hydrocarbons, and is characterized by an oily odor (Acree & Arn, 2026). δ-Muurolene has been identified in the leaves of *Piper sarmentosum* (Rameshkumar et al., 2017). However, its occurrence specifically in *Piper nigrum* has not been confirmed in the literature sources considered. Therefore, the identification of δ-muurolene in the studied pâté should be regarded as preliminary. If confirmed, this compound may contribute to oily and spicy odor notes in the aroma profile of the product.

Peak No 8 (RI_{exp} = 1344.399) was most probably assigned to α-cubebene (RI_{lit} = 1345) within the search criterion of ±5 RI units. The compound belongs to the terpenes and is characterized by herbaceous and waxy odor notes (Acree & Arn, 2026). Its occurrence in the mushroom pâté may be associated with plant-derived formulation components. α-Cubebene has been reported in carrot (*Daucus carota*) (Tian et al., 2024) and in black pepper (*Piper nigrum*) (Dosoky et al., 2019; Feitosa et al., 2024; Nurjanah et al., 2025). Thus, α-cubebene may contribute to the herbaceous, waxy, and spicy odor characteristics of the product.

Peak No 9 (RI_{exp} = 1346.271) was also most probably assigned to α-cubebene (RI_{lit} = 1345) within the search criterion of ±5 RI units, with a difference of 1.271 RI units. The compound belongs to the terpenes and is characterized by herbaceous and waxy odor notes (Acree & Arn, 2026). The close experimental retention indices of peaks No 8 and No 9 may indicate possible coelution or incomplete chromatographic separation of components with similar physicochemical properties. Probable sources of α-cubebene include carrot (*Daucus carota*) (Tian et al., 2024) and black pepper (*Piper nigrum*) (Dosoky et al., 2019; Feitosa et al., 2024; Nurjanah et al., 2025).

Peak No 10 (RI_{exp} = 1350.024) was most probably assigned to 2-undecenal (RI_{lit} = 1350) within the search criterion of ±5 RI units, with a difference of only 0.024 RI units. The compound belongs to the aldehydes and is characterized by a sweet odor (Acree & Arn, 2026). Its occurrence in the mushroom pâté may be associated with thermal oxidation of sunflower oil (Huang et al., 2021; Liu et al., 2019), as well as with volatile compounds reported in onion (*Allium cepa*) (Arena et al., 2024) and beans (*Phaseolus vulgaris*) (Khrisanapant et al., 2022). The compound may have formed during frying of the formulation components and subsequent sterilization. Thus, 2-undecenal may contribute to the sweet and fatty odor characteristics of the mushroom pâté.

Peak No 11 (RI_{exp} = 1357.102) was most probably assigned to citronellyl acetate (RI_{lit} = 1357) within the search criterion of ±5 RI units, with a difference of only 0.102 RI units. The compound belongs to the esters and is characterized by a rose-like odor with a slight dusty note (Acree & Arn, 2026). Its occurrence in the studied pâté may be associated with plant-derived ingredients. Although black pepper (*Piper nigrum*) was the main spice in the formulation, the occurrence of citronellyl acetate in this species has not been confirmed in the literature sources considered. The compound has been identified in *Piper sarmentosum* (Nugroho et al., 2020). Therefore, its presence in the mushroom pâté may be associated with other plant-derived ingredients or with thermal transformations during processing. Citronellyl acetate may contribute to subtle floral and sweet odor notes in the overall aroma profile of the pâté.

Peak No 12 (RI_{exp} = 1363.307) was most probably assigned to eugenol (RI_{lit} = 1364) within the search criterion of ±5 RI units, with a difference of 0.693 RI units. The compound belongs to the phenolic compounds and is characterized by a clove-like odor with honey notes (Acree & Arn, 2026). Probable sources among the formulation components include paprika (*Capsicum annuum*) (Izcara et al., 2022; Mateo et al., 1997), carrot (*Daucus carota*) (Buttery & Takeoka, 2013; Tian et al., 2024), black pepper (*Piper nigrum*) (Nurjanah et al., 2025), allspice (Götz et al., 2023), and onion (*Allium cepa*) (Arena et al., 2024). Thus, eugenol may contribute to the clove-like, spicy, and honey-like odor characteristics of the mushroom pâté.

Peak No 13 (RI_{exp} = 1363.950) was also most probably assigned to eugenol (RI_{lit} = 1364)

within the search criterion of ±5 RI units, with a difference of only 0.050 RI units. The compound belongs to the phenolic compounds and is characterized by clove-like and honey-like odor notes (Acree & Arn, 2026). Probable sources among the formulation components include paprika (*Capsicum annuum*) (Izcara et al., 2022; Mateo et al., 1997), carrot (*Daucus carota*) (Buttery & Takeoka, 2013; Tian et al., 2024), black pepper (*Piper nigrum*) (Nurjanah et al., 2025), allspice (Götz et al., 2023), and onion (*Allium cepa*) (Arena et al., 2024). The occurrence of two closely spaced peaks, No 12 and No 13, assigned to the same literature RI may indicate possible coelution of eugenol with other components exhibiting similar chromatographic behavior. Therefore, their identification should be regarded as preliminary and requires confirmation by mass spectrometric analysis or comparison with an authentic standard. Eugenol may contribute to the clove-like, honey-like, and spicy-sweet odor characteristics of the pâté.

Peak No 14 (RI_{exp} = 1365.778) was most probably assigned to (E)-2-undecenal (RI_{lit} = 1366) within the search criterion of ±5 RI units, with a difference of 0.222 RI units. The compound belongs to the aldehydes and is characterized by soapy, fatty, and green odor notes (Acree & Arn, 2026). Its occurrence may be associated with thermal oxidation of lipids, particularly sunflower oil (Liu et al., 2019). In combination with other aldehydes, (E)-2-undecenal may contribute to the fatty and fresh green odor characteristics of the sterilized mushroom pâté.

Peak No 15 (RI_{exp} = 1369.459) was most probably assigned to undecanol (1-undecanol) (RI_{lit} = 1371) within the search criterion of ±5 RI units, with a difference of 1.541 RI units. The compound belongs to the alcohols and is characterized by a mandarin-like odor (Acree & Arn, 2026). Its occurrence in the studied pâté may be associated with thermal transformations of the lipid phase and products of sunflower oil oxidation (Liu et al., 2019). Undecanol may contribute to subtle fresh, fruity, and citrus-like odor notes in the overall aroma profile of the mushroom pâté.

Peak No 16 (RI_{exp} = 1370.199) was most probably assigned to decanoic acid (RI_{lit} = 1373) within the search criterion of ±5 RI units, with a difference of 2.801 RI units. The compound belongs to the fatty acids and is characterized by rancid and fatty odor notes (Acree & Arn, 2026). Its occurrence in the mushroom pâté may be associated with the lipid fraction of the formulation, particularly butter (Demirkol et al., 2016), as well as with lipid oxidation and thermal transformations during processing and sterilization. Decanoic acid may contribute to the fatty background of the aroma profile of the product.

Peak No 17 (RI_{exp} = 1375.942) was most probably assigned to α-copaene (RI_{lit} = 1377) within the search criterion of ±5 RI units, with a difference of 1.058 RI units. The compound belongs to the terpenes and is characterized by woody and spicy odor notes (Acree & Arn, 2026). Probable sources of α-copaene among the formulation components include paprika (*Capsicum annuum*) (Serio et al., 2024) and carrot (*Daucus carota*) (Tian et al., 2024). α-Copaene has also been reported in black pepper (*Piper nigrum*) (Feitosa et al., 2024; Nurjanah et al., 2025). Thus, α-copaene may contribute to the woody and spicy odor characteristics of the mushroom pâté.

Peak No 18 (RI_{exp} = 1378.189) was most probably assigned to hexyl hexanoate (RI_{lit} = 1379) within the search criterion of ±5 RI units, with a difference of 0.811 RI units. The compound belongs to the esters and is characterized by apple peel and peach odor notes (Acree & Arn, 2026). Its occurrence in the studied sample may be associated with plant-derived formulation components. However, the presence of hexyl hexanoate specifically in beans (*Phaseolus vulgaris*) was not directly confirmed in the literature sources considered (Khrisanapant et al., 2022; Mishra et al., 2017, 2019; Oomah et al., 2007; Romero-Castillo et al., 2025). Therefore, the origin of this compound in the mushroom pâté remains uncertain and may reflect a contribution from beans or other plant-based ingredients. Hexyl hexanoate may contribute subtle fruity, apple-like, and peach-like odor notes to the overall aroma profile of the product.

Peak No 19 (RI_{exp} = 1380.335) was most probably assigned to epoxy-2-decenal (RI_{lit} = 1380) within the search criterion of ±5 RI units, with a difference of only 0.335 RI units. The compound

belongs to the aldehydes and is characterized by metallic and green odor notes (Acree & Arn, 2026). The formation of 4,5-epoxy-2-decenal has been associated with thermal oxidation of lipids in sunflower oil (Goicoechea et al., 2008; Guillén & Goicoechea, 2008). Therefore, the occurrence of this compound in the mushroom pâté may be associated with thermal transformations of the lipid fraction during processing and subsequent sterilization. It may contribute to the green and metallic odor characteristics of the volatile profile of the product.

Peak No 20 (RI_{exp} = 1381.083) was most probably assigned to geranyl acetate (RI_{lit} = 1382) within the search criterion of ±5 RI units, with a difference of 0.917 RI units. The compound belongs to the esters and is characterized by rose-like odor notes (Acree & Arn, 2026). Its occurrence in the studied pâté may be associated with plant-derived formulation components, including carrot (*Daucus carota*) (Alves-Silva et al., 2016; Tian et al., 2024). Geranyl acetate may contribute subtle floral odor notes to the overall aroma profile of the sterilized pâté.

Peak No 21 (RI_{exp} = 1382.998) was most probably assigned to (E,Z)-3,6-nonadien-1-ol (RI_{lit} = 1383) within the search criterion of ±5 RI units, with a difference of only 0.002 RI units. The compound belongs to the alcohols and is characterized by a fishy odor (Acree & Arn, 2026). Its possible occurrence in the studied pâté may be associated with mushrooms (Liu et al., 2024). Despite the close agreement between the experimental and literature retention indices, the identification remains preliminary because it is based on retention-index data and requires confirmation by mass spectrometric analysis or comparison with an authentic standard. (E,Z)-3,6-Nonadien-1-ol may contribute specific odor characteristics to the volatile profile of the product.

Peak No 22 (RI_{exp} = 1386.386) was most probably assigned to β-damascenone (RI_{lit} = 1386) within the search criterion of ±5 RI units, with a difference of 0.386 RI units. According to Acree and Arn (2026), the compound belongs to the ketones and is characterized by apple-, rose-, and honey-like odor notes. Its presence in the studied sample may be associated with carrot (*Daucus carota*) (Buttery & Takeoka, 2013) and with the thermal degradation of carotenoids during thermal processing of the formulation components. β-Damascenone may contribute to the formation of subtle floral-fruity and sweet odor notes in the aroma profile of the mushroom pâté.

Peak No 23 (RI_{exp} = 1390.479) was most probably assigned to dehydro-ar-ionene (RI_{lit} = 1389) within the search criterion of ±5 RI units, with a difference of 1.479 RI units. The compound belongs to the terpenes and is characterized by a licorice-like odor (Acree & Arn, 2026). According to literature data, its presence may be associated with mushroom raw materials, as dehydro-ar-ionene has been identified in dried mushrooms (Zhang et al., 2024). As part of the volatile fraction, this compound may potentially contribute to the formation of specific spicy and sweet odor notes in the aroma profile of the mushroom pâté.

Peak No 24 (RI_{exp} = 1391.085) was most probably assigned to β-elemene (RI_{lit} = 1393) within the search criterion of ±5 RI units, with a difference of 1.915 RI units. According to Acree and Arn (2026), β-elemene belongs to the terpenes and is characterized by herbaceous, waxy, and fresh odor notes. Probable sources of this compound among the formulation components include paprika (*Capsicum annuum*) (Serio et al., 2024), carrot (*Daucus carota*) (Muchlinski et al., 2020; Tian et al., 2024), and black pepper (*Piper nigrum*) (Dosoky et al., 2019; Jirovetz et al., 2002). The presence of β-elemene may contribute to the formation of fresh, herbaceous, and spicy odor notes and complement the overall mushroom-spicy aroma profile of the product.

Peak No 25 (RI_{exp} = 1392.271) was most probably assigned to isobornyl propionate (RI_{lit} = 1393) within the search criterion of ±5 RI units, with a difference of 0.729 RI units. The compound belongs to the esters and is characterized by a fruity odor with a turpentine-like note (Acree & Arn, 2026). Its probable origin may be associated with mushroom raw materials, as isobornyl propionate has been detected in fungal mycelium (Wang et al., 2020). As part of the volatile fraction, this compound may potentially contribute subtle fruity and resinous odor notes, increasing the complexity of the aroma profile of the mushroom pâté.

Peak No 26 (RI_{exp} = 1395.454) was most probably assigned to ethylfuranone (RI_{lit} = 1397) within the search criterion of ±5 RI units, with a difference of 1.546 RI units. The compound belongs to the furans and is characterized by a spicy odor (Acree & Arn, 2026). Its formation may be associated with thermal transformation and oxidation processes involving lipid components of vegetable oils, as 5-ethyl-2(5H)-furanone has been reported among the products of thermal oxidation of vegetable oils (Gómez-Cortés et al., 2015). Prolonged thermal processing and sterilization of the mushroom pâté may have promoted the formation of this compound. Ethylfuranone may potentially contribute to spicy and thermally generated odor notes in the aroma profile of the product.

Peak No 27 (RI_{exp} = 1396.409) was most probably assigned to ethyl decanoate (RI_{lit} = 1398) within the search criterion of ±5 RI units, with a difference of 1.591 RI units. The compound belongs to the esters and is characterized by a grape-like odor (Acree & Arn, 2026). Its occurrence in the studied sample may be associated with thermal transformations of the lipid phase of the formulation. Thermal treatment of vegetable oils can result in the formation of various volatile compounds, including esters (Park et al., 2022). As part of the volatile fraction, ethyl decanoate may potentially contribute subtle fruity odor notes that complement the mushroom, fatty, and spicy aroma profile of the pâté.

Peak No 28 (RI_{exp} = 1398.175) was most probably assigned to methylene bis(methyl sulfide), also known as bis(methylthio)methane (RI_{lit} = 1400), within the search criterion of ±5 RI units, with a difference of 1.825 RI units. The compound belongs to sulfur-containing volatile compounds and is characterized by garlic-like and sulfurous odor notes (Acree & Arn, 2026). Its occurrence in the studied pâté may be associated with mushroom raw materials, as sulfur-containing volatile compounds have been identified in mushrooms (Splivallo et al., 2011). Despite their potentially low concentrations, sulfur-containing compounds can substantially influence the aroma profile because of their low odor detection thresholds. Therefore, methylene bis(methyl sulfide) may contribute characteristic sulfurous, garlic-like, and pungent odor notes to the volatile aroma profile of the mushroom pâté.

Peak No 29 (RI_{exp} = 1401.425) was most probably assigned to tetradecane (RI_{lit} = 1400) within the search criterion of ±5 RI units, with a difference of 1.425 RI units. The compound belongs to the alkanes and is characterized by a typical hydrocarbon odor (Acree & Arn, 2026). Probable sources of tetradecane among the formulation components include ghee, particularly its fat fraction (Lee et al., 1991), oyster mushroom (*Pleurotus ostreatus*) (Sarıyer et al., 2024), and onion (*Allium cepa*) (Arena et al., 2024; Kjeldsen et al., 2003). In the aroma profile, alkanes generally have limited sensory significance; however, their presence may reflect the composition of the lipid and wax fractions of the formulation components.

Peak No 30 (RI_{exp} = 1405.256) was most probably assigned to methyleugenol (RI_{lit} = 1407) within the search criterion of ±5 RI units, with a difference of 1.744 RI units. The compound belongs to the phenolic compounds and is characterized by clove-like and spicy odor notes (Acree & Arn, 2026). Its occurrence in the studied sample may be associated with plant-derived formulation components, particularly carrot leaves (*Daucus carota*) (Yahyaa et al., 2019). Methyleugenol has also been reported in allspice (Götz et al., 2023); however, allspice was not included in the formulation of the studied pâté, and this source therefore cannot be directly attributed to the product. The presence of methyleugenol may be associated with other plant-derived components or thermal transformations during processing, but this requires further confirmation. Based on its reported odor characteristics, methyleugenol may contribute spicy and clove-like notes to the overall aroma profile of the product.

Peak No 31 (RI_{exp} = 1406.723) was most probably assigned to decyl alcohol, or 1-decanol (RI_{lit} = 1408), within the search criterion of ±5 RI units, with a difference of 1.277 RI units. The compound belongs to the alcohols and is characterized by orange-like and oily odor notes (Acree

& Arn, 2026). Its occurrence in the studied pâté may be associated with mushroom raw materials, as 1-decanol has been detected in oyster mushroom (*Pleurotus ostreatus*) (Jung et al., 2019). As part of the volatile fraction, this compound may potentially contribute soft oily and subtle citrus-like odor notes to the overall aroma profile of the mushroom pâté.

Peak No 32 (RI_{exp} = 1414.250) was most probably assigned to (E)-β-damascone (RI_{lit} = 1415) within the search criterion of ±5 RI units, with a difference of 0.750 RI units. The compound belongs to the ketones and is characterized by an apple-like odor (Acree & Arn, 2026). Its formation may be associated with the thermal degradation of β-carotene (Zepka et al., 2014), which may occur during intensive thermal processing of plant-based raw materials containing carotenoids, particularly carrot and paprika. (E)-β-Damascone may potentially contribute subtle fruity and sweet odor notes that complement the complex aroma profile of the mushroom pâté.

Peak No 33 (RI_{exp} = 1415.980) was most probably assigned to β-caryophyllene (RI_{lit} = 1417) within the search criterion of ±5 RI units, with a difference of 1.020 RI units. The compound belongs to the terpenes and is characterized by spicy and clove-like odor notes (Acree & Arn, 2026). Probable sources of β-caryophyllene among the formulation components include paprika (*Capsicum annuum*) (Serio et al., 2024), carrot (*Daucus carota*) (Alasalvar et al., 1999; Kjeldsen et al., 2003; Tian et al., 2024), and black pepper (*Piper nigrum*) (Dosoky et al., 2019). The occurrence of this compound is consistent with the presence of spice and plant-derived raw materials in the formulation. β-Caryophyllene may potentially contribute to the formation of characteristic spicy, woody, and clove-like odor notes in the aroma profile of the mushroom pâté.

According to the data presented in Table 2, the volatile profile of the mushroom pâté comprises a complex mixture of compounds of different chemical natures, including ketones, esters, aldehydes, alcohols, phenolic compounds, terpenes, fatty acids, furans, and sulfur-containing compounds, while alkanes were also detected, some of which were used as reference standards. Among the most characteristic components of the aroma profile, acetoin, δ-muurolene, α-cubebene, 2-undecenal, eugenol, (E)-2-undecenal, α-copaene, β-damascenone, β-elemene, methyleugenol, and β-caryophyllene should be highlighted, along with products of thermal transformations of lipid and plant-based raw materials.

Buttery and creamy notes in the aroma profile are likely formed with the involvement of acetoin (3-hydroxy-2-butanone), the origin of which may be associated with the use of butter, oyster mushroom (*Pleurotus ostreatus*), carrot (*Daucus carota*), paprika (*Capsicum annuum*), and beans (*Phaseolus vulgaris*). Fatty, fried, and waxy notes may also be associated with aldehydes and products of lipid oxidation, particularly decadienal, oxodecanal, 2-undecenal, (E)-2-undecenal, and epoxy-2-decenal. Their formation is likely associated with thermal oxidation of the lipid fraction of sunflower oil and other fat components of the formulation during thermal processing.

Terpene compounds may contribute to the formation of spicy-woody, herbaceous, and waxy notes (δ-muurolene, α-cubebene, α-copaene, dehydro-ar-ionene, β-elemene, β-caryophyllene). Their presence may be associated predominantly with plant-based raw materials used in the formulation, particularly carrot (*Daucus carota*), paprika (*Capsicum annuum*), and black pepper (*Piper nigrum*). The phenolic compounds eugenol and methyleugenol complement the aroma profile with clove-like, spicy, and sweetish notes.

A separate group comprises esters (citronellyl acetate, hexyl hexanoate, geranyl acetate, isobornyl propionate, ethyl decanoate), which may contribute floral, fruity, apple, peach, rose-like, and grape-like aroma notes. Their origin is likely associated with plant-based formulation components, mushroom and legume raw materials, as well as products of thermal lipid transformations.

Fruity-floral and sweetish notes may also be formed with the involvement of β-damascenone and (E)-β-damascone, whose formation is associated with the thermal degradation of carotenoids,

particularly β-carotene, which is consistent with the presence of carrot in the formulation. The presence of ethylfuranone may result from thermal transformations of plant oil components and contribute to the formation of spicy notes in the aroma profile.

The mushroom-derived component of the aroma profile is also represented by alcohols and other volatile compounds associated with mushroom raw materials, particularly (E,Z)-3,6-nonadien-1-ol, dehydro-ar-ionene, decyl alcohol, and the sulfur-containing compound bis(methylthio)methane. The latter is characterized by garlic-like and sulfurous notes and may contribute to the specific complex aroma of the mushroom pâté.

Thus, the aroma profile of the studied mushroom pâté is formed not by a single group of compounds or one type of raw material, but by the combined action of volatile components originating from mushrooms, vegetables, spices, legumes, and fat components of the formulation, as well as products of their thermal transformations. The interaction of aldehydes, ketones, terpenes, phenolic compounds, esters, alcohols, and lipid oxidation products contributes to the formation of a complex combination of mushroom, buttery-creamy, fatty, spicy, woody, herbaceous, green, fruity, and floral aroma notes.

To summarize, all compounds were grouped according to their chemical classes, and the distribution of their relative peak areas is presented in Figure 3.

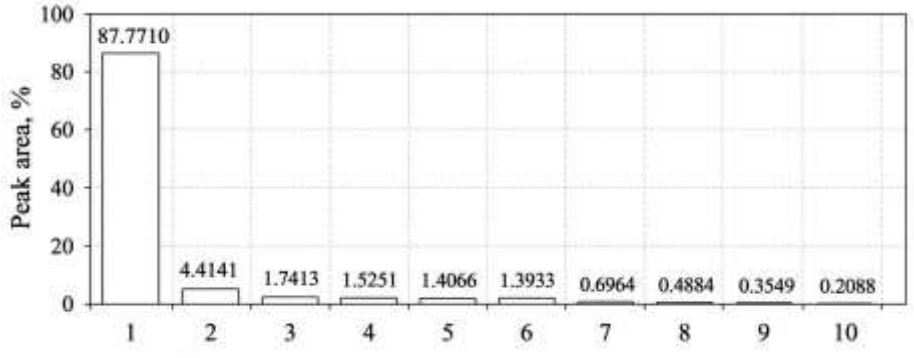

Figure 3. Distribution of the relative peak area of chromatographic peaks of volatile aroma compounds of the mushroom pâté (A, %):
1 – ketones; 2 – esters; 3 – aldehydes; 4 – alcohols; 5 – phenolic compounds; 6 – terpenes; 7 – fatty acids; 8 – furans; 9 – sulfur-containing compounds; 10 – alkanes

Distribution of volatile compounds by chemical groups

According to the results of chromatographic analysis, the ketone group had the largest relative peak area (A, 87.7710%). Based on the identification results, this group included acetoin (3-hydroxy-2-butanone) (Roosta et al., 2014), β-damascenone (Buttery & Takeoka, 2013), and (E)-β-damascone (Zepka et al., 2014). Acetoin is characterized by butter- and cream-like odor notes, whereas β-damascenone has apple-, rose-, and honey-like notes, and (E)-β-damascone is associated with an apple-like odor. The occurrence of these compounds indicates that ketones made the predominant contribution to the volatile fraction of the studied pâté.

The second group comprised esters (A, 4.4141%). It included citronellyl acetate (Nugroho et al., 2020), hexyl hexanoate (Karolkowski et al., 2021), geranyl acetate (Tian et al., 2024), isobornyl propionate (Wang et al., 2020), and ethyl decanoate (Park et al., 2022). These compounds were characterized by rose-, dust-, apple peel-, peach-, fruit-, turpentine-, and grape-like odor notes, respectively. The presence of esters therefore contributed additional fruity, floral, and sweet aromatic nuances to the volatile profile of the pâté.

The third group comprised aldehydes (A, 1.7413%). This group included decadienal (Sun et al., 2020), oxodecanal (Takeoka et al., 1995), 2-undecenal (Khrisanapant et al., 2022), (E)-2-undecenal (Liu et al., 2019), and epoxy-2-decenal (Goicoechea et al., 2008). The identified aldehydes were characterized by fried-, fatty-, sweet-, green-, waxy-, and metallic odor notes. Their occurrence is consistent with the formation of aldehydes during thermal and oxidative transformations of lipids, particularly in the fat-containing components of the formulation.

Alcohols constituted the fourth group in terms of relative peak area (A, 1.5251%). This group included 1-undecanol (Liu et al., 2019), (E,Z)-3,6-nonadien-1-ol (Liu et al., 2024), and 1-decanol (Jung et al., 2019). These compounds were associated with mandarin-, fish-, orange-, and oil-like odor characteristics, respectively. Their occurrence may reflect the volatile composition of mushroom raw materials and transformations of lipid-derived precursors during processing.

Phenolic compounds constituted the fifth group (A, 1.4066%). This group included eugenol (Izcara et al., 2022) and methyleugenol (Yahyaa et al., 2019), with a coelution peak also detected for eugenol. Eugenol is characterized by clove- and honey-like odor notes, whereas methyleugenol is associated with clove- and spice-like characteristics. The presence of these compounds may be related to the spice-containing ingredients used in the pâté formulation, particularly paprika and black pepper.

Terpenes constituted the sixth group (A, 1.3933%). This group included δ-muurolene (Rameshkumar et al., 2017), α-cubebene (Dosoky et al., 2019), α-copaene (Feitosa et al., 2024), dehydro-ar-ionene (Zhang et al., 2024), β-elemene (Muchlinski et al., 2020), and β-caryophyllene (Dosoky et al., 2019). The identified terpenes exhibited woody, spicy, herbaceous, waxy, fresh, and licorice-like odor characteristics. Their presence may be associated primarily with plant-based and spice ingredients incorporated into the formulation.

The seventh group comprised fatty acids, represented by decanoic acid, with a relative area (A) of 0.6964%. Decanoic acid has been reported among volatile compounds of butter and is characterized by rancid and fatty odor notes (Demirkol et al., 2016). Its occurrence in the studied pâté may therefore be associated with the lipid-containing components of the formulation and transformations of fatty constituents during processing. Owing to its relatively small peak area, its contribution to the overall volatile profile was limited.

The eighth group comprised furans (A, 0.4884%). This group included ethylfuranone, which has been reported among products associated with the thermal oxidation of vegetable oils (Gómez-Cortés et al., 2015). This compound was characterized by a spicy odor note and may therefore have contributed to the thermally derived aromatic background of the pâté.

The ninth group comprised sulfur-containing compounds (A, 0.3549%). The detected compound was methylene bis(methyl sulfide), which has been reported among volatile compounds associated with mushrooms (Splivallo et al., 2011). Its garlic- and sulfur-like odor characteristics indicate a possible contribution to the characteristic mushroom and savory nuances of the product despite the relatively small relative peak area of this group.

The tenth group comprised alkanes (A, 0.2088%). This category included hexane (Acree & Arn, 2026), heptane (Acree & Arn, 2026), decane (Acree & Arn, 2026), and tetradecane (Lee et al., 1991). Hexane, heptane, and decane were used as reference n-alkanes for the determination of retention indices and therefore should not be considered full-fledged components of the aroma profile. Tetradecane, in contrast, was detected as a volatile compound and may be associated with lipid- or wax-derived fractions of the raw materials.

Thus, the volatile profile of the studied mushroom pâté was characterized by a pronounced predominance of ketones (87.7710%), which accounted for the major part of the chromatographic profile. Esters (4.4141%), aldehydes (1.7413%), alcohols (1.5251%), phenolic compounds (1.4066%), and terpenes (1.3933%) accounted for substantially smaller proportions. Fatty acids

(0.6964%), furans (0.4884%), sulfur-containing compounds (0.3549%), and alkanes (0.2088%) represented the remaining identified chemical groups.

The identified compounds indicate a multicomponent volatile profile comprising butter- and cream-like notes associated with acetoin (Roosta et al., 2014), fruity and floral nuances associated with β-damascenone (Buttery & Takeoka, 2013) and esters such as geranyl acetate (Tian et al., 2024), spicy and clove-like notes associated with eugenol (Izcara et al., 2022), woody and spicy nuances associated with terpenes such as β-caryophyllene (Dosoky et al., 2019), and fried, fatty, and green notes associated with lipid-derived aldehydes such as decadienal (Sun et al., 2020). The sulfur-containing compound methylene bis(methyl sulfide) may additionally contribute garlic- and sulfur-like nuances characteristic of mushroom volatile profiles (Splivallo et al., 2011).

At the same time, the retention indices determined by GC-FID provide a basis only for the preliminary identification of volatile compounds. Therefore, the relationships established between individual compounds and sensory characteristics should be interpreted as probable, taking into account the literature data on their odor characteristics, chemical nature, and possible origin from the formulation components. The use of retention indices supports tentative identification, but does not provide the same degree of structural confirmation as GC-MS or authentic reference standards.

Thus, the chromatographic analysis makes it possible to associate the characteristic organoleptic properties of the mushroom pâté with a complex of volatile compounds belonging to different chemical groups. Their formation and occurrence may be related both to the properties of the raw materials and to transformations occurring during technological processing.

Organoleptic properties

The organoleptic properties of the sterilized mushroom pâté based on oyster mushroom and beans were evaluated according to six parameters: appearance, color, consistency, taste, aftertaste, and odor. The evaluation results are presented in Table 3.

Table 3

Results of the tasting evaluation of mushroom pâté based on oyster mushroom and beans

Parameter	Characteristic
Appearance	A homogeneous pâté mass with an even distribution of oyster mushroom and beans, a smooth surface, and occasional small inclusions of sautéed carrot and onion; the appearance was characteristic of pâté products
Color	Deep brown, more intense as a result of prolonged high-temperature processing, uniform, and characteristic of mushroom pâté
Consistency	Homogeneous, dense, paste-like, moderately plastic; retained its shape well and spread easily over the surface, without pronounced phase separation
Taste	Rich and balanced, with pronounced umami and meaty notes complemented by liver-like and fatty notes
Aftertaste	Pronounced, long-lasting, and multicomponent, with rich vegetable and thermally generated notes complemented by characteristic meaty nuances
Odor	Pleasant, pronounced, and multicomponent, with mushroom, nutty, and rich vegetable-spicy notes

Appearance. The sterilized mushroom pâté was characterized by a homogeneous pâté mass with an even distribution of oyster mushroom and beans. The surface of the product was smooth, with occasional small inclusions of sautéed carrot and onion. The overall appearance was characteristic of pâté products and indicated adequate comminution and mixing of the formulation components.

Color. The pâté had a deep brown color, uniform throughout the mass and characteristic of mushroom pâté after sterilization. The more intense coloration may have been caused by prolonged high-temperature processing, during which thermal transformations of the formulation components occur.

Consistency. The consistency of the product was homogeneous, dense, and paste-like, with moderate plasticity. The pâté retained its shape well and spread easily over the surface. No pronounced separation of the pâté mass was observed, indicating sufficient structural stability of the finished product.

Taste. The taste of the pâté was rich and balanced. The overall taste profile was characterized by pronounced umami and meaty notes complemented by liver-like and fatty notes. This taste profile contributed to the complex and rich character of the product and resulted from the combination of the formulation components and their transformations during high-temperature processing.

Aftertaste. The aftertaste was characterized as pronounced, long-lasting, and multicomponent. Rich vegetable and thermally generated notes predominated, complemented by characteristic meaty nuances. This combination of characteristics provided a prolonged and rich taste perception of the product.

Odor. The odor of the pâté was pleasant, pronounced, and multicomponent. Its structure combined mushroom and nutty notes with rich vegetable-spicy nuances. The resulting aroma was determined by the combined contribution of oyster mushroom, beans, sautéed vegetables, and spices, as well as aromatic compounds formed or transformed during technological processing.

Thus, according to the results of the organoleptic evaluation, the sterilized mushroom pâté based on oyster mushroom and beans was characterized by a homogeneous appearance, deep brown color, dense paste-like consistency, and a complex multicomponent taste and aroma profile. To provide a more detailed characterization of the intensity of individual sensory properties, the next stage of the study involved descriptive evaluation of the product according to individual taste and aroma characteristics.

Sensory profile

The sensory profile of the sterilized mushroom pâté based on oyster mushroom and beans was determined using 13 descriptors, with intensity evaluated on a 5-point scale (Figure 4).

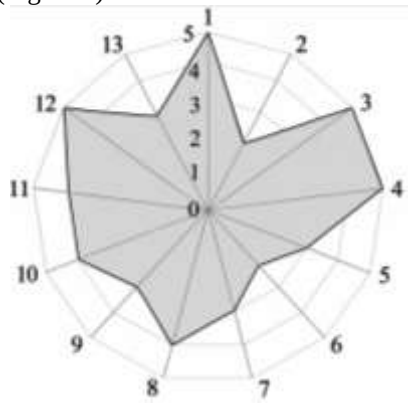

Figure 4. Sensory profile of mushroom pâté based on oyster mushroom and beans:
1 – pleasant; 2 – sweetish; 3 – harmonious; 4 – balanced; 5 – tender; 6 – ingredient-characteristic; 7 – nutty; 8 – umami; 9 – mushroom; 10 – liver-like; 11 – beef-like; 12 – sun-dried tomato; 13 – fatty

The descriptor «pleasant» received the maximum score of 5 points, corresponding to the characteristic «highly perceptible» and indicating a pronounced positive overall perception of the product. The descriptor «sweetish» was rated at 2 points, meaning that it was barely perceptible and was not among the main characteristics of the sensory profile. The descriptor «harmonious» received 5 points and was characterized as highly perceptible. This indicates a consistent combination of individual taste and aroma characteristics of the product. The descriptor «balanced» also received the maximum score of 5 points, corresponding to high intensity and characterizing the overall sensory perception of the pâté. The descriptor «tender» was rated at 3 points, meaning that it was moderately perceptible. This characteristic is consistent with the homogeneous and paste-like consistency of the product. The descriptor «ingredient-characteristic» received 2 points and was barely perceptible. Thus, the direct characteristics of the raw materials used were not dominant in the overall sensory profile of the finished product.

The descriptor «nutty» was characterized by moderate intensity – 3 points. It was present in the sensory profile but was not among its dominant characteristics. The descriptor «umami» received 4 points, corresponding to the characteristic «clearly perceptible». The pronounced nature of this characteristic may be associated with the combined influence of taste-forming components of the mushroom and bean raw materials. The descriptor «mushroom» was rated at 3 points, meaning that it was moderately perceptible. This indicates that the mushroom component was retained in the sensory profile of the finished product, although it was not dominant. The descriptor «liver-like» received 4 points and was clearly perceptible. Its presence indicates a pronounced meaty note in the overall sensory profile of the pâté. The descriptor «beef-like» also received 4 points, corresponding to the characteristic «clearly perceptible». Thus, the meaty character was sufficiently pronounced and complemented the overall taste profile of the product. The descriptor «sun-dried tomato» received the maximum score of 5 points and was highly perceptible. It was among the most pronounced characteristics of the sensory profile and imparted a rich vegetable-thermal note to the product. The descriptor «fatty» was rated at 3 points, corresponding to moderate intensity. Its manifestation is consistent with the presence of a fat phase in the formulation and represents one of the components of the overall sensory perception of the product.

Thus, the most pronounced characteristics of the mushroom pâté were the descriptors «pleasant», «harmonious», «balanced», and «sun-dried tomato», with an intensity of 5 points corresponding to the characteristic «highly perceptible». The descriptors «umami», «liver-like», and «beef-like» received 4 points and were characterized as clearly perceptible. The descriptors «tender», «nutty», «mushroom», and «fatty» were rated at 3 points, corresponding to moderate intensity. The descriptors «sweetish» and «ingredient-characteristic» received 2 points and were characterized as barely perceptible.

Comparison of the volatile composition and sensory profile

At the final stage of the study, the volatile composition preliminarily identified in the mushroom pâté was compared with the sensory profile obtained by descriptive analysis. The comparison considered the chemical groups of volatile compounds, their relative peak areas, characteristic aroma properties, and the sensory descriptors recorded for the pâté. This approach was used to assess whether the identified volatile components could provide a plausible explanation for the sensory characteristics of the product. The results of this comparison are summarized in Table 4.

Table 4

Comparison of sensory descriptors with preliminarily identified volatile components of the mushroom pâté

No	Compound group	A, %	Peak No	Compounds	Aroma	Sensory descriptors
1	Ketones	87.77	3; 22; 32	acetoin (3-hydroxy-2-butanone); β-damascenone; (E)-β-damascone	buttery; apple, rose, honey	pleasant; sweetish; harmonious; balanced; tender; ingredient-characteristic; nutty; umami; liver-like; beef-like; sun-dried tomato
2	Esters	4.41	11; 18; 20; 25; 27	citronellyl acetate; hexyl hexanoate; geranyl acetate; isobornyl propionate; ethyl decanoate	rose-like, dusty; apple peel, peach; rose-like; fruity, turpentine-like; grape-like	pleasant; harmonious; balanced; tender; sun-dried tomato
3	Aldehydes	1.75	5; 6; 10; 14; 19	decadienal; oxodecanal; 2-undecenal; (E)-2-undecenal; epoxy-2-decenal	fried, waxy, fatty; fatty; sweet; soapy, fatty, green; metallic, green	sweetish; fatty
4	Alcohols	1.53	15; 21; 31	undecanol (1-undecanol); (E,Z)-3,6-nonadien-1-ol; decyl alcohol (1-decanol)	mandarin-like; fishy; orange-like, oily	tender; ingredient-characteristic; mushroom; fatty
5	Phenolic compounds	1.41	12; 13; 30	eugenol; eugenol (coelution); methyleugenol	clove-like, honey; clove-like, honey; clove-like, spicy	pleasant; harmonious; balanced; ingredient-characteristic; nutty
6	Terpenes	1.39	7; 8; 9; 17; 23; 24; 33	δ-muurolene; α-cubebene; α-cubebene (coelution); α-copaene; dehydro-ar-ionene; β-elemene; β-caryophyllene	oily; herbaceous, waxy; herbaceous, waxy; woody, spicy; licorice-like; herbaceous, waxy, fresh; spicy, clove-like	pleasant; harmonious; balanced; ingredient-characteristic; nutty; mushroom; sun-dried tomato
7	Fatty acids	0.697	16	decanoic acid	rancid, fatty	fatty
8	Furans	0.48	26	ethylfuranone	spicy	umami; liver-like; beef-like
9	Sulfur-containing compounds	0.35	28	methylene bis(methyl sulfide) (bis(methylthio)methane)	garlic-like, sulfurous	umami; mushroom; liver-like; beef-like
10	Alkanes	0.20	1; 2; 4; 29	hexane; heptane; decane; tetradecane	alkane-like	–
Σ		**100.00**				

Comparison of the sensory descriptors with the characteristic aroma properties of the preliminarily identified volatile components showed overall consistency between sensory perception and the qualitative composition of the volatile fraction of the mushroom pâté. The high scores for the descriptors «pleasant», «harmonious», and «balanced» (5 points each) are consistent with the combination of buttery, fruity-floral, spicy, and woody aroma characteristics represented by ketones, esters, phenolic compounds, and terpenes. The descriptor «sun-dried tomato» had the highest intensity (5 points). Its pronounced character may be associated with the combined action of compounds with sweet, fruity, spicy, and thermally generated aroma nuances, particularly β-damascenone, (E)-β-damascone, geranyl acetate, α-copaene, and β-caryophyllene (Alves-Silva et al., 2016; Buttery & Takeoka, 2013; Serio et al., 2024; Tian et al., 2024; Zepka et al., 2014). This character of the volatile fraction is consistent with the formation of the rich vegetable-thermal note detected during sensory evaluation.

The descriptors «umami», «liver-like», and «beef-like», each rated at 4 points, have a complex character and cannot be unambiguously associated with a single volatile compound. Their manifestation cannot be unambiguously attributed to an individual volatile compound; however, the formation of rich meaty and thermally generated notes may be consistent with the presence of acetoin, sulfur-containing compounds, furan derivatives, and lipid oxidation products identified in the studied volatile fraction (Demirkol et al., 2016; Gómez-Cortés et al., 2015; Splivallo et al., 2011; Sun et al., 2020).

The descriptors «nutty», «mushroom», «tender», and «fatty» were characterized by moderate intensity (3 points). The moderately pronounced «nutty» descriptor may be associated with a combination of spicy-woody and warm aroma notes characteristic of α-cubebene, α-copaene, β-caryophyllene, and eugenol (Dosoky et al., 2019; Feitosa et al., 2024; Izcara et al., 2022; Mateo et al., 1997; Nurjanah et al., 2025; Serio et al., 2024; Tian et al., 2024). This relationship should be regarded as probable, since the nutty note results from complex sensory perception rather than the action of a single volatile compound. The mushroom character may be consistent with the presence of (E,Z)-3,6-nonadien-1-ol, dehydro-ar-ionene, and the sulfur-containing compound methylene bis(methyl sulfide) (Liu et al., 2024; Splivallo et al., 2011; Zhang et al., 2024), whereas nutty notes may be associated with the combined spicy-woody characteristics of terpenes and phenolic compounds. The descriptor «fatty» is consistent with the presence in the volatile fraction of products of thermal lipid oxidation, particularly oxodecanal, (E)-2-undecenal, epoxy-2-decenal, undecanol, and decanoic acid, which are characterized by fatty, waxy, or oily notes (Demirkol et al., 2016; Goicoechea et al., 2008; Guillén and Goicoechea, 2008; Liu et al., 2019; Takeoka et al., 1995). Their presence may complement the direct contribution of the fat phase of the formulation to the taste and aroma properties of the product.

The descriptor «sweetish» had low intensity (2 points), which is consistent with the presence of individual sweet, apple, honey, and rose-like aroma characteristics, particularly β-damascenone, (E)-β-damascone, and 2-undecenal.

Overall, comparison of the two analytical approaches showed that the sensory profile of the sterilized mushroom pâté was compatible with the qualitative characteristics of the preliminarily identified volatile fraction. The predominance of ketones, particularly acetoin, together with the presence of esters, terpenes, phenolic compounds, aldehydes, alcohols, furans, and sulfur-containing compounds provides a chemical background consistent with the simultaneously perceived pleasant, harmonious, balanced, mushroom-like, umami, nutty, fatty, and vegetable-spicy characteristics. However, these associations should be considered interpretative rather than causal because the study did not include statistical correlation analysis between individual volatile compounds and sensory descriptors, and compound identification was based on retention indices without mass-spectrometric confirmation or authentic standards.

Conclusions

Gas chromatographic analysis with preliminary identification based on experimental and literature retention indices revealed a volatile fraction dominated by ketones (87.77%), followed by esters (4.41%), aldehydes (1.74%), alcohols (1.53%), phenolic compounds (1.41%), and terpenes (1.39%), with smaller proportions of other compound classes.

The sterilized mushroom pâté based on oyster mushroom and beans had a homogeneous, paste-like consistency, uniform deep brown color, pleasant, harmonious and balanced taste, and a complex aroma. The most intense sensory descriptors were "pleasant," "harmonious," "balanced," and "sun-dried tomato" (5 points), while umami, liver-like, beef-like, mushroom, nutty, and fatty notes were also detected.

The aroma profile was probably associated with the combined contribution of volatile compounds from different chemical classes and their possible transformations during processing. Mushroom-like, fruity-floral, spicy-woody, and fatty/waxy aroma characteristics were potentially related to specific preliminarily identified compounds, including (E,Z)-3,6-nonadien-1-ol, dehydro-ar-ionene, methylene bis(methyl sulfide), β-damascenone, (E)-β-damascone, α-copaene, β-caryophyllene, eugenol, methyleugenol, aldehydes, alcohols, and decanoic acid. These relationships should be considered probable because compound identities were not confirmed by mass spectrometry or authentic standards.

Overall, the sensory profile was consistent with the qualitative composition of the volatile fraction, indicating that the characteristic aroma of the sterilized mushroom pâté results from the combined contribution of volatile compounds of different chemical natures.

Acknowledgments. The authors gratefully acknowledge ESMASH-3 LLC (Ukraine) for cooperation and support in the production validation of the developed formulation and technology for sterilized mushroom pâté based on oyster mushroom and beans within the framework of the scientific and technical consulting agreement with the National University of Food Technologies (2021–2026). The authors also acknowledge the Institute of Food Resources of the National Academy of Agrarian Sciences of Ukraine and the National University of Food Technologies for their cooperation in the development and approval of TU U 10.3-00419880-194:2025, "Canned foods. Mushroom pâtés. Technical specifications" (Bakhlukova et al., 2025).

References

Acree, T., & Arn, H. (2026). *FlavorNet: An aroma compound database*. Retrieved August 2, 2026, from https://www.flavornet.org/flavornet.html

Ahn, J., Choi, E. & Lee, K. G. (2025). Analysis of volatiles and α-dicarbonyl compounds in Maillard reaction products derived from 2′-fucosyllactose and amino acids. *Food Research International, 205*, 115975. https://doi.org/10.1016/j.foodres.2025.115975

Alasalvar, C., Grigor, J. M. & Quantick, P. C. (1999). Method for the static headspace analysis of carrot volatiles. *Food Chemistry, 65*(3), 391–397. https://doi.org/10.1016/S0308-8146(98)00202-7

Alves-Silva, J. M., Zuzarte, M., Gonçalves, M. J., Cavaleiro, C., Cruz, M. T., Cardoso, S. M. & Salgueiro, L. (2016). New claims for wild carrot (*Daucus carota* subsp. *carota*) essential oil. *Evidence-Based Complementary and Alternative Medicine, 2016*, 9045196. https://doi.org/10.1155/2016/9045196

Arena, D., Ben Ammar, H., Major, N., Kovačević, T. K., Goreta Ban, S., Al Achkar, N., Rizzo, G. F. & Branca, F. (2024). Diversity of the morphometric and biochemical traits of *Allium cepa* L. varieties. *Plants, 13*(13), 1727. https://doi.org/10.3390/plants13131727

Bakhlukova, K. V., Khomichak, L. M., Sheiko, T. V., Bakhlukov, D. O., Arsenieva, L. Iu.,

Kuzmin, O. V. & Velikanov, O. O. (2025). *Canned mushroom pâtés. Technical specifications TU U 10.3-00419880-194:2025*. Registration No 45166702/000427. Kyiv: Institute of Food Resources of the National Academy of Agrarian Sciences of Ukraine; 31 p. (in Ukrainian).

Buttery, R. G. & Takeoka, G. R. (2013). Cooked carrot volatiles. AEDA and odor activity comparisons. Identification of linden ether as an important aroma component. *Journal of Agricultural and Food Chemistry*, *61*(38), 9063–9066. https://doi.org/10.1021/jf402827e

Chen, X., Yu, J., Cui, H., Xia, S., Zhang, X. & Yang, B. (2018). Effect of temperature on flavor compounds and sensory characteristics of Maillard reaction products derived from mushroom hydrolysate. *Molecules*, *23*(2), 247. https://doi.org/10.3390/molecules23020247

Demirkol, A., Guneser, O. & Karagul Yuceer, Y. (2016). Volatile compounds, chemical and sensory properties of butters sold in Çanakkale. *Journal of Agricultural Sciences Journal*, *22*(1), 99–108. https://doi.org/10.1501/Tarimbil_0000001372

Dippong, T., Senila, L. & Muresan, L. E. (2023). Preparation and characterization of the composition of volatile compounds, fatty acids and thermal behavior of paprika. *Foods*, *12*(10), 2041. https://doi.org/10.3390/foods12102041

Dosoky, N. S., Satyal, P., Barata, L. M., da Silva, J. K. R. & Setzer, W. N. (2019). Volatiles of black pepper fruits (*Piper nigrum* L.). *Molecules*, *24*(23), 4244. https://doi.org/10.3390/molecules24234244

Dubova, H., Dotsenko, N., Mykchaylova, O., & Poyedinok, N. (2021). Study of aromatic components in the course of initiating enzymatic reactions in the edible mushroom *Pleurotus ostreatus*. *Food Science and Technology*, *15*(4), 12–21. https://doi.org/10.15673/fst.v15i4.2254

Dudarev, I. & Kuzmin, O. (2023). Influence of plant-based ingredients on the sensory and physicochemical indicators of salad dressings. *Scientific Works of NUFT*, *29*(2), 124–138. https://doi.org/10.24263/2225-2924-2023-29-2-12

Feitosa, B. d. S., Ferreira, O. O., Franco, C. d. J. P., Karakoti, H., Kumar, R., Cascaes, M. M., Jawarkar, R. D., Mali, S. N., Cruz, J. N., de Menezes, I. C., de Oliveira, M. S., & de Aguiar Andrade, E. H. (2024). Chemical composition of *Piper nigrum* L. cultivar guajarina essential oils and their biological activity. *Molecules*, *29*(5), 947. https://doi.org/10.3390/molecules29050947

Goicoechea, E., Van Twillert, K., Duits, M., Brandon, E. D. F. A., Kootstra, P. R., Blokland, M. H. & Guillén, M. D. (2008). Use of an in vitro digestion model to study the bioaccessibility of 4-hydroxy-2-nonenal and related aldehydes present in oxidized oils rich in omega-6 acyl groups. *Journal of Agricultural and Food Chemistry*, *56*(18), 8475–8483. https://doi.org/10.1021/jf801212k

Gómez-Cortés, P., Sacks, G. L. & Brenna, J. T. (2015). Quantitative analysis of volatiles in edible oils following accelerated oxidation using broad spectrum isotope standards. *Food Chemistry*, *174*, 310–318. https://doi.org/10.1016/j.foodchem.2014.11.015

Götz, M. E., Eisenreich, A., Frenzel, J., Sachse, B., & Schäfer, B. (2023). Occurrence of alkenylbenzenes in plants: Flavours and possibly toxic plant metabolites. *Plants*, *12*(11), 2075. https://doi.org/10.3390/plants12112075

Guillén, M. D. & Goicoechea, E. (2008). Formation of oxygenated α,β-unsaturated aldehydes and other toxic compounds in sunflower oil oxidation at room temperature in closed receptacles. *Food Chemistry*, *111*(1), 157–164. https://doi.org/10.1016/j.foodchem.2008.03.052

Huang, S., Liu, Y., Sun, X., & Li, J. (2021). Application of artificial neural network based on traditional detection and GC-MS in prediction of free radicals in thermal oxidation of vegetable oil. *Molecules*, *26*(21), 6717. https://doi.org/10.3390/molecules26216717

Izcara, S., Perestrelo, R., Morante-Zarcero, S., Sierra, I. & Câmara, J.S. (2022). Spices volatilomic fingerprinting – A comprehensive approach to explore its authentication and bioactive properties. *Molecules*, *27*(19), 6403. https://doi.org/10.3390/molecules27196403

Jirovetz, L., Buchbauer, G., Ngassoum, M. B. & Geissler, M. (2002). Aroma compound analysis of *Piper nigrum* and *Piper guineense* essential oils from Cameroon using solid-phase microextraction–gas chromatography, solid-phase microextraction–gas chromatography–mass spectrometry and olfactometry. *Journal of Chromatography A*, *976*(1–2), 265–275. https://doi.org/10.1016/S0021-9673(02)00376-X

Jung, M. Y., Lee, D. E., Cheng, H. Y., Chung, I. M., Kim, S. H., Han, J. G. & Kong, W. S. (2019). Characterization of volatile profiles of six popular edible mushrooms using headspace-solid-phase

microextraction coupled with gas chromatography combined with chemometric analysis. *Journal of Food Science*, *84*(3), 421–429. https://doi.org/10.1111/1750-3841.14481

Karolkowski, A., Guichard, E., Briand, L. & Salles, C. (2021). Volatile compounds in pulses: A review. *Foods*, *10*(12), 3140. https://doi.org/10.3390/foods10123140

Khrisanapant, P., Kebede, B., Leong, S. Y. & Oey, I. (2022). Effects of hydrothermal processing on volatile and fatty acids profile of cowpeas (*Vigna unguiculata*), chickpeas (*Cicer arietinum*) and kidney beans (*Phaseolus vulgaris*). *Molecules*, *27*(23), 8204. https://doi.org/10.3390/molecules27238204

Kim, J. H., Park, Y. J. & Jang, M. J. (2026). Analysis of volatile organic compounds and comparison of heat resistance related gene expression in *Pleurotus ostreatus* under heat stress. *Mycobiology*, *54*(1), 100–111. https://doi.org/10.1080/12298093.2025.2599029

Kjeldsen, F., Christensen, L. P. & Edelenbos, M. (2003). Changes in volatile compounds of carrots (*Daucus carota* L.) during refrigerated and frozen storage. *Journal of Agricultural and Food Chemistry*, *51*(18), 5400–5407. https://doi.org/10.1021/jf030212q

Koretska, I., Kuzmin, O., Polyovyk, V., Deinychenko, L., Berezova, G. & Stukalska, N. (2021). Quality rating of desserts based on fruit and berry raw materials. *Ukrainian Journal of Food Science*, *9*(1), 71–87. https://doi.org/10.24263/2310-1008-2021-9-1-8

Kuzmin, O., Kiiko, V., Khareba, O., Gavrylenko, O., Ianchyk, M. & Melnyk, N. (2023). Ryazhanka with pumpkin puree and flax seeds. *Ukrainian Food Journal*, *12*(1), 65–79. https://doi.org/10.24263/2304-974X-2023-12-1-7

Kuzmin, O., Velikanov, O., Melnyk, O., Kiiko, V., Bakhlukova, K. & Kuzmin, A. (2025). Research on the sensory and antioxidant properties of functional pastes based on shiitake mushrooms. *Food Science and Technology*, *19*(2), 79–89. https://doi.org/10.15673/fst.v19i2.3192

Lee, S.R., Macku, C. & Shibamoto, T. (1991). Isolation and identification of headspace volatiles formed in heated butter. *Journal of Agricultural and Food Chemistry*, *39*(11), 1972–1975. https://doi.org/10.1021/jf00011a017

Liu, Y., Li, J., Cheng, Y. & Liu, Y. (2019). Effect of frying oils' fatty acid profile on quality, free radical and volatiles over deep-frying process: A comparative study using chemometrics. *LWT – Food Science and Technology*, *101*, 331–341. https://doi.org/10.1016/j.lwt.2018.11.033

Liu, H., Cheng, Z. & Xie, J. (2024). Formation of special odors driven by volatile compounds during the growth and maturation in edible fungi (*Phallus impudicus*). *Food Chemistry: X*, *22*, 101288. https://doi.org/10.1016/j.fochx.2024.101288

Lohinova, A., & Petrusha, O. (2023). Maillard reaction in food technologies. *Ukrainian Journal of Food Science*, *11*(2), 81–109. https://doi.org/10.24263/2310-1008-2023-11-2-4

Mateo, J., Aguirrezábal, M., Domínguez, C. & Zumalacárregui, J.M. (1997). Volatile compounds in Spanish paprika. *Journal of Food Composition and Analysis*, *10*(3), 225–232. https://doi.org/10.1006/jfca.1997.0535

Mishra, P. K., Tripathi, J., Gupta, S. & Variyar, P. S. (2017). Effect of cooking on aroma profile of red kidney beans (*Phaseolus vulgaris*) and correlation with sensory quality. *Food Chemistry*, *215*, 401–409. https://doi.org/10.1016/j.foodchem.2016.07.149

Mishra, P. K., Tripathi, J., Gupta, S. & Variyar, P. S. (2019). GC-MS olfactometric characterization of odor active compounds in cooked red kidney beans (*Phaseolus vulgaris*). *Heliyon*, *5*(9), e02459. https://doi.org/10.1016/j.heliyon.2019.e02459

Muchlinski, A., Ibdah, M., Ellison, S., Yahyaa, M., Nawade, B., Laliberte, S., Senalik, D., Simon, P., Whitehead, S. R. & Tholl, D. (2020). Diversity and function of terpene synthases in the production of carrot aroma and flavor compounds. *Scientific Reports*, *10*, 9989. https://doi.org/10.1038/s41598-020-66866-1

Nugroho, L. H., Lexinta, E. C., Priyono, Y. & Susandarini, R. (2020). Short communication: Composition of terpenoid compounds in essential oils extracted from stems of eight *Piper* species and their role in taxonomic relationships. *Biodiversitas Journal of Biological Diversity*, *21*(8), 3438–3443. https://doi.org/10.13057/biodiv/d210804

Nurjanah, S., Suryadi, E., Thoriq, A., Ainina, N., Mardawati, E., Ramadhan, M. G., Rosmiati, R., Akili, A. W. R., Permadi, N. & Julaeha, E. (2025). Essential oils from different parts of *Piper nigrum* L.: Chemical composition, antibacterial, and antioxidant activities. *Food Science & Nutrition*, *13*(11),

e71205. https://doi.org/10.1002/fsn3.71205

Oomah, B. D., Liang, L. S. Y. & Balasubramanian, P. (2007). Volatile compounds of dry beans (*Phaseolus vulgaris* L.). *Plant Foods for Human Nutrition*, *62*(4), 177–183. https://doi.org/10.1007/s11130-007-0059-3

Park, S. Y., Kim, M. J. & Lee, J. H. (2022). Physicochemical properties and volatile formation mechanism of medium-chain triacylglycerols during heating. *Journal of Food Science*, *87*(6), 2616–2625. https://doi.org/10.1111/1750-3841.16162

Peterson, D. G. & Reineccius, G. A. (2003). Determination of the aroma impact compounds in heated sweet cream butter. *Flavour and Fragrance Journal*, *18*(4), 320–324. https://doi.org/10.1002/ffj.1228

Politowicz, J., Lech, K., Sánchez-Rodríguez, L., Figiel, A., Szumny, A., Grubor, M. & Carbonell-Barrachina, A. A. (2018). Volatile composition and sensory profile of oyster mushroom as affected by drying method. *Drying Technology*, *36*(6), 685–696. https://doi.org/10.1080/07373937.2016.1274903

Rameshkumar, K. B., Nandu, T. G., Anu Aravind, A. P., Mathew, S. P. & Shiburaj, S. (2017). Chemical composition and FtsZ GTPase inhibiting activity of the essential oil of *Piper sarmentosum* from Andaman Islands, India. *Journal of Essential Oil Research*, *29*(5), 430–435. https://doi.org/10.1080/10412905.2017.1303405

Romero-Castillo, R., Rivera, A., Roselló, S., Beltran, J., Campo, S., Casañas, F. & Casals, J. (2025). The odor and flavor of cooked common beans (*Phaseolus vulgaris* L.): Sensory lexicon, chemical background and diversity in the Spanish Core collection. *LWT*, *232*, 118453. https://doi.org/10.1016/j.lwt.2025.118453

Roosta, M., Ghaedi, M. & Daneshfar, A. (2014). Optimisation of ultrasound-assisted reverse micelles dispersive liquid–liquid micro-extraction by Box–Behnken design for determination of acetoin in butter followed by high performance liquid chromatography. *Food Chemistry*, *161*, 120–126. https://doi.org/10.1016/j.foodchem.2014.03.043

Sarıyer, T., Gündoğdu, M.A., Kaya, Ç., Çiftci, H.N., ªahin, E., Kuzucu, F.C. & Alkan, Y. (2024). Determination of the effects of different tree logs on some important volatile aroma components in the oyster mushroom (*Pleurotus ostreatus* Jacq Kumm). *International Journal of Innovative Approaches in Science Research*, *8*(3), 113–122. https://doi.org/10.1080/10.29329/ijiasr.2024.1087.1

Selli, S., Guclu, G., Sevindik, O. & Kelebek, H. (2021). Variations in the key aroma and phenolic compounds of champignon (*Agaricus bisporus*) and oyster (*Pleurotus ostreatus*) mushrooms after two cooking treatments as elucidated by GC-MS-O and LC-DAD-ESI-MS/MS. *Food Chemistry*, *354*, 129576. https://doi.org/10.1016/j.foodchem.2021.129576

Serio, A., Maggio, F., Ben Hsouna, A., Ben Saad, R., Taiti, C. & Garzoli, S. (2024). Exploring the metabolome and antimicrobial properties of *Capsicum annuum* L. (baklouti and paprika) dried powders from Tunisia. *Molecules*, *29*(22), 5236. https://doi.org/10.3390/molecules29225236

Splivallo, R., Ottonello, S., Mello, A. & Karlovsky, P. (2011). Truffle volatiles: from chemical ecology to aroma biosynthesis. *New Phytologist*, *189*(3), 688–699. https://doi.org/10.1111/j.1469-8137.2010.03523.x

Stabnikova, O., Stabnikov, V. & Paredes-López, O. (2024). Wild and cultivated mushrooms as food, pharmaceutical and industrial products. *Ukrainian Food Journal*, *13*(1), 20–59. https://doi.org/10.24263/2304-974X-2024-13-1-4

Stabnikova, O., Stabnikov, V., & Paredes-López, O. (2025). Wild edible plants, berries, mushrooms and seaweeds in food production. In S. Gubsky, O. Stabnikova, V. Stabnikov, & O. Paredes-López (Eds.), *Wild edible plants: Improving foods nutritional value and human health through biotechnology* (pp. 1–47). Boca Raton, FL: CRC Press. https://doi.org/10.1201/9781003486794-1

Sun, H., Peng, X., Li, C., Zhang, W. M. & Cao, J. (2020). Determination of 2,4-decadienal in edible oils using reversed-phase liquid chromatography and its application as an alternative indicator of lipid oxidation. *Journal of Food Science*, *85*(5), 1418–1426. https://doi.org/10.1111/1750-3841.15132

Tagkouli, D., Bekiaris, G., Pantazi, S., Anastasopoulou, M.E., Koutrotsios, G., Mallouchos, A., Zervakis, G.I. & Kalogeropoulos, N. (2021). Volatile profiling of *Pleurotus eryngii* and *Pleurotus ostreatus* mushrooms cultivated on agricultural and agro-industrial by-products. *Foods*, *10*(6), 1287. https://doi.org/10.3390/foods10061287

Takeoka, G.R., Buttery, R.G. & Perrino, C.T. (1995). Synthesis and occurrence of oxoaldehydes in used frying oils. *Journal of Agricultural and Food Chemistry*, *43*(1), 22–26. https://doi.org/10.1021/jf00049a006

Tian, Z., Dong, T., Wang, S., Sun, J., Chen, H., Zhang, N. & Wang, S. (2024). A comprehensive review on botany, chemical composition and the impacts of heat processing and dehydration on the aroma formation of fresh carrot. *Food Chemistry: X*, *22*, 101201. https://doi.org/10.1016/j.fochx.2024.101201

Timaná, R., Arango, O., Osorio, O. & Benavides, O. (2024). Effect of different drying methods on the physicochemical characteristics and volatile compound profile of *Pleurotus ostreatus*. *Engenharia Agrícola*, *44*, e20240026. https://doi.org/10.1590/1809-4430-eng.agric.v44e20240026/2024

Tokitomo, Y. (1995). Volatile components of cooked onions. *Nippon Shokuhin Kagaku Kogaku Kaishi*, *42*(4), 279–287. https://doi.org/10.3136/nskkk.42.279

Tovstonoh, D., Niemirich, O., Kuzmin, O., Ushchapovskyi, A., Nakonechna, A., Roiko, O., Bakhlukova, K., Zaslavskyi, O., Kuzmin, A. & Yastreba, S. (2026). Development of a vegetable oil blend with improved oxidative stability for emulsion semi-finished products. *Technology Audit and Production Reserves*, *3/3*(89), 69–76. https://doi.org/10.15587/2706-5448.2026.364684

Villière, A., Le Roy, S., Fillonneau, C., Guillet, F., Falquerho, H., Boussely, S. & Prost, C. (2015). Evaluation of aroma profile differences between sué, sautéed, and pan-fried onions using an innovative olfactometric approach. *Flavour*, *4*, 24. https://doi.org/10.1186/s13411-015-0034-0

Wang, D., Huang, C., Zhao, Y., Wang, L., Yang, Y., Wang, A., Zhang, Y., Hu, G. & Jia, J. (2020). Comparative studies on polysaccharides, triterpenoids, and essential oil from fermented mycelia and cultivated sclerotium of a medicinal and edible mushroom. *Poria Cocos*. *Molecules*, *25*(6), 1269. https://doi.org/10.3390/molecules25061269

Wang, J., Qiao, L., Wang, R., Zhang, N., Liu, Y., Chen, H., Sun, J., Wang, S. & Zhang, Y. (2023). Effect of frying process on the flavor variations of *Allium* plants. *Foods*, *12*(7), 1371. https://doi.org/10.3390/foods12071371

Yahyaa, M., Berim, A., Nawade, B., Ibdah, M., Dudareva, N. & Ibdah, M. (2019). Biosynthesis of methyleugenol and methylisoeugenol in *Daucus carota* leaves: Characterization of eugenol/isoeugenol synthase and O-Methyltransferase. *Phytochemistry*, *159*, 179–189. https://doi.org/10.1016/j.phytochem.2018.12.020

Yin, C., Fan, X., Fan, Z., Shi, D., Yao, F. & Gao, H. (2019). Comparison of non-volatile and volatile flavor compounds in six *Pleurotus* mushrooms. *Journal of the Science of Food and Agriculture*, *99*(4), 1691–1699. https://doi.org/10.1002/jsfa.9358

Zepka, L. Q., Garruti, D. S., Sampaio, K. L., Mercadante, A. Z. & Da Silva, M. A. A. P. (2014). Aroma compounds derived from the thermal degradation of carotenoids in a cashew apple juice model. *Food Research International*, *56*, 108–114. https://doi.org/10.1016/j.foodres.2013.12.015

Zhang, F., Lu, B., He, X. & Yu, F. (2024). Flavor variations in precious *Tricholoma matsutake* under different drying processes as detected with HS-SPME-GC-MS. *Foods*, *13*(13), 2123. https://doi.org/10.3390/foods13132123

Zhao, Q., Liu, X., Cui, L. & Ma, C. (2024). Extraction and bioactivities of the chemical composition from *Pleurotus ostreatus*: A review. *Journal of Future Foods*, *4*(2), 111–118. https://doi.org/10.1016/j.jfutfo.2023.06.001

Cite:

Kuzmin, O., Niemirich, O., Podobii, O., Zaporozhets, Y., & Velikanov, O. (2026). Aroma characteristics and volatile composition of sterilized mushroom pâté. *Ukrainian Food Journal*, *15*(3), 802–830. https://doi.org/10.24263/2304-974X-2026-15-3-13

Physicochemical stability of cooked sausages during frozen storage under different cryostabilisation conditions

Olena Tunik, Iryna Shevchenko

National University of Food Technologies, Kyiv, Ukraine

Keywords:

Cooked sausages
Frozen
Storage
Cryostabilising
Mixture
Microstructure
Water activity
Lipid oxidation

Article history:

Received 30.11.2025
Received in revised form 15.03.2026
Accepted 30.09.2026

Corresponding author:

Olena Tunik
E-mail:
tunikov@nuft.edu.ua

DOI:
10.24263/2304-974X-2026-15-3-14

Abstract

Introduction. The aim of the study was to evaluate the effect of frozen storage on the physicochemical properties and microstructure of cooked sausages, with particular focus on the stability of the lipid phase, the water-binding system, and the progression of hydrolytic and oxidative processes.

Materials and methods. Cooked sausages were studied, including control samples and samples with a cryostabilising mixture (2%). Water activity, acid value, peroxide value, pH, and organoleptic properties were determined. The samples were frozen at –30 °C and stored at –18 °C for 90 days. Microstructure was analyzed using light microscopy (×600) with semi-quantitative porosity assessment and morphometric analysis based on image analysis.

Results and discussion. During 90 days of frozen storage at −18 °C, the physicochemical parameters of cooked sausages showed no pronounced deterioration. Water activity decreased from 0.982 to 0.958 in the beef control and from 0.972 to 0.952 in the pork control, while samples containing the cryostabilis ing mixture showed lower values, decreasing from 0.881 to 0.852 and from 0.894 to 0.860, respectively. The pH decreased from 6.45 to 5.65 in the beef control and from 6.35 to 5.40 in the pork control, while samples with the cryostabilis ing mixture retained higher values (6.00–6.10 after 90 days), indicating greater pH stability. The acid value remained within 4.14–4.61 mg KOH/g. The peroxide value remained unchanged throughout storage, indicating no detectable accumulation of primary lipid oxidation products under the studied conditions.

Microstructural analysis revealed pronounced cryodestruction in control samples, including the formation of large pores and disruption of the protein–fat matrix, whereas cryostabilis ed samples had a more uniform and dense structure, with lower porosity and significantly smaller pore size. Sensory evaluation confirmed the improved consumer properties of cryostabilis ed samples, particularly in terms of texture, appearance, and overall acceptability after thawing.

Overall, cryostabilis ation enhanced the structural integrity and quality of cooked sausages during frozen storage. The reduction in water activity contributed to microbiological stability and shelf-life extension, while freezing suppressed autooxidation processes and thus maintained high oxidative stability.

Conclusions. Cryostabilising mixtures improve the structural stability and quality of cooked sausages during frozen storage by enhancing water binding and reducing cryodestruction. Freezing suppresses oxidative processes, while reduced water activity contributes to extended shelf life. The combined effects of freezing and cryostabilisation help maintain product quality after thawing.

Introduction

Contemporary technological development in the meat processing industry is accompanied by a growing interest in stabilising the quality of cooked sausage products under low-temperature storage conditions (Rybachuk & Shevchenko, 2025). Freezing and subsequent thawing of finished products cause significant changes in their structural, mechanical, and rheological properties (Sher et al., 2015), which negatively affect the texture, juiciness, and overall consumer characteristics of the products (Jeong et al., 2025; Ladikos & Lougovois, 1990; Zhang et al., 2023).

A promising approach to preserving the quality of such products is the use of cryostabilising mixtures, whose effectiveness is largely determined by their ability to maintain the structural integrity of multicomponent minced meat systems and preserve their structural and mechanical properties during freezing and subsequent storage.

The properties of minced meat used in cooked sausages are largely determined by the nature and organisation of its protein-fat-water matrix. Myofibrillar proteins, which are capable of hydration, gel formation, and the formation of a three-dimensional protein network, play a key role in determining structural and mechanical characteristics (Tornberg, 2005; Vorontsov et al., 2025). Freezing and subsequent storage at low temperatures can disrupt intermolecular interactions and the structural organisation of the protein matrix, resulting in reduced minced meat viscosity, impaired water- and fat-holding capacity, and increased weight loss during subsequent heat treatment (Martino & Zaritzky, 1988).

Cryostabilising mixtures containing hydrocolloids, phosphates, protein ingredients, and low-molecular-weight cryoprotectants have a significant effect on the rheological properties of minced meat. Their use contributes to an increase in effective viscosity, elastic modulus, and the stability of the system's structural characteristics both before and after freeze–thaw cycles. Chou and Lin (2010) found that the addition of xylo-oligosaccharides to model systems of pork myofibrillar proteins increased their stability during freeze–thaw cycles; at a protein concentration of 60 mg/mL, gel strength increased with increasing XOS concentration up to 6%, whereas concentrations above 8% resulted in a decrease in gel strength. A similar protective effect was demonstrated by Walayat et al. (2020) for a mixture of egg white protein and β-cyclodextrin (EWP/βCD) in a model system of *Culter alburnus* myofibrillar proteins. The study was conducted for 60 days at −18 °C using EWP/βCD concentrations of 0%, 2%, 4%, and 6%. The highest concentration, 6%, promoted the formation of a denser and more interconnected protein network, increased the water-holding capacity, hardness, springiness, cohesiveness, and gumminess of the gel, and also increased the storage (G′) and loss (G″) moduli compared with the control (Walayat et al., 2020).

This effect is associated with enhanced protein hydration, the formation of additional hydrogen and ionic bonds, and reduced mobility of free water. The formation of large ice crystals can cause significant damage to structural elements of the product, whereas the formation of small and uniformly distributed crystals promotes better structural preservation during freezing (Kiani & Sun, 2011). At the same time, the formation of a stable protein network is determined by environmental conditions. According to Sun and Holley (2011), optimal gel-forming characteristics of myofibrillar proteins are observed at approximately pH 6.0 and an ionic strength of 0.6 M, highlighting the importance of controlling acidity and ionic composition in the meat system (Sun et al., 2011).

Plant fibre and hydrocolloids (guar gum, xanthan gum, and carrageenans), which exhibit pronounced rheological properties (Sun et al., 2022), contribute to the formation of pseudoplastic systems with increased structural viscosity. This increased structural viscosity reduces mechanical damage to the protein matrix during ice crystallisation and ensures a

more uniform distribution of moisture in minced meat (Verbeken et al., 2005). Phosphates, as components of cryostabilising systems, increase the ionic strength of the medium, promote the extraction of myofibrillar proteins, and enhance their gel-forming ability, thereby contributing to the formation of a more stable protein structure (Stabnikova et al., 2022).

Despite the numerous studies devoted to the use of cryoprotectants and functional ingredients in meat systems, the mechanisms of cryostabilisation of minced meat in cooked sausages under freeze–thaw cycles remain insufficiently understood. In particular, data on the relationship between the structural behaviour of minced meat, the stability of the protein matrix, and the quality parameters of finished products after low-temperature storage remain limited.

The aim of this study is to comprehensively evaluate the effect of frozen storage on the physicochemical parameters (water activity, acid value, and peroxide value) and microstructure of cooked sausages in order to determine the stability of the lipid phase and water-binding system, as well as the patterns of hydrolytic and oxidative processes.

Materials and methods

Materials and formulations

The objects of the study were cooked sausage products manufactured using standard technology. Four recipe variants were compared: Beef Control, Pork Control, Beef CS, and Pork CS. The Beef Control and Pork Control samples did not contain a cryostabilising mixture, whereas the Beef CS and Pork CS samples contained the cryostabilising mixture.

The Beef Control sample contained prime beef (35%), chicken fillet (10%), ground chicken (25%), and side fat (30%). The Pork Control sample was composed of semi-fat pork (35%), chicken fillet (15%), ground chicken (25%), and side fat (25%). The Beef CS sample formulation included prime beef (35%), chicken fillet (8%), ground chicken (25%), side fat (30%), and a cryostabilising mixture (2%). The Pork CS sample contained semi-fat pork (35%), chicken fillet (13%), ground chicken (25%), side fat (25%), and a cryostabilising mixture (2%). The cryostabilising mixture was incorporated during ground meat preparation, replacing 2% of the chicken fillet.

Cryostabilising mixture

The 2% dosage was selected based on previous studies that evaluated the technological effectiveness of the mixture and its ability to stabilize the properties of the meat system during freezing and subsequent storage. The use of the mixture at this concentration was reported to provide an optimal balance between its cryostabilising effect and the technological properties of the ground meat (Shevchenko & Tunik, 2024). The rationale for the composition of the cryostabilising mixture is described in a previous study (Tunik & Shevchenko, 2025).

Frozen storage conditions

The samples were rapidly cooled to −30 °C using a shock-freezing method in a rapid-cooling chamber equipped with a forced-air circulation system. This mode ensured a high rate of heat removal and reduced the duration of exposure of the product to the critical temperature range of maximum ice crystallization (−1 to −5 °C). Freezing was continued

until the temperature at the geometric center of the sample reached a value below the cryoscopic point of ground meat (−18 °C).

After freezing, the samples were stored at −18 °C until the scheduled time of analysis. The physicochemical parameters were evaluated in freshly prepared products (day 0) and after 30, 60, and 90 days of frozen storage at −18 °C.

Methods

Given the high content of fatty raw materials (approximately 30%) and moisture (62%) in the sausage formulations, the following physicochemical parameters were determined to assess the effect of the cryostabilising mixtures: water activity (a_w), pH, acid value, and peroxide value. Water activity characterized moisture availability and the stability of the aqueous phase; pH reflected changes in the acid–base state of the meat system; acid value characterized the degree of hydrolytic changes in lipids; and peroxide value characterized the intensity of primary oxidative processes in the fat phase. The comprehensive determination of these parameters allowed the assessment of the physicochemical and lipid stability of cooked sausages during prolonged frozen storage and the effectiveness of the cryostabilising mixtures.

Water activity (a_w) was determined in accordance with ISO 18787:2017 using a water activity analyzer (AquaLab 4TE/4TEV, Meter Group, USA).

To facilitate analysis, the samples were meticulously ground to ensure a homogeneous consistency, with particular attention paid to avoid heating and moisture loss during the process. The prepared sample was meticulously transferred into a pristine, dry measuring cup of the a_w analyzer, ensuring that the material was distributed uniformly across the bottom of the cup. The sample quantity should provide a sufficient evaporation area while maintaining a distance from the instrument's sensor. The cup containing the sample was subsequently placed within the analyzer's measuring chamber and securely sealed. Subsequent to the attainment of equilibrium, the instrument measured the relative humidity and temperature above the sample surface and automatically calculated the water activity value.

Water activity was defined as the ratio of the partial pressure of water vapor above the sample to the saturated vapor pressure of water above pure water at the same temperature. The results were expressed in dimensionless units of a_w.

The uncertainty of the measurement results is given in accordance with the data from the laboratory's test reports and is presented as the expanded uncertainty U for a coverage factor k = 2, corresponding to a confidence level P = 0.95.

Acid value of the fat extracted from sausage products was determined by titrimetric analysis in accordance with DSTU EN ISO 660:2019 (EN ISO 660:2009, IDT). The method is predicated on the neutralization of free fatty acids with a standard potassium hydroxide solution.

The analysis was initiated by extracting fat from the sausage products through melting. Subsequently, the resultant fat underwent filtration to eliminate mechanical impurities. A 5.0 g sample of fat was meticulously placed in a conical flask, where it was thoroughly dissolved in a pre-neutralized mixture of ethanol and diethyl ether. Subsequently, a few drops of phenolphthalein were added to the resulting solution to serve as an indicator. The mixture was then titrated with a standard alcoholic KOH solution at a concentration of 0.1 mol/dm³ until a faint pink color appeared that did not fade within 30 seconds. During the titration process, potassium hydroxide was utilized to neutralize the free fatty acids present in the fat phase.

The acid value was determined by the amount of KOH solution consumed to neutralize the free fatty acids and was expressed in milligrams of KOH required to neutralize the free fatty acids contained in 1 g of fat.

The values of the parameters are based on the results of laboratory tests. The error bars correspond to the expanded measurement uncertainty (U) specified in the test reports; the coverage factor and confidence level are provided by the laboratory in accordance with its uncertainty assessment procedures.

Peroxide value of fat extracted from sausage products was determined using the iodometric titration method in accordance with ISO 3960:2017. The method is predicated on the oxidation of iodide ions by peroxide compounds in the fat, followed by titration of the released iodine with a sodium thiosulfate solution.

The initial extraction of fat from the samples was conducted through a process of melting, followed by a purification step that involved the filtration of mechanical impurities. A precise mass of fat was meticulously placed in a conical flask and thoroughly dissolved in a mixture of acetic acid and isooctane. Following complete dissolution, a potassium iodide solution was introduced. The peroxides present in the fat oxidize the iodide ions, resulting in the release of iodine.

The released iodine was then titrated with a standard sodium thiosulfate solution. During the titration process, iodine is reduced to iodide ions, and the amount of thiosulfate consumed is directly proportional to the content of peroxide compounds present in the fat. At the conclusion of the titration process, a starch indicator was incorporated, which undergoes a color change to blue when reacting with iodine. The titration process is considered complete when the blue color is no longer visible. According to ISO 3960:2017, the value expressed in mmol of active oxygen per 1 kg is equivalent to half the value expressed in meq of active oxygen per 1 kg. The peroxide value was expressed in mmol of active oxygen per 1 kilogram of fat (mmol ½O/kg).

The pH value of sausages was determined by the potentiometric method in accordance with DSTU ISO 2917:2001 using a laboratory pH meter. Prior to measurement, the pH meter was calibrated using standard buffer solutions. The electrode was immersed in the prepared samples, and the pH value was recorded after the instrument readings stabilized**.**

The microstructure of the frozen samples was examined using a MICROmed Fusion FS-7630 light microscope at a magnification of ×600. The size and distribution of voids, the degree of homogeneity of the protein-fat matrix, the presence of zones of destruction, and signs of fat phase coalescence were assessed**.**

Cooked sausage samples were prepared according to the experimental protocol, which included a control formulation and a formulation with the addition of a cryostabilising mixture at a concentration of 2%. After heat treatment and cooling to 12°C, the samples were frozen at −30°C and stored at −18°C for 90 days, after which they were thawed at 4°C.

Representative samples were taken from the central part of the sausage links for microscopic analysis. The samples were cut into thin sections 1–2 mm thick with minimal mechanical disturbance to preserve their natural structure. The examination was conducted using optical light microscopy at a magnification of ×600.

During the microstructural analysis, the integrity of the protein matrix, the distribution pattern of fat inclusions, the presence and size of pores formed as a result of ice crystallization, and the degree of structural damage following freezing and thawing were

evaluated. The resulting microphotographs were then utilized for a comparative qualitative assessment of the microstructure of the control and experimental samples.

Microphotographs were captured under identical lighting conditions and magnification using a digital camera. The results were then subjected to a comprehensive analysis, with particular attention devoted to the functional, technological, and quality characteristics of the sausage systems.

A semi-quantitative analysis of porosity was conducted to assess the extent of microstructural damage in cooked sausage products after freeze-thaw cycles and to determine the effectiveness of cryostabilising compositions. The study was conducted using microphotographs obtained by light microscopy at a magnification of ×600 (Pearson & Dutson, 1994). For each variant, at least seven images from different areas of the sample were analyzed.

Porosity was assessed based on the number, size, and distribution of pores in the protein-fat matrix, which were identified as irregular cavities formed as a result of ice crystallization. A three-point scale was used: 1 point–low porosity (dense structure with isolated small pores); 2 points–moderate porosity (medium-sized pores, partial disruption of the matrix); 3 points–high porosity (numerous large pores, pronounced destruction). The final value was determined as the arithmetic mean of the scores obtained. In addition, a morphometric analysis was performed to quantitatively assess structural changes. Pore diameters were measured on micrographs using image analysis tools (Adobe Photoshop, Adobe Inc., USA) by manually determining the linear dimensions of the pores. For each sample, at least 20 pores were measured, and the average pore diameter was calculated and expressed as the mean±standard deviation. This approach allows for both qualitative and quantitative assessment of structural damage in protein-fat matrices caused by freezing processes.

Determination of the organoleptic characteristics of sausages involves evaluating the quality of sausage products based on six criteria: appearance, cross-section, texture, taste, smell, and color. Each of these indicators is rated on a five-point scale, where 5 is excellent and 1 is unsatisfactory. The evaluation is conducted by a group of experts who analyze the product according to established parameters to determine its compliance with quality standards (Fudali et al., 2021; Savinok et al., 2017).

Results and discussion

Effect of cryostabilisation on the physicochemical parameters of cooked sausages

The results of the water activity measurements indicate a gradual decrease in a_w values in all studied samples during 90 days of frozen storage (Figure 1). In the beef control sample, a_w decreased from 0.982 to 0.958, while in the pork control sample it decreased from 0.972 to 0.952. In the beef and pork samples containing cryostabilising mixtures, water activity was already lower at the beginning of storage and decreased from 0.881 to 0.852 and from 0.894 to 0.860, respectively. Thus, all studied samples showed a tendency toward decreasing water activity during storage, while samples containing cryostabilising mixtures were characterized by lower a_w values compared with the corresponding control samples. This may indicate lower availability of unbound water in the product structure and potentially contribute to its stability during storage.

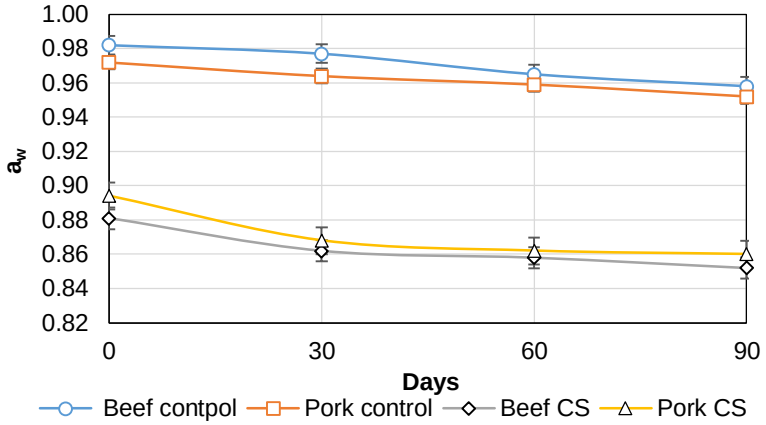

Figure 1. Dynamics of water activity (a_w) in cooked sausages during frozen storage

The observed trend toward decreasing water activity in samples containing cryostabilising mixtures is consistent with the findings reported by Tunik et al. (2025), where an increase in the content of the cryostabilising mixture from 2% to 4% resulted in a decrease in a_w in model sausage products from 0.952 to 0.924, compared with 0.972 in the control sample. The authors associated this change with the ability of the components of the cryostabilising mixture to retain moisture within the meat system.

In the present study, a_w was also lower in samples containing cryostabilising mixtures: after 90 days of storage, it was 0.852 in the beef sample and 0.860 in the pork sample, whereas in the corresponding beef and pork control samples it was 0.958 and 0.952, respectively. These results can be considered a trend consistent with the available literature data. A low water activity value is an important factor in the stability of food products, as it characterizes the fraction of water available for microbial activity and for a range of chemical and biochemical reactions. Therefore, a decrease in a_w and maintenance of a relatively low level throughout the studied period can be considered a positive characteristic of frozen cooked sausages and may contribute to extending their storage life (Tapia et al., 2020).

The stability of water activity in the studied samples may be associated with the specific conditions of frozen storage. At low temperatures, part of the free moisture changes into a crystalline state, reducing its availability for physicochemical and biochemical processes (Leygonie et al., 2012). In addition, water in cooked sausages is largely bound within the protein–fat–carbohydrate matrix, which further limits its migration even during prolonged storage. Rahman noted that the properties of frozen food products depend on the amount and state of different types of water. Therefore, maintaining a stable temperature regime during frozen storage contributes to maintaining a relatively stable a_w level in the product (Rahman, 2009). The obtained data indicate the absence of intensive moisture redistribution processes and the stability of the water-binding system of the product under frozen storage conditions.

The pH value decreased in all samples during frozen storage. This may be explained by the fact that enzymatic and hydrolytic reactions do not cease completely at low temperatures but are only slowed down, resulting in the gradual accumulation of free fatty acids, peptides, and amino acids (Liu et al., 2024) (Figure 2).

Measurements of pH in the sausages were performed after thawing the samples, which could have additionally affected the measured values due to moisture redistribution and the release of soluble components into the intercellular space. An additional factor is the

concentration effect resulting from the transition of water into the crystalline state and the increased concentration of dissolved substances in the unfrozen phase, which may cause a decrease in pH. In addition, structural changes in proteins associated with their partial denaturation also affect the acid–base equilibrium of the system.

Particular attention should be paid to the pattern of pH changes in the control samples, where the decrease during frozen storage was more pronounced compared with the samples containing the cryostabilising mixture. Excessive or prolonged decreases in pH in frozen meat systems may have undesirable consequences for the functional state of proteins, since, in combination with an increased concentration of dissolved substances in the unfrozen phase, they promote denaturation of myofibrillar proteins and reduce their water-holding capacity after thawing (Zhang & Ertbjerg, 2021). Thus, the more pronounced decrease in pH in the control sample may indicate lower stability of its protein–water system during prolonged frozen storage and may potentially result in greater moisture losses during thawing and subsequent technological processing.

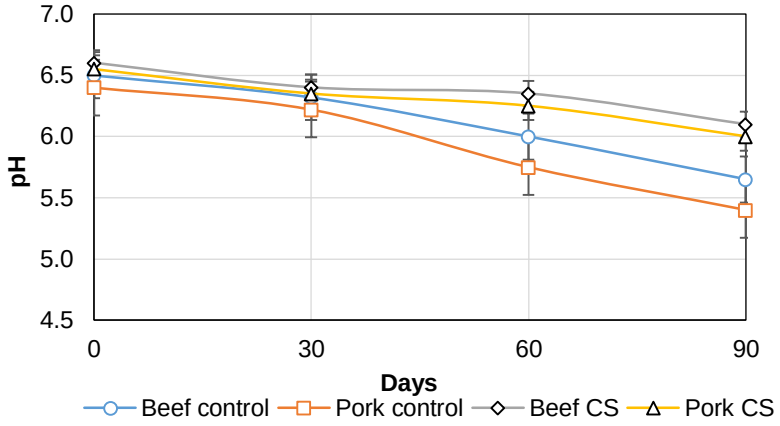

Figure 2. Changes in pH of cooked sausages during frozen storage

The acid value varied from 4.14 to 4.61 mg KOH/g during 90 days of frozen storage, with no consistent upward trend (Figure 3). In the beef control sample, the value increased from 4.40 mg KOH/g at the beginning of storage to 4.60 mg KOH/g on day 30, after which it decreased to 4.15 mg KOH/g on day 60 and reached 4.26 mg KOH/g after 90 days. In the pork control sample, the acid value increased slightly from 4.55 to 4.61 mg KOH/g during the first 60 days, after which it decreased to 4.26 mg KOH/g by day 90.

In the Beef CS sample, the acid value decreased from 4.40 to 4.15 mg KOH/g on day 30 and subsequently remained practically stable, reaching 4.16 and 4.14 mg KOH/g on days 60 and 90, respectively. In the Pork CS sample, the value decreased to 4.14 mg KOH/g on day 30, followed by an increase to 4.61 mg KOH/g on day 60. By day 90, the value had decreased again to 4.14 mg KOH/g.

The acid value is an indicator of the amount of free fatty acids formed as a result of the hydrolytic breakdown of lipids. During frozen storage, lipolytic processes do not necessarily cease completely, as low temperatures reduce the activity of lipolytic enzymes but do not always completely inactivate them. Thus, studies of pork have shown that lipid changes and the formation of free fatty acids may continue during frozen storage, although their intensity varies depending on storage duration (Feng et al., 2022). At the same time, the pattern of such changes may depend on the composition and structural state of the meat system.

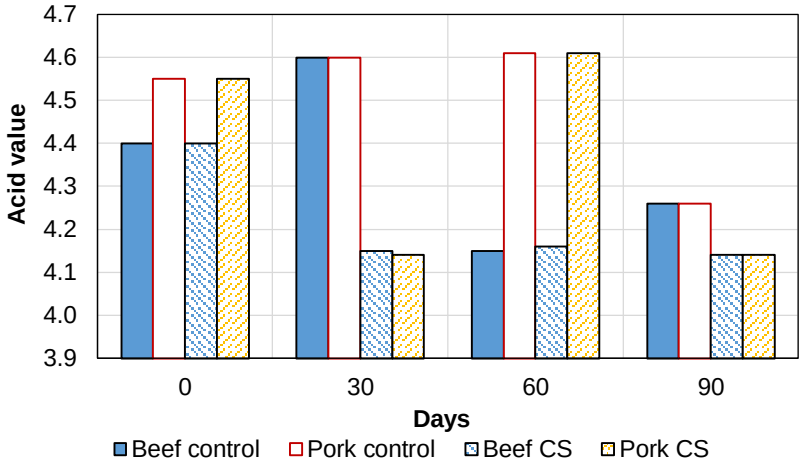

Figure 3. Changes in the acid value of cooked sausages during frozen storage

In the studied samples, no sustained accumulation of free fatty acids was observed over the 90-day period. On the contrary, the final acid values were lower than the initial values in all variants: 4.26 mg KOH/g in the beef control sample, 4.26 mg KOH/g in the pork control sample, 4.14 mg KOH/g in the beef CS sample, and 4.14 mg KOH/g in the pork CS sample. This indicates the absence of pronounced hydrolytic changes in lipids under the studied frozen storage conditions.

Individual fluctuations in the acid value, particularly the increase to 4.61 mg KOH/g in the pork CS on day 60, were not followed by a further increase in the parameter and may be associated with the uneven progression of lipolytic processes or variability in sample composition and sampling. Overall, the obtained results indicate relative stability of the lipid phase of the studied sausages during 90 days of frozen storage.

The absence of a further increase in the acid value indicates that the observed increase was not accompanied by sustained accumulation of free fatty acids. Minor fluctuations in the acid value may be associated with the progression of lipolytic processes; however, their intensity was low and did not result in pronounced accumulation of lipid hydrolysis products. This is also supported by literature data on the stability of fats in frozen meat products (Hui, 2012).

The obtained results are consistent with current understanding of lipolysis in meat products during frozen storage: freezing slows hydrolytic processes but does not necessarily stop them completely (Tatiyaborworntham et al., 2022). At the same time, the absence of a sustained increase in the acid value in our samples indicates the limited intensity of hydrolytic changes during the 90-day storage period.

The peroxide value remained at zero throughout the 90-day frozen storage period in both the control and experimental samples, indicating no detectable accumulation of primary lipid oxidation products under the conditions of the study. Lipid oxidation is a temperature-dependent process, and under freezing conditions the rate of autooxidation decreases sharply. In addition, the limited mobility of oxygen and reaction substrates in the frozen system substantially inhibits peroxide formation. It is known that the rate of lipid oxidation in meat systems decreases considerably at temperatures below −18 °C (Utrera et al., 2013). An additional factor is the prior heat treatment of the sausage products, which partially inactivates pro-oxidant enzymes.

The obtained results indicate that, under the frozen storage conditions of cooked sausages, the use of antioxidants is not critical for preventing primary lipid oxidation within the studied

period. Similar conclusions have been reported in studies of the stability of meat products at low temperatures, where the effectiveness of antioxidants is reported to decrease substantially under freezing conditions (Hęś et al., 2000).

During the 90-day frozen storage period, water activity, pH, and acid value changed only slightly, indicating relative stability of the water and acid–lipid components of the studied sausages. The peroxide value remained at zero in all samples, indicating no detectable accumulation of primary lipid oxidation products under the studied conditions. Frozen storage with the use of cryostabilising mixtures may contribute to maintaining the quality of cooked sausages, with the observed changes being associated predominantly with structural rather than oxidative transformations of the system.

Microstructural analysis of frozen sausage products

Microstructural analysis of the cooked sausage products was performed to assess the effect of cryostabilising compositions on the structural integrity of the protein-fat-carbohydrate matrix after freezing. The analysis was performed using light microscopy at ×600 magnification. Control samples and samples containing the cryostabilising mixture were compared (Figure 4).

In the samples produced with the cryostabilising mixture, a fine, uniformly distributed porous structure was observed. The pores were relatively uniform in size, with no formation of large cavities. The protein-fat-carbohydrate matrix was characterized by high density and homogeneity. No signs of pronounced coalescence of the fat phase or disruption of the protein network were detected, indicating preservation of the integrity of the emulsion system after freezing and being consistent with the findings of Xiong (2005) regarding the role of functional ingredients in stabilizing meat emulsions.

In the control samples (Figure 4), which were produced without the cryostabilising mixture, pronounced structural disturbances were observed, including large cavities, matrix heterogeneity, and local disruptions of the protein network. These changes are associated with the formation and growth of large ice crystals during freezing. The variation in pore size indicates an uncontrolled crystallization process and a higher degree of cryodestruction, which is consistent with the findings of Leygonie (2012), who described the effects of freezing on the microstructure of meat products.

The results of the semi-quantitative porosity analysis showed that the control samples without the cryostabilising mixture had a higher porosity score (2.43), indicating pronounced cryodestruction processes. In contrast, the samples containing the cryostabilising mixture had a lower porosity score (1.29), indicating preservation of the structural integrity of the protein–carbohydrate matrix and reduced microstructural damage. Morphometric analysis of the micrographs showed that the mean pore diameter was larger in the control sample (43.7±5.1 pixels) than in the sample containing the cryostabilising mixture (17.5±2.1 pixels). The control sample was characterized by large and unevenly distributed pores, indicating pronounced structural damage caused by ice crystal formation. In contrast, the sample containing the cryostabilis ing mixture had smaller and more uniformly distributed pores, confirming improved structural integrity and reduced cryodestruction.

The use of the cryostabilising mixture contributes to reducing ice crystal size, preserving the structural integrity of the product, stabilizing the protein-fat system, and forming a more homogeneous microstructure after thawing. Similar effects have been described by Sun et al. (2023) and Dang et al. (2021), who reported that proteins, sugars, and polysaccharides can limit ice crystal growth and improve the water-holding capacity of meat systems.

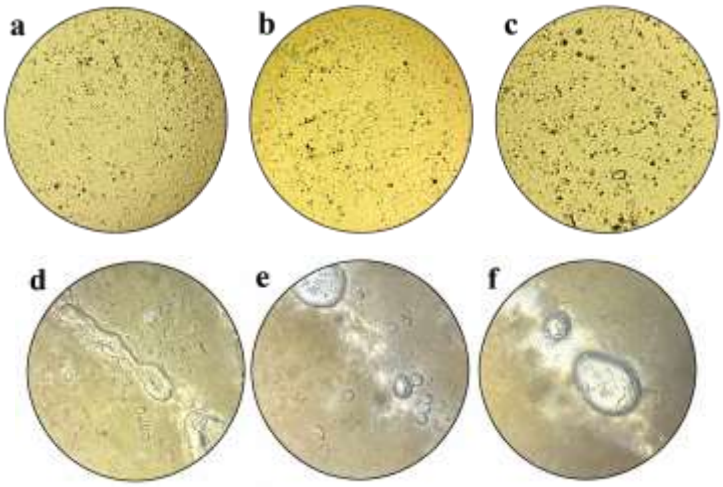

Figure 4. Representative micrographs of cooked sausages after freezing:
a, b, c – three samples containing the cryostabilising functional mixture;
d, e, f – three samples without the cryostabilising functional mixture (control)

The absence of cryostabilising components leads to the formation of larger ice crystals, mechanical damage to the matrix, and potentially reduced water-holding capacity and overall destabilization of the product structure, as confirmed by previous studies (Damodaran et al., 2007; Medić et al., 2018). Samples containing the cryostabilising mixture were characterized by a more stable, fine-grained, and uniform microstructure compared with the control samples, which exhibited pronounced cryodestruction. Microscopic analysis confirms the effectiveness of the cryostabilising mixture in improving the structural stability of frozen sausage products.

Relationship between water activity and cryoscopic temperature

The values of water activity and cryoscopic temperature (Figure 5) indicate changes in the state of water in the studied samples depending on the formulation. In the beef control, water activity was 0.982, while the cryoscopic temperature was −2.5 °C. In the beef CS, water activity decreased to 0.894, whereas the cryoscopic temperature was −4.2 °C. In the pork control, water activity was 0.972 and the cryoscopic temperature was −2.1 °C, whereas in the pork CS, water activity decreased to 0.881 and the cryoscopic temperature to −3.5 °C.

Thus, the incorporation of cryostabilising mixtures into the formulations was accompanied by a decrease in water activity and a shift in the onset of freezing toward lower temperatures. There is a relationship between these parameters, as the state and availability of water in a food system influence its phase transition during freezing.

The obtained results indicate that the incorporation of cryostabilising mixtures may contribute to an increased degree of moisture binding in the protein–fat–carbohydrate system and, consequently, to a decrease in the onset temperature of freezing. This promotes the formation of smaller ice crystals and reduces structural damage to the product during freezing (Zhu et al., 2019). Previous studies have established that the use of cryostabilising mixtures contributes to the preservation of the structural, mechanical, and sensory properties of cooked sausages after freeze–thaw cycles (Tunik & Shevchenko, 2025).

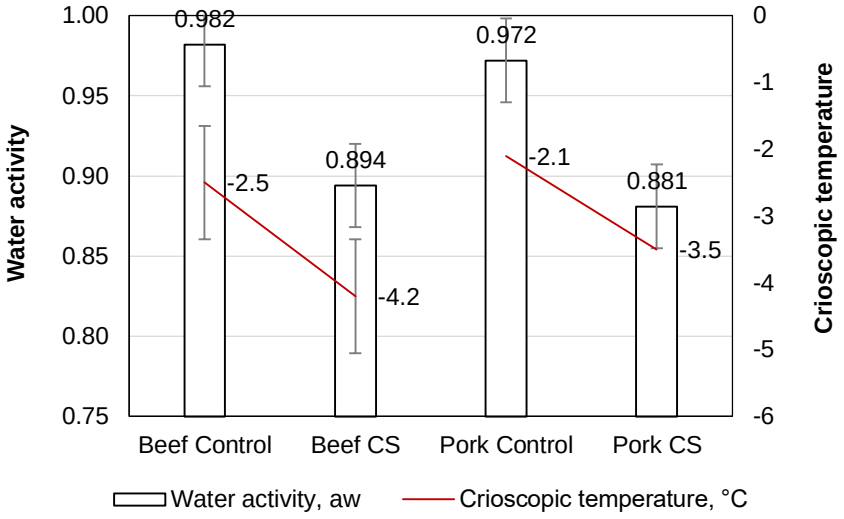

Figure 5. Effect of water activity on cryoscopic temperature

Sensory evaluation of cooked sausages

Sensory evaluation was performed to assess the quality and consumer properties of the finished products after the freeze–thaw cycle. The evaluation results are presented in Figure 6.

The beef control, produced without the cryostabilising mixture, was characterized by the lowest sensory scores. The appearance score was 2.5 points, while the cross-section appearance and texture scores were 1.0 point each; the taste score was 2.5 points, the odour score was 3.8 points, and the colour score was 4.2 points. The most pronounced deterioration was observed in the cross-section appearance and texture, indicating substantial disruption of the product structure after thawing.

The pork control, also produced without the cryostabilising mixture, was characterized by low sensory scores: appearance – 2.2 points, cross-section appearance and texture – 1.0 point each, taste – 1.8 points, odour – 3.2 points, and colour – 4.0 points. The lowest scores were obtained for cross-section appearance, texture, and taste, which may indicate substantial deterioration of the structural and sensory properties of the product after thawing.

The beef CS, containing the cryostabilising mixture, was characterized by considerably higher sensory scores. The appearance was rated at 4.8 points, cross-section appearance – 5.0 points, texture – 4.8 points, taste and odour – 4.5 points each, and colour – 4.8 points. The pork CS also demonstrated high sensory scores: appearance – 5.0 points, cross-section appearance – 4.8 points, texture – 5.0 points, taste and odour – 4.8 points each, and colour – 5.0 points.

Thus, the beef CS and pork CS containing the cryostabilising mixture were characterized by higher sensory scores after freezing–thawing compared with the corresponding control samples. The most pronounced differences were observed in cross-section appearance, texture, and taste, indicating better preservation of the structural and sensory properties of the products when the cryostabilising mixture was used.

The results of the sensory evaluation are supported by the visual changes observed in the studied samples (Figure 7).

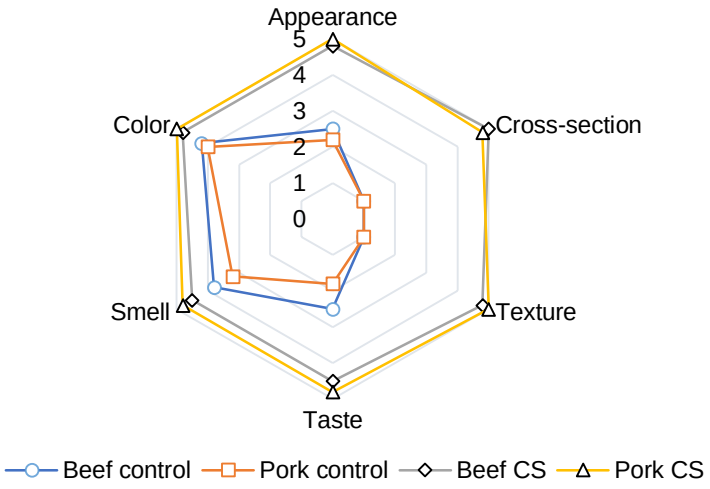

Figure 6. Sensory characteristics of cooked sausages after thawing



Figure 7. Appearance of the sausages after thawing (left – samples without the cryostabilising mixture; right – samples containing the cryostabilising mixture)

After thawing, the cooked sausage samples containing the cryostabilising mixture were characterized by a dense and homogeneous texture, a smooth cut surface, and a uniform distribution of structural components. In contrast, the control samples exhibited cavities and defects on the cut surface, a less dense texture, and signs of structural disruption.

The identified differences are associated with cryodestructive processes occurring during freezing. The formation and growth of ice crystals may cause mechanical damage to the structural elements of the minced meat, disruption of the integrity of the protein–fat–carbohydrate matrix, and a reduction in its water-holding capacity. The use of the cryostabilising mixture contributes to stabilisation of the product structure and reduction of adverse changes during freezing–thawing. Previous studies have established that its use in cooked sausages contributes to increased water-holding capacity and preservation of the structural, mechanical, and sensory properties of the

products after freezing and thawing (Shevchenko & Tunik, 2024). The obtained results are consistent with these findings and confirm the effectiveness of the cryostabilising mixture in preserving the quality of cooked sausages.

Thus, the use of the cryostabilising mixture ensures better preservation of the sensory characteristics of cooked sausages after thawing, particularly texture and cross-section appearance, which deteriorated most markedly in the control samples. This indicates its effectiveness in maintaining the structural integrity and consumer properties of the product during frozen storage.

Conclusions

Frozen storage of cooked sausages at −18 °C is not accompanied by intensive lipid oxidation or substantial changes in water activity, indicating high physicochemical stability of the product. At the same time, it was established that the main quality changes during freezing are associated not with oxidative processes but with structural transformations of the system.

Freezing without the use of cryostabilising components leads to the development of cryodestructive processes, manifested by reorganisation of the protein matrix, formation of cavities, coalescence of the fat phase, and disruption of system integrity. These changes result from ice crystal growth and mechanical damage to the product structure. Freezing negatively affects the microstructure of cooked sausages, as manifested by disruption of the protein matrix, formation of cavities, and coalescence of the fat phase. At the same time, the use of the cryostabilising mixture ensures preservation of structural integrity, formation of a more homogeneous protein–fat system, and reduction of destructive changes caused by water crystallisation, which is consistent with current concepts of stabilisation of emulsion systems during low-temperature storage. This is manifested in the formation of a more homogeneous, finely dispersed structure with a uniform distribution of the fat phase and a minimal number of defects.

The use of the cryostabilising mixture has a positive effect not only on the microstructural characteristics but also on the sensory properties of the products after thawing, particularly by providing better texture, homogeneity, and preservation of the taste and appearance of the product.

Thus, the use of cryostabilising mixtures is an effective technological approach for preserving the quality of cooked sausages during frozen storage, allowing structural damage to be minimised and enabling the subsequent use of the products after thawing without substantial loss of consumer properties. This makes it possible to use thawed sausage products for further processing.

References

Ali, S., Zhang, W., Rajput, N., Khan, M. A., Li, C., & Zhou, G. (2015). Effect of multiple freeze–thaw cycles on the quality of chicken breast meat. *Food Chemistry*, *173*, 808–814. https://doi.org/10.1016/j.foodchem.2014.09.095

Chou, Y. T., & Lin, K. W. (2010). Effects of xylooligosaccharides and sugars on the functionality of porcine myofibrillar proteins during heating and frozen storage. *Food Chemistry*, *121*(1), 127–131. https://doi.org/10.1016/j.foodchem.2009.12.017

Damodaran, S., Parkin, K. L., & Fennema, O. R. (Eds.). (2007). *Fennema's food chemistry* (4th ed.). Boca Raton, FL: CRC Press. https://doi.org/10.1201/9781420028010

Dang, D., Bastarrachea, L., Martini, S., & Matarneh, S. (2021). Crystallization behavior and quality of frozen meat. *Foods*, *10*(11), 2707. https://doi.org/10.3390/foods10112707

Feng, X., Li, J., Zhang, L., Rao, Z., Feng, S., Wang, Y., Liu, H., & Meng, Q. (2022). Integrated lipidomic and metabolomics analysis revealing the effects of frozen storage duration on pork lipids. *Metabolites*, *12*(10), 977. https://doi.org/10.3390/metabo12100977

Fudali, E., Kaczyński, Ł., Urbaniak, M., & Dolatowski, Z. J. (2021). Sensory quality assessment of meat products using a five-point evaluation scale. *Applied Sciences*, *11*(14), 6409. https://doi.org/10.3390/app11146409

Hęś, M., Korczak, J., Gramza-Michałowska, A., & Jędrusek-Golińska, A. (2006). Changes of lipid oxidation degrees and their influence on protein nutritional value in frozen meat products. *Polish Journal of Food and Nutrition Sciences*, *15*/56(1), 37–40.

Hui, Y. H. (Ed.). (2012). *Handbook of meat and meat processing* (2nd ed.). Boca Raton, FL: CRC Press. https://doi.org/10.1201/b11479

Jeong, S., Jo, K., Lee, S., Jeon, H., Kim, S., Han, S., Woo, M., Choi, Y., & Jung, S. (2025). Changes in the properties of frozen meat with freezing and storage conditions and non-destructive analyses for monitoring meat quality. *Food Science of Animal Resources*, *45*(3), 711–726. https://doi.org/10.5851/kosfa.2025.e15

Kiani, H., & Sun, D. W. (2011). Water crystallization and its importance to freezing of foods: A review. *Trends in Food Science & Technology*, *22*(8), 407–426. https://doi.org/10.1016/j.tifs.2011.04.011

Ladikos, D., & Lougovois, V. (1990). Lipid oxidation in muscle foods: A review. *Food Chemistry*, *35*(4), 295–314. https://doi.org/10.1016/0308-8146(90)90019-Z

Leygonie, C., Britz, T., & Hoffman, L. (2012). Impact of freezing and thawing on the quality of meat: Review. *Meat Science*, *91*(2), 93–98. https://doi.org/10.1016/j.meatsci.2012.01.013

Liu, J., Wang, H., Zhang, X., Kong, B., & Chen, Q. (2024). Deterioration mechanism of and improvement strategies for frozen meat. *Food Science*, *45*(8), 321–330. https://doi.org/10.7506/spkx1002-6630-20230627-210

Martino, M. N., & Zaritzky, N. E. (1988). Ice crystal size modifications during frozen beef storage. *Journal of Food Science*, *53*(6), 1631–1637. https://doi.org/10.1111/j.1365-2621.1988.tb07802.x

Medić, H., Djurkin, J., Pleadin, J., Kozačinski, L., Njari, B., Hengl, B., & Kušec, G. (2018). Frozen storage duration influence on physical, chemical and microbiological properties of pork. *Meat Science*, *140*, 119–127. https://doi.org/10.1016/j.meatsci.2018.03.006

Pearson, A., & Dutson, T. (1994). Quality attributes and their measurement in meat, poultry and fish products. *Advances in Meat Research Series*, *9*. New York, NY: Springer Science+Business Media.

Puolanne, E., Ruusunen, M., & Vainionpää, J. (2000). Combined effects of NaCl and raw meat pH on water-holding in cooked sausage with and without added phosphate. *Meat Science*, *58*(1), 1–7. https://doi.org/10.1016/S0309-1740(00)00103-6

Rahman, M. (2009). *Food properties handbook* (2nd ed.). Boca Raton, FL: CRC Press. https://doi.org/10.1201/9781420003093

Rybachuk, O., & Shevchenko, I. (2025). Biological hurdles as modern strategy for extending shelf life of cooked sausages. *Ukrainian Food Journal, 14(4),* 607–637. https://doi.org/10.24263/2304-974X-2025-14-4-3

Savinok, O., Pastyukov, S., Kuzelov, A., & Shepelenko, D. (2017). Sensory and functional parameters of sausages with reduced sodium nitrite content. *Scientific Works of University of Food Technologies*, *64*(1), 32–40.

Shevchenko, I., & Tunik, O. (2024). Cryoprotective properties of functional mixtures in cooked sausage products. *Ukrainian Journal of Food Science*, *13*(3), 33–44. https://doi.org/10.24263/2310-1008-2024-12-1-5

Stabnikova, O., Danylenko, S., Kryzhska, T., Shang, F., & Duan, Z. (2022). Effects of different phosphate content on the quality of wheat bran chicken sausage. *Ukrainian Food Journal*, *11*(4), 588–600. https://doi.org/10.24263/2304-974X-2022-11-4-8

Sun, L., Zhu, Z., & Sun, D. (2023). Regulating ice formation for enhancing frozen food quality: Materials, mechanisms and challenges. *Trends in Food Science & Technology*, *139*, 104116. https://doi.org/10.1016/j.tifs.2023.07.013

Sun, X., & Holley, R. (2011). Factors influencing gel formation by myofibrillar proteins in muscle foods. *Comprehensive Reviews in Food Science and Food Safety*, *10*(1), 33–51. https://doi.org/10.1111/j.1541-4337.2010.00137.x

Sun, X., Wu, Y., Song, Z., & Chen, X. (2022). A review of natural polysaccharides for food cryoprotection: Ice crystals inhibition and cryo-stabilization. *Bioactive Carbohydrates and Dietary Fibre*, *27*, 100291. https://doi.org/10.1016/j.bcdf.2021.100291

Tapia, M. S., Alzamora, S. M., & Chirife, J. (2020). Effects of water activity (a_w) on microbial stability as a hurdle in food preservation. In G. V. Barbosa-Cánovas, A. J. Fontana, S. J. Schmidt, & T. P. Labuza (Eds.), *Water activity in foods*. https://doi.org/10.1002/9781118765982.ch14

Tatiyaborworntham, N., Oz, F., Richards, M. P., & Wu, H. (2022). Paradoxical effects of lipolysis on the lipid oxidation in meat and meat products. *Food Chemistry: X*, *14*, 100317. https://doi.org/10.1016/j.fochx.2022.100317

Tornberg, E. (2005). Effects of heat on meat proteins–Implications on structure and quality of meat products. *Meat Science*, *70*(3), 493–508. https://doi.org/10.1016/j.meatsci.2004.11.021

Tunik, O., & Shevchenko, I. (2025). Effect of cryostabilising mixtures on quality of cooked sausages. *Ukrainian Food Journal*, *14*(1), 8–21. https://doi.org/10.24263/2304-974X-2025-14-1-4

Utrera, M., & Estévez, M. (2013). Oxidative damage to poultry, pork, and beef during frozen storage through the analysis of novel protein oxidation markers. *Journal of Agricultural and Food Chemistry*, *61*(33), 7987–7993. https://doi.org/10.1021/jf402220q

Vorontsov, M., Galenko, O., & Topchii, O. (2025). Thermal stability and technological performance of fibre-fortified protein-fat emulsions for meat and fish products. *Ukrainian Food Journal, 14(3),* 448–463. https://doi.org/10.24263/2304-974X-2025-14-3-7

Verbeken, D., Neirinck, N., Van Der Meeren, P., & Dewettinck, K. (2005). Influence of κ-carrageenan on the thermal gelation of salt-soluble meat proteins. *Meat Science*, *70*(1), 161–166. https://doi.org/10.1016/j.meatsci.2004.12.007

Walayat, N., Xiong, Z., Xiong, H., Moreno, H. M., Niaz, N., Ahmad, M. N., Hassan, A., Nawaz, A., Ahmad, I., & Wang, P. K. (2020). Cryoprotective effect of egg white proteins and xylooligosaccharides mixture on oxidative and structural changes in myofibrillar proteins of *Culter alburnus* during frozen storage. *International Journal of Biological Macromolecules, 158*, 865–874. https://doi.org/10.1016/j.ijbiomac.2020.04.093

Xiong, Y. *L.* (2005). Role of myofibrillar proteins in water-binding in brine-enhanced meats. *Food Research International*, *38*(3), 281–287. https://doi.org/10.1016/j.foodres.2004.03.013

Zhang, Y., & Ertbjerg, P. (2021). Effect of pH at high ionic strength on myofibrillar protein denaturation in frozen-thawed pork. *Food Chemistry*, *338*, 128011. https://doi.org/10.1016/j.foodchem.2020.128017

Zhu, Z., Zhou, Q., & Sun, D. W. (2019). Measuring and controlling ice crystallization in frozen foods: A review of recent developments. *Trends in Food Science & Technology*, *90*, 13–25. https://doi.org/10.1016/j.tifs.2019.05.012

Cite:

Tunik, O., & Shevchenko, I. (2026). Physicochemical stability of cooked sausages during frozen storage under different cryostabilisation conditions. *Ukrainian Food Journal*, *15*(3), 831–846. https://doi.org/10.24263/2304-974X-2026-15-3-14

Biotechnological potential of iron-adapted *Saccharomyces cerevisiae* for producing bakery products enriched with bioaccessible iron

Hanna Bondar, Oleksandra Parkhomova, Viktoriia Krasinko, Olena Bilyk

National University of Food Technologies, Kyiv, Ukraine

Keywords:

Saccharomyces cerevisiae
Iron
Biotechnology
Iron-adapted yeast
Dough
Bread
Bioaccumulation

Article history:

Received 23.12.2025
Received in revised form 21.05.2026
Accepted 30.06.2026

Corresponding author:

Viktoriia Krasinko
E-mail: krasinkovo@nuft.edu.ua

DOI:
10.24263/2304-974X-2026-15-3-15

Abstract

Introduction. The aim of this study was to evaluate the biotechnological potential of the iron-adapted yeast strain *Saccharomyces cerevisiae* M437Fe for the production of bakery products with enhanced Fe bioaccessibility.

Materials and methods. Commercial baker's yeast was used as the technically pure culture (TPC), while the iron-adapted *S. cerevisiae* M437Fe served as the experimental strain. Both cultures were grown in a molasses-based medium with $FeSO_4$. Growth, yeast properties, dough and bread quality, and in vitro bioaccessible iron were evaluated.

Results and discussion. After $FeSO_4$ supplementation at 24 h of cultivation, the iron-adapted culture *S. cerevisiae* M437Fe exhibited higher OD_{540} and biomass levels. After 72 h, the OD_{540} was 14.7% higher, and the dry biomass reached 7.30 g/L compared with 6.29 g/L in the TPC. During the 24–48 h period, biomass increased from 4.89 to 6.08 g/L in TPC and from 5.66 to 7.15 g/L in M437Fe. At 48 h, the biomass of M437Fe in the $FeSO_4$-supplemented variant was approximately 1.2-fold higher than that in the control; however, after Holm correction, this difference showed only a tendency toward significance. At the same time, it was confirmed a significant overall effect of culture type on biomass accumulation during the 24–72 h post-supplementation interval, indicating that M437Fe maintained a higher general biomass level in the presence of $FeSO_4$. $FeSO_4$ supplementation enhanced cell aggregation, as indicated by increases in Dx(50) and Dx(90) particle sizes, and improved flotation ability, with maximum Flo values after 72 h of cultivation of 46.4% for M437Fe compared with 26.6% for TPC. Iron enrichment improved fermentative activity: the time required to release 10 mL of CO_2 decreased by 47.6% for M437Fe and 29.2% for TPC, while leavening power increased 2.3-fold and 1.5-fold, respectively. Osmotic sensitivity decreased by 18.5% in M437Fe. Bread produced using M437Fe had a higher specific volume (2.8 mL/g) compared with 2.3 mL/g in the control, as well as higher crumb porosity (80% compared with 76% in the control produced with TPC). The proportion of iron released into the soluble fraction after *in vitro* digestion of bread produced with M437Fe was $72.3 \pm 0.7\%$.

Conclusions. The iron-adapted culture *S. cerevisiae* M437Fe retained its growth activity, exhibited improved technological properties, and enabled the production of bread with increased Fe release after *in vitro* digestion. These results indicate its potential for producing bakery products enriched with biogenic iron.

Introduction

Iron deficiency is the main cause of anemia, which affects roughly one-third of the world's population (World Health Organization, 2017). Recently, iron in the form of nanoparticles (Tsykhanovska et al., 2023, 2024), plant ferritin induced in legume sprouts by germination in an $FeSO_4$ solution (Zielińska-Dawidziak et al., 2023), lactic acid bacteria as carriers of iron nanoparticles adsorbed onto the cells (Ciont et al., 2023; Garces et al., 2018), and heme iron (Jarzębski et al., 2023; Xing et al., 2022) have been considered as potential ingredients for food fortification.

Saccharomyces cerevisiae yeasts are among the most important microorganisms in industrial biotechnology and are widely used in food production due to their high technological activity, safety, and ability to synthesize and accumulate biologically valuable compounds. One promising direction in modern food biotechnology is the use of yeast biomass as a natural carrier of essential micronutrients, particularly iron, for the development of functional foods with enhanced biological value. In this context, bread and bakery products are considered an effective matrix for functional micronutrient enrichment, as they are regularly consumed foods and may ensure a stable dietary intake of nutrients. However, in the case of iron, the effectiveness of such an approach is determined not only by the total Fe content in the final product, but also by its chemical form, interactions with dough components, stability during baking, and ability to be converted into an accessible form after digestion (Nikolaou et al., 2026; Rengifo et al., 2025). This issue is particularly relevant for cereal-based products, since iron may bind to phytates, proteins, polysaccharides, and other bread components, thereby limiting its release in the gastrointestinal tract (Rodriguez-Ramiro et al., 2017).

Traditional fortification of bread with iron salts is known to substantially affect the physicochemical and sensory properties of the product, as well as the predicted bioaccessibility of Fe (Majeed et al., 2025). Different iron forms have been shown to modify the specific volume, crust and crumb colour, hardness, aftertaste, and overall consumer acceptability of wheat and gluten-free bread (Kiskini et al., 2010). In addition, iron accessibility is influenced by the technological process, primarily the biotechnological stage of yeast fermentation, during which the activity of *S. cerevisiae*, dough acidity, and fermentation time determine the ratio between bound and soluble Fe forms (Rodriguez-Ramiro et al., 2017). Therefore, the evaluation of bread iron enrichment requires consideration not only of the form of the added micronutrient, but also of its behaviour within the final food matrix.

A promising alternative to conventional iron fortification with iron salts is the biotechnological accumulation of micronutrients by yeast biomass. *S. cerevisiae* possesses well-developed mechanisms for interacting with metal ions, including their uptake, transport, intracellular binding, and biotransformation. For example, when cultivated in a medium containing inorganic selenium, *S. cerevisiae* can accumulate selenium in organic forms with high nutritional value, such as selenomethionine and selenocysteine (Stabnikova et al., 2022), or as selenium nanoparticles containing elemental selenium (Se^0), which are characterized by high bioavailability and lower toxicity (Skrotska et al., 2025). The ability of a cell-free aqueous extract of *S. cerevisiae* M437 to produce silver nanoparticles through the reduction of silver nitrate has also been demonstrated (Skrotska et al., 2021). These properties of yeast cells provide a basis for their use not only as conventional technological agents but also as biological platforms for the accumulation of essential micronutrients. In particular, *S. cerevisiae* can actively take up Fe from the culture medium, transport it into the cells, and accumulate it in forms associated with cellular biomolecules (Tafazzoli et al., 2024). As a

result, yeast biomass may simultaneously serve as a technological agent in breadmaking and as a natural carrier of bioaccessible iron. The practical relevance of this approach is supported by studies in which iron-enriched yeasts have been used for the production of bakery products with acceptable sensory characteristics and increased Fe content (Nowosad & Sujka, 2021), and have also been considered as a promising source of organically associated iron (Chen et al., 2024).

Despite the considerable interest in iron biofortification of yeast biomass, most studies have focused either on micronutrient accumulation by yeast cells or on the quality assessment of final bakery products. In contrast, comprehensive biotechnological evaluation of iron-adapted *S. cerevisiae* cultures that simultaneously considers the physiological characteristics of the producer strain, its technological performance during breadmaking, and the bioaccessibility of accumulated iron after baking remains scarce.

Therefore, the aim of this study was to provide a comprehensive biotechnological evaluation of the iron-adapted *S. cerevisiae* strain M437Fe as a promising source of bioaccessible iron for the production of functional bakery products. To achieve this aim, the growth characteristics of TPC and iron-adapted *S. cerevisiae* M437Fe were compared, their technological properties were assessed, the effect of iron-adapted yeast application on bread quality parameters was determined, and the proportion of iron released into the soluble fraction after *in vitro* digestion was established.

Materials and Methods

Materials

The iron-adapted strain *Saccharomyces cerevisiae* M437Fe, obtained by sequential subculturing on a nutrient medium supplemented with an iron source, and a technically pure culture (TPC) of active dry baker's yeast commercially available under the trademark "Lvivski Drizhdzhi" and produced by PJSC "Enzym Company" (Ukraine), were used in the study.

Molasses (Zhdanivka Sugar Plant, Ukraine) and iron(II) sulfate heptahydrate, potassium chloride, ammonium sulfate, potassium dihydrogen phosphate, dextrose, peptone, and yeast extract (Sigma-Aldrich) were used to prepare three culture media with the following compositions:

(1) a molasses-based medium containing (g/L): molasses, 20.0; ammonium sulfate, 6.0; potassium dihydrogen phosphate, 10.0; potassium chloride, 0.1; pH 5.0. This medium served as the basal cultivation medium for producing iron-enriched yeast biomass and was used in the experiments aimed at evaluating growth, biomass accumulation, iron enrichment, and technological properties of the studied yeast cultures.

(2) yeast extract–peptone–dextrose (YPD) medium used for maintenance of the TPC and cultivation of the inoculum, containing (g/L): dextrose, 20.0; peptone, 20.0; yeast extract, 10.0;

(3) agarized yeast extract–peptone–glucose (YPG) medium used for maintenance of the *S. cerevisiae* M437Fe culture and cultivation of the inoculum, containing (g/L): glucose, 30.0; peptone, 20.0; yeast extract, 10.0; agar, 20.0. Iron(II) sulfate was added to obtain an iron concentration of 50 mg/L.

The iron(II) sulfate stock solution was prepared in distilled water. To ensure sterility, the solution was passed through a 0.22 μm membrane filter and aseptically added to medium 1 to obtain a final iron concentration of 1.3 mM.

The medium components were dissolved in drinking water, and the final volume was adjusted to 1 L. The media were sterilized by autoclaving, whereas the iron(II) sulfate solution was sterilized by membrane filtration.

The control variant consisted of the culture medium without the addition of iron compounds (i.e., without an exogenous Fe source).

Iron adaptation of *Saccharomyces cerevisiae* M437

The iron-adapted culture *Saccharomyces cerevisiae* M437Fe was obtained from the strain *S. cerevisiae* M437, obtained from the Collection of Live Microbial Cultures of the Department of Biotechnology and Microbiology, National University of Food Technologies, by sequential subculturing on an iron-containing nutrient medium. For this purpose, the parental culture was transferred three consecutive times onto medium 3.

Each subculturing step was performed under aseptic conditions. After incubation, actively growing colonies were transferred to fresh iron-containing medium of the same composition. The three-step sequential subculturing procedure was used to gradually expose the yeast culture to iron and obtain a culture capable of maintaining growth in the presence of an increased Fe concentration. The resulting culture was designated *S. cerevisiae* M437Fe and was further used in experiments on biomass accumulation, iron enrichment, technological characterization, and bread production. The *S. cerevisiae* M437Fe culture was stored on medium 3 at 4 ± 1 °C in the dark.

Preparation of inoculum

The TPC culture was maintained on slants of medium 2 at 4°C. Strain *Saccharomyces cerevisiae* M437Fe was maintained on medium 3 at 4 ± 1°C.

Prior to inoculum preparation, the yeast was streaked onto Petri dishes containing the same medium using the depletion streak method to obtain isolated colonies and incubated at 30 ± 1°C for 48 h. Colonies located at least 1 cm apart on the plate were selected for inoculum preparation. The selected colonies were transferred to tubes containing slants of medium 3. The cultures were subsequently incubated at 30 ± 1°C for 24 h. All yeast transfers were performed under aseptic conditions.

The inoculum for all cultivation variants was prepared by washing off and suspending a 24 h cell suspension in sterile physiological saline. An aliquot of the resulting inoculum was aseptically transferred using a sterile pipette into flasks containing 150 mL of medium 1. The inoculum accounted for 10% of the medium volume. All operations involving yeast cultures were performed under aseptic conditions.

Yeast cultivation

Cultivation was carried out in 750-mL Erlenmeyer flasks with a working volume of 150 mL. The cultures were incubated at 30 ± 2 °C for 72 h to study biomass growth kinetics and for 48 h in all other experiments.

Iron was added as an iron(II) sulfate solution 24 h after the start of cultivation, following preliminary biomass accumulation. The time point for iron addition was determined in preliminary experiments as optimal in terms of the balance between biomass accumulation and iron content in yeast cells (Bondar & Krasinko, 2026).

Monitoring of yeast culture growth by OD_{540} measurement

At predetermined time intervals, 0.5 mL of culture broth was collected from each flask and diluted to a final volume of 10 mL with distilled water. Optical density (OD) was measured at a wavelength of $\lambda = 540$ nm using a photoelectric colorimeter. Distilled water was used as the blank.

Determination of iron-enriched yeast dry biomass

Dry biomass of both the technically pure culture of *S. cerevisiae* and the iron-adapted culture *S. cerevisiae* M437Fe was determined according to the method described by Bondar and Krasinko (2025). The results were expressed as dry weight (DW), g/L of culture medium.

The specific growth rate (μ), h^{-1}, was estimated by the following equation:

$$\mu = (\ln X_1 - \ln X_0)/(t_1 - t_0),$$

where X_0 and X_1 are the initial and final concentrations of yeast biomass at time t_0 and t_1, respectively.

Determination of iron content

The following reagents were used to determine the content of accumulated iron: iron (II) sulfate heptahydrate, nitric acid, Certipur® MS multi-element standard solution (Sigma-Aldrich) containing Fe at a concentration of 1000 ppm, and Milli-Q chromatography-grade water (Millipore). Sample preparation and determination of intracellular iron content were performed according to the method described by Bondar and Krasinko (2025).

Determination of yeast flotation ability

The flotation assay was performed in a 100 mL graduated cylinder used as a flotation chamber. Briefly, 50 mL of culture broth was aerated by bubbling air through the suspension for 2 min using a microcompressor, with the aerator positioned at the bottom of the cylinder. Cell concentration was determined before flotation, after flotation, and in the foam fraction. Cell concentration was measured photocolorimetrically at a wavelength of 540 nm. Flotation ability (Flo, %) was calculated using the following equation:

$$Flo(\%) = \left[\frac{(C_p - C_r)}{C_p}\right] \times 100,$$

where C_p is the cell concentration before flotation and C_r is the cell concentration after flotation (Palmieri et al., 1996).

Determination of yeast cell and aggregate size

The size distribution of yeast biomass cells and aggregates was determined by laser diffraction using a Mastersizer 3000 particle size analyzer (Malvern Instruments, United Kingdom). Granulometric characteristics were evaluated based on Dx(10), Dx(50), and Dx(90) values, expressed in μm.

Determination of yeast fermentative activity

The fermentative, or zymase, activity of the yeasts was determined using a modified procedure based on the time required to release 10 mL of CO_2 during glucose fermentation. The method was adapted from the classical assay used to determine the zymase activity of baker's yeast.

The CO_2 volume was recorded using a sealed gas-measuring system consisting of a 150 mL reaction flask and a 150 mL gasometric flask. The gasometric flask was equipped with a graduated gasometric tube, which was used to determine the volume of displaced indicator solution corresponding to the volume of released CO_2. A 0.17 g portion of dry yeast was placed into the reaction flask and suspended in 10 mL of water preheated to 35 °C, after which 10 mL of 10% glucose solution was added.

The gasometric flask was filled with a saturated NaCl solution stained with methylene blue, which served as the indicator liquid for CO_2 volume determination by displacement. After sealing the system, the initial level of the indicator liquid was adjusted to the zero mark, and the system was incubated at 35 °C. Fermentative, or zymase, activity was evaluated as the time required to release 10 mL of CO_2, determined by displacement of the corresponding volume of indicator solution.

Determination of yeast leavening power and osmotic sensitivity

The leavening power of the yeasts was determined using the floating dough ball method. A 0.31 g portion of yeast was suspended in 4.8 mL of water preheated to 35°C, after which 7.5 g of wheat flour was added and the dough was kneaded until a homogeneous ball was formed. The resulting dough ball was immersed in water at 35°C and incubated at the same temperature. Leavening power was evaluated as the time from immersion of the dough ball to its flotation on the surface.

Yeast osmotic sensitivity was determined using the same procedure, except that 4.8 mL of 3.85% (w/v) NaCl solution was used instead of water. Osmotic sensitivity was expressed as the time required for the dough ball to float under increased osmotic pressure, reflecting changes in the gas-forming activity of yeasts under osmotic stress.

Determination of dough specific volume

Dough specific volume was determined to assess its viscoelastic properties during fermentation. The assay was performed using 250 mL graduated cylinders. After kneading, 50 g of dough was placed into the cylinders and incubated at 30°C. Changes in dough volume were recorded immediately after kneading and then every 30 min during 3 h of fermentation. The obtained values were used to assess dough leavening capacity and gas-retention ability during fermentation.

Preparation of dough samples

Dough samples were prepared according to the following formulation, expressed as a percentage of flour weight: high-grade wheat flour – 100.0; tested yeast biomass – 3.0; and salt – 1.5. Iron-enriched biomass of *Saccharomyces cerevisiae* M437Fe and biomass of the technically pure culture (TPC) of active dry baker's yeast commercially available under the trademark "Lvivski drizhdzhi" were used as the yeast component.

The dough was prepared by the straight-dough method at a moisture content of 44.0%, with a fermentation time of 180 min. Dough kneading was performed using a two-speed Escher dough mixer (Italy): 2 min at the first speed and 10 min at the second speed. Proofing was carried out in a proofing cabinet at 35–40°C for 45 min. Baking was performed without a lid in a Sveba-Dahlen deck oven (Italy) at 180–200°C for 20–25 min.

Specific volume of bread

The grain is filled with excess, which is raked with the edge of the ruler into the receiving container and removed through the hole. After that, the curtains of the main capacity with grain are opened manually and put through the hole into the bucket. This grain is used for determination. A small amount of grain is put into the main container, bread is put on it, carefully, without passing the grain, and the rest of grain is put in excess of the capacity. Grain is raked with the edge of the ruler and put into the receiving container, and then, after opening the latch – into the measuring cylinder. The volume of grain in a cylinder (mL) is equal to the volume of bread. Measurements are performed twice, deviations between parallel determinations should not exceed 5%.

The specific volume of bread is determined by dividing the volume of bread by its weight and expressed to the nearest 0.01 mL/g (Zhu et al., 2016).

Porosity of bread

The porosity of bread reflects the volume of the pores in a certain volume of the crumb, expressed as a percentage to the total volume (Verheyen et al., 2015).

Bread shape stability (H/D)

The height and diameter of hearth bread were measured using a ruler or a specialized measuring device. The shape stability index (H/D) was calculated as the ratio of product height (H) to product diameter (D) (Drobot et al., 2015).

Bread crumb moisture content

Two metal weighing dishes were each loaded with 5 g of ground bread crumb. The dishes containing the crumb were placed in a drying oven (SESh-3M) and dried for 45 min at a temperature of 130°C. After drying, the dishes were transferred to a desiccator and cooled for 20–120 min. The cooled dishes were then weighed, and the mass fraction of moisture in the bread crumb was calculated (Drobot et al., 2015).

$$W = ((m_1 - m_2)/m) \times 100\%,$$

where m is the mass of the bread crumb sample before drying; m_1 is the mass of the box with the sample before drying; m_2 is the mass of the box with the sample after drying.

Crust and crumb color of bread

The bread slice crumb and crust colour were analysed using a colorimeter Chroma meter CR-200 (Minolta, Osaka, Japan). Three colour-coordinates were recorded: (1) $L*$ (dark-light); (2) $a*$ (green-red) and (3) $b*$ (blue-yellow) as well as the total colour difference ($\Delta E*$) which was subsequently recorded to understand human perceivable differences (e.g., less than one: non-perceivable differences, one to three: minor perceivable differences and more than three: perceivable differences) (Norton et al., 2025)

$$\Delta E = \sqrt{(L^* - L_0^*)^2 + (a^* - a_0^*)^2 + (b^* - b_0^*)^2},$$

where L_0*, a_0*, and b_0* are the color parameters of the control sample, and L*, a*, and b* are those of the experimental sample. Each parameter was measured at five different points, and the mean value was used for calculations.

Bread quality assessment

Bread quality was assessed by determining organoleptic and physicochemical parameters that characterize the consumer properties and technological quality of the final product.

Determination of *in vitro* iron bioaccessibility from enriched bread

The following reagents were used to determine *in vitro* iron bioaccessibility from bread using the INFOGEST method: sodium hydrogen carbonate, α-amylase from porcine pancreas type VI-B, pepsin from porcine gastric mucosa, trypsin from porcine pancreas type IX-S, α-chymotrypsin from bovine pancreas type II, lipase from porcine pancreas type II, porcine bile extract, potassium chloride, potassium dihydrogen phosphate, sodium chloride, magnesium chloride hexahydrate, ammonium carbonate, calcium chloride dihydrate, as well as sodium hydroxide and hydrochloric acid solutions for pH adjustment. All reagents were purchased from Sigma-Aldrich.

Simulated salivary fluid (SSF), simulated gastric fluid (SGF), and simulated intestinal fluid (SIF) were prepared according to the procedure described by Minekus et al. (2014).

In vitro iron bioaccessibility was assessed in bread samples produced using the technically pure culture of *S. cerevisiae* as the control sample and the iron-enriched, iron-adapted culture *S. cerevisiae* M437Fe. After baking, the bread was cooled to room temperature and stored for 24 h under identical conditions, after which the crumb was homogenized. For each determination, 5.00 g of the homogenized sample was used.

Digestion was performed according to the standardized static INFOGEST protocol described by Minekus et al. (2014), with sequential simulation of the oral, gastric, and intestinal phases. The oral phase was carried out using simulated salivary fluid (SSF) at a final α-amylase activity of 75 U/mL, pH 7.0, for 2 min at 37°C. The gastric phase was performed using simulated gastric fluid (SGF) at a final pepsin activity of 2000 U/mL, pH 3.0, for 2 h at 37°C. The intestinal phase was carried out using SIF containing trypsin, α-chymotrypsin, lipase, and bile extract, pH 7.0, for 2 h at 37°C.

After digestion, the digestate was centrifuged at 6000 rpm for 20 min at 20ºC, and the supernatant was collected as the soluble fraction, in which iron content was determined by AAS. The total iron content in the initial bread sample after mineralization was also determined by AAS according to the method described by Bondar and Krasinko (2025). *In vitro* iron bioaccessibility (%) was calculated as follows:

$$\text{Bioaccessibility (\%)} = \left[\frac{\text{Fesoluble}}{\text{Fetotal}}\right] \times 100,$$

where Fesoluble is the iron content in the soluble fraction after INFOGEST digestion, and Fetotal is the total iron content in the corresponding bread sample before digestion.

Statistical analysis

Statistical processing of the results was performed using descriptive and inferential statistics. Mean values, graphical representation, and assessment of data normality were carried out in Microsoft Excel 2016. One-way ANOVA was used to compare experimental variants within a single regime, for example, within one agitation speed or one culture medium. When a significant effect was detected, pairwise comparisons were performed using Welch's t-test, due to the possible inequality of variances between groups, with Holm correction applied to control the error rate associated with multiple comparisons. For multifactorial analysis and assessment of relationships between variables, regression analysis was performed using the Data Analysis ToolPak in Microsoft Excel 2016.

Each experiment was performed in three independent replicates, and mean values were used as the response. Statistical significance was accepted at $p < 0.05$.

Results and discussion

Comparative study of biomass growth kinetics of the TPC and *Saccharomyces cerevisiae* M437Fe in the presence and absence of iron

One of the key indicators of the biotechnological potential of iron-adapted cultures is their ability to maintain active growth after iron accumulation. Therefore, a comparative assessment of the growth kinetics of the technically pure culture (TPC) of *Saccharomyces cerevisiae* and the iron-adapted culture *S. cerevisiae* M437Fe was performed based on the optical density of the culture broth (OD_{540}) in the medium without iron addition (Figure 1) and after $FeSO_4$ supplementation at 24 h of cultivation (Figure 2).

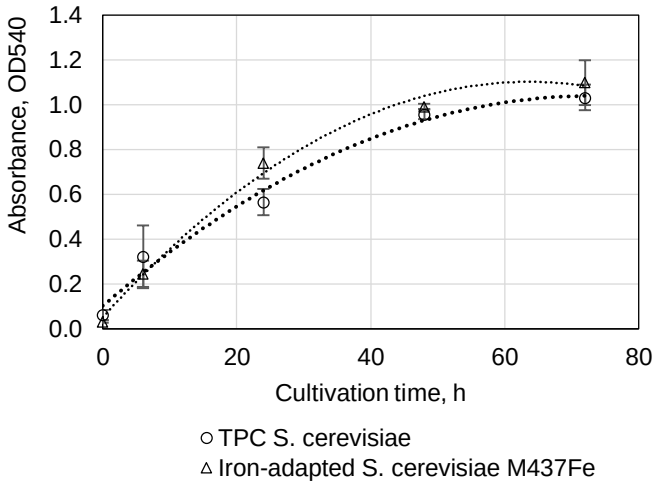

Figure 1. Optical density dynamics of the TPC and iron-adapted *Saccharomyces cerevisiae* M437Fe without $FeSO_4$ supplementation

During cultivation in the medium without iron supplementation, both cultures showed a growth pattern typical of batch cultivation, with an intensive increase in optical density at the early stages, followed by a gradual slowdown after 48 h of cultivation. The maximum specific growth rate values were observed during the initial cultivation interval and reached 0.27 h^{-1} for the TPC and 0.34 h^{-1} for *S. cerevisiae* M437Fe. Subsequently, μ gradually decreased to 0.003–0.004 h^{-1} by the end of cultivation, indicating the completion of the active growth phase and transition of the cultures to the stationary state.

Statistical analysis confirmed that cultivation time was the main factor affecting OD_{540} in the control variant (two-way ANOVA, $F = 251.93$; $p < 0.001$). The effect of culture type was not statistically significant ($F = 1.90$; $p = 0.183$), indicating that, under control conditions, the overall optical density levels of the TPC and *S. cerevisiae* M437Fe did not differ significantly. At the same time, the "culture × time" interaction was statistically significant ($F = 3.03$; $p = 0.042$), suggesting that the dynamics of OD_{540} changes over time were not completely identical between the two cultures. However, pairwise comparisons between the TPC and *S. cerevisiae* M437Fe at individual time points did not reveal statistically significant differences after Holm correction ($pHolm > 0.05$). Thus, in the absence of an exogenous iron source, iron adaptation did not lead to statistically confirmed differences in OD_{540} at individual cultivation time points.

After $FeSO_4$ supplementation at 24 h of cultivation, optical density continued to increase in both cultures (Figure 2).

The 24 h time point was considered the baseline immediately before iron exposure, whereas the 48 and 72 h time points reflected the post-supplementation period. The iron-adapted culture *S. cerevisiae* M437Fe showed higher mean OD_{540} values during the 24–72 h interval. At 72 h, the optical density of the M437Fe culture was approximately 14.7% higher than that of the TPC. The specific growth rate decreased progressively in both cultures after 24 h, indicating their gradual transition toward the stationary phase.

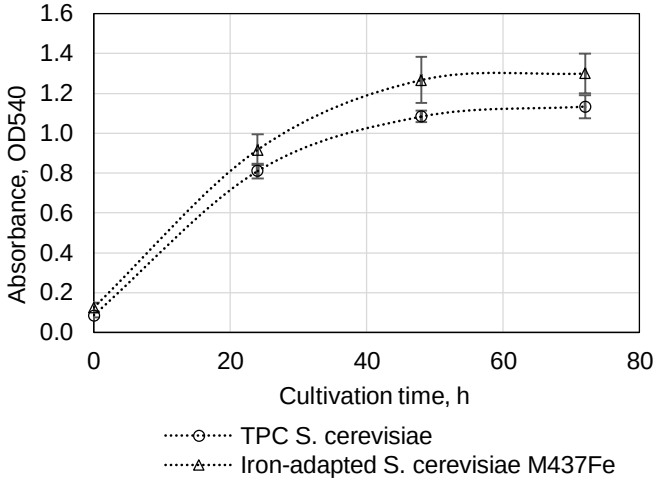

Figure 2. Optical density dynamics of the TPC and iron-adapted *Saccharomyces cerevisiae* M437Fe after $FeSO_4$ supplementation at 24 h of cultivation

Since $FeSO_4$ was added after 24 h of cultivation, statistical interpretation of the $FeSO_4$-supplemented variant was focused on the 24–72 h interval. Two-way ANOVA showed that cultivation time significantly affected OD_{540} during this period ($F = 38.76$; $p < 0.001$). Culture type also had a statistically significant effect on the overall OD_{540} level ($F = 18.06$; $p = 0.001$), whereas the "culture × time" interaction was not statistically significant ($F = 0.42$; $p = 0.665$). This indicates that the iron-adapted culture M437Fe was characterized by higher overall OD_{540} values during the post-supplementation period, while the temporal pattern of OD_{540} changes remained similar for both cultures.

Pairwise comparisons between the cultures at individual time points during the 24–72 h interval did not reveal statistically significant differences after Holm correction (pHolm = 0.247). Therefore, the higher OD_{540} values observed for M437Fe after $FeSO_4$ supplementation should be interpreted as an overall culture-dependent effect confirmed by two-way ANOVA, rather than as statistically significant differences at separate time points.

Comparison of the control and $FeSO_4$-supplemented variants showed that $FeSO_4$ addition most clearly affected the TPC of *S. cerevisiae*. After iron supplementation, a statistically significant increase in OD_{540} was observed for the TPC at 48 h of cultivation, whereas by 72 h this difference was no longer statistically significant. For the iron-adapted culture *S. cerevisiae* M437Fe, $FeSO_4$ supplementation was associated with higher mean OD_{540} values after iron addition; however, these differences were not statistically significant after Holm correction. This may indicate that prior adaptation to iron reduced the magnitude of the culture response to additional Fe^{2+} supply in the nutrient medium.

Overall, the results showed that iron adaptation did not suppress the growth of *S. cerevisiae* and did not disrupt the general pattern of transition between growth phases. The iron-adapted culture maintained active growth both under control conditions and after $FeSO_4$ supplementation. The higher overall OD_{540} values observed for M437Fe during the post-supplementation period suggest a stable physiological response to cultivation in the presence of iron, which is an important prerequisite for further use of this culture as a biotechnological agent for food biofortification.

Since optical density is an indirect indicator of growth and may be affected by cell aggregation and the turbidity of the culture suspension, the next stage of the study was to determine dry biomass accumulation by the TPC of *S. cerevisiae* and the iron-adapted culture *S. cerevisiae* M437Fe under control conditions (Table 1) and after $FeSO_4$ supplementation at 24 h of cultivation (Table 2). Dry biomass concentration was used as an additional parameter characterizing cell mass accumulation and complementing OD_{540}-based growth assessment.

Table 1

Dry biomass accumulation and growth kinetic parameters of the TPC and iron-adapted *Saccharomyces cerevisiae* during cultivation without iron supplementation

t, h	*S. cerevisiae* TPC		*S. cerevisiae* M437Fe		pHolm between cultures
	X, g/L	μ, h^{-1}	X, g/L	μ, h^{-1}	
0	2.00 ± 0.00	–	1.84 ± 0.23	–	1.000
6	2.67 ± 1.15	0.048	3.00 ± 1.73	0.183	1.000
24	3.33 ± 0.58	0.012	4.67 ± 0.58	0.011	0.237
48	5.34 ± 1.53	0.020	5.87 ± 0.58	0.012	1.000
72	6.33 ± 0.58	0.007	6.67 ± 0.58	0.006	1.000

Note. t – cultivation time; μ – specific growth rate. X – dry biomass, values are presented as mean ± standard deviation, n = 3. pHolm values indicate pairwise comparisons between the TPC and *S. cerevisiae* M437Fe at the same cultivation time point according to Welch's t-test with Holm correction.

Table 2

Dynamics of dry biomass accumulation and growth kinetic parameters of the TPC and iron-adapted *Saccharomyces cerevisiae* yeasts following $FeSO_4$ supplementation after 24 h of cultivation

t, h	*S. cerevisiae* TPC		*S. cerevisiae* M437Fe		pHolm between cultures
	X, g/L	μ, h^{-1}	X , g/L	μ, h^{-1}	
0	1.77 ± 0.05	–	2.30 ± 0.09	–	n/a
24	4.89 ± 0.16	0.042	5.66 ± 0.33	0.038	0.105
48	6.08 ± 0.13	0.009	7.15 ± 0.49	0.010	0.105
72	6.29 ± 0.25	0.001	7.30 ± 0.43	0.001	0.105

Note. t – cultivation time; μ – specific growth rate. X – dry biomass, values are presented as mean ± standard deviation, n = 3. pHolm values indicate pairwise comparisons between the TPC and S. cerevisiae M437Fe at the same cultivation time point during the 24–72 h interval according to Welch's t-test with Holm correction. n/a – not included in the post-supplementation statistical comparison.

During cultivation in the medium without iron supplementation, both cultures demonstrated a gradual increase in dry biomass concentration during cultivation. Relative to the initial time point, dry biomass increased approximately 3.2-fold after 72 h for the TPC of *S. cerevisiae* and approximately 3.6-fold for *S. cerevisiae* M437Fe. Two-way ANOVA showed that cultivation time was the main factor affecting dry biomass accumulation under control conditions ($F = 25.68$; $p < 0.001$). In contrast, the effect of culture type was not statistically significant ($F = 2.02$; $p = 0.171$), and the "culture x time" interaction was also not significant ($F = 0.53$; $p = 0.715$). This indicates that, in the absence of an exogenous iron source, both cultures exhibited a similar overall pattern of biomass accumulation.

Pairwise comparisons between the TPC of *S. cerevisiae* and *S. cerevisiae* M437Fe at individual time points did not reveal statistically significant differences after Holm correction (pHolm > 0.05). Thus, although some differences in mean biomass values were observed between the cultures, they were not statistically confirmed under control cultivation conditions.

In the variant in which $FeSO_4$ was added after 24 h of cultivation, the 24 h time point was considered the baseline immediately before iron exposure, whereas the 48 and 72 h points reflected the post-supplementation period. During the 24–48 h interval, biomass increased from 4.89 to 6.08 g/L in the TPC of *S. cerevisiae* and from 5.66 to 7.15 g/L in *S. cerevisiae* M437Fe. This corresponded to an approximately 1.2-fold increase for the TPC and 1.3-fold increase for M437Fe. During the subsequent 48–72 h interval, biomass concentration changed only slightly, reaching 6.29 g/L in the TPC and 7.30 g/L in M437Fe.

Since $FeSO_4$ was added after 24 h of cultivation, statistical interpretation of the $FeSO_4$-supplemented variant was focused on the 24–72 h interval. Two-way ANOVA showed that cultivation time significantly affected dry biomass accumulation during this period ($F = 39.17$; $p < 0.001$). Culture type also had a statistically significant effect on the overall biomass level ($F = 38.46$; $p < 0.001$), whereas the "culture × time" interaction was not statistically significant ($F = 0.36$; $p = 0.703$). This indicates that the iron-adapted culture M437Fe generally maintained higher dry biomass values during the post-supplementation period, while the temporal pattern of biomass accumulation remained similar for both cultures.

Pairwise comparisons between the cultures at individual time points during the 24–72 h interval did not reveal statistically significant differences after Holm correction (pHolm = 0.105). Therefore, the higher dry biomass values observed for M437Fe after $FeSO_4$ supplementation should be interpreted as an overall culture-dependent effect confirmed by two-way ANOVA, rather than as statistically significant differences at separate time points.

Comparison of the control and $FeSO_4$-supplemented variants showed that $FeSO_4$ addition was associated with higher mean biomass accumulation, especially for the iron-adapted culture. At 48 h, dry biomass concentration increased from 5.34 to 6.08 g/L for the TPC of *S. cerevisiae* and from 5.87 to 7.15 g/L for *S. cerevisiae* M437Fe. However, after Holm correction, pairwise differences between the control and $FeSO_4$-supplemented variants did not reach statistical significance. For M437Fe at 48 h, the difference showed only a tendency toward significance (pHolm = 0.089).

Thus, based on dry biomass concentration, cultivation time was the main factor determining yeast biomass accumulation in both cultivation variants. $FeSO_4$ supplementation after 24 h was associated with a higher overall biomass level of the iron-adapted culture M437Fe, as confirmed by the significant culture effect in two-way ANOVA for the 24–72 h interval. The absence of a significant culture x time interaction indicates that iron adaptation did not substantially alter the general temporal pattern of biomass accumulation after $FeSO_4$ addition. These results indicate that iron adaptation did not impair biomass formation and may support stable growth of *S. cerevisiae* M437Fe in the presence of an exogenous iron source.

Flotation ability of the TPC and iron-adapted *Saccharomyces cerevisiae*

Since yeast flocculation ability is an important technological characteristic that determines the efficiency of cell separation from the culture broth and may influence the course of fermentation processes, the next stage of the study involved a comparative investigation of the flotation ability of the TPC and iron-adapted cultures.

The flotation ability of the TPC of *Saccharomyces cerevisiae* and *S. cerevisiae* M437Fe was evaluated immediately after cultivation and after an additional 72 h of cell retention in the culture broth (Table 3).

Table 3

Comparative characterization of the flotation ability of iron-adapted and TPC *S. cerevisiae*

Yeast	Cultivation variant	OD (C_p)	OD (C_r)	Flo, %	K_t
Flotation ability immediately after cultivation					
S. cerevisiae M437Fe	without Fe supplementation	1.21±0.03	1.11±0.06	8.3	-
	with Fe supplementation	1.42±0.11	1.24±0.05	14.3	-
TPC *S. cerevisiae*	without Fe supplementation	1.13±0.08	1.13±0.03	0.0	-
	with Fe supplementation	1.23±0.01	1.13±0.08	8.3	-
Flotation ability after 72 h of post-cultivation retention					
S. cerevisiae M437Fe	without Fe supplementation	1.25±0.16	1.11±0.09	20.0	0.24
	with Fe supplementation	1.41±0.11	0.75±0.12	46.4	0.50
TPC *S. cerevisiae*	without Fe supplementation	1.05±0.12	0.95±0.05	9.5	0.14
	with Fe supplementation	1.22±0.10	0.88±0.09	26.6	0.30

Note. OD (C_p) – optical density before flotation; OD (C_r) – optical density after flotation; K_t – coefficient of transition to the flocculated state.

The obtained results showed that the ability of yeast cells to transfer into the foam fraction depended both on the culture type and on the presence of $FeSO_4$ in the cultivation medium. Immediately after cultivation, the flotation ability of both cultures remained low. However, even at this stage, the iron-adapted culture was characterized by a higher proportion of cells transferred to the foam fraction, with $FeSO_4$ supplementation further enhancing this effect. In the TPC, the effect of iron was less evident.

Flocculation is also known to be a physiologically controlled process that intensifies after the completion of active culture growth and is accompanied by the expression of FLO genes and remodeling of the cell surface (Soares, 2011). This is consistent with our results, since the most substantial increase in the proportion of aggregates and flotation ability was observed at the later stages of cultivation. After 72 h of post-cultivation retention, flotation ability increased markedly in both cultures; however, this effect was considerably stronger in the iron-adapted *S. cerevisiae* M437Fe. This was particularly evident during cultivation in the presence of $FeSO_4$, when the proportion of cells transferred to the foam fraction was almost twice as high as that of the TPC.

A similar trend was observed for the coefficient of transition of cells to the flocculated state. In the iron-adapted culture, this coefficient was higher regardless of cultivation conditions and reached its maximum value after growth in the presence of an exogenous iron source. This indicates more intensive removal of cells from the liquid phase and the formation of larger cell aggregates.

The increase in flotation ability after 72 h may be attributed to physiological changes in yeast cells during the late stages of cultivation. Studies have shown that cells in the active growth phase have more hydrophilic surfaces than cells in the stationary phase exhibit higher surface hydrophobicity (Stabnikova et al., 1990, 1991). In *S. cerevisiae*, the transition to the stationary phase is also associated with reduced budding, changes in cell wall structure, and activation of *FLO* gene expression. The resulting flocculins promote cell–cell adhesion and aggregate formation (Seibel et al., 2021; Soares, 2011). Increased surface hydrophobicity and

aggregation during the later stages of cultivation may therefore contribute to enhanced flotation.

An additional factor in the $FeSO_4$-supplemented variants may be the effect of Fe^{2+} ions on the surface properties of yeast cells. Cells in the exponential growth phase exhibit a more negative surface charge, which decreases with aging (Stabnikova et al., 1991). The resulting reduction in electrostatic repulsion, together with increased hydrophobicity, may favor cell adhesion and aggregate formation. In addition, interactions between positively charged Fe^{2+} ions and negatively charged groups on the cell surface may facilitate intercellular contacts and aggregation (Soares, 2011).

A further indirect effect of iron may be associated with its role as a cofactor of enzymes involved in energy metabolism and antioxidant defense. This may support cell viability during the later stages of cultivation and thereby influence flocculation behavior (Soares, 2011).

The observed increase in flotation ability was consistent with the granulometric analysis, which showed a higher proportion of larger cell aggregates in samples cultivated in the presence of $FeSO_4$. Overall, these findings suggest that iron adaptation affects not only Fe accumulation by yeast cells but also their surface properties and intercellular interactions, which may be relevant to the technological processing of yeast biomass.

Thus, the increased flotation ability of the iron-adapted culture *S. cerevisiae* M437Fe indicates that the process of iron adaptation is accompanied by changes in cell surface properties without signs of loss of technological potential. Together with the results of growth and biomass accumulation analyses, these findings support the feasibility of using iron-adapted yeasts as a promising biotechnological agent for obtaining iron-enriched yeast biomass and functional food products.

Analysis of yeast cell and aggregate size by laser diffraction

Laser-based optical methods are increasingly used to characterize yeast cells and their aggregates. In addition to determining the particle size distribution of suspensions, modern approaches involve the analysis of laser scattering patterns combined with machine learning algorithms for high-accuracy identification of different yeast species (Liu et al., 2026). This supports the potential of non-contact optical methods for assessing the dispersed state and other properties of yeast cultures.

The granulometric analysis showed that $FeSO_4$ supplementation altered the dispersed state of yeast suspensions, as evidenced by an increase in characteristic particle sizes and changes in the shape of their distribution (Table 4).

Table 4

Granulometric characteristics of suspensions of the TPC and iron-adapted *S. cerevisiae* yeasts cultivated with and without $FeSO_4$ supplementation

Yeasts	Cultivation variant	Dx (10), μm	Dx (50), μm	Dx (90), μm
S. cerevisiae M437Fe	without Fe supplementation	3.69	5.79	8.98
	with Fe supplementation	3.83	10.80	22.90
TPC *S. cerevisiae*	without Fe supplementation	3.31	5.41	8.91
	with Fe supplementation	4.18	13.20	25.30

In the control variants, when yeasts were cultivated without Fe supplementation, both cultures were characterized by similar granulometric parameters. The Dx(50) and Dx(90) values differed only slightly, indicating a similar dispersed composition of the suspensions in the absence of an exogenous iron source. At the same time, the distribution curves were narrow and showed a single clearly defined maximum, characteristic of the predominance of particles of similar size, approximately 9 μm.

After cultivation in the presence of $FeSO_4$, the distribution pattern changed substantially. In both cultures, Dx(50) and Dx(90) increased almost twofold or more compared with the control, with the effect being slightly stronger in the technically pure culture. In contrast, Dx(10) changed only slightly, indicating relative stability of the fine particle fraction.

The obtained results indicate that $FeSO_4$ supplementation was associated not so much with an increase in the size of individual cells, but rather with changes in the dispersed composition of yeast suspensions and the formation of a larger proportion of aggregated particles, most likely corresponding to cell aggregates. This is supported by the substantial increase in Dx(50) and Dx(90), the relatively minor changes in Dx(10), and the appearance of an additional maximum on the particle size distribution curves.

Similar patterns were described by Patel et al. (2011), who showed that enhanced yeast flocculation is accompanied by the formation of larger and more compact aggregates and is associated with changes in cell surface properties, particularly a reduction in electrostatic repulsion between cells. Although the ζ-potential of the cells was not determined in the present study, the increased proportion of large aggregates in the presence of $FeSO_4$ may indicate a similar enhancement of intercellular interactions.

The application of laser diffraction for the quantitative characterization of yeast flocs has been demonstrated in a study on the particle size distribution of yeast material during flocculation using a Mastersizer analyzer. In that study, a shift in the particle size distribution toward larger diameters was observed, and two fractions with mean sizes of approximately 3 and 25 μm were identified (Radhakrishnan et al., 2018).

The Dx(90) values obtained in the present study were of the same order of magnitude as the larger fraction reported by these authors. However, this comparison is only qualitative, since the cited study analyzed a yeast homogenate supplemented with a polymeric flocculant (Radhakrishnan et al., 2018).

In the present study, the increase in Dx(50) and Dx(90) values, together with the appearance of a second fraction of larger particles, may indicate enhanced cell aggregation in the presence of $FeSO_4$, although the mechanisms underlying this phenomenon require further investigation.

The obtained results are in good agreement with the flotation analysis data. $FeSO_4$ supplementation was accompanied by both an increased proportion of large aggregates and enhanced flotation ability in both cultures. At the same time, despite the slightly higher Dx(50) and Dx(90) values observed for the TPC of *S. cerevisiae*, the iron-adapted culture exhibited higher flotation indices. This indicates that the efficiency of cell transfer into the foam fraction is determined not only by the geometric size of aggregates, but also by their surface properties, the strength of intercellular contacts, and the nature of cell–cell interactions.

Taken together, the results of granulometric and flotation analyses indicate that adaptation of *S. cerevisiae* to iron was not accompanied by a substantial increase in the size of individual cells, but promoted the formation of cell aggregates, which is likely one of the factors contributing to the increased flotation ability of the yeasts.

Fermentative activity, leavening power, and osmotic sensitivity of TPC and iron-adapted yeasts

The functional activity of the TPC of *S. cerevisiae* and the iron-adapted culture *S. cerevisiae* M437Fe was evaluated using a set of parameters directly relevant to the application of yeasts in breadmaking: fermentative, or zymase, activity; leavening power; and osmotic sensitivity (Table 5). Zymase activity characterizes the intensity of alcoholic fermentation and the ability of cells to produce CO_2 during glucose fermentation. A shorter time required to release 10 mL of CO_2 corresponds to higher zymase activity. Leavening power reflects the practical ability of yeasts to ensure gas production in dough (Liu et al., 2025). A shorter time required for dough ball flotation corresponds to higher yeast leavening power, whereas osmotic sensitivity allows assessment of the preservation of fermentative activity under increased osmotic pressure. A lower osmotic sensitivity coefficient indicates higher yeast tolerance to osmotic stress.

Table 5

Fermentative activity, leavening power, and osmotic sensitivity of TPC and iron-adapted *Saccharomyces cerevisiae*

Yeasts	Cultivation variant	t_1, min	t_2, min	t_3, min	K_{osm}
S. cerevisiae M437Fe	without Fe supplementation	42	49.0	66.5	1.35
	with Fe supplementation	22	21.0	24.5	1.10
TPC *S. cerevisiae*	without Fe supplementation	48	70.0	98.0	1.40
	with Fesupplementation	34	45.5	58.0	1.27

Note. t_1 – CO_2 release time for 10 mL; t_2 – dough ball flotation time; t_3 – dough ball flotation time in 3.85% NaCl; K_{osm} – osmotic sensitivity coefficient. Osmotic sensitivity was determined based on the time required for dough ball flotation in a 3.85% NaCl solution.

In terms of zymase activity, cultivation in the presence of $FeSO_4$ was accompanied by an increase in the intensity of alcoholic fermentation in both studied cultures. For the iron-adapted culture *S. cerevisiae* M437Fe, the time required to release 10 mL of CO_2 decreased by 47.6%, whereas for the TPC of *S. cerevisiae* it decreased by 29.2%. Thus, the positive effect of $FeSO_4$ on zymase activity was stronger in M437Fe, which may indicate more intensive utilization of glucose as a fermentation substrate.

A similar pattern was observed for yeast leavening power. In the presence of $FeSO_4$, the time required for dough ball flotation decreased 2.3-fold for M437Fe and 1.5-fold for the TPC of *S. cerevisiae*. Since a shorter dough flotation time corresponds to increased gas-forming activity, the obtained results indicate better technological performance of the iron-adapted culture, especially after cultivation with $FeSO_4$.

The assessment of osmotic sensitivity also demonstrated the advantage of the M437Fe culture. Upon $FeSO_4$ supplementation, the osmotic sensitivity coefficient decreased by 18.5% for M437Fe and by only 9.3% for the TPC of *S. cerevisiae*. A lower value of this coefficient indicates less inhibition of gas formation in a saline medium; therefore, the obtained data point to higher osmotolerance of the iron-adapted culture.

Thus, $FeSO_4$ positively affected the technological properties of both cultures; however, the strongest changes were observed for *S. cerevisiae* M437Fe. This suggests that prior adaptation to iron may have contributed to the formation of a culture with higher fermentative activity, better leavening power, and greater resistance to osmotic load.

The reduced osmotic sensitivity observed in the $FeSO_4$ -supplemented variants may be associated with improved cellular energy supply and maintenance of enzymatic system activity under stress conditions. Under increased osmotic pressure, yeast cells expend part of their energy resources on maintaining water balance, stabilizing membranes, and synthesizing osmoprotectants. Therefore, the ability of cells to maintain gas production in the presence of NaCl is an important indicator of their technological robustness.

The obtained results may be explained by the role of iron in yeast metabolism. Iron is a component of cytochromes, Fe–S proteins, and antioxidant defense enzymes; therefore, its availability may affect cellular respiration, electron transport, ATP generation, and maintenance of metabolic activity during fermentation (Lindahl, 2019; Walker and Stewart, 2016). In the iron-adapted culture, these processes may have been more effectively balanced, which was reflected in faster CO_2 release, better leavening power, and lower osmotic sensitivity.

The higher tolerance of M437Fe to osmotic stress may also be associated with more efficient activation of adaptive mechanisms, particularly the HOG pathway, which regulates the response of yeast cells to increased medium osmolarity. One consequence of this response is the accumulation of glycerol and trehalose, which contribute to the stabilization of proteins, membranes, and intracellular water balance under dehydration and salt stress conditions (Hounsa et al., 1998; de Nadal and Posas, 2022).

Thus, the iron-adapted culture *S. cerevisiae* M437Fe was characterized by higher zymase activity, better leavening power, and lower osmotic sensitivity compared with the TPC of *S. cerevisiae*. Cultivation in the presence of $FeSO_4$ improved all three functional parameters; however, the strongest effect was observed for M437Fe. This indicates that iron adaptation did not impair the technological activity of the yeasts, but, on the contrary, may have enhanced their functional suitability for breadmaking applications.

Effect of TPC and iron-adapted yeasts on dough fermentation

To evaluate the breadmaking activity of the technically pure culture of *S. cerevisiae* and the iron-adapted culture *S. cerevisiae* M437Fe, changes in dough volume were monitored during 3 h of fermentation. This parameter reflects the intensity of yeast gas production and the ability of the dough system to retain CO_2 formed during fermentation.

In the dough sample prepared using *S. cerevisiae* M437Fe, the volume increased from 46 to 136 mL, whereas in the sample containing the TPC of *S. cerevisiae*, it increased from 49 to 134 mL. The absolute volume increase was 90 and 85 mL, respectively (Table 6). Thus, both cultures ensured active gas production in the dough; however, the sample containing iron-adapted yeasts showed a slightly greater increase in volume.

The obtained results are consistent with the data on zymase activity and yeast leavening power. The iron-adapted culture M437Fe was characterized by faster CO_2 release and a shorter dough ball flotation time, which may have contributed to more intensive accumulation of the gas phase during fermentation. At the same time, the difference between the final dough volumes was small; therefore, these data should be interpreted as confirmation that the breadmaking activity of iron-adapted yeasts was maintained, rather than as evidence of a marked improvement in fermentation.

Visual assessment of dough structure showed the formation of more distinct gas pores in the sample containing *S. cerevisiae* M437Fe. This may result from more active CO_2 formation and its retention by the gluten network of the dough. Thus, the use of iron-adapted yeasts did not impair the fermentative properties of the dough and provided a level of gas formation comparable to, or slightly higher than, that of the control sample.

Table 6

Changes in dough volume during fermentation using TPC and iron-adapted *S. cerevisiae*

Yeasts	Cultivation variant	Initial dough volume, mL	Dough volume after 3 h, mL	Volume increase, mL	Volume increase, %
TPC *S. cerevisiae*	without Fe supplementation	49	134	85	173.5
S. cerevisiae M437Fe	with Fe supplementation	46	136	90	195.7

Note. The volume increase was calculated relative to the initial dough volume. The values are presented as experimental indicators for comparison of the fermentative activity of the studied yeasts.

Quality assessment of bread produced using TPC and iron-adapted yeasts

To evaluate the effect of iron-adapted *S. cerevisiae* M437Fe biomass on the quality of the final product, a comparative analysis was performed for bread produced using the TPC of *S. cerevisiae* and iron-enriched iron-adapted yeasts. Organoleptic characteristics, specific volume, shape stability, moisture content, and acidity were assessed (Table 7).

Bread produced using *S. cerevisiae* M437Fe was characterized by a higher specific volume compared with the control sample: 2.8 versus 2.3 cm^3/g. This is consistent with the results obtained for zymase activity, leavening power, and dough fermentation, where the iron-adapted culture demonstrated higher gas-forming activity. The more developed crumb porosity in the M437Fe sample may also be associated with more intensive CO_2 production during fermentation.

The results showed that the use of iron-adapted yeasts did not lead to changes in crumb moisture or to the formation of an excessively moist and sticky texture in the final product. The acidity of bread produced with M437Fe was lower than that of the control sample, which may indicate differences in the course of fermentation processes and the accumulation of acidic metabolites.

The shape stability of bread produced with *S. cerevisiae* M437Fe was 0.49, compared with 0.59 in the control sample. Both values substantially exceeded the normative level for hearth bread; therefore, the observed difference should be interpreted not as a weakening of the structural and mechanical properties of the dough, but rather as a change in the commercial appearance of the product. The flour used was characterized by a high content and satisfactory quality of wet gluten (30.20%, gluten deformation index 61.2 units), which enabled the gluten network to retain a considerably larger gas volume than that produced by the TPC yeasts. As a result, the control sample had an excessively convex shape ($H/D > 0.5$), approaching a hemispherical form, which is not typical of hearth bread.

The increased gas-forming capacity of the iron-adapted strain was confirmed by a 21.7% increase in dough specific volume and a 5.3% increase in porosity. The product acquired a shape typical of hearth bread while maintaining an adequate shape stability margin relative to the normative requirement (Figure 3).

Organoleptic assessment showed that bread produced with iron-adapted yeasts had a more pronounced porous crumb structure. In the M437Fe sample, a weak metallic aftertaste was noted after prolonged chewing, which may be associated with the increased iron content in the yeast biomass.

Table 7

Organoleptic and physicochemical quality parameters of bread produced using TPC and iron-adapted *S. cerevisiae*

Parameter	Bread produced with the TPC *S. cerevisiae*	Bread produced with iron-enriched *S. cerevisiae* M437Fe
Shape and surface	Regular shape, surface without cracks or ruptures	Regular shape, surface without cracks or ruptures
Crust colour	Golden-yellow	Golden-yellow
Crumb colour	White	White with a slight greyish shade
Crumb condition	Well-baked, elastic crumb with small, uniformly distributed pores	Well-baked, elastic crumb with uniformly distributed medium-sized pores
Odour	Characteristic bread odour, without any off-odour	Characteristic bread odour, without any off-odour
Taste	No bitter or sour aftertaste	No bitter or sour aftertaste; a weak metallic aftertaste was noted after prolonged chewing
Specific volume, mL/g	2.3	2.8
Shape stability	0.59	0.49
Moisture content, %	42.0	42.0
Acidity, degrees	3.6	2.4
Porosity, %	76	80
Crust colour:		
L*	56.53	53.2
a*	10.58	8.95
b*	17.65	14.6
ΔE	-	4.8
Crumb colour:		
L*	70.22	67.74
a*	-0.56	1.72
b*	14.10	10.88
ΔE	-	4.66

According to the organoleptic assessment, the crust colour of both samples was the same, namely golden-yellow; therefore, no qualitative differences were detected by visual inspection. However, the colorimetric parameters revealed objective differences between the samples. In bread produced with the M437Fe strain, all three parameters decreased: L* (from 56.53 to 53.20), a* (from 10.58 to 8.95), and b* (from 17.65 to 14.60). The decrease in L* indicates darkening of the crust, while the simultaneous decrease in a* and b* indicates reduced colour saturation. Thus, the crust became a slightly darker and less saturated, or more muted, version of the same golden colour, which may result from the catalytic acceleration of the Maillard reaction by iron ions (Nowosad and Sujka, 2021). The total colour difference, ΔE = 4.8, corresponds to a difference that may be noticeable when the samples are carefully compared side by side, although according to the general organoleptic scale it remains within the golden-yellow colour category.

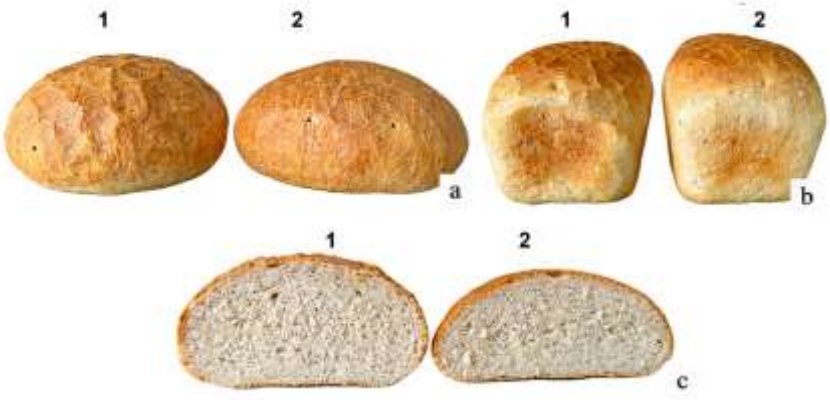

Figure 3. Bread samples:
a – hearth bread; b – pan bread; c – bread cross-section;
1 – bread produced using the TPC *S. cerevisiae* yeasts;
2 – bread produced using iron-adapted *S. cerevisiae* M437Fe yeasts

Analysis of the crumb showed that the difference was more evident in this part of the product. The control sample was described as white, whereas the sample produced with M437Fe was described as white with a slight greyish shade. Colorimetric analysis confirmed this observation: L* decreased from 70.22 to 67.74, indicating crumb darkening, while chroma decreased from approximately 14.1 to 11.0 units, i.e., by approximately 22%, indicating that the colour became more neutral and desaturated. Notably, a* shifted from a negative value of −0.56, corresponding to a slight greenish shade, to a positive value of +1.72, while b* decreased markedly from 14.10 to 10.88. This indicates a shift in hue from a purely yellowish or cream tone toward a warmer, muted brownish nuance against the background of overall darkening and desaturation. The combination of lower lightness, reduced saturation, and a slight warm-grey undertone was perceived sensorially as a greyish shade. The change in crumb colour may be associated with carotenoid oxidation and the formation of iron–phenolic complexes, leading to darkening and loss of the natural yellowish tone of the crumb.

Thus, the use of the iron-enriched, iron-adapted culture *S. cerevisiae* M437Fe enabled the production of bread with a higher specific volume, more developed porosity, and preservation of the main physicochemical quality parameters. At the same time, the appearance of a weak metallic aftertaste indicates the need for further optimization of the amount of iron-enriched biomass incorporated into the bread formulation in order to combine increased iron content with acceptable sensory characteristics.

In vitro bioaccessible iron fraction from bread produced using iron-adapted yeasts

The *in vitro* bioaccessible iron fraction was assessed in two bread samples: the control sample produced using the TPC *S. cerevisiae* and the experimental sample produced using the iron-enriched, iron-adapted culture *S. cerevisiae* M437Fe (Table 8). The control sample was used to account for the background content of endogenous iron in bread, whereas the experimental sample was used to evaluate the release of iron associated with yeast biomass into the soluble fraction after simulated digestion using the INFOGEST method.

To further assess the nutritional value of the experimental sample, the theoretical iron content in the daily bread portion was calculated. According to the dough formulation, which included 100 g of flour, 3 g of yeast, 1.5 g of salt, and 50 g of water, the total dough mass was 154.5 g. Taking into account technological losses during baking of 14%, the mass of the final bread was 132.87 g. Accordingly, this amount of bread contained 2.58 g of yeast. Assuming consumption of 277 g of bread, the amount of yeast in the daily portion was 5.37 g. Since the iron content in the iron-adapted yeasts was 16.20 mg/g, the theoretical total iron content in the daily bread portion was 86.99 mg.

Atomic absorption spectrometry showed that, for bread produced using *S. cerevisiae* M437Fe yeasts, the proportion of iron released into the soluble fraction after INFOGEST digestion was 72.3 ± 0.7%. This indicates that most of the iron accumulated by the yeast biomass and incorporated into the bread matrix was released into a soluble form after sequential oral, gastric, and intestinal digestion.

Taking into account the theoretically calculated total iron content in the daily bread portion, the amount of iron corresponding to the soluble fraction after INFOGEST digestion was:

$$86.99 \times 0.723 = 62.89 \text{ mg}$$

Thus, for the theoretical daily bread portion of 277 g, the amount of iron released into the soluble fraction after *in vitro* digestion was 62.89 mg. This value should be interpreted strictly as a theoretical, model-based estimate of iron released into the soluble fraction under in vitro INFOGEST conditions. It does not represent the amount of iron absorbed in vivo and should not be considered a recommended daily intake level.

Table 8

Parameters of iron release into the soluble fraction from bread after INFOGEST digestion

Sample	Theoretical total Fe content in the daily bread portion, mg	Proportion of Fe in the soluble fraction, %	Fe content in the soluble fraction, mg
Bread produced with iron-enriched *S. cerevisiae* M437Fe	86.99	72.3 ± 0.7	62.89

The obtained value indicates a high release of iron into the soluble fraction under *in vitro* digestion conditions and suggests that iron associated with yeast biomass largely retained its bioaccessibility in the digestion model. These results support the feasibility of further investigating iron-adapted *S. cerevisiae* yeasts as an ingredient for bakery products enriched with biogenic iron.

Conclusions

The iron-adapted yeast strain *Saccharomyces cerevisiae* M437Fe retained its ability to grow and accumulate biomass in the presence of $FeSO_4$. The observed growth characteristics indicated that iron adaptation did not negatively affect yeast growth under the conditions studied.

The iron-adapted culture *S. cerevisiae* M437Fe exhibited higher technological activity than the technically pure culture, as evidenced by increased fermentative activity and leavening power, together with reduced osmotic sensitivity. $FeSO_4$ supplementation further enhanced these properties.

The use of the iron-adapted M437Fe culture promoted the formation of larger cell aggregates and increased yeast flotation ability. The combined granulometric and flotation characteristics

indicate changes in the dispersed state and intercellular interactions of yeast cells in the presence of $FeSO_4$.

Application of the M437Fe strain in bread production increased the specific volume and crumb porosity of the bread while maintaining the main physicochemical quality parameters. At the same time, the weak metallic aftertaste detected in the product indicates the need for further optimization of the amount of iron-adapted biomass added to the formulation.

After *in vitro* digestion of bread produced using the M437Fe strain, $72.3 \pm 0.7\%$ of iron was released into the soluble fraction, indicating high iron bioaccessibility under the applied digestion model.

The obtained results support the feasibility of using iron-adapted *S. cerevisiae* M437Fe as a functional ingredient for the production of bakery products enriched with biogenic iron.

Acknowledgments. The authors gratefully acknowledge Andrii Marynin, Head of the Problem Research Laboratory, for providing access to the Mastersizer 3000 instrument and conducting particle size analysis of the samples.

References

Abdul Majeed, S., Said, S., Hassan, D. A., Sadiq, F., Alhosani, M., Al-Jawaldeh, A., El-Obeid, T., & Tayyem, R. (2025). Evaluating the effectiveness and risks of bread fortification programs in the Middle Eastern region: A comprehensive review. *Frontiers in Public Health, 13*, 1-13. https://doi.org/10.3389/fpubh.2025.1530380

Bondar, H., & Krasinko, V. (2025). Rapid spectrophotometric method for the determination of iron content in yeast. *Ukrainian Journal of Food Science, 13*, 80–90, https://doi.org/10.24263/2310-1008-2025-13-1-9

Bondar, H., & Krasinko, V. (2026). Iron accumulation in yeast under different cultivation conditions. *Ukrainian Food Journal, 15*(2), 518–531. https://doi.org/10.24263/2304-974X-2026-15-2-14

Chen, Y., Pang, Y., Wan, H., Zhou, X., Wan, M., Li, S., & Liu, X. (2024). Production of iron-enriched yeast and its application in the treatment of iron-deficiency anemia. *BioMetals, 37*(4), 1023–1035. https://doi.org/10.1007/s10534-024-00592-3

Ciont, C., Mesaroș, A., Pop, O. L., & Vodnar, D. C. (2023). Iron oxide nanoparticles carried by probiotics for iron absorption: A systematic review. *Journal of Nanobiotechnology, 21*(1), 124. https://doi.org/10.1186/s12951-023-01880-9

Drobot, V. I., Yurchak, V. H., Bilyk, O. A., Bondarenko, Yu. V., & Hryshchenko, A. M. (2015). Technochemical control of raw materials and bakery and pasta products. Kyiv, Kondor.

Garces, V., Rodriguez-Nogales, A., Gonzalez, A., Galvez, N., Rodriguez-Cabezas, M. E., Garcia-Martin, M. L., Gutierrez, L., Rondon, D., Olivares, M., Galvez, J., & Dominguez-Vera, J. M. (2018). Bacteria-carried iron oxide nanoparticles for treatment of anemia. *Bioconjugate Chemistry, 29*(5), 1785–1791. https://doi.org/10.1021/acs.bioconjchem.8b00245

Hounsa, C. G., Brandt, E. V., Thevelein, J., Hohmann, S., & Prior, B. A. (1998). Role of trehalose in survival of *Saccharomyces cerevisiae* under osmotic stress. *Microbiology, 144*(3), 671-680. https://doi.org/10.1099/00221287-144-3-671

Jarzębski, M., Wieruszewski, M., Kościński, M., Rogoziński, T., Kobus-Cisowska, J., Szablewski, T., Perła-Kaján, J., Waszkowiak, K., & Jakubowicz, J. (2023). Heme iron as potential iron fortifier for food application – Characterization by material techniques. *Reviews on Advanced Materials Science, 62*, 20230128–20230142. https://doi.org/10.1515/rams-2023-0128

Kiskini, A., Kapsokefalou, M., Yanniotis, S., & Mandala, I. (2010). Effect of different iron compounds on wheat and gluten-free breads. *Journal of the Science of Food and Agriculture, 90*, 1136–1145. https://doi.org/10.1002/jsfa.3927

Minekus, M., Alminger, M., Alvito, P., Ballance, S., Bohn, T., Bourlieu, C., Carrière, F., Boutrou, R., Corredig, M., Dupont, D., Dufour, C., Egger, L., Golding, M., Karakaya, S., Kirkhus, B., Le Feunteun, S., Lesmes, U., Macierzanka, A., Mackie, A., Marze, S., McClements, D. J., Ménard, O., Recio, I., Santos, C. N., Singh, R. P., Vegarud, G. E., Wickham, M. S., Weitschies, W., & Brodkorb, A. (2014). A standardised static in vitro digestion method suitable for food: An

international consensus. *Food & Function, 5*(6), 1113–1124. https://doi.org/10.1039/C3FO60702J

Lindahl, P. A. (2019). A comprehensive mechanistic model of iron metabolism in *Saccharomyces cerevisiae*. *Metallomics*, *11*(11), 1779-1799. https://doi.org/10.1039/c9mt00199a

Liu, J., Yang, L., Wang, Y., Wang, M., Qian, Q., Lou, L., Wu, Z., Zhu, J., Fu, X., Xing, J., Tu, Y., & Liu, Y. G. (2025). Effect of mixed yeast strains and additives on the quality of long-term refrigerated fermented doughs. *Foods, 14*(5), 717. https://doi.org/10.3390/foods14050717

Liu, X., Shankarnarayan, S., Cheng, Z., Gupta, M., Rozmus, W., Mandal, M., Charlebois, D. A., & Tsui, Y. Y. (2026). Machine Learning-Assisted Classification of Pathogenic Yeasts Using Laser Light Scattering and Conventional Microscopy. *Journal of Imaging*, *12*(3), 136. https://doi.org/10.3390/jimaging12030136

de Nadal, E., & Posas, F. (2022). The HOG pathway and the regulation of osmoadaptive responses in yeast. *FEMS Yeast Research, 22*(1), foac013. https://doi.org/10.1093/femsyr/foac013

Nikolaou, A., Assunção, R., Cvetković, B., Fardet, A., Gamero, A., Gandía, M., Mojsova, S., Yilmaz, B., Kütt, M. L., Santa, D., Chassard, C., Praćer, S., Vergères, G., Karakaya, S., & Syrpas, M. (2026). Effects of sourdough- or regular-bread fermentation, and phytate reduction on iron bioavailability, absorption, and iron status in humans: A systematic review of intervention studies. *Frontiers in Nutrition, 13*, 1-14. https://doi.org/10.3389/fnut.2026.1778997

Norton, V., Rodriguez-Garcia, J., Wagstaff, C., Lovegrove, A., Shewry, P., Charlton, M., Gillett, N., Tindall, M., Prins, A., & Lignou, S. (2025). Exploring the relationship between physical properties and sensory characteristics of newly developed white breads with improved nutritional composition: Initial insights. *LWT*, 230, 118297. https://doi.org/10.1016/j.lwt.2025.118297

Nowosad, K., & Sujka, M. (2021). The use of iron-enriched yeast for the production of flatbread. *Molecules, 26*(17), 5204. https://doi.org/10.3390/molecules26175204

Palmieri, M. C., Greenhalf, W., & Laluce, C. (1996). Efficient flotation of yeast cells grown in batch culture. *Biotechnology and Bioengineering, 50*(3), 248–256. https://doi.org/10.1002/(sici)1097-0290(19960505)50:3%3c248::aid-bit3%3e3.0.co;2-g

Patel, J. K., Speers, R. A., & Lake, J. C. (2011). Colloidal examination of worts associated with premature yeast flocculation. *Journal of the American Society of Brewing Chemists, 69*(2), 81–90. https://doi.org/10.1094/ASBCJ-2011-0225-01

Radhakrishnan, A. N. P., Marques, M. P. C., Davies, M. J., O'Sullivan, B., Bracewell, D. G., & Szita, N. (2018). Flocculation on a chip: A novel screening approach to determine floc growth rates and select flocculating agents. *Lab on a Chip, 18*(4), 585–594. https://doi.org/10.1039/C7LC00793K

Rengifo, E., Vela-Paredes, R., Rios-Mera, J. D., Cabrera, F., Saldaña, E., Guerra, W., Arce, T., Vásquez, J., Vásquez, J., & Tello Célis, F. (2025). Nutritional value and acceptability of heme iron microparticles-fortified bread. *CyTA - Journal of Food, 23*(1), 2502533. https://doi.org/10.1080/19476337.2025.2502533

Rodriguez-Ramiro, I., Brearley, C. A., Bruggraber, S. F., Perfecto, A., Shewry, P., & Fairweather-Tait, S. (2017). Assessment of iron bioavailability from different bread making processes using an in vitro intestinal cell model. *Food Chemistry, 228*, 91–98. https://doi.org/10.1016/j.foodchem.2017.01.130

Seibel, K., Schmalhaus, R., Haensel, M., & Weiland, F. (2021). Molecular basis and regulation of flocculation in *Saccharomyces cerevisiae* and *Saccharomyces pastorianus*: A review. *BrewingScience, 74*(3/4), 39–50. https://doi.org/10.23763/BrSc21-03seibel

Skrotska, O., Kharchenko, Y., Laziuka, Y., Marynin, A., & Kharchuk, M. (2021). Biosynthesis and characterictics of silver nanoparticles obtained using *Saccharomyces cerevisiae* M437. *Ukrainian Food Journal, 10*(3), 615-631. https://doi.org/10.24263/2304-974X-2021-10-3-14

Skrotska, O., Protsenko, M., Zholobko, M., & Marynin, M. (2025). Biosynthesis and characterization of selenium nanoparticles by *Saccharomyces cerevisiae* M437, *Ukrainian Journal of Food Science, 13*(1), 91-110. https://doi.org/10.24263/2310-1008-2025-13-1-10

Soares, E. V. (2011). Flocculation in *Saccharomyces cerevisiae*: A review. *Journal of Applied Microbiology, 110*(1), 1–18. https://doi.org/10.1111/j.1365-2672.2010.04897.x

Stabnikova, E. V., Gordienko, A. S., Ksenofontov, B. S., Poberezhniy, V. Y., Stavskaya, T. Z., & Ivanov, V. N. (1991). *Interaction between the cells and water–air interface*. Naukova Dumka.

Stabnikova, E. V., Polyatevich, E. V., Pindrus, A. A., & Ivanov, V. N. (1990). Flotation, hydrophobicity, and survival of yeast cells of different ages. *Microbiological Journal, 52*(2), 46–50.

Stabnikova, O., Stabnikov, V., Antoniuk, M., Arsenieva, L., & Ivanov, V. (2022). Bakery products enriched with organoselenium compounds. In O. Paredes-López, V. Stabnikov, O. Shevchenko, & V. Ivanov (Eds.), *Bioenhancement and fortification of foods for a healthy diet* (pp. 89–111). CRC Press. https://doi.org/10.1201/9781003225287

Tafazzoli, K., Ghavami, M., & Khosravi-Darani, K. (2024). Production of iron-enriched *Saccharomyces boulardii*: Impact of process variables. *Scientific Reports, 14*, 4844. https://doi.org/10.1038/s41598-024-55433-7

Tsykhanovska, I., Lazarieva, T., Stabnikova, O., Kupriyanov, O., Litvin, O., & Yevlash, V. (2023). Potential benefits of functional antianemic energy bars. *Ukrainian Food Journal, 12*(4), 578–598. https://doi.org/10.24263/2304-974X-2023-12-4-7

Tsykhanovska, I., Stabnikova, O., Oliinyk, S., Lazarieva, T., & Gubsky, S. (2024). Application of combined food additive based on iron oxide nanoparticles and kombu in a rye-wheat bread technology. *Ukrainian Food Journal, 13*(3), 576–596. https://doi.org/10.24263/2304-974X-2024-13-3-10

Verheyen, C., Albrecht, A., Elgeti, D., Jekle, M., & Becker, T. (2015). Impact of gas formation kinetics on dough development and bread quality. *Food Research International*, 76(3), 860–866. https://doi.org/10.1016/j.foodres.2015.08.013

Walker, G. M., & Stewart, G. G. (2016). *Saccharomyces cerevisiae* in the production of fermented beverages. *Beverages, 2*(4), 30. https://doi.org/10.3390/beverages2040030

World Health Organization. (2017). *Nutritional anaemias: Tools for effective prevention and control*. World Health Organization. https://www.who.int/publications/i/item/9789241513067

Xing, Y., Gao, S., Zhang, X., & Zang, J. (2022). Dietary heme-containing proteins: Structures, applications, and challenges. *Foods*, *11*(22), 3594–3614. https://doi.org/10.3390/foods11223594

Zhu, F., Sakulnak, R., & Wang, S. (2016). Effect of black tea on antioxidant, textural, and sensory properties of Chinese steamed bread. *Food Chemistry*, 194, 1217–1223. https://doi.org/10.1016/j.foodchem.2015.08.110

Zielińska-Dawidziak, M., Białas, W., Piasecka-Kwiatkowska, D., Staniek, H., & Niedzielski, P. (2023). Digestibility of protein and iron availability from enriched legume sprouts. *Plant Foods for Human Nutrition, 78*(2), 270–278. https://doi.org/10.1007/s11130-023-01045-x

Cite:

Bondar, H., Parkhomova, O., Krasinko, V., & Bilyk, O. (2026). Biotechnological potential of iron-adapted *Saccharomyces cerevisiae* for producing bakery products enriched with bioaccessible iron. *Ukrainian Food Journal, 15*(3), 847–870. https://doi.org/10.24263/2304-974X-2026-15-3-15

Current advances in biosynthesis of selenium nanoparticles using microorganisms

Oksana Skrotska, Oleksandr Zholobko, Maria Protsenko, Iryna Kovshar

National University of Food Technologies, Kyiv, Ukraine

Keywords:

Selenium
Nanoparticle
Biosynthesis
Microorganism
Biotechnology
Food product

Article history:

Received 10.10.2025
Received in revised form 16.04.2026
Accepted 30.06.2026

Corresponding author:

Oksana Skrotska
E-mail: skrotskaoi@nuft.edu.ua

DOI:
10.24263/2304-974X-2026-15-3-16

Abstract

Introduction. Biogenic selenium nanoparticles are characterized by a wide range of biological properties that make them promising for application in the food industry. One promising approach for their production is microbial biosynthesis using microorganisms from different taxonomic groups, including bacteria, fungi, yeasts, and archaea.

Materials and methods. The present review was based on a systematic examination of scientific publications indexed in international bibliographic databases. The analysis included the collection, critical evaluation, comparison, and synthesis of research findings related to the biosynthesis of selenium nanoparticles. The review primarily covered studies published from 2020 to 2026.

Results and discussion. Microorganisms are used for the biosynthesis of selenium nanoparticles due to their ability to transform toxic inorganic selenium compounds into elemental selenium. The biosynthesis of nanoparticles can occur intracellularly or extracellularly and involves various microbial metabolites, including proteins, enzymes, polysaccharides, and low-molecular-weight compounds. Bacteria remain the most extensively studied group of microorganisms for the biosynthesis of selenium nanoparticles. At the same time, yeasts and fungi have significant potential due to the diversity of their metabolic activities and their ability to produce biomolecules that influence the formation and functional properties of nanoparticles. Archaea are a relatively understudied but promising group of microorganisms for the biosynthesis of selenium nanoparticles. The efficiency of microbial synthesis, as well as the physicochemical characteristics and biological properties of the resulting nanoparticles, depends on the microorganism species and strain, the mechanisms of selenium reduction, the localization of the process, and the biosynthesis conditions. Analysis of current studies highlights the potential of microorganisms as biological systems for producing functional selenium nanoparticles with specific properties. Particular attention is given to their potential applications in the food industry, where their antioxidant and antimicrobial properties may be used in functional foods, selenium-enriched products, and active packaging materials, as well as in technologies aimed at improving food quality and extending shelf life.

Conclusions. The results of the review highlight the potential of microorganisms for the environmentally safe production of functional selenium nanoparticles and provide a basis for optimizing biosynthesis conditions and their further application in the food industry.

Introduction

Selenium nanoparticles (SeNPs) attract considerable attention from researchers due to their combination of high biological activity, relatively low toxicity, and a wide range of potential practical applications. Their physicochemical and functional properties differ significantly from those of traditional inorganic and organic forms of selenium, which is attributed to their nanoscale size, high surface-area-to-volume ratio, morphological features, and surface functionalization. Therefore, in recent years, the number of studies on the development of various methods for SeNP synthesis and the investigation of their potential applications in different fields has increased significantly (Jothinathan et al., 2025; Ruiz-Fresneda et al., 2023; Zhang et al., 2023).

The use of SeNPs in the food industry is of particular interest. Selenium is an essential trace element necessary for the functioning of the body's antioxidant system. Therefore, SeNPs have potential for use in functional food products and active packaging materials aimed at extending food shelf life (Ao et al., 2023; Ndwandwe et al., 2021).

At the same time, most review papers on SeNPs have a broad interdisciplinary focus. They mainly consider physical, chemical, and biological methods for the synthesis of SeNPs, as well as their physicochemical properties, biological activity, and potential biomedical applications (Sampath et al., 2024; Ullah et al., 2022). Although microorganisms are often presented as one of the possible biological systems for SeNP synthesis (Escobar-Ramírez et al., 2021), comparative information on the use of bacteria, yeasts, fungi, and archaea for SeNP biosynthesis remains scattered across the literature.

The relationships among the properties of microorganisms, biosynthesis conditions, and the characteristics of SeNPs also require further systematization (Sarkar et al., 2023). The concentration and chemical form of the selenium precursor, pH, temperature, duration, and other biosynthesis parameters can significantly affect the nucleation, growth, and stabilization of nanoparticles (Senthamarai et al., 2024).

Thus, there is a need for a comprehensive review considering microorganisms from different taxonomic groups, including bacteria, fungi, yeasts, and archaea, as biological systems for the synthesis of SeNPs. Systematization of data on the diversity of microorganisms, mechanisms of bioreduction, biosynthesis conditions, and the properties of the resulting nanoparticles may contribute to a better understanding of microbial SeNP synthesis and the development of controlled and scalable biotechnologies. This is particularly relevant in view of the potential use of biogenic selenium nanoparticles in the food industry for selenium enrichment of products, the development of functional food systems and active packaging materials, and technologies aimed at extending food shelf life.

Materials and methods

The search and analysis of scientific sources were conducted using the international scientometric databases Scopus, Web of Science, ScienceDirect, PubMed, and Google Scholar. Scientific articles published between 2020 and 2026 were primarily used for the preparation of this review, focusing on the biosynthesis of selenium nanoparticles using microorganisms, including bacteria, fungi, yeast and archaea. Full texts of relevant articles were obtained for further assessment. The selected publications were analyzed according to the following criteria: type of biological material, conditions of nanoparticle biosynthesis, nanoparticle size and morphology, nanoparticle properties, and their potential practical applications. The obtained experimental data were systematized and summarized in order to identify different strategies for the biosynthesis of selenium nanoparticles and the prospects for their practical application in food technology.

Results and discussion

Bacteria for the biosynthesis of selenium nanoparticles

Bacteria of the genus *Acinetobacter*

An analysis of scientific studies published over the past 5–6 years identified three studies addressing the biosynthesis of selenium nanoparticles (SeNPs) using bacteria of the genus *Acinetobacter*. The limited number of studies may be related to the fact that some representatives of this genus are pathogenic, form persistent biofilms, and exhibit multidrug resistance to antibiotics (Shi et al., 2024).

The strain *Acinetobacter* sp. SX5 has been investigated as a potential agent for environmental bioremediation. This strain was isolated from selenium-rich soil in Anhui, China, and exhibited high resistance to sodium selenite. At a selenite concentration of 10 mM, its growth was nearly indistinguishable from that of the control. When *Acinetobacter* sp. SX5 was used for SeNP biosynthesis, spherical nanoparticles were obtained, with their size increasing from 143.8 to 374.1 nm over 12–36 h of biosynthesis. The enzymes arsenate reductase and NAD(P)-dependent alcohol dehydrogenase were identified as playing a key role in SeNP biosynthesis (Huang et al., 2025).

Isolates of the pathogenic bacterium *A. baumannii* were obtained from biological samples collected from individuals with burns and wound infections (Salman et al., 2024). These bacteria produce a bacteriocin-like inhibitory substance, bumanniicin. This compound was used for the cell-free biosynthesis of SeNPs, during which bacteriocin molecules acted as both reducing and stabilizing agents. As a result, spherical SeNPs with an average diameter of 81.23 nm were obtained (Salman et al., 2025).

Bacteria of the genus *Bacillus*

Recent scientific literature contains numerous studies on the biosynthesis of selenium nanoparticles using bacteria of the genus *Bacillus* (Table 1).

Selenium-reducing *Bacillus* strains have been isolated from a wide range of contaminated environments and waste materials, including heavy metal-contaminated soils, industrial effluents, mining waste dumps, mine drainage waters, electronic waste disposal sites, and fermented agricultural wastes. Examples include *B. subtilis* AL43 and AS12, *B. cabrialesii* Se1, *B. paramycoides* SP3 and MF-14, *B. cereus* YB1806, and *B. subtilis* SE201412 (Abdel-Moneim et al., 2022; Borah et al., 2021; Ghosh et al., 2025; Hossny et al., 2025; Huang et al., 2023; Saad et al., 2022; Yadav et al., 2023). Several of these strains demonstrate high tolerance to selenite and the ability to reduce selenium oxyanions to elemental selenium. For example, *B. paramycoides* SP3 exhibited tolerance to selenite concentrations of up to 1000 mM, whereas *Bacillus subtilis* SE201412 tolerated selenite concentrations of up to 66,000 mg/L (Borah et al., 2021; Huang et al., 2023). Wastewater and sewage sludge have also been used as sources of selenium-reducing *Bacillus* strains, including *B. niabensis* OAB2 and other *Bacillus* spp. capable of intracellular SeNP accumulation (Al-Hagar et al., 2021).

Marine environments represent another source of selenium-reducing *Bacillus* strains. The high salinity, fluctuating temperatures, and elevated osmotic pressure characteristic of these environments may select for microorganisms with enhanced tolerance to selenium oxyanions. *B. amyloliquefaciens* SRB04 was isolated from the coastal zone of the Caspian Sea and was capable of reducing selenite to elemental selenium under aerobic conditions (Ashengroph & Hosseini, 2021). *Bacillus* sp. Q33, isolated from marine sediments of the Arctic Ocean, demonstrated a high rate of selenite reduction and tolerance to concentrations exceeding 100 mM (Zhang et al., 2022a). A moderately halophilic strain, *Bacillus* sp. D54, isolated from saline soils, was also capable of intracellular SeNP synthesis (Abdollahnia et al., 2020).

Table 1

Biosynthesis of selenium nanoparticles using bacteria of the genus *Bacillus*

Bacteria	Biosynthesis conditions	Characteristics of nanoparticles	Reference
Bacillus amyloliquefaciens Endo 4	Liquid culture, 8 mM Na_2SeO_3, 30 °C, 96 h, 150 rpm	Spherical, 122.31 nm (DLS), 22–89 nm (TEM), zeta potential -7.3 mV, PDI 0.334	Ibrahim et al., 2025
Bacillus amyloliquefaciens SRB04	Biomass, 2 mM Na_2SeO_3, 30 °C, 60 h	Spherical, 45.4–68.3 nm (DLS)	Ashengroph and Hosseini, 2021
Bacillus altitudinis LH18	Liquid culture, 5 mM Na_2SeO_3, 37 °C, 48 h, 180 rpm, pH 7.0	Spherical, 228.5 nm (DLS), zeta potential -31.5 mV, PDI 0.412	Li et al., 2024a
Bacillus cereus YB1806	Liquid culture, 300 mg/L Na_2SeO_4, 30 °C, 48 h, 200 rpm, pH 7.0	Spherical, 76.1 nm (TEM), 48–115 nm (FESEM)	Ghosh et al., 2025
Bacillus coagulans	Cell-free supernatant, 4 mM Na_2SeO_3, 40 °C, 3 h, 350 rpm	Spherical, 70–120 nm, zeta potential -16.1 mV, PDI 0.279	Khaledizade et al., 2024
Bacillus cabrialesii Se1	Liquid culture, 7.6 g/L Na_2SeO_4, 3.6 g/L sodium lactate, 31 °C, 240 h, 150 rpm, pH 7.8	Spherical, 19.9–25 nm (TEM)	Hossny et al., 2025
Bacillus licheniformis F1	Liquid culture, 100 mM/L Na_2SeO_3, 37 °C, 48 h, 180 rpm	Spherical, 110–170 nm (SEM), zeta potential -46.59 mV	Wang et al., 2024c
Bacillus megaterium ATCC55000	Cell-free supernatant, 1 mM Na_2SeO, 25 °C, 48 h	Spherical, 45.9 nm (DLS), 29.72–74.36 nm (TEM)	Hashem et al., 2021a
Bacillus niabensis OAB2	Liquid culture, 20 mM Na_2SeO_4, 30 °C, 72 h, 1 kGy of gamma irradiation	Rod-shaped, 399,4 nm, zeta potential -19.5 mV	Al-Hagar et al., 2021
Bacillus paramycoides 24522	Liquid culture, 2 mM Na_2SeO_3, 37 °C, 24 h, 140 rpm, pH 6.0	Spherical, 150 nm (DLS), 100–180 nm (SEM), zeta potential -29.9 mV	Liu et al., 2023
Bacillus paramycoides MCCC 1A04098	Cell-free supernatant 20 mL, 20 mL 4 mM SeO_2, 25 kGy of gamma irradiation	Spherical, 118.6 nm (DLS), 18.27–21.72 nm (TEM)	El Refai et al., 2024
Bacillus paramycoides MF-14	Liquid culture, 5 mM Na_2SeO_3, 35 °C, 48 h, 150 rpm	Spherical, 703.98 nm (DLS), zeta potential -30.9 mV	Yadav et al., 2023
Bacillus paramycoides SP3	Liquid culture, 10 mM Na_2SeO_3, 30 °C, 48 h, 150 rpm	Spherical, 149.1 nm (DLS), 120–170 nm (SEM), zeta potential -29.9 mV	Borah et al., 2021
Bacillus paralicheniformis Y4	Liquid culture, 50 mM Na_2SeO_3, 37 °C, 48 h, 180 rpm, pH 7.0	Spherical, 70–120 nm (SEM), zeta potential -35.8 mV	Wang et al., 2022d
Bacillus subtilis AL43	Liquid culture, 1–2 mM Na_2SeO_3, 30 °C, 24 h, 150 rpm, pH 7.2	Spherical, 65.24 nm (DLS), 45–80 nm (TEM), zeta potential -22.7 mV	Abdel-Moneim et al., 2022
Bacillus subtilis AS12	Liquid culture, 5 mM Na_2SeO_3, 30 °C, 48 h, 180 rpm, pH 7.0	Spherical, 77.47 nm (DLS), 25–85 nm (TEM), zeta potential -26.33 mV	Saad et al., 2022

Bacillus subtilis BSN313	Liquid culture, 200 μg/mL Na_2SeO_3, 37 °C, 24 h, 200 rpm, pH 7.0	Spherical, 530 nm (DLS), 280–630 nm (TEM), zeta potential -26.9 mV	Ullah et al., 2021
Bacillus subtilus DA20	Cell-free supernatant, 6 mM Na_2SeO_3, 30 °C, 72 h, 180 rpm	Spherical, 56 nm (DLS), 20–65 nm (TEM), zeta potential -22.35 mV	Al-Quwaie, 2023
Bacillus subtilis L11	Liquid culture, 4 mM Na_2SeO_3, 37 °C, 48 h, 180 rpm, pH 6.0	Spherical, 50–200 nm (TEM/SEM)	Guo et al., 2024
Bacillus subtilis NT147	Liquid culture, 0.5 mM Na_2SeO_3, 37 °C, 18–24 h, 150 rpm	Spherical, 335.2 nm (TEM)	Likidtaveesin et al., 2025
Bacillus subtilis SE201412	Liquid culture, 500 mg/L Na_2SeO_3, 30 °C, 18–24 h, 190 rpm, pH 6.0	Spherical, 126 nm	Huang et al., 2023
Bacillus subtilis T5	Liquid culture, 5 mM Na_2SeO_3, 37 °C, 48 h, 200 rpm	Spherical, 167.8 nm (DLS), 100–200 nm (SEM), zeta potential -31.1 mV	Duan et al., 2022
Bacillus sp. B2	Cell-free supernatant, 5 mM Na_2SeO_3, 18-20 °C, 2–3 h	Spherical, 33.2 nm (XRD), 20–50 nm (SEM)	Bharathi et al., 2020
Bacillus sp. D54	Liquid culture, 5 mM Na_2SeO_3, 40 °C, 168 h, 150 rpm	Spherical, 161.9 nm (DLS), 141.7 nm (SEM), zeta potential -29.34 mV, PDI 0.36	Abdollahnia et al., 2020
Bacillus sp. EKT1	Cell-free supernatant, 6.4 mM SeO_2, 33 °C, 72 h, 120 rpm, pH 9.0	Spherical, 31–335 nm (FESEM), mean size 126 nm	Akcay & Avci, 2020
Bacillus sp. Q33	Liquid culture, 5 mM Na_2SeO_3, 33 °C, 48 h, 180 rpm	Spherical, 159.2 nm, zeta potential -42.0 mV	Zhang et al., 2022a

Note: DLS, dynamic light scattering; FESEM, field-emission scanning electron microscopy; PDI, polydispersity index; SEM, scanning electron microscopy; TEM, transmission electron microscopy; XRD, X-ray diffraction.

Endophytic *Bacillus* bacteria combine selenium biotransformation with other potentially useful properties, including plant growth promotion and biocontrol activity. The strain *B. amyloliquefaciens* Endo 4 was isolated from wheat (*Triticum aestivum*) roots and demonstrated high tolerance to selenite and the ability to produce SeNPs (Ibrahim et al., 2025). Such strains may have potential for applications involving selenium biotransformation in plant-associated systems.

Several studies have also investigated *Bacillus* strains obtained from food and feed-related sources. *B. subtilis* BSN313, isolated from the traditional Chinese starter culture Jiuqu, demonstrated selenium reduction at concentrations up to 200 μg/mL (Ullah et al., 2021). *B. subtilis* T5 exhibited high selenite tolerance and simultaneous production of SeNPs and selenium-containing polysaccharides (Duan et al., 2022). *Bacillus licheniformis* F1 was investigated for SeNP biosynthesis using low-cost substrates such as corn and soybean flour (Wang et al., 2024c). *B. subtilis* NT147, isolated from fermented soybeans, produced intracellular spherical SeNPs (Likidtaveesin et al., 2025). In addition, *B. subtilis* L11, isolated from fermented feed, produced SeNPs mainly in the periplasmic space, on the cell membrane, and within the cell wall. The complex of L11 cells and SeNPs has been investigated as a feed additive to enhance animal immunity (Guo et al., 2024).

Bacteria of the genus *Enterococcus*

Bacteria of the genus *Enterococcus* belong to a large group of lactic acid bacteria that includes members of the normal human microbiota, probiotic strains, and opportunistic pathogens

(Krawczyk et al., 2021). *Enterococcus* strains used for the biosynthesis of SeNPs have been isolated from various ecological niches, including humans, animals, and food products. The strain *E. durans* A8-1, which demonstrated a high capacity for intracellular SeNP biosynthesis, was isolated from fecal samples of a healthy infant (Liu et al., 2022). *Enterococcus* spp. strains were also isolated from a selenium-containing medium (Tendenedzai et al., 2022).The strain *E. faecium* MC-5 was isolated from the intestine of mirror carp (Tilwani et al., 2023), indicating the potential of aquatic-derived enterococci for SeNP biosynthesis. The strain *E. durans* LAB18s was isolated from traditional Brazilian cheese. The strains *E. faecalis* CH121 and CH124 have been investigated for selenium enrichment of dairy and fermented products because of their ability to convert soluble selenium forms into nanoparticulate selenium (Liu et al., 2022).

Enterococci are characterized by relatively high resistance to selenium compounds compared with many other lactic acid bacteria. For example, *E. faecium* CCDM 922A did not show significant growth inhibition at a sodium selenite concentration of 100 mg/L. Certain enterococcal strains have also been reported to tolerate selenium concentrations exceeding 600 mg/L (Hyrslova et al., 2022).

Bacteria of the genus *Halomonas*

Bacteria of the genus *Halomonas* can adapt to extreme environmental conditions and reduce toxic selenium ions to elemental selenium. Representatives of this genus capable of SeNP biosynthesis have been isolated from diverse natural ecosystems (Table 2).

Table 2

Biosynthesis of selenium nanoparticles using bacteria of the genus *Halomonas*

Bacteria	Biosynthesis conditions	Characteristics of nanoparticles	Reference
Halomonas boliviensis H-10	Liquid culture, 1 mM Na_2SeO_3, 25 °C, 24 h	Spherical, 80–300 nm (TEM)	Bravo et al., 2024
Halomonas elongata (IBRC-M 10433)	Cell-free supernatant, 0.8 mg/mL Na_2SeO_3, 30 °C, 48 h, 140 rpm	Spherical, 5–25 nm (TEM), 11 nm (SEM)	Safaei et al., 2022
Halomonas elongata QW6 He10214	Liquid culture, 8 mM Na_2SeO_3, 30 °C, 72 h, 150 rpm, pH 7.2	Spherical, 50–100 nm (TEM), zeta potential -51.2 mV	Tabibi et al., 2023
Halomonas eurihalina	Liquid culture, 5 mM Na_2SeO_3, 40 °C, 24 h	Spherical, 200–400 nm (DLS), PDI 0.2	Shakeri et al., 2022
Halomonas venusta GUSDM4	Liquid culture, 4 mM Na_2SeO_3, 25 °C, 34 h, 150 rpm, pH 7.0	Spherical, 20–80 nm (TEM)	Vaigankar et al., 2022
Halomonas sp. SF2000	Liquid culture, 5 mM Na_2SeO_3, 37 °C, 48 h, 150 rpm, pH 7.3	Spherical, 351.3 nm (DLS), 200–500 nm (TEM), zeta potential -47.8 mV	Liu et al., 2025

Note: DLS, dynamic light scattering; PDI, polydispersity index; SEM, scanning electron microscopy; TEM, transmission electron microscopy.

These strains have been isolated from diverse environments, including saline lakes, desert regions, high-altitude salt flats, industrial wastewater, and selenium-enriched organic fertilizers. *Halomonas elongata* QW6 IBRC-M 10,214 and *H. eurihalina* were isolated from saline environments (Shakeri et al., 2022; Tabibi et al., 2023). The strain *H. boliviensis* H-10 was isolated from a salt flat in the Atacama Desert, Chile (Bravo et al., 2023). In addition to natural habitats, *H. elongata* was isolated from textile industry wastewater, whereas *Halomonas* sp. SF2000 was isolated from selenium-enriched organic fertilizer (Liu et al., 2025).

Representatives of the genus *Halomonas* are characterized by high resistance to sodium selenite. For example, *H. venusta* GUSDM4 tolerates selenite concentrations of up to 100 mM (Vaigankar et al., 2022), whereas *H. boliviensis* H-10 demonstrates resistance to concentrations of up to 128 mM (Bravo et al., 2024). The highest reported tolerance was observed for *Halomonas* sp. SF2000, which retained the ability to grow and synthesize SeNPs at selenite concentrations of up to 1200 mM (Liu et al., 2025).

Lactic acid bacteria

Following the 2020 phylogenomic revision, the former broad genus *Lactobacillus* was divided into several genera, including *Lactiplantibacillus* and *Limosilactobacillus*, while *Lactobacillus* remained a separate genus (Qiao et al., 2022). Recent studies have increasingly focused on the biogenic synthesis of selenium nanoparticles using safe and environmentally friendly microorganisms (Stabnikova et al., 2023). Lactic acid bacteria are of particular interest due to their widespread use in food fermentation and their potential as probiotic microorganisms for the development of functional foods (Starovoitova et al., 2023, 2024), as well as for the synthesis of metal nanoparticles (Gregirchak et al., 2023; Stabnikov et al., 2025). Their ability to reduce selenite and form stable SeNPs makes them promising biological systems for selenium biotransformation and nanoparticle production (Ghosh et al., 2022). At the same time, the efficiency of SeNP biosynthesis by lactic acid bacteria depends largely on strain-specific characteristics and process parameters, emphasizing the importance of producer selection and optimization of biosynthesis conditions to obtain nanoparticles with specific properties (Khonkiv et al., 2026). Their ability to reduce selenite and form stable SeNPs makes them promising biological systems for selenium biotransformation and nanoparticle production (Ghosh et al., 2022), as summarized in Table 3.

Table 3

Biosynthesis of selenium nanoparticles using lactic acid bacteria (*Lactobacillus, Lactiplantibacillus, and Limosilactobacillus*)

Bacteria	Biosynthesis conditions	Characteristics of nanoparticles	Reference
Lactobacillus acidophilus	Cell-free supernatant, 15 mM Na_2SeO_3, 37 °C, 48 h	Spherical, 34.13 nm (DLS), 2–15 nm (TEM), zeta potential +37.86 mV, PDI 0.28	Alam et al., 2020
Lactobacillus casei 393	Liquid culture, 200 µg/mL Na_2SeO_3, 37 °C, 24 h	150–200 nm (TEM)	Sendani et al., 2024
Lactobacillus casei 6904	Cell-free supernatant, 4 mM Na_2SeO_3, 40 °C, 3 h, 350 rpm	Spherical, mean size 90.78 nm (DLS), zeta potential -17.3 mV, PDI 0.28	Haji Mehdi Nouri et al., 2024
Lactobacillus casei ATCC 393	Liquid culture, 20 mg/mL $NaHSeO_3$, 37 °C, 96 h	Spherical, 170–550 nm (SEM)	Spyridopoulou et al., 2021
Lactobacillus casei ZK-AS 1.1482	Liquid culture, 0.17 mg/mL Na_2SeO_3, 37 °C, 48 h	Spherical, 52–103 nm (SEM), zeta potential -20 mV, PDI 0.239	Xu et al., 2023
Lactobacillus delbrueckii subsp. *bulgaricus* CICC 20247	Liquid culture, 1 mg/mL Na_2SeO_3, 37 °C, 48–60 h, 120 rpm	Spherical, 20–180 nm, mean size 92.4 nm (TEM/SEM)	Wang et al., 2025

Lactobacillus paracasei HM1	Liquid culture, 4 mM Na_2SeO_3, 35 °C, 32 h, 160 rpm, pH 6	Spherical, mean size 56.91 nm (DLS), 3–50 nm (TEM), zeta potential -20.1 mV	El-Saadony et al., 2021
Lactobacillus reuteri	Liquid culture, 15 µg/mL Na_2SeO_3, 37 °C, 10 h, 200 rpm, pH 7	Spherical, 70–110 nm, mean size 80 nm (TEM), zeta potential -25 mV	Sun et al., 2024b
Lactiplantibacillus pentosus S1	Liquid culture, 100 mg/mL $NaHSeO_3$, 37 °C, 72 h, 120 rpm	Spherical, 40.5–95.02 nm (TEM), PDI 0.31	Fadel et al., 2025
Lactiplantibacillus plantarum CXG-4	Liquid culture, 16 µg/mL Na_2SeO_3, 37 °C, 24 h	Spherical, 35–240 nm (TEM)	Li et al., 2025c
Lactiplantibacillus plantarum KNF-5	Liquid culture, 100 µg/mL Na_2SeO_3, 37 °C, 36 h	Spherical, mean size 270 nm (SEM), zeta potential -38.79 mV, PDI 0.432	Si et al., 2024
Lactiplantibacillus plantarum NML21	Liquid culture, 200 mg/L Na_2SeO_3, 34 °C, 30 h	Spherical, mean size 160 nm, zeta potential -37.82 mV	Wang et al., 2024b
Limosilactobacillus fermentum ATCC 14931	Cell-free supernatant, 0.75 mM $Na_2SeO_3 \times 5 H_2O$, 37 °C, 72 h, pH 7.4	Spherical, mean size 92.52 nm (DLS), zeta potential -32.2 mV, PDI 0.134	Aminisough et al., 2024
Limosilactobacillus fermentum OR553490	Cell-free supernatant, 5 mM Na_2SeO_3, 37 °C, 72 h, 150 rpm	Rod-shaped, 17–30 nm (TEM), zeta potential -11.8 mV	Mohamed and El-Zahed, 2024

Note: DLS, dynamic light scattering; PDI, polydispersity index; SEM, scanning electron microscopy; TEM, transmission electron microscopy.

The data presented in Table 3 show that lactic acid bacteria can produce SeNPs under a wide range of cultivation conditions and using different selenium precursors. Most studies used sodium selenite (Na_2SeO_3), although the applied concentrations, cultivation temperatures, and incubation times varied considerably among strains. SeNPs were predominantly spherical, with particle sizes ranging from several nanometers to several hundred nanometers. Differences in particle size and surface charge indicate that the properties of the resulting SeNPs are strongly influenced by the microorganism strain and biosynthesis conditions.

Among the studied lactic acid bacteria, *Lactobacillus*, *Lactiplantibacillus*, and *Limosilactobacillus* demonstrated the ability to reduce selenium oxyanions and accumulate or release SeNPs. The reported results indicate that strain selection and optimization of cultivation conditions are important for controlling selenium transformation and the physicochemical characteristics of the resulting nanoparticles.

Bacteria of the genus *Lactobacillus*

The strains of *Lactobacillus* used for SeNP biosynthesis have been isolated from various sources, including fermented dairy products. For example, *L. acidophilus* was isolated from fermented dairy products such as curd, yogurt, and fermented milk and investigated as an industrial starter culture (Alam et al., 2020). The strain *L. reuteri* is a natural inhabitant of the gastrointestinal tract of humans and animals and has been investigated for its ability to biosynthesize SeNPs (Sun et al., 2024b). The strain *L. paracasei* HM1 was isolated from human breast milk and demonstrated the ability to produce SeNPs (El-Saadony et al., 2021).

The toxicity of selenium ions, particularly selenite (Se^{4+}) and selenate (Se^{6+}), is an important factor affecting the ability of lactic acid bacteria to biosynthesize SeNPs. Sodium selenite is a toxic selenium compound that can induce oxidative stress and disrupt cellular redox balance (Wang et al., 2025). In response to selenium stress, some lactic acid bacteria can reduce selenium oxyanions to elemental selenium, resulting in the formation and accumulation of SeNPs. This process may represent an adaptive response to selenium exposure. Lactobacillus strains generally show moderate resistance to sodium selenite, with concentrations of approximately 1–15 mM reported in the literature, whereas higher concentrations may inhibit growth and metabolic activity (Spyridopoulou et al., 2021).

Bacteria of the genus *Lactiplantibacillus*

Representatives of *Lactiplantibacillus* and *Lactobacillus* were previously classified within a single genus, *Lactobacillus*. However, in 2020, following a phylogenomic revision, the taxonomy was restructured, and the genus was divided into several new taxa, including *Lactiplantibacillus* (Qiao et al., 2022). Bacteria of the genus *Lactiplantibacillus* are typical representatives of the microbiota of fermented products and are considered promising agents for selenium biotransformation (Table 3). From traditional fermented products of the Gannan Tibetan area, the strains *L. plantarum* NML21 and NML22 were isolated; these strains demonstrated tolerance to selenium ions and high efficiency in biotransforming them into SeNPs. In particular, the strain *L. plantarum* NML21 retains metabolic activity and the ability to form selenium nanoparticles at sodium selenite concentrations of 500 mg/L (Wang et al., 2024b). During the study of traditional Chinese fermented foods, among 69 isolated strains, a high-performing strain, *L. plantarum* CXG-4, was identified and characterized for enhanced selenium biotransformation into nanoparticles (Li et al., 2025c).

Plant materials also serve as a common source of *Lactiplantibacillus* isolates. In particular, the highly tolerant strain *L. plantarum* BSe was isolated from citrus fruits. These bacteria exhibit ultra-high resistance to selenium ions and can grow and convert selenium at concentrations up to 100 mM/L (Zhong et al., 2024b).

Cow's milk is another source of novel strains with selenium-reducing activity. From it, strains of *L. pentosus* and *L. plantarum* were isolated, capable of reducing selenium ions to the elemental state, leading to nanoparticle formation (Fadel et al., 2025).

Bacteria of the genus *Limosilactobacillus*

Bacteria of the genus *Limosilactobacillus* are widely distributed in nature and include species associated with milk and dairy products (Qiao et al., 2022).

An analysis of the scientific literature from 2020 to 2026 indicates that studies on the biosynthesis of SeNPs using bacteria of this genus are scarce, with only two relevant publications identified (Table 3). Available data suggest that *Limosilactobacillus* strains can tolerate certain concentrations of selenium ions and participate in their biotransformation. However, selenium concentrations above 5 mM may negatively affect cellular metabolism and reduce the efficiency of nanoparticle biosynthesis (Mohamed and El-Zahed, 2024).

Bacteria of the genera *Lysinibacillus* and *Paenibacillus*

Bacteria of the genus *Lysinibacillus* belong to the family *Bacillaceae* and were previously classified within the genus *Bacillus*. They were later reclassified as a separate genus based on differences in cell wall composition and phylogenetic characteristics. Representatives of the genus *Paenibacillus* were also formerly classified within *Bacillus* but were separated into a distinct genus in 1993 based on 16S rRNA phylogenetic analysis (Jamal and Ahmad, 2022).

Bacteria of the genera *Lysinibacillus* and *Paenibacillus* used for the biosynthesis of selenium nanoparticles have been isolated from a wide range of natural and anthropogenically influenced environments, including soils, plant rhizosphere, food products, and wastewater treatment systems (Table 4).

Table 4

Biosynthesis of selenium nanoparticles using bacteria of the genera *Lysinibacillus* and *Paenibacillus*

Bacteria	Biosynthesis conditions	Characteristics of nanoparticles	Reference
Lysinibacillus sp. NOSK	Cell-free supernatant, 1 mM $Na_2SeO_3 \times 4\ H_2O$, 37 °C, 48 h, 150 rpm, pH 10	Spherical, 130 nm (DLS), zeta potential -26.3 mV, PDI 0.27	San Keskin et al., 2020
Lysinibacillus odysseyi PP112153	Cell-free supernatant, 15 mM Na_2SeO_3, 37 °C, 48 h	Spherical, 85.8 nm (DLS), zeta potential -70.1 mV	Mangudi and Pappu, 2025
Lysinibacillus sphaericus RS3E	Cell-free supernatant, 10 mM Na_2SeO_3, 35 °C, 72 h	Spherical, 16.7 nm (TEM/SEM)	Babajide et al., 2025
Lysinibacillus xylanilyticus DS3, *Lysinibacillus macrolides* DS15	Liquid culture, 1 mM Na_2SeO_3, 35 °C, 36 h, 180 rpm	Spherical, 80–200 nm, mean size 162 nm (SEM)	Zhang et al., 2019
Paenibacillus motobuensis LY5201	Liquid culture, 5 g/L Na_2SeO_3, 37 °C, 24 h, 200 rpm	Spherical, 130.4 nm (DLS), 100 nm (TEM), zeta potential -21.6 mV, PDI 0.227	Long et al., 2023
Paenibacillus polymyxa MS 411	Liquid culture, 4 mM Na_2SeO_3, 30 °C, 48 h, 220 rpm	Spherical, 26 nm (DLS), zeta potential -25 mV	Alsulami and El-Saadony, 2023
Paenibacillus terreus	Liquid culture, 1 mM Na_2SeO_3, 37 °C, 6–48 h, 150 rpm	Spherical, 200–220 nm (DLS), 220–240 nm (FESEM), zeta potential -37.44 mV, PDI 0.265	Nile et al., 2023

Note: DLS, dynamic light scattering; PDI, polydispersity index; SEM, scanning electron microscopy; TEM, transmission electron microscopy

The strains *Lysinibacillus xylanilyticus* DS3 and *L. macrolides* DS15 were isolated from selenium-rich tea plantation soils and demonstrated high tolerance to selenite, up to 120 and 220 mmol/L, respectively (Zhang et al., 2019). *L. sphaericus* RS3E was isolated from the rhizosphere of *Samanea saman* (Babajide et al., 2025), while *Lysinibacillus* sp. NOSK was obtained from a wastewater treatment system (San Keskin et al., 2020).

The strain *Paenibacillus polymyxa* MS 411 was isolated from the maize rhizosphere and demonstrated the ability to synthesize SeNPs with anticoccidial properties (Alsulami & El-Saadony, 2023). *P. motobuensis* LY5201 was isolated from fermented cabbage and tolerated selenite concentrations of up to 173 mmol/L (Long et al., 2023).

Bacteria of the genus *Proteus*

The genus *Proteus* includes motile bacteria widely distributed in the environment, including soil and water, as well as in the intestinal microbiota of humans and animals. These microorganisms are considered opportunistic pathogens. *Proteus* strains capable of SeNP biosynthesis have been isolated from various natural environments. In particular, *P. mirabilis* QZB-2 (Huang et al., 2022) and *P. penneri* LAB-1 (Wang et al., 2022b) were isolated from selenium-rich soils. The strain *Proteus* sp. YS02 was also isolated from selenium-rich soil (Wang et al., 2022c) (Table 5).

Table 5

Biosynthesis of selenium nanoparticles using bacteria of the genera *Proteus*, *Providencia* and *Pseudomonas*

Bacteria	Biosynthesis conditions	Characteristics of nanoparticles	Reference
Proteus sp. YS02	Liquid culture, 5 mM Na_2SeO_3, 30 °C, 24 h, 180 rpm	Spherical, mean size 140 nm (DLS), zeta potential -34.2 mV	Wang, et al., 2022c
Proteus mirabilis PQ350419	Cell-free supernatant, 5 mM Na_2SeO_3, 35 °C, 72 h, 150 rpm, pH 6	Spherical, 88–98 nm (TEM), zeta potential -24.27 mV	Elshikiby et al., 2025
Proteus mirabilis QZB-2	Liquid culture, 2 mM Na_2SeO_3, 30 °C, 18 h, 150 rpm	Spherical, mean size 152 nm (DLS)	Huang et al., 2022
Proteus penneri LAB-1	Liquid culture, 2 mM Na_2SeO_3, 30 °C, 18 h, 150 rpm, pH 7	Spherical, mean size 274.9 nm (DLS)	Wang et al., 2022b
Providencia sp. BM-2	Liquid culture, 2 mM Na_2SeO_3, 30 °C, 36 h, 150 rpm, pH 7	Spherical, 210–222 nm (DLS), 100–150 nm (SEM), zeta potential -43.02 mV	Li et al., 2025b
Providencia sp. DCX	Liquid culture, 2 mM Na_2SeO_3, 30 °C, 48 h	Spherical, 120 nm (DLS), 46–333 nm (TEM), zeta potential -25.6 mV	Zhang et al., 2021
Providencia rettgeri HF16	Liquid culture, 5 mM Na_2SeO_3, 30 °C, 24 h, 180 rpm, pH 7	Spherical, 120–295 nm (DLS), zeta potential -23.5 mV	Huang et al., 2021
Pseudomonas libanensis SDKVG 28	Liquid culture, 4 mM Na_2SeO_3, 32 °C, 48 h	Spherical, 50–150 nm (SEM)	Sonali et al., 2024
Pseudomonas putida KT2440	Liquid culture, 1 mM Na_2SeO_3, 30 °C, 24 h, 150 rpm	Spherical, 90–120 nm (TEM)	Hosseini et al., 2025
Pseudomonas stutzeri MH191156	Liquid culture, 2 mM Na_2SeO_3, 37 °C, 48 h, pH 6.5	Spherical, 75–200 nm (SEM), zeta potential -46.2 mV	Rajkumar et al., 2020

Note: DLS, dynamic light scattering; PDI, polydispersity index; SEM, scanning electron microscopy; TEM, transmission electron microscopy

Representatives of the genus *Proteus* exhibit very high tolerance to selenium ions, particularly selenite (SeO_3^{2-}), making them among the most resistant microorganisms to this compound. However, at elevated concentrations, selenite exerts toxic effects by inhibiting bacterial growth and metabolic activity. The level of tolerance depends on the species and specific strain. For example, *P. mirabilis* QZB-2 can tolerate selenite concentrations up to 300 mM (Huang et al., 2022). For the strain *P. mirabilis* PQ350419, high concentrations (40-50 mM) significantly inhibit biosynthetic processes, whereas an optimal concentration for growth and nanoparticle synthesis is around 5 mM (Elshikiby et al., 2025). Even higher resistance is observed in *P. penneri* LAB-1, which tolerates up to 500 mM selenite. For comparison, most other selenium-reducing bacteria typically exhibit tolerance limits of no more than 100 mM (Wang et al., 2022b).

Bacteria of the genus *Providencia*

Bacteria of the genus *Providencia* are opportunistic enterobacteria widely distributed in the environment. Representatives of this genus capable of SeNP biosynthesis have been isolated from various natural sources (Table 5). In particular, the strain *Providencia* sp. DCX was isolated from coastal marine sediments (Zhang et al., 2021). The highly selenite-tolerant strain *P. rettgeri* HF16 was isolated from coal mine soil (Huang et al., 2021), while *Providencia* sp. BM-2 was isolated from selenium-rich soil (Li et al., 2025b).

Representatives of the genus *Providencia* demonstrate high resistance to selenium ions, particularly selenite (SeO_3^{2-}). For example, *P. rettgeri* HF16 tolerated selenite concentrations of up to 800 mM (Huang et al., 2021), while *Providencia* sp. BM-2 tolerated concentrations of up to 400 mM (Li et al., 2025b).

The high resistance of these bacteria to selenium ions may be associated with efficient detoxification mechanisms. Selenite reduction can generate reactive oxygen species and induce oxidative stress, leading to activation of protective enzymes involved in maintaining cellular redox homeostasis. An important detoxification mechanism is the reduction of toxic selenite (Se^{4+}) to elemental selenium (Se^0), accompanied by SeNP formation. This process may involve sulfite reductase and increased availability of reducing equivalents through the pentose phosphate pathway (Huang et al., 2021).

Bacteria of the genus *Pseudomonas*

Bacteria of the genus *Pseudomonas* capable of biosynthesizing selenium nanoparticles have been isolated from various sources (Table 5). The strain *Pseudomonas stutzeri* MH191156 was isolated from freshwater (Rajkumar et al., 2020), while *P. putida* KT2440 is a typical soil microorganism (Avendano et al., 2023). The strain *P. libanensis* SDKVG 28 was isolated from the rhizosphere of tea and coffee plants (Sonali et al., 2024). *P. aeruginosa* strains capable of SeNP biosynthesis were isolated from clinical samples from individuals with wounds and burns. These bacteria are opportunistic pathogens commonly associated with the respiratory, gastrointestinal, and urogenital tracts (Jassim & Al-Shibly, 2024).

The studied *Pseudomonas* strains demonstrate moderate to high resistance to selenium ions. In studies involving *P. aeruginosa* and *P. putida*, sodium selenite concentrations of 1–5 mM were used for SeNP biosynthesis. The highest tolerance among the strains considered was reported for *P. libanensis* SDKVG 28, which tolerated sodium selenite concentrations of up to 20 mM (Sonali et al., 2024).

Bacteria of the genus *Staphylococcus*

The genus *Staphylococcus* comprises bacteria, many of which are pathogenic or opportunistic human pathogens (Touaiti et al., 2025). Their pathogenicity may explain the limited number of studies investigating their use as bioagents for the synthesis of selenium nanoparticles. Moreover, in most studies, the investigated strains were isolated from clinical samples. A review of recent scientific literature revealed only a few publications reporting the biosynthesis of SeNPs using *Staphylococcus* species.

In studies using *Staphylococcus aureus* (MTCC 96), the minimum inhibitory concentration (MIC) of sodium selenate (Na_2SeO_4) was determined to be 75 mM. At this concentration, approximately 40% of cells remain viable, indicating relatively high tolerance to selenium compounds. *Staphylococcus* species can survive at elevated metal ion concentrations due to various adaptive mechanisms, including efflux systems (active ion export), extracellular complexation, and specific metal transport systems (Sahoo et al., 2023).

Two approaches to SeNPs biosynthesis have been investigated: using whole bacterial cells (Salimi et al., 2024) or their metabolic products – bacteriocins, or bacteriocin-like inhibitory substances (Fawzi and Ahmed, 2025). The biosynthesis conditions and the size of the resulting selenium nanoparticles differ depending on the approach (Table 6).

Table 6

Biosynthesis of selenium nanoparticles using bacteria of the genus *Staphylococcus*

Bacteria	Biosynthesis conditions	Characteristics of nanoparticles	Reference
Staphylococcus aureus	Liquid culture, 0.1 M Na_2SeO_3, 37 °C, 48 h, 150 rpm	Spherical, 119.59 nm (SEM), zeta potential -77.4 mV	Salimi et al., 2024
Staphylococcus aureus (MTCC 96)	Liquid culture, 75 mM Na_2SeO_3, 37 °C, 48 h, 120 rpm	Spherical, 119 nm (FESEM), zeta potential -47.1 mV	Sahoo et al., 2023
Staphylococcus warneri F7	20 mL bacteriocin, 1.5 g Na_2SeO_3, 37 °C, 48 h	Spherical, 48.59 nm (AFM)	Fawzi & Ahmed, 2025

Note: SEM, scanning electron microscopy; FESEM, field-emission scanning electron microscopy; AFM, Atomic Force Microscopy.

Bacteria of the genus *Streptomyces*

Actinobacteria of the genus *Streptomyces* used for SeNPs biosynthesis are isolated from diverse natural habitats, primarily soils and marine ecosystems (Table 7).

Table 7

Biosynthesis of selenium nanoparticles using bacteria of the genus *Streptomyces*

Bacteria	Biosynthesis conditions	Characteristics of nanoparticles	Reference
Streptomyces sp.	Cell-free supernatant, 4 mM Na_2SeO_3, 37 °C, 48 h	Spherical, 20–100 nm (TEM), zeta potential -40 mV	Shawky et al., 2025
Streptomyces sp. M10A65	Biomass, 1 mM Na_2SeO_3, 28 °C, 48 h	Spherical, 20–150 nm (FESEM/ AFM), 100 nm (DLS)	Ramya et al., 2020
Streptomyces sp. MA4	Cell-free supernatant, 5 mM Na_2SeO_3, 24 h	Spherical, 50–70 nm (SEM)	Sumithra et al., 2023
Streptomyces diastaticus KA-21	Cell-free supernatant, 1 mM H_2SeO_3, 2 mM ascorbic acid, 37 °C, 24 h	Spherical, 130 nm (DLS), 8–21 nm (TEM), zeta potential -25 mV, PDI 0.326	Kalpana et al., 2025b
Streptomyces microflavus	Cell-free supernatant, 1 mM H_2SeO_3, 27 °C, 24 h	Spherical, 224.1 nm (DLS), 7–36 nm (TEM), zeta potential -28.7 mV, PDI 0.328	Kalpana et al., 2025a
Streptomyces parvulus MAR4	Cell-free supernatant, 4 mM Na_2SeO_3, 37 °C, 48 h	Spherical, mean size 196.2 nm (DLS), 48.8–129 nm (TEM), zeta potential +37.08 mV, PDI 0.252	Hassan et al., 2024
Streptomyces vinaceusdrappus AMG31	Cell-free aqueous extract, 5 mM Na_2SeO_3, 40 °C (1 h), 25 °C (12 h), pH 8	Spherical, 460.1 nm (DLS), 20–80 nm (TEM), zeta potential -37.9 mV, PDI 0.384	Ghareeb et al., 2025

Note: DLS, dynamic light scattering; FESEM, field-emission scanning electron microscopy; AFM, Atomic Force Microscopy; PDI, polydispersity index; SEM, scanning electron microscopy; TEM, transmission electron microscopy.

Strains of the genus *Streptomyces* have been isolated from various environments. The strain *S. diastaticus* KA-21 was isolated from soil samples collected in India. *Streptomyces* sp. M10A65 was obtained from magnesite mine soil characterized by high alkalinity and elevated temperatures, representing an extreme environment for microbial life (Ramya et al., 2020). The strain *Streptomyces* sp. MA4 was isolated from coastal marine sediments (Sumithra et al., 2023). From Red Sea sediments, *S. parvulus* MAR4 (Hassan et al., 2024) and *S. vinaceusdrappus* AMG31 (Ghareeb et al., 2025) were isolated. Marine actinobacteria are considered promising microorganisms for the biogenic synthesis of SeNPs due to their ability to produce a wide range of secondary metabolites (Ramya et al., 2020).

Selenium ions can exert toxic effects on *Streptomyces* species. In most studies, *Streptomyces* strains maintain viability and the ability to reduce selenium at concentrations of 1–5 mM. In particular, *S. vinaceusdrappus* AMG31 (Ghareeb et al., 2025) and *Streptomyces* sp. MA4 (Sumithra et al., 2023) effectively reduced selenium salts at a concentration of 5 mM. The tolerance of *Streptomyces* strains to selenium may be influenced by their ecological origin, as strains isolated from environments with high levels of chemical stress may exhibit greater tolerance to metals and metalloids.

Cyanobacteria

Cyanobacteria are a group of photosynthetic prokaryotic microorganisms that play an important role in biotechnology due to their high metabolic activity and ability to synthesize a wide range of biologically active compounds. They produce photosynthetic pigments, including phycocyanin, phycoerythrin, chlorophylls, and carotenoids (Saad et al., 2024), as well as various proteins, vitamins, and polysaccharides. The surface polysaccharides of cyanobacteria contain functional groups, including hydroxyl and carboxyl groups, which can interact with metal ions (Abbas et al., 2021). Cyanobacteria also produce secondary metabolites, including alkaloids, amines, phenolic compounds, and polyunsaturated fatty acids. The biosynthesis of selenium nanoparticles by cyanobacteria (Table 8) may represent an adaptive response to selenium exposure, as these organisms can detoxify toxic selenium ions by reducing them to elemental selenium (Nowruzi et al., 2023).

Table 8

Biosynthesis of selenium nanoparticles using cyanobacteria

Bacteria	Biosynthesis conditions	Characteristics of nanoparticles	Reference
Alborzia kermanshahica	Cell-free aqueous extract, 1 mM Na_2SeO_3, magnetic fields 60 mT, 32 °C, 24 h	Spherical, 87.7 nm (DLS), zeta potential -40.5 mV, PDI 0.338	Eydelkhani et al., 2024
Anabaena sp. PCC 7120	Biomass, 1 mM Na_2SeO_3, 24 °C, 72 h	Spherical, 5–50 nm (TEM)	Pandey et al., 2021
Anabaena variabilis NCCU-441	Cell-free aqueous extract, 1 mM Na_2SeO_3, 30 °C, 24 h	Spherical, 6.4–15.8 nm, mean size 10.8 nm (TEM)	Afzal et al., 2021
Desmonostoc alborizicum 1387	Cell-free aqueous extract, 5 mM Na_2SeO_3, 60 °C, 10 min	Spherical, 58.77 nm (DLS), 29.4–110 nm (TEM), zeta potential +22.7 mV, PDI 0.635	Nowruzi et al., 2023
Leptolyngbya sp. SSI24	Phycocyanin extract, 2 mM $Na_2SeO_3 \times 5\ H_2O$, 30 °C, 48 h, 120 rpm, pH 7.2	Spherical, 44.45–209 nm (TEM), zeta potential -17 mV, PDI 0.1	Saad et al., 2024
Spirulina platensis (abdf2224)	Liquid culture, 8 mM Na_2SeO_3, 25 °C, 168 h (24 h dark / 24 h light), 120 rpm, pH 7	Spherical, 145 nm (DLS), 100 nm (SEM), zeta potential -50.4 mV, PDI 1.3	Alipour et al., 2021
Spirulina platensis	Supernatant of cell lysate, 10 mM Na_2SeO_3, 30 °C, 72 h	Spherical, 255 nm (DLS), mean size 79.4 nm (TEM), zeta potential -32.9 mV	Abbas et al., 2021
Spirulina platensis	Cell-free aqueous extract, 1 mM Na_2SeO_3, 25 °C, 72 h	Spherical, 2.8–38.9 nm (TEM), zeta potential -37.4 mV	ElSaied et al., 2021
Spirulina platensis	Cell-free aqueous extract, 1 mM Na_2SeO_3, 37 °C, 144 h, 130 rpm, pH 9	Spherical, 411.3 nm (DLS), 65 nm (TEM), zeta potential -16.7 mV, PDI 0.548	Yassein et al., 2025
Spirulina platensis	Biomass, 8 mM Na_2SeO_3, 25 °C, 168 h, 120 rpm	Spherical, 249.4 nm (DLS), 253.74 nm (SEM), zeta potential -67.07 mV, PDI 1.08	Sadeghi et al., 2025

Note: DLS, dynamic light scattering; PDI, polydispersity index; SEM, scanning electron microscopy; TEM, transmission electron microscopy.

Cyanobacteria capable of SeNP biosynthesis have been isolated from various natural sources. The strain *Leptolyngbya* sp. SSI24 was isolated from the waters of the River Nile (Saad et al., 2024). *Spirulina platensis* was isolated from the brackish waters of the Wadi El Natrun valley (Abbas et al., 2021). The strains *Desmonostoc alborizicum* (Nowruzi et al., 2023) and *Alborzia kermanshahica* (Eydelkhani et al., 2024) were isolated from a water supply system in Iran.

The maximum concentration of selenium ions tolerated by cyanobacteria varies considerably among species and strains. *Anabaena* sp. PCC 7120 demonstrated high resistance to sodium selenite. Concentrations of up to 100 mM did not inhibit growth but stimulated cell proliferation and the synthesis and accumulation of chlorophyll and carotenoids. The yield of synthesized SeNPs increased with increasing sodium selenite concentration up to 120 mM. However, further increases in concentration to 150–200 mM resulted in a sharp decrease in pigment content and overall cellular metabolic activity (Pandey et al., 2021).

Bacteria of other genera

Regarding other bacterial genera used for SeNPs biosynthesis, their sources of isolation are highly diverse. Among natural sources, mangrove ecosystems and marine sediments serve as reservoirs of halophilic and halotolerant microorganisms (Table 9).

Table 9

Biosynthesis of selenium nanoparticles using other bacteria

Bacteria	Biosynthesis conditions	Characteristics of nanoparticles	Reference
Alcaligenes sp. HZ-9-3-3	Liquid culture, 1000 µg/mL Na_2SeO_3, 28 °C, 168 h, 150 rpm, pH 7	Spherical	Hassan et al., 2025
Bifidobacterium animalis subsp. *lactis* H15	Liquid culture, 100 µg/mL Na_2SeO_3, 37 °C, 24 h	Spherical, 122.37 nm (DLS), 40–200 nm (TEM), zeta potential -25.4 mV, PDI 0.03	Li et al., 2024b
Citrobacter sp. BM-1	Liquid culture, 2 mM Na_2SeO_3, 30 °C, 24 h, 150 rpm	Spherical, 221.23 nm (DLS), 100–150 nm (SEM), zeta potential -43.77 mV	Li et al., 2025b
Escherichia coli RN-10	Liquid culture, 100 mM Na_2SeO_3, 37 °C, 48 h, 160 rpm, pH 8	Spherical, 46.71–71.91 nm (SEM), zeta potential -60 mV	Yasir and Zaki, 2024
Geobacillus sp ARB04	Supernatant of cell lysate, 10 mM Na_2SeO_3, 24 °C	Spherical, 30–60 nm (TEM)	Kumar et al., 2020
Metasolibacillus sp. ES129	Liquid culture, 5 mM Na_2SeO_3, 30 °C, 48 h, 150 rpm	Spherical, 100–300 nm (SEM/TEM)	Ge et al., 2024
Oceanobacillus sp. ES111		Spherical, 50–200 nm (SEM/TEM)	
Pediococcus acidilactici DSM20284	Liquid culture, 100 mg/L Na_2SeO_3, 35 °C, 48 h	Spherical, 100–500 nm (DLS), 50–400 nm (TEM), zeta potential -26.9 mV, PDI 0.096	Wang et al., 2023
Shewanella sp.	Cell-free supernatant, 1 mM Na_2SeO_3, 28 °C, 72 h, 150 rpm	Spherical, mean size 49 nm (SEM)	Annamalai et al., 2024
Stutzerimonas sp. MSB9	Cell-free supernatant, 5 mM Na_2SeO_3, 12 h	Spherical, mean size 85.2 nm (FESEM)	Ashwin et al., 2025
Xenorhabdus cabanillasii GU480990	Cell-free supernatant, 5 mM Na_2SeO_3, 24 °C, 48 h, 200 rpm	Spherical, 80–200 nm (TEM), zeta potential -24.17 mV	Raja et al., 2024

Note: DLS, dynamic light scattering; FESEM, field-emission scanning electron microscopy; SEM, scanning electron microscopy; TEM, transmission electron microscopy.

In particular, *Shewanella* sp. (Annamalai et al., 2024), *Stutzerimonas* sp. (Ashwin et al., 2025), and *Kocuria* sp. (Babavalian et al., 2025) were isolated from mangrove sediments. These ecosystems are characterized by high microbial diversity and specific environmental conditions that may favor microorganisms capable of biotransforming inorganic compounds, including selenium compounds.

Another important source is selenium-enriched soil. Several bacterial strains capable of selenite reduction and SeNP formation have been isolated from selenium-rich regions such as Enshi County and Bama County, China. These include representatives of the genera *Alcaligenes* (Hassan et al., 2025), *Metasolibacillus* and *Oceanobacillus* (Ge et al., 2024), as well as *Citrobacter* and *Brucella* (Li et al., 2025b). High selenium concentrations in such soils may select for microbial communities with efficient selenium detoxification mechanisms.

Bacteria capable of selenium biotransformation into SeNPs have also been isolated from agricultural soils and plants. For example, *Pediococcus acidilactici* (Wang et al., 2023) was isolated from alfalfa rhizosphere soil and plant samples.

Bacteria capable of synthesizing SeNPs have also been isolated from the human body. The probiotic strain *Bifidobacterium animalis* subsp. *lactis* H15 was isolated from the feces of breastfed infants (Li et al., 2024b).

The toxicity of selenium ions is an important factor affecting the efficiency of SeNP biosynthesis. Although selenium is an essential trace element for many organisms, its soluble oxyanions, selenite (SeO_3^{2-}, Se(IV)) and selenate (SeO_4^{2-}, Se(VI)), are highly bioavailable and can exert toxic effects on cells (Wang et al., 2023). The toxic effects of selenium ions on bacterial cells are mediated through several mechanisms, including the induction of oxidative stress. Selenite can react with sulfhydryl (thiol) groups in cellular proteins, leading to the formation of reactive oxygen species, such as superoxide anions and hydrogen peroxide. The accumulation of these reactive compounds can damage cellular membranes, proteins, and nucleic acids, ultimately inhibiting growth or causing cell death (Ge et al., 2024). Microorganisms possess various selenium detoxification mechanisms, among which reduction to elemental selenium (Se^0) plays an important role. The formation of insoluble elemental selenium nanoparticles can reduce selenium toxicity and facilitate its sequestration within cells. In response to selenium-induced stress, cellular defense systems may also be activated, including chaperone proteins such as GroEL, which are involved in maintaining proper protein folding under stress conditions (Li et al., 2024b).

The ability of bacteria to tolerate selenium toxicity varies considerably among species and strains. High tolerance is often observed in strains isolated from selenium-rich environments. For example, *Alcaligenes* sp. HZ-9-3-3 can tolerate sodium selenite concentrations of up to 231 mM (Hassan et al., 2025), while *Oceanobacillus* sp. ES111 tolerates concentrations exceeding 700 mM (Ge et al., 2024). *Citrobacter* sp. can tolerate selenite concentrations of up to 400 mM (Li et al., 2025b).

Archaea for the biosynthesis of selenium nanoparticles

Archaea constitute a distinct domain of prokaryotic microorganisms characterized by unique physiological, metabolic, and structural features that enable them to survive in extreme environmental conditions. One of the key features of archaea is the specific structure of their cell membrane and cell wall. Their membranes are composed of isoprenoid chains linked to glycerol-1-phosphate via ether bonds, providing increased stability at high temperatures, in extreme salinity, and under other stress conditions. In haloarchaea, the cell

wall is additionally adapted to function under hypersaline conditions and elevated concentrations of toxic compounds (Aparici-Carratalá et al., 2023).

Currently, only a limited number of studies report the use of archaea in the production of selenium nanoparticles. The main sources of archaeal isolates capable of producing SeNPs are extremely saline environments, such as salt pans, hypersaline lakes, and marine sediments. From salt flats in Goa (India), the strains *Haloferax alexandrinus* GUSF-1 (Alvares & Furtado, 2022), *Haloferax volcanii* BBK2, and *Haloarcula japonica* BS2 (Nagar et al., 2022) were isolated. The strain *Halogeometricum borinquense* E3 was isolated from salt pans in Mar-akkanam (Tamil Nadu, India) (Nagar et al., 2022). From the Santa Pola salterns (Alicante, Spain), the strain *Haloferax mediterranei* R-4 was isolated (Guijarro-Ramírez et al., 2025). *Halogeometricum* sp. E118 was isolated from crystallizer ponds of the Tic saltern (coast of the Gulf of Oman) (Abdollahnia et al., 2020). These ecosystems are characterized by extremely high salinity, making them natural selective niches for microorganisms with unique enzymatic systems for detoxifying and transforming selenium compounds.

Archaea generally tolerate sodium selenite concentrations of 1-5 mM (Abdollahnia et al., 2020), although tolerance levels vary by species and strain. For example, *Haloferax volcanii* BBK2, *Haloarcula japonica* BS2, and *Halogeometricum borinquense* E3 retain growth capability at sodium selenite concentrations from 2 to 100 mM. However, at concentrations of 50-100 mM, significant inhibition of cell division and metabolic activity is observed. The most favorable concentrations for active growth and efficient SeNPs biosynthesis are 2-8 mM, providing an optimal balance between induction of reduction processes and toxic stress (Nagar et al., 2022).

Archaea can synthesize nanoparticles with diverse morphologies (Table 10) that are rarely observed in other microorganisms. For example, *H. alexandrinus* GUSF-1 produces unique pentagonal SeNPs (Alvares and Furtado, 2022). In *H. volcanii* BBK2 and *H. japonica* BS2, extracellular synthesis of nanostructures in the form of rosette-like aggregates composed of nanoneedles has been observed. The formation of such morphotypes is associated with specific physicochemical mechanisms, including Ostwald ripening, which accounts for the assembly of extracellular nanoneedles into rosettes (Nagar et al., 2022). Meanwhile, many archaea, such as *H. borinquense*, predominantly produce spherical nanoparticles, which represent the most common SeNPs morphology (Abdollahnia et al., 2020).

A distinctive feature of haloarchaea, particularly *Haloferax alexandrinus*, is the involvement of the carotenoid pigment bacterioruberin in selenite reduction and nanoparticle formation. During cultivation, interaction between selenite and pigment molecules is accompanied by a decrease or disappearance of characteristic bacterioruberin spectral peaks, suggesting its involvement in redox reactions. Bacterioruberin may have a dual function, acting as a reducing agent and antioxidant that protects cells against selenium-induced oxidative stress. Due to its long hydrocarbon chains with conjugated double bonds, this pigment can participate in electron transfer and interact with metal ions, potentially facilitating their reduction (Alvares et al., 2025).

Some archaea, particularly methanogenic species such as *Methanosarcina acetivorans* C2A, may employ an additional selenium detoxification mechanism involving methylation. Through the action of methyltransferase enzymes, selenium compounds can be converted into volatile organoselenium compounds, such as dimethyl selenide and dimethyl diselenide. This process may be accompanied by a characteristic garlic-like odor during cultivation, indicating the formation of volatile methylated selenium derivatives (Liu et al., 2024b).

Table 10

Biosynthesis of selenium nanoparticles using archaea

Archaea	Biosynthesis conditions	Characteristics of nanoparticles	Reference
Haloferax alexandrinus GUSF-1	Liquid culture, 5 mM Na_2SeO_3, 37 °C, 168 h	Pentagonal, mean size 11.6 nm (TEM)	Alvares et al., 2025
Halogeometricum borinquense E3	Liquid culture, 4 mM Na_2SeO_3, 37 °C, 240 h, 110 rpm	Spherical, mean size 163 nm (DLS), 50–175 nm (FESEM), zeta potential -22.01 mV, PDI 0.215	Nagar et al., 2022
Haloferax mediterranei R-4	Liquid culture, 0.25–1 mM Na_2SeO_3, 42 °C, 48–72 h	Spherical, mean size 80–100 nm (TEM)	Guijarro-Ramírez et al., 2025
Halogeometricum sp. E118	Liquid culture, 5 mM Na_2SeO_3, 40 °C, 168 h, 150 rpm	Spherical, mean size 118.3 nm (DLS), mean size 111.6 nm (TEM), zeta potential -31.2 mV, PDI 0.27	Abdollahnia et al., 2020
Haloferax volcanii BBK2	Liquid culture, 4 mM Na_2SeO_3, 37 °C, 240 h, 110 rpm	Nanoneedles (extracellular), spherical (intracellular), 152.1 nm (DLS), 55–410 nm (FESEM), zeta potential -24.93 mV, PDI 0.213	Nagar et al., 2022

Note: DLS, dynamic light scattering; FESEM, field-emission scanning electron microscopy; TEM, transmission electron microscopy; PDI, polydispersity index.

Fungi for the biosynthesis of selenium nanoparticles

Fungi of the genus *Aspergillus*

Fungi of the genus *Aspergillus* are widely distributed in nature and are extensively used in biotechnology for the production of a broad range of enzymes, including lipases, proteases, peptidases, and glycosidases (Pocsi et al., 2024). Genetically modified *Aspergillus* strains are also used for the production of recombinant proteins (Li et al., 2022). In addition, these fungi are an important source of secondary metabolites that are widely used in the food, agrochemical, and medical industries. As of 2022, more than 3,100 secondary metabolites produced by *Aspergillus* species had been described, including polyketides (Bai et al., 2023) and antimicrobial compounds (Li et al., 2023). However, some *Aspergillus* species are phytopathogens that infect agricultural crops and may cause significant economic losses (Zakaria, 2024). Moreover, some representatives of this genus produce mycotoxins, including aflatoxins and ochratoxins, which can contaminate cereals and other food products, posing risks to food and feed safety and human and animal health (Xue et al., 2025).

Aspergillus fungi used for the microbial synthesis of SeNPs (Table 11) have been isolated from a wide range of natural and anthropogenic environments. Soil is one of the main sources of such strains. For example, *A. terreus* isolate ASE1 was obtained from cultivated soil (Saied et al., 2023), while *A. carneus* MAK 259 was also isolated from cultivated soil (Fahmy et al., 2025). In addition, *A. niger* SS4 was isolated from soil and used to optimize chitosan biosynthesis and subsequently produce SeNPs (Kavitha et al., 2024).

Marine-derived *Aspergillus* species are also considered promising for the biosynthesis of SeNPs, as they can produce unique bioactive metabolites. For instance, *Aspergillus candidus* TU-65 was isolated from the roots of sand lily (*Pancratium maritimum* L.) growing in coastal ecosystems (Alsehli et al., 2025).

Table 11

Biosynthesis of selenium nanoparticles using fungi of the genus *Aspergillus*

Fungi	Biosynthesis conditions	Characteristics of nanoparticles	Reference
Aspergillus candidus TU-65	Cell-free ethyl acetate extract, 0.7% w/v Na_2SeO_3, 121 °C (autoclaving), 1 h	Spherical, 108.58 nm (DLS), 6.1–28.1 nm (TEM), zeta potential -42.96 mV, PDI 0.33	Alsehli et al., 2025
Aspergillus carneus MAK 259	Cell-free aqueous extract, 1 mM Na_2SeO_3, 28 °C, 24 h	Spherical, 20–77 nm (TEM), zeta potential -25.7 mV	Fahmy et al., 2025
Aspergillus flavus	Cell-free aqueous extract, 1 mM Na_2SeO_3, 30 °C, 24 h, 130 rpm, pH 6.5	Spherical, mean size 49.72 nm (DLS), 28–78 nm (TEM)	Mohammed et al., 2024
Aspergillus fumigatus TIMML-025	Fungal biomass filtrate, 1 mM Na_2SeO_3, 48 h	Spherical, 37–46 nm (FESEM)	Bafghi et al., 2022
Aspergillus niger KP	Liquid culture, 10 mg/L Na_2SeO_3, 30 °C, 168 h, pH 3.5	Spherical, 65–100 nm (FETEM)	Negi et al., 2020
Aspergillus niger SS4	Fungil chitosan, 50 mM Na_2SeO_3, 50 mM ascorbic acid, 28–32 °C, 24 h	Spherical, mean size 62.84 nm (TEM), zeta potential +17 mV	Kavitha et al., 2024
Aspergillus oryzae A02	Liquid culture, 20 mg/mL Na_2SeO_3, 30 °C, 96 h, 200 rpm, pH 6	Spherical, 500–600 nm (SEM)	Gao et al., 2024
Aspergillus terreus ASE1	Cell-free aqueous extract, 1 mM Na_2SeO_3, 28 °C	Spherical, mean size 50 nm (DLS), 10–100 nm (TEM), PDI 0.022	Saied et al., 2023

Note: DLS, dynamic light scattering; FESEM, field-emission scanning electron microscopy; TEM, transmission electron microscopy; PDI, polydispersity index.

A separate group includes strains isolated from specialized environments where microorganisms have adapted to elevated concentrations of metals and metalloids. For example, *Aspergillus niger* KP was isolated from a laboratory-scale inverse fluidized-bed bioreactor used for the treatment of selenium-containing wastewater (Negi et al., 2020). Another strain, *Aspergillus* sp. 3A was isolated from bentonite clay samples collected in Cabo de Gata (Spain) and studied in microcosms simulating deep geological repositories for radioactive waste (Ruiz-Fresneda et al., 2024).

Some *Aspergillus* strains exhibit high tolerance to selenite. For example, *Aspergillus oryzae* A02 can grow at sodium selenite concentrations up to 115 mM (Gao et al., 2024), while the minimum inhibitory concentration (MIC) for *Aspergillus* sp. 3A exceeds 32 mM (Ruiz-Fresneda et al., 2024). However, most representatives of this genus are considerably more sensitive, with growth inhibition occurring at selenite concentrations of 1-5 mM.

Fungi of the genus *Fusarium*

Members of the genus *Fusarium* exhibit remarkable species diversity and a wide geographic distribution. Many of them are phytopathogens causing substantial economic losses in agriculture. Numerous *Fusarium* species produce a wide range of mycotoxins, including zearalenone, trichothecenes, and fumonisins, which can contaminate staple crops and pose serious risks to human and animal health (Bugingo et al., 2025). At the same time, these fungi attract increasing attention in nanobiotechnology due to their metabolic potential and ability to biosynthesize nanomaterials with unique physicochemical properties. For

instance, SeNPs synthesized using *F. oxysporum* biomass exhibit strong fluorescence, indicating their potential application as biosensors and bioimaging agents (Islam et al., 2022).

Fusarium species used for the biosynthesis of SeNPs (Table 12) are isolated from various ecological niches. One common source is infected plant tissues. For example, *F. semitectum* currently referred to as F. incarnatum)) was isolated from roots and tissues of *Moringa oleifera* affected by wilt disease (Abbas & Abou, 2020). Another phytopathogen, *F. fujikuroi*, infects crops such as maize, sugarcane, wheat, and asparagus (El-Fawal et al., 2025). The phytopathogen *F. solani* was isolated from soil samples collected from pots used in experimental studies at the Laboratory of Insect Natural Enemies, Kyushu University, Japan (Helmy et al., 2023a). Fungi of the genus *Fusarium* were also isolated from animal and poultry feed, specifically *F. oxysporum* CCASU-2023-F9 (Gharieb et al., 2024). It should be noted that *Fusarium* species can also be isolated from healthy plant tissues; for instance, *F. equiseti* was obtained from branches of *Hibiscus rosa-sinensis* (Hussein et al., 2022).

Table 12

Biosynthesis of selenium nanoparticles using fungi of the genera *Fusarium* and *Monascus*

Fungi	Biosynthesis conditions	Characteristics of nanoparticles	Reference
Fusarium equiseti	Liquid culture, 1 mM Na_2SeO_3, 30 °C, 168 h	Spherical and rod-shaped, 20–90 nm (DLS), zeta potential -12.4 mV, PDI 0.786	Hussein et al., 2022
Fusarium fujikuroi MED14	Fungal biomass filtrate, 0.03 M Na_2SeO_3, 30 °C, 48–72 h, 150 rpm	Spherical, 10–19 nm (TEM), zeta potential -43 mV	El-Fawal et al., 2025
Fusarium oxysporum	Biomass, 2 mM $SeCl_4$, 72 h	Spherical, mean size 42 nm (TEM)	Islam et al., 2022
Fusarium semitectum	Fungal biomass filtrate, 2 g/L Na_2SeO_3, 28 °C, 72 h	Spherical, 92.33 nm (DLS), 32.8–103.82 nm (TEM), PDI 0.3	Abbas and Abou Baker, 2020
Monascus purpureus ATCC 16436	Cell-free ethanol extract, 1 mM Na_2SeO_3, 0.5 h	Spherical, 45.65 nm (DLS), 30–70 nm (TEM), zeta potential -24.01 mV, PDI 0.205	El-Sayed et al., 2020

Note: DLS, dynamic light scattering; TEM, transmission electron microscopy; PDI, polydispersity index.

Fungi of the genus *Monascus*

Fungi of the genus *Monascus* are widely distributed in nature and have long been used in Asian countries for food fermentation. They are capable of producing a wide range of secondary metabolites, including natural pigments (red, orange, and yellow) and biologically active compounds such as monacolins. However, some strains may also produce the mycotoxin citrinin, which requires careful monitoring in food and biotechnological applications (Arruda et al., 2025).

Recent literature contains a limited number of studies on the use of *Monascus* species for the biosynthesis of SeNPs (Qi et al., 2024) (Table 12). These fungi are mainly isolated from traditional fermented products and certain types of agro-industrial waste. A common source is red koji rice, where *Monascus* develops during fermentation. They are also frequently isolated from fermented industrial residues, such as *Monascus* distillers' grains and *Monascus* vinegar-fermented grains. For example, *M. purpureus* M12, isolated from fermented food products, demonstrated enhanced selenium tolerance and was considered a promising microorganism for the biosynthesis of SeNPs and the bioconversion of inorganic selenium into organic forms (Sun et al., 2022).

Fungi of the genus *Nigrospora*

Representatives of the genus *Nigrospora* synthesize a wide range of biologically active secondary metabolites, most of which belong to the polyketide group. These include quinones, furanones, pyrans, monophenyl derivatives, and other compounds. These secondary metabolites exhibit antibacterial, antifungal, antiviral, antioxidant, and anti-inflammatory activities. Some species of the genus *Nigrospora* may act as phytopathogens; however, many representatives occur in symbiotic or saprotrophic associations with plants (Xu et al., 2022).

Analysis of scientific publications from 2020 to 2026 shows that studies on the use of fungi of the genus *Nigrospora* for the biosynthesis of SeNPs are limited. In particular, only two studies describing the use of representatives of this genus for SeNP synthesis were identified. These studies showed that metabolic products of *N. guilinensis* OP248797, particularly exopolysaccharides and secondary metabolites, play an important role in SeNP biosynthesis.

In both studies, SeNPs were biosynthesized in a cell-free system. In the first study, exopolysaccharides from strain OP248797 were used to synthesize nanoparticles in combination with ascorbic acid and 5 mM sodium selenite. As a result, spherical selenium nanoparticles with a hydrodynamic diameter of approximately 91 nm and a zeta potential of −28.2 mV were obtained (Singh et al., 2025). In the second study, an extract of secondary metabolites from strain OP248797 was used for the biosynthesis of SeNPs together with ascorbic acid and 5 mM sodium selenite. Spherical selenium nanoparticles with a hydrodynamic diameter of approximately 122 nm and a zeta potential of −27 mV were obtained (Singh et al., 2024).

In both cases, a combined approach to SeNP biosynthesis was used, in which ascorbic acid served as the reducing agent for the conversion of selenite to elemental selenium, while the biological components of *N. guilinensis* OP248797 acted as stabilizing agents. Fungal exopolysaccharides and secondary metabolites may form a protective layer on the nanoparticle surface, thereby reducing aggregation and increasing the stability of the colloidal system. Their potential contribution to the biological activity of the synthesized SeNPs also requires further investigation.

Fungi of the genus *Penicillium*

Fungi of the genus *Penicillium* play an important role in biotechnology due to their ability to synthesize a wide range of secondary metabolites, including alkaloids, polyketides, terpenoids (Lv & Zeng, 2024), steroids (Lindsay et al., 2023), and other biologically active compounds. A significant proportion of these metabolites exhibits pharmacological activity, which has attracted interest in representatives of this genus as potential producers of antibiotics, antioxidants, and antitumor compounds (Zhang et al., 2022b). Representatives of the genus *Penicillium* also demonstrate potential for environmental bioremediation. Due to their diverse enzymatic systems, these fungi can utilize various xenobiotics as carbon sources, making them promising agents for environmentally safe wastewater treatment technologies (Wolski, 2023). However, some *Penicillium* species produce mycotoxins, including ochratoxin A and patulin, which pose risks to food safety and human health (Shen et al., 2025).

Soil is one of the main sources of *Penicillium* fungi used to obtain biogenic SeNPs. In soil ecosystems, these fungi contribute to the decomposition of organic matter and element cycling, which may be associated with their high metabolic activity and ability to transform various inorganic compounds. The strain *P. tardochrysogenum* OR059437 was isolated from cultivated soil (El-Sayed et al., 2024). The strain *P. corylophilum* As-1 was also isolated from soil (Salem et al., 2021).

Some representatives have been isolated from the internal tissues of healthy plants. The strain *P. verhagenii* AR.1 was isolated from the roots of garlic (*Allium sativum*) (Nassar et al., 2023). *P. citrinum* OQ443236 was isolated from the roots and leaves of wild plants, including

periwinkle (*Catharanthus roseus*) and crown of thorns (*Euphorbia milii*) (Gharieb et al., 2025b). The strain *P. crustosum* EP-1 was isolated from the leaves of the medicinal plant *Ephedra pachyclada* (Fouda et al., 2022).

Coastal and marine ecosystems are also sources of *Penicillium* strains adapted to increased salinity and other environmental stress factors. For example, *P. chrysogenum* MZ945518 was isolated from the surface of stones collected on the southern Mediterranean coast (Morad et al., 2022).

Some *Penicillium* strains used for the biosynthesis of SeNPs have been isolated from atypical anthropogenic environments, including cultural heritage objects. The strain *P. chrysogenum* F9 was isolated from a historical manuscript (Amin et al., 2021).

In most studies on the biosynthesis of SeNPs using fungi of the genus *Penicillium*, cell-free systems are used (Table 13). Therefore, the effects of selenium ions on the growth and viability of *Penicillium* representatives have been studied to a limited extent. The strain *P. citrinum* OQ443236 exhibits relatively high resistance to sodium selenite, tolerating concentrations of up to 40 mM. At the same time, increasing the selenite concentration gradually decreases the efficiency of selenium ion reduction. In particular, at a selenite concentration of 40 mM, the selenium reduction rate of strain OQ443236 decreases to 76.98% (Gharieb et al., 2025b).

Table 13

Biosynthesis of selenium nanoparticles using fungi of the genus *Penicillium*

Fungi	Biosynthesis conditions	Characteristics of nanoparticles	Reference
Penicillium chrysogenum	Fungal biomass filtrate, 1 mM Na_2SeO_3, 10.0 kGy (gamma rays)	Spherical, 46.3 nm (DLS), 12.12–84.15 nm (TEM)	El-Sayyad et al., 2020
Penicillium chrysogenum F9	Fungal biomass filtrate, 2 mM Na_2SeO_3, 32 °C, 24 h, 150 rpm, pH 7	Spherical, 3–15 nm (TEM), PDI 0.03	Amin et al., 2021b
Penicillium chrysogenum MZ945518	Fungal biomass filtrate, 3 mM Na_2SeO_3, 40 °C, 0.5 h	Spherical, 213 nm (DLS), 30–78 nm (TEM), zeta potential -30.1 mV, PDI 0.35	El-Sayed et al., 2023
Penicillium citrinum	Biomass (gamma radiation 30 Gy), 10 mM $NaHSeO_3$, 37 °C, 48 h, 120 rpm	Spherical, 19.76 nm (TEM)	Amin et al., 2021a
Penicillium citrinum OQ443236	Biomass, 3 mM Na_2SeO_3, 28 °C, 96 h, 150 rpm, pH 9	Spherical, 50–80 nm (TEM)	Gharieb et al., 2025b
Penicillium corylophilum As-1	Fungal biomass filtrate, 2 mM Na_2SeO_3, ascorbic acid, 30 °C, 24 h, 150 rpm, pH 6.5	Spherical, mean size 72 nm (DLS), 29.1–48.9 nm (TEM)	Salem et al., 2021
Penicillium crustosum EP-1	Fungal biomass filtrate, 3 mM Na_2SeO_3, 38 °C, 24 h, pH 8	Spherical, 3–22 nm (TEM)	Fouda et al., 2022
Penicillium expansum ATTC 36200	Fungal biomass filtrate, 2 mM SeO_2, 30 °C, 24 h, 150 rpm	Spherical, 4–12.7 nm (TEM)	Hashem et al., 2021b
Penicillium tardochrysogenum OR059437	Cell-free aqueous extract, 1 mM Na_2SeO_3, 28 °C, 72 h, 150 rpm	Spherical, 60.21–104.41 nm (TEM), zeta potential -17 mV	El-Sayed et al., 2024
Penicillium verhagenii AR.1	Cell-free aqueous extract, 5 mM Na_2SeO_3, 40 °C, 24 h, pH 8	Spherical, mean size 91.2 nm (DLS), 25–75 nm (TEM), zeta potential -32 mV	Nassar et al., 2023

Note: DLS, dynamic light scattering; PDI, polydispersity index; TEM, transmission electron microscopy.

Fungi of the genus *Trichoderma*

The genus *Trichoderma* comprises numerous species of microscopic fungi that are widely distributed in various ecosystems, including soils, the plant rhizosphere, and organic substrates. In general, representatives of the genus *Trichoderma* are considered nonpathogenic to humans, animals, and plants, which supports their safety and widespread use in agriculture and industrial biotechnology (Chen et al., 2025). These fungi synthesize a wide range of biologically active secondary metabolites, including butenolides, koninginins, peptaibols, pyridones, and polyketides, which play an important role in suppressing the development of phytopathogenic microorganisms (Yadav & Khare, 2025). Fungi of the genus *Trichoderma* are also known for their ability to synthesize a complex of lignocellulolytic enzymes, including cellulases and hemicellulases. This makes them important agents in the bioconversion of lignocellulosic biomass, particularly agro-industrial waste (Lima et al., 2024).

Fungi of the genus *Trichoderma* used for the biosynthesis of SeNPs (Table 14) can be isolated from various ecological niches. One of the main habitats of the genus *Trichoderma* is the plant rhizosphere, where fungi actively interact with plants and other soil microorganisms, thereby contributing to the development of their diverse metabolic potential (Arunthirumeni et al., 2022). *Trichoderma* strains were also isolated from wetland soils (Saravanakumar et al., 2022). Another source of isolation of fungi of this genus is technogenic environments. For example, the strain *Trichoderma* sp. WL-Go, which demonstrated high efficiency in the biosynthesis of SeNPs, was isolated from activated sludge samples of an antibiotic-contaminated bioreactor. The authors studied the resistance of strain WL-Go to selenium compounds (selenium oxide IV) in the concentration range from 0.5 to 7.0 mM. An increase in selenium concentration to 7 mM was accompanied by changes in the reduction mechanisms: SeNPs biosynthesis occurred predominantly intracellularly. This is likely associated with the activation of fungal intracellular protective mechanisms in response to increased toxic stress (Diko et al., 2020).

Table 14

Biosynthesis of selenium nanoparticles using fungi of the genus *Trichoderma*

Fungi	Biosynthesis conditions	Characteristics of nanoparticles	Reference
Trichoderma harzianum	Cell-free aqueous extract, 10 mM Na_2SeO_3, 28 °C, 24 h	Spherical and oval, 80–100 nm (SEM)	Kashisaz et al., 2024
Trichoderma harzianum RCMB 017009	Cell-free aqueous extract, 10 mM Na_2SeO_3, 28 °C, 48 h, 150 rpm, pH 6.5	Spherical, 16 nm (TEM)	Helmy et al., 2023b
Trichoderma harzianum SKCGW012	Cell-free aqueous extract, 25 mM Na_2SeO_3, 28 °C, 120 h, 180 rpm	Oval, 145.3 nm (DLS), 26.45 nm (TEM), zeta potential -37.8 mV, PDI 0.22	Saravanakumar et al., 2022
Trichoderma sp.	Fungal biomass filtrate, 20 mM Na_2SeO_3, 27 °C, 72 h, 120 rpm, pH 8–12	Square, spherical, pentagons, hexagons, 40–100 nm (DLS), 137 nm (SEM), PDI 0.287	Arunthirumeni et al., 2022
Trichoderma sp. WL-Go	Liquid culture, 2 mM SeO_2, 30 °C, 48 h, 150 rpm, pH 8	Spherical, 147.1 nm (DLS), 20–220 nm (SEM), zeta potential -24.6 mV	Diko et al., 2020
Trichoderma viride	Fungal biomass filtrate, 2 mM Na_2SeO_3, pH 6	Spherical, 25.4–80.6 nm (TEM)	Abd-Elkhalek et al., 2024

Note: DLS, dynamic light scattering; PDI, polydispersity index; SEM, scanning electron microscopy; TEM, transmission electron microscopy.

Fungi of other genera

Representatives of other fungal genera that can be used for the biosynthesis of SeNPs (Table 15) were isolated from various ecological niches. One of the main sources of their isolation is soil. Many species, including *Trichoderma harzianum*, *Aspergillus niger*, and representatives of the genus *Talaromyces*, are typical inhabitants of soil ecosystems (Rasheed et al., 2024). In addition, several species, including *Mucor circinelloides*, *Curvularia lunata*, and *Clonostachys rosea*, were isolated from the plant rhizosphere (Wu et al., 2024).

Table 15

Biosynthesis of selenium nanoparticles using other fungi

Fungi	Biosynthesis conditions	Characteristics of nanoparticles	Reference
Alternaria alternata AUMC15177	Cell-free ethanol extract, 1 mM Na_2SeO_3, 6 h	Spherical, 25–86 nm (DLS), zeta potential -21.89 mV, PDI 0.107	Mohamed et al., 2025
Aureobasidium pullulans IMI 45533	Fungal biomass filtrate, 20 mM Na_2SeO_3, 25 °C, 72 h, 125 rpm	Spherical, 20–120 nm (SEM/TEM)	Liang et al., 2022
Colletotrichum fructicola KL19	Biomass, 4.56 mM Na_2SeO_3, 28 °C, 120 h, 150 rpm, pH 6.25	Spherical, mean size 144.8 nm (DLS), zeta potential -18.3 mV, PDI 0.316	Wu et al., 2024
Curvularia sp. LCJ413	Fungal biomass filtrate, 30 mM Na_2SeO_3, 24 h	Rod-shaped, mean size 111.5 nm (DLS), 25–100 nm (SEM), zeta potential -2.77 mV, PDI 0.271	Kathiravan et al., 2023
Eurotium cristatum H-7	Liquid culture, 1.2 mM Na_2SeO_3, 28 °C, 216 h, 120 rpm	Spherical, mean size 231.7 nm (DLS), zeta potential -20.8 mV, PDI 0.277	Li et al., 2025a
Paraphaeosphaeria sporulosa	Liquid culture, 0.1/0.5 mM Se^{4+}, 21 °C, 32 days	Spherical, 500 nm	Santelli et al., 2023
Phoma glomerata	Fungal biomass filtrate, 1 mM Na_2SeO_3, 25 °C, 30 days, 125 rpm	Spherical, 100–200 nm (SEM)	Liang et al., 2020
Rhizopus oryzae MG518370	Fungal biomass filtrate, 2 mM SeO_2, 30 °C, 24 h, 150 rpm	Spherical, 20–200 nm (SEM), zeta potential -9.8 mV	Abu-Elghait et al., 2021
Serendipita indica	Fungal biomass filtrate, 100 mM Na_2SeO_3, 70 °C, 20 min	Spherical, 20–80 nm (TEM), zeta potential -31.6 mV, PDI 0.267	Chauhan et al., 2024
Talaromyces haitouensis	Fungal biomass filtrate, 1 mM Na_2SeO_3, 45 °C, 24 h	Spherical, mean size 150 nm (DLS), zeta potential 200 mV	Rasheed et al., 2024

Note: DLS, dynamic light scattering; PDI, polydispersity index; TEM, transmission electron microscopy.

Various fungal species used to obtain biogenic SeNPs were also isolated from the internal tissues of healthy plants. In particular, *Rhizopus arrhizus* was isolated from plant tissues (Gharieb et al., 2025b). The strain *Colletotrichum fructicola* KL19 was isolated from plants *Kadsura angustifolia* and *Schisandra sphenanthera* (Wu et al., 2024). The species *Alternaria alternata* was isolated from the bark of *Citrus medica* (Mohamed et al., 2025), and *Curvularia* sp. LCJ413 from the stem of *Vitex negundo* (Kathiravan et al., 2023).

Some fungal strains capable of reducing selenium compounds can also be isolated from food products. For example, the strain *Eurotium cristatum* H-7 was isolated from Fuzhuan brick tea, China (Li et al., 2025a).

Yeast for the biosynthesis of selenium nanoparticles

Yeast of the genus *Saccharomyces*

One of the most-studied eukaryotic microorganisms is the yeast genus *Saccharomyces*. They are used in biotechnology, the food industry, and other fields. Representatives of this genus are characterized by high adaptability to various environmental stressors, particularly low pH, elevated ethanol concentrations, and high osmotic pressure (Elhalis, 2024). An important property of *Saccharomyces* yeasts is also their ability to interact with metal ions and accumulate them within their cells, thereby creating opportunities for the use of yeast cultures in biofortification technologies (Bondar & Krasinko, 2025; 2026). Such physiological and biochemical features enable them to survive under conditions that are inhibitory to many other microorganisms.

Yeasts of the genus *Saccharomyces* exhibit resistance to toxic selenium ions and are capable of effective bioaccumulation. In yeast cells, inorganic forms of selenium can be transformed into organic selenium-containing compounds such as selenomethionine and selenocysteine, as well as into biogenic SeNPs (Table 16). This is associated with specific mechanisms in yeast cells for detoxification, reduction, and metabolic transformation of selenium compounds (Sęk et al., 2025).

Table 16

Biosynthesis of selenium nanoparticles using yeast of the genus *Saccharomyces*

Yeast	Biosynthesis conditions	Characteristics of nanoparticles	Reference
Saccharomyces boulardii CCDM 2020	Liquid culture, 10 mg/L Na_2SeO_3, 25 °C, 24 h	Spherical, ovoid, 167 nm	Hyrslova et al., 2024
Saccharomyces boulardii (mutant strain)	Liquid culture, 300 µg/mL Na_2SeO_3, 30 °C, 48 h, 250 rpm	Spherical, 164.2 nm (DLS), <100 nm (TEM), zeta potential -14.7 mV	Nie et al., 2023
Saccharomyces cerevisiae ATCC 7090	Liquid culture, Na_2SeO_3 (10 mg/L Se^{4+}), 28 °C, 24 h, 150 rpm	Spherical, 60–180 nm	Kieliszek et al., 2025
Saccharomyces cerevisiae GDMCC 2.90	Liquid culture (death-phase), 11 mM Na_2SeO_3, UV irradiation (20 min)	Spherical, 0–150 nm	Cui et al., 2025
Saccharomyces cerevisiae YW16	Liquid culture, 2 g/L Na_2SeO_3, 30 °C, 48 h	Spherical, 120–190 nm (TEM)	Sun et al., 2024a
Saccharomyces boulardii	Liquid culture, 74 ppm Na_2SeO_3, 37 °C, 9–48 h	Spherical, 100–200 nm (TEM)	González-Salitre et al., 2023
Saccharomyces cerevisiae	Cell-free aqueous extract, 200 mg/L SeO_2, microwave irradiation, 10 min	Spherical, 60–140 nm	Borowska et al., 2023
Saccharomyces cerevisiae	Cell-free aqueous extract, 2 mM Na_2SeO_3, 30 °C, 24 h, 150 rpm	Spherical, mean size 83.3 nm (DLS), 4–51 nm (TEM), zeta potential -11.9 mV	Salem, 2022
Saccharomyces cerevisiae	Cell-free supernatant, 2 mM $NaHSeO_3$, 3 h	Spherical, 30.89–50.01 nm (SEM)	Farouq and Shehab, 2026
Saccharomyces cerevisiae	Yeast glucan, 20 mM $NaHSeO_3$, ascorbic acid	Spherical, 100–300 nm (TEM), zeta potential +37 mV	Sun et al., 2023
Saccharomyces cerevisiae	Liquid culture, Na_2SeO_3 (5 µg/ 200 mL), 32 °C, 96 h, 120 rpm	Spherical, mean size 50 nm (TEM), zeta potential -10.3 mV, PDI 0.989	Faramarzi et al., 2020
Saccharomyces cerevisiae	Liquid culture, 1 mg/mL Na_2SeO_3, 30 °C, 36 h	Spherical, mean size 71.14 nm, zeta potential -34 mV	Wu et al., 2021

Note: DLS, dynamic light scattering; TEM, transmission electron microscopy.

An effective tool for increasing biosynthesis productivity, controlling morphological characteristics, and improving the colloidal stability of SeNPs is the genetic and metabolic engineering of yeasts of the genus *Saccharomyces*. One of the key directions of genetic optimization is the enhancement of the glutathione biosynthesis pathway, which plays a major role in reducing selenite to elemental selenium (Sun et al., 2024a). Mutagenesis methods are also used to generate strains with improved phenotypic characteristics. Thus, mutant yeasts *S. boulardii* demonstrate increased tolerance to selenite and the ability to synthesize SeNPs with a significantly smaller average size (55.8-58.8 nm) compared to non-modified yeasts (134.6-164.2 nm) (Yang et al., 2024).

The biosynthesis of SeNPs using glucans from *S. cerevisiae* is another promising approach for producing stable, bioactive nanomaterials. Native yeast β-glucan is almost insoluble in water, which complicates its practical use. Therefore, it is chemically modified by amination. Aminated yeast glucans acquire a positive charge, which improves their ability to stabilize and disperse nanoparticles. Glucans form a stabilizing layer around SeNPs, preventing their aggregation. Stabilization is achieved through hydrogen bonding between the glucan hydroxyl groups and the nanoparticle surface, as well as electrostatic interactions arising from the presence of amino groups (Sun et al., 2023).

Yeasts of other genera

The search for new yeast strains for the biosynthesis of SeNPs is usually conducted in specific natural ecosystems, where microorganisms have evolved over time under various stress factors. Such conditions contribute to the development of metabolic mechanisms for detoxifying and transforming toxic compounds, particularly selenium.

Yeasts of different genera were isolated from marine ecosystems. In particular, *Candida pseudojiufengensis* was isolated from samples of coastal sand and seawater of the Red Sea near Giftun Island (Hurghada, Egypt) (Ali et al., 2024). Another example is a new yeast species, *Magnusiomyces ingens* LH-F1. Strain LH-F1 was isolated from marine mud sampled in the city of Dalian (China) (Lian et al., 2019). From seawater near Mumbai (India), the strain *Yarrowia lipolytica* NCIM 3589 was isolated. This strain has high tolerance to selenium ions, withstanding up to 8 mM sodium selenite (Hamza et al., 2017).

Promising selenium-resistant yeasts are also isolated from freshwater ecosystems. The strain *Rhodotorula mucilaginosa* R-8441 was isolated from water samples collected from a waterfall in Kurdistan Province (Iran). When using biomass from strain R-8441 for SeNPs biosynthesis, a pronounced dependence of nanoparticle morphology on sodium selenite concentration was observed. At concentrations of 1-4 mM, predominantly spherical nanoparticles are formed. Increasing the concentration of sodium selenite to 5 mM leads to the formation of rod-shaped structures. It is assumed that such a change in morphology is associated with the Ostwald ripening process and the limited availability of stabilizing biomolecules at elevated selenium concentrations (Ashengroph and Tozandehjani, 2022).

The strain *Pichia kudriavzevii* 1845 was identified as the dominant microorganism during the fermentation process of fruit wine (Wang et al., 2024a). From tulum cheese, the strain *Kluyveromyces marxianus* M59 was isolated. β-glucans were isolated from these yeasts, which can be used as biopolymeric matrices or natural stabilizers in the processes of SeNPs biosynthesis. At the same time, natural yeast β-glucans are practically insoluble in water, which complicates their use in nanomaterial synthesis processes. Therefore, to enhance their functionality, chemical modification, in particular carboxymethylation, is applied. Such modification is an important step in preparing the polysaccharide matrix for subsequent SeNPs formation. Due to their natural origin, biodegradability, and biological

activity, the obtained nanocomposites may have broad prospects for application in the food industry (Cinar-Acar, 2025).

Genetically modified yeasts *Pichia pastoris* X-33 are used for the biosynthesis of SeNPs, in which the gene of *Mucor racemosus*, encoding the cytochrome b5 reductase enzyme (Cyb5R), is functioning. This is an NADH-dependent enzyme that catalyzes the intracellular reduction of selenium ions to zero-valent elemental selenium (Se^0). As a result of this process, elemental selenium accumulates in cells as nanoparticles. The recombinant strain X-33 exhibits high resistance to toxic selenium ions and can grow even at concentrations up to 10 mM. At the same time, natural strains of *Pichia pastoris* usually do not withstand selenium ion concentrations above 1 mM (Elahian et al., 2017).

The characteristics of SeNP biosynthesis using different yeast genera are presented in Table 17.

Table 17

Biosynthesis of selenium nanoparticles using other yeast

Yeast	Biosynthesis conditions	Characteristics of nanoparticles	Reference
Candida albicans TIMML-1306	Cell-free supernatant, Na_2SeO_4, 28 °C, 24 h, 140 rpm	Spherical, 50 nm (FESEM), zeta potential -19 mV	Bafghi et al., 2021
Candida pseudojiufengensis	Cell-free aqueous extract, 0.8 mM SeO_2, 40 °C, 48 h, 200 rpm, pH 7	Spherical, 14 nm (DLS), 12 nm (TEM), zeta potential -34 mV, PDI 0.15	Ali et al., 2024
Kluyveromyces lactis GG799	Liquid culture, 1.2 mM Na_2SeO_3, 30 °C, 24 h, 200 rpm	Spherical, 80–150 nm (TEM)	Song et al., 2021
Kluyveromyces marxianus M59	Yeast carboxymethylated β-glucan (1 mg/mL), 20 mM SeO_2, 60 mM ascorbic acid	Spherical, 83–180 nm (SEM)	Cinar-Acar, 2025
Magnusiomyces ingens LH-F1	Supernatant of cell lysate, 2 mM SeO_2, 30 °C, 132 h	Spherical, quasi-spherical, 70–90 nm (TEM)	Lian et al., 2019
Nematospora coryli	Biomass, 1 mM $Na_2SeO_3 \times 5H_2O$, 28 °C, 48 h, 130 rpm	Spherical, 50–250 nm (TEM)	Rasouli, 2019
Pichia kudriavzevii 1845	Liquid culture, 8 μg/mL Na_2SeO_3, 28 °C, 36 h,	Spherical, mean size 197 nm (DLS), PDI 0.232	Wang et al., 2024a
Pichia pastoris X-33 (genetically modified)	Liquid culture, 4 mM SeO_2, 30 °C, 72 h	Spherical, 70–180 nm (TEM)	Elahian et al., 2017
Rhodotorula glutinis CCY 20–2-26	Liquid culture, Na_2SeO_3 (10 mg/L Se^{4+}), 28 °C, 24 h, 150 rpm	Spherical, 40–260 nm	Kieliszek et al., 2025
Rhodotorula mucilaginosa R-8441	Biomass, 5 mM Na_2SeO_3, 25 °C, 72 h, 200 rpm	Rod-shaped, 478 nm (DLS), 363 nm (FESEM)	Ashengroph and Tozandehjani, 2022
Yarrowia lipolytica ATCC 18942	Liquid culture, 2 mM Na_2SeO_3, 30 °C, 48 h, 160 rpm	Spherical, mean size 110 nm (DLS), zeta potential -34.51 mV, PDI 1	Lashani et al., 2024

Note: DLS, dynamic light scattering; FESEM, field-emission scanning electron microscopy; PDI, polydispersity index; SEM, scanning electron microscopy; TEM, transmission electron microscopy.

Mechanisms of microbial biosynthesis of selenium nanoparticles

The biosynthesis of SeNPs is considered an important mechanism of cellular detoxification, enabling microorganisms to convert toxic soluble selenium oxyanions into insoluble and significantly less toxic elemental selenium. Such biotransformation may be part of the adaptive response of microorganisms to elevated selenium concentrations in the environment. The reduction process can occur both intracellularly, in the cytoplasm or periplasmic space, and extracellularly, depending largely on the species and cultivation conditions of the microorganisms (Likidtaveesin et al., 2025). In addition, SeNP synthesis is possible in cell-free systems due to the activity of secreted enzymes, proteins, and other biomolecules (Hashem et al., 2021a).

Enzymatic reduction mechanisms play an important role in the biosynthesis of SeNPs. Various reductase enzymes are involved in this process, including NADH- or NADPH-dependent nitrate reductases, fumarate reductase, and membrane-bound reductases (Abdollahnia et al., 2020). In representatives of the genera *Bacillus* and *Lactiplantibacillus*, selenite reduction may be catalyzed by thioredoxin reductase, which uses NADPH as an electron donor and reduces selenium oxyanions to the elemental state. In addition, oxidoreductases of the SDR (short-chain dehydrogenase/reductase) family, which use NADH as an electron donor, may contribute to the reduction of selenium ions to the elemental state. Such enzymatic systems are components of cellular redox pathways and contribute to maintaining cellular redox homeostasis (Huang et al., 2023; Li et al., 2025c). Selenate reductase catalyzes the reduction of selenate to selenite, whereas selenite reductase catalyzes the reduction of selenite to elemental selenium, followed by SeNP formation (Nowruzi et al., 2023).

The biosynthesis of SeNPs in yeast cells involves various enzymes. Superoxide dismutase may contribute to nucleation processes, resulting in the formation of smaller nanoparticles. Glutathione peroxidase participates in maintaining the glutathione antioxidant system and in the formation of intermediate selenium-containing compounds, particularly glutathioneselenol. Thioredoxin reductases maintain the activity of the thioredoxin system, which is involved in regulating cellular redox homeostasis, protecting yeast cells against oxidative stress, and detoxifying toxic forms of selenium (Yang et al., 2024).

In addition to enzymatic processes, low-molecular-weight thiol compounds play an important role in selenium reduction. These include glutathione and, particularly in many Gram-positive bacteria, bacillithiol (Yadav et al., 2023). These compounds can interact with selenite through a Painter-type reaction, leading to the formation of intermediate thiol-selenium complexes, particularly selenodiglutathione. Further reduction of these intermediates results in the formation of elemental selenium atoms, which can serve as primary nucleation centers for SeNP formation (Nile et al., 2023).

Specific bacterial proteins may also participate in the biosynthesis of SeNPs. In particular, the intracellular protein elongation factor Tu has been reported to participate in the formation of primary nanoparticle nuclei and to influence their morphology and size (Liu et al., 2024a). The functional groups of phycocyanin, a water-soluble protein pigment (phycobiliprotein) in cyanobacteria, may participate in the reduction of inorganic selenium (selenite) to elemental selenium (Saad et al., 2024). In archaea, the carotenoid pigment bacterioruberin has been reported to contribute to the reduction of selenium ions (Alvares et al., 2025).

The formation of SeNPs usually occurs in several successive stages (Figure 1). At the initial stage, selenite is transported into the microbial cell via specific or nonspecific membrane transporters, particularly those involved in sulfate transport. This is followed by

the reduction of selenium ions to Se^0 atoms and the formation of primary nucleation nuclei. In the case of intracellular synthesis, these nuclei can be transported to the periplasmic space or outside the cell. The next stage involves the aggregation and growth of nanoparticles, which often occurs via the Ostwald ripening process, when small nuclei aggregate into larger spherical structures (Liu et al., 2024a).

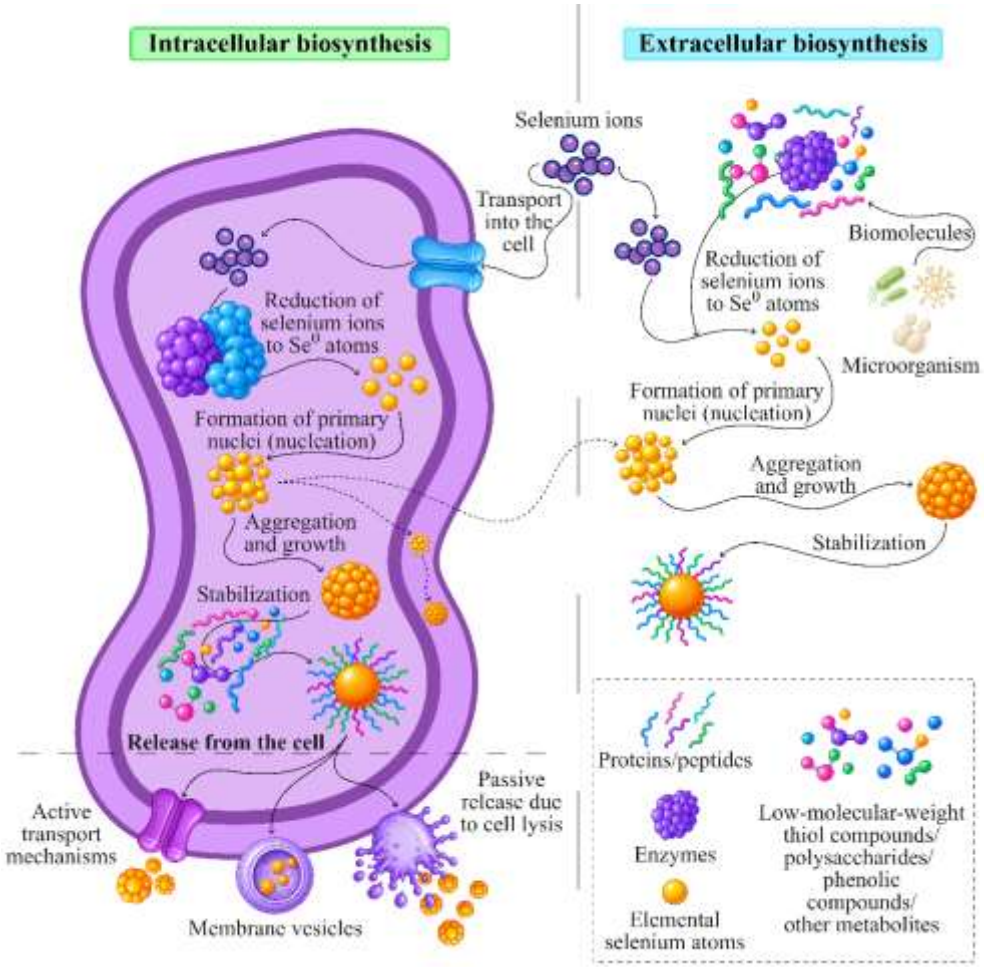

Figure 1. Proposed mechanisms of intracellular and extracellular biosynthesis of selenium nanoparticles by microorganisms

Original conceptual figure designed and assembled by the authors in Inkscape, incorporating selected graphical elements created with the assistance of AI-based tools. The figure was not reproduced or adapted from previously published sources

The release of nanoparticles from microbial cells can occur through various pathways, including active transport mechanisms, release through membrane vesicles, or passive release resulting from partial cell lysis. In some cases, the accumulation of intracellular SeNPs may lead to mechanical disruption of the cell wall, thereby contributing to their release into the extracellular environment. At later stages of microbial growth, selenium reduction in

the periplasmic or extracellular space may also occur, allowing nanoparticles to form without disrupting the microbial cell. Such a mechanism may be more favorable for the long-term survival and functioning of microorganisms in environments with elevated selenium concentrations (Zhong et al., 2024b).

An important stage is the stabilization of nanoparticles. After formation, the surface of SeNPs can become covered with various microbial metabolites, including proteins, peptides, and exopolysaccharides. These biomolecules form a natural organic shell that acts as a capping layer. Such a shell can contribute to the electrostatic stabilization of the colloidal system. The resulting negative zeta potential may reduce particle aggregation and contribute to the stability of biogenic SeNPs in aqueous environments (Ibrahim et al., 2025).

Prospects for the use of biogenic selenium nanoparticles in the food industry

Food fortification and biofortification

In recent years, the potential use of biogenic SeNPs in the production of fermented dairy products, probiotic preparations, and dietary supplements has been investigated. Technologies for producing selenium-containing yogurt powder and liquid yogurt enriched with biogenic SeNPs have been described. The use of probiotic cultures, including *Lactobacillus rhamnosus*, has enabled the production of products with high selenium content and acceptable technological properties (Rao and Poonia, 2024). At the same time, the incorporation of SeNPs into yogurt requires comprehensive evaluation of their effects on the microbiological and physicochemical characteristics of the finished product, which is important for the development of stable functional dairy products (Khonkiv et al., 2025). Powder based on selenium-enriched *Limosilactobacillus reuteri* has been investigated as a potential functional additive for use in products intended to support gastrointestinal health (Sun et al., 2024b). Similarly, bacteria of the genus *Enterococcus* are capable of transforming inorganic selenium into organic forms or elemental selenium nanoparticles, indicating their potential use as selenium sources in the production of fermented dairy products and other functional foods (Liu et al., 2022).

The strain *Saccharomyces cerevisiae* CNCM I-3060 is authorized in the European Union as a food and feed additive. The organic forms of selenium accumulated in yeast cells are characterized by high bioavailability, reported to reach 90–95%, which is higher than that of inorganic selenium salts (Hyrslova et al., 2024). In addition, *S. cerevisiae*, traditionally used in the baking industry, can accumulate 1559–4270 μg Se/g of dry biomass, converting selenium predominantly into organic compounds and biogenic nanoparticles (Faramarzi et al., 2020). This may provide an opportunity to produce bakery products with controlled selenium content without substantial changes to the baking process.

A separate area of research is the development of functional fermented beverages. One example is craft beer produced using the probiotic yeast *Saccharomyces boulardii*. During cultivation, yeast cells accumulated up to 5.92 mg Se/g of dry mass, while the selenium content of the finished beverage reached 0.642 mg/L. The obtained beer contained approximately 2.4% alcohol and had a pH of approximately 4.5 (González-Salitre et al., 2025). The combination of the probiotic properties of *S. boulardii* with the antioxidant properties of biogenic SeNPs may contribute to the functional characteristics of the beverage. However, the potential health effects of such products require further investigation. The ability of *S. boulardii* to survive acidic conditions in the gastrointestinal tract also supports its investigation as a carrier of selenium for functional food applications (González-Salitre et al., 2023).

An important area of application of biogenic SeNPs is the biofortification of agricultural crops, which can promote selenium accumulation in edible plant tissues. This approach may

increase the nutritional value of plant products during cultivation. One method involves treating plants with preparations containing biogenic selenium nanoparticles. For example, foliar spraying with the culture liquid of *Bacillus subtilis* SE201412 increased selenium accumulation in wheat and rice grains. In wheat grains, the proportion of organic selenium after treatment was 80–94.6%, whereas in rice, the total selenium content increased by 212.5–587.5% compared with the control (Huang et al., 2023). Pre-sowing treatment of soybean (*Glycine max*) seeds with low concentrations of SeNPs (0.5–1.0 μM) stimulated seed germination, improved seedling development, and promoted selenium accumulation in soybean grains. Given the widespread use of soybeans in the production of soy milk, sauces, and other products, such biofortification may increase the selenium content of the resulting food products. Similarly, the application of biogenic SeNPs to wheat and rapeseed (*Brassica napus*) has been reported to improve plant physiological parameters and promote selenium accumulation in grains (Abdelsalam et al., 2023). Foliar application of SeNPs at a concentration of 20 ppm during sunflower (*Helianthus annuus*) cultivation was associated with increased contents of proteins, carbohydrates, and carotenoids, suggesting potential effects on the nutritional composition of the plant material (Amin et al., 2021b).

The use of biogenic SeNPs for food fortification should comply with applicable requirements for the safe intake of selenium. In the European Union, selenium-containing food supplements are regulated under relevant EU legislation, including Regulation (EC) No. 1170/2009, which specifies permitted vitamin and mineral substances and their forms for use in foods and food supplements (Hyrslova et al., 2024). Selenium fortification should therefore be designed to provide an appropriate intake without exceeding established upper intake levels.

Extension of the storage period for fruits and vegetables

Biosynthesized SeNPs demonstrate potential for extending the shelf life of fruits and vegetables due to their antifungal, antioxidant, and protective properties. Their application may reduce postharvest losses, suppress the development of phytopathogenic microorganisms, slow ripening processes, and help maintain the nutritional quality of plant products. Thus, treatment of strawberries with SeNPs allowed the berries to be stored for 16 days at 6 °C and was associated with reduced physiological weight loss, maintenance of moisture content, and a lower incidence of decay. An increase in the activity of antioxidant defense enzymes, particularly catalase and peroxidase, as well as an increase in the total content of phenolic compounds, was also observed (Aftab et al., 2023). The effectiveness of SeNP treatment in maintaining the postharvest quality of strawberries has also been demonstrated under conditions of *Botrytis cinerea* (gray mold) infection (Hamouda et al., 2024).

The protective effects of SeNPs have also been investigated in citrus fruits. Treatment with nanoparticles suppressed the development of *Penicillium digitatum*, a major causal agent of postharvest decay in citrus fruits. A particularly pronounced protective effect was observed when a SeNP nanocomposite with nanochitosan was used. Treatment of infected oranges completely suppressed the growth of *P. digitatum* and maintained their marketable appearance. Pronounced lysis and deformation of fungal hyphae were observed as early as 12 h after treatment, indicating rapid antifungal activity of the nanocomposite (Salem et al., 2022).

Biogenic SeNPs also exhibited antifungal activity against *Fusarium oxysporum* and *Fusarium moniliforme* in tomato plants. Treatment of infected fruits completely suppressed the growth of both pathogens and allowed tomato freshness to be maintained for 25 days at 25 °C and up to 35 days at 5 °C. Significant morphological damage to the fungal mycelium,

including deformation and lysis, was observed as early as 18 h after SeNP application. In addition to the antifungal effect, the nanoparticles reduced physiological weight loss and pH and increased the contents of carotenoids and lycopene, which contributed to maintaining tomato quality during storage (Manaa et al., 2023).

The potential of SeNPs has also been investigated in other fruit crops. An edible coating based on a composite of polyvinyl alcohol, chitosan, and biosynthesized selenium nanoparticles effectively extended the shelf life of plums. The coating reduced weight loss and helped maintain fruit firmness and was also associated with a decrease in titratable acidity and increases in the contents of soluble solids, L-ascorbic acid, and anthocyanins (Abdelaziz et al., 2025).

Exogenous application of biosynthesized SeNPs to mango plants affected by malformation disease increased chlorophyll content, membrane stability index, proline levels, and soluble sugar content. The most effective concentration under the conditions of the study was 30 μg/mL. Treatment with nanoparticles was associated with reduced biotic stress, increased activities of antioxidant defense enzymes, including superoxide dismutase and peroxidase, and increased accumulation of phenolic compounds and flavonoids. In *in vitro* studies, SeNPs at a concentration of 300 μg/mL showed the highest inhibition of *Fusarium mangiferae*, the causal agent of mango malformation disease (Shahbaz et al., 2023).

A positive effect of SeNPs was also observed during the storage of button mushrooms (*Agaricus bisporus*). Treatment with nanoparticles reduced the intensity of enzymatic browning, apparently by attenuating oxidative processes, and contributed to maintaining the postharvest quality of the mushrooms (Wang et al., 2024b).

The antioxidant properties of SeNPs may help protect fruit and vegetable tissues against oxidative stress, maintain the activity of antioxidant enzymes, and promote the accumulation of phenolic compounds. In addition, SeNP-based coatings can form a semipermeable physical barrier that limits gas exchange and moisture loss, thereby reducing respiration rate and slowing ripening and biochemical degradation. The combination of these effects may contribute to extending shelf life and maintaining the nutritional and marketable quality of fruit and vegetable products (Shahbaz et al., 2023).

Action on foodborne pathogens

Biosynthesized SeNPs exhibit antimicrobial activity against a broad range of bacterial and fungal pathogens that contribute to foodborne diseases, food spoilage, and mycotoxin production. Numerous studies indicate that the antimicrobial effectiveness of SeNPs depends on the microorganisms used for nanoparticle biosynthesis, their physicochemical characteristics, and the target microorganisms. High antibacterial activity has been reported for SeNPs synthesized using various microorganisms. In particular, nanoparticles obtained using an extract of baker's yeast, *Saccharomyces cerevisiae*, inhibited the growth of *Escherichia coli* (MIC, 125 μg/mL) and *Staphylococcus aureus* (MIC, 62.5 μg/mL) and also exhibited antifungal activity against *Aspergillus fumigatus* (MIC, 250 μg/mL) and *Aspergillus niger* (MIC, 500 μg/mL) (Salem, 2022). Similar results were obtained for SeNPs synthesized using the yeast *Yarrowia lipolytica*. The nanoparticles inhibited the growth of *Serratia marcescens*, *Klebsiella pneumoniae*, *Escherichia coli*, *Pseudomonas aeruginosa*, and *Bacillus subtilis* at concentrations of 160–640 μg/mL (Lashani et al., 2024).

High antimicrobial activity has also been reported for SeNPs synthesized using the phototrophic microorganism *Arthrospira platensis*. Their application inhibited the growth of *Staphylococcus aureus* (inhibition zone, 18.7 mm; MIC, 17.5 μg/mL) and *Salmonella Typhimurium* (inhibition zone, 15.3 mm; MIC, 22.5 μg/mL) (ElSaied et al., 2021).

Biogenic SeNPs obtained using the lactic acid bacterium *Lactobacillus casei* have also demonstrated antimicrobial activity. These nanoparticles were active against the psychrotrophic bacterium *Pseudomonas fluorescens* (MIC, 0.1 mg/mL), which is associated with spoilage of refrigerated food products, particularly raw milk, fish, and meat (Xu et al., 2023).

Particular attention has been given to the antifungal activity of biogenic SeNPs, since fungi can cause food spoilage and produce mycotoxins. SeNPs obtained using the endophytic bacterium *Bacillus amyloliquefaciens* completely inhibited the growth of *Fusarium graminearum* at a concentration of 10 μg/mL and also reduced the accumulation of the mycotoxin deoxynivalenol (Ibrahim et al., 2025). Using the supernatant of *Bacillus megaterium*, SeNPs were synthesized that effectively inhibited the development of *Rhizoctonia solani*, with a maximum inhibition zone of 45 mm at a concentration of 1 mM and an MIC of 0.0625 mM (Hashem et al., 2021a). SeNPs synthesized by *Bacillus subtilis* exhibited antifungal activity against fungi of the genus *Aspergillus*, particularly *A. niger* (inhibition zone, 27.5 mm; MIC, 55 μg/mL) (Abdel-Moneim et al., 2022). Antifungal activity has also been reported for SeNPs synthesized using fungi. For example, nanoparticles obtained using *Trichoderma harzianum* inhibited the growth of *Fusarium culmorum* by 84% at a concentration of 100 mg/L and were also effective against *Fusarium oxysporum*, *Alternaria solani*, *Pyricularia grisea*, and *Colletotrichum capsici* (Kashisaz et al., 2024).

The antimicrobial activity of biogenic SeNPs is associated with several interconnected mechanisms. One important mechanism is the generation of reactive oxygen species (ROS), which can cause oxidative damage to proteins, lipids, and nucleic acids in microbial cells. In addition, SeNPs can interact with thiol groups of cellular proteins, affecting cell wall integrity and membrane function. These interactions may increase membrane permeability and disrupt the respiratory chain and ATP synthesis, thereby inhibiting cell growth and potentially leading to cell death or lysis (Meenambigai et al., 2022).

The antimicrobial activity of SeNPs is also influenced by their physicochemical properties. Biogenically synthesized nanoparticles are often reported within a size range of approximately 3–50 nm. Smaller particles have a greater specific surface area, which may facilitate interactions with microbial cells and contribute to increased antimicrobial activity. Surface charge is also important because it influences colloidal stability, particle aggregation, and electrostatic interactions with microbial cell surfaces. In addition, the biosynthesis method and composition of the SeNP surface coating can affect their biological activity. Proteins, polysaccharides, lipids, and other biomolecules can act as natural stabilizing agents, contributing to nanoparticle stability and interactions with microbial cells and thereby potentially affecting their antimicrobial activity (Al-Saggaf et al., 2020; Yuan et al., 2023).

Active packaging

A wide range of natural and synthetic polymers is used to create active packaging materials incorporating biosynthesized SeNPs, which can serve both structural and functional roles. Polymer matrices facilitate the uniform distribution and stabilization of nanoparticles, reducing their aggregation, and form films or coatings with the required mechanical, barrier, and functional properties. The combination of SeNPs with a polymer matrix makes it possible to obtain active packaging materials that not only protect products from mechanical damage but also exhibit antimicrobial and antioxidant activity, increased resistance to ultraviolet radiation, and potential to extend the shelf life of food products (Ndwandwe et al., 2021).

One of the most common biopolymers used to create active packaging is starch due to its low cost, biodegradability, availability, and high film-forming ability. Nanocomposite films based on cassava starch modified with SeNPs have been studied. Such materials exhibit

pronounced antimicrobial activity against major foodborne pathogens, particularly *Listeria monocytogenes*, *Salmonella* spp., and *Escherichia coli*. In addition to suppressing the growth of microorganisms, the use of such films resulted in a slowdown of fruit ripening and spoilage processes, as demonstrated during the storage of cherry tomatoes (Nogueira et al., 2024). Potato starch is also a promising basis for creating packaging materials. Packaging materials containing SeNPs can be used for the storage of potato chips. Such active packaging slows the oxidation of fatty acids and the formation of hexanal, thereby helping maintain the quality of the food product (Ndwandwe et al., 2022).

Another promising biopolymer is chitosan, which is characterized by biocompatibility, natural antimicrobial activity, and high film-forming ability. The incorporation of SeNPs into a nanochitosan matrix can result in stable nanocomposites with improved functional properties. Of particular interest are edible coatings based on nanochitosan, SeNPs, and natural plant extracts, particularly pomegranate peel and cinnamon extracts. The use of such packaging materials suppresses the development of phytopathogenic fungi on citrus fruit surfaces, which may reduce product losses during storage (Gharieb et al., 2025a; Hassan et al., 2024).

Among polymers of microbial origin, γ-polyglutamic acid (γ-PGA) attracts attention as a promising water-soluble, edible, and non-toxic biopolymer. Complexes of γ-PGA with SeNPs are characterized by high biocompatibility and functional activity. Se-γ-PGA-based materials can be used as components of active packaging coatings and have also been investigated for seed treatment, fertilizer production, and functional food supplements (Likidtaveesin et al., 2025). Another promising material is polylactic acid (PLA), which, due to its high mechanical strength, transparency, thermoplasticity, and suitability for food-contact applications, is widely used to manufacture packaging films. PLA-SeNP composites exhibit antibacterial activity against *Staphylococcus aureus* and *Escherichia coli* and are characterized by antioxidant properties, increased water resistance, and resistance to ultraviolet radiation (Lu et al., 2020).

A promising direction is the use of microbial exopolysaccharides (EPS), which can serve as natural nanoparticle stabilizers. Functionalization of SeNPs with exopolysaccharides can increase their colloidal stability and antioxidant activity and may facilitate their incorporation into biopolymer packaging materials (Wang et al., 2022a).

In addition to the main polymer matrices, auxiliary components that improve their structural and functional characteristics are also used to create nanocomposite packaging materials. In particular, alginate is often combined with chitosan to form multicomponent composites with high mechanical strength and the potential for controlled release of SeNPs. Carboxymethyl cellulose, glucomannan, and gum arabic can be used to increase the stability of dispersions and reduce nanoparticle aggregation. The incorporation of gelatin or cellulose nanofibers can improve the mechanical strength, elasticity, and barrier properties of films against gases and water vapor. A separate modern direction is the development of multilayer active packaging systems, in which SeNPs are integrated into separate functional layers of the polymer structure. This approach may allow controlled release of biologically active components, improve the stability of the packaging material, and provide more effective protection for food products during transportation and long-term storage (Mohamed & El Zahed, 2024; Nogueira et al., 2024).

Overall, biogenic selenium nanoparticles have significant potential for application in the food industry, ranging from food fortification and biofortification to extending the shelf life of food products, controlling foodborne pathogens, and developing active packaging materials.

Conclusions

The analysis of current scientific studies indicates that the biosynthesis of selenium nanoparticles using microorganisms is a promising direction in modern biotechnology and nanobiotechnology, combining environmental advantages, relative simplicity of the technological process, and the possibility of obtaining biocompatible nanomaterials with a wide range of functional properties. Bacteria represent the most extensively studied and diverse group of microorganisms used for the biosynthesis of SeNPs. Of particular interest are strains isolated from extreme, technologically contaminated, and selenium-containing environments, as their adaptation to high concentrations of toxic selenium compounds may contribute to the development of effective mechanisms for their reduction and detoxification. Yeasts and fungi also represent an important group of eukaryotic microorganisms used for SeNP biosynthesis. Of particular interest are representatives of the genus *Saccharomyces*, which are characterized by high technological suitability and potential for genetic and metabolic optimization. Despite the relatively small number of studies, archaea also represent a promising group of microorganisms for the development of SeNP biosynthesis technologies. Their adaptation to extreme conditions, including high salinity, temperature, and osmotic pressure, is associated with specific enzymatic and metabolic systems that may provide opportunities for obtaining nanoparticles with specific morphological and functional properties.

The characteristics of biogenic SeNPs are determined not only by the microorganism species but also by strain-specific features and biosynthesis conditions. The concentration and chemical form of the precursor, temperature, pH of the medium, process duration, stirring rate, and other technological parameters can substantially affect the size, shape, dispersity, surface charge, stability, and biological activity of nanoparticles. This highlights the need for optimization of biosynthesis conditions for individual microbial producers to obtain SeNPs with reproducible physicochemical characteristics.

A promising direction for further research is the elucidation of the molecular mechanisms underlying microbial selenium reduction and nanoparticle formation. Complex systems involved in maintaining cellular redox homeostasis participate in this process, including antioxidant defense enzymes, various reductases, and low-molecular-weight reducing agents. Further application of genomics, transcriptomics, proteomics, and metabolomics may facilitate the identification of key genes, enzymes, and metabolic pathways involved in selenium biotransformation. This may provide a basis for the rational selection of highly productive natural strains and the development of microbial producers with specific properties.

An important area of practical application of biogenic SeNPs is the food industry. Due to their biological activity and antioxidant and antimicrobial properties, SeNPs may be used for selenium enrichment of food products, the development of functional foods, and increasing their biological value. The use of biogenic SeNPs as components of active packaging materials and coatings for extending the shelf life of food products is also promising. At the same time, widespread application of biogenic SeNPs in food technologies requires further comprehensive studies of their toxicological safety, bioavailability, metabolism, and potential long-term effects.

References

Abbas, H., & Abou Baker, D. (2020). Biological evaluation of selenium nanoparticles biosynthesized by *Fusarium semitectum* as antimicrobial and anticancer agents. *Egyptian Journal of Chemistry*, *63*(4), 1119–1133. https://doi.org/10.21608/ejchem.2019.15618.1945

Abbas, H. S., Abou Baker, D. H., & Ahmed, E. A. (2021). Cytotoxicity and antimicrobial efficiency of selenium nanoparticles biosynthesized by *Spirulina platensis*. *Archives of Microbiology*, *203*(2), 523–532. https://doi.org/10.1007/s00203-020-02042-3

Abd-Elkhalek, H. F., Badawy, A. A., Al-Askar, A. A., Abd Elgawad, H., Hashem, A. H., & Salem, S. S. (2024). Biosynthesis and characterization of selenium and silver nanoparticles using *Trichoderma viride* filtrate and their impact on *Culex pipiens*. *Green Processing and Synthesis*, *13*(1), 20240025. https://doi.org/10.1515/gps-2024-0025

Abdel-Moneim, A. M. E., El-Saadony, M. T., Shehata, A. M., Saad, A. M., Aldhumri, S. A., Ouda, S. M., & Mesalam, N. M. (2022). Antioxidant and antimicrobial activities of *Spirulina platensis* extracts and biogenic selenium nanoparticles against selected pathogenic bacteria and fungi. *Saudi Journal of Biological Sciences*, *29*(2), 1197–1209. https://doi.org/10.1016/j.sjbs.2021.09.046

Abdelaziz, H. T., Seif Mohamed, E. M., Younis, S. K., Ahmed, N., Michaeel, M. N., Abu-Hussien, S. H., Bakry, A., Ebeed, N. M., Nasser, M. A., El-Nasr, M. K. A., Ali, M. A. A., Hemdan, B., Salah, M., & El-Sayed, S. M. (2025). Selenium nanoparticle loaded on PVA/chitosan biofilm synthesized from orange peels: antimicrobial and antioxidant properties for plum preservation, *BMC chemistry*, 19(1), 245, https://doi.org/10.1186/s13065-025-01608-w

Abdelsalam, A., El-Sayed, H., Hamama, H. M., Morad, M. Y., Aloufi, A. S., & Abd El-Hameed, R. M. (2023). Biogenic selenium nanoparticles: Anticancer, antimicrobial, insecticidal properties and their impact on soybean (Glycine max L.) seed germination and seedling growth. *Biology*, *12*(11), 1361. https://doi.org/10.3390/biology12111361

Abdollahnia, M., Makhdoumi, A., Mashreghi, M., & Eshghi, H. (2020). Exploring the potentials of halophilic prokaryotes from a solar saltern for synthesizing nanoparticles: the case of silver and selenium. *PLoS One*, *15*(3), e0229886. https://doi.org/10.1371/journal.pone.0229886

Abu-Elghait, M., Hasanin, M., Hashem, A. H., & Salem, S. S. (2021). Ecofriendly novel synthesis of tertiary composite based on cellulose and myco-synthesized selenium nanoparticles: Characterization, antibiofilm and biocompatibility. *International Journal of Biological Macromolecules*, *175*, 294–303. https://doi.org/10.1016/j.ijbiomac.2021.02.040

Aftab, A., Ali, M., Yousaf, Z., Binjawhar, D. N., Hyder, S., Aftab, Z. E. H., Maqbool, Z., Shahzadi, Z., Eldin, S. M., Iqbal, R., & Ali, I. (2023). Shelf-life extension of *Fragaria× ananassa* Duch. using selenium nanoparticles synthesized from *Cassia fistula* Linn. leaves. *Food Science & Nutrition*, *11*(6), 3464-3484. https://doi.org/10.1002/fsn3.3336

Afzal, B., Yasin, D., Naaz, H., Sami, N., Zaki, A., Rizvi, M. A., Kumar, R., Srivastava, P., & Fatma, T. (2021). Biomedical potential of *Anabaena variabilis* NCCU-441 based selenium nanoparticles and their comparison with commercial nanoparticles. *Scientific Reports*, *11*(1), 13507. https://doi.org/10.1038/s41598-021-91738-7

Akcay, F. A., & Avci, A. (2020). Effects of process conditions and yeast extract on the synthesis of selenium nanoparticles by a novel indigenous isolate *Bacillus* sp. EKT1 and characterization of nanoparticles. *Archives of Microbiology*, *202*(8), 2233–2243. https://doi.org/10.1007/s00203-020-01942-8

Alam, H., Khatoon, N., Khan, M. A., Husain, S. A., Saravanan, M., & Sardar, M. (2020). Synthesis of selenium nanoparticles using probiotic bacteria *Lactobacillus acidophilus* and their enhanced antimicrobial activity against resistant bacteria. *Journal of Cluster Science*, *31*(5), 1003–1011. https://doi.org/10.1007/s10876-019-01705-6

Al-Hagar, O. E., Abol-Fotouh, D., Abdelkhalek, E. S., Elsoud, M. M. A., & Sidkey, N. M. (2021). *Bacillus niabensis* OAB2: Outstanding bio-factory of selenium nanoparticles. *Materials Chemistry and Physics*, *273*, 125147. https://doi.org/10.1016/j.matchemphys.2021.125147

Ali, B. A., Allam, R. M., Hasanin, M. S., & Hassabo, A. A. (2024). Biosynthesis of selenium nanoparticles as a potential therapeutic agent in breast cancer: G2/M arrest and apoptosis induction. *Toxicology Reports*, *13*, 101792. https://doi.org/10.1016/j.toxrep.2024.101792

Alipour, S., Kalari, S., Morowvat, M. H., Sabahi, Z., & Dehshahri, A. (2021). Green synthesis of selenium nanoparticles by cyanobacterium *Spirulina platensis* (abdf2224): cultivation condition quality controls. *BioMed Research International*, *2021*(1), 6635297. https://doi.org/10.1155/2021/6635297

Al-Quwaie, D. A. (2023). The influence of bacterial selenium nanoparticles biosynthesized by *Bacillus subtilis* DA20 on blood constituents, growth performance, carcass traits, and gut microbiota of broiler chickens. *Poultry Science*, *102*(9), 102848. https://doi.org/10.1016/j.psj.2023.102848

Al-Saggaf, M. S., Tayel, A. A., Ghobashy, M. O., Alotaibi, M. A., Alghuthaymi, M. A., Moussa, S. H. (2020). Phytosynthesis of selenium nanoparticles using the costus extract for bactericidal application against foodborne pathogens. *Green Processing and Synthesis*, *9*(1), 477–487. https://doi.org/10.1515/gps-2020-0038

Alsehli, B. R., Al-Hakkani, M. F., Alluhayb, A. H., Saleh, S. M., Mohamed, H., Hassane, A. M., & Hassan, M. H. (2025). Facile mycosynthesis of selenium nanoparticles by *Aspergillus candidus* extract: unveiling characterization, potent antimicrobial properties, and cytotoxic activities. *BioNanoScience*, *15*(2), 234. https://doi.org/10.1007/s12668-025-01845-2

Alsulami, M. N., & El-Saadony, M. T. (2023). Supplementing broiler diets with bacterial selenium nanoparticles enhancing performance, carcass traits, blood indices, antioxidant status, and caecal microbiota of *Eimeria tenella*-infected broiler chickens. *Poultry Science*, *102*(12), 103111. https://doi.org/10.1016/j.psj.2023.103111

Alvares, J., Gaonkar, S., D'costa, A., Shyama, S. K., Furtado, I. (2025). Antimicrobial potential and alleviation of arsenic toxicity in human lymphocytes by bacterioruberin and selenium nanoparticles from *Haloferax alexandrinus* GUSF-1 (KF796625). *Discover Applied Sciences*, *7*(8), 919. https://doi.org/10.1007/s42452-025-07602-0

Alvares, J. J., & Furtado, I. J. (2022). Conversion of selenite by *Haloferax alexandrinus* GUSF-1 (KF796625) to pentagonal selenium nanoforms which *in vitro* modulates the formation of calcium oxalate crystals. *Journal of applied microbiology*, *132*(3), 1900–1913. https://doi.org/10.1111/jam.15309

Amin, B. H., Ahmed, H. Y., El Gazzar, E. M., & Badawy, M. M. (2021a). Enhancement the mycosynthesis of selenium nanoparticles by using gamma radiation. *Dose-Response*, *19*(4), 15593258211059323. https://doi.org/10.1177/155932582110593

Amin, M. A., Ismail, M. A., Badawy, A. A., Awad, M. A., Hamza, M. F., Awad, M. F., Fouda, A. (2021b). The potency of fungal-fabricated selenium nanoparticles to improve the growth performance of *Helianthus annuus* L. and control of cutworm *Agrotis ipsilon*. *Catalysts*, *11*(12), 1551. https://doi.org/10.3390/catal11121551

Aminisough, S. A., Daneshjou, S., & Khajeh, K. (2024). Biosynthesis, characterization, and investigation of cytotoxic activities of selenium nanoparticles utilizing *Limosilactobacillus fermentum*. *Green Processing and Synthesis*, *13*(1), 20240030. https://doi.org/10.1515/gps-2024-0030

Annamalai, K. K., Selvaraj, B., Subramanian, K., Binsuwaidan, R., & Saeed, M. (2024). Antibiofilm and antivirulence activity of selenium nanoparticles synthesized from cell-free extract of moderately halophilic bacteria. *Microbial Pathogenesis*, *193*, 106740. https://doi.org/10.1016/j.micpath.2024.106740

Ao, B., Du, Q., Liu, D., Shi, X., Tu, J., & Xia, X. (2023). A review on synthesis and antibacterial potential of bio-selenium nanoparticles in the food industry. *Frontiers in microbiology*, *14*, 1229838. https://doi.org/10.3389/fmicb.2023.1229838

Aparici-Carratala, D., Esclapez, J., Bautista, V., Bonete, M. J., & Camacho, M. (2023). Archaea: current and potential biotechnological applications. *Research in Microbiology*, *174*(7), 104080. https://doi.org/10.1016/j.resmic.2023.104080

Arruda, G. L., Reis, W. S., Raymundo, M. T. F., Shibukawa, V. P., Cruz-Santos, M. M., Silos, N. O., Prado, C. A., Marcelino, P. R. F., da Silva, S. S., & Santos, J. C. (2025). Biotechnological potential of *Monascus*: biological aspects, metabolites of interest, and opportunities for new products. *Microbiological Research*, *297*, 128177. https://doi.org/10.1016/j.micres.2025.128177

Arunthirumeni, M., Veerammal, V., & Shivakumar, M. S. (2022). Biocontrol efficacy of mycosynthesized selenium nanoparticle using *Trichoderma* sp. on insect pest *Spodoptera litura*. *Journal of Cluster Science*, *33*(4), 1645–1653. https://doi.org/10.1007/s10876-021-02095-4

Ashengroph, M., & Hosseini, S. R. (2021). A newly isolated *Bacillus amyloliquefaciens* SRB04 for the synthesis of selenium nanoparticles with potential antibacterial properties. *International Microbiology*, *24*(1), 103–114. https://doi.org/10.1007/s10123-020-00147-9

Ashengroph, M., & Tozandehjani, S. (2022). Optimized resting cell method for green synthesis of selenium nanoparticles from a new *Rhodotorula mucilaginosa* strain. *Process Biochemistry*, *116*, 197–205. https://doi.org/10.1016/j.procbio.2022.03.014

Ashwin, S. P., Shah, K. K., Dhanraj, G., Ramasubburayan, R., & Bharathi, S. (2025). Biosynthesis of selenium nanoparticles from marine *Stutzerimonas* sp. and their biomedical implications. *BioNanoScience*, *15*, 543. https://doi.org/10.1007/s12668-025-02163-3

Avendano, R., Munoz-Montero, S., Rojas-Gatjens, D., Fuentes-Schweizer, P., Vieto, S., Montenegro, R., Salvador, M., Frew, R., Kim, J., Chavarria, M., & Jimenez, J. I. (2023). Production of selenium nanoparticles occurs

through an interconnected pathway of sulphur metabolism and oxidative stress response in *Pseudomonas putida* KT2440. *Microbial Biotechnology*, *16*(5), 931–946. https://doi.org/10.1111/1751-7915.14215

Babajide, A. M., Adebami, G. E., & Adebayo-Tayo, B. C. (2025). Screening of rhizobacteria from monkey pod trees for plant growth promoters and evaluating the antifungal potential of the biosynthesized selenium nanoparticles. *Scientific Reports*, *15*(1), 16797. https://doi.org/10.1038/s41598-025-96330-x

Babavalian, H., Shakeri, F., Safarpour, A., Hassankhani, I., Nasrollahzadeh, Z., & Amoozegar, M. A. (2025). Biosynthesis and characterization of selenium nanoparticles by *Kocuria* strain Bm3: evaluating their synergistic antimicrobial activity with *Chlorella vulgaris* crude extract against multidrug-resistant bacteria. *Iranian Journal of Pharmaceutical Research: IJPR*, *24*(1), e164350. https://doi.org/10.5812/ijpr-164350

Bafghi, M. H., Darroudi, M., Zargar, M., Zarrinfar, H., & Nazari, R. (2021). Biosynthesis of selenium nanoparticles by *Aspergillus flavus* and *Candida albicans* for antifungal applications. *Micro & Nano Letters*, *16*(14), 656–669. https://doi.org/10.1049/mna2.12096

Bafghi, M. H., Nazari, R., Darroudi, M., Zargar, M., & Zarrinfar, H. (2022). The effect of biosynthesized selenium nanoparticles on the expression of *CYP51A* and *HSP90* antifungal resistance genes in *Aspergillus fumigatus* and *Aspergillus flavus*. *Biotechnology Progress*, *38*(1), e3206. https://doi.org/10.1002/btpr.3206

Bai, X., Sheng, Y., Tang, Z., Pan, J., Wang, S., Tang, B., ... & Zhang, H. (2023). Polyketides as secondary metabolites from the genus *Aspergillus*. *Journal of Fungi*, *9*(2), 261. https://doi.org/10.3390/jof9020261

Bharathi, S., Kumaran, S., Suresh, G., Ramesh, M., Thangamani, V., Pugazhvendan, S. R., & Sathiyamurthy, K. (2020). Extracellular synthesis of nanoselenium from fresh water bacteria *Bacillus* sp., and its validation of antibacterial and cytotoxic potential. *Biocatalysis and Agricultural Biotechnology*, *27*, 101655. https://doi.org/10.1016/j.bcab.2020.101655

Bondar, H., & Krasinko, V. (2026). Iron accumulation in yeast under different cultivation conditions. *Ukrainian Food Journal*, *15*(2), 518–531. https://doi.org/10.24263/2304-974X-2026-15-2-14

Bondar, H., & Krasinko, V. (2025). Rapid spectrophotometric method for the determination of iron content in yeast. *Ukrainian Journal of Food Science*, *13*(1), 80–90. https://doi.org/10.24263/2310-1008-2025-13-1-9

Borah, S. N., Goswami, L., Sen, S., Sachan, D., Sarma, H., Montes, M., Peralta-Videa, J. R., Pakshirajan, K., & Narayan, M. (2021). Selenite bioreduction and biosynthesis of selenium nanoparticles by *Bacillus paramycoides* SP3 isolated from coal mine overburden leachate. *Environmental Pollution*, *285*, 117519. https://doi.org/10.1016/j.envpol.2021.117519

Bravo, F., Moraga, R., Valenzuela, C., Aguayo, P., Smith, C. T., Contreras, F., Gugliandolo, C., Zammuto, V., & Campos, V. L. (2024). Arsenic biomineralization and selenium nanoparticles biosynthesis by *Halomonas boliviensis* strain H-10 isolated from the high-altitude Salar de Huasco salt flat (Chile). *Environmental Technology & Innovation*, 34, 103575. https://doi.org/10.1016/j.eti.2024.103575

Bugingo, C., Infantino, A., Okello, P., Perez-Hernandez, O., Petrović, K., Turatsinze, A. N., & Moparthi, S. (2025). From morphology to multi-omics: A new age of *Fusarium* research. *Pathogens*, *14*(8), 762. https://doi.org/10.3390/pathogens14080762

Chauhan, R., Bhargava, P., Singh, A., Prasad, R., & Goel, A. (2024). Exploring the impact of mycogenic selenium nanoparticles on production of exopolysaccharides from arid zone bacteria. *Biocatalysis and Agricultural Biotechnology*, *60*, 103313. https://doi.org/10.1016/j.bcab.2024.103313

Chen, X., Lu, Y., Liu, X., Gu, Y., & Li, F. (2025). *Trichoderma*: dual roles in biocontrol and plant growth promotion. *Microorganisms*, *13*(8), 1840. https://doi.org/10.3390/microorganisms13081840

Cinar-Acar, B. (2025). Size reduction of selenium nanoparticles synthesized from yeast beta glucan using cold atmospheric plasma. *Scientific Reports*, *15*(1), 25875. https://doi.org/10.1038/s41598-025-09192-8

Cui, Y., Chen, Y., Shi, Q., Feng, J., Song, Y., Yao, J., & Xie, X. (2025). UV assisted nano-selenium synthesis using *Saccharomyces cerevisiae* and *Escherichia coli* waste. *Environmental Technology & Innovation*, *39*, 104325. https://doi.org/10.1016/j.eti.2025.104325

Diko, C. S., Zhang, H., Lian, S., Fan, S., Li, Z., & Qu, Y. (2020). Optimal synthesis conditions and characterization of selenium nanoparticles in *Trichoderma* sp. WL-Go culture broth. *Materials Chemistry and Physics*, *246*, 122583. https://doi.org/10.1016/j.matchemphys.2019.122583

Duan, Y., Li, M., Zhang, S., Wang, Y., Deng, J., Wang, Q., Yi, T., Dong, X., Cheng, S., He, Y., Gao, C., & Wang, Z. (2022). Highly efficient biotransformation and production of selenium nanoparticles and polysaccharides using potential probiotic *Bacillus subtilis* T5. *Metabolites*, *12*(12), 1204. https://doi.org/10.3390/metabo12121204

Elahian, F., Reiisi, S., Shahidi, A., & Mirzaei, S. A. (2017). High-throughput bioaccumulation, biotransformation, and production of silver and selenium nanoparticles using genetically engineered *Pichia pastoris*. *Nanomedicine: Nanotechnology, Biology and Medicine*, *13*(3), 853–861. https://doi.org/10.1016/j.nano.2016.10.009

El-Fawal, M. F., El-Fallal, A. A., Abou-Dobara, M. I., El-Sayed, A. K., & El-Zahed, M. M. (2025). *In vitro* antibacterial activity of myco-synthesized selenium nanoparticles against a multidrug-resistant *E. coli* isolated from clinical specimens. *Discover Materials*, *5*(1), 130. https://doi.org/10.1007/s43939-025-00330-7

Elhalis, H. (2024). Expanding the horizons of *Saccharomyces cerevisiae*: nutrition, oenology, and bioethanol production. *Sustainability*, *16*(24), 11151. https://doi.org/10.3390/su162411151

El Refai, H. A., Mohamed, S. I., Naser, A. F. A., Saleh, A. M., Gomaa, S. K., Zaki, R. A., & Hamed, M. A. (2024). Biogenic synthesized SeONPs by *Bacillus paramycoides* as antimicrobial, anticancer, antioxidant, apoptotic and hepatorenal treating agent. *Biocatalysis and Agricultural Biotechnology*, *57*, 103080. https://doi.org/10.1016/j.bcab.2024.103080

El-Saadony, M. T., Saad, A. M., Taha, T. F., Najjar, A. A., Zabermawi, N. M., Nader, M. M., AbuQamar, S. F., El-Tarabily, K. A., & Salama, A. (2021), Selenium nanoparticles from *Lactobacillus paracasei* HM1 capable of antagonizing animal pathogenic fungi as a new source from human breast milk. *Saudi Journal of Biological Sciences*, *28*(12), 6782–6794. https://doi.org/10.1016/j.sjbs.2021.07.059

ElSaied, B. E., Diab, A. M., Tayel, A. A., Alghuthaymi, M. A., Moussa, S. H. (2021). Potent antibacterial action of phycosynthesized selenium nanoparticles using *Spirulina platensis* extract. *Green Processing and Synthesis*, *10*(1), 49–60. https://doi.org/10.1515/gps-2021-0005

El-Sayed, A. I., El-Sheekh, M. M., & Abo-Neima, S. E. (2024). Mycosynthesis of selenium nanoparticles using *Penicillium tardochrysogenum* as a therapeutic agent and their combination with infrared irradiation against Ehrlich carcinoma. *Scientific Reports*, *14*(1), 2547. https://doi.org/10.1038/s41598-024-52982-9

El-Sayed, E. S. R., Abdelhakim, H. K., & Ahmed, A. S. (2020). Solid-state fermentation for enhanced production of selenium nanoparticles by gamma-irradiated *Monascus purpureus* and their biological evaluation and photocatalytic activities. *Bioprocess and Biosystems Engineering*, *43*(5), 797–809. https://doi.org/10.1007/s00449-019-02275-7

El-Sayed, H., Morad, M. Y., Sonbol, H., Hammam, O. A., Abd El-Hameed, R. M., Ellethy, R. A., Ibrahim, A. M., & Hamada, M. A. (2023). Myco-synthesized selenium nanoparticles as wound healing and antibacterial agent: an in vitro and in vivo investigation. *Microorganisms*, *11*(9), 2341. https://doi.org/10.3390/microorganisms11092341

El-Sayyad, G. S., El-Bastawisy, H. S., Gobara, M., & El-Batal, A. I. (2020). Gentamicin-assisted mycogenic selenium nanoparticles synthesized under gamma irradiation for robust reluctance of resistant urinary tract infection-causing pathogens. *Biological Trace Element Research*, *195*(1), 323–342. https://doi.org/10.1007/s12011-019-01842-z

Elshikiby, L. A., Baka, Z. A., & El-Zahed, M. M. (2025). Biological activities of optimized biosynthesized selenium nanoparticles using *Proteus mirabilis* PQ350419 alone or combined with chitosan and ampicillin against common multidrug-resistant bacteria. *Microbial Cell Factories*, *24*(1), 159. https://doi.org/10.1186/s12934-025-02783-0

Escobar-Ramírez, M. C., Castañeda-Ovando, A., Pérez-Escalante, E., Rodríguez-Serrano, G. M., Ramírez-Moreno, E., Quintero-Lira, A., Contreras-López, E., Añorve-Morga, J., Jaimez-Ordaz, J., & González-Olivares, L. G. (2021). Antimicrobial activity of Se-nanoparticles from bacterial biotransformation. *Fermentation*, *7*(3), 130. https://doi.org/10.3390/fermentation7030130

Eydelkhani, M., Kiabi, S., & Nowruzi, B. (2024). In vitro assessment of the effect of magnetic fields on efficacy of biosynthesized selenium nanoparticles by *Alborzia kermanshahica*. *BMC Biotechnology*, *24*(1), 27. https://doi.org/10.1186/s12896-024-00855-4

Fadel, N., Abu-Elghait, M., Gebreel, H., Zendo, T., & Youssef, H. (2025). Lactic acid bacteria-mediated synthesis of selenium nanoparticles: A smart strategy against multidrug-resistant pathogens. *Applied Microbiology*, *5*(4), 121. https://doi.org/10.3390/applmicrobiol5040121

Fahmy, N. F., Abdel-Kareem, M. M., Ahmed, H. A., Helmy, M. Z., & Mahmoud, E. A. R. (2025). Evaluation of the antibacterial and antibiofilm effect of mycosynthesized silver and selenium nanoparticles and their synergistic effect with antibiotics on nosocomial bacteria. *Microbial Cell Factories*, *24*(1), 6. https://doi.org/10.1186/s12934-024-02604-w

Faramarzi, S., Anzabi, Y., Jafarizadeh-Malmiri, H. (2020). Nanobiotechnology approach in intracellular selenium nanoparticle synthesis using *Saccharomyces cerevisiae* – fabrication and characterization. *Archives of Microbiology*, *202*(5), 1203–1209. https://doi.org/10.1007/s00203-020-01831-0

Farouq, M. M., & Shehab, Z. H. (2026). Biological activity of the selenium nanoparticles prepared by *Saccharomyces cerevisiae* extract against methicillin-resistant *Staphylococcus aureus*. *Iraqi Journal of Science*, 679–700. https://doi.org/10.24996/ijs.2026.67.2.9

Fawzi, F. H., & Ahmed, M. E. (2025). Green synthesis and characterization of selenium nanoparticles via *Staphylococcus warneri* approach: Antimicrobial and on PhzM pyocyanin gene expression in *Pseudomonas aeruginosa*. *Plasmonics*, *20*(3), 1455–1471. https://doi.org/10.1007/s11468-024-02378-2

Fouda, A., Hassan, S. E. D., Eid, A. M., Abdel-Rahman, M. A., & Hamza, M. F. (2022). Light enhanced the antimicrobial, anticancer, and catalytic activities of selenium nanoparticles fabricated by endophytic fungal strain, *Penicillium crustosum* EP-1. *Scientific Reports*, *12*(1), 11834. https://doi.org/10.1038/s41598-022-15903-2

Gao, L., Li, X., Li, Y., Zhang, Z., Wang, J., Xu, C., Wu, X. (2024). Biochemical characterization, biosynthesis mechanism, and functional evaluation of selenium-enriched *Aspergillus oryzae* A02. *International Journal of Biological Macromolecules*, *275*, 133714. https://doi.org/10.1016/j.ijbiomac.2024.133714

Ge, M., Zhou, S., Li, D., Song, D., Yang, S., & Xu, M. (2024). Reduction of selenite to selenium nanoparticles by highly selenite-tolerant bacteria isolated from seleniferous soil. *Journal of Hazardous Materials*, *472*, 134491. https://doi.org/10.1016/j.jhazmat.2024.134491

Ghareeb, A., Fouda, A., Kishk, R. M., & El Kazzaz, W. M. (2025). Marine actinobacterium *Streptomyces vinaceusdrappus* mediated nano-selenium: biosynthesis and biomedical activities. *BMC Complementary Medicine and Therapies*, *25*(1), 329. https://doi.org/10.1186/s12906-025-05073-9

Gharieb, M. M., Hassan, E. M., & Soliman, A. M. (2024). Nutritional conditions affecting of selenium nanoparticles synthesized by *Fusarium oxysporum* (CCASU-2023-F9), and their biological activities against mycotoxin-producing fungi isolated from animal feed. *Brazilian Journal of Microbiology*, *55*(4), 3465–3476. https://doi.org/10.1007/s42770-024-01494-9

Gharieb, M. M., Omara, M. S., Soliman, A. M. (2025a). Antifungal activity of mycogenic selenium nanoparticles conjugated with fungal nano chitosan against three important phytopathogenic fungi. *BioNanoScience*, *15*(2), 229. https://doi.org/10.1007/s12668-025-01836-3

Gharieb, M. M., Soliman, A. M., & Omara, M. S. (2025b). Biosynthesis of selenium nanoparticles by potential endophytic fungi *Penicillium citrinum* and *Rhizopus arrhizus*: characterization and maximization. *Biomass Conversion and Biorefinery*, *15*(2), 2319-2328. https://doi.org/10.1007/s13399-023-05084-x

Ghosh, S., Mahanty, S., Das, S., Purkait, S., Darbha, G. K., Pal, R., & Majumder, S. (2025). Eco-friendly synthesis and characterization of crystalline selenium nanoparticles via *Bacillus cereus*. https://doi.org/10.21203/rs.3.rs-7492605/v1

Ghosh, S., Sarkar, B., Kaushik, A., & Mostafavi, E. (2022). Nanobiotechnological prospects of probiotic microflora: Synthesis, mechanism, and applications. *Science of the Total Environment*, *838*, 156212. https://doi.org/10.1016/j.scitotenv.2022.156212

González-Salitre, L., Castañeda-Ovando, A., Basilio-Cortés, U. A., del Carmen García-Contreras, A., Serrano, G. M. R., Cardelle-Cobas, A., Román-Gutiérrez, A. D., & González-Olivares, L. G. (2023). Biogenic production of seleno-amino acids and seleno-nanoparticles by *Saccharomyces boulardii*. *Food Bioscience*, *53*, 102552. https://doi.org/10.1016/j.fbio.2023.102552

González-Salitre, L., González-Olivares, L. G., Salazar-Navarro, A. A., Cervantes-García, D., Durán-Hernández, D., Torres-Ramos, R., Beleño-Cabarcas, M. T., & Basilio-Cortes, U. A. (2025). Spectroscopic analysis of selenium nanoparticles synthesized by *Saccharomyces boulardii* for the production of craft beer. *Fermentation*, *11*(3), 144. https://doi.org/10.3390/fermentation11030144

Gregirchak, N., Syniavska, D., Khonkiv, M., & Stabnikov, V. (2023), Lactic acid bacteria for the synthesis of metals nanoparticles, *Ukrainian Food Journal*, *12*(4), 599–626, http://doi.org/10.24263/2304-974X-2023-12-4-8

Guijarro-Ramírez, N., Sáez-Zamacona, I., Torregrosa, D., Grindlay, G., Gras, L., Pire, C., Mora, J., & Martínez-Espinosa, R. M. (2025). Characterization of biogenic selenium nanoparticles in hypersaline media by single particle inductively coupled plasma mass spectrometry: *Haloferax mediterranei* case. *Analytica Chimica Acta*, *1335*, 343453. https://doi.org/10.1016/j.aca.2024.343453

Guo, W., Shi, X., Wang, L., Cong, X., Cheng, S., Li, L., & Cheng, H. (2024). Optimization of the conditions for the transformation of a *Bacillus subtilis* strain L11 to prepare nano selenium and its preliminary application in sheep feed. *Microbiology Research*, *15*(1), 326–341. https://doi.org/10.3390/microbiolres15010022

Haji Mehdi Nouri, Z., Tafvizi, F., Amini, K., Khandandezfully, N., & Kheirkhah, B. (2024). Enhanced induction of apoptosis and cell cycle arrest in MCF-7 breast cancer and HT-29 colon cancer cell lines via low-dose biosynthesis of selenium nanoparticles utilizing *Lactobacillus casei*. *Biological Trace Element Research*, *202*(3), 1288–1304. https://doi.org/10.1007/s12011-023-03738-5

Hamouda, R. A., Abdel-Hamid, M. S., Hagagy, N., & Nofal, A. M. (2024). The potent effect of selenium nanoparticles: insight into the antifungal activity and preservation of postharvest strawberries from gray mold diseases. *Journal of the Science of Food and Agriculture*, *104*(11), 6756–6768. https://doi.org/10.1002/jsfa.13502

Hamza, F., Vaidya, A., Apte, M., Kumar, A. R., & Zinjarde, S. (2017). Selenium nanoparticle-enriched biomass of *Yarrowia lipolytica* enhances growth and survival of *Artemia salina*. *Enzyme and Microbial Technology*, *106*, 48–54. https://doi.org/10.1016/j.enzmictec.2017.07.002

Hassan, M. G., Hawwa, M. T., Baraka, D. M., El-Shora, H. M., & Hamed, A. A. (2024). Biogenic selenium nanoparticles and selenium/chitosan-Nanoconjugate biosynthesized by *Streptomyces parvulus* MAR4 with antimicrobial and anticancer potential. *BMC Microbiology*, *24*(1), 21, https://doi.org/10.1186/s12866-023-03171-7

Hashem, A. H., Abdelaziz, A. M., Askar, A. A., Fouda, H. M., Khalil, A. M., Abd-Elsalam, K. A., & Khaleil, M. M. (2021a). *Bacillus megaterium*-mediated synthesis of selenium nanoparticles and their antifungal activity against *Rhizoctonia solani* in faba bean plants. *Journal of Fungi*, *7*(3), 195. https://doi.org/10.3390/jof7030195

Hashem, A. H., Khalil, A. M. A., Reyad, A. M., & Salem, S. S. (2021b). Biomedical applications of mycosynthesized selenium nanoparticles using *Penicillium expansum* ATTC 36200. *Biological Trace Element Research*, *199*(10), 3998-4008. https://doi.org/10.1007/s12011-020-02506-z

Hassan, O. H. A., Wei, Y. R., Feng, Z. P., Pei, J. M., Xu, J. N., Du, W. T., Gou, Q. Q., Wang, W. D., Zhao, X., Shi, Q. C., & Zhang, X. G. (2025). Efficient microbial production of selenium nanoparticles by selenium-tolerant *Alcaligenes* sp. HZ-9-3-3. *Current Microbiology*, *82*(9), 394. https://doi.org/10.1007/s00284-025-04389-6

Helmy, E. A. M., San, P. P., Zhang, Y. Z., Adarkwah, C., & Tuda, M. (2023a). Entomotoxic efficacy of fungus-synthesized nanoparticles against immature stages of stored bean pests. *Scientific Reports*, *13*(1), 8508. https://doi.org/10.1038/s41598-023-35697-1

Helmy, E. A., Salah, R. A., El-Shazly, M. M., Alqhtani, A. H., Pokoo-Aikins, A., & Yosri, M. (2023b). Investigation of the impact of mycogenic titanium and selenium nanoparticles on *Fusarium* wilt infection of tomato plant. *Journal of Pure & Applied Microbiology*, *17*(3). https://doi.org/10.22207/JPAM.17.3.45

Hosseini, M., Mashreghi, M., Eshghi, H., & Kosanjian, F. (2025). Antibacterial and antibiofilm activity of biogenic Se-Au nanoparticles against most prevalent pathogenic bacteria. *Advances in Natural Sciences: Nanoscience and Nanotechnology*, *16*(1), 015009. https://doi.org/10.1088/2043-6262/ada0b5

Hossny, N. E., Ismaeil, M., & Saeed, A. M. (2025). Bioremediation and optimization of selenate reduction by a novel *Bacillus cabrialesii* strain (Se1) producing red selenium nanoparticles with potential antibacterial activity. *BMC Microbiology*, *25*(1), 746. https://doi.org/10.1186/s12866-025-04417-2

Huang, J., Jiang, D., Wang, M., & Huang, X. (2022). Highly selenite-tolerant strain *Proteus mirabilis* QZB-2 rapidly reduces selenite to selenium nanoparticles in the cell membrane. *Frontiers in Microbiology*, *13*, 862130. https://doi.org/10.3389/fmicb.2022.862130

Huang, S., Yu, K., Wen, L., Long, X., Sun, J., Liu, Q., Zheng, Z., Zheng, W., Luo, H., & Liu, J. (2023). Development and application of a new biological nano-selenium fermentation broth based on *Bacillus subtilis* SE201412. *Scientific Reports*, *13*(1), 2560. https://doi.org/10.1038/s41598-023-29737-z

Huang, S., Wang, Y., Tang, C., Jia, H., & Wu, L. (2021). Speeding up selenite bioremediation using the highly selenite-tolerant strain *Providencia rettgeri* HF16-A novel mechanism of selenite reduction based on proteomic analysis. *Journal of Hazardous Materials*, *406*, 124690. https://doi.org/10.1016/j.jhazmat.2020.124690

Huang, S. W., Yao, Y. Y., Zhang, H. X., Guo, W. Y., Fang, M. H., Wang, H. B., Sun, Y. J., & Li, M. H. (2025). Novel mechanisms for selenite biotransformation and selenium nanoparticles biogenesis in *Acinetobacter* sp. SX5 isolated from seleniferous soil. *Journal of Hazardous Materials*, *489*, 137694. https://doi.org/10.1016/j.jhazmat.2025.137694

Hussein, H. G., El-Sayed, E. S. R., Younis, N. A., Hamdy, A. E. H. A., & Easa, S. M. (2022). Harnessing endophytic fungi for biosynthesis of selenium nanoparticles and exploring their bioactivities. *AMB Express*, *12*(1), 68. https://doi.org/10.1186/s13568-022-01408-8

Hyrslova, I., Kana, A., Kantorova, V., Krausova, G., Mrvikova, I., & Doskocil, I. (2022). Selenium accumulation and biotransformation in *Streptococcus*, *Lactococcus*, and *Enterococcus* strains. *Journal of Functional Foods*, *92*, 105056. https://doi.org/10.1016/j.jff.2022.105056

Hyrslova, I., Kana, A., Nesporova, V., Mrvikova, I., Doulgeraki, A. I., Lampova, B., Doskocil, I., Musilova, S., Kieliszek, M., & Krausova, G. (2024). In vitro digestion and characterization of selenized *Saccharomyces cerevisiae*, *Pichia fermentans* and probiotic *Saccharomyces boulardii*. *Journal of Trace Elements in Medicine and Biology*, *83*, 127402. https://doi.org/10.1016/j.jtemb.2024.127402

Ibrahim, E., Fang, Y., Nasser, R., Wang, D., Kafsheer, D. A. E. M. K., Ayoade, S. O., Hafeez, R., Al-Megrin, W. A. I., Li, B., & Lin, H. (2025). Biogenic synthesis of selenium nanoparticles by *Bacillus amyloliquefaciens*: A promising method for mitigating mycotoxin contamination and fighting *Fusarium graminearum*. *Journal of Hazardous Materials*, 140267. https://doi.org/10.1016/j.jhazmat.2025.140267

Islam, S. N., Naqvi, S. M. A., Raza, A., Jaiswal, A., Singh, A. K., Dixit, M., Barnwal, A., Gambhir, S., & Ahmad, A. (2022). Mycosynthesis of highly fluorescent selenium nanoparticles from *Fusarium oxysporum*, their antifungal activity against black fungus *Aspergillus niger*, and in-vivo biodistribution studies. *3 Biotech*, *12*(11), 309. https://doi.org/10.1007/s13205-022-03383-0

Jamal, Q. M. S., & Ahmad, V. (2022). *Lysinibacilli*: A biological factories intended for bio-insecticidal, bio-control, and bioremediation activities. *Journal of Fungi*, *8*(12), 1288 https://doi.org/10.3390/jof8121288

Jassim, T., & Al-Shibly, M. K. A. (2024). Antimicrobial effect of biosynthesis of selenium nanoparticles by *Pseudomonas aeruginosa* on bacteria isolated from wounds and burns. *Wasit Journal for Pure Sciences*, *3*(1), 143–151. https://doi.org/10.31185/wjps.304

Jothinathan, M. K. D., Behera, A., Ramalingam, S., Alam, M. M., Amanullah, M., & Karunakaran, R. (2025). Review on bio-selenium nanoparticles: Synthesis, protocols, and applications in biomedical processes. *Nanotechnology Reviews*, *14*(1), 20250183. https://doi.org/10.1515/ntrev-2025-0183

Kalpana, M., Raguvaran, K., Manimegalai, T., Kalaivani, S., Devapriya, P., & Maheswaran, R. (2025a). Eco-friendly synthesis of selenium nanoparticles using *Streptomyces microflavus* and their efficacy against the larvae of *Culex quinquefasciatus*, *Aedes aegypti*, and *Anopheles stephensi*. *Environmental Science and Pollution Research*, *32*(17), 10800–10817. https://doi.org/10.1007/s11356-025-36285-8

Kalpana, M., Raguvaran, K., Manimegalai, T., Kalaivani, S., Devapriya, P., & Maheswaran, R. (2025b). Evaluation of the larvicidal potential of selenium nanoparticles synthesized using *Streptomyces diastaticus* (KA-21)(OM758168) and their toxicity against the larvae of *Culex quinquefasciatus*, *Aedes aegypti* and *Anopheles stephensi*. *Journal of Sol-Gel Science and Technology*, *116*(2), 1024–1040. https://doi.org/10.1007/s10971-025-06953-9

Kashisaz, M., Enayatizamir, N., Fu, P., & Eslahi, M. (2024). Synthesis of nanoparticles using *Trichoderma harzianum*, characterization, antifungal activity and impact on plant growth promoting bacteria. *World Journal of Microbiology and Biotechnology*, *40*(4), 107. https://doi.org/10.1007/s11274-024-03920-4

Kathiravan, A., Udayan, E., Rajeshkumar, S., & Gnanadoss, J. J. (2023). Unveiling the biological potential of mycosynthesized selenium nanoparticles from endophytic fungus *Curvularia* sp. LCJ413. *Bionanoscience*, *13*(4), 2232–2251. https://doi.org/10.1007/s12668-023-01223-w

Kavitha, K., Bharathi, S., Rajalakshmi, A., Ramesh, M., Padmini, P., Suresh, G., Guruchandran, V., Prakash, M., Puvanakrishnan, R., & Ramesh, B. (2024). Selenium nanoparticles stabilized by fungal chitosan with antibacterial activity – synthesis and characterization. *Particulate Science and Technology*, *42*(2), 311–323. https://doi.org/10.1080/02726351.2023.2237438

Khaledizade, E., Tafvizi, F., & Jafari, P. (2024). Anti-breast cancer activity of biosynthesized selenium nanoparticles using *Bacillus coagulans* supernatant. *Journal of Trace Elements in Medicine and Biology*, *82*, 127357. https://doi.org/10.1016/j.jtemb.2023.127357

Khonkiv, M., Dmytrenko, I., Marynin, A., Polishchuk, G., & Stabnikov, V. (2025). Influence of functional additives on microbiological and physicochemical characteristics of yogurt. *Ukrainian Food Journal*, *14*(4), 727–742. https://doi.org/10.24263/2304-974X-2025-14-4-10

Khonkiv, M., Kovshar, I., Danylenko, S., & Stabnikov, V. (2026). Improved production of selenium nanoparticles using lactic acid bacteria: Role of strain selection and process parameters. *Ukrainian Food Journal*, *15*(1), 195. https://doi.org/10.24263/2304-974X-2026-15-1-15

Kieliszek, M., Sęk, W., Angaïts, A., & Szpunar, J. (2026). Biotransformation of selenium in yeast – speciation and nanostructural analysis. *Biological Trace Element Research*, *204*(3), 1329–1342. https://doi.org/10.1007/s12011-025-04751-6

Krawczyk, B., Wityk, P., Gałęcka, M., & Michalik, M. (2021). The many faces of *Enterococcus* spp. – commensal, probiotic and opportunistic pathogen. *Microorganisms*, *9*(9), 1900. https://doi.org/10.3390/microorganisms9091900

Kumar, A., Prasad, B., Manjhi, J., & Prasad, K. S. (2020). Antioxidant activity of selenium nanoparticles biosynthesized using a cell-free extract of *Geobacillus*. *Toxicological & Environmental Chemistry*, *102*(10), 556–567. https://doi.org/10.1080/02772248.2020.1829623

Lashani, E., Moghimi, H., Turner, R. J., & Amoozegar, M. A. (2024). Characterization and biological activity of selenium nanoparticles biosynthesized by *Yarrowia lipolytica*. *Microbial Biotechnology*, *17*(10), e70013. https://doi.org/10.1111/1751-7915.70013

Li, H., Fu, Y., & Song, F. (2023). Marine *Aspergillus*: a treasure trove of antimicrobial compounds. *Marine Drugs*, *21*(5), 277. https://doi.org/10.3390/md21050277

Li, M., Yang, R., Li, N., Zhao, S., Wei, S., Zhang, S., Gong, J., Song, J., Kim, J. R., He, Y., Gao, C., Wang, Z., & Cheng, S. (2024a). Effect of different selenium species on indole-3-acetic acid activity of selenium nanoparticles producing strain *Bacillus altitudinis* LH18. *Molecules*, *29*(11), 2463. https://doi.org/10.3390/molecules29112463

Li, N., Yang, Y., Qi, J., Li, J., Cheng, Y., Li, Z., Yue, T., & Yuan, Y. (2025a). Selenium nanoparticles biosynthesized by *Eurotium cristatum* with antimicrobial activity. *Food Science and Human Wellness*, *14*(7), 9250158. https://doi.org/10.26599/FSHW.2024.9250158

Li, Q., Lu, J., Zhang, G., Liu, S., Zhou, J., Du, G., & Chen, J. (2022). Recent advances in the development of *Aspergillus* for protein production. *Bioresource Technology*, *348*, 126768. https://doi.org/10.1016/j.biortech.2022.126768

Li, R., Chen, W., Huang, S., Jiang, D., Zhu, Z., Li, C., & Huang, X. (2025b). Three bacterial strains efficiently reduce selenite to selenium nanoparticles in cell membranes. *BMC Microbiology*, *25*(1), 564. https://doi.org/10.1186/s12866-025-04304-w

Li, T., Zhu, K., Wang, L., Dong, Y., & Huang, J. (2024b). Stabilization by chaperone GroEL in biogenic selenium nanoparticles produced from *Bifidobacterium animalis* H15 for the treatment of DSS-induced colitis. *ACS Applied Materials & Interfaces*, *16*(11), 13439–13452. https://pubs.acs.org/doi/10.1021/acsami.3c16340

Li, Y., Wang, T., Liu, D., Zhang, C., Wu, W., Yi, H., & Zhang, J. (2025c). Biotransformation of inorganic selenium into selenium nanoparticles and organic selenium by *Lactiplantibacillus plantarum* CXG4. *Food Bioscience*, *65*, 106060. https://doi.org/10.1016/j.fbio.2025.106060

Lian, S., Diko, C. S., Yan, Y., Li, Z., Zhang, H., Ma, Q., & Qu, Y. (2019). Characterization of biogenic selenium nanoparticles derived from cell-free extracts of a novel yeast *Magnusiomyces ingens*. *3 Biotech*, *9*(6), 221. https://doi.org/10.1007/s13205-019-1748-y

Liang, X., Perez, M. A. M. J., Zhang, S., Song, W., Armstrong, J. G., Bullock, L. A., Feldmann, J., Parnell, J., Csetenyi, L., & Gadd, G. M. (2020). Fungal transformation of selenium and tellurium located in a volcanogenic sulfide deposit. *Environmental Microbiology*, *22*(6), 2346–2364. https://doi.org/10.1111/1462-2920.15012

Liang, X., Zhang, S., Gadd, G. M., McGrath, J., Rooney, D. W., & Zhao, Q. (2022). Fungal-derived selenium nanoparticles and their potential applications in electroless silver coatings for preventing pin-tract infections. *Regenerative Biomaterials*, *9*, rbac013. https://doi.org/10.1093/rb/rbac013

Likidtaveesin, S., Changtong, N., Jarussophon, N., & Chunhachart, O. (2025). Biosynthesis of selenium nanoparticles and selenium-enriched g-polyglutamic acid (Se-PGA) by *Bacillus subtilis*. *Trends in Sciences*, *22*(4), 9391–9391. https://doi.org/10.48048/tis.2025.9391

Lima, P. C., Karimian, P., Johnston, E., & Hartley, C. J. (2024). The use of *Trichoderma* spp. for the bioconversion of agro-industrial waste biomass via fermentation: a review. *Fermentation*, *10*(9), 442. https://doi.org/10.3390/fermentation10090442

Lindsay, C. A., Kinghorn, A. D., & Rakotondraibe, H. L. (2023). Bioactive and unusual steroids from *Penicillium* fungi. *Phytochemistry*, *209*, 113638. https://doi.org/10.1016/j.phytochem.2023.113638

Liu, J., Shi, L., Tuo, X., Ma, X., Hou, X., Jiang, S., Lv, J., Cheng, Y., Guo, D., & Han, B. (2022). Preparation, characteristic and anti-inflammatory effect of selenium nanoparticle-enriched probiotic strain *Enterococcus durans* A8-1. *Journal of Trace Elements in Medicine and Biology*, *74*, 127056. https://doi.org/10.1016/j.jtemb.2022.127056

Liu, P., Long, H., Cheng, H., Liang, M., Liu, Z., Han, Z., Guo, Z., Shi, H., Sun, M., & He, S. (2023). Highly-efficient synthesis of biogenic selenium nanoparticles by *Bacillus paramycoides* and their antibacterial and antioxidant activities. *Frontiers in Bioengineering and Biotechnology*, *11*, 1227619. https://doi.org/10.3389/fbioe.2023.1227619

Liu, P., Long, H., He, S., Cheng, H., Li, E., Cheng, S., Liang, M., Liu, Z., Guo, Z., & Shi, H. (2024a). Unveiling the innovative green synthesis mechanism of selenium nanoparticles by exploiting intracellular protein elongation factor Tu from *Bacillus paramycoides*. *Journal of Zhejiang University-Science B*, *25*(9), 789–795. https://doi.org/10.1631/jzus.B2300738

Liu, S., Gu, Q., Gao, J., Li, Z., & Yu, X. (2025). Characterization, antioxidant properties and transcriptome analysis of selenium nanoparticles biosynthesized by the high selenite tolerance strain *Halomonas* sp. SF2000. *Environmental Technology & Innovation*, 104373. https://doi.org/10.1016/j.eti.2025.104373

Liu, X. Y., Ma, J. Y., Wang, Y., Duan, J. L., Feng, L. J., Zhu, F. P., Sun, X. D., Yan, Z., & Yuan, X. Z. (2024b). Chemical dynamics of selenium nanoparticles in archaeal systems. *ACS Nano*, *18*(24), 15661–15670. https://doi.org/10.1021/acsnano.4c01596

Long, Q., Cui, L. K., He, S. B., Sun, J., Chen, Q. Z., Bao, H. D., Liang, T. Y., Liang, B. Y., & Cui, L. Y. (2023). Preparation, characteristics and cytotoxicity of green synthesized selenium nanoparticles using *Paenibacillus motobuensis* LY5201 isolated from the local specialty food of longevity area. *Scientific Reports*, *13*(1), 53. https://doi.org/10.1038/s41598-022-26396-4

Lv, F., & Zeng, Y. (2024). Novel bioactive natural products from marine-derived *Penicillium* fungi: a review (2021-2023). *Marine Drugs*, *22*(5), 191. https://doi.org/10.3390/md22050191

Manaa, H. M., Hamza, E. M., & Sorour, N. M. (2023). Post-harvest biocontrol of Fusarium infection in tomato fruits using bio-mediated selenium nanoparticles. *Amb Express*, *13*(1), 119. https://doi.org/10.1186/s13568-023-01622-y

Mangudi, S., & Pappu, S. (2025). Biologically synthesized selenium nanoparticles from cell-free supernatant of *Lysinibacillus odysseyi* with therapeutic potential. *Microbial Pathogenesis*, 108109. https://doi.org/10.1016/j.micpath.2025.108109

Meenambigai, K., Kokila, R., Chandhirasekar, K., Thendralmanikandan, A., Kaliannan, D., Ibrahim, K. S., Kumar, S., Liu, W., Balasubramanian, B., & Nareshkumar, A. (2022). Green synthesis of selenium nanoparticles mediated by Nilgirianthus ciliates leaf extracts for antimicrobial activity on foodborne pathogenic microbes and pesticidal activity against *Aedes aegypti* with molecular docking. *Biological Trace Element Research*, *200*(6), 2948–2962. https://doi.org/10.1007/s12011-021-02868-y

Mohamed, A., El-Sayed, E. S. R., Zakaria, Z., Mohamed, M. H., & Elhakim, H. K. (2025). Enhanced myco-synthesis of selenium and zinc oxide nanoparticles and evaluating their anticancer activities and role against antibiotic resistance genes in certain bacterial strains. *Microbial Cell Factories*, *24*(1), 214. https://doi.org/10.1186/s12934-025-02795-w

Mohamed, E. A., & El-Zahed, M. M. (2024). Anticandidal applications of selenium nanoparticles biosynthesized with *Limosilactobacillus fermentum* (OR553490). *Discover Nano*, *19*(1), 115. https://doi.org/10.1186/s11671-024-04055-z

Mohammed, E. J., Abdelaziz, A. E., Mekky, A. E., Mahmoud, N. N., Sharaf, M., Al-Habibi, M. M., Khairy, N. M., Al-Askar, A. A., Youssef, F. S., Gaber, M. A., Saied, E., AbdElgayed, G., Metwally, S. A., & Shoun, A. A. (2024). Biomedical promise of *Aspergillus flavus*-biosynthesized selenium nanoparticles: a green synthesis approach to antiviral, anticancer, anti-biofilm, and antibacterial applications. *Pharmaceuticals*, *17*(7), 915. https://doi.org/10.3390/ph17070915

Morad, M. Y., El-Sayed, H., Elhenawy, A. A., Korany, S. M., Aloufi, A. S., & Ibrahim, A. M. (2022). Myco-synthesized molluscicidal and larvicidal selenium nanoparticles: a new strategy to control *Biomphalaria alexandrina* snails and larvae of *Schistosoma mansoni* with an in silico study on induced oxidative stress. *Journal of Fungi*, *8*(3), 262. https://doi.org/10.3390/jof8030262

Nagar, D. N., Ghosh, N. N., & Braganca, J. M. (2022). Green synthesis of selenium nanospheres and nanoneedles by halophilic archaea. *Applied Nanoscience*, *12*(12), 3983–3994. https://doi.org/10.1007/s13204-022-02665-6

Nassar, A. R. A., Eid, A. M., Atta, H. M., El Naghy, W. S., & Fouda, A. (2023). Exploring the antimicrobial, antioxidant, anticancer, biocompatibility, and larvicidal activities of selenium nanoparticles fabricated by endophytic fungal strain *Penicillium verhagenii*. *Scientific Reports*, *13*(1), 9054. https://doi.org/10.1038/s41598-023-35360-9

Ndwandwe, B. K., Malinga, S. P., Kayitesi, E., & Dlamini, B. C. (2021). Advances in green synthesis of selenium nanoparticles and their application in food packaging. *International Journal of Food Science and Technology*, *56*(6), 2640–2650. https://doi.org/10.1111/ijfs.14916

Ndwandwe, B. K., Malinga, S. P., Kayitesi, E., & Dlamini, B. C. (2022). Selenium nanoparticles–enhanced potato starch film for active food packaging application. *International Journal of Food Science and Technology*, *57*(10), 6512–6521. https://doi.org/10.1111/ijfs.15990

Negi, B. B., Sinharoy, A., & Pakshirajan, K. (2020). Selenite removal from wastewater using fungal pelleted airlift bioreactor. *Environmental Science and Pollution Research*, *27*(1), 992–1003. https://doi.org/10.1007/s11356-019-06946-6

Nie, X., Zhu, Z., Lu, H., Xue, M., Tan, Z., Zhou, J., Xin, Y., Mao, Y., Shi, H., & Zhang, D. (2023). Assembly of selenium nanoparticles by protein coronas composed of yeast protease A. *Process Biochemistry*, *129*, 140–149. https://doi.org/10.1016/j.procbio.2023.03.025

Nile, S. H., Thombre, D., Shelar, A., Gosavi, K., Sangshetti, J., Zhang, W., Sieniawska, E., Patil, R., & Kai, G. (2023). Antifungal properties of biogenic selenium nanoparticles functionalized with nystatin for the inhibition of *Candida albicans* biofilm formation. *Molecules*, *28*(4), 1836. https://doi.org/10.3390/molecules28041836

Nogueira, M. H., de Carvalho, L., Peron dos Santos, A. R., Furlaneto, M. C., & Maia, L. F. (2024). Cassava starch-based film infused with biogenic selenium nanoparticles (bio-SeNPs) to reduce foodborne pathogens. *International Journal of Food Science and Technology*, *59*(10), 7541–7549. https://doi.org/10.1111/ijfs.17519

Nowruzi, B., Jalil, B. S., & Metcalf, J. S. (2023). Antifungal screening of selenium nanoparticles biosynthesized by microcystin-producing *Desmonostoc alborizicum*. *BMC Biotechnology*, *23*(1), 41. https://doi.org/10.1186/s12896-023-00807-4

Pandey, S., Awasthee, N., Shekher, A., Rai, L. C., Gupta, S. C., & Dubey, S. K. (2021). Biogenic synthesis and characterization of selenium nanoparticles and their applications with special reference to antibacterial, antioxidant, anticancer and photocatalytic activity. *Bioprocess and Biosystems Engineering*, *44*(12), 2679–2696. https://doi.org/10.1007/s00449-021-02637-0

Pocsi, I., Dijksterhuis, J., Houbraken, J., & De Vries, R. P. (2024). Biotechnological potential of salt tolerant and xerophilic species of *Aspergillus*. *Applied Microbiology and Biotechnology*, *108*(1), 521. https://doi.org/10.1007/s00253-024-13338-5

Qiao, N., Wittouck, S., Mattarelli, P., Zheng, J., Lebeer, S., Felis, G. E., & Gänzle, M. G. (2022). After the storm – perspectives on the taxonomy of *Lactobacillaceae*. *JDS Communications*, *3*(3), 222–227. https://doi.org/10.3168/jdsc.2021-0183

Qi, J., Guo, X., Han, W., Chang, M., Yuan, Y., & Yue, T. (2024). The potency of *Monascus purpureus* to achieve the transformation from inorganic selenium into organic selenium during the fermentation process. *Food Bioscience*, *62*, 105091. https://doi.org/10.1016/j.fbio.2024.105091

Raja, R. K., Seetharaman, P. K., Kalidass, B., Ananth, S., Bo, L., Kamaraj, C., Cimen H., & Hazir, S. (2024). Biosynthesis of selenium nanoparticles using cell-free extract of *Xenorhabdus cabanillasii* GU480990 and their potential mosquito larvicidal properties against yellow fever mosquito *Aedes aegypti*. *Journal of Invertebrate Pathology*, *203*, 108045. https://doi.org/10.1016/j.jip.2023.108045

Rajkumar, K., Mvs, S., Koganti, S., & Burgula, S. (2020). Selenium nanoparticles synthesized using *Pseudomonas stutzeri* (MH191156) show antiproliferative and anti-angiogenic activity against cervical cancer cells. *International Journal of Nanomedicine*, 4523–4540. https://doi.org/10.2147/IJN.S247426

Ramya, S., Shanmugasundaram, T., & Balagurunathan, R. (2020). Actinobacterial enzyme mediated synthesis of selenium nanoparticles for antibacterial, mosquito larvicidal and anthelminthic applications. *Particulate Science and Technology*, *38*(1), 63–72. https://doi.org/10.1080/02726351.2018.1508098

Rao, V., & Poonia, A. (2024). Microbial biosynthesis of selenium nanoparticles using probiotic strain and its characterization. *Journal of Food Measurement and Characterization*, *18*(7), 5477–5488. https://doi.org/10.1007/s11694-024-02581-z

Rasheed, R., Bhat, A., Singh, B., & Tian, F. (2024). Biogenic synthesis of selenium and copper oxide nanoparticles and inhibitory effect against multi-drug resistant biofilm-forming bacterial pathogens. *Biomedicines*, *12*(5), 994. https://doi.org/10.3390/biomedicines12050994

Rasouli, M. (2019). Biosynthesis of selenium nanoparticles using yeast *Nematospora coryli* and examination of their anti-candida and anti-oxidant activities. *IET Nanobiotechnology*, *13*(2), 214–218. https://doi.org/10.1049/iet-nbt.2018.5187

Ruiz-Fresneda, M. A., Morales-Hidalgo, M., Povedano-Priego, C., Jroundi, F., Hidalgo-Iruela, J., Cano-Cano, M., Pérez-Muelas, E., Merroun, M. L., & Martín-Sanchez, I. (2024). Unlocking the key role of bentonite fungal isolates in tellurium and selenium bioremediation and biorecovery: implications in the safety of radioactive waste disposal. *Science of the Total Environment*, *912*, 169242. https://doi.org/10.1016/j.scitotenv.2023.16924

Ruiz-Fresneda, M. A., Staicu, L. C., Lazuén-López, G., & Merroun, M. L. (2023). Allotropy of selenium nanoparticles: Colourful transition, synthesis, and biotechnological applications. *Microbial Biotechnology*, *16*(5), 877-892. https://doi.org/10.1111/1751-7915.14209

Saad, A. M., Sitohy, M. Z., Sultan-Alolama, M. I., El-Tarabily, K. A., & El-Saadony, M. T. (2022). Green nanotechnology for controlling bacterial load and heavy metal accumulation in Nile tilapia fish using biological selenium nanoparticles biosynthesized by *Bacillus subtilis* AS12. *Frontiers in Microbiology*, *13*, 1015613. https://doi.org/10.3389/fmicb.2022.1015613

Saad, S., Abdelghany, A. M., Abou-ElWafa, G. S., Aldesuquy, H. S., & Eltanahy, E. (2024). Bioactivity of selenium nanoparticles biosynthesized by crude phycocyanin extract of *Leptolyngbya* sp. SSI24 cultivated on recycled filter cake wastes from sugar-industry. *Microbial Cell Factories*, *23*(1), 211. https://doi.org/10.1186/s12934-024-02482-2

Sadeghi, M. M., Alipour, S., Morowvat, M. H., Salehi, M. S., Das, S. S., & Dehshahri, A. (2025). Green biosynthesized selenium nanoparticles using whole cell and cell lysate of *Spirulina platensis*: characterizations and *in vitro* wound healing studies. *BioNanoScience*, *15*(1), 100. https://doi.org/10.1007/s12668-024-01753-x

Safaei, M., Mozaffari, H. R., Moradpoor, H., Imani, M. M., Sharifi, R., & Golshah, A. (2022). Optimization of green synthesis of selenium nanoparticles and evaluation of their antifungal activity against oral *Candida albicans* infection. *Advances in Materials Science and Engineering*, *2022*(1), 1376998. https://doi.org/10.1155/2022/1376998

Sahoo, B., Panigrahi, L. L., Jena, S., Jha, S., & Arakha, M. (2023). Oxidative stress generated due to photocatalytic activity of biosynthesized selenium nanoparticles triggers cytoplasmic leakage leading to bacterial cell death. *RSC Advances*, *13*(17), 11406–11414. https://doi.org/10.1039/d2ra07827a

Saied, E., Mekky, A. E., Al-Askar, A. A., Hagag, A. F., El-bana, A. A., Ashraf, M., Walid, A., Nour, T., Fawzi, M. M., Arishi, A. A., & Hashem, A. H. (2023). Aspergillus terreus-mediated selenium nanoparticles and their antimicrobial and photocatalytic activities. *Crystals*, *13*(3), 450. https://doi.org/10.3390/cryst13030450

Salem, M. F., Abd-Elraoof, W. A., Tayel, A. A., Alzuaibr, F. M., & Abonama, O. M. (2022). Antifungal application of biosynthesized selenium nanoparticles with pomegranate peels and nanochitosan as edible coatings for citrus green mold protection. *Journal of Nanobiotechnology*, *20*(1), 182. https://doi.org/10.1186/s12951-022-01393-x

Salem, S. S. (2022). Bio-fabrication of selenium nanoparticles using baker's yeast extract and its antimicrobial efficacy on food borne pathogens. *Applied Biochemistry and Biotechnology*, *194*(5), 1898–1910. https://doi.org/10.1007/s12010-022-03809-8

Salem, S. S., Fouda, M. M., Fouda, A., Awad, M. A., Al-Olayan, E. M., Allam, A. A., & Shaheen, T. I. (2021). Antibacterial, cytotoxicity and larvicidal activity of green synthesized selenium nanoparticles using *Penicillium corylophilum*. *Journal of Cluster Science*, *32*(2), 351–361. https://doi.org/10.1007/s10876-020-01794-8

Salimi, T., Hajarian, H., Karamishabankareh, H., & Soltani, L. (2024). Effects of sodium selenite, cysteamine, bacterially synthesized Se-NPs, and cysteamine loaded on Se-NPs on ram sperm cryopreservation. *Scientific Reports*, *14*(1), 852. https://doi.org/10.1038/s41598-023-50221-1

Salman, M. F., Al-Mudallal, N. H., & Ahmed, M. E. (2025). Cytotoxic effect of biogenic selenium nanoparticles using bacteriocin of *Acinetobacter baumannii* isolated from burns and wound infections. *Iraqi Journal of Science*, *66*(4), 1535–1549. https://doi.org/10.24996/ijs.2025.66.4.13

Salman, M. F., Al-Mudallal, N. H., & Ahmed, M. E. (2024). The effect of selenium nanoparticles on the expression of MexB gene of *Pseudomonas aeruginosa* isolated from wound and burn infections. *Iraqi Journal of Medical Sciences*, *22*(1), 79–92. https://doi.org/10.22578/IJMS.22.1.10

Sampath, S., Sunderam, V., Manjusha, M., Dlamini, Z., & Lawrance, A. V. (2024). Selenium nanoparticles: a comprehensive examination of synthesis techniques and their diverse applications in medical research and toxicology studies. *Molecules*, *29*(4), 801. https://doi.org/10.3390/molecules29040801

Sarkar, J., Mridha, D., Davoodbasha, M. A., Banerjee, J., Chanda, S., Ray, K., Roychowdhury, T., Acharya, K., & Sarkar, J. (2023). A state-of-the-art systemic review on selenium nanoparticles: Mechanisms and factors influencing biogenesis and its potential applications. *Biological Trace Element Research*, *201*(10), 5000-5036. https://doi.org/10.1007/s12011-022-03549-0

San Keskin, N. O., Akbal Vural, O., & Abaci, S. (2020). Biosynthesis of noble selenium nanoparticles from *Lysinibacillus* sp. NOSK for antimicrobial, antibiofilm activity, and biocompatibility. *Geomicrobiology Journal, 37*(10), 919–928. https://doi.org/10.1080/01490451.2020.1799264

Santelli, C. M., Sabuda, M. C., & Rosenfeld, C. E. (2023). Time-resolved examination of fungal selenium redox transformations. *ACS Earth and Space Chemistry, 7*(5), 960–971. https://doi.org/10.1021/acsearthspacechem.2c00288

Saravanakumar, K., Sathiyaseelan, A., Zhang, X., Park, S., & Wang, M. H. (2022). Purinoceptor targeted cytotoxicity of adenosine triphosphate-conjugated biogenic selenium nanoparticles in human colon cancer cells. *Pharmaceuticals, 15*(5), 582. https://doi.org/10.3390/ph15050582

Sęk, W., Kot, A. M., & Kieliszek, M. (2025). The impact of selenium on the physiological activity of yeast cells *Saccharomyces cerevisiae* ATCC 7090 and *Rhodotorula glutinis* CCY 20-2-26. *Frontiers in Bioscience-Landmark, 30*(1), 26692. https://doi.org/10.31083/FBL26692

Sendani, A. A., Farmani, M., Jahankhani, K., Kazemifard, N., Ghavami, S. B., Houri, H., Ashrafi, F., & Sadeghi, A. (2024). Exploring the anti-inflammatory and antioxidative potential of selenium nanoparticles biosynthesized by *Lactobacillus casei* 393 on an inflamed Caco-2 cell line. *Cell Biochemistry and Biophysics, 82*(4), 3265–3276. https://doi.org/10.1007/s12013-024-01356-z

Senthamarai, M. D., Hillary, V. E., Rajan, M. R., & Ceasar, S. A. (2024). Biosynthesis of selenium nanoparticles and its biological applications: A systematic review. *Nano-Structures & Nano-Objects, 39*, 101261. https://doi.org/10.1016/j.nanoso.2024.101261

Shahbaz, M., Akram, A., Raja, N. I., Mukhtar, T., Mehak, A., Fatima, N., Ajmal, M., Ali, K., Mustafa, N., & Abasi, F. (2023). Antifungal activity of green synthesized selenium nanoparticles and their effect on physiological, biochemical, and antioxidant defense system of mango under mango malformation disease. *PLoS ONE, 18*(2), e0274679. https://doi.org/10.1371/journal.pone.0274679

Shakeri, F., Zaboli, F., Fattahi, E., & Babavalian, H. (2022). Biosynthesis of selenium nanoparticles and evaluation of its antibacterial activity against *Pseudomonas aeruginosa*. *Advances in Materials Science and Engineering, 2022*(1), 4118048. https://doi.org/10.1155/2022/4118048

Shawky, M., Kalaba, M. H., & El-Sherbiny, G. M. (2025). Combined impact of biosynthesized selenium nanoparticles and imipenem against carbapenem-resistant *Pseudomonas aeruginosa* and their associated virulence factors. *BMC Microbiology, 25*(1), 235. https://doi.org/10.1186/s12866-025-03932-6

Shen, Y., Ma, N., Liu, S., Xu, G., & Zhang, J. (2025). Mycotoxins and secondary metabolites from fruit postharvest pathogenic *Penicillium* species. *Food Chemistry, 488*, 144880. https://doi.org/10.1016/j.foodchem.2025.144880

Shi, J., Cheng, J., Liu, S., Zhu, Y., & Zhu, M. (2024). *Acinetobacter baumannii*: An evolving and cunning opponent. *Frontiers in Microbiology, 15*, 1332108. https://doi.org/10.3389/fmicb.2024.1332108

Si, B., Yang, Y., Naveed, M., Wang, F., & Chan, M. W. H. (2024). Characterizations of biogenic selenium nanoparticles and their anti-biofilm potential against *Streptococcus mutans* ATCC 25175. *Journal of Trace Elements in Medicine and Biology, 84*, 127448. https://doi.org/10.1016/j.jtemb.2024.127448

Singh, A., Dey, P., Mihara, H., Prakash, N. T., & Prakash, R. (2025). Facile synthesis of selenium nanoparticles and stabilization using exopolysaccharide from endophytic fungus, *Nigrospora gullinensis*, and their bioactivity study. *Biomass Conversion and Biorefinery, 15*(6), 9581–9598. https://doi.org/10.1007/s13399-024-05870-1

Singh, A., Jaiswal, S. K., Prakash, R., Mihara, H., & Prakash, N. T. (2024). Selenium nanoparticles synthesized and stabilized by fungal extract exhibit enhanced bioactivity. *Journal of Cluster Science, 35*(5), 1425–1437. https://doi.org/10.1007/s10876-024-02600-5

Sonali, J. M. I., Gayathri, K. V., Rangasamy, G., Kumar, P. S., & Rajagopal, R. (2024). Efficacy of biogenic selenium nanoparticles from *Pseudomonas libanensis* towards growth enhancement of okra. *Waste and Biomass Valorization, 15*(3), 1793–1806. https://doi.org/10.1007/s12649-023-02233-1

Song, X., Qiao, L., Yan, S., Chen, Y., Dou, X., & Xu, C. (2021). Preparation, characterization, and in vivo evaluation of anti-inflammatory activities of selenium nanoparticles synthesized by *Kluyveromyces lactis* GG799. *Food & Function, 12*(14), 6403–6415. https://doi.org/10.1039/D1FO01019K

Spyridopoulou, K., Tryfonopoulou, E., Aindelis, G., Ypsilantis, P., Sarafidis, C., Kalogirou, O., & Chlichlia, K. (2021). Biogenic selenium nanoparticles produced by *Lactobacillus casei* ATCC 393 inhibit colon cancer cell growth in vitro and in vivo. *Nanoscale Advances, 3*(9), 2516–2528. https://doi.org/10.1039/D0NA00984A

Stabnikov, V., Kovshar, I., & Stabnikova, O. (2025). Recent advances in the study of the properties and applications of lactic acid bacteria. *World Journal of Microbiology and Biotechnology*, *41*, 287. https://doi.org/10.1007/s11274-025-04499-0

Stabnikova, O., Khonkiv, M., Kovshar, I., & Stabnikov, V. (2023). Biosynthesis of selenium nanoparticles by lactic acid bacteria and areas of their possible applications. *World Journal of Microbiology and Biotechnology*, *39*(9), 230. https://doi.org/10.1007/s11274-023-03673-6

Starovoitova, S. O., Kishko, K. M., Demchenko, O. M., & Bila, V. V. (2023). Encapsulated probiotic microorganisms in functional food products. *Microbiological Journal*, *85*(6), 77–94. https://doi.org/10.15407/microbiolj85.06.077

Starovoitova, S. O., Lazarenko, L. M., Babenko, L. P., Demchenko, O. M., & Kishko, K. M. (2024). Selection of probiotic microorganisms and their compositions as a basis of line functional food products with hypocholesterolemic properties. *Microbiological Journal*, *86*(3), 3–17. https://doi.org/10.15407/microbiolj86.03.003

Sumithra, D., Bharathi, S., Kaviyarasan, P., & Suresh, G. (2023). Biofabrication of selenium nanoparticles using marine *Streptomyces* sp. and assessment of its antibacterial, antibiofilm, antioxidant, and in vivo cytotoxic potential. *Geomicrobiology Journal*, *40*(5), 485–492. https://doi.org/10.1080/01490451.2023.2196280

Sun, J., Wang, Y., Zheng, Y., Yuan, M., Zhang, H., Huo, G., Weng, M., Jiang, R., Zhang, Y., & Wang, Y. (2024a). Improved titer and stability of selenium nanoparticles produced by engineered *Saccharomyces cerevisiae*. *Enzyme and Microbial Technology*, *173*, 110367. https://doi.org/10.1016/j.enzmictec.2023.110367

Sun, L., Liu, S. M., Ding, Y., Yang, R., & Zeng, H. J. (2024b). Preparation and structural characterization of selenium nanoparticles from *Lactobacillus reuteri* and their protective effects on DSS-induced ulcerative colitis in mice. *Food Bioscience*, *62*, 105293. https://doi.org/10.1016/j.fbio.2024.105293

Sun, Y., Gan, Y., Zhang, L., Shi, Y., Yue, T., & Yuan, Y. (2022). Isolation and identification of *Monascus* and evaluation of its selenium accumulation. *LWT*, *154*, 112887. https://doi.org/10.1016/j.lwt.2021.112887

Sun, Y., Liang, L., Yi, Y., Meng, Y., Peng, K., Jiang, X., & Wang, H. (2023). Synthesis, characterization and anti-inflammatory activity of selenium nanoparticles stabilized by aminated yeast glucan. *International Journal of Biological Macromolecules*, *245*, 125187. https://doi.org/10.1016/j.ijbiomac.2023.125187

Tabibi, M., Aghaei, S., Amoozegar, M. A., Nazari, R., & Zolfaghari, M. R. (2023). Characterization of green synthesized selenium nanoparticles (SeNPs) in two different indigenous halophilic bacteria. *BMC Chemistry*, *17*(1), 115. https://doi.org/10.1186/s13065-023-01034-w

Tendenedzai, J. T., Chirwa, E. M., & Brink, H. G. (2022). *Enterococcus* spp. cell-free extract: An abiotic route for synthesis of selenium nanoparticles (SeNPs), their characterisation and inhibition of *Escherichia coli*. *Nanomaterials*, *12*(4), 658. https://doi.org/10.3390/nano12040658

Tilwani, Y. M., Lakra, A. K., Domdi, L., Jha, N., & Arul, V. (2023). Preparation, physicochemical characterization, and in vitro biological properties of selenium nanoparticle synthesized from exopolysaccharide of *Enterococcus faecium* MC-5. *BioNanoScience*, *13*(2), 413–425. https://doi.org/10.1007/s12668-023-01077-2

Touaitia, R., Mairi, A., Ibrahim, N. A., Basher, N. S., Idres, T., & Touati, A. (2025). *Staphylococcus aureus*: A review of the pathogenesis and virulence mechanisms. *Antibiotics*, *14*(5), 470. https://doi.org/10.3390/antibiotics14050470

Ullah, A., Mu, J., Wang, F., Chan, M. W. H., Yin, X., Liao, Y., Mirani, Z. A., Sebt-e-Hassan, S., Aslam, S., Naveed, M., Khan, M. N., Khatoon, Z., & Kazmi, M. R. (2022). Biogenic selenium nanoparticles and their anticancer effects pertaining to probiotic bacteria – A review. *Antioxidants*, *11*(10), 1916. https://doi.org/10.3390/antiox11101916

Ullah, A., Yin, X., Wang, F., Xu, B., Mirani, Z. A., Xu, B., Chan, M. W. H., Ali, A., Usman, M., Ali, N., & Naveed, M. (2021). Biosynthesis of selenium nanoparticles (via *Bacillus subtilis* BSN313), and their isolation, characterization, and bioactivities. *Molecules*, *26*(18), 5559. https://doi.org/10.3390/molecules26185559

Vaigankar, D. C., Mujawar, S. Y., Mohanty, A. K., & Dubey, S. K. (2022). Biogenesis of selenium nanospheres using *Halomonas venusta* strain GUSDM4 exhibiting potent environmental applications. *Archives of Microbiology*, *204*(7), 372. https://doi.org/10.1007/s00203-022-02977-9

Wang, F., Du, M., Kai, L., Du, S., Hu, W., Wang, Y., & Cheng, Y. (2022a). Exopolymer-functionalized nanoselenium from *Bacillus subtilis* SR41: Characterization, monosaccharide analysis and free radical scavenging ability. *Polymers*, *14*(17), 3523. https://doi.org/10.3390/polym14173523

Wang, H., Shi, D., Chen, Y., Chen, K., Wang, Z., Yuan, Y., & Yue, T. (2024a). Selenium accumulation characteristics and biotransformation potentiality in *Pichia kudriavzevii*. *Food Bioscience*, *59*, 104119. https://doi.org/10.1016/j.fbio.2024.104119

Wang, L., Song, L., Wang, P., Zhang, H., Li, Y., Song, J., Zhong, L., Liu, C., Zhang, W., & Wen, P. (2024b). Bioreduction of Se(IV) by *Lactiplantibacillus plantarum* NML21 and synthesis of selenium nanospheres Se(0). *Food Chemistry*, *452*, 139595. https://doi.org/10.1016/j.foodchem.2024.139595

Wang, M., Jiang, D., & Huang, X. (2022b). Selenium nanoparticle rapidly synthesized by a novel highly selenite-tolerant strain *Proteus penneri* LAB-1. *iScience*, *25*(9), 104904. https://doi.org/10.1016/j.isci.2022.104904

Wang, Q., Wang, C., Kuang, S., Wang, D., & Shi, Y. (2023). Biological selenite reduction, characterization and bioactivities of selenium nanoparticles biosynthesised by *Pediococcus acidilactici* DSM20284. *Molecules*, *28*(9), 3793. https://doi.org/10.3390/molecules28093793

Wang, Y., Li, K., Zhu, W., Xi, H., Qi, M., Chen, P., Chen, H., Zhang, C. E., & Luo, Y. (2025). Characteristics analysis and intestinal effects of probiotic-derived nano-selenium by *Lactobacillus bulgaricus* CICC 20247. *eFood*, *6*(4), e70074. https://doi.org/10.1002/efd2.70074

Wang, Y., Ye, Q., Sun, Y., Jiang, Y., Meng, B., Du, J., Chen, J., Tugarova, A. V., Kamnev, A. A., & Huang, S. (2022c). Selenite reduction by *Proteus* sp. YS02: New insights revealed by comparative transcriptomics and antibacterial effectiveness of the biogenic Se0 nanoparticles. *Frontiers in Microbiology*, *13*, 845321. https://doi.org/10.3389/fmicb.2022.845321

Wang, Y., Yu, Y., Duan, Y., Wang, Q., Cong, X., He, Y., Gao, C., Hafeez, M., Jan, S., Rasheed, S. M., Cheng, S., & Wang, Z. (2022d). Enhancing the activity of carboxymethyl cellulase enzyme using highly stable selenium nanoparticles biosynthesized by *Bacillus paralicheniformis* Y4. *Molecules*, *27*(14), 4585. https://doi.org/10.3390/molecules27144585

Wang, Z., Li, N., Zhou, X., Wei, S., Zhu, Y., Li, M., Gong, J., He, Y., Dong, X., Gao, C., & Cheng, S. (2024c). Optimization of fermentation parameters to improve the biosynthesis of selenium nanoparticles by *Bacillus licheniformis* F1 and its comprehensive application. *BMC Microbiology*, *24*(1), 271. https://doi.org/10.1186/s12866-024-03410-5

Wolski, E. A. (2023). The versatility of *Penicillium* species to degrade organic pollutants and its use for wastewater treatment. *Studies in Fungi*, *8*(1), 2. https://doi.org/10.48130/SIF-2023-0002

Wu, Y., Huang, S., Tian, W., Yang, S., Shen, W., & Dong, J. (2024). Endophytic *Colletotrichum fructicola* KL19 and its derived SeNPs mitigate Cd-stress-associated damages in *Spinacia oleracea* L. *Plants*, *13*(17), 2359. https://doi.org/10.3390/plants13172359

Wu, Z., Ren, Y., Liang, Y., Huang, L., Yang, Y., Zafar, A., Hasan, M., Yang, F., & Shu, X. (2021). Synthesis, characterization, immune regulation, and antioxidative assessment of yeast-derived selenium nanoparticles in cyclophosphamide-induced rats. *ACS Omega*, *6*(38), 24585–24594. https://doi.org/10.1021/acsomega.1c03205

Xue, M., Qu, Z., Moretti, A., Logrieco, A. F., Chu, H., Zhang, Q., Sun, C., Ren, X., Cui, L., Chen, Q., An, Y., Li, C., Zhong, H., Cao, Z., Wang, F., Sun, Y., Wang, L., Hou, J., Zhang, C., Yang, M., Ding, Y., Yao, Y., Li, P., & Zhu, Y. G. (2025). *Aspergillus* mycotoxins: The major food contaminants. *Advanced Science*, *12*(9), 2412757. https://doi.org/10.1002/advs.202412757

Xu, T., Song, Z., Hou, Y., Liu, S., Li, X., Yang, Q., & Wu, S. (2022). Secondary metabolites of the genus *Nigrospora* from terrestrial and marine habitats: Chemical diversity and biological activity. *Fitoterapia*, *161*, 105254. https://doi.org/10.1016/j.fitote.2022.105254

Xu, Y., Zhang, T., Che, J., Yi, J., Wei, L., & Li, H. (2023). Evaluation of the antimicrobial mechanism of biogenic selenium nanoparticles against *Pseudomonas fluorescens*. *Biofouling*, *39*(2), 157–170. https://doi.org/10.1080/08927014.2023.2199932

Yadav, K., & Khare, P. (2025). Exploring the multifaceted roles of *Trichoderma* secondary metabolites. *Canadian Journal of Microbiology*, *71*, 1–10. https://doi.org/10.1139/cjm-2025-0045

Yadav, P., Pandey, S., & Dubey, S. K. (2023). Selenite bioreduction with concomitant green synthesis of selenium nanoparticles by a selenite resistant EPS and siderophore producing terrestrial bacterium. *Biometals*, *36*(5), 1027–1045. https://doi.org/10.1007/s10534-023-00503-y

Yang, X., Song, W., Gao, F., Luo, H., Liu, P., Tan, Z., Zhou, J., Wang, D., Nie, X., Lai, C., Shi, H., Li, X., & Zhang, D. (2024). Superoxide dismutase catalyzed size-adjustable selenium nanoparticles in *Saccharomyces boulardii*. *Journal of Agricultural and Food Chemistry*, *72*(8), 4257–4266. https://doi.org/10.1021/acs.jafc.3c08507

Yasir, R. M., & Zaki, N. H. (2024). Preparation, characterization of selenium nanoparticles from *E. coli* and study its effect on pathogenic bacteria. *Journal of Physico-Chemical Material (JPCM)*, *1*(1), 30–38. https://doi.org/10.64820/AEPJPCM.11.30.38.122024

Yassein, A. S., Elamary, R. B., & Alwaleed, E. A. (2025). Biogenesis, characterization, and applications of *Spirulina* selenium nanoparticles. *Microbial Cell Factories*, *24*(1), 39. https://doi.org/10.1186/s12934-025-02656-6

Yuan, Q., Xiao, R., Afolabi, M., Bomma, M., & Xiao, Z. (2023). Evaluation of antibacterial activity of selenium nanoparticles against food-borne pathogens. *Microorganisms*, *11*(6), 1519. https://doi.org/10.3390/microorganisms11061519

Zakaria, L. (2024). An overview of *Aspergillus* species associated with plant diseases. *Pathogens*, *13*(9), 813. https://doi.org/10.3390/pathogens13090813

Zhang, H., Li, Z., Dai, C., Wang, P., Fan, S., Yu, B., & Qu, Y. (2021). Antibacterial properties and mechanism of selenium nanoparticles synthesized by *Providencia* sp. DCX. *Environmental Research*, *194*, 110630. https://doi.org/10.1016/j.envres.2020.110630

Zhang, L., Li, Z., Zhang, L., Lei, Z., Jin, L., Cao, J., & Quan, C. (2022a). High-efficiency reducing strain for producing selenium nanoparticles isolated from marine sediment. *International Journal of Molecular Sciences*, *23*(19), 11953. https://doi.org/10.3390/ijms231911953

Zhang, J., Wang, Y., Shao, Z., Li, J., Zan, S., Zhou, S., & Yang, R. (2019). Two selenium tolerant *Lysinibacillus* sp. strains are capable of reducing selenite to elemental Se efficiently under aerobic conditions. *Journal of Environmental Sciences*, *77*, 238–249. https://doi.org/10.1016/j.jes.2018.08.002

Zhang, T., Qi, M., Wu, Q., Xiang, P., Tang, D., & Li, Q. (2023). Recent research progress on the synthesis and biological effects of selenium nanoparticles. *Frontiers in Nutrition*, *10*, 1183487. https://doi.org/10.3389/fnut.2023.1183487

Zhang, X., Yin, Q., Li, X., Liu, X., Lei, H., & Wu, B. (2022b). Structures and bioactivities of secondary metabolites from *Penicillium* genus since 2010. *Fitoterapia*, *163*, 105349. https://doi.org/10.1016/j.fitote.2022.105349

Zhong, B., Xu, W., Wu, H., Xian, W., Gong, M., & Wu, Z. (2024a). Differences in slow-release characteristics and release kinetics of three selenium nanoparticles from different synthesis strategies: Revealing the advantages synthesized by *Lactiplantibacillus plantarum*. *Food Bioscience*, *62*, 105307. https://doi.org/10.1016/j.fbio.2024.105307

Zhong, B., Xu, W., Xie, H., & Wu, Z. (2024b). Biosynthesis and characterization of selenium nanoparticles by Se-tolerant *Lactiplantibacillus plantarum*. *Food Bioscience*, *59*, 104061. https://doi.org/10.1016/j.fbio.2024.104061

Cite:

Skrotska, O., Zholobko, O., Protsenko, M., & Kovshar, I. (2026). Current advances in biosynthesis of selenium nanoparticles using microorganisms. *Ukrainian Food Journal*, *15*(3), 871–920. https://doi.org/10.24263/2304-974X-2026-15-3-16

Effect of viscoelastic properties on layer thickness distribution in coextruded packaging films

Viktor Vytvytskyi[1], Oleksandr Sokolskyi[1], Ihor Mikulionok[1,2], Oleksandr Gavva[2], Vladyslav Vytvytskyi[1]

1 – National Technical University of Ukraine "Igor Sikorsky Kyiv Polytechnic Institute", Kyiv, Ukraine
2 – National University of Food Technologies, Kyiv, Ukraine

Keywords:

Packaging
Multilayer
Polymer
Films
Coextrusion
Viscoelasticity

Article history:

Received 12.12.2025
Received in revised form 01.05.2026
Accepted 30.06.2026

Corresponding author:

Viktor Vytvytskyi
E-mail: vytvytskyi.v@gmail.com

DOI:
10.24263/2304-974X-2026-15-3-17

Abstract

Introduction. The effect of the viscoelastic properties of polymer melts on the spatial distribution of layer thickness in coextruded packaging films was determined to ensure the specified barrier and mechanical characteristics.

Materials and methods. Numerical simulation of polymer flow kinetics was performed for the two-dimensional axisymmetric geometry of the coextrusion die. The interaction of a basic viscoelastic flow (Oldroyd-B model) with a variable flow described by non-Newtonian (Cross model) and differential viscoelastic (Giesekus model) rheological models was investigated.

Results and discussion. An increase in the variable flow viscosity within the range of 5000...25000 Pa·s causes a systematic shift of the phase interface. A displacement of the maximum velocity zone by 1.1 mm was recorded, while the actual shift of the interface is 0.3 mm. For the calculated annular die gap, this is equivalent to a 3% change in the thickness of the functional extrudate layer. An inversion of kinetics was revealed: at a minimum viscosity (5000 Pa·s), the flow according to the Giesekus model is slower than the flow described by the Cross model, however, at 25000 Pa·s it becomes faster. This is explained by the influence of elastic effects, macromolecule mobility, and the presence of a normal stress gradient, which generate additional deformations and deviate the profile from the classical parabolic shape. The established thickness redistribution significantly affects the operational performance of PE/PA/EVOH multilayer films: even a 3% change in the barrier layer proportion proportionally increases the elastic modulus and puncture resistance, but can increase the oxygen and moisture permeability of the film. The functional dependencies obtained in the form of third-order polynomials allow for the quantitative prediction of these structural changes.

Conclusions. The influence of viscoelastic effects on the spatial redistribution of layer thicknesses during coextrusion has been quantitatively proven. The established dependencies provide a basis for predicting the structure of multilayer packaging films.

Introduction

Most polymer packaging films, particularly for vacuum and modified atmosphere packaging, are manufactured using a high-performance extrusion method (Mikulenok, 2014). Coextrusion technology allows for the formation of multifunctional structures (with barrier, mechanical, and sealing layers) in a single technological cycle (Apicella et al., 2023; Garofalo et al., 2017). Studies on films containing recycled low-density polyethylene prove that, provided the layer structure is rationally designed, the necessary mechanical strength is ensured at low overall migration rates (Badeka et al., 2003).

Optimization of thickness, layer sequence, and melt flow regimes during coextrusion increases the stiffness of polymer films by 55% without loss of transparency and barrier properties (Garofalo et al., 2017). Specifically, polyamide-based nanocomposite systems and biodegradable blends are promising for hot-fill packaging due to their high strength and barrier characteristics (Apicella et al., 2023). According to that study (Alias et al., 2022), mechanical strength, stiffness, and puncture resistance are the critical criteria that directly depend on the structure of the multilayer film.

Numerical simulation is actively used to analyze the multilayer flow of polymer melts. It has been established that the phenomena of viscous encapsulation and elastic layer thickness redistribution significantly deform the phase interfaces in the forming channel of the die (Dooley et al., 2003). Three-dimensional numerical models of viscoelastic flow demonstrate the sensitivity of velocity profiles and layer thicknesses to the rheological parameters of the flow (Mu et al., 2007; Sunwoo et al., 2001). Dynamic simulation of blown film extrusion confirms a direct relationship between melt rheology, stress distribution, and the final mechanical properties of the film (Pirkle et al., 2003). The scientific and methodological basis of this study also includes the authors' previous works on the modeling of polymer processes and equipment (Karvatskii et al., 2019; Vytvytskyi et al., 2017).

Despite the available results, studies on coextrusion predominantly focus on the overall flow stability, shaping, and the influence of channel geometry (Alias et al., 2022; Dooley et al., 2003). At the same time, the quantitative analysis of the effect of polymer viscoelastic properties on the spatial distribution of layer thickness, especially considering the mechanical requirements of food packaging, remains insufficiently studied.

The aim of the study is to determine the effect of the viscoelastic properties of polymer melts on the layer thickness distribution in coextruded packaging films using numerical simulation methods.

Materials and methods

Methodology of numerical simulation

Numerical simulation of the coextrusion of two polymer flows in the coextrusion die of a multilayer packaging film production line was performed. Channel geometry was designed in SolidWorks, and calculations were executed using the Ansys Polyflow software package.

The isothermal interaction of flows with different rheological properties was investigated. The study included two cases: the first modeled the interaction between a non-Newtonian and a viscoelastic flow, while the second modeled the interaction of two viscoelastic flows with different characteristics.

In each case, a series of calculations was performed wherein the viscosity of the first flow was varied from 5000 to 25000 Pa·s with a step of 5000 Pa·s, while a constant viscosity of 5000 Pa·s was set for the second flow.

Characteristics of the investigated packaging films

The objects whose forming processes were investigated in this study are typical multilayer coextruded packaging films for food products. The structure of such films is based on a combination of conditionally "rigid" and "soft" polymer layers. Barrier layers based on polyamide or ethylene-vinyl alcohol copolymers form the structural framework of the film, ensuring low gas permeability, as well as increased stiffness and puncture resistance (Briassoulis et al., 2017; Scarfato et al., 2017).Polyolefin layers (primarily various grades of polyethylene) provide the material with the necessary plasticity, water impermeability, and heat sealability, and are also responsible for the formation of the package seam (Garofalo et al., 2017).

Photographs of actual samples of multilayer packaging films, whose coextrusion forming kinetics were modeled in this study, are presented in Figure 1 (FoodIngredients, 2020).



Figure 1. Samples of multilayer coextruded packaging films

Flow properties

In the first case (see Table 1), the first polymer flow was assigned the rheological properties of a non-Newtonian flow according to the Cross model (Cross, 1965), and the second – of a differential viscoelastic flow according to the Oldroyd-B model (Castillo et al., 2022). In the second case (Table 2), both flows were assigned the rheological properties of a differential viscoelastic flow: the first – according to the Giesekus model (Moayed et al., 2010), and the second – according to the Oldroyd-B model (Castillo et al., 2022).

Table 1

Properties of the first case

First polymer flow			Second polymer flow		
Flow type	Non-Newtonian (Cross model)		**Flow type**	Differential viscoelastic (Oldroyd-B model)	
Flow parameters	Zero-shear viscosity, Pa·s	5000	**Flow parameters**	Viscosity, Pa·s	5000
		10000			
		15000			
		20000		Relaxation time, s	0.1
		25000			
	Relaxation time, s	0.24		Ratio of Newtonian viscosity to total shear viscosity	0.11
	P	0.32			

Table 2

Properties of the second case

First polymer flow			Second polymer flow		
Flow type	Differential viscoelastic (Giesekus model)		**Flow type**	Differential viscoelastic (Oldroyd-B model)	
Flow parameters	Viscosity, Pa·s	5000	**Flow parameters**	Viscosity, Pa·s	5000
		10000			
		15000			
		20000			
		25000			
	Relaxation time, s	0.1		Relaxation time, s	0.1
	Material constant	0.5		Ratio of Newtonian viscosity to total shear viscosity	0.11
	Ratio	0.11			

Geometry and mesh

The polymer flow channels of the axisymmetric coextrusion die for the production of multilayer polymer film were designed as a two-dimensional geometry of the lower half of the die (see Figure 2), specifying the corresponding symmetry plane.

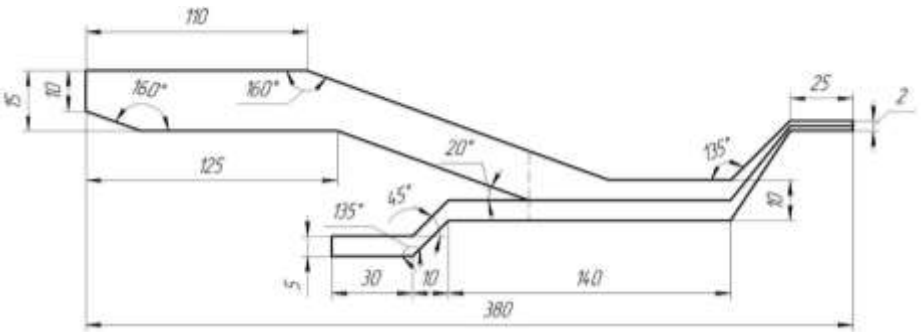

Figure 2. Geometry of coextrusion die channels

The finite element mesh of the two-dimensional geometry of the coextrusion die channels was generated with a finite element size of 0.2 mm. For the numerical model, the obtained number of mesh nodes is 43,210 and the number of mesh elements is 42,250. The choice of the mesh domain parameters was justified by comparing the simulation results for different element sizes until an acceptable convergence within 5% was achieved.

Initial and boundary conditions

Figure 3 shows the computational scheme of the die with boundaries for setting the initial and boundary conditions. For both cases, the following common parameters were set:

— volumetric flow rate of the inlet polymer flows $Q = 5 \cdot 10^{-6}$ m^3/s with an evolution $f(S) = S$ (zero-order method: $S_{initial} = 0.01$; $S_{final} = 1$);

- symmetry plane at boundary *1*;
- moving interface along boundary *5*, upwinding in the kinetic equation, position imposed at the beginning of the interface;
- zero wall velocity at boundary *4*;
- inlet of the first polymer flow at boundary *2*;
- inlet of the second polymer flow at boundary *3*;
- outlet of the two-layer polymer flow at boundary 6 with normal and tangential forces $f_n = f_s = 0$.

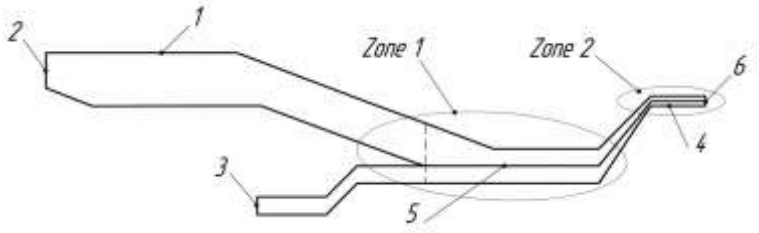

Figure 3. Schematic of coextrusion die showing boundaries and studied zones:
1 – symmetry plane boundary;
2, 3 – polymer flow inlet boundaries;
4 – solid walls with zero flow velocity;
5 – moving interface;
6 – two-layer polymer flow outlet boundary.

During the study, the main attention was paid to two zones of the coextrusion die where the interaction of flows and the formation of the layer profile occur: the zone of the initial merging of polymer melts (Figure 3, Zone 1) and the zone of the two-layer flow outlet (Figure 3, Zone 2).

Results and discussion

Under conditions of laminar flow in an axisymmetric coextrusion die, the application of a two-dimensional numerical model is justified, as it correctly reproduces the velocity fields and the flow merging mechanism (Pirkle et al., 2003; Tang et al., 2019). This approach significantly reduces computational costs, simplifies the setup of initial and boundary conditions, and ensures obtaining reliable simulation results. Furthermore, it allows for a detailed investigation of the velocity distribution in the planar cross-section of the channel, which is important for optimizing the coextrusion process and provides a basis for further expansion to a three-dimensional model.

Case 1. Interaction of non-Newtonian and viscoelastic flows (Cross model and Oldroyd-B model)

Based on the results of the first case (interaction of the non-Newtonian flow according to the Cross model and the viscoelastic flow according to the Oldroyd-B model, parameters in Table 1), the velocity distributions in Zone 1 and Zone 2 were obtained for five values of the first flow viscosity (5000, 10000, 15000, 20000, 25000 Pa·s).

Figure 4 shows the velocity distribution in Zone 1 at the minimum viscosity of the first flow (5000 Pa·s), and in Figure 5 – at the maximum (25000 Pa·s). Figures 6–7 show the analogous results for Zone 2.

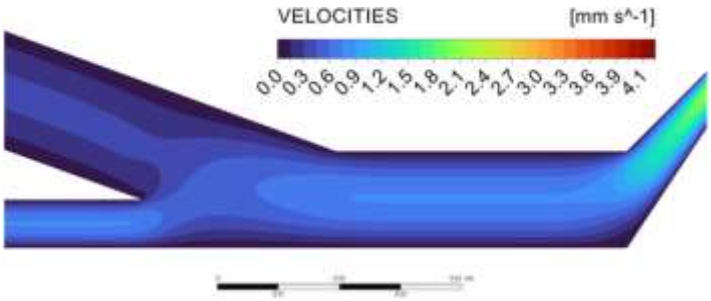

Figure 4. Velocity distribution in Zone 1 at minimum viscosity of the first flow (5000 Pa·s)

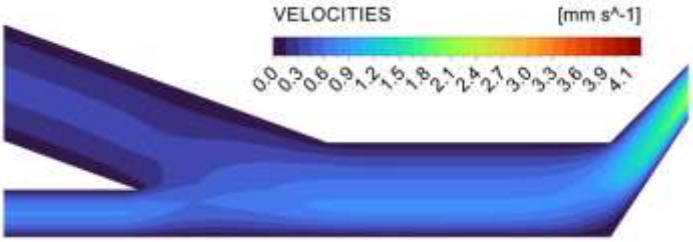

Figure 5. Velocity distribution in Zone 1 at maximum viscosity of first flow (25000 Pa·s)

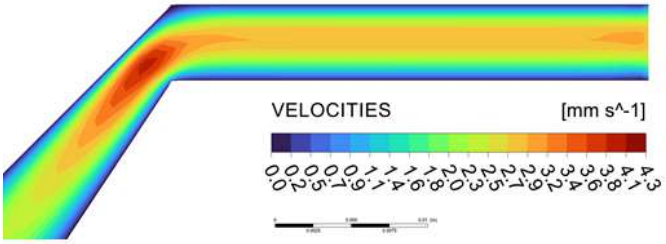

Figure 6. Velocity distribution in Zone 2 at minimum viscosity of first flow (5000 Pa·s)

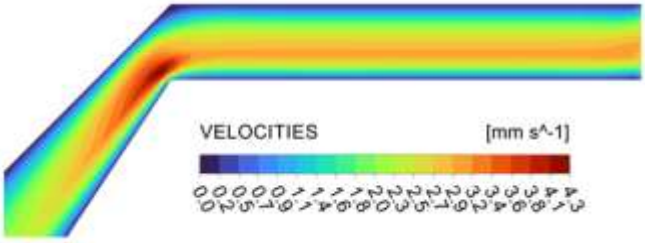

Figure 7. Velocity distribution in Zone 2 at maximum viscosity of first flow (25000 Pa·s)

Based on the results of the considered case, the dependencies of the two-layer polymer flow velocity on the channel width coordinate for five variants of the first flow viscosity (Figure 8) and the maximum velocity of the two-layer polymer flow on the position of its maximum across the channel width (Figure 9) were plotted.

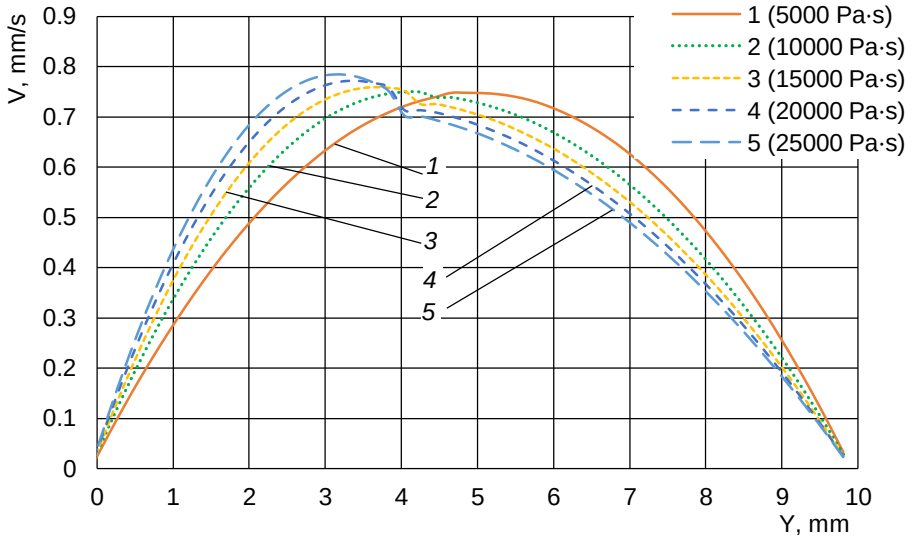

Figure 8. Dependence of polymer flow velocity on channel width coordinate in Zone 1

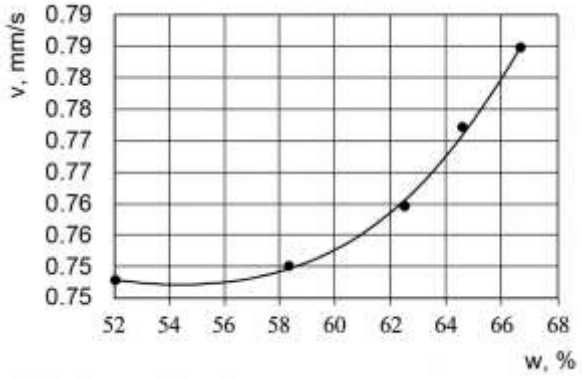

Figure 9. Dependence of maximum polymer flow velocity on position of its maximum across channel width

From the obtained results of the first case (Figures 4–7), it is evident that the two-layer polymer flow shifts downward (to the right) as the viscosity of the first polymer increases. The velocity distribution graph (Figure 8) visually demonstrates this shift: the peaks of the velocity profiles for the higher viscosity of the first flow are located at lower values of the Y coordinate compared to the minimum viscosity, which corresponds to the aforementioned flow shift. The local minimum at the coordinate $Y \approx 13$ mm indicates the boundary between the flows.

Figure 9 shows the increase in velocities resulting from the displacement of the layers. Additionally, an approximating line is plotted on it, which is described by a 3rd-order polynomial equation

$$V = 11.306w^3 - 17.303w^2 + 8.7853w - 0.7317.$$

The obtained dependence describes this process with high accuracy ($R^2 = 0.997$) and allows for the prediction of the further shift of the flows given a larger viscosity difference.

This shift of the phase interface has a clear physical justification: according to the principle of minimizing the internal energy of the system, the less viscous flow tends to displace the more viscous one into the zone of lower shear rates. Similar phenomena of layer redistribution and viscous encapsulation (when the less viscous component becomes "trapped" within the more viscous one) have been previously recorded during experimental and numerical studies of the coextrusion process (Anderson et al., 2006; Dooley et al., 2003). Physically, such an interface shift implies a change in the layer thickness ratio in the finished extrudate. According to previous studies (Briassoulis et al., 2017; Hoffman et al., 2024), deviations in the layer geometry directly affect the operational characteristics of the packaging (stiffness, barrier properties, and puncture resistance). Our obtained results are consistent with the conclusions of (Mu et al., 2007; Sunwoo et al., 2001), which confirm that the correct selection of rheological properties is important for the accurate prediction of the structure of multilayer films.

Case 2. Interaction of two viscoelastic flows (Giesekus and Oldroyd-B models)

Based on the results of the second case (interaction of two viscoelastic flows according to the Giesekus and Oldroyd-B models, parameters in Table 2), the velocity distributions in Zone 1 and Zone 2 were obtained for five values of the first flow viscosity (5000, 10000, 15000, 20000, 25000 Pa·s).

Figure 10 shows the velocity distribution in Zone 1 at the minimum viscosity of the first flow (5000 Pa·s), and in Figure 11 – at the maximum (25000 Pa·s). Figures 12–13 show the analogous results for Zone 2.

Based on the results of the considered case, the dependencies of the two-layer polymer flow velocity on the channel width coordinate for five variants of the first flow viscosity (Figure 14) and the maximum velocity of the two-layer polymer flow on the position of its maximum across the channel width (Figure 15) were plotted.

Analysis of the obtained results of the second case (Figures 12–15) indicates a trend similar to the first case: the two-layer polymer flow shifts downward (to the right) with an increase in the viscosity of the first polymer. The velocity distribution graph (Figure 14) visually demonstrates this shift: the peaks of the velocity profiles for the higher viscosity of the first flow are located at lower values of the Y coordinate, compared to the minimum viscosity. The local minimum at the coordinate $Y \approx 13$ mm indicates the boundary between the flows.

Figure 15 shows the increase in velocities resulting from the displacement of the layers. Additionally, an approximating line is plotted on it, which is described by a 3rd-order polynomial equation

$$V = -13.858w^3 + 26.772w^2 - 16.842w + 4.2175.$$

The obtained dependence ($R^2 = 0.9885$) allows for predicting the shift of the flows given a larger viscosity difference. A certain decrease in the coefficient of determination compared to the first case indicates a more complex, non-linear nature of the interaction between two purely viscoelastic media.

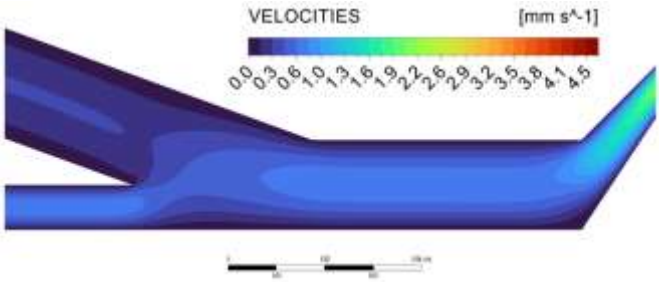

Figure 10. Velocity distribution in Zone 1 at minimum viscosity of first flow (5000 Pa·s)

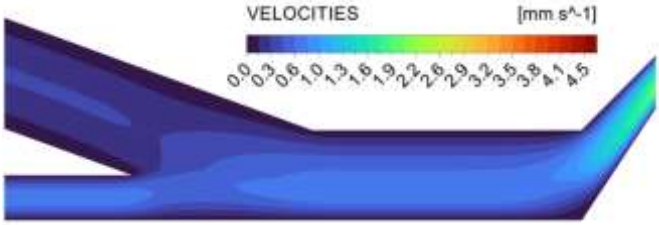

Figure 11. Velocity distribution in Zone 1 at maximum viscosity of first flow (25000 Pa·s)

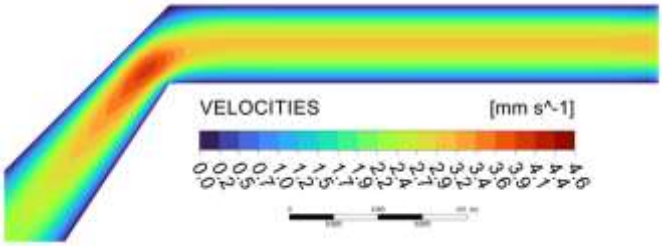

Figure 12. Velocity distribution in Zone 2 at minimum viscosity of first flow (5000 Pa·s)

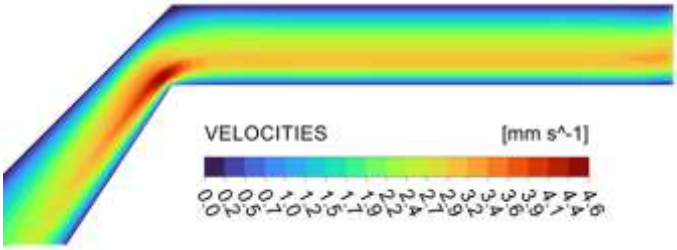

Figure 13. Velocity distribution in Zone 2 at maximum viscosity of first flow (25000 Pa·s)

Taking into account viscoelastic effects simultaneously for both flows complicates the flow kinetics. As noted in the study (Dooley et al., 2003), the presence of a discrepancy in the values of the first normal stress difference at the phase interface generates additional local deformations of the interface. The Giesekus model, unlike purely viscous models, takes into account not only the dependence of viscosity on the shear rate but also the effects of polymer macromolecule mobility, which makes the velocity profile more sensitive to changes in rheological properties (Moayed et al., 2010; Park et al., 2021). According to studies (Sunwoo et al., 2001), the use of a combination of differential viscoelastic models allows for the most adequate description of the real behavior of multilayer polymer systems under extrusion conditions, which is important for controlling the layer thickness uniformity of coextruded packaging films.

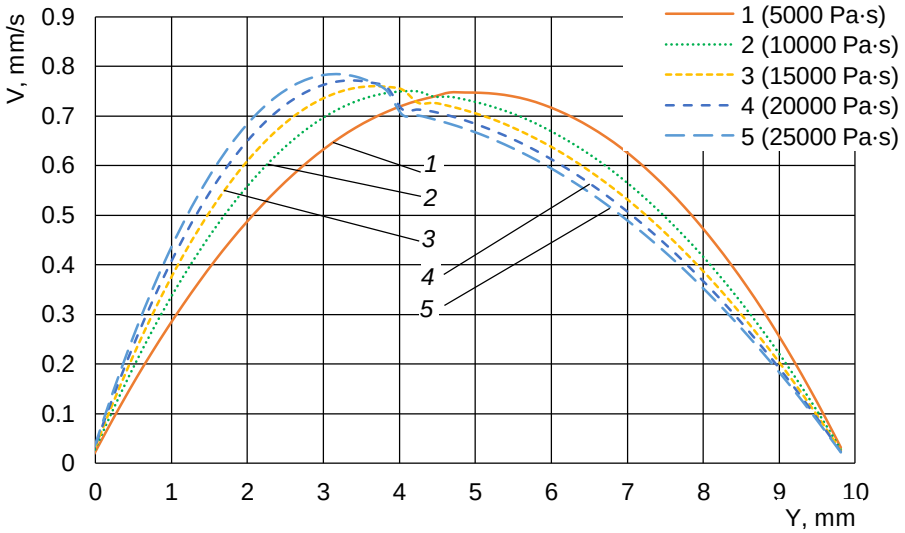

Figure 14. Dependence of polymer flow velocity on channel width coordinate in Zone 1

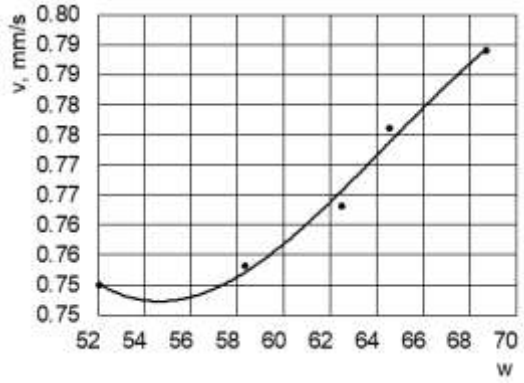

Figure 15. Dependence of maximum polymer flow velocity on position of its maximum across channel width

Comparative analysis of flow kinetics

For a comparative analysis of both cases, a graph of the dependence of the difference in flow velocities (ΔV) in Zone 1 on the coordinate across the channel width (Y) was plotted (Figure 16). The conditional boundary between the flows is located at the coordinate $Y \approx 13$ mm, where the velocity difference ΔV approaches zero.

Analysis of the left part of the graph (Figure 16) indicates that under the condition of minimum viscosity (5000 Pa·s), the first flow, described by the Giesekus model (second case), moves slower compared to the flow according to the Cross model (first case). This is confirmed by the negative values of ΔV. The maximum discrepancy in velocities is observed precisely at the beginning of the calculation series. With a sequential increase in the viscosity of the first polymer to 25000 Pa·s in both cases, the velocity difference decreases, however, an inversion of kinetics occurs: the flow according to the viscoelastic Giesekus model begins to flow faster than the flow according to the Cross model.

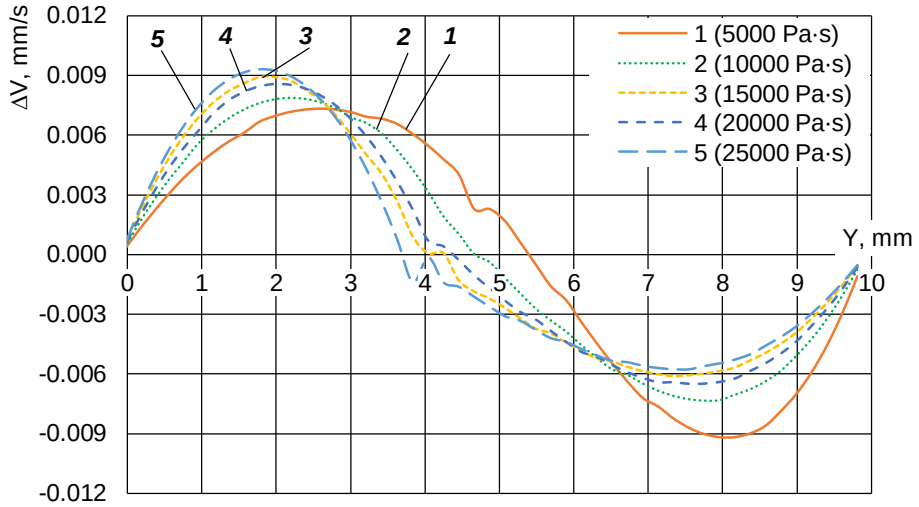

Figure 16. Dependence of difference in polymer flow velocities on channel width in Zone 1

Such behavior is explained by the fundamental differences in the rheological models. The Cross model exclusively describes the effect of viscosity reduction with increasing shear rate, whereas the differential Giesekus model additionally takes into account the anisotropy of polymer macromolecule mobility and relaxation processes (Moayed et al., 2010; Park et al., 2021). At low viscosity values, elastic forces decelerate the flow, but with an increase in viscosity and shear stresses, the mechanism of macromolecule "slip" is activated, which accelerates the flow in the near-wall layers.

Furthermore, the presence of elastic effects simultaneously in both layers (second case) leads to the emergence of more complex, non-monotonic velocity and stress profiles at the phase interface. According to previous studies (Anderson et al., 2006; Dooley et al., 2003), the normal stress difference generates secondary flows that deviate the velocity profile from the classical parabolic shape. This precisely explains the somewhat lower coefficient of determination ($R^2 \approx 0.9885$) for the polynomial approximation of the second case compared to the first one ($R^2 \approx 0.997$). As noted in (Raps et al., 2018), polynomial models well reproduce the general nature of such flows, but the decrease in accuracy confirms the more complex, non-linear structure of the interaction of purely viscoelastic media. The specific model used to approximate the rheological behavior of a particular polymer and its grade depends on its nature and the specifics of its production technology, and is determined from experimental studies.

Prediction of structural and mechanical properties of films

The established patterns of changes in flow kinetics allow for the quantitative prediction of the structural characteristics of multilayer packaging films. According to the obtained numerical simulation data, an increase in the viscosity of the first flow from 5000 to 25000 Pa·s in both cases leads to a displacement of the maximum velocity zone of the second layer by 1.1 mm, while the actual shift of the phase interface is 0.3 mm. On the scale of the calculated annular die gap (width of 10 mm), this is equivalent to a 3% change in the thickness of the functional extrudate layer.

Data regarding experimental multilayer PE films with EVOH or PA barrier layers (Barbosa et al., 2025) show that increasing the thickness of the conditionally "rigid" barrier layer even by 3–5% increases the overall elastic modulus and puncture resistance in proportion (up to 10–15%), but can increase the oxygen and moisture permeability of the film. The thickness of the "soft" polyethylene layers determines the ability of the film to withstand local deformations and compensate for the brittleness of the barrier layer. Studies of copolyamide nanocomposite films confirm that a deviation in the layer arrangement of more than 8–10% from the nominal value leads to an increase in the permeability of the multilayer film (Russo et al., 2006; Scarfato et al., 2017), which can cause a reduction in the shelf life of the products.

Thus, the phenomenon of thickness redistribution between the "rigid" and "soft" flows recorded as a result of numerical simulation is of significant importance. For a quantitative assessment of this effect, polynomial dependencies (Figures 9, 15) were obtained in the study, which serve as a tool for linking the rheological properties of the melt flow and the shift of the layer boundary. These regularities complement general models of the mechanical behavior of polymer materials, including the numerical simulation of the properties of reinforced polymers developed by the authors earlier (Vytvytskyi et al., 2026), and allow for the optimization of the rheological regimes of the coextrusion process to achieve the target balance of strength and deformability of the packaging without conducting a significant volume of full-scale experiments.

Conclusions

Numerical simulation of the coextrusion of two polymer melt flows with different rheological properties, including non-Newtonian flow according to the Cross model and viscoelastic flows according to the Oldroyd-B and Giesekus models, was performed in a two-dimensional axisymmetric coextrusion die. It was shown that an increase in the viscosity of the first flow from 5000 to 25000 Pa·s leads to a systematic shift of the two-layer flow and the layer interface, as confirmed by changes in the spatial position of the velocity profile maxima and the coordinates of the phase interface in the channel cross-section. A significant influence of the rheological model on the flow behavior was established. At low viscosity values, the flow described by the Giesekus model had a lower velocity within its layer than the flow described by the Cross model, while this difference decreased with increasing viscosity. Third-order polynomial dependencies were obtained that describe the changes in the maximum velocity and its position across the channel width depending on the viscosity of the first flow with high accuracy (R^2 = 0.9885–0.997). These dependencies allow interpolation of the layer interface shift within the studied parameter range. With increasing viscosity of the first flow, the velocity difference between the models decreased, and the Giesekus flow became faster than the Cross-model flow, reflecting changes in the distribution of deformations and stresses between the layers. This indicates that consideration of both viscous non-Newtonian and viscoelastic properties of the melt, particularly the normal stress difference, is important for accurate determination of the layer thickness distribution. The established dependencies can be used to predict the structural characteristics and mechanical behavior, including stiffness and resistance to local loads, of multilayer packaging films without conducting a large number of full-scale experiments. The proposed numerical model provides a basis for further extension to three-dimensional non-isothermal coextrusion conditions, including film drawing and cooling, and for integration with experimental mechanical testing of multilayer packaging films.

References

Alias, A. R., Wan, M. K., & Sarbon, N. M. (2022). Emerging materials and technologies of multi-layer film for food packaging application: A review. *Food Control, 136*, 108875. https://doi.org/10.1016/j.foodcont.2022.108875

Anderson, P. D., Dooley, J., & Meijer, H. E. H. (2006). Viscoelastic effects in multilayer polymer extrusion. *Applied Rheology, 16*(4), 198–205. https://doi.org/10.1515/arh-2006-0014

Apicella, A., Scarfato, P., & Incarnato, L. (2023). Tailor-made coextruded blown films based on biodegradable blends for hot filling and frozen food packaging. *Food Packaging and Shelf Life, 37*, 101096. https://doi.org/10.2139/ssrn.4389362

Badeka, A., Goulas, A. E., Adamantiadi, A., & Kontominas, M. G. (2003). Physicochemical and mechanical properties of experimental coextruded food-packaging films containing a buried layer of recycled low-density polyethylene. *Journal of Agricultural and Food Chemistry, 51*(8), 2426–2431. https://doi.org/10.1021/jf025709z

Barbosa, F. D., Staffa, L. H., & Costa, L. C. (2025). Recycling of PE/PA/EVOH multilayer flexible packaging films via reactive extrusion. *Journal of Applied Polymer Science, 142*(33), 57332. https://doi.org/10.1002/app.57332

Briassoulis, D., Tserotas, P., & Hiskakis, M. (2017). Mechanical and degradation behaviour of multilayer barrier films. *Polymer Degradation and Stability, 143*, 214–230. https://doi.org/10.1016/j.polymdegradstab.2017.07.019

Castillo Sánchez, H. A., Jovanović, M. R., Kumar, S., Morozov, A., Shankar, V., Subramanian, G., & Wilson, H. J. (2022). Understanding viscoelastic flow instabilities: Oldroyd-B and beyond. *Journal of Non-Newtonian Fluid Mechanics, 302*, 104742. https://doi.org/10.1016/j.jnnfm.2022.104742

Cross, M. M. (1965). Rheology of non-Newtonian fluids: A new flow equation for pseudoplastic systems. *Journal of Colloid Science, 20*(5), 417–437. https://doi.org/10.1016/0095-8522(65)90022-X

Dooley, J., & Rudolph, L. (2003). Viscous and elastic effects in polymer coextrusion. Journal of Plastic Film & Sheeting, 19(2), 81–102. https://doi.org/10.1177/8756087903039575

FoodIngredients. (2020). Iskusstvennaya obolonka. FoodIngredients.com.ua. https://foodingredients.com.ua/obolonka

Garofalo, E., Scarfato, P., Di Maio, L., & Incarnato, L. (2017). Tuning of co-extrusion processing conditions and film layout to optimize the performances of PA/PE multilayer nanocomposite films for food packaging. *Polymer Composites, 39*(9), 3157–3167. https://doi.org/10.1002/pc.24323

Hoffman, J., & Otten, C. (2024). *Multilayer packaging film characterization* (Application note M-082324). EAG Laboratories. https://www.eag.com/app-note/multilayer-packaging-film-characterization

Karvatskii, A., Panov, Y., Vasylchenko, G., Vytvytskyi, V., & Korolenko, K. (2019). Determining efficient values for the thermophysical properties of bulk materials. *Eastern-European Journal of Enterprise Technologies, 2*(5), 55–62. https://doi.org/10.15587/1729-4061.2019.164791

Mikulenok, I. (2014). Intensification of fabrication of extruded polymeric shapes. *Chemical and Petroleum Engineering, 50*(7–8), 483–488. https://doi.org/10.1007/s10556-014-9927-5

Moayed, M., Kamali, R., & Fattahi, E. (2010). Viscoelastic fluid behavior in annulus using Giesekus model. *Journal of Non-Newtonian Fluid Mechanics, 165*(21–22), 1505–1511. https://doi.org/10.1016/j.jnnfm.2010.07.012

Mu, Y., Zhao, G., Chen, A., & Wu, X. (2007). Numerical simulation of three-dimensional polymer extrusion flow with differential viscoelastic model. *Polymers for Advanced Technologies, 18*(11), 913–923. https://doi.org/10.1002/pat.959

Park, G., Yun, J., Lee, C., & Jung, H. W. (2021). Effect of material parameter of viscoelastic Giesekus fluids on extensional properties in spinline and draw resonance instability in isothermal melt spinning process. *Polymers, 13*(1), 139–148. https://doi.org/10.3390/polym13010139

Pirkle, C. J., & Braatz, R. D. (2003). Dynamic modeling of blown-film extrusion. *Polymer Engineering and Science, 43*(2), 398–418. https://doi.org/10.1002/pen.10033

Raps, D., Goodarzi Hosseinabadi, H., Heymann, L., Köppl, T., & Altstädt, V. (2018). Rheological properties of thermoplastic polymers with dissolved gases for foaming applications. In *Polymer rheology*. Retrieved from https://arxiv.org/pdf/1804.0795

Russo, G. M., Simon, G. P., & Incarnato, L. (2006). Correlation between rheological, mechanical, and barrier properties in new copolyamide-based nanocomposite films. *Macromolecules, 39*(11), 3855–3864. https://doi.org/10.1021/ma052178h

Scarfato, P., Garofalo, E., Di Maio, L., & Incarnato, L. (2017). Transport, mechanical and global migration data of multilayer copolyamide nanocomposite films with different layouts. *Data in Brief, 12*, 540–545. https://doi.org/10.1016/j.dib.2017.04.025

Sunwoo, K. B., Park, S. J., Lee, S. J., Ahn, K. H., & Lee, S. J. (2001). Numerical simulation of three-dimensional viscoelastic flow using the open boundary condition method in coextrusion process. *Journal of Non-Newtonian Fluid Mechanics, 99*(2–3), 125-444. https://doi.org/10.1016/S0377-0257(01)00115-X

Tang, D., Marchesini, F. H., D'hooge, D. R., & Cardon, L. (2019). Isothermal flow of neat polypropylene through a slit die and its die swell: Bridging experiments and 3D numerical simulations. *Journal of Non-Newtonian Fluid Mechanics, 266*, 33–45. https://doi.org/10.1016/j.jnnfm.2019.02.004

Vytvytskyi, V., Mikulionok, I., Sokolskyi, O., & Gavva, O. (2017). Pressure and temperature influence on the friction coefficient of granular polymeric materials on the metal surfaces. *Ukrainian Food Journal, 6*(3), 543–552. https://doi.org/10.24263/2304-974X-2017-6-3-14

Vytvytskyi, V., Sokolskyi, O., & Mikulionok, I. (2026). Numerical analysis of the ultimate load-bearing capacity of polymer pipes reinforced with continuous longitudinal fibers. *Bulletin of Kremenchuk Mykhailo Ostrohradskyi National University, 2*(1(156)), 83–90. https://doi.org/10.32782/1995-0519.2026.1.2.10

Cite:

Vytvytskyi, V., Sokolskyi, O., Mikulionok, I., Gavva, O., & Vytvytskyi, V. (2026). Effect of viscoelastic properties on layer thickness distribution in coextruded packaging films. *Ukrainian Food Journal, 15*(3), 921–934. https://doi.org/10.24263/2304-974X-2026-15-3-17

International business activities of food enterprises in the Slovak Republic considering current trends and business sustainability

Mariana Dubravská[1], Elena Širá[1], Ladislav Mura[2]

University of Prešov, Slovakia
Bratislava University of Economics and Business,Slovakia

Keywords:

Food industry
Internationalization
Enterprises
Slovak republic
Sustainability

Article history:

Received 17.03.2026
Received in revised form 16.05.2026
Accepted 30.06.2026

Corresponding author:

Ladislav Mura
E-mail:
ladislav.mura@euba.sk

DOI:
10.24263/2304-974X-2026-15-3-18

Abstract

Introduction. The aim of the research is to identify management practices in food businesses following periods of crisis and the Russian invasion, which led to widespread uncertainty and economic consequences.

Materials and methods. The objectives were achieved through the following methodological procedures: the collection of domestic and foreign data, analysis, synthesis and comparison of data, which were processed into tabular, graphical and textual forms, mathematical and statistical calculations, including a model solution for calculating, investment needs in the food sector, and expert estimates.

Results and discussion. The Slovak food industry has undergone significant changes since the establishment of the independent Slovak Republic. Last decades has brought many opportunities for the Slovak food industry, but also threats – imports of foreign food, exports of Slovak food, the entry of foreign investors, the military conflict in Ukraine and the further periods of crisis. Over the past twenty years, foreign trade has been one of the most significant drivers of global economic growth and an effective tool for mitigating the negative effects of limited resources. Current data confirms that over-reliance on the domestic market poses a severe threat during crises. This article examines selected areas of the Slovak food industry's international business in the context of recent events—the pandemic, the war conflict, and their economic impacts. It focuses on the factors influencing international business activities and the strategies that enterprises employ in carrying them out. 80% of Slovak food industry enterprises are owned by multinational corporations. 78.3% of the surveyed enterprises engaged in international business, while 21.7% did not. The volume of international business increased during the searched period for 69.9% of enterprises, remained unchanged for 29% of enterprises, and decreased for 1.4% of enterprises. Based on the results of the Friedman test ($p<0.05$), we conclude that enterprises perceive the various factors influencing their operations in foreign markets differently; in other words, they are not motivated by the same reasons to internationalise their business activities, as a statistically significant difference between the individual factors has been demonstrated.

Conclusions. One way the Slovak food industry can strengthen its competitiveness, and how Slovak food enterprises can survive despite Slovakia's small size through its business activities in an international environment and the resources derived therefrom.

Introduction

Political and economic changes in many European countries have laid the foundations for the formation of a new geographical area characterised by economic activities and business relationships within a market environment. Businesses must build sustainable long-term commercial relationships that enable them to develop and strengthen their market position, thereby gaining a competitive advantage over other market players. The food industry has historically held an irreplaceable position amongst the industrial sectors of the Slovak economy. This applies in particular to the small and medium-sized enterprise sector (Koraus et al., 2020). The main roles of the food industry include ensuring food supply and the processing of agricultural produce.

Globalisation has begun to break down the barriers that traditionally distinguished local business opportunities and local firms from their international counterparts. Local markets are becoming part of wider global markets. As a result, internationally-oriented entrepreneurs now have a wider range of options at their disposal, unhindered by national borders. In this increasingly integrated global environment, entrepreneurs face both new opportunities and new challenges (Balsiūnaitė et al., 2026; Kordos & Habanik, 2018). A company that views the world as a single global market and employs global marketing is based on capitalising on the common traits and characteristics of customers and their needs. One of the principles is the global standardisation of the company's business activities and the provision of standardised products. Globalisation is accompanied by increasing global interdependence, in the sense of a deepening interdependence between economic actors, countries and integration groups (Hečková & Chapčáková, 2021; Horalíková, 2000; Horská & Ubrežiová, 2001; Tiruneh et al., 2009).

The main benefit of globalisation in the food market is the cross-border sharing of agricultural and production practices and their efficiency. This is leading to the global modernisation of agriculture and food production (Kita & Cvirik, 2024; Wang & Xu, 2026). The situation in Slovakia is characterised by thirty years of efforts to bring about the transformation and restructuring of the Slovak economy and to adapt to new market conditions and dynamic changes. For the primary agricultural production sector, the ongoing changes and trends present major challenges; however, they also bring new possibilities offering opportunities both within the European Union and on a global scale (Kočanová et al., 2023). The global agri-food market has entered a period of unprecedented and historically high growth. Consequently, the Slovak agricultural sector is not only taking note of this phenomenon but, within the framework of the EU's Common Agricultural Policy, must effectively capitalise on the benefits of globalisation and eliminate its drawbacks. The globalisation of economic activities is a more advanced and complex form of internationalisation, which also encompasses the functional integration of internationally dispersed activities (Blcháč, 2001; Dicken, 1998; Manuell, 2017)

Internationalization offers enterprises the opportunity to strengthen their position, achieve organic growth, and improve the return on their capital. It is evident that internationalization can bring many benefits to businesses, but here, too, every situation has two sides: positive and negative. The positive and negative aspects of business internationalization can be summarized as shown in Table 1.

The internationalisation of the economy has reached such an advanced stage that this process cannot be halted. The same is true for the agri-food sector where internationalization has taken full effect, driving the movement of inputs and outputs on a global scale, ensuring food supply, and influencing managerial decisions in primary agricultural production, the processing industry, distribution, and trade. There are numerous theoretical approaches to defining the internationalization of business, proposed by various authors from different countries, each of whom offers a different perspective and emphasizes a different factor. Most authors view internationalization as a process (Chandra and Wilkonson, 2017; Mura & Löster, 2011; Zadražilová, 2017). In stage models, firms typically expand first to neighbouring markets, and food producers form one of the larger groups of foreign investors among manufacturing firms (Kłysik-Uryszek & Kuna-Marszałek, 2015).

Table 1

Advantages and disadvantages of business internationalization

Advantages	Disadvantages
Deepening of the international division of labour	Increased intensity of competition
Blurring of national borders	Greater losses in the event of failure in foreign markets than in the domestic business environment
Elimination of trade barriers	Disappearance of entities that were unable to adapt
Better utilization of company resources	Greater investment requirements for business internationalization compared with operating in the domestic market
Growth and profit potential of the company	
Opportunity to gain experience in international business	
Possibility of diversifying business risk	
Opportunity to acquire know-how	
Possibility of acquiring new customers and entering new markets	

Baran (2018) examined the internationalization of food enterprises in Poland. Nearly all of the enterprises surveyed identified export activities as their primary form of internationalization, and nearly 50% of the enterprises surveyed reported that they engage in imports. Joint ventures were mentioned by 13% of the surveyed enterprises.

An analysis of the German food retail sector and its development in recent years reveals structural changes. While 25 years ago, it was typical for enterprises in the food retail sector to operate only at the national level, over time these enterprises have transformed into multinational groups (Hanf et al., 2009).

Serrano et al. (2015) conducted a long-term analysis of the factors determining the internationalization process of the Spanish agri-food industry. The results suggest that the existence of a "home market effect" is a determining factor in the intensifying process of internationalization in most subsectors of the food industry. In a survey of 1,585 SMEs from the V4 countries, strategic management was significantly associated with internationalization, innovation mattered mainly in combination with it, and exporting SMEs perceived differences in tax policy as the most significant barrier (Virglerová et al., 2025).

Tha aim of research is to identify the management practices used by Slovak food companies in conducting foreign trade activities during uncertain times.

Materials and methods

Materials. The material on which this study is based, and which contributes to the achievement of its objective, consists of primary and secondary sources. Primary sources comprise information obtained through original research – specifically through a questionnaire survey. The research focused on mapping business activity during a succession of crises, notably the coronavirus pandemic, followed by war and an energy crisis. These factors shaped business practices. The method of selecting the research sample was based on the defined research task, the subject of the study and the factors under investigation.

The target group for the questionnaire survey consisted of the 200 largest enterprises in the food industry, based on their revenue for the year 2022. These are food industry enterprises in the Slovak Republic with annual revenue exceeding €3 million, which in 2022

accounted for 85% of the total revenue of the Slovak food industry through their production. These food businesses include both non-family and family-owned enterprises. The food industry in Slovakia is characterised by a higher proportion of family-owned businesses; however, the Statistical Office does not record the exact proportion. Only ongoing research by academics highlights the activities of these businesses (MPRV SR, 2022).

Secondary sources of information include: analytical and conceptual studies by the Ministry of Labor, Social Affairs, and Family of the Slovak Republic (MPSR), analytical and outlook reports from the European Union, materials and data published by the VÚEPP, specialized publications and journals (both domestic and foreign), primarily those indexed in the prestigious scientific databases Web of Science and Scopus, proceedings from international conferences and specialized seminars, and others.

Statistical analysis. The subgoals were quantified using Friedman's test. Statistical analysis was performed using SPSS. $p<0.05$ indicates a statistically significant difference between the individual factors (Rimarčík 2007).

Results and discussion

The year 2020 and the years that followed were exceptionally volatile, uncertain and marked by numerous crises and challenges, many of which were unexpected. The pandemic crisis had a profound social and economic impact on the entire planet and its inhabitants. The measures adopted by governments to combat the coronavirus had a devastating effect on the global economy. And that was only the beginning. This was followed by another crisis in the form of the war in Ukraine and the energy crisis. This led to a period of devastating crises for businesses and national economies alike. Global markets collapsed, unemployment rose and the incomes of tens of millions of people fell sharply (Bernat & Duda, 2024). In 2022, Russia launched a military operation against Ukraine. This military operation had a profound impact not only on Ukraine itself, but also on the global economy. Market stability was disrupted, the energy market was thrown into turmoil, and trade routes and international markets were adversely affected, leading to widespread uncertainty and economic repercussions. The war has devastated Ukraine's transport infrastructure, and regulatory fragmentation and underinvestment in digitalisation are among the barriers to rebuilding its logistics system (Vovk et al., 2025). The resulting situation caused significant volatility in price levels, particularly energy prices, which in turn affected consumers, industry and countries across the globe (Liu & Su, 2024).

The pandemic crisis has had a particularly negative impact, both socially and economically, on every country in the world without exception. The measures that governments were forced to adopt in the fight to contain the coronavirus pandemic have had a devastating impact on local, regional and global economies. The armed conflict has once again had negative economic consequences for many countries around the world and has affected various sectors of the economy. As a result of these events, the economies of several countries were adversely affected, leading to increased economic instability. In Slovakia, these shocks occurred within a macroeconomic environment in which inflation dynamics were shaped, amongst other things, by globalisation, monetary policy conditions, labour market developments and external economic shocks (Senci & Afful, 2025; Stehlikova et al., 2026).

Slovak food industry

A fundamental objective of food industry is to guarantee the manufacturing of hygienically safe food products. Once the production process is complete, it is essential to focus on the distribution network, as this is responsible for supplying the population. Distribution relies on a functioning network of wholesale logistics centres. From these, goods are distributed to end consumers via the next level of the distribution network – retail channels. The final output of food production comprises a diverse portfolio of approximately eight thousand distinct product types, varying in weight, packaging, and quality specifications (Prytulska et al., 2021; Tóthová & Tóth, 2019). As a vital component of Slovakia's industrial framework and national economy, the food industry generates substantial added value through accompanying services, employment opportunities, regional development stimulation, and public nutrition. Therefore, this sector must be classified as a strategic asset indispensable for maintaining the food sovereignty of the Slovak Republic. This domain builds upon a long-standing domestic tradition of high-quality manufacturing, which is tightly regulated by rigorous legislative standards, reinforcing its position as one of the cornerstone pillars of the country's manufacturing economy (MPRV SR, 2014).

The Slovak food industry has undergone significant changes over the past thirty years. Slovakia’s accession to the European Union opened up our market to foreign products and, conversely, created conditions for the export of Slovak food products abroad.

According to a report by the Ministry of Agriculture and Rural Development (MPRV), the dairy and meat industries are the mainstays of the food industry in Slovakia; the bakery, confectionery, and pastry sectors are also well represented, as are the brewing and malting industries. The distilling, winemaking, and fat processing industries continue to account for a small share of total food production.

The food industry is the second-largest industrial sector, in which primarily agricultural raw materials are processed into a wide range of foods, condiments, beverages, and semi-finished products. The financial position of the largest Slovak food processing companies has been compared across regions at the NUTS II level (Jencová et al., 2022). It is a relatively evenly distributed sector across the entire territory of Slovakia, and its individual sub-sectors are located in different regions (see Figure 1).



Figure 1. Location of the most significant enterprises in selected sectors of the food industry in Slovakia

High demands have been placed on food producers over the years. The most fundamental changes were brought about by the restructuring of the food industry and, subsequently, Slovakia's accession to the EU. Food producers were now required to comply with European standards, directives, regulations, and food quality requirements. Not all enterprises were able to meet these conditions, which significantly shook the industry's foundation. As an example, it was used to have eleven sugar refineries, and today it was only two. In the past, we were a food-self-sufficient country. Today, the situation is different, particularly because 80% of the food industry is owned by multinational corporations.

The Slovak Republic is far from realising the full potential of the Slovak food industry, which is by no means being fully utilised. This is also the case for half of the EU Member States. Although the food industry is not one of the key sectors, it plays a very important role in meeting the nutritional needs of the population (Majerník & Majerník, 2018). High-quality technologies and a knowledge base of key information are essential for identifying, evaluating and managing the spatio-temporal conditions of production. Optimising costs, productivity, profitability, sustainability and food safety are key determinants (Erdei-Gally & Vágány 2022; Jarossova et al., 2025; Vrabcova et al. 2022).

Global history shows that pandemics are recurring phenomena rather than unprecedented crises, with each outbreak invariably causing serious disruptions to the international economic landscape. The food supply chain is a cornerstone of the global economy. It is here that the full impact of the pandemic crisis has been felt, as it comprises a long chain stretching from primary agricultural production to consumer markets. Current research highlights significant fragility and sensitivity in the areas of food production, processing operations, distribution networks and changing consumer demand. The pandemic crisis has led to critical restrictions on labour mobility, volatile consumer behaviour, the temporary closure of production facilities, protectionist trade policies and escalating financial pressures throughout the supply chain (Aday & Aday, 2020).

The pandemic crisis has destabilised not only the economy but also other sectors. On the other hand, it can also be seen as a systemic and comprehensive stress test for the countries of Central and Eastern Europe. Despite maintaining its trajectory of sustainable growth and previous stability, the agri-food sector was not immune to these shocks (Andrejovska & Glova, 2022), although it demonstrated greater resilience compared with other sectors. Two pilot surveys of Slovak employees (302 respondents in autumn 2020 and 284 in early 2021) found that about four in five reported their company had been affected by the pandemic (80.8% and 78.2%), and the share reporting lower income was higher in small than in large companies (Habánik et al., 2021). During the pandemic, the processing of agricultural raw materials by the food industry emerged as the most resilient component of the region's economy. Weighted average GDP stood at 101 per cent of the previous year's baseline in July (EIT Food, 2021). Primary agricultural production was severely disrupted by a critical labour shortage in the agricultural sector. Other factors proved to be of less significance. Demand for food rose sharply at the start of the crisis, which can be attributed to panic buying. Households sought to stock up on at least basic foodstuffs (Plutzer, 2021).

Armed conflict is not merely a local or regional crisis. It has negative and far-reaching consequences. Armed conflict has had a profound impact on the functioning of the global economy, leading to rising inflation and a decline in economic performance (Galiani, 2023).

It is widely assumed that the several crisis situations such as pandemic crisis, the war in Ukraine and energy crisis were the main drivers of the global increase in prices, particularly food inflation. Prices of goods and services across the European Union (EU) and worldwide began rising in the summer of 2021 (see Figure 2). Food inflation in EU member states reached significantly higher levels than overall inflation. In July 2023, the average annual food inflation rate across the EU stood at 12.4%, more than twice the overall inflation rate of 6.1%. In Slovakia, food inflation reached 16.5%, which was 1.6 times higher than the overall inflation rate of 10.3% (European Commission). Between 2021 and 2023, food inflation rose to one of the highest levels in the EU's history and affected all member states.

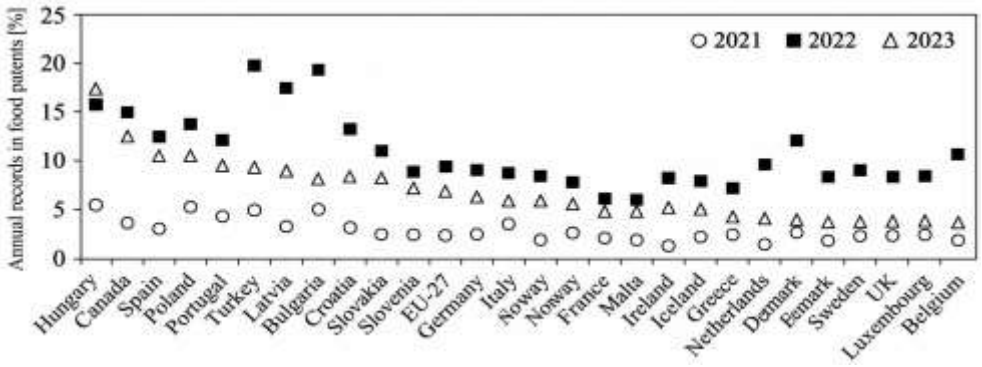

Figure 2. Annual rate of change in food prices

A study by the International Monetary Fund (Ahn & Tan, 2025), using a general equilibrium model, demonstrates that deliberately spreading the purchase of critical inputs across multiple countries significantly mitigates the impact of local shocks. Research highlights the so-called resilience-efficiency trade-off. While a broader network of foreign suppliers slightly increases operating costs, it has been shown to safeguard a country's overall well-being and the continuity of its production in the event of a crisis.

A global study on the impact of epidemics and health crises (Kumar, 2022) confirms that unexpected crises lead to long-term or even irreversible changes in global market shares. The study proposes the implementation of international business strategies that enable enterprises to rapidly divert trade to geographically safer regions if a crisis in the original partner country persists for an extended period.

A publication on fragmented global trade recommends nearshoring (shifting trade to neighboring countries) and international agreements on the strategic stockpiling of critical commodities among allied governments as key international business measures to mitigate risk (Azim et al., 2025).

Belova et al. (2020) developed a methodology for determining the strategic position of an industry or company by identifying and quantitatively assessing factors that exert both positive and negative effects. The methodology also evaluates a company's readiness to adopt the Blue Ocean Strategy.

Recent studies agree that passive dependence on developments in the domestic market can be devastating in times of crisis. The solution lies in international diversification, regional contracting (nearshoring), and the technological integration of business systems (Horvathova & Cvirik, 2026; Qureshi & Ali, 2025). Diversification also has an operational side. Deliveries of raw materials and products have to be planned so that they stay on time

at the lowest economic and environmental cost, and a study of Ukrainian bakery enterprises shows that the preferred delivery plan can differ between delivery zones (Ivashkiv et al., 2019). Supply chain agility, understood as responsiveness, flexibility, visibility and resilience, is likewise presented as a strategic enabler of competitiveness in volatile markets (Mogaka & Njururi, 2024).

Management of food industry enterprises in the Slovak Republic in the context of the impacts of recent events

80% of food industry enterprises are owned by multinational corporations. In our questionnaire survey, enterprises that are not part of larger corporations were overrepresented. 78.3% of the surveyed enterprises engaged in international business, while 21.7% did not. The volume of international business increased during the searched period for 69.9% of enterprises, remained unchanged for 29% of enterprises, and decreased for 1.4% of enterprises.

Factors influencing international business of the Slovak food enterpises

Factors indicating possible reasons for operating in foreign markets shed light on the process of business internationalization. Our research shows that the main factors influencing the enterprises surveyed in their internationalization activities are: management's interest in territorial expansion, efforts to build a promising market position abroad, and demand in foreign markets. On the other hand, the factors that influence them the least are a lack of subcontractors in the domestic market and the company's involvement in an international network of partner enterprises. The factors examined influence the sustainability of business activity.

Empirical findings have highlighted that internationalisation processes are positively influenced primarily by proactive and strategic motivating factors. These include, for example, the organisation's management's desire to expand, a commitment to sustainability, and the aim of building a strong competitive position in the international arena. On the other hand, this process is negatively influenced by reactive stimuli, which may include a low level of domestic demand or a small number of subcontractors.

Using Friedman's test it was examined whether the differences observed in the sample of responses to individual questions regarding the factors driving the surveyed enterprises' operations in foreign markets could be merely random or are statistically significant. The following hypothesis were tested:

H_10: There is no statistically significant difference among the reported factors that explain why the surveyed enterprises operate in foreign markets.

H_11: There is a statistically significant difference among the reported factors that explain why the surveyed enterprises operate in foreign markets (Table 2).

The Friedman test revealed a statistically significant difference in the perceived importance of the ten factors influencing enterprise internationalization, $\chi^2(9, N = 54) = 153.313$, $p < .001$. Therefore, the null hypothesis that all factors were evaluated equally can be rejected.

Relational resources can also contribute to sustainability and the improvement of business development. This view is based on empirical evidence gathered from several countries. Practical experience has shown that social relationships, access to information, additional capital and social commitments contribute to a positive increase in business success (Bayoumy et al., 2025).

Table 2

Results of calculations of the statistical significance of differences between individual factors that account for the performance of the enterprises under study in the foreign market

Factor	**Mean Rank**
Enterprise management's interest in territorial expansion	8.06
Insufficient demand in the domestic market	4.54
Growing competition in the domestic market	5.45
Demand in foreign markets	6.58
Efforts to build a promising market position abroad	7.40
Competitors' success in foreign markets	4.99
Acceptance of internationalization as a current trend in an increasingly globalized world	5.79
The enterprise's involvement in an international network of cooperating enterprises	3.85
Enterprise management's experience of operating in international markets	4.99
Shortage of subcontractors in the domestic market	3.35
Test statistic	**Value**
Number of observations (N)	54
Chi-square	153.313
Degrees of freedom (df)	9
Asymptotic significance (p-value)	< .001

Business strategies with regard to business internationalization

Current trends in international trade call for a reassessment of existing national and corporate strategies and their adaptation to the conditions of the global economic environment. The management of every company must think ahead and develop a long-term growth strategy to adapt to changing conditions in its sector of the food industry. There is no universal, one-size-fits-all business strategy or corporate policy that applies to all enterprises.

In practice, the competitive advantage strategy is regarded as a common and important strategy, as it reflects the very needs of customers. Other proven strategies implemented by the companies under study include a focus on differentiating themselves from competitors through, for example, quality, brand, innovation and product range. The focus on building strategic long-term relationships with foreign partners is also significant. The choice of sales channels can itself be formalised, for example through an integral indicator of how efficiently they are organised (Ivashkiv et al., 2019). Findings from the hospitality sector highlight the importance of innovation in relation to sustainability, which in turn helps to strengthen customer loyalty and satisfaction. This merely demonstrates the strategic importance of differentiation, which requires innovation and long-term, high-quality and promising relationships with customers (Ruiz-Molina et al., 2025).

Using Friedman's test, it was examined whether the differences observed in the sample of responses to individual questions regarding the strategies employed by individual firms in connection with future-oriented business internationalization could be merely random or are statistically significant. The following hypothesis were tested:

H_20: There is no statistically significant difference between the declared strategies implemented by the enterprises under study.

$H_2$1: There is a statistically significant difference between the declared strategies implemented by the enterprises under study (Table 3).

The Friedman test revealed a statistically significant difference in the perceived importance of the seven aspects of competitive strategy, $\chi^2(6, N = 69) = 40.449$, $p < .001$. Therefore, the null hypothesis that all seven aspects received equal evaluations can be rejected.

Table 3

Business strategies with regard to business internationalization

Strategy	**Mean Rank**
Our competitive advantage strategy is based on understanding customer needs	4.69
We consider our products to be price-competitive	4.09
We strive to differentiate ourselves from competitors through quality, branding, innovation, and product range	4.44
We strive to make our products accessible to the broadest possible segments of the population	3.43
Our company responds promptly to information concerning customer dissatisfaction	3.49
We strive to build long-term relationships with our foreign customers (buyers)	4.38
Top management focuses on developing the resources required to achieve objectives in foreign markets	3.48
Test statistic	**Value**
Number of observations (N)	69
Chi-square	40.449
Degrees of freedom (df)	6
Asymptotic significance (p-value)	< .001

Conclusions

Research carried out to date highlights the fact that focusing solely on developments in the domestic market can have significant negative consequences for both businesses and the country's economy. This is particularly true during periods of economic crisis. For effective management, international diversification, nearshoring as a platform for regional sourcing, and the integration of business systems are essential in order to have the most up-to-date information.

This article examines selected areas of the Slovak food industry's international business in the context of recent events, the pandemic, the war conflict, and their economic impacts. It focuses on the factors influencing international business activities and the strategies that enterprises employ in carrying them out.

Various factors stemming from their position motivate enterprises to internationalize their business activities. Based on the findings of our survey, it can be concluded that by accepting the internationalization of business as a current trend and adapting their activities to this trend, enterprises can contribute to increasing their competitiveness and thereby improve their position in both domestic and foreign markets. Taking into account the other factors evaluated by the enterprises, varying degrees of impact were observed, but each factor

was perceived to some extent by the surveyed enterprises. The internationalization of business activities represents a way to address the problems posed by these individual factors.

The implementation of different strategies stems from the established goals. Enterprises must make strategic decisions regarding changes in business strategy, human resources, investments, production, organizational structure, environmental protection, and finance, taking into account their potential or current operations in foreign markets. This strategic balancing is particularly important in resource-constrained enterprises, as sustainability-oriented environmental and governance practices may generate short-term operational and financial trade-offs (Nicoara-Popescu, 2026). These decisions must necessarily be preceded by preparations at the operational level.

Acknowledgements. This research was funded by the Grant Agency for Management Research at the Faculty of Management, University of Prešov in Prešov under grant GAMA/25/3 "The economic and social impacts of the Covid-19 pandemic on the management of companies in the food industry of the Slovak Republic" and project VEGA 1/0812/25 "Sustainable family business in the context of the challenges of the 21st century", funded by the Ministry of Education, Research, Development and Youth of the Slovak Republic.

References

Aday, S., & Aday, M. S. (2020). Impact of COVID-19 on the food supply chain. *Food Quality and Safety*, *4*(4), 167–180. https://doi.org/10.1093/fqsafe/fyaa024

Agriculture Switzerland, *12* (11), 1884. https://doi.org/10.3390/agriculture12111884

Ahn, J., & Tan, B. J. (2025). *Supply chain diversification and resilience* (IMF Working Paper No. WP/25/102). International Monetary Fund.

Andrejovská, A., & Glova, J. (2022). Sustainability of farms in EU countries in the context of income indicators: Regression analysis based on a new classification. *Agriculture*, *12*(11), 1884. https://doi.org/10.3390/agriculture12111884

Azim, S., Rooh, S., Malik, M., & Shah, S. M. A. (2025). The fragmentation of global trade: From protectionism to gated globalization. *Social Sciences & Humanity Research Review, 3*(2), 015. https://doi.org/10.63468/sshrr.015

Balsiūnaitė, R., Petrusevičienė, I., & Lekavičius, V. (2026). Measuring the economic impact of environmental sustainability practices: A systematic literature review. *Transformations in Business & Economics, 25*(2(68), 261-303. https://doi.org/10.15388/Tibe.2026.25.2.4

Baran, J. (2018). Reasons for internationalization of Polish food industry companies. *Economic Sciences for Agribusiness and Rural Economy*, *2*, 203–208. https://doi.org/10.22630/ESARE.2018.2.26

Bayoumy, M. S. A., Abou-Shouk, M., Al-Taii, A., Al-Leheabi, S. M. Z. M., & Youssef, E. (2025). The contribution of social capital to entrepreneurial activities' success: Across-country field study in the light of social capital theory. *Journal of Tourism and Services, 16*(31), 65–89. https://doi.org/10.29036/3350h252

Belova, T., Krainiuchenko, O., Rozumei, S., & Pietukhova, O. (2020). Methodical approaches to the determination of readiness of introduction of "blue ocean" strategy on the enterprises of food industry. *Ukrainian Food Journal, 9*(4),917-929. https://doi.org/10.24263/2304-974X-2020-9-4-15

Bernat, T., & Duda, J. (Eds.). (2024). *Business impacts of COVID-19: International business, crisis management and the global economy*. Routledge.

Blcháč, J. (2001). Management of a food company in the context of globalization. In *Economic and management aspects of sustainable agricultural development: Proceedings of the MVD 2001 International Scientific Conference* (p. 16). SAU.

Chandra, Y., & Wilkinson, I. F. (2017). Firm internationalization from a network-centric complex-systems perspective. *Journal of World Business, 52*(5), 691–701. https://doi.org/10.1016/j.jwb.2017.06.001

Dicken, P. (1998). *Global shift: Transforming the world economy* (3rd ed.). Guilford Publications.

EIT Food. (2021). *Food Foresight: Impact of the COVID-19 pandemic on the food sector in Central and Eastern Europe*. Country report: Slovakia. Retrieved from https://www.eitfood.eu/

Erdei-Gally, S., & Vágány, J. (2022). Role of precision agriculture in food supply. *Ukrainian Food Journal, 11*(3), 458–473. https://doi.org/10.24263/2304-974X-2022-11-3-10

European Commission, Eurostat. (n.d.). *Harmonised index of consumer prices (HICP)* Retrieved from https://ec.europa.eu/eurostat/cache/metadata/en/prc_hicp_esms.htm

Galiani, S. (2023). How the war in Ukraine changes the economic and business landscapes of countries, regions and the world. *Forbes Ukraine*. Retrieved from https://forbes.ua/money/velika-ekonomichna-perebudova-25082023-15642

Habánik, J., Grenčíková, A., Šramka, M., & Huževka, M. (2021). Changes in the organization of work under the influence of COVID-19 pandemic and Industry 4.0. *Economics and Sociology, 14*(4), 228-241. https://doi.org/10.14254/2071-789X.2021/14-4/13

Hanf, J. H., Kruckemeier, K., & Hanf, C. H. (2009). Internationalisation of the food retailing industry and its impact on the agricultural and food industries. *Berichte über Landwirtschaft, 87*(2), 343–352.

Hečková, J., & Chapčáková, A. (2021). *World economy*. Equilibria.

Horalíková, M. (2000). Global managers in agri-businesses. In *Globalization and competitiveness*, 1–7.

Horská, E., & Ubrežiová, I. (2001). *Management and marketing in an international environment*. SAU.

Horvathova, K., & Cvirik, M. (2026). The post-covid adaptation and transformation model of retail food units based on customer behaviour: what constitutes the new normal for marketing management? *Central European Business Review, 15*(1), 135 – 149. https://doi.org/10.18267/j.cebr.409

Ivashkiv, I., Kupalova, H., Goncharenko, N., Khrutba, Y., & Vovk, I. (2019). Optimization of commodity flows: The case of bakery enterprises of Ukraine. *Montenegrin Journal of Economics, 15*(3), 205-216. https://doi.org/10.14254/1800-5845/2019.15-3.15

Jarossova, M. A., Krnacova, P., Solis, J. W., Prokeinová, B. R., Sikorska, J. S., Krajewska, M. S., Malinowski, M., & Rojik, S. (2025). Factors influencing the purchasing of organic food by Slovak consumers: Quality or promotion? *Scifood, 19*(1), 451–466. https://doi.org/10.5219/scifood.67

Jencova, S., Vasanicova, P., Gavurova, B., & Bacik, R. (2022). Financial position of companies operating in food processing industry of Slovakia by using multidimensional scaling. *Economics and Sociology, 15*(2), 253-273. https://doi.org/10.14254/2071-789X.2022/15-2/16

Kabát, L. & Lincenyi, M. (2024). Economic Development and Business Environment in EU Countries under the Social Media Support. *Acta Polytechnica Hungarica, 21*(11), 29 – 48. https://doi.org/10.12700/APH.21.11.2024.11.2

Kita, P., & Cvirik, M. (2024). Retailer processes centred on the food market as the main determinate of business models in the context of retail size. *Journal of Retailing and Consumer Services, 81*, 103937. https://doi.org/10.1016/j.jretconser.2024.103937

Kłysik-Uryszek, A., & Kuna-Marszałek, A. (2015). Geographical breakdown of Polish OFDI– explanatory potential of Uppsala model. *Journal of International Studies*, *8*(1), 150-163. https://doi.org/10.14254/2071-8330.2015/8-1/13

Kočanová, D., Kováč, V., Serzhanov, V., & Buleca, J. (2023). Differences and Similarities in Patterns of Ageing Society in the European Union, *E + M Ekonomie a management*, *26* (1), 45-64. https://doi.org/10.15240/tul/001/2023-1-003

Koraus, A., Haviernikova, K., Gombar, M., Cernak, F., & Miroslav, F. (2020). Dimensions and their elements affecting the innovative activities of agricultural SMEs toward their sustainable development. *Entrepreneurship and Sustainability Issues*, *8*(2), 1142 – 1157. https://doi.org/10.9770/jesi.2020.8.2(68)

Kordos, M., & Habanik, J.(2018). Corporate culture interplay issues in global economy. *Problems and Perspectives in Management*, *16*(3). https://doi.org/10.21511/ppm.16(3).2018.24

Kumar, S. (2022). The global impact of pandemics on world economy and public health response. In *Pandemic India: Coronavirus and the uses of history*, 30–50. Elsevier.

Liu, N., & Su, Y. (2024). Russia-Ukraine war's effects on the world economy. *Highlights in Business, Economics and Management, 24*, 1105–1113. https://doi.org/10.54097/hbem.v24i.16475

Majerník, M., & Majerník, Š. (2018). The economic challenges of the enterprises in the food industry] In *Globálne existenčné riziká 2018: Zborník z VIII. medzinárodnej vedeckej konferencie*, 123–129. STRIX; SSŽP. Retrieved from https://www.sszp.eu/wp-content/uploads/2018_conference_GER__p-123__MajernikM_MajernikS__f4e.pdf

Manuell, R. (2017). Is globalisation good for food? New Food Magazine. Retrieved from https://www.newfoodmagazine.com/article/40883/globalisation-food/

Mazur, G., & Takemura, M. (2020). The evolution of merchandise trade between the Visegrad Group countries and Japan in the 21st century. *Journal of International Studies*, *13*(3), 9-24. https://doi.org/10.14254/2071-8330.2020/13-3/1

Ministry of Agriculture and Rural Development of the Slovak Republic. (2014). *The concept of food industry development 2014–2020*. Retrieved from https://www.mpsr.sk/

Ministry of Agriculture and Rural Development of the Slovak Republic. (2022). *Zelená správa 2022* [Green report 2022]. mpsr.sk

Mogaka, C. O., & Njururi, A. (2024). A systematic review and conceptual framework of supply chain agility as a strategic enabler of firm competitiveness. *Journal of Sustainable Development of Transport and Logistics*, *9*(2), 109-125. https://doi.org/10.14254/jsdtl.2024.9-2.8

Mura, L., & Löster, T. (2011). Manifestations of business internationalization in a selected sector of the food industry. *Economics and Management*, *4*(1), 29–42. Retrieved from https://vse.cz/eam/vse.cz/eam/124.html

Nicoara-Popescu, D. (2026). Assessing the interplay between financial trade-offs and ESG practices in small restaurants. *Journal of Tourism and Services, 17*(32), 202–222. https://doi.org/10.29036/57eca570

Plutzer, V. (2021). *Industry in the time of corona: The impact of the first wave of the corona crisis on industrial activity in Slovakia* (Commentary 2021/3). Institute for Financial Policy, Ministry of Finance of the Slovak Republic. Retrieved from https://sszp.eu/

Prytulska, N., Motuzka, I., Koshelnyk, A., Motuzka, O., Yashchenko, L., Jarossová, M., Krnáčová, P., Wyka, J., Malczyk, E., & Habánová, M. (2021). Consumer preferences on the market of plant-based milk analogues. *Potravinarstvo Slovak Journal of Food Sciences*, *15*, 131–142. https://doi.org/10.5219/1485

Qureshi, N., & Ali, S. (2025). The impact of supplier diversification on supply chain resilience in the post-COVID era. *The Critical Review of Social Sciences Studies*, *3*, 2234–2242. https://doi.org/10.59075/gtef5x07

Rimarčík, M. (2007). *Štatistika pre prax [Statistics for practice]*. Enigma.

Ruiz-Molina, M. E., Gil Saura, I., Berenguer-Contri, G., & Marín García, A. (2025). Does the generational cohort influence the effects of sustainability-oriented service innovation? *Journal of Tourism and Services, 16*(30), 262–277. https://doi.org/10.29036/kszmz846

Senci, M., & Afful, C. R. (2025). Inflation and unemployment in Slovakia: Is the Phillips curve still relevant? *International Journal of Entrepreneurial Knowledge, 13*(1), 95–105. https://doi.org/10.37335/ijek.v13i1.304

Serrano, R., García-Casarejos, N., Gil-Pareja, S., Llorca-Vivero, R., & Pinilla, V. (2015). The internationalisation of the Spanish food industry: The home market effect and European market integration. *Spanish Journal of Agricultural Research, 13*(3), https://doi.org/10.5424/sjar/2015133-7501

Stehlikova, B., Caganova, D., Kolenak, J., & Cvirik, M. (2026). Analyzing the Effects of the COVID-19 Pandemic on Family and Non-family-Owned Enterprises in Slovakia. *Eai Springer Innovations in Communication and Computing*, 57–77. https://doi.org/10.1007/978-3-032-10833-3_5

Tiruneh, M. W., Morvay, K., Okáli, I., Frank, K., & Gabrielová, H. (2009). *Developments and prospects for the world economy: The global financial and economic crisis: Causes, costs, and solutions*. Institute of Economic Research, Slovak Academy of Sciences.

Tóthová, A., & Tóth, M. (2019). Selected indicators of the food industry in the Slovak Republic. *Ekonomika a manažment, 16*(4), 93–111.

Virglerova, Z., Kovács, S., Belas, J., & Olah, J. (2025). Factors influencing internationalization of micro-enterprises and SMEs in Central Europe. *Journal of International Studies, 18*(1), 179-195. https://doi.org/10.14254/2071-8330.2025/18-1/11

Vovk, Y., Vovk, I., Plekan, U., Tson, O., & Oleksyuk, V. (2025). Sustainable and smart logistics centers: Challenges and opportunities for Ukraine's transport system. *Journal of Sustainable Development of Transport and Logistics, 10*(1), 116–124. https://doi.org/10.14254/jsdtl.2025.10-1.8

Vrabcova, P.,Urbancova, H., & Hudakova M. (2022). Strategic Trends of Organizations in the Context of New Perspectives of Sustainable Competitiveness. *Journal of Competitiveness, 14* (2), https://doi.org/10.7441/joc.2022.02.10

Wang, L., & Xu, J. (2026). Equity incentive mechanism for an alliance-based agricultural product logistics model under digital-intelligence platforms. *Transformations in Business & Economics, 25*(1(67)), 292–310. https://doi.org/10.15388/Tibe.2026.25.1.15

Zadražilová, D. (2017). *International management*. Oeconomica.

Cite:

Dubravská, M., Širá, E., & Mura, L. (2026). International business activities of food enterprises in the Slovak Republic considering current trends and business sustainability. *Ukrainian Food Journal, 15*(3), 935–948. https://doi.org/10.24263/2304-974X-2026-15-3-18

Impact of retail food loss on undernourishment in developing countries

Andrii Dankevych[1], Meherun Nesa Mitu[2], Nurul Mohammad Zayed[3], Vitalii Nitsenko[4], Keisha LaRaine Ingram[5]

1 – National University of Food Technologies, Kyiv, Ukraine
2 – Daffodil International University, Dhaka, Bangladesh
3 – INTI International University, Nilai, Malaysia
4 – Kauno kolegija Higher Education Institution, Kaunas, Lithuania
5 – Mykolas Romeris University, Vilnius, Lithuania

Keywords:

Retail food loss
Undernourishment
Food security
Supply chain
Sustainability

Article history:

Received 3.03.2026
Received in revised form 18.07.2026
Accepted 30.09.2026

Corresponding author:

Andrii Dankevych
E-mail: dankevichie@nuft.edu.ua

DOI:
10.24263/2304-974X-2026-15-3-19

Abstract

Introduction. This study aims to examine the relationship between caloric losses at the retail distribution level and the prevalence of undernourishment in developing countries, while accounting for key agricultural and macroeconomic factors.

Materials and methods. The effect of caloric losses at the retail distribution level (ICLRD) on the prevalence of undernourishment (POU) was examined using a balanced panel of 30 developing countries from 2010 to 2022. Data were obtained from United Nations databases and the World Development Indicators. The food price index (FPI), inflation, agricultural value added, and gross domestic product per capita were included as control variables. Pooled ordinary least squares, fixed effects, random effects, and the Hausman test were applied.

Results and discussion. The empirical findings reveal a positive relationship between retail food losses and undernourishment. The coefficient of caloric losses at the retail distribution stage (ICLRD) is 1.6469 ($p < 0.01$) in the Fixed Effects model and 1.3742 ($p < 0.05$) in the Random Effects model. These results indicate that greater caloric losses at the retail distribution stage are associated with higher undernourishment. The positive and statistically significant coefficient in the preferred model suggests that food losses before reaching consumers may reduce food availability and contribute to food insecurity in developing countries. However, Pooled OLS shows an inverse relationship between ICLRD and the prevalence of undernourishment, highlighting the importance of accounting for country-specific factors. Among the control variables, GDP per capita has a statistically significant negative effect on undernourishment, indicating that higher economic development is associated with better access to food and lower vulnerability to undernourishment. Inflation, the FPI, and agricultural value added do not have statistically significant effects in the selected specification. Overall, the findings highlight the importance of minimizing food losses during retail distribution as part of broader food security strategies. Retail food losses represent not only resource waste but also a food security concern in developing countries. Improving retail distribution efficiency could help preserve food availability and reduce unnecessary caloric losses.

Conclusions. Reducing retail food losses through efficient supply chains, cold-chain management, and food redistribution may improve food security and contribute to Sustainable Development Goals 2 (Zero Hunger) and 12 (Responsible Consumption and Production).

Introduction

Food shortages have never been the only reason for food insecurity around the world. Despite there being enough food production globally to fulfill the nutritional needs of the entire population of the planet, hundreds of millions of people have still remained deprived of adequate nourishment. This has been among the greatest enigmas in the discourse on food security: how is it possible that hunger is rampant amid the wastage of almost a third of the total amount of food production worldwide? The majority of the academic literature sees the disparity between developing and developed nations' economies as a sharp, almost geographical law. According to Gustavsson et al. (2011) food losses occur upstream, at the farm and post-harvest stage in poor countries due to ineffective cold chains and storage systems, whereas in rich countries, they do not happen during the production stage and take place at retailers and consumers due to their habits and purchasing behaviors. Moreover, Sheahan and Barrett (2017) and Aragie et al. (2018) summarize the evidence and conclude that food losses in sub-Saharan Africa and at the level of ten agrarian nations (Benin, Chad, Ethiopia, Kenya, Madagascar, Malawi, Mali, Mozambique, Niger, and Rwanda) account for about 28 percent of calories per capita per day, respectively. It was also established that the countries in question lose approximately 38 percent of produce at the pre-harvest stage and 34 percent at the post-harvest stage. Indeed, in the countries mentioned, fruit losses resulting from improper storage and a lack of necessary skills in handling refrigeration technologies range from 30% to 80% (James & Zikankuba, 2017). Kumar and Kalita (2017) add that grain losses in developing countries due to inefficient storage technologies can reach 50-60%. Thus, poor postharvest handling and storage can lead to the loss of one-third of the produce and, in extreme cases involving cereal storage, even more than half of the harvest.

Despite substantial research on food loss, food waste, and food security, the direct link between retail-stage food loss and the prevalence of undernourishment in developing countries has received scant attention (Shynkaruk et al., 2025). The existing literature covers various aspects of food loss and waste, including cost analysis (Nahman & De Lange, 2013), nutritional analysis (Khan et al., 2024), country-specific studies (Mirzoieva et al., 2024), econometric analysis of factors influencing undernourishment (Kramer & Allen, 2015), and circular economy approaches, including the conversion of waste into value-added products (Stabnikova et al., 2023). However, these research areas have not adequately addressed the direct relationship between retail-stage food loss and undernourishment in developing countries. Existing studies either aggregate food losses and waste across the supply chain without considering the specific role of retail-stage losses (Alexander et al., 2013), focus on retail losses in developed economies, where infrastructure, consumer behaviour, and policy environments differ from those in developing countries (Joardder & Masud, 2019), or model undernourishment using macroeconomic and institutional indicators without incorporating supply-chain losses disaggregated by stage (Hodges et al., 2011).

Furthermore, the broad variation in the magnitude of global food losses from 1.3 to 1.6 billion tons of food (Ishangulyyev et al., 2019) and 263 billion to 2.6 trillion US dollars (Wang et al., 2023) in value across different studies clearly emphasizes the uncertain empirical base of this field, necessitating a need for a targeted examination of this issue at each individual stage of the food cycle. The novelty of the current research lies in the fact that it considers the food losses at the retail stage as an independent variable, as compared to considering them as an essential component of food loss and waste in general, with respect to tackling undernourishment in developing countries. Whereas earlier works (James & Zikankuba, 2017; Kumar & Kalita, 2017) have concentrated on food losses and waste in general, this paper will look into retail-stage calorie losses and their effect on undernourishment in developing nations using panel data methods. The significance of this methodology derives from it directly, and this is because retail stage is the point in the food chain at which the nutritious food gets disposed of the nearest to the consumer,

meaning that the food would have been available to be consumed by the hungry ones before the food was taken out of the system; something which cannot be said about food loss at the farm level which happens earlier in the process. In order to systematically analyze such empirical irregularities, the present paper aims to achieve three specific objectives as follows: firstly, to empirically investigate the degree to which retail food losses impact on hunger in developing nations; secondly, to compare the relative importance of this link versus other major macroeconomic and agricultural factors determining undernourishment, such as income, food production, inflation, and agriculture's contribution to value added; and Thirdly, to ascertain whether this link still exists when controlling for any potential unobserved heterogeneity in each country using diagnostic tests for panel data.

To realize these objectives, the study uses a cross-country panel dataset of 30 developing economies from Sub-Saharan Africa, Latin America and the Caribbean (LAC), Southeast Asia, Middle East and North Africa (MENA), and South Asia, covering 2010–2022. In this context, the empirical strategy adopted is focused on isolating the impact of the prevalence of calorie losses at the retail distribution level on the level of undernourishment while holding constant some shifting variables at the macroeconomic and sector levels, which include: Food Production Index, Agriculture, Forestry and Fishing Value Added, Inflation Rate, and Per Capita GDP.

Materials and Methods

Materials

The research utilizes the quantitative method to conduct an analysis on the link between food loss and undernourishment within different nations. The quantitative method is ideal for conducting this research since the use of numeric values in this research will help in examining the correlation between food loss, economy, agriculture, and its impact on food security. The use of numeric values will help in measuring, estimating, and empirically testing the effect of food loss. This paper uses secondary data analysis since all data used in the research come from international databases instead of being gathered by the researcher. Secondary data are data that have already been collected, compiled, and published by certain institutions for statistical and research purposes. The data were gathered using two major sources of secondary data: the United Nations database and the World Bank's World Development Indicators database.

Sample selection

The dataset comprises a balanced panel of 30 countries from Southeast Asia, South Asia, the Middle East and North Africa (MENA), Latin America and the Caribbean (LAC), and Sub-Saharan Africa over the period 2010–2022. The countries included in the analysis are Bolivia, Nicaragua, Malaysia, Peru, Paraguay, Thailand, Ecuador, Cameroon, Sri Lanka, Egypt, Nepal, Cambodia, Ghana, Indonesia, Senegal, the Philippines, Jordan, Benin, India, Honduras, Pakistan, Bangladesh, Malawi, Ethiopia, Togo, Kenya, Uganda, Mozambique, Rwanda, and Zambia. The countries were selected based on the availability of complete data for all variables included in the study. These regions were chosen because they continue to face significant food security challenges, including food insecurity, food losses, agricultural constraints, and economic vulnerability. Panel data are suitable for this study because they combine cross-sectional and time-series dimensions, increasing the number of observations and potentially improving the efficiency of econometric estimates. Furthermore, panel data methods allow researchers to account for unobserved country-specific characteristics and time effects, thereby helping to control for heterogeneity across countries and changes over time (Table 1).

Table 1

Definition, measurement, classification and data sources of variables

Type	Variables	Abbreviation	Definition and measurement	Source
Dependent	Prevalence of undernourishment	POU	% of population	World Bank
Control	Inflation	INF	Annual, %	
Independent	Incidence of caloric losses at retail distribution level	ICLRD	Caloric losses at the retail distribution stage	UN Database
Control	GDP per capita	GDPPC	Constant 2015, US$	World Bank
Control	Food production index	FPI	Index (2014–2016 = 100)	
Control	Agriculture, forestry and fishing value	AFV	% of GDP	

Source: compiled by the authors based on (World Bank Group, 2025)

Conceptual structure

Figure 1 provides the conceptual framework for this study.

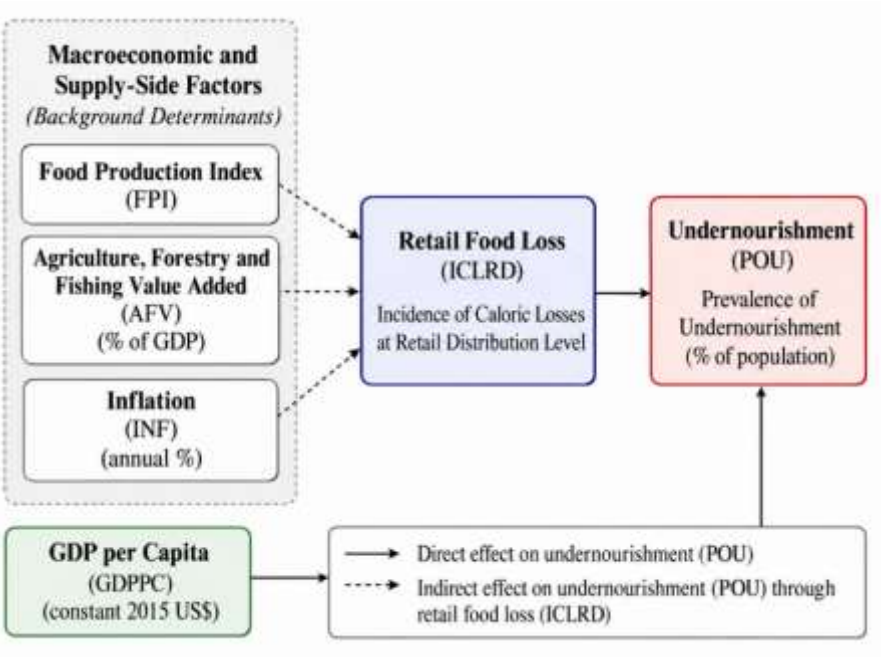

Figure 1. Conceptual structure

Source: Developed by the authors based on the literature review and study framework

The conceptual framework highlights Retail Food Loss, measured in terms of the Incidence of Caloric Losses at the Retail Distribution Level (ICLRD), as the major independent variable affecting the Prevalence of Undernourishment (POU). The Food Production Index (FPI), Agriculture, Forestry and Fishing Value Added (AFV), and Inflation (INF) have been included as macroeconomic and supply-side factors that could potentially affect undernourishment indirectly through their impact on retail food loss. On the other hand, GDP per Capita (GDPPC) has been shown to have a direct relationship with undernourishment, which is in line with the empirical results obtained in this study, wherein GDPPC had a statistically significant negative effect on POU. The framework reflects the study's empirical model while emphasizing ICLRD as the central mechanism linking food system conditions to undernourishment.

To reduce the calorie deficit in the population, it is necessary to consider the traditional food security indicator POU together with calorie losses at the retail distribution level (ICLRD). These indicators can help identify the need for measures to increase food production, as reflected by the FPI indicator. The relationship between ICLRD and FPI reflects the need to maintain a balance between the population's food requirements and the efficiency of the food production and distribution system. For example, if FPI increases without a corresponding improvement in the population's food security and access to sufficient calories, retailers may be unable to sell the additional food products, which, in turn, may increase ICLRD.

The loss of calories at the retail stage results in a loss of the corresponding food value. Thus, the AFV indicator, without accounting for calorie losses at the retail stage, may not fully reflect the actual state of food security. The relationships between AFV, ICLRD, and POU may also help characterize the strength of the regional food system. Inflation (INF) changes food prices, which may affect the supply and availability of food products at the retail stage. These changes may contribute to an increase in POU.

The relationships between FPI, ICLRD, and POU; AFV, ICLRD, and POU; and INF, ICLRD, and POU reflect the functioning of the national food system. As mentioned above, GDP per capita and POU are directly related, although the relationship is inverse. In countries with higher GDP per capita, the proportion of people who may experience a calorie deficit is generally lower than in countries with lower GDP per capita.

At the same time, as shown in Fig. 1, the FPI, AFV, and INF indicators are assumed to affect POU indirectly through ICLRD rather than directly. The POU indicator is estimated on the basis of the availability of dietary energy for the population. Changes in food production and inflation may affect food prices and consumer purchasing behaviour. As food prices increase, consumers may buy less food or switch to cheaper products. This may also change the composition of their diets, including the proportions of protein, fat, fruit, and vegetables consumed. Since these food groups differ in their energy content, changes in dietary composition may affect total calorie intake. For example, potatoes have an energy content of approximately 0.77 kcal/g. Changes in the demand for perishable products, such as fruit and vegetables, may also increase retail food losses if storage and distribution infrastructure is insufficient. This may, in turn, increase ICLRD. These considerations support the proposed mediating role of ICLRD in the relationships between FPI, AFV, INF, and POU.

This led to the development of Equation (2), which mathematically formalizes the proposed mediation of the relationships between POU and FPI, AFV, and INF. The significance of retail-stage calorie losses for POU is further formalized in Equations (3)–(5).

Model specification and estimation procedure

To investigate the relationship between food loss and undernourishment, the following panel-data regression model is estimated:

Basic model:

$$e_{it}=a_0+a_1v_1+a_2v_2+a_3v_3+a_4v_4+a_5v_5+\mu_{it} \quad (1)$$

In this linear regression model, e_{it} represents the outcome of the dependent variable at time t and country i, a_0 intercept, which is constant, a_1 to a_5 are the coefficients, independent variables v_1 to v_5 and μ_{it} are the error terms.

Overall model (Based on selective variables):

$$POU_{it}=a_0+a_1ICLRD_{it}+a_2FPI_{it}+a_3AFV_{it}+a_4INF_{it}+a_5GDPPC_{it}+\mu_t \quad (2)$$

where:

POU_{it} represents the Prevalence of Undernourishment in the country i during the year t,

$ICLRD_{it}$ represents the Incidence of Caloric Losses at Retail Distribution Level in the country i during the year t,

FPI_{it} represents the Food Production Index in the country i during the year t,

AFV_{it} represents Agriculture, Forestry and Fishing Value Added as a percentage of GDP in the country i during the year t,

INF_{it} represents Inflation measured by Consumer Prices in the country i during the year t,

$GDPPC_{it}$ represents GDP per Capita in the country i during the year t,

Firstly, descriptive statistics along with the Jarque-Bera normality test will be used to analyze the distribution properties of the variables. After that, a correlation analysis will be performed to analyze the connection between the factors and identify any potential issues with multicollinearity. Data organization and preparation will be done using Microsoft Excel software, whereas statistical analysis will be carried out using EViews. Next, Levin-Lin-Chu (LLC), Im–Pesaran–Shin (IPS), and Fisher-ADF panel unit root tests will be used to ensure that the variables are stationary. The empirical model will be estimated using Pooled Ordinary Least Squares (OLS), Fixed Effects (FE), and Random Effects (RE) estimators. Additionally, the Hausman specification test will be done to find out which estimation technique is the best suited one for panel data. Finally, heteroskedasticity and cross-sectional dependence tests are conducted to check the assumptions of the model.

Potential food-energy recovery from retail loss reduction equation

The calculation begins with the annual food-energy availability of each country. For country (i) in year (t), total annual food calories available are calculated as:

$$TFC_{it}=FS_{it} \times POP_{it} \times 365 \quad (3)$$

where:

FS_{it} is Per-capita daily food supply in kcal/person/day

POP_{it} is Country's population

Retail-stage calorie losses are then estimated from the ICLRD measure:

$$CL_{it}=TFC_{it} \times \frac{ICLRD_{it}}{365} \quad (4)$$

where CL_{it} is Calories lost at the retail distribution stage

To reflect the reviewer's observation that natural and operational losses cannot realistically be reduced to zero, the analysis assumes a 50% reduction in the observed retail calorie loss:

$$RC_{it}=CL_{it} \times 50\% \quad (5)$$

where RC_{it} is potentially recoverable calories under the 50% reduction scenario

Therefore, the counterfactual does not assume that all food losses are completely replaceable. Rather, the counterfactual poses the more conservative policy question of what the food/energy equivalents would be if one-half of existing retail losses were to be eliminated?

The recovered energy is transformed into a feeding-equivalent measure using a reference requirement of 2,000 kcal per person per day, according to Dietary Guidelines for Americans (2020-2025), for cross-national and cross-year comparison (U.S. Department of Agriculture, 2020). Accordingly, the annual reference requirement is:

$$ARC=2{,}000\times365=730{,}000 \text{ (kcal/person/year)}$$

where ACR ıii Annual Calorie Requirement

And the number of annual person-equivalents associated with the recoverable calories is:

$$PE_{it}=\frac{RC_{it}}{730{,}000} \quad (6)$$

This 2,000 kcal/day figure is used only as a standard reference energy requirement but not as a claim that all people have identical physiological energy requirement. Energy requirement differs depending on age, gender, body mass, and level of physical activity. Therefore, the use of the standard figure is intended to provide a point of comparison for the magnitude of the loss of food energy between different nations and years.

Bangladesh had a total annual food-calorie availability of 1.58829×10^4 kcal in 2021 and 1.61966×10^{14} kcal in 2022. With an ICLRD of 2.64%, the corresponding retail-stage calorie losses were:

$$CL_{2021}=1.58829\times10^{14}\times\frac{2.64}{100}=4.19309\times10^{12} \text{ kcal}$$

$$CL_{2022}=1.61966\times10^{14}\times\frac{2.64}{100}=4.27590\times10^{12} \text{ kcal}$$

Under the 50% reduction scenario:

$$RC_{2021}=4.19309\times10^{12} \text{ kcal}\times50\%=2.09654\times10^{12} \text{ kcal}$$

$$RC_{2022}=4.27590\times10^{12} \text{ kcal}\times50\%=2.13795\times10^{12} \text{ kcal}$$

Thus, the corresponding annual person-equivalents are:

$$PE_{2021}=\frac{2.09654\times10^{12} \text{ kcal}}{730{,}000}\approx2.87 \text{ millions}$$

$$PE_{2021}=\frac{2.13795\times10^{12} \text{ kcal}}{730{,}000}\approx2.93 \text{ millions}$$

So, in the case where one-half of the retail-calorie loss recorded in Bangladesh is prevented, then the resulting amount of energy saved in 2022 will be equal to the yearly calorie needs of 2.93 million people.

For the broader study, the same calculation is performed separately for each country and year. The country-specific estimates can then be summed for a given year:

$$PE_{total,t}=\sum_{i=1}^{28}PE_{it} \quad (7)$$

$PE_{total,2022}$= 57.62 millions

The corresponding average across the 28 countries is:

$$\frac{57.62}{28}=2.06 \text{ million annual person-equivalents per country}$$

Results and discussion

Descriptive statistics of study variables

Descriptive statistics provide a preliminary analysis of the distribution of the variables in question across countries and over time before conducting any panel estimates (Baltagi, 2021;

Wooldridge, 2021). Undernourishment (POU) is 13.6 percent on average, varying between 2.5 and 43.9 percent with a standard deviation of 9.1, thus showing true cross-country heterogeneity rather than being driven by outliers. Inflation (INF) is the most volatile variable, varying between -1.1 and 49.7 percent with a skewness of 2.73 and kurtosis of 14.64, which is much higher than normal.

The core independent variable in the study, ICLRD, shows the least variability (mean 2.50, skewness -0.50, kurtosis 3.42). GDP per capita varies between USD 421 and USD 11,192, with an average of USD 2,615, which is significantly below the range median, showing that most of the countries in the panel belong to the low-income group. Variables of FPI and AFV display similar right-skewed distributions, while AFV shows the distribution closest to a normal one with kurtosis of 3.19. None of the six variables follows a normal distribution, confirming the heterogeneous nature of the panel (Table 2).

Table 2

Descriptive statistics

Variable	Mean	Max	Min	SD	Skew	Kurt
POU	13.616	43.900	2.500	9.105	1.249	4.054
INF	6.001	49.721	-1.139	5.869	2.728	14.641
ICLRD	2.505	3.750	0.026	0.636	-0.501	3.417
GDPPC	2615.010	11191.650	421.899	2193.644	1.510	5.067
FPI	104.401	183.450	62.400	15.526	1.405	7.597
AFV	16.356	44.331	2.861	7.880	0.637	3.186

Note: POU – Prevalence of Undernourishment; INF – Inflation; ICLRD – Incidence of Caloric Losses at Retail Distribution Level; GDPPC – GDP per Capita; FPI – Food Production Index; AFV – Agriculture, Forestry and Fishing, Value Added. SD – standard deviation; Max – maximum; Min – minimum; Skew – skewness; Kurt – kurtosis.
Source: estimated by the authors

Cross-country and regional patterns of food security and economic development

Malnutrition is unevenly distributed across the developing countries in the world. There are certain countries where malnutrition is more prevalent than others, and it is imperative to note some of the underlying factors for this trend before making sense out of the data presented below. Malnutrition is highly prevalent in Zambia, Rwanda, Mozambique, and Uganda, with more than 27% undernourishment, and there are also Kenya, Ethiopia, Malawi, Bolivia, and Nicaragua that have undernourishment rates ranging from 16% to 24%. Bolivia and Nicaragua should be highlighted as countries that belong to the same level of malnutrition prevalence as several other East African countries despite being part of a completely different geographical region, in line with Aragie et al. (2018), who reported that ten sub-Saharan countries lose up to 28% of per capita calorie intake in the production and post-harvest stages alone.

This paper aims to show that this specific level of malnutrition is a structural problem, not a Sub-Saharan one, and this assertion holds true in line with Ishangulyyev et al. (2019), who pointed out that developing countries lose more food during the production, handling, and storage stages than at the consumption stage regardless of the region they are located in (Figure 2). For this purpose, the methodology for calculating the ICLRD indicator proposed by Thayyil and Manogna (2026) was used. This indicator measures the loss of food energy content (as a percentage) within the retail sector relative to its total value.

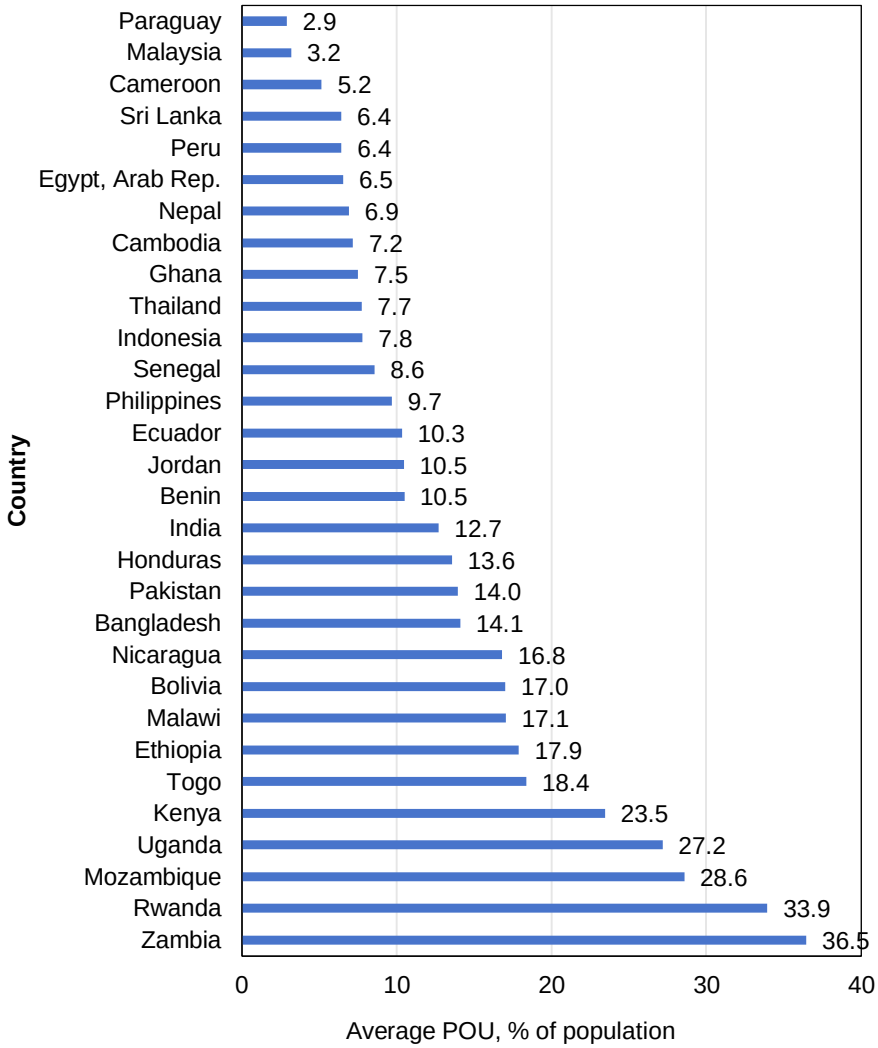

Figure 2. Country-level average prevalence of undernourishment across 30 developing countries (2010–2022)
Source: Authors' calculations based on (World Bank Group, 2025)

GDP per capita offers a second dimension instead of merely repeating that income inequality creates food inequality. The near $9,700 average for Malaysia is nearly twice that of the following bracket (Peru, Paraguay, Thailand, Ecuador, near $5,800-$6,200), but it also marks a prelude to how Malaysia will turn out to be one of the least undernourished nations in the data set. As noted by Baykoca and Yılmaz (2025), using a typology of 105 nations based on their GDP, there is an identical trend where richer nations have their food lost later in the line, i.e., at consumption, whereas poorer nations have theirs lost much earlier in the process, at the harvest/production stage – and it is precisely that separation between Malaysia

and Bolivia/Nicaragua. But income cannot offer the full explanation on its own, as Bolivia and Nicaragua remain as lower middle-income nations and yet record undernourishment rates more consistent with East Africa than with their income counterparts (Figure 3).

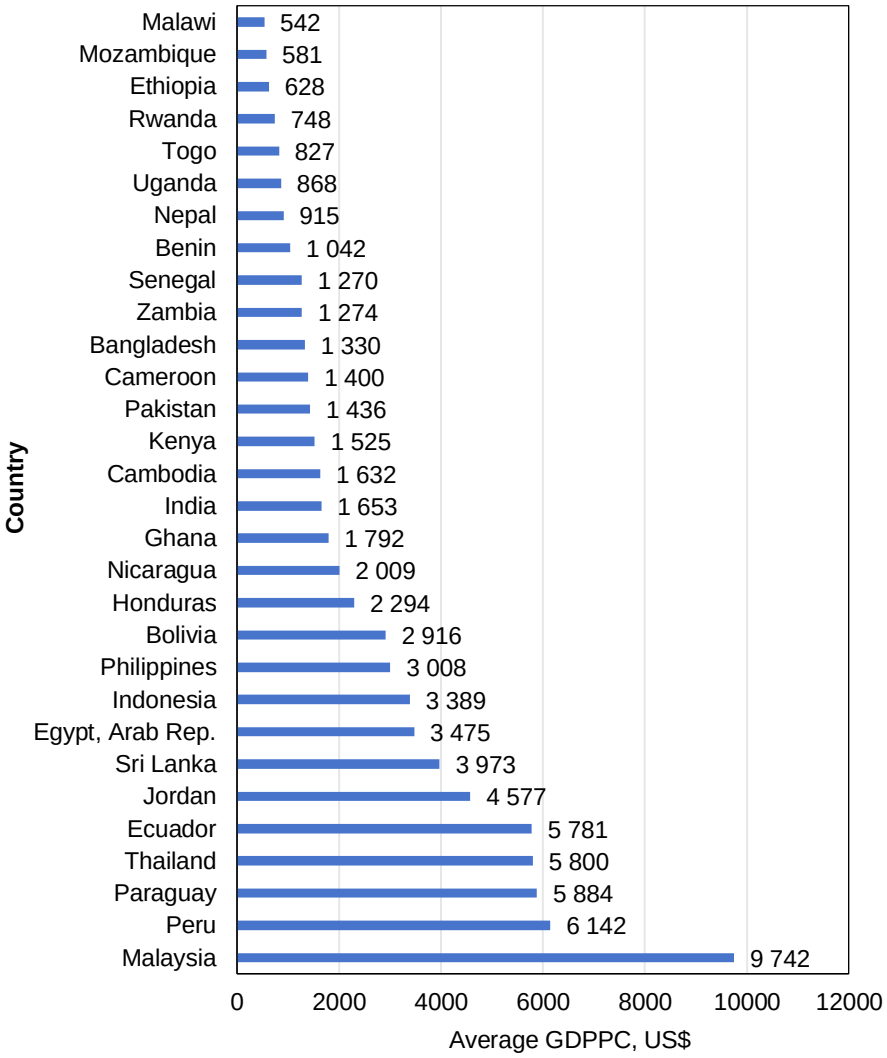

Figure 3. Average GDP per capita across sample countries
Source: Authors' calculations based on based on (World Bank Group, 2025)

It is here that the ICLRD comparison makes its mark as the most innovative contribution of the paper, since neither of the above rankings is followed. Ecuador, Jordan, Indonesia, Rwanda and Cameroon show up with the largest numbers of calorie losses, above 3.2, while Zambia and Malawi, burdened with the highest rate of undernourishment in the entire sample, and score the lowest (Figure 4).

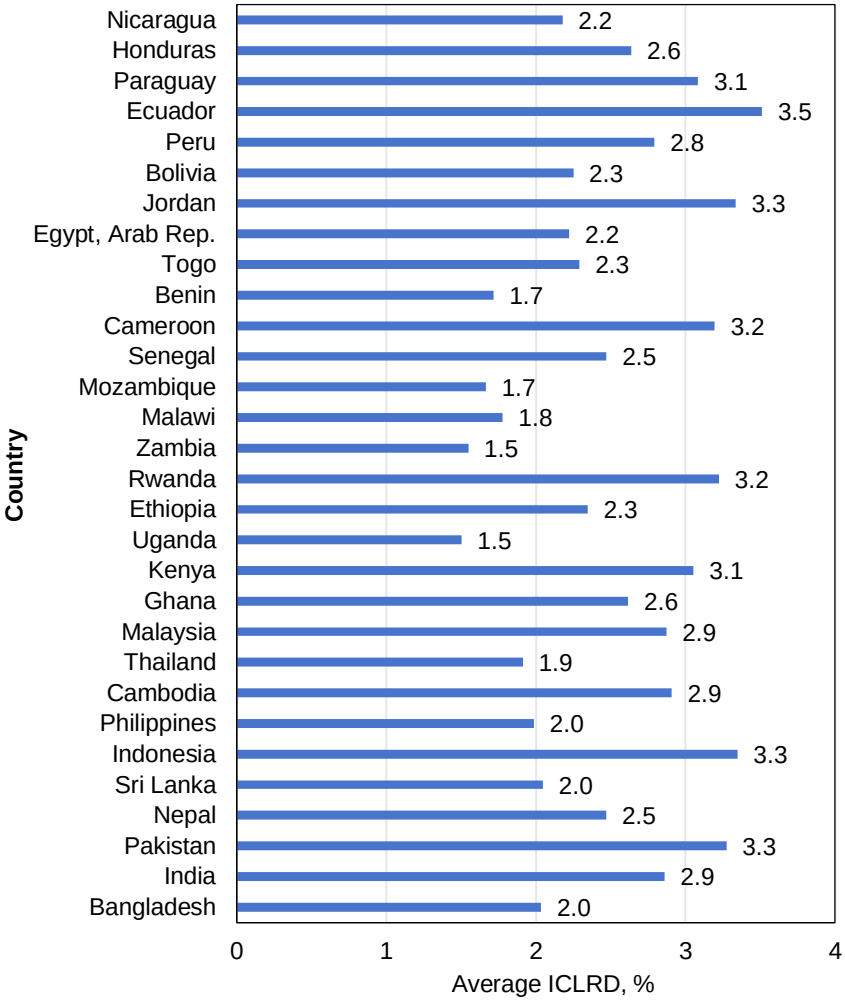

Figure 4. Average level of calorie losses at the retail stage in the countries included in the sample

Source: Authors' calculations based on (UNEP, 2024)

Pakistan's relatively favourable position on this particular indicator is not an anomaly. Khalid et al. (2019) estimated that Pakistani households lost approximately 2.6% of their daily calorie requirements due to food losses, even before wider retail-stage losses were taken into account. Abbade (2020) demonstrated that annual global food losses contained sufficient calories to feed more people than the number of undernourished people worldwide in that year. Thus, the caloric content of food losses, rather than their total volume alone, may be relevant to understanding their relationship with undernourishment. Furthermore, Porat et al. (2018) linked fruit and vegetable losses at the retail stage to cold-chain and inventory management problems rather than to a country's poverty level alone. This may help explain why Ecuador, a middle-income country, also has a high ICLRD value (Figure 4).

This comparison highlights an aspect of the problem that has received limited attention in the existing literature. Both Sub-Saharan Africa and the MENA region experience similar levels of undernourishment, approximately 19–20%. This similarity may be overlooked because the two regions are not frequently compared in the literature. Abiad and Meho (2018) examined the problem of food waste in the Arab world but considered it separately, focusing on the extensive import of food from other countries rather than comparing it with food losses at the production stage in Africa. As the comparison of these regions shows, similar levels of undernourishment may result from different underlying processes. Therefore, solutions should be adapted to the specific conditions and causes of undernourishment in each region (Figure 5).

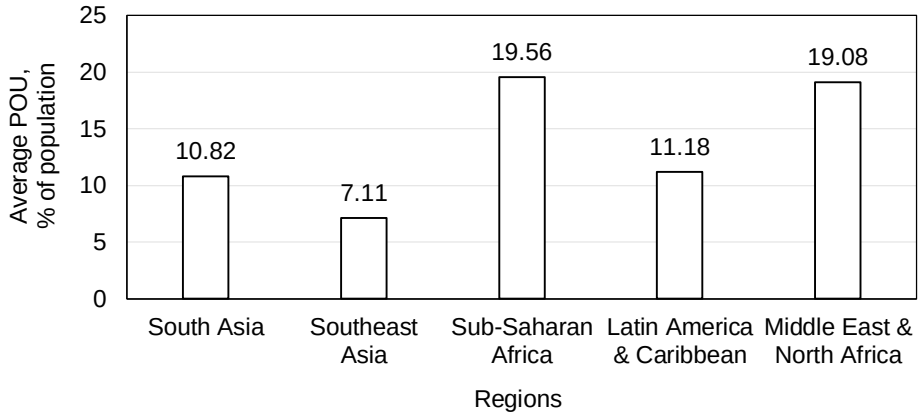

Figure 5. Average prevalence of malnutrition by region
Source: **Authors' calculations based on (World Bank Group, 2025)**

The relationship between GDP per capita and undernourishment can be seen clearly in the scatterplot. Countries having more than 25% undernourishment have GDP per capita below $2,000, and countries having GDP above $5,000 have undernourishment below 11%, making it a threshold rather than a smooth trend. Malaysia is the outlier in terms of being both wealthy and low-undernourished, while Zambia, Rwanda, and Mozambique represent the other extreme of the spectrum. Bolivia and Nicaragua stand out as outliers in this regard, and their importance cannot be understated because according to Kuiper & Cui (2021), food waste reduction produces the most significant food security gains when performed in poor nations where the loss of food is a structural issue rather than a coincidence – in other words, the positioning of Bolivia and Nicaragua on the graph is not an anomaly, but rather represents the only clear message that the income does not explain undernourishment when the loss of food in the retail sector is ignored (Figure 6).

Assessment of data normality

The Jarque-Bera test (Table 3) validates non-normality based on the skewness and kurtosis results in Table 2. All six variables prove not to be normally distributed at $p<0.01$, with INF exhibiting the largest lack of normality (JB = 2685.96), consistent with its extremely high kurtosis, due to its sporadic inflationary peaks in the data set. The lack of normality detected here calls for care in future analyses based on distributional assumptions.

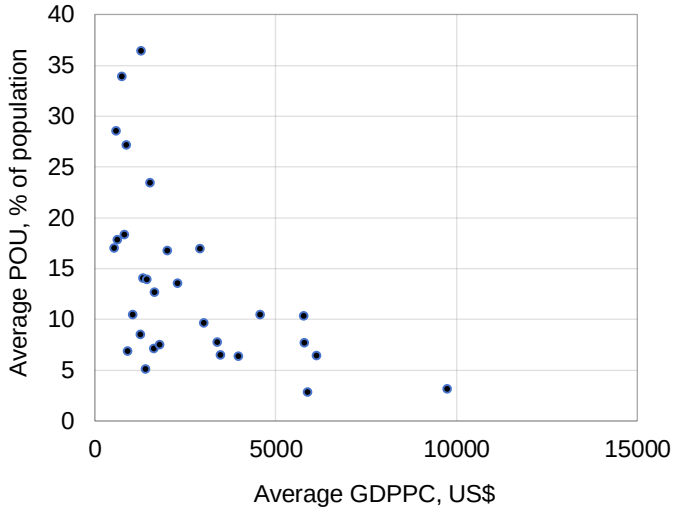

Figure 6. Scatter Plot of GDP per Capita and Prevalence of Undernourishment
Source: Authors' calculations based on (UNEP, 2024; World Bank Group, 2025)

Table 3

Jarque-Bera Normality Test

Variable	Jarque Bera Statistics	Probability
POU	119.5147	0.00000
INF	2685.955	0.00000
ICLRD	19.74016	0.000052
GDPPC	217.5667	0.00000
FPI	471.7217	0.00000
AFV	26.93107	0.000001

Note: POU - Prevalence of Undernourishment; INF - Inflation; ICLRD - Incidence of Caloric Losses at Retail Distribution Level; GDPPC - GDP per Capita; FPI - Food Production Index; AFV - Agriculture, Forestry and Fishing, Value Added.
Source: estimated by the authors

Correlation analysis

As shown in Table 4, none of the correlations between the independent variables exceeds 0.80, suggesting that multicollinearity is not a serious concern (Gujarati & Porter, 2009). The strongest correlation is observed between GDPPC and AFV ($r = -0.6696$), which is below the commonly used threshold.

Panel unit root tests (LLC, IPS, and Fisher-ADF) were performed before estimation to assess the stationarity of the variables and avoid spurious regression (Choi, 2001; Im et al., 2003; Levin et al., 2002). The variables POU, ICLRD, INF, and AFV are stationary at level [I(0)], whereas FPI and GDPPC are stationary at first difference [I(1)]. Since none of the variables is integrated of order two, the results satisfy a condition commonly considered when selecting appropriate methods for panel data analysis. The estimation was therefore conducted using Pooled OLS, Fixed Effects, and Random Effects models (Table 5).

Table 4

Correlation matrix

Correlation	POU	INF	ICLRD	GDPPC	FPI	AFV
POU	1.0000					
INF	0.1821	1.0000				
ICLRD	-0.2849	-0.1874	1.0000			
GDPPC	-0.5227	-0.2470	-0.2947	1.0000		
FPI	0.1343	0.0188	-0.1359	-0.1693	1.0000	
AFV	0.2903	0.3112	-0.1600	-0.6696	0.0810	1.0000

Note: POU - Prevalence of Undernourishment; INF - Inflation; ICLRD - Incidence of Caloric Losses at Retail Distribution Level; GDPPC - GDP per Capita; FPI - Food Production Index; AFV - Agriculture, Forestry and Fishing, Value Added.
Source: estimated by the authors

Table 5

Unit Root Test

Variable	LLC	IPS	Fisher-ADF	Decision
POU	I(0)	I(0)	I(0)	I(0)
FPI	I(1)	I(1)	I(1)	I(1)
GDPPC	I(1)	I(1)	I(1)	I(1)
ICLRD	I(0)	I(0)	I(0)	I(0)
INF	I(0)	I(0)	I(0)	I(0)
AFV	I(0)	I(0)	I(0)	I(0)

Note: POU - Prevalence of Undernourishment; INF - Inflation; ICLRD - Incidence of Caloric Losses at Retail Distribution Level; GDPPC - GDP per Capita; FPI - Food Production Index; AFV - Agriculture, Forestry and Fishing, Value Added.
Source: estimated by the authors

Baseline Pooled OLS regression

Pooled OLS regression (Table 6) reveals that ICLRD and GDP per capita are the major determinants of undernourishment. GDP per capita is statistically significant (β=-0.0022, p<0.01), but ICLRD, while being statistically significant, has a negative sign (β=-1.873, p<0.01), a finding which should be considered with caution due to the fact that pooled OLS does not account for unobserved country-specific heterogeneity. The model is statistically significant (F=32.89, p<0.01) and accounts for about 30 percent of the variance.

Estimated Fixed Effects Equation:

$$POU_{it}=23.7467-1.8730ICLRD_{it}+0.0195FPI_{it}-0.1239AFV_{it}+0.0662INF_{it}-0.0022GDPPC_{it}+\mu_t$$

Fixed effects model

Table 7 demonstrates how the Fixed Effects regression directly addresses cross-country heterogeneity.

Estimated Fixed Effects Equation:

$$POU_{it}=23.7467-1.8730ICLRD_{it}+0.0195FPI_{it}-0.1239AFV_{it}+0.0662INF_{it}-0.0022GDPPC_{it}+\mu_t$$

Fixed effects model

Table 7 demonstrates how the Fixed Effects regression directly addresses cross-country heterogeneity.

Table 6

Baseline Pooled OLS regression results

Variable	Coefficient	Std. Error	t-Statistic	Probability
C	23.74669	3.670719	6.469220	0.0000
INF	0.066244	0.070620	0.938026	0.3488
ICLRD	-1.873007	0.648720	-2.887233	0.0041
GDPPC	-0.002235	0.000249	-8.963139	0.0000
FPI	0.019488	0.025549	0.762846	0.4460
AFV	-0.123859	0.067739	-1.828480	0.0683

R-squared	0.299861	Mean dependent var	13.61615
Adjusted R-squared	0.290745	S.D. dependent var	9.104516
S.E. of regression	7.667576	Akaike info criterion	6.927143
Sum squared resid	22576.02	Durbin-Watson stat	0.039386
Log likelihood	-1344.793	Schwarz criterion	6.988161
F-statistic	32.89255	Hannan-Quinn criter.	6.951331
Prob(F-statistic)	0.000000		

Note: INF - Inflation; ICLRD - Incidence of Caloric Losses at Retail Distribution Level; GDPPC - GDP per Capita; FPI - Food Production Index; AFV - Agriculture, Forestry and Fishing, Value Added.
Source: estimated by the authors

Table 7

Fixed Effects (FE) Model

Variable	Coefficient	Std. Error	t-Statistic	Probability
C	12.44546	2.878314	4.323873	0.0000
INF	-0.006742	0.034754	-0.193999	0.8463
ICLRD	1.646918	0.605402	2.720370	0.0068
GDPPC	-0.001483	0.000551	-2.689395	0.0075
FPI	-0.017866	0.011386	-1.569154	0.1175
AFV	0.172905	0.088899	1.944958	0.0526

R-squared	0.908098	Mean dependent var	13.61615
Adjusted R-squared	0.899296	S.D. dependent var	9.104516
S.E. of regression	2.889215	Akaike info criterion	5.045305
Sum squared resid	2963.385	Durbin-Watson stat	0.264221
Log likelihood	-948.8345	Schwarz criterion	5.401241
F-statistic	103.17	Hannan-Quinn criter.	5.186400
Prob(F-statistic)	0.000000		

Note: INF - Inflation; ICLRD - Incidence of Caloric Losses at Retail Distribution Level; GDPPC - GDP per Capita; FPI - Food Production Index; AFV - Agriculture, Forestry and Fishing, Value Added.
Source: estimated by the authors

Random effects model

The Random Effects model (Table 8) reveals that ICLRD is a substantial driver of undernourishment (β=1.3742, p<0.05), similar to Aragie et al. (2018) and Gatto and Chepeliev (2024). GDP per capita is still negative and extremely significant (β=-0.0017, p<0.01). Inflation and FPI are not statistically significant, although AFV has a weak positive correlation at the 10% level.

Table 8

Random effects (RE) model

Variable	Coefficient	Std. Error	t-Statistic	Probability
C	14.13689	3.038406	4.652732	0.0000
INF	-0.004406	0.034612	-0.127283	0.8988
ICLRD	1.374184	0.583693	2.354295	0.0191
GDPPC	-0.001744	0.000439	-3.968425	0.0001
FPI	-0.015901	0.010906	-1.457944	0.1457
AFV	0.139660	0.083620	1.670169	0.0957

R-squared	0.106999	Mean dependent var	1.436114
Adjusted R-squared	0.095372	*S.D.* dependent var	3.043675
S.E. of regression	2.894898	Durbin-Watson stat	0.241418
Sum squared resid	3218.087	Prob(F-statistic)	0.000000
F-statistic	9.202175		

Effects Specification	*S.D*	Rho
Cross-Section random	7.555175	0.8724
Idiosyncratic random	2.889215	0.1276

Note: INF - Inflation; ICLRD - Incidence of Caloric Losses at Retail Distribution Level; GDPPC - GDP per Capita; FPI - Food Production Index; AFV - Agriculture, Forestry and Fishing, Value Added.
Source: estimated by the authors

Estimated Random Effects Equation:

$$POU_{it} = 14.1369 + 1.3742ICLRD_{it} - 0.0159FPI_{it} + 0.1397AFV_{it} - 0.0044INF_{it} - 0.001744GDPPC_{it} + \mu_t$$

Both FE and RE models show that ICLRD is significantly positive, which means that the pooled OLS model suffers from omitted country-specific heterogeneity. In case such heterogeneity is considered, the actual positive impact of food waste at the retail level on undernourishment becomes apparent. The lack of statistical significance in the coefficients of the Food Production Index (FPI), Agriculture, Forestry, and Fishing Value Added (AFV), and Inflation (INF) imply that these macroeconomic and agricultural variables do not have any direct effect on undernourishment once food loss is taken into consideration. They might actually have an indirect effect on undernourishment via the availability of food and purchasing power among others. The decision to choose either the FE or RE model depends on the result of the Hausman test below.

However, this neat distinction is not applicable to all datasets. For instance, Laso et al. (2021), and Campoy-Muñoz et al. (2021), analyzing the supply chain of Spain, discovered that 53.3 percent of food losses caused by economic and nutritional factors took place at the stage of agricultural production, rather than at the retail and domestic stages, thus challenging the idea that food waste in developed countries takes place downstream. According to Karwowska et al. (2021), another important nuance related to meat industry should be taken into consideration: while in the industrialized regions, 64 percent of losses take place during the consumption of meat, in the developing regions, the same product is lost mainly at the production and storage stages; hence, this distinction between developed and developing countries can be applied to meat products despite the fact that it does not hold for some other products. Finally, Gatto and Chepeliev (2024) offer another perspective, arguing that in low-income regions, food exports lead to farm-level food loss. Among the numerous stages of the food supply chain, the retail sector merits special attention because it is the point at which food is closest to being consumed.

According to Gustavsson et al. (2011), the amount is equal to 1.3 billion tonnes per year, and this figure was later repeated almost verbatim by Alexander et al. (2013), Vilariño et al. (2017), Wunderlich and Martinez (2018), and Shafiee-Jood and Cai (2016), which may imply that a considerable part of the field relies on one FAO estimate without re-measuring the phenomenon in an independent way. On the other hand, Ishangulyyev et al. (2019) state the amount to be 1.6 billion tonnes, while Durán-Sandoval et al. (2023) reached 1,498 million tonnes using the top-down mass-balance method, and Paraschivu et al. (2022) decided on one billion tonnes. Even the economic value attached to this loss varies by an order of magnitude depending on who is counting and what they include: Ishangulyyev et al. (2019), and Eastham and Creedon (2023) cite figures near 750 and 936 billion dollars respectively, Spang et al. (2019), Vilariño et al. (2017) and Kechagias et al. (2024) converge on roughly one trillion dollars, and Mokrane et al. (2023) with Berjan et al. (2018) push the number to 2.6 trillion once hidden environmental and social costs are folded in. None of this disagreement is trivial; it tells a reader, before a single policy recommendation is offered, that while these estimates emphasize the worldwide extent of food loss, they offer little insight into how losses at various levels of the food supply chain affect food security and nutritional outcomes.

Retail itself, the stage most relevant to the present study, has attracted a smaller and more geographically lopsided body of work than either farm-level or household-level loss. Nahman and de Lange (2013) costed the entire South African food value chain at roughly 7.7 billion US dollars, or 2.1 percent of national GDP, tracing the bulk of that cost to processing, distribution and agricultural production rather than the retail shelf, a finding at odds with the developed-country retail-dominance narrative given that South Africa is a middle-income economy. Moraes et al. (2020), synthesising 54 studies on retail food waste, catalogued 34 distinct causes and 32 mitigation practices, from forecasting errors to inadequate inventory management, yet almost all their underlying studies were conducted in Europe or North America. Busetti and Pace (2023), and Todd and Faour(2024), offer one of the few frameworks built specifically around the retail supply chain, reporting that 13 percent of food is lost before reaching retail and a further 17 percent wasted domestically and in food services, yet their analysis, like Chalak et al. (2018) study of hospitality, restaurant and retail waste across 33 developed countries, is again anchored in wealthy-economy data. However, Porat et al. (2018) discussed post-harvest losses for fruits and vegetables at retail level as well as at household levels; yet again, this study is based on limited evidence from industrialized retail settings. Collectively, this group of papers reveals one thing that is not commonly mentioned in the literature regarding the underdeveloped countries: Retail losses have been studied mostly in cases where the retail system is modernized. Retail food loss has significant nutritional repercussions that may directly affect undernourishment and food security outcomes in addition to its economic ramifications.

A number of studies step back from measuring loss altogether and instead model the broader determinants of undernourishment, and it is here that a genuine gap in the literature becomes visible. Nugroho et al. (2022), using system GMM estimation across 57 developing countries, found that corruption control, institutional quality and food-system factors jointly shape the number of undernourished people, while Baykoca and Yılmaz (2025) built a typology of 105 countries by GDP, growth and health expenditure and confirmed that developing countries lose food earlier in the chain while developed countries lose it later, and Jayadevan (2022) found across 165 countries that food wastage depresses economic growth while raising poverty. None of these econometric studies, however, isolates retail-stage loss as a distinct explanatory variable; they either treat food loss and waste as a single undifferentiated aggregate or examine wastage alongside unrelated macroeconomic controls.

Smith (1998) adds an important qualification from an earlier era of this literature, arguing that hunger can persist in cities even where aggregate food supply is adequate, because access and distribution, not production volume, determine who actually eats, a point Gómez and Ricketts (2013) extend by showing that modern and traditional food value chains affect undernourishment, micronutrient deficiency and over-nutrition in genuinely opposite directions depending on which population is served. Popkin et al. (2020) and Schmidhuber and Shetty (2005), writing fifteen years apart, both describe a "double burden" in which undernutrition and rising obesity coexist within the same developing populations, a phenomenon that plain calorie-loss accounting cannot explain and that Kramer and Allen (2015) and Pollard and Booth (2019) show is not confined to poor countries alone, since food insecurity affects 8 to 20 percent of populations even in some of the wealthiest nations on earth. To address these difficulties, a growing body of literature has recommended different legislative and administrative measures aimed at minimizing food loss and boosting food-system efficiency.

The nutritional consequences of loss, as distinct from its economic cost, form a third strand of evidence smaller in size but arguably more directly relevant to undernourishment. Wang et al. (2023) calculated that China's annual per-capita food loss and waste contain enough nutrients to sustain a person for 66.2 days, with losses of vitamin K, copper, and vitamin C exceeding 74 percent of the dietary reference intake, a demonstration that nutrient loss and calorie loss do not move together.

Eastham and Creedon (2023) push this further, insisting that counting tonnes lost tells us little unless nutrient density at each stage of degradation is also tracked, since storage, processing and temperature exposure erode micronutrient content even when bulk mass is preserved. Abbade (2020), who introduced the Nutritional Loss and Waste and Feeding Potential indicators, calculated that in 2017 food loss could have fed up to 940 million adults on the planet, surpassing almost all contemporary estimates of undernourishment in the world, while Chen et al. (2020), studying 151 countries, concluded that on average annually food waste per capita would be sufficient for maintaining a healthy nutrition regime for about 18 days, and losses of vitamin C, vitamin K, zinc, copper, manganese and selenium were equal or exceeded one quarter of daily recommended intake.

In the context of household level losses Khalid et al. (2019), who studied Pakistan, and Chalak et al. (2019), who studied Lebanon, calculated daily caloric and micronutrient losses from kitchen waste and came to quite similar figures of daily energy and protein losses reaching several hundred kilocalories and tens of grams respectively, proving that the issue of nutritional loss occurs not only at the household level but through the whole chain. The question of micronutrient malnutrition and insufficient protein quality in developing regions was considered by Miller and Welch (2013) and Schönfeldt and Hall (2012).

This last point brings the discussion to its central weakness. Chaboud and Daviron (2017), Xue et al. (2017), Shalash et al. (2025), and Imran et al. (2025) independently diagnose the same underlying problem from different angles: the former shows that inconsistent definitions of loss and waste undermine cross-study comparison, and the latter demonstrates empirically that global data on food loss remain narrow in temporal, geographic, and supply-chain coverage, concentrated overwhelmingly in a handful of industrialized countries such as the United Kingdom and the United States. Van der Werf and Gilliland (2017), compiling 55 estimates from prior research, directly confirm this bias, since their entire sample is drawn from developed-country studies. The consequence of this concentration is that the retail segment specifically, as opposed to food loss and waste in general, has been measured almost exclusively in contexts where retail systems are already efficient, formalized and data-rich, while the developing-country literature has instead

concentrated its attention on farm-level and post-harvest losses, treating retail as a secondary or even negligible stage simply because that is where losses happen to be smaller in absolute terms.

This asymmetry matters because retail systems in developing countries are neither absent nor uniform: informal markets, inconsistent cold-chain access, and rapidly urbanizing consumer bases mean that retail-level loss in these settings may behave very differently from either the mature retail systems of Europe and North America or the on-farm losses that dominate existing developing-country research. Thi et al. (2015) come closest to acknowledging this blind spot, noting that urbanization and rising incomes are reshaping food waste generation in developing economies in ways the existing farm-centric literature was not designed to capture, yet even their review stops short of isolating retail loss as a distinct variable and testing its relationship to undernourishment directly.

A distinct but related body of economic modelling asks not how much is lost but what would happen if losses were reduced, and here the literature disagrees quite openly about where intervention would do the best. Okawa (2015), using the OECD-FAO Aglink-Cosimo model, found that demand-side reductions in consumer waste in wealthy countries exert far greater downward pressure on international prices than supply-side gains from reduced producer losses, generating cumulative consumer savings of 2.52 trillion US dollars over a decade alongside 421 billion dollars in producer revenue losses concentrated in China's pigmeat sector.

Munesue et al. (2015) and Munesue and Masui (2019) obtained a complementary conclusion from a different perspective, which estimated that a reduction in food loss and waste by half in developed areas would decrease the number of undernourished people in developing nations by about 63 million people, thereby showing that there is a spill-over effect of policies from rich nations on poor nations. Kuiper and Cui (2021), on the other hand, using a global economy-wide modeling approach, showed that reducing losses during the initial production stage will yield the maximum benefit in terms of increased availability and access to food in low-income regions. Lopez Barrera and Hertel (2021) complicate matters further with evidence of a non-linear relationship between income and food waste across 158 countries, projecting that household waste will rise sharply in emerging economies such as China and South Asia as incomes grow, which suggests that today's low-waste developing countries may not remain low-waste for long.

Rutten (2013) offers perhaps the most sobering caution among this group, showing through supply-and-demand theory that reducing losses does not automatically produce uniform welfare gains at all, since producers can suffer short-run losses even as consumers benefit, a nuance that much of the more descriptive literature overlooks entirely. Xia et al. (2026), applying multi-regional input-output modelling, add a distributive-justice dimension by showing that production-based accounting understates the responsibility of import-dependent nations for global food loss and waste, shifting an average of 31 percent of responsibility back onto importing countries. While global modelling studies provide useful insights, country-specific research is still crucial since the causes and consequences of food loss vary across economic and institutional contexts.

Country-based case studies present valuable insight into the diverse manifestations of food losses and food insecurity in developing nations. Research from countries such as China, South Africa, Pakistan, India, Turkey, Lebanon, and others reveals that food loss impacts food availability, nutrition, and food security through inefficient supply chains, poor infrastructure for storage, post-harvest food losses, and food access issues.

The negative consequences of armed conflicts have a significant impact on food security (Dankevych et al., 2024). While the extent and causes of food losses differ in different

countries, most research studies suggest that food losses have been shown to help improve food availability and nutrition and make food security more attainable. In essence, the findings emphasize the need to understand the impact of losses in particular parts of the food supply chain that cause undernutrition in developing countries (Wang et al., 2023). Although country-level studies provide comprehensive contextual evidence, they do not fully explain why undernutrition occurs in nations with diverse economic and food-system situations.

A further cluster of work addresses solutions rather than causes, and even here consensus is partial. Garrone et al. (2014) proposed an availability–surplus–recoverability–waste model, Vilariño et al. (2017) and de Oliveira et al. (2021) frame circular-economy principles as the organising solution, and Tchonkouang et al. (2023) with Aschemann-Witzel et al. (2023) argue for valorisation and upcycling of food that would otherwise be discarded. Yet Dudziak et al. (2022), examining gendered and regional patterns in self-reported food waste, expose a methodological weakness running through much of this literature: self-declared waste behaviour is vulnerable to social desirability bias, so the demographic differences circular-economy interventions target may not hold under objective, diary-based measurement. Manzoor et al. (2024), Chauhan et al. (2021), reviewing hundreds of studies between them, converge on the observation that stakeholder coordination and standardised measurement are repeatedly recommended but rarely implemented at scale, while Akkerman and Cruijssen (2024), Zayed et al. (2026), argue that even the underlying convention of counting loss by weight or volume is flawed, since it ignores how nutrient density differs across food types. Horák et al. (2023) emphasize the importance of efficient agricultural resource use for sustainable development and food security. Nitsenko et al. (2024) emphasize the need for ethical and social incentives when analyzing approaches. Von Braun et al. (2023) frame the coexistence of loss and hunger as a fundamental failure of contemporary food systems, a framing broad enough to be difficult to disagree with but also too broad to say where, within the supply chain, action should begin. Despite these essential advances, there are considerable conceptual and empirical gaps in understanding the precise role of retail-stage food losses in influencing undernutrition outcomes in developing countries.

Model selection: the Gausman specification test

The Hausman specification test has been carried out in Table 9 so as to identify the optimal approach to estimate the panel data model. The chi-squared value was 6.512, with a p-value of 0.2595. It indicates that we cannot reject the null hypothesis. It can be seen from the results that the Random Effects model is superior to the Fixed Effects model since there is no systematic relationship between the unobserved country effects and the explanatory variables. The opposite sign of the coefficients in pooled OLS vs. panel estimates indicates that there is country-specific heterogeneity omitted. Those countries that have better economic and institutional performance might at the same time experience higher retail loss while having low levels of undernourishment. Having controlled for this hidden heterogeneity using Fixed and Random Effects estimations, the actual positive relationship becomes clear. This conclusion emphasizes the need to take into account cross-country heterogeneity in the analysis of the food security problem of food losses at the retail stage.

Table 9

Hausman test result

Test	Chi-Sq. Statistics	Chi-Sq. *d.f*	Probability
Cross Section Random	6.512157	5	0.2595

Source: estimated by the authors

Diagnostic tests

Panel heteroskedasticity LR test rejects the null hypothesis of homoskedasticity (statistic=467.772, p<0.01), thus verifying the use of robust standard errors (Table 10).

Table 10

Panel Cross-Section Heteroskedasticity LR Test

Test	Statistics	*d.f.*	P-value	Decision
Panel Cross-Section Heteroskedasticity LR Test	467.772	30	0.0000	Reject H_0

Source: estimated by the authors

Panel cross-sectional dependence test results in Table 11 exhibit highly significant Breusch-Pagan LM and Pesaran Scaled LM statistics (p<0.01), although the Pesaran *CD* test is insignificant (p=0.1474). There seems to be little cross-sectional correlation on an average basis.

Table 11

Cross-sectional dependence test

Test	Statistics	*d.f.*	*P*-value
Breusch-Pagan LM	2133.243	435	0.0000
Pesaran Scaled LM	57.576	-	0.0000
Pesaran CD	-1.449	-	0.1474

Source: estimated by the authors

Potential food-energy recovery from retail loss reduction

Econometrics confirms the existence of a statistically significant association between calorie losses at the retail stage and undernutrition; yet, the scale of this relationship becomes more comprehensible in light of its translation into the possible consequences for food security. To answer the question of how much food would actually be recovered, this research conducts a counterfactual calorie recovery analysis. It does not aim to assume that all food losses can be eliminated but to consider a more realistic case scenario when half of retail-stage calorie losses are saved.

Based on the findings, there is a positive impact of reducing the retail stage calories losses on food security. Under the 50 percent reduction assumption, the recoverable calories were equal to 57.62-million-person equivalents per year in 2022 for 28 countries, averaging 2.06-million-person equivalents for each country. It means that the reduction of retail stage losses will have the positive impact on the volume of food energy available for human consumption, thereby contributing to food security improvement. These findings are supported by the literature review where it is stated that food loss and waste reduction can lead to food availability increase and, therefore, to food security improvement. Nevertheless, these person equivalents are the potential food energy but not the number of people who will become free from undernutrition.

Summary of novelty and contribution

Overall, the findings presented in this paper differ from the food loss literature in three aspects. First, whereas previous studies (Aragie et al., 2018; Ishangulyyev et al., 2019) reveal

very significant upstream losses in one specific region, this paper reveals the same degree of losses in geographically different regions (East Africa and the Bolivia-Nicaragua Cluster). In doing so, undernourishment ceases to be a geographically determined problem and becomes a structural one. Second, the adoption of the retail-level calorie loss index (ICLRD) as the key explanatory variable addresses another issue with the data.

Namely, the correlation between ICLRD and undernourishment is clear only when controlling for heterogeneity through the Random Effects model; otherwise, it appears that the countries with high ICLRD values are not necessarily the most undernourished. Third, direct comparison of Sub-Saharan Africa with the Middle East and North Africa rather than region-siloed comparison, which is typical of the literature (Abiad & Meho, 2018), demonstrates that despite structurally different reasons for food loss, they can result in the same outcomes of undernourishment. In summary, the findings clearly show that food loss continues to play an important role in causing under-nutrition, even after accounting for the effects of income, prices, and cross-country variation.

Policy implications

With retail-level loss and income being separate, balancing factors of undernourishment, policies to reduce hunger should focus specifically on improving retail efficiency without relying on the automatic result of income generation or agricultural output, especially considering that the SDG Target 12.3 aims to reduce retail and consumer food losses by half by 2030. Since undernourishment prevalence has more of a structural than a regional pattern, retail and cold chain policies known to be successful in one country, for instance, East African nations, can be adopted in similarly structured nations, like Bolivia and Nicaragua, without having to create a new policy for each region. Nevertheless, the similar level of undernourishment found in Sub-Saharan Africa and MENA is due to different causes, namely production-stage inefficiency in one and dependence on imports in the other, thus requiring the development of policies for each path separately. Digital retail monitoring systems, enhanced inventory management, cold-chain development, and food donation initiatives are examples of practical approaches.

Limitations

The primary drawbacks of this study are associated with the availability of data and research scope. The choice of the ICLRD as the main explanatory variable is justified due to the lack of similar cross-country data on previous stages of the food supply chain: production, harvesting, post-harvesting, storage, and transportation of food products. Hence, the results of the study present the correlation between the caloric losses during the retail stage and the level of undernourishment, but not the overall impact of the losses throughout the food supply chain. The lack of data also prevents the inclusion of institutional variables that would allow assessing their possible moderating role in the examined relationship. Despite the geographical diversity of the panel of 30 countries, the differences in food supply systems, infrastructure, and retail structure can influence the applicability of the study's results. Lastly, only 28 countries have data for the assessment of the food energy recovery and person-equivalent; therefore, this measure is estimated only within this subsample.

Future research directions

Based on the limitations highlighted above, Future research should focus on the comparison between the Food Loss Index (FLI) and Food Waste Index (FWI), as well as the retail food loss index, in order to determine the stage that has the biggest effect on

malnutrition. The reason is that such studies would provide much more information in support of the development of specific food security policy measures, especially in developing nations. Lastly, using dummy variables or interaction of ICLRD and regions would turn the current regional descriptive comparison into a more rigorous testing process. Extending the panel data to years beyond 2022 and including a larger number of countries would validate the pattern observed in the current study. Future research should also use more extensive and harmonized food-supply data to expand the food-energy recovery evaluation to the entire study sample and increase the precision of person-equivalent estimations.

Conclusions

This paper analyzes the effect of retail food waste on undernutrition in 30 developing countries from Sub-Saharan Africa, MENA, South Asia, Southeast Asia, and Latin America and the Caribbean over the period of 2010–2022 using Pooled OLS, Fixed Effects, and Random Effects panel data models. The empirical results suggest that allowing for unobservable differences between countries significantly alters the relationship between retail food waste and undernutrition. According to the Pooled OLS, the relationship is negative, while both Fixed Effects ($\beta = 1.6469$, $p < 0.01$) and Random Effects ($\beta = 1.3742$, $p < 0.05$) models indicate a positive and statistically significant relationship, implying that omission of unobserved country heterogeneity results in biased results. In line with the results of the Hausman test, the Random Effects model is chosen as the preferred estimator.

On the control variables, the variable GDP per capita is seen to be highly significant in having a negative impact on undernourishment. Although Food Production Index (FPI), Agriculture, Forestry and Fishing Value Added (AFV), and Inflation (INF) were not statistically significant in the estimated models, these variables remain important background determinants of food security. Their influence is likely to be indirect, operating through production capacity, agricultural productivity, food prices, purchasing power, and supply-chain conditions rather than exerting an immediate direct effect on undernourishment.

The results of the descriptive comparison show that undernourishment is not only affected by the geographic position of the country. Different countries in various regions can have an equal degree of undernourishment despite having various economic and institutional conditions, while different countries in the same region can reach the same outcome due to various mechanisms. It means that reduction of retail food loss by the optimization of logistics, cold chain infrastructure, stock management, and redistribution of the food can be considered together with economic development measures. Such a combination of policy measures will help to accomplish SDG2 (zero hunger) and SDG12.3 on food loss reduction.

References

Abbade, E. B. (2020). Estimating the nutritional loss and the feeding potential derived from food losses worldwide. *World Development, 134*, 105038. https://doi.org/10.1016/j.worlddev.2020.105038

Abiad, M. G., & Meho, L. I. (2018). Food loss and food waste research in the Arab world: A systematic review. *Food Security, 10*, 311–322. https://doi.org/10.1007/s12571-018-0782-7

Akkerman, R., & Cruijssen, F. (2024). Food loss, food waste, and sustainability in food supply chains. In *Sustainable supply chains: A research-based textbook on operations and strategy* (pp. 219–239). Springer. https://doi.org/10.1007/978-3-031-45565-0_9

Alexander, C., Gregson, N., & Gille, Z. (2013). Food waste. In A. Murcott, W. Belasco, & P. Jackson (Eds.), *The handbook of food research* (pp. 471–484). Bloomsbury Academic. https://doi.org/10.5040/9781350042261-ch-0028

Aragie, E., Balié, J., & Morales-Opazo, C. (2018). Does reducing food losses and wastes in sub-Saharan Africa make economic sense? *Waste Management & Research, 36*(6), 483–494. https://doi.org/10.1177/0734242X18770247

Aschemann-Witzel, J., Asioli, D., Banovic, M., Perito, M. A., Peschel, A. O., & Stancu, V. (2023). Defining upcycled food: The dual role of upcycling in reducing food loss and waste. *Trends in Food Science & Technology, 132*, 132–137. https://doi.org/10.1016/j.tifs.2023.01.001

Baltagi, B. H. (2021). *Econometric analysis of panel data* (6th ed.). Springer, Cham, Switzerland. https://doi.org/10.1007/978-3-030-53953-5

Baykoca, B., & Yılmaz, S. (2025). Understanding food loss patterns across developed and developing countries using a GDP, growth rate, and health expenditure-based typology. *Scientific Reports, 15*, 27597. https://doi.org/10.1038/s41598-025-13156-3

Berjan, S., Capone, R., Debs, P., & El Bilali, H. (2018). Food losses and waste: A global overview with a focus on Near East and North Africa region. *International Journal of Agricultural Management and Development, 8*(1), 1–16. https://doi.org/10.22004/ag.econ.292516

Busetti, S., & Pace, N. (Eds.). (2023). *Food loss and waste policy: From theory to practice*. Routledge, London. https://doi.org/10.4324/9781003226932

Campoy-Muñoz, P., Cardenete, M. A., Delgado, M. C., & Sancho, F. (2021). Food losses and waste: A needed assessment for future policies. *International Journal of Environmental Research and Public Health, 18*(21), 11586. https://doi.org/10.3390/ijerph182111586

Chaboud, G., & Daviron, B. (2017). Food losses and waste: Navigating the inconsistencies. *Global Food Security, 12*, 1–7. https://doi.org/10.1016/j.gfs.2016.11.004

Chalak, A., Abiad, M. G., Diab, M., & Nasreddine, L. (2019). The determinants of household food waste generation and its associated caloric and nutrient losses: The case of Lebanon. *PLOS ONE, 14*(12), e0225789. https://doi.org/10.1371/journal.pone.0225789

Chalak, A., Abou-Daher, C., & Abiad, M. G. (2018). Generation of food waste in the hospitality and food retail and wholesale sectors: Lessons from developed economies. *Food Security, 10*, 1279–1290. https://doi.org/10.1007/s12571-018-0841-0

Chauhan, C., Dhir, A., Akram, M. U., & Salo, J. (2021). Food loss and waste in food supply chains: A systematic literature review and framework development approach. *Journal of Cleaner Production, 295*, 126438. https://doi.org/10.1016/j.jclepro.2021.126438

Chen, C., Chaudhary, A., & Mathys, A. (2020). Nutritional and environmental losses embedded in global food waste. *Resources, Conservation and Recycling, 160*, 104912. https://doi.org/10.1016/j.resconrec.2020.104912

Choi, I. (2001). Unit root tests for panel data. *Journal of International Money and Finance, 20*(2), 249–272. https://doi.org/10.1016/S0261-5606(00)00048-6

Dankevych, A., Stoyanova-Koval, S., Polova, O., Los, Z., Burdeina, N., & Kazak, O. (2024). State of economic security and directions of restoration socio-economic development and food security in the conditions of war. *Financial and Credit Activity Problems of Theory and Practice, 2*(55), 441–460. https://doi.org/10.55643/fcaptp.2.55.2024.4170

de Oliveira, M. M., Lago, A., & Dal' Magro, G. P. (2021). Food loss and waste in the context of the circular economy: A systematic review. *Journal of Cleaner Production, 294*, 126284. https://doi.org/10.1016/j.jclepro.2021.126284

Dudziak, A., Stoma, M., & Derkacz, A. J. (2022). Circular economy in the context of food losses and waste. *Sustainability, 14*(16), 10116. https://doi.org/10.3390/su141610116

Durán-Sandoval, D., Durán-Romero, G., & Uleri, F. (2023). How much food loss and waste do countries with problems with food security generate? *Agriculture, 13*(5), 966. https://doi.org/10.3390/agriculture13050966

Eastham, J., & Creedon, A. (2023). Food losses, food waste, and beyond in food supply chains: Retaining optimum nutrient density. *Food Frontiers, 4*, 971–979. https://doi.org/10.1002/fft2.271

Garrone, P., Melacini, M., & Perego, A. (2014). Opening the black box of food waste reduction. *Food Policy, 46*, 129–139. https://doi.org/10.1016/j.foodpol.2014.03.014

Gatto, A., & Chepeliev, M. (2024). Global food loss and waste estimates show increasing nutritional and environmental pressures. *Nature Food, 5*, 136–147. https://doi.org/10.1038/s43016-023-00915-6

Gómez, M. I., & Ricketts, K. D. (2013). Food value chain transformations in developing countries: Selected hypotheses on nutritional implications. *Food Policy, 42*, 139–150. https://doi.org/10.1016/j.foodpol.2013.06.010

Gustavsson, J., Cederberg, C., Sonesson, U., van Otterdijk, R., & Meybeck, A. (2011). *Global food losses and food waste: Extent, causes and prevention*. Food and Agriculture Organization of the United Nations, Rome. https://www.fao.org/4/mb060e/mb060e00.pdf

Hodges, R. J., Buzby, J. C., & Bennett, B. (2011). Postharvest losses and waste in developed and less developed countries: Opportunities to improve resource use. *The Journal of Agricultural Science, 149*(S1), 37–45. https://doi.org/10.1017/S0021859610000936

Horák, J., Bilan, Y., Dankevych, A., Nitsenko, V., Kucher, A., & Streimikiene, D. (2023). Bioenergy production from sunflower husk in Ukraine: Potential and necessary investments. *Journal of Business Economics and Management, 24*(1), 1–19. https://doi.org/10.3846/jbem.2023.17756

Imran, M., Tufail, M., Mo, C., Wahab, S., Khan, M. K., Chee Hoo, W., & Ling, Z. (2025). From resources to resilience: Understanding the impact of standard of living and energy consumption on natural resource rent in Asia. *Energy Strategy Reviews, 57*, 101590. https://doi.org/10.1016/j.esr.2024.101590

Ishangulyyev, R., Kim, S., & Lee, S. H. (2019). Understanding food loss and waste: Why are we losing and wasting food? *Foods, 8*(8), 297. https://doi.org/10.3390/foods8080297

James, A., & Zikankuba, V. (2017). Postharvest management of fruits and vegetables: A potential for reducing poverty, hidden hunger and malnutrition in sub-Sahara Africa. *Cogent Food & Agriculture, 3*(1), 1312052. https://doi.org/10.1080/23311932.2017.1312052

Joardder, M. U. H., & Masud, M. H. (2019). *Food preservation in developing countries: Challenges and solutions*. Springer, Cham, Switzerland. https://doi.org/10.1007/978-3-030-11530-2

Karwowska, M., Łaba, S., & Szczepański, K. (2021). Food loss and waste in meat sector: Why the consumption stage generates the most losses? *Sustainability, 13*(11), 6227. https://doi.org/10.3390/su13116227

Kechagias, E. P., Gayialis, S. P., Panayiotou, N., & Papadopoulos, G. A. (2024). A holistic framework for evaluating food loss and waste due to marketing standards across the entire food supply chain. *Foods, 13*(20), 3273. https://doi.org/10.3390/foods13203273

Khalid, S., Naseer, A., Shahid, M., Shah, G. M., Ullah, M. I., Waqar, A., Abbas, T., Imran, M., & Rehman, F. (2019). Assessment of nutritional loss with food waste and factors governing this waste at household level in Pakistan. *Journal of Cleaner Production, 206*, 1015–1024. https://doi.org/10.1016/j.jclepro.2018.09.138

Khan, A. A., Siddiqui, Y., Siddique, K. H. M., Bobo, J. A., & Ali, A. (2024). Minimizing postharvest food losses: A vital strategy to alleviate food insecurity and malnutrition in developing nations: A review. *Discover Food, 4*, 145. https://doi.org/10.1007/s44187-024-00129-0

Kramer, C. V., & Allen, S. (2015). Malnutrition in developing countries. *Paediatrics and Child Health, 25*(9), 422–427. https://doi.org/10.1016/j.paed.2015.04.002

Kuiper, M., & Cui, H. D. (2021). Using food loss reduction to reach food security and environmental objectives: A search for promising leverage points. *Food Policy, 98*, 101915. https://doi.org/10.1016/j.foodpol.2020.101915

Kumar, D., & Kalita, P. (2017). Reducing postharvest losses during storage of grain crops to strengthen food security in developing countries. *Foods, 6*(1), 8. https://doi.org/10.3390/foods6010008

Levin, A., Lin, C.-F., & Chu, C.-S. J. (2002). Unit root tests in panel data: Asymptotic and finite-sample properties. *Journal of Econometrics, 108*(1), 1–24. https://doi.org/10.1016/S0304-4076(01)00098-7

Lopez Barrera, E., & Hertel, T. (2021). Global food waste across the income spectrum: Implications for food prices, production and resource use. *Food Policy, 98*, 101874. https://doi.org/10.1016/j.foodpol.2020.101874

Manzoor, S., Fayaz, U., Dar, A. H., Dash, K. K., Shams, R., Bashir, I., Pandey, V. K., & Abdi, G. (2024). Sustainable development goals through reducing food loss and food waste: A comprehensive review. *Future Foods, 9*, 100362. https://doi.org/10.1016/j.fufo.2024.100362

Miller, D. D., & Welch, R. M. (2013). Food system strategies for preventing micronutrient malnutrition. *Food Policy, 42*, 115–128. https://doi.org/10.1016/j.foodpol.2013.06.008

Mokrane, S., Buonocore, E., Capone, R., & Franzese, P. P. (2023). Exploring the global scientific literature on food waste and loss. *Sustainability, 15*(6), 4757. https://doi.org/10.3390/su15064757

Moraes, C. C. D., Costa, F. H. D. O., Pereira, C. R., Silva, A. L. D., & Delai, I. (2020). Retail food waste: Mapping causes and reduction practices. *Journal of Cleaner Production, 256*, 120124. https://doi.org/10.1016/j.jclepro.2020.120124

Munesue, Y., & Masui, T. (2019). The impacts of Japanese food losses and food waste on global natural resources and greenhouse gas emissions. *Journal of Industrial Ecology, 23*(5), 1196–1210. https://doi.org/10.1111/jiec.12863

Munesue, Y., Masui, T., & Fushima, T. (2015). The effects of reducing food losses and food waste on global food insecurity, natural resources, and greenhouse gas emissions. *Environmental Economics and Policy Studies, 17*, 43–77. https://doi.org/10.1007/s10018-014-0083-0

Nahman, A., & De Lange, W. (2013). Costs of food waste along the value chain: Evidence from South Africa. *Waste Management, 33*(11), 2493–2500. https://doi.org/10.1016/j.wasman.2013.07.012

Nitsenko, V., Dankevych, A., Dzoba, O., Ustenko, A., Bashynska, Yu. (2024). Ethical and social incentives for the transformation of the business model of enterprise management in conditions of sustainable development. *Naukovyi Visnyk Natsionalnoho Hirnychoho Universytetu*, 4, 172-179. https://doi.org/10.33271/nvngu/2024-4/172.

Nugroho, A. D., Cubillos Tovar, J. P., Bopushev, S. T., Bozsik, N., Fehér, I., & Lakner, Z. (2022). Effects of corruption control on the number of undernourished people in developing countries. *Foods, 11*(7), 924. https://doi.org/10.3390/foods11070924

Okawa, K. (2015). *Market and trade impacts of food loss and waste reduction* (OECD Food, Agriculture and Fisheries Papers No. 75). OECD Publishing, Paris. https://doi.org/10.1787/5js4w29h0wr2-en

Paraschivu, M., Cotuna, O., Matei, G., & Sărățeanu, V. (2022). Are food waste and food loss a real threat for food security? *Scientific Papers Series Management, Economic Engineering in Agriculture and Rural Development, 22*(1), 479–484. https://managementjournal.usamv.ro/pdf/vol.22_1/Art56.pdf

Pollard, C. M., & Booth, S. (2019). Food insecurity and hunger in rich countries: It is time for action against inequality. *International Journal of Environmental Research and Public Health, 16*(10), 1804. https://doi.org/10.3390/ijerph16101804

Popkin, B. M., Corvalan, C., & Grummer-Strawn, L. M. (2020). Dynamics of the double burden of malnutrition and the changing nutrition reality. *The Lancet, 395*(10217), 65–74. https://doi.org/10.1016/S0140-6736(19)32497-3

Porat, R., Lichter, A., Terry, L. A., Harker, R., & Buzby, J. C. (2018). Postharvest losses of fruit and vegetables during retail and in consumers' homes: Quantifications, causes, and means of prevention. *Postharvest Biology and Technology, 139*, 135–149. https://doi.org/10.1016/j.postharvbio.2017.11.019

Rutten, M. M. (2013). What economic theory tells us about the impacts of reducing food losses and/or waste: Implications for research, policy and practice. *Agriculture & Food Security, 2*, 13. https://doi.org/10.1186/2048-7010-2-13

Schmidhuber, J., & Shetty, P. (2005). The nutrition transition to 2030: Why developing countries are likely to bear the major burden. *Acta Agriculturae Scandinavica, Section C—Food Economics, 2*(3–4), 150–166. https://doi.org/10.1080/16507540500534812

Schönfeldt, H. C., & Gibson Hall, N. (2012). Dietary protein quality and malnutrition in Africa. *British Journal of Nutrition, 108*(S2), S69–S76. https://doi.org/10.1017/S0007114512002553

Shafiee-Jood, M., & Cai, X. (2016). Reducing food loss and waste to enhance food security and environmental sustainability. *Environmental Science & Technology, 50*(16), 8432–8443. https://doi.org/10.1021/acs.est.6b01993

Sheahan, M., & Barrett, C. B. (2017). Review: Food loss and waste in Sub-Saharan Africa. *Food Policy, 70*, 1–12. https://doi.org/10.1016/j.foodpol.2017.03.012

Shlash, A. A. M., Al-Ramadan, A. M., Ibrahim Mohammad, S., Al Oraini, B., Vasudevan, A., Turki Alshurideh, M., Chen, Q., & Ali, I. (2025). Enhancing metadata management and data-driven decision-making in sustainable food supply chains using blockchain and AI technologies. *Data and Metadata, 4*, 683. https://doi.org/10.56294/dm2025683

Shynkaruk, L., Dielini, M., Vlasenko, T., Svyrydenko, D., Nitsenko, V., Kondratyev, Y., & Salii, I. (2025). Food security and the agri-food sector of Ukraine: An inclusive approach. *Rocznik Ochrona Środowiska, 27*, 553–570. https://doi.org/10.54740/ros.2025.045

Smith, D. W. (1998). Urban food systems and the poor in developing countries. *Transactions of the Institute of British Geographers, 23*(2), 207–219. https://doi.org/10.1111/j.0020-2754.1998.00207.x

Spang, E. S., Moreno, L. C., Pace, S. A., Achmon, Y., Donis-Gonzalez, I., Gosliner, W. A., Jablonski-Sheffield, M. P., Momin, M. A., Quested, T. E., Winans, K. S., & Tomich, T. P. (2019). Food loss and waste: Measurement, drivers, and solutions. *Annual Review of Environment and Resources, 44*, 117–156. https://doi.org/10.1146/annurev-environ-101718-033228

Stabnikova, O., Shevchenko, O., Stabnikov, V., & Paredes-López, O. (Eds.). (2023). *Bioconversion of waste to value-added products*. CRC Press. https://doi.org/10.1201/9781003329671

Tchonkouang, R. D., Onyeaka, H., & Miri, T. (2023). From waste to plate: Exploring the impact of food waste valorisation on achieving zero hunger. *Sustainability, 15*(13), 10571. https://doi.org/10.3390/su151310571

Thayyil, A., & Manogna, R. L. (2026). Impact of climate change mitigation finance on food security in emerging and developing economies of Global South. *Discover Food*. https://doi.org/10.1007/s44187-026-01202-6

Thi, N. B. D., Kumar, G., & Lin, C.-Y. (2015). An overview of food waste management in developing countries: Current status and future perspective. *Journal of Environmental Management, 157*, 220–229. https://doi.org/10.1016/j.jenvman.2015.04.022

Todd, E. C. D., & Faour-Klingbeil, D. (2024). Impact of food waste on society, specifically at retail and foodservice levels in developed and developing countries. *Foods, 13*(13), 2098. https://doi.org/10.3390/foods13132098

U.S. Department of Agriculture, & U.S. Department of Health and Human Services. (2020). *Dietary guidelines for Americans, 2020–2025* (9th ed.). U.S. Department of Agriculture; U.S. Department of Health and Human Services, Washington, DC. https://www.dietaryguidelines.gov/

United Nations Environment Programme. (2024). *Food waste index report 2024*. https://www.unep.org/resources/publication/food-waste-index-report-2024

van der Werf, P., & Gilliland, J. A. (2017). A systematic review of food losses and food waste generation in developed countries. *Proceedings of the Institution of Civil Engineers—Waste and Resource Management, 170*(2), 66–77. https://doi.org/10.1680/jwarm.16.00026

Vilariño, M. V., Franco, C., & Quarrington, C. (2017). Food loss and waste reduction as an integral part of a circular economy. *Frontiers in Environmental Science, 5*, 21. https://doi.org/10.3389/fenvs.2017.00021

von Braun, J., Sánchez Sorondo, M., & Steiner, R. (2023). Reduction of food loss and waste: The challenges and conclusions for actions. In J. von Braun, M. Sánchez Sorondo, & R. Steiner (Eds.), *Science and innovations for food systems transformation* (pp. 569–578). Springer, Cham, Switzerland. https://doi.org/10.1007/978-3-031-15703-5_31

Wang, R., Lu, S., Zhou, L., Yang, Z., Tang, Z., Zhao, M., & Cheng, G. (2023). Assessing nutritional and economic aspects of food loss and waste in China. *Sustainable Production and Consumption, 42*, 95–105. https://doi.org/10.1016/j.spc.2023.09.010

Wooldridge, J. M. (2021). *Introductory econometrics: A modern approach* (7th ed.). Cengage Learning, Boston, MA.

World Bank Group. (2025). *World development indicators*. https://databank.worldbank.org/source/world-development-indicators

Wunderlich, S. M., & Martinez, N. M. (2018). Conserving natural resources through food loss reduction: Production and consumption stages of the food supply chain. *International Soil and Water Conservation Research, 6*(4), 331–339. https://doi.org/10.1016/j.iswcr.2018.06.002

Xue, L., Liu, G., Parfitt, J., Liu, X., Van Herpen, E., Stenmarck, Å., O'Connor, C., Östergren, K., & Cheng, S. (2017). Missing food, missing data? A critical review of global food losses and food waste data. *Environmental Science & Technology, 51*(12), 6618–6633. https://doi.org/10.1021/acs.est.7b00401

Cite:

Dankevych, A., Mitu, M. N., Zayed, N. M., Nitsenko, V., & Ingram, K. L. (2026). Impact of retail food loss on undernourishment in developing countries. *Ukrainian Food Journal, 15*(3), 949–976. https://doi.org/10.24263/2304-974X-2026-15-3-19

Competitiveness of Visegrad Countries' sugar sectors after EU sugar quota abolition and under EU-Mercosur Agreement

Patrik Rovny[1], Lubos Smutka[2] , Inna Cabelkova[3]

1 – Slovak University of Agriculture in Nitra, Nitra, Slovakia
2 – Institute of Agricultural Economics and Information, Prague, Czech Republic
3 – Mendel University in Brno, Faculty of Business and Economics, Czechia

Keywords:

Sugar
Visegrad Group
Mercosur
Trade
Self-sufficiency
Resilience

Article history:

Received 16.03.2026
Received in revised form 02.06.2026
Accepted 30.06.2026

Corresponding author:

Patrik Rovny
E-mail: patrik.rovny@uniag.sk

DOI:
10.24263/2304-974X-2026-15-3-20

Abstract

Introduction. The EU–Mercosur interim Trade Agreement has applied provisionally since 1 May 2026, changing preferential sugar access. This paper asks whether the four Visegrad (V4) sugar sectors entered the new regime with comparable capacity to absorb competitive pressure.

Materials and methods. Annual 2010–2024 data on beet area, production, yield, consumption and HS1701 trade are assessed using the Trade Specialisation Index (TSI), export/import coverage (CR), self-sufficiency ratio (SSR), trade balance (TB) and an equal-weight min–max Composite Competitiveness Index (CI). Means for 2010–2016 and 2018–2024 are compared with Welch tests; 2017 is treated as a transition year.

Results and discussion. The analysis revealed substantial differences within the V4 sugar sector. In 2024, the Composite Competitiveness Index (CI) reached 0.980 in Poland and 0.731 in Czechia, compared with 0.377 in Slovakia and only 0.097 in Hungary. Poland and Czechia combined high self-sufficiency, positive trade balances and strong export performance, whereas Slovakia showed moderate competitiveness despite maintaining production surpluses. Hungary remained the least competitive country, characterized by import dependence and persistent trade deficits. Following the abolition of EU sugar quotas in 2017, mean CI increased by 36.3% in Poland and 10.6% in Czechia, but declined by 11.6% in Slovakia and 61.3% in Hungary, indicating a widening divergence within the region. Direct sugar trade between the V4 countries and Mercosur remained limited and volatile; however, the integrated nature of the EU sugar market suggests that future impacts of the EU-Mercosur agreement may occur through indirect competitive pressures, price transmission and intra-EU trade adjustments rather than through bilateral imports alone. The results indicate that Poland and Czechia are currently the most resilient sugar producers in the region, while Slovakia occupies an intermediate position and Hungary remains the most vulnerable. These findings provide a useful baseline for assessing future market developments after the implementation of the EU-Mercosur agreement and for evaluating the capacity of individual V4 sugar sectors to adapt to increased international competition.

Conclusions. The EU-Mercosur agreement may affect V4 sugar sectors unevenly. Poland and Czechia show the strongest competitiveness, Slovakia remains moderately resilient, while Hungary is the most vulnerable. Direct Mercosur imports alone do not adequately capture risks within the integrated EU sugar market.

Introduction

The global sugar market is characterised by a strong concentration of production and exports, with Brazil playing a dominant role due to its large-scale sugarcane sector and growing export capacity (OECD-FAO, 2025). The European Union is the world's largest sugar-beet producing region, but its sugar sector has undergone substantial reforms over the past two decades. The 2006 reform reduced institutional support and encouraged restructuring, while the abolition of production quotas in 2017 increased the exposure of growers and processors to market forces. Previous studies suggest that quota removal favoured more efficient production regions and altered trade patterns both within the EU and in international markets (Nolte et al., 2012; Haß, 2022). These changes intensified competition among producers and increased the importance of productivity, processing efficiency and export orientation as determinants of sectoral performance.

These developments are particularly relevant for the Visegrad countries (V4), whose sugar sectors have evolved differently. Poland and Czechia strengthened their production and export performance, Slovakia maintained a smaller but largely self-sufficient sector, whereas Hungary became increasingly dependent on imports. Consequently, the V4 cannot be regarded as a homogeneous production region. Import dependence in a food sector is not merely a statistical feature but a structural vulnerability with policy implications. Evidence from Azerbaijan's food industry shows that even when a processing sector holds significant weight within the broader manufacturing base, heavy reliance on imports to meet domestic demand constrains sustainable growth and requires targeted measures, including internal-market protection and raw-material supply security, to reduce that dependence (Sadikhov, 2024). Hungary's position within the V4 sugar sector, where domestic production covers only a minority of consumption, illustrates the same structural exposure documented in other import-dependent food industries. Differences in sugar beet acreage, processing capacity and trade performance suggest varying abilities to respond to changing market conditions and external competitive pressures. At the same time, the world sugar market is shaped by interactions between agricultural production, energy markets and trade policy. In Brazil, sugarcane can be diverted between sugar and ethanol production, making export availability sensitive to developments in fuel and commodity markets (Serra & Zilberman, 2013). As a result, OECD-FAO (2025) projects a further increase in Brazil's share of global sugar exports, reinforcing its importance as a key supplier in world markets.

The external policy environment changed further with the implementation of the EU-Mercosur Trade Agreement in 2026. The agreement grants duty-free access for 180,000 tonnes of Brazilian raw sugar within an existing WTO quota and establishes a new duty-free quota of 10,000 tonnes for Paraguay (European Commission, 2026a; European Commission, 2026b). Although these volumes represent only around 1.1% of EU sugar production, their economic significance extends beyond direct imports because the European Union functions as an integrated market. Consequently, the effects of Mercosur liberalisation should be assessed not only through bilateral trade flows but also through indirect transmission mechanisms affecting prices, intra-EU trade and processing-capacity utilisation. Sugar imported through refineries or trading hubs in one Member State may influence market conditions across the entire Union, creating indirect competitive pressures even in countries with limited direct imports from Mercosur.

Because sugar trade continues to be influenced by tariffs, quota systems and other policy instruments, competitiveness cannot be captured by a single indicator. Observed trade performance reflects a combination of productivity, market access, processing capacity and policy conditions. For this reason, competitiveness is treated here as a multidimensional

concept rather than being measured solely through comparative-advantage indicators (Balassa, 1965; Vollrath, 1991; Siggel, 2006). A broader assessment is particularly important in the sugar sector, where production self-sufficiency does not necessarily correspond to strong export competitiveness or favourable trade performance.

This distinction between self-sufficiency and broader trade performance echoes a wider concern in food-security research. Cross-country evidence shows that self-sufficiency indicators, share of agriculture in GDP, and food-production levels can move independently of a country's structural capacity to compete internationally, meaning that adequate domestic supply does not automatically translate into resilience against external market pressure (Vasylieva & James, 2021; García-Perez et al., 2023; Belas et al, 2024). The Slovak case in this study, where high self-sufficiency coexists with comparatively weak export performance, illustrates precisely this decoupling.

For decades, the EU sugar sector operated under a system of production quotas, administered prices and border protection (Galović & Bezić, 2019). The abolition of quotas in 2017 marked a major transition towards a more market-oriented environment. Modelling studies predicted that production would expand in competitive regions, while less efficient producers would face greater adjustment pressures (Nolte et al., 2012). Subsequent research has shown that liberalisation may generate uneven outcomes across countries and exporters, redistributing production, trade opportunities and market rents rather than producing uniform gains (Haß, 2022; Kopp et al., 2016). Consequently, countries characterised by higher productivity, stronger processing industries and export surpluses are expected to be more resilient than import-dependent producers. These findings suggest that the effects of future trade liberalisation are likely to differ substantially among individual V4 countries.

The dataset used in this study covers the period 2010-2024 and therefore predates the implementation of the EU-Mercosur agreement. Rather than estimating its actual effects, the study establishes a pre-liberalisation benchmark and evaluates whether V4 sugar sectors entered the new trade regime from comparable competitive positions. The analysis combines indicators of production, trade performance and self-sufficiency within a single analytical framework, compares developments before and after the abolition of EU sugar quotas by contrasting the periods 2010-2016 and 2018-2024, and evaluates potential exposure to Mercosur competition through both bilateral trade relations and broader EU market integration. The objective is not to simulate the agreement itself but to identify which V4 sugar sectors entered the post-2026 environment with stronger competitive buffers and greater adaptive capacity. Furthermore, the study provides a baseline for future assessments of how the EU-Mercosur agreement may influence competitiveness, trade flows and market resilience in the Central European sugar sector.

Materials and methods

Data and scope

The empirical analysis covers Czechia, Hungary, Poland and Slovakia for 2010–2024. Foreign trade is defined at Harmonised System heading HS1701 (cane or beet sugar and chemically pure sucrose, in solid form). Trade values were drawn from Eurostat and cross-checked against ITC Trade Map / UN Comtrade series used in the original dataset. Sugar-beet area, beet production and yield were obtained from the national statistical offices of the four V4 countries. Sugar production and consumption information used to calculate self-sufficiency was compiled from FAOSTAT, OECD–FAO and national sources. The data

horizon ends in 2024 because it is the latest complete common year in the assembled dataset and predates the 2026 implementation of the EU–Mercosur interim Trade Agreement.

The analysis deliberately retains HS1701 rather than attempting to isolate only refined white sugar. This is consistent with the original trade dataset but requires careful interpretation because HS1701 includes both cane and beet sugar and other solid sucrose categories. The indicator set therefore describes sector-level trade competitiveness, not the profitability of a single sugar product or factory.

Competitiveness indicators

The Trade Specialisation Index (TSI) measures whether a country is export- or import-oriented in HS1701:

$$TSI = (X - M) / (X + M)$$

where X is the value of HS1701 exports and M is the value of HS1701 imports. TSI ranges from −1 to +1; positive values indicate net export specialisation.

Export/import coverage (CR) measures the extent to which exports finance imports:

$$CR = (X / M) \times 100$$

Values above 100% indicate that exports exceed imports. The trade balance (TB) is calculated as X − M and is reported in million EUR.

The self-sufficiency ratio (SSR) measures the relationship between domestic sugar production (P) and domestic sugar consumption (C):

$$SSR = (P / C) \times 100$$

Values above 100% indicate a production surplus relative to domestic use. Because self-sufficiency and trade competitiveness capture different dimensions, both are retained in the analysis.

A Composite Competitiveness Index (CI) combines TSI, CR, SSR and TB. Each indicator is min–max normalised over the 2010–2024 V4 panel, $z = (x - xmin)/(xmax - xmin)$, and the four normalised indicators are averaged with equal weights. Higher values represent a stronger relative combination of export orientation, import coverage, self-sufficiency and trade surplus. The equal-weight construction is transparent but not presented as a unique structural measure of competitiveness; robustness is assessed by checking whether the country ordering is also visible in the underlying indicators.

Structural comparison around the 2017 quota abolition

To increase the analytical value beyond a year-by-year description, the study compares two seven-year windows: 2010–2016 (pre-abolition) and 2018–2024 (post-abolition). The year 2017 is excluded because the quota system ended during that year and is treated as a transition period. For each country, mean TSI, CR, SSR, TB and CI are compared between the two windows. Welch two-sample t-tests are used as an exploratory test because the annual series are short and variances may differ. These p-values are interpreted as descriptive evidence of structural change, not as causal estimates: annual observations may be serially correlated and other shocks, including weather, energy prices and the COVID-19 period, are not controlled for.

Exposure to Mercosur and limitations

Direct exposure is measured from bilateral HS1701 trade between the V4 and Argentina, Brazil, Paraguay and Uruguay. Systemic exposure is interpreted conceptually:

because the EU single market transmits price and trade shocks across Member States, a country can be affected without recording large direct imports from Mercosur. This distinction is particularly important after 1 May 2026, when the new preferences began to apply.

Four limitations should be noted. First, the study provides a pre-implementation baseline and cannot identify the realised effect of the 2026 agreement. Second, HS1701 is broader than refined sugar. Third, the CI depends on min–max scaling and equal weights, so it is best interpreted as a comparative summary rather than an absolute measure. Fourth, the dataset does not include plant-level costs, sugar-factory capacity utilisation, contract prices or farm profitability. These variables would be necessary for a complete microeconomic impact assessment.

Results and discussion

Production base and demand

The area of sugar beet is one of the most important factors influencing the production potential of the sugar sector. The level of cultivated areas determines the volume of sugar beet production, the utilization of sugar factories' processing capacities and, to a large extent, the self-sufficiency of countries in sugar production.

The largest sugar beet grower in the V4 countries was Poland throughout the entire period under review. The area increased from 206,225 ha in 2010 to 277,920 ha in 2024. After a slight decrease between 2013 and 2015, there was a significant increase after 2017, when EU sugar production quotas were abolished, creating more scope for production to respond to market conditions. Particularly significant growth was recorded between 2017 and 2021, when the area increased from 231,716 ha to 250,570 ha. The highest value was recorded in 2024.

A similar development can be observed in the Czech Republic. The area of sugar beet increased from 56,388 ha in 2010 to 65,910 ha in 2024. The growth was relatively continuous until 2017, when the maximum value of 66,101 ha was reached. Subsequently, there was a slight reduction in the sown areas, but growth began again from 2023. The Czech Republic maintained a stable position as the second largest sugar beet producer within the V4 throughout the entire monitored period.

In Slovakia, the development of the area of sugar beet was relatively stable. While in 2010 the area was 17,932 ha, in 2024 it reached 23,550 ha. Growth was recorded mainly in the period from 2010 to 2017, when the area increased by more than 4 thousand hectares. In the years from 2018 to 2022, the cultivation areas fluctuated around the level of 20 to 22 thousand ha, while in 2022 there was a temporary decrease to 19,480 ha. Subsequently, growth was recorded again and in 2024 the highest value was reached during the entire monitored period.

The most significant fluctuations in the area were recorded in Hungary. Between 2010 and 2013, the area gradually increased from 13,859 ha to 18,810 ha, which was the maximum of the entire monitored period. However, there was a significant decrease afterwards, and in 2022 only 9,710 ha were recorded, which was the lowest value of all years. From 2023, the area under cultivation grew again, and in 2024 the area reached 16,130 ha. The development indicates a higher sensitivity of the Hungarian sugar sector to economic and market conditions compared to other V4 countries.

Sugar beet production is one of the key performance indicators of the sugar sector, as it directly affects the volume of raw material available for sugar production. The development of production is determined not only by the extent of cultivated areas, but also by the yields achieved per hectare, the course of the weather and the technological level of cultivation.

In 2010, Poland produced 9,972.6 thousand tons of sugar beet. During the period under review, a significant increase in production was recorded, accompanied by some year-on-year fluctuations. The decline was recorded mainly in 2015, when production reached 9,364.5 thousand tons, which represented the lowest value of the entire period. However, production subsequently grew again and after 2017, it expanded significantly. In 2024, production reached a record 18,430.3 thousand tons. Compared to 2010, this represented an increase of 8,457.7 thousand tons and the 2024/2010 index reached 184.81%. Sugar beet production in Poland thus increased by approximately 85% over the period under review.

The second largest producer was the Czech Republic. Production increased from 3,065.0 thousand tons in 2010 to 4,584.7 thousand tons in 2024. During the monitored period, production mostly ranged from 3.5 to 4.5 million tons. Significant growth was recorded in particular in 2014, 2017 and 2024, with 2024 representing the highest production value in the entire time series. The growth index reached 149.58%, which means an increase in production by almost 50% compared to 2010.

Slovakia showed a relatively stable development during the monitored period with some fluctuations caused by weather conditions and yield fluctuations. Production ranged from a minimum of 894.5 thousand tons in 2012 to a maximum of 1,550.2 thousand tons in 2014. In 2024, production reached a level of 1,388.7 thousand tons. Compared to 2010, when production amounted to 977.7 thousand tons, this is an increase of 411 thousand tons. The 2024/2010 index reached 142.04%, which represents an increase of approximately 42%.

The Hungarian economy was the smallest producer throughout the period. Sugar beet production was also characterized by the highest degree of fluctuation. After a gradual increase to a maximum of 1,121.2 thousand tons in 2016, there was a decline, which culminated in 2022 with a production of only 470.2 thousand tons. In the following years, however, the sector partially recovered and in 2024 production reached 856.3 thousand tons. Despite significant fluctuations, production in 2024 was slightly higher than in 2010. The growth index reached 104.57%, which represents an increase in production of only 4.57%.

In terms of growth dynamics, the highest index was achieved in Poland, where production increased almost twice the original level. The second-strongest production growth was recorded in the Czech Republic, followed by Slovakia. Hungary showed only minimal production growth, with significant fluctuations indicating higher instability of the sector compared to other V4 countries.

The total sugar beet production in all V4 countries together increased from 14.83 million tonnes in 2010 to 25.26 million tonnes in 2024 (Table 1). This represents an increase of more than 10.4 million tonnes and an index of 170.35%. The results show a significant strengthening of the production base of the V4 sugar sector in the period under review, with Poland and partly the Czech Republic being the main drivers of growth. The development also suggests that after the abolition of sugar quotas in 2017, the most competitive producers were able to expand production and increase their position in the European sugar market.

Sugar beet yield is one of the most important indicators of cultivation efficiency, as it reflects the level of utilization of the production potential of the soil, the quality of agricultural technology, the course of weather conditions and the technological maturity of growers. High yields per hectare have a direct impact on the economics of sugar beet cultivation and consequently on the competitiveness of the entire sugar sector.

Table 1

Sugar beet area and production in V4 countries, 2010 and 2024

Country	Area 2010 (ha)	Area 2024 (ha)	Beet production 2010 (kt)	Beet production 2024 (kt)
Czechia	56,388	65,910	3,065.0	4,584.7
Slovakia	17,932	23,550	977.7	1,388.7
Hungary	13,859	16,130	818.9	856.3
Poland	206,225	277,920	9,972.6	18,430.3

Source: national statistical offices of the V4 countries; original dataset; own compilation.

The Czech Republic achieved the highest stability and, at the same time, the highest average yields during the monitored period. The yield increased from 54.36 t ha^{-1} in 2010 to 69.56 t ha^{-1} in 2024. During most of the monitored period, Czech yields were above 60 t ha^{-1}, with the maximum value recorded in 2014 (70.28 t ha^{-1}). High values were also recorded in 2021, 2022 and 2024, which confirms the long-term stability of Czech sugar beet cultivation.

Slovakia has experienced more significant yield fluctuations. The lowest value was recorded in 2012, when the yield reached only 45.31 t ha^{-1}. On the contrary, the maximum was recorded in 2016 at 70.15 t ha^{-1}. After 2018, yields stabilized mainly in the interval of 56 to 64 t ha^{-1}. In 2024, the yield reached 58.97 t ha^{-1}, which represented a slight increase compared to 2010.

In Hungary, the development of yields was most affected by year-on-year fluctuations. In the period from 2014 to 2017, yields reached very high values, exceeding 67 t ha^{-1}, and in 2016 they reached a maximum of 70.09 t ha^{-1}. However, a significant decrease subsequently occurred, with the lowest yields recorded in 2012 (47.10 t ha^{-1}) and in 2022 (48.42 t ha^{-1}). Hungary ended 2024 with a yield of 53.09 t ha^{-1}, i.e. at a level lower than most other V4 countries.

Poland has shown continuous growth in sugar beet productivity over the period under review. The yield increased from 48.36 t ha^{-1} in 2010 to 66.32 t ha^{-1} in 2024. 2014 was a particularly favourable year, when a yield of 68.25 t ha^{-1} was recorded. In the last years of the period under review, yields have been steadily above 60 t ha^{-1}, which has significantly contributed to the growth of sugar beet production in the country.

The results show that the highest growth in per hectare yields was recorded in Poland, where the yield increased by more than 37%. Significant growth was also recorded in the Czech Republic, where the index reached almost 128%. Slovakia recorded a moderate growth of 8.16%. The only country that achieved a lower yield in 2024 than in 2010 was Hungary, where the index was 89.85%.

Despite growing criticism of the excessive consumption of simple sugars, sugar remains a significant part of the food basket of the population in all V4 countries. The development of sugar consumption per capita in the period from 2010 to 2024 is presented in Table 4. The data show that the highest consumption was achieved in Poland throughout the entire period under review, while the lowest values were recorded in Hungary and Slovakia. At the same time, different development trends can be observed between individual countries.

Poland was the country with the highest per capita sugar consumption throughout the entire period under review. In 2010, consumption amounted to 39.9 kg·inhabitant^{-1}·year^{-1} and in the following years it showed a predominantly increasing trend. The maximum was reached in 2018, when consumption reached 47.0 kg·inhabitant^{-1}·year^{-1}. In the following years, consumption decreased slightly and in 2024 it amounted to 39.8 kg·inhabitant^{-1}·year^{-1}. Compared to 2010, it remained practically at the same level, with the 2024/2010 index reaching 99.75%.

The development in the Czech Republic was relatively stable. Consumption ranged between 35 and 37 kg·inhabitant^{-1}·year^{-1} for most of the monitored period. The highest value was recorded

in 2017 (36.8 kg·inhabitant^{-1}·year^{-1}), while after 2021 there was a more significant decrease. In 2024, consumption reached 30.8 kg·inhabitant^{-1}·year^{-1}. Compared to 2010, this is a decrease of 4.7 kg per capita, with the 2024/2010 index representing 86.76%.

In Slovakia, sugar consumption showed a slightly decreasing trend throughout the period. In 2010, it amounted to 34.3 kg·inhabitant^{-1}·year^{-1}, while in the following years it fluctuated mainly between 29 and 32 kg·inhabitant^{-1}·year^{-1}. The highest value was recorded in 2010, while the lowest in 2024, when consumption fell to 28.9 kg·inhabitant^{-1}·year^{-1}. Compared to the base year, there was a decrease of 5.4 kg per capita, with the 2024/2010 index reaching a value of 84.26%.

A different development was recorded in Hungary. Sugar consumption at the beginning of the monitored period was below 30 kg·inhabitant^{-1}·year^{-1}, while in 2010 it reached 29.2 kg·inhabitant^{-1}·year^{-1}. Subsequently, there was a gradual increase, while after 2014 consumption stabilized at a level of approximately 30 to 32 kg·inhabitant^{-1}·year^{-1}. In 2024, it reached 32.1 kg·inhabitant^{-1}·year^{-1}, which represents the highest level of the monitored period. Compared to 2010, consumption increased by 2.9 kg per capita and the 2024/2010 index reached 109.93%, which represents the only increase in consumption among the V4 countries.

From a long-term perspective, it can be stated that sugar consumption has been decreasing or stagnating in most V4 countries. The most significant decline was recorded in Slovakia and the Czech Republic, while Poland maintained a stable level of consumption. The only country that recorded an increase in consumption was Hungary.

When comparing countries for 2024, the highest consumption was recorded in Poland (39.8 kg·inhabitant^{-1}·year^{-1}), followed by Hungary (32.1 kg·inhabitant^{-1}·year^{-1}), the Czech Republic (30.8 kg·inhabitant^{-1}·year^{-1}) and Slovakia (28.9 kg·inhabitant^{-1}·year^{-1}). The difference between the country with the highest and lowest consumption was 10.9 kg per capita. The results indicate that despite common historical and economic conditions, there are significant differences in consumer behavior and demand for sugar among the V4 countries. These differences subsequently affect the size of the domestic market, the degree of self-sufficiency, the creation of production surpluses and the position of individual countries in international sugar trade.

Table 2

Sugar beet yields and sugar consumption in V4 countries, 2010 and 2024

Country	Yield 2010 (t/ha)	Yield 2024 (t/ha)	Sugar consumption 2010 (kg/cap.)	Sugar consumption 2024 (kg/cap.)
Czechia	54.36	69.56	35.5	30.8
Slovakia	54.52	58.97	34.3	28.9
Hungary	59.09	53.09	29.2	32.1
Poland	48.36	66.32	39.9	39.8

Source: national statistical offices of the V4 countries; original dataset; own compilation.

From a regional perspective, it can be stated that the V4 countries have a strong production base for sugar production. Poland and the Czech Republic in particular are among the major producers of sugar beet within the European Union and have been increasing their competitiveness in the long term. Slovakia, despite its smaller area, maintains stable production and good harvest levels. On the contrary, the Hungarian sugar sector is more sensitive to changes in the market and production environment.

Direct V4–Mercosur sugar trade

Mercosur countries, the HS 1701 commodity group was analyzed, which includes cane and beet sugar, chemically pure sucrose and other products belonging to the sugar group. For this reason, the presented results do not include exclusively refined sugar trade, but capture the total trade exchange of products of the sugar commodity group.

The analyzed data show that the trade of the V4 countries with Mercosur countries was characterized by a significant imbalance between imports and exports during the years 2010 to 2024. While imports of HS 1701 products from Mercosur to the V4 countries reached several million in some years, exports from the V4 countries to Mercosur countries remained only marginal throughout the entire period. Trade relations were thus predominantly one-sided in favor of the Mercosur countries.

The most significant importer of HS 1701 products was Poland. In 2010, the value of imports amounted to only 1.2 thousand EUR, but in 2011 it increased to more than 10.4 million EUR. The peak of imports was recorded in 2013, when the value of imports reached approximately 18.7 million EUR. After a subsequent decline, imports increased again in 2017, 2020 and 2023. In 2023, the value of imports reached approximately 12.9 million EUR and in 2024 it amounted to 418 thousand EUR. The development indicates significant volatility of trade flows, which may be associated with the current situation on the sugar market, price developments and the need to secure additional volumes of raw materials for the domestic processing sector.

Czechia became a more visible importer from Mercosur in the later years of the series. Imports were negligible or irregular in the first half of the period, but rose to EUR 4.7 million in 2021 and EUR 9.7 million in 2022 before falling sharply again. The pattern is therefore better described as episodic than as a stable dependence on South American sugar.

A different situation was recorded in Slovakia. Imports of HS 1701 products from Mercosur countries were practically non-existent during the analyzed period. After isolated trade operations recorded before 2010, Slovak imports remained minimal and did not reach significant values during the monitored period. This development indicates a high orientation of the Slovak market towards the internal market of the European Union and minimal dependence on supplies from South American countries.

A similar trend was also observed in Hungary. Significant trade transactions were only recorded at the beginning of the period under review. In 2010, imports were practically non-existent, but in 2011 they reached approximately EUR 9.2 million and in 2012 more than EUR 5.6 million. This period was followed by a sharp decline and import values remained negligible for most of the years 2013 to 2024. Compared to Poland and the Czech Republic, the importance of Mercosur countries for the Hungarian sugar market was significantly lower.

In the case of exports of HS 1701 products from the V4 countries to the Mercosur countries, only isolated trade transactions were recorded. Exports reached very low values throughout the period, often at the level of several tens or hundreds of euros. The most significant exporter was Poland, but even in its case, exports to the Mercosur countries did not represent a significant trade activity. Slovakia, the Czech Republic and Hungary showed zero or only symbolic exports in most years.

From a regional perspective, it can be stated that trade with Mercosur countries represented only a marginal part of the total foreign trade in sugar and sugar products for the V4 countries. At the same time, however, the growing importance of imports can be identified, especially for Poland and the Czech Republic. The results also confirm a significant trade asymmetry between the two regions, as Mercosur countries act mainly as

suppliers of sugar to the V4 market, while exports from the V4 countries to South America remain negligible.

As a result of significantly higher imports than exports, the V4 countries had a negative trade balance with Mercosur throughout the period under review. Despite the persistent deficit, the total financial volumes of trade remained relatively low compared to the total sugar trade within the European Union.

Mercosur countries cannot currently be considered as decisive trading partners of the V4 countries in the sugar sector. Most trade flows are oriented towards the internal market of the European Union, where the dominant part of exports and imports of sugar and sugar products is realized.

The results show that Brazil clearly occupies a dominant position in trade exchange, while the importance of other Mercosur countries remains relatively low.

Data for the entire period under review show that the majority of imports of sugar and sugar products into the V4 countries came from Brazil. In individual years, Brazil's share of total imports was very high and in some years it represented practically the only trading partner of the V4 countries within Mercosur. Significant values of imports from Brazil were recorded especially in 2011 (19.68 million EUR), 2013 (18.74 million EUR), 2023 (12.90 million EUR) and 2024 (2.66 million EUR). These results are logical given the fact that Brazil is the largest producer and exporter of sugar in the world and has significant comparative advantages in the production of sugar from sugar cane.

Argentina was the second most visible partner, but its role was far below Brazil’s and highly irregular. The strongest values were concentrated in a few years, whereas Paraguay and Uruguay remained marginal. This concentration matters because the relevant external competitive shock is overwhelmingly Brazilian rather than evenly distributed across Mercosur.

Paraguay's position was only marginal throughout the period under review. Imports were recorded only sporadically, reaching a peak of approximately EUR 13.7 thousand in 2012. In recent years, trade operations have been minimal or non-existent. Nevertheless, it should be noted that Paraguay is a major producer of organic cane sugar, which is mainly aimed at specialized market segments.

During most of the monitored period, practically no trade in products of the HS 1701 group was recorded. The only significant trade operation was the import in 2018 worth approximately 8.8 thousand EUR. Therefore, from the perspective of the V4 countries, Uruguay cannot be considered a significant trading partner in the sugar sector.

Exports of HS 1701 products from the V4 countries to Mercosur countries were negligible throughout the period. If exports were made, they were mainly directed to Brazil or Argentina, with their values reaching only symbolic levels. In the case of Paraguay and Uruguay, exports were practically zero. This situation confirms the one-sidedness of trade relations between the analyzed regions.

To better assess the territorial structure of trade, it can be stated that more than 90% of the total value of sugar and sugar products imports from Mercosur countries to the V4 region were realized via Brazil. Argentina played a complementary role, while Paraguay and Uruguay were of only marginal importance. The results therefore confirm that the potential impacts of the EU–Mercosur agreement on the sugar sector of the V4 countries will depend to a decisive extent on the development of trade relations with Brazil.

From the perspective of further analysis, this finding is extremely important. Although the agreement applies to the entire Mercosur bloc, real trade flows in the sugar sector are concentrated almost exclusively in one country. The potential increase in imports after the implementation of the agreement will therefore not represent pressure from the entire

Mercosur region, but primarily from the Brazilian sugar sector, which is among the most competitive in the world. Such a concentration of trade flows also increases the sensitivity of the V4 market to possible changes in production, export policy or price developments in Brazil.

The original bilateral series therefore supports two simultaneous conclusions. Direct V4 dependence on Mercosur sugar was limited before implementation of the 2026 agreement, but Brazil dominated the transactions that did occur. The first result tempers claims of an immediate physical import shock; the second identifies the supplier most capable of transmitting a price shock when preferential access improves.

Table 3

Selected direct HS1701 import values from Mercosur into the V4 (EUR)

Year	Czechia	Slovakia	Hungary	Poland
2011	0	0	9,206,829	10,477,196
2013	0	0	0	18,739,660
2017	1,043,501	0	0	0
2021	4,680,862	0	2	119,667
2022	9,727,783	0	295	469,524
2023	127,541	0	0	12,904,749
2024	2,243,164	0	0	418,317

Source: Eurostat 2026;
values reproduced from the original V4–Mercosur dataset.

Trade competitiveness and self-sufficiency

Sugar is one of the traditional agricultural commodities of the V4 countries, and the importance of the sector is determined not only by the production potential of sugar beet cultivation, but also by the ability to assert itself on international markets. The competitiveness of the sugar sector can be assessed through business performance, export orientation, production self-sufficiency and the ability to create trade surpluses. In the conditions of a globalized market, the ability of producers to respond to growing competition from low-cost producers, primarily from Brazil and other Mercosur countries, also plays a significant role.

The Trade Specialisation Index (TSI) identifies the degree of export or import orientation of a country. Values close to +1 indicate strong export specialisation, while values close to −1 signal dependence on imports.

The 2024 results show significant differences between the V4 countries. The highest TSI value was achieved by Poland (0.78), followed by Czechia (0.60). Both countries thus stand out as significant net exporters of sugar. Moreover, Poland significantly strengthened its position during the monitored period, when the value of exports increased from 186.58 million EUR in 2010 to 655.14 million EUR in 2024. Similarly, Czechia has been showing a stable positive trade balance and a strong export orientation for a long time.

Slovakia achieved a TSI of only 0.03 in 2024, indicating almost balanced trade. Although the country remained a net exporter, its trade performance weakened more significantly compared to Czechia and Poland. In contrast, Hungary achieved a TSI of −0.51, the lowest level among the V4 countries. Negative TSI values since 2011 point to long-term import dependence and loss of competitiveness of the Hungarian sugar sector.

In the long term, the results indicate a widening gap between the countries in the region. While Poland and Czechia are consolidating their position as competitive exporters, Slovakia is stagnating and Hungary is becoming increasingly dependent on foreign sugar supplies.

The export-import coverage ratio is an important indicator of a country's trade performance and ability to finance imports through its own exports.

The best results were achieved by Poland, where exports covered imports at a level of approximately 803% in 2024. This means that Polish sugar exports were more than eight times higher than imports. Czechia also showed favourable results, with export/import coverage reaching approximately 405%. In both cases, these are values characteristic of highly competitive export-oriented sectors.

Slovakia achieved an import-export coverage of approximately 107% in 2024, which represents only a minimal surplus above the trade balance threshold. The development also shows increasing volatility in foreign trade, with the trade balance even being negative in 2020 and 2023.

Hungary recorded the worst results. In 2024, exports covered only about 32% of the value of imports. Such low values indicate the country's high dependence on foreign supplies and the low competitiveness of the domestic sector.

The results obtained confirm that Poland and Czechia have stable export performance, while Slovakia and especially Hungary show a lower ability to assert themselves in international markets.

An important indicator of production resilience is the Self-Sufficiency Ratio (SSR), which expresses a country's ability to cover domestic sugar consumption with its own production. The 2010–2024 results show substantial differences across the V4. Czechia recorded the highest and most stable self-sufficiency, producing substantially more sugar than it consumed domestically throughout the period. Its SSR increased from 114.9% in 2010 to 191% in 2024. In 2024, sugar production reached 641.86 thousand tonnes while domestic consumption was 336.03 thousand tonnes, implying a surplus of more than 305 thousand tonnes. This confirms the strong production base of the Czech sugar sector and its long-term export orientation.

Trade balance of V4 countries in sugar trade (HS 1701)

The development of the trade balance indicates significant differences between the individual V4 countries. The most stable and long-term highest positive trade balance was achieved by Poland, which throughout the entire monitored period was profiled as the most important producer and exporter of sugar in the Central European region. The high production capacities of the Polish sugar industry allowed for the creation of significant export surpluses, which were reflected in positive values of the trade balance. The development also indicates a growing strengthening of the export orientation of the Polish sector after the abolition of sugar quotas in the EU.

Relatively positive developments can also be observed in the case of Czechia. The Czech sugar sector maintained a positive trade balance for most of the period under review, reflecting a relatively high level of production self-sufficiency and the ability to export to foreign markets. Although the size of the trade surplus lagged behind Poland, Czechia demonstrated a stable competitive position within the regional market.

Slovakia showed a significantly more volatile development. In the first years of the monitored period, the trade balance fluctuated around balanced values, with some years also recording slight surpluses. However, the increasing dependence of the domestic market on imports gradually became apparent, which was related to limited production capacities and a lower production base compared to Poland and Czechia. The result was lower and less stable values of the trade balance.

Hungary performed the worst. After the restructuring of the sugar sector in previous decades, the country became heavily dependent on sugar imports. The trade balance was therefore negative in most years, which documents the weakened competitiveness of the Hungarian sugar industry and its limited ability to generate export surpluses.

When assessing the entire period, it can be stated that the trade balance confirms the existence of a significant differentiation of the sugar sectors of the V4 countries. While Poland and Czechia act as net exporters of sugar and have sufficient production potential to satisfy both domestic needs and foreign demand, Slovakia shows a transitional position and Hungary is among the countries with high import dependence.

The position of the V4 countries towards potential competition from Mercosur

The results indicate that the most competitive sugar sectors throughout the period under review were Poland and Czechia. This pattern is consistent with broader evidence that national resilience to economic shocks is closely linked to a country's competitive position within international trade. A methodology measuring resilience through industrial-portfolio performance finds a direct mathematical correlation between national resilience and competitiveness, indicating that sectors capable of compensating losses in one trade channel with gains in another display significantly stronger resistance to external disruption (Montrimas et al., 2024). Applied to the sugar sector, this suggests that Poland's and Czechia's export diversification and processing scale function as structural buffers against the type of shock the EU-Mercosur opening represents. While Czechia showed a high and relatively stable level of competitiveness since the beginning of the period under review, Poland saw a significant strengthening of its position, especially after 2017. The index value in Poland increased from 0.434 in 2010 to 0.980 in 2024, which was related to the growth of production, export performance and trade surpluses.

The Czechia maintained stable index values throughout the period, mostly in the range of 0.50 to 0.60. In 2024, it reached a value of 0.731, confirming its strong position among export-oriented sugar producers in Central Europe.

Slovakia showed a medium level of competitiveness. The index values ranged from approximately 0.33 to 0.45, reflecting a relatively high level of production self-sufficiency, but also lower export performance and weaker trade results compared to Czechia and Poland. At the same time, the development of the index in Slovakia was significantly more stable than in the other countries.

The lowest values were recorded in Hungary. After 2014, there was a systematic weakening of the competitiveness of the sector, with the minimum being reached in 2022 (0.017). The low values of the index reflect a combination of low production self-sufficiency, persistent dependence on imports and long-term unfavorable trade results.

Long-term average CI values place Poland and Czechia at the top of the V4. Their mean values over 2010–2024 were relatively close, but Poland showed more dynamic growth in production and trade indicators in recent years and therefore entered 2024 in the leading position. Czechia ranked second, supported by high self-sufficiency, a stable trade surplus and persistent export orientation.

A significant gap can be observed between Czechia and Slovakia. The average index value in Slovakia reached only 69% of Czechia's level and approximately 67% of the Polish level. Despite the high self-sufficiency of the Slovak sector, its international competitiveness remains limited by a lower degree of export orientation and a smaller scale of production.

The lowest value of the index was achieved by Hungary. The average competitiveness index was only a quarter of the Slovak level and less than a third of the level achieved by Poland and Czechia. The results thus point to significant structural problems in the Hungarian sugar sector.

Table 4

Competitiveness indicators in 2024

Country	TSI	Export/import coverage (%)	SSR (%)	Trade balance (EUR million)	CI
Czechia	0.60	405	191	221.34	0.731
Slovakia	0.03	107	124	4.39	0.377
Hungary	-0.51	32	39	-130.96	0.097
Poland	0.78	803	177	573.53	0.980

Source: Eurostat and own calculations based on the original dataset.

Table 5

Composite Competitiveness Index (CI), 2010–2024

Year	Czechia	Slovakia	Hungary	Poland
2010	0.473	0.356	0.280	0.434
2011	0.541	0.390	0.234	0.407
2012	0.536	0.425	0.250	0.528
2013	0.538	0.408	0.260	0.518
2014	0.545	0.419	0.145	0.467
2015	0.505	0.445	0.134	0.516
2016	0.560	0.392	0.121	0.479
2017	0.566	0.416	0.175	0.657
2018	0.558	0.358	0.162	0.666
2019	0.522	0.352	0.089	0.542
2020	0.499	0.333	0.087	0.557
2021	0.559	0.381	0.055	0.664
2022	0.610	0.352	0.017	0.459
2023	0.612	0.353	0.044	0.695
2024	0.731	0.377	0.097	0.980

Source: own calculations from TSI, CR, SSR and TB.

On the basis of the long-term CI and the underlying indicators, the relative resilience ordering is Poland and Czechia at the top, Slovakia in an intermediate position, and Hungary substantially below the other three countries.

This ranking confirms that Poland and Czechia are best placed to cope with a potential increase in sugar imports from Mercosur. Slovakia has a relatively favourable production base, but weaker trade performance. The most vulnerable sector within the V4 remains Hungary, which, due to its low level of self-sufficiency and high dependence on imports, is most exposed to the potential negative consequences of trade liberalisation between the EU and Mercosur.

Structural comparison before and after the 2017 quota abolition

The window comparison adds a structural perspective to the year-by-year results. Poland's average CI rose from 0.478 in 2010–2016 to 0.652 in 2018–2024, an increase of 36.3%. Czechia also improved, from 0.528 to 0.584 (+10.6%). By contrast, Slovakia declined from 0.405 to 0.358 (−11.6%) and Hungary from 0.203 to 0.079 (−61.3%). Welch tests

indicate statistically significant differences for Poland, Slovakia and Hungary at the 5% level; the Czech change is positive but not statistically significant in this short annual sample.

The underlying indicators explain these movements. In Poland, post-2017 mean export/import coverage increased by about 76% relative to the 2010–2016 mean and mean SSR rose from approximately 104% to 137%. Czechia strengthened its TSI and import coverage while remaining strongly self-sufficient. Slovakia moved in the opposite direction in trade performance: mean TSI fell from about 0.21 to 0.04 and mean export/import coverage from 157% to 110%, even though mean SSR increased slightly. Hungary combined a deterioration in trade specialisation with a decline in mean self-sufficiency from 45% to 36%.

These results are consistent with the mechanism anticipated in earlier EU sugar-market research: once quota constraints are removed, production can concentrate in more competitive regions (Nolte et al., 2012; Haß, 2022). The analysis does not prove that quota abolition caused every observed change, but it shows that the previous market reform widened rather than closed the competitiveness gap within the V4. This is directly relevant to the 2026 trade opening because external competition enters a region whose internal capacity to absorb shocks is already uneven.

Table 6

Mean CI before and after EU sugar quota abolition

Country	2010–2016 mean	2018–2024 mean	Change	Change (%)	Welch p-value
Czechia	0.528	0.584	+0.056	+10.6	0.110
Slovakia	0.405	0.358	-0.047	-11.6	0.004
Hungary	0.203	0.079	-0.125	-61.3	0.002
Poland	0.478	0.652	+0.173	+36.2	0.034

Source: own calculations. 2017 excluded as a transition year. Tests are exploratory and do not establish causality.

Implications of the 2026 EU–Mercosur trade opening

The direct-trade data could be read as evidence that the V4 has little to fear from Mercosur because bilateral flows were small. Such an interpretation is incomplete. The European Commission's 2026 sugar provisions are EU-wide, not V4-specific, and the common market allows imported sugar to affect price formation and intra-EU allocation. The appropriate question is therefore not simply "how much Brazilian sugar enters each V4 country?" but "how capable is each national sector of remaining competitive if the EU-wide price and trade environment changes?"

Poland enters this environment with the strongest combination of scale, export orientation and improving self-sufficiency. Its 2024 beet production was about 18.4 million tonnes, TSI 0.78, export/import coverage 803% and CI 0.980. These values do not eliminate exposure to price pressure, but they provide more room for adjustment through exports, processing scale and domestic supply.

Czechia has a smaller production base but similarly strong indicators. This connects to a broader finding in food-manufacturing competitiveness research: functional integration across procurement, processing, and distribution stages shows a significant positive relationship with firms' competitive advantage, independent of overall production scale (Mogaka et al., 2022). This is consistent with Czechia's profile in the present analysis, where

high self-sufficiency and processing efficiency, rather than sheer production volume, appear to underpin its trade resilience relative to Poland. A 2024 yield of 69.56 t/ha, SSR of 191%, export/import coverage of 405% and CI of 0.731 indicate a substantial buffer. The main difference from Poland is scale: the Czech sector is competitive but less able to influence regional trade volumes.

Slovakia is more ambiguous. Its 2024 SSR of 124% indicates that domestic production can cover consumption, yet TSI was only 0.03 and export/import coverage 107%. This is precisely why self-sufficiency should not be used as a synonym for competitiveness. A sector can produce enough sugar for its own market and still possess limited capacity to absorb a sustained external price shock through exports.

Hungary is structurally different. In 2024, SSR was only 39%, TSI −0.51, export/import coverage 32% and CI 0.097. Because the country is already import-dependent, the immediate effect of cheaper imported sugar may not be a loss of a large export surplus; the more relevant concern is whether remaining domestic beet and processing capacity can be maintained when price competition intensifies.

The trade agreement should also be placed in scale. The duty-free treatment for 180,000 tonnes of Brazilian raw cane sugar under the existing quota, plus 10,000 tonnes for Paraguay, is limited relative to total EU production (European Commission, 2026b). This argues against dramatic "market flooding" narratives. At the same time, sugar-market models show that even constrained preference changes can alter trade diversion and price relationships when the EU market is integrated (Haß, 2022). The practical transmission of any preferential trade opening also depends on customs and logistics efficiency at the point of entry. Evidence on cross-border logistics performance shows that customs clearance efficiency and supply chain coordination are significant determinants of how effectively trade flows translate into competitive pressure, with institutional quality further amplifying the returns to logistics performance in cross-border trade integration (Njuguna et al., 2025). This suggests that the speed and consistency with which the new Mercosur sugar quotas are administered at EU entry points, not only their nominal volume, will shape how quickly price pressure reaches V4 producers. A nuanced interpretation is therefore more defensible than either alarmism or dismissal. How this moderate exposure is absorbed will depend partly on the governance arrangements linking beet growers, processors, and downstream buyers. Evidence from agricultural supply chains subject to external trade pressure shows that price-stabilisation mechanisms, certification requirements, and supplier-level stewardship provisions can reduce input-price volatility and cushion producers against competitive shocks, but only where compliance costs are shared across the chain rather than imposed unilaterally on growers (Tyozenda & Ahemen, 2025). This points to a further monitoring dimension beyond trade statistics: how contract and pricing arrangements between V4 beet growers and processors evolve once Mercosur preferences take effect.

Discussion

The results confirm substantial heterogeneity within the V4 sugar sector. Poland and Czechia achieved consistently higher competitiveness, while Slovakia showed relatively strong production self-sufficiency but weaker trade performance, and Hungary remained the least competitive among the analyzed countries. Similar patterns of divergence following CAP reforms and market liberalization have been identified by Swinnen and Van Herck (2017), Frandsen et al. (2011), Grethe et al. (2018), and Nolte and Grethe (2019).

The period after the abolition of EU sugar quotas in 2017 reinforced these differences. Poland and Czechia improved their competitive position, whereas Slovakia and Hungary

experienced weaker performance. These findings are consistent with studies suggesting that liberalization tends to favor producers with higher productivity, larger processing capacities and stronger economies of scale (Matthews, 2015; Bureau et al., 2017; Swinnen and Knops, 2018; Grethe et al., 2018).

The analysis further demonstrates that self-sufficiency should not be interpreted as a direct measure of competitiveness. Slovakia maintained SSR values above 100%, yet its export specialization remained weaker than in Poland and Czechia. Conversely, Hungary exhibited low self-sufficiency together with persistent trade deficits. Similar conclusions regarding the multidimensional nature of competitiveness were reported by Balassa (1965), Vollrath (1991), Lafay (1992), Siggel (2006), and Widodo (2009). The trade-off between specialisation and diversification identified in this competitiveness literature also has a production-structure counterpart. Farm-level evidence shows that specialised production typically achieves higher economic efficiency through economies of scale, though this advantage can be offset by greater exposure to price fluctuations in a single output market compared with diversified operations (Czyżewski & Smędzik-Ambroży, 2015). Poland's and Czechia's concentration on sugar-beet specialisation with strong export orientation therefore carries a structural trade-off: superior current competitiveness against a potential vulnerability to sustained price pressure in that single commodity.

Another important finding concerns the distinction between direct trade exposure and systemic market vulnerability. This distinction between direct exposure and systemic vulnerability parallels findings on supply chain resilience under disruption more broadly. Evidence on lean-agile supply chain strategies shows that responsiveness, integration, and organisational flexibility, rather than the scale of a single disruptive shock, determine whether a supply system absorbs shocks smoothly or experiences cascading disruption (Nyile et al., 2025). For the V4 sugar sector, this reinforces the argument that resilience to the EU-Mercosur opening will depend less on the direct volume of Brazilian imports and more on each country's processing flexibility and capacity to reallocate resources across production stages. Although current trade flows between the V4 and Mercosur countries remain relatively limited, competitive pressures may emerge indirectly through the integrated EU market. Previous studies emphasize that resilience depends not only on import exposure but also on productivity, processing capacity, trade integration and the ability to generate exportable surpluses (Beghin and Elobeid, 2015; Blanco et al., 2021; Nowak et al., 2025).

This resilience-oriented framing is consistent with broader panel evidence on economic recovery capacity. A global analysis covering 87 countries over eleven years finds that the quality of public governance and administration, alongside the scale of public intervention, has a clear and statistically robust impact on an economy's ability to recover from external shocks (Paun et al., 2021). Applied to the V4 sugar sector, this suggests that Hungary's weaker resilience may reflect not only trade and production fundamentals but also the institutional and policy environment supporting sectoral adjustment after the 2017 quota abolition.

The potential effects of the EU-Mercosur agreement should therefore be interpreted cautiously. The analyzed dataset largely predates the implementation of the agreement, and the study cannot provide evidence of actual impacts on prices, production or farm incomes. Rather, it offers a baseline assessment of sectoral resilience before the introduction of the new trade regime. This approach corresponds with recommendations presented by Josling (2021), Grieger (2025), and the European Commission (2025), Zaremba & Asakowska (2026).

Overall, the findings support previous evidence that the post-quota EU sugar market has become increasingly differentiated, with competitiveness concentrated among the most

efficient producers (Frandsen et al., 2011; Swinnen and Van Herck, 2017; Grethe et al., 2018; Nolte and Grethe, 2019). Within the V4, Poland and Czechia appear best positioned to adapt to future market changes, Slovakia occupies an intermediate position, and Hungary remains the most vulnerable to additional competitive pressures.

Conclusions

This paper analysed the competitiveness of the V4 sugar sector over 2010–2024 and used the results to assess pre-implementation resilience to the EU–Mercosur trade opening that began provisionally on 1 May 2026. The evidence confirms marked differentiation between the four national sectors. Poland achieved the strongest overall position, Czechia followed closely, Slovakia occupied an intermediate position and Hungary remained structurally weak and import-dependent.

The added structural analysis shows that the divergence was not static. Comparing 2010–2016 with 2018–2024, mean CI increased by 36.3% in Poland and 10.6% in Czechia, but declined by 11.6% in Slovakia and 61.3% in Hungary. The previous major liberalisation step – abolition of EU sugar quotas – was therefore followed by greater differentiation within the V4. This makes heterogeneous responses to the new Mercosur preferences more plausible.

Direct V4–Mercosur sugar trade was too small and irregular to justify a simple bilateral-import narrative. Brazil nevertheless dominated the transactions that did occur, and the 2026 preferences target precisely the supplier with the greatest ability to affect global sugar flows. Because the EU is a single market, the economic transmission can occur through EU-wide prices and intra-EU trade even when direct Mercosur imports into a particular V4 country remain low.

The central policy conclusion is consequently twofold. First, the agreed sugar quantities are limited and do not support extreme claims about an unlimited import shock. Second, the capacity to absorb even a moderate market shock differs substantially across the V4. Poland and Czechia have stronger production and trade buffers; Slovakia's production base is more robust than its trade performance; Hungary is the most exposed through chronic import dependence. Monitoring of the 2026 agreement should therefore be country-specific and should combine import data with prices, margins, beet area and processing-capacity indicators.

References

Balassa, B. (1965). Trade liberalisation and revealed comparative advantage. The Manchester School, 33(2), 99-123. https://doi.org/10.1111/j.1467-9957.1965.tb00050.x

Belas, J., Kubalek, J., Hlawiczka, R., Bencsik, A., & Metzker, Z. (2024). The impact of selected financial factors on business ethics in the SMEs segment in the V4 countries. Economics and Sociology, 17(2), 173-193. doi:10.14254/2071-789X.2024/17-2/8

Beghin, J. C., & Elobeid, A. (2015). The impact of changing policies and market conditions on the world sugar market. Journal of Agricultural Economics, 66(2), 233-250.

Blanco, M., Fellmann, T., Witzke, P., Himics, M., Salputra, G., Jansson, T., & Weiss, F. (2021). Cumulative economic impact of trade agreements on EU agriculture. European Commission, Joint Research Centre. Publications Office of the European

Union. https://agriculture.ec.europa.eu/system/files/2021-01/jrc-cumulative-economic-impact-of-trade-agreements-on-eu-agriculture_en_0.pdf

Bureau, J. C., Disdier, A. C., & Jean, S. (2017). Market impacts of agricultural trade liberalisation in the European Union. Food Policy, 68, 33-45.

Czech Statistical Office. (2025). Agricultural statistics database. Prague, Czechia.

Czyżewski, A., & Smędzik-Ambroży, K. (2015). Specialization and diversification of agricultural production in the light of sustainable development. *Journal of International Studies, 8*(2), 63–73. https://doi.org/10.14254/2071-8330.2015/8-2/6

European Commission. (2024). Short-term outlook for EU agricultural markets. Brussels: European Commission.

European Commission. (2025). EU-Mercosur Agreement: Economic Assessment and Agricultural Implications. Brussels: European Commission.

European Commission. (2026a). EU-Mercosur agreement: Status and text of the agreement. Directorate-General for Trade, Brussels. https://policy.trade.ec.europa.eu/eu-trade-relationships-country-and-region/countries-and-regions/mercosur/eu-mercosur-agreement_en

European Commission. (2026b). EU-Mercosur Partnership Agreement: Opening opportunities for European farmers - sugar provisions. Directorate-General for Trade, Brussels. https://policy.trade.ec.europa.eu/eu-trade-relationships-country-and-region/countries-and-regions/mercosur/eu-mercosur-agreement/factsheet-eu-mercosur-partnership-agreement-opening-opportunities-european-farmers_en

European Commission. (2026c). Sugar Market Observatory. Directorate-General for Agriculture and Rural Development, Brussels. https://agriculture.ec.europa.eu/data-and-analysis/markets/overviews/market-observatories/sugar_en

Eurostat. (2026). International trade in goods database. Luxembourg: European Commission.

Food and Agriculture Organization of the United Nations. (2025). FAOSTAT statistical database. Rome: FAO.

Frandsen, S. E., Jensen, H. G., & Vanzetti, D. (2011). Effects of the reform of the EU sugar regime. Food Policy, 36(5), 722-732.

Galović, T., & Bezić, H. (2019). The competitiveness of the EU sugar industry. Zbornik radova Ekonomskog fakulteta u Rijeci: Časopis za ekonomsku teoriju i praksu / Proceedings of Rijeka Faculty of Economics: Journal of Economics and Business. Retrieved from https://api.semanticscholar.org/CorpusID:226921121

García-Perez, A.M., Román-Cervantes, C., González-Dávila, E., & YanesEstévez, V. (2023). Social capital in cooperatives: A typology and their influence on performance. Economics and Sociology, 16(4), 155-177. doi:10.14254/2071-789X.2023/16-4/7

Grethe, H., Tangermann, S., & Nolte, S. (2018). The future of the EU sugar sector after quota abolition. EuroChoices, 17(2), 18-25.

Grieger, G. (2025). EU-Mercosur Partnership Agreement: State of play and outlook. European Parliamentary Research Service.

Haß, M. (2022). Liberalising the EU sugar market: What are the effects on third countries? Australian Journal of Agricultural and Resource Economics, 66(4), 638-667. https://doi.org/10.1111/1467-8489.12475

Hungarian Central Statistical Office. (2025). Agricultural statistics database. Budapest, Hungary.

International Sugar Organization. (2024). World Sugar Statistics 2024. London: ISO.

International Trade Centre. (2026). Trade Map: International trade statistics. Geneva: ITC.

Josling, T. (2021). Agricultural provisions in preferential trade agreements. ICTSD Working Paper Series.

Kopp, T., Prehn, S., & Brümmer, B. (2016). Preference erosion: The case of Everything But Arms and sugar. The World Economy, 39(9), 1339-1359. https://doi.org/10.1111/twec.12374

Lafay, G. (1992). The measurement of revealed comparative advantages. In M. G. Dagenais & P. A. Muet (Eds.), International Trade Modelling (pp. 209-234). Chapman & Hall.

Matthews, A. (2015). The economic consequences of EU sugar policy reform. EuroChoices, 14(1), 16-22.

Mogaka, C. O., Odari, S., & Arani, W. (2022). Functional integration and competitive advantage of food and beverages manufacturing firms in Kenya. *Journal of Sustainable Development of Transport and Logistics*, *7*(1), 99-111. https://doi.org/10.14254/jsdtl.2022.7-1.9

Montrimas, A., Bruneckienė, J., Navickas, V., & Martinkienė, J. (2024). Measuring national economic resilience through industrial portfolios. *Journal of International Studies, 17*(1), 124–154. https://doi.org/10.14254/2071-8330.2024/17-1/8

Njuguna, A.W., Githae, P., & Nyile, E.K. (2025). Cross-border logistics and shipping company performance in East Africa: Empirical evidence from Mombasa Port. *Journal of Sustainable Development of Transport and Logistics, 10*(2), 134–172. https://doi.org/10.14254/jsdtl.2025.10-2.8

Nolte, S., & Grethe, H. (2019). Impacts of sugar quota abolition in the European Union. Agricultural Economics, 50(6), 695-708.

Nolte, S., Buysse, J., & Van Huylenbroeck, G. (2012). Modelling the effects of an abolition of the EU sugar quota on internal prices, production and imports. European Review of Agricultural Economics, 39(1), 75-94. https://doi.org/10.1093/erae/jbr043

Nowak, A., Gradziuk, P., & Jarosz-Angowska, A. (2025). Comparative analysis of the competitiveness of agriculture and agri-food trade in Visegrad Group countries under the European Union frameworks. Wieś i Rolnictwo, 2(207), 49-77. https://doi.org/10.53098/wir.2025.2.207/03

Nyile, E., Shale, N.I., & Osoro, A. (2025). Optimizing humanitarian aid in Kenya: The synergy between lean-agile supply chains and organizational characteristics. *Journal of Sustainable Development of Transport and Logistics, 10*(1), 152–177. https://doi.org/10.14254/jsdtl.2025.10-1.10

OECD/FAO. (2025). OECD-FAO Agricultural Outlook 2025-2034. Paris: OECD Publishing and Rome: FAO. https://doi.org/10.1787/601276cd-en

Paun, C., Musetescu, R., Isaic, R., Manea, G.C., & Shayb, H. (2021). Economic resilience and the state: A global panel analysis. *Economics, Management and Sustainability, 6*(2), 34–45. https://doi.org/10.14254/jems.2021.6-2.3

Sadikhov, S. (2024). Development potential and prospects of Azerbaijan's food industry. *Economics, Management and Sustainability, 9*(1), 6–20. https://doi.org/10.14254/jems.2024.9-1.1

Serra, T., & Zilberman, D. (2013). Biofuel-related price transmission literature: A review. Energy Economics, 37, 141-151. https://doi.org/10.1016/j.eneco.2013.02.014

Siggel, E. (2006). International competitiveness and comparative advantage: A survey and a proposal for measurement. Journal of Industry, Competition and Trade, 6(2), 137-159. https://doi.org/10.1007/s10842-006-8430-x

Statistical Office of the Slovak Republic. (2025). DATAcube statistical database. Bratislava, Slovakia.

Statistics Poland. (2025). Agriculture Statistics Yearbook and statistical database. Warsaw, Poland.

Swinnen, J., & Knops, L. (2018). The political economy of agricultural and food policies in Europe. CEPS Policy Insights.

Swinnen, J., & Van Herck, K. (2017). Agricultural reforms and structural adjustment in the European Union. European Review of Agricultural Economics, 44(2), 185-214.

Tyozenda, A.J., & Ahemen, M. (2025). Enhancing sustainability in Nigerian agricultural supply chains through fair trade practices. *Economics, Management and Sustainability, 10*(1), 82–100. https://doi.org/10.14254/jems.2025.10-1.6

United Nations. (2026). UN Comtrade database: International trade statistics. New York: United Nations Statistics Division.

Vasylieva, N., & James, H. (2021). The effect of urbanization on food security and agricultural sustainability. *Economics and Sociology*, *14*(1), 76–88. https://doi.org/10.14254/2071-789X.2021/14-1/5

Vollrath, T. L. (1991). A theoretical evaluation of alternative trade intensity measures of revealed comparative advantage. Review of World Economics, 127(2), 265-280. https://doi.org/10.1007/BF02707986

Widodo, T. (2009). Comparative advantage: Theory, empirical measures and case studies. Review of Economic and Business Studies, 4(2), 57-82.

Zaremba, Ł., & Asakowska, W. (2026). The EU-Mercosur agreement: An opportunity or a threat to the sustainability of the European and Polish fruit and vegetable sector? Sustainability, 18(2), 724. https://doi.org/10.3390/su18020724

Cite:

Rovný, P., Smutka, L., & Cabelková, I. (2026). Competitiveness of Visegrad countries' sugar sectors after EU sugar quota abolition and under EU-Mercosur Agreement.. *Ukrainian Food Journal, 15*(3), 977–997. https://doi.org/10.24263/2304-974X-2026-15-3-20

Instructions for authors

Dear colleagues!

The Editorial Board of scientific periodical
Ukrainian Food Journal
invites you to publish your research findings in our journal

Manuscripts should present original research that has not been previously published and is not under consideration for publication elsewhere. Submission of the manuscript implies that its publication has been approved by all co-authors and by the appropriate institutional authorities at the organization where the research was conducted.

A cover letter to the editor is mandatory and should include a brief description of the research topic, its novelty and significance. The letter must also confirm that all authors agree to submit the manuscript to the Ukrainian Food Journal and that the work is original and authored solely by the listed contributors.

Manuscript requirements

Authors must prepare the manuscript according to the guide for authors. Editors reserve the right to adjust the style to certain standards of uniformity.

Language – English

Manuscripts should be submitted in Word.

Use 1.0 spacing and 2 cm margins.

Use a normal font 14-point Times New Roman for text, tables, and in the figure captions.

Present tables and figures in the text of manuscript.

Consult a recent issue of the journal for a style check.

Number all pages consecutively.

Abbreviations should be defined on first appearance in text and used consistently thereafter. No abbreviation should be used in title and section headings.

Please submit math equations as editable text and not as images (It is recommend software application MathType or Microsoft Equation Editor).

Minimal size of the article (without the Abstract and References) is 10 pages. For review article is 25 pages (without the Abstract and References).

Manuscript should include:

Title (should be concise and informative). Avoid abbreviations in it.

Authors' information: the name(s) of the author(s); the affiliation(s) of the author(s), city, country. One author has been designated as the corresponding author with e-mail address. If available, the 16-digit ORCID of the author(s) information on the title page.

Declaration of interest

Author Contribution Statement

Abstract. The **abstract** should contain the following mandatory parts:

Introduction provides a rationale for the study (2–3 lines).

Materials and methods briefly describe the materials and methods used in the study (3–5 lines).

Results and discussion describe the main findings (20–26 lines).

Conclusions provides the main conclusions (2–3 lines).

The abstract should not contain any undefined abbreviations or references to the articles.

Keywords. Immediately after the abstract provide 4 to 6 keywords.

Text of manuscript

References

Manuscripts should be divided into the following sections:

- **Introduction**
- **Materials and methods**
- **Results and discussion**
- **Conclusions**
- **References**

Introduction. Provide a background avoiding a detailed review of literature and declare the aim of the present research. Identify unexplored questions, prove the relevance of the topic. The Introduction section should not exceed 1.5 pages in length.

Materials and methods. Provide sufficient detail to enable an independent researcher to replicate the study. For methods that are already published, cite the original source and summarize the procedure briefly. Detailed descriptions are required only for new techniques or significant modifications of existing methods.

Results and discussion. Results should be presented clearly and concisely, supported by appropriate tables and/or figures. The significance of the findings should be discussed in the context of existing literature, highlighting similarities, differences, and potential implications.

Conclusions. Conclusions should be clearly derived from the study's findings and summarized briefly in a separate Conclusion section.

Acknowledgments (if necessary). Acknowledgments of individuals, grants, or funding sources should be included in a separate section. List all persons who contributed assistance during the research. Names of funding organizations must be written in full.

Organize your article into clearly defined sections and, if necessary, subsections. Each subsection should have a concise and descriptive heading.

References

Please, check references carefully.

The list of references should include works that are cited in the text and that have been published or accepted for publication.

All references mentioned in the reference list are cited in the text, and vice versa.

Citation

Cite references in the text by surname and year in parentheses:

- One author: (Smith, 2026)
- Two authors: (Smith & Jones, 2025)
- More than two authors: (Smith et al., 2021)

Some examples:

- The application of plant additives for food products is indeed a modern trend if the food industry (Ivanov et al., 2021).
- These results confirm the findings of Beker and Smith (2024).
- This effect has been widely studied (Feng et al., 2022a, b; Liu and Cheng, 2025; Lorenzo et al., 2005, 2012; Shevchenko, 2024).

Reference list

Reference list entries should be alphabetized by the last name of the first author. If available, DOIs should always be included as full DOI links (e.g., https://doi.org/xxxxx).

Journal article. Authors: surname + initials, separated by commas, & before last author; the publication year is in parentheses; the article title is in sentence case (only first word capitalized), no italics; the journal title is italicized, full name; volume number is italicized; issue number is in parentheses (not italicized); the page range (e.g., 7–36); DOI (if available) in URL format.

Example:

Ivanov, V., Shevchenko, O., Marynin, A., Stabnikov, V., Gubenia, O., Stabnikova, O., Shevchenko, A., Gavva, O., & Saliuk, A. (2021). Trends and expected benefits of the breaking edge food technologies in 2021–2030. *Ukrainian Food Journal*, *10*(1), 7–36. https://doi.org/10.24263/2304-974X-2021-10-1-3

Book. Authors formatted the same as journal articles. Author, A. A. – surname followed by initials, if there are multiple authors, they are separated by commas, and an ampersand (&) is used before the last author; year of publication in parentheses, followed by a full stop (Year); book title italicized, sentence case; edition only if not first (e.g., 2nd ed., 4th ed.); place of publication required (City, Country); Publisher name written clearly (no "Inc." or "Ltd." if not needed).

Author, A. A. (Year). *Title of the book* (Edition). Place of publication: Publisher.

Examples:

Fellows, P. J. (2017). *Food processing technology: Principles and practice* (4th ed.). Cambridge, England: Woodhead Publishing.

Damodaran, S., & Parkin, K. L. (2017). *Fennema's food chemistry* (5th ed.). Boca Raton, FL: CRC Press.

Edited Book.

Editor, A. A. (Ed.). (Year). *Title of the book*. Place: Publisher.

Editor, A. A., & Editor, B. B. (Eds.). (Year). *Title of the book*. Place: Publisher.

Example:

Stabnikova, O., Shevchenko, O., Stabnikov, V., & Paredes-López, O. (Eds.). (2023). *Bioconversion of waste to value-added products.* Boca Raton, London, New York: CRC Press. https://doi.org/10.1201/9781003329671

Book Chapter. Author, A. A., & Author, B. B. (Year). Title of chapter. In Editor A. A. & Editor B. B. (Eds.), *Book title* (pp. xx–xx). Place: Publisher.

Example:

Topchii, O., Pasichniy, V., Marynin A., & Stabnikova, O. (2023). Biotransformation of collagen-containing meat materials into valuable product. In Stabnikova O., Shevchenko O., Stabnikov V., & Paredes-López O. (Eds.), *Bioconversion of waste to value-added products*, (pp. 37-68). Boca Raton, London, New York: CRC Press. https://doi.org/10.1201/9781003329671-2

Online document. Author, A. A. (Year). *Title of document*. Retrieved from https://xxxxxx or (if DOI is available):

Author, A. A. (Year). *Title of document*. https://doi.org/xxxxx

Examples:

Food and Agriculture Organization of the United Nations. (2019). *Food loss and waste reduction*. Retrieved from http://www.fao.org/food-loss-and-food-waste/en/

World Health Organization. (2020). *Food safety*. https://www.who.int/news-room/fact-sheets/detail/food-safet

Published conference paper (in proceedings).

Author, A. A., Author, B. B., & Author, C. C.**;** year in parentheses; paper title: sentence case, not italicized; "In" + editors (if available); *Proceedings title*, italicized; page range included (if available); Place of publication: Publisher.

Author, A. A., & Author, B. B. (Year). Title of paper. In Editor E. E. (Ed.), *Title of proceedings* (pp. xx–xx). Place: Publisher.

Example:

Marynin, A., & Pasychnyi, V. (2026). Biotechnological approaches in food packaging. In A. Brown & M. Smith (Eds.), Proceedings of the International Food Engineering Conference (pp. 120–128). London, England: Springer.

Conference paper (online proceedings). Author, A. A. (Year). Title of paper. In Title of conference proceedings. Retrieved from URL

Example:

Marynin, A., & Pasychnyi, V. (2026). Biotechnological approaches in food packaging. In *Proceedings of the International Food Engineering Conference*. Retrieved from https://www.ifec2026.org/proceedings

Dissertation retrieved from an institutional repository. Author, A. A. (Year). Title of dissertation (Doctoral dissertation or Master's thesis). Name of Institution. Retrieved from URL

Example:

Smith, J. A. (2020). *Development of biodegradable edible coatings for fresh produce preservation (*Doctoral dissertation). University of California, Davis. Retrieved from https://escholarship.org/uc/item/xxxxx

Figures

All figures must be created using a graphic editor with Arial font.

The font size on the figures and the text of the article should be the same.

Black and white graphic with no shading should be used.

The figure elements (lines, grid, and text) should be presented in black (not gray) colour.

Figure parts should be denoted by lowercase letters (a, b, etc.).

All figures are to be numbered using Arabic numerals.

Figures should be cited in text in consecutive numerical order.

Place figure after its first mentioned in the text.

Figure captions begin with the term Figure in bold type, followed by the figure number, also in bold type.

Each figure should have a caption describing what the figure depicts in bold type.

Submit all figures along with the corresponding Excel files containing the graph data as separate attachments.

If your manuscript includes figures previously published elsewhere, you must obtain permission from the copyright owner(s) prior to submission.

Tables

Number tables consecutively in accordance with their appearance in the text.

Place footnotes to tables below the table body and indicate them with superscript lowercase letters.

Place table after its first mentioned in the text.

Ensure that the data presented in tables do not duplicate results described elsewhere in the article.

Suggesting / excluding reviewers

Authors may suggest reviewers and/or request the exclusion of certain individuals when submitting their manuscripts.

When suggesting reviewers, authors should make sure they are totally independent and not connected to the work in any way. When suggesting reviewers, the Corresponding Author must provide an institutional email address for each suggested reviewer. Please note that the Journal may not use the suggestions, but suggestions are appreciated and may help facilitate the peer review process.

Submission

Email for all submissions and other inquiries:

ufj_nuft@meta.ua

Шановні колеги!

Редакційна колегія наукового періодичного видання «**Ukrainian Food Journal**» запрошує Вас до публікації результатів наукових досліджень.

Вимоги до оформлення статей

Мова статей – англійська.

Мінімальний обсяг статті – **10 сторінок** формату А4 (без врахування анотацій і списку літератури)**.**

Для всіх елементів статті шрифт – **Times New Roman**, кегль – **14**, інтервал – 1.

Всі поля сторінки – по 2 см.

Структура статті:

1. **Назва статті.**
2. Автори статті (ім'я та прізвище повністю, приклад: Денис Озерянко).
3. *Установа, в якій виконана робота*.
4. Анотація. **Обов'язкова** структура анотації:
   - Вступ (2–3 рядки).
   - Матеріали та методи (до 5 рядків)
   - Результати та обговорення (пів сторінки).
   - Висновки (2–3 рядки).
6. Ключові слова (3–5 слів, але не словосполучень).

Пункти 2–6 виконати англійською і українською мовами.

7. Основний текст статті. Має включати такі обов'язкові розділи:
   - Вступ
   - Матеріали та методи
   - Результати та обговорення
   - Висновки
   - Література.

За необхідності можна додавати інші розділи та розбивати їх на підрозділи.

8. Авторська довідка (Прізвище, ім'я та по батькові, вчений ступінь та звання, місце роботи, електронна адреса або телефон).
9. Контактні дані автора, до якого за необхідності буде звертатись редакція журналу.

Рисунки виконуються якісно. Скановані рисунки не приймаються. Розмір тексту на рисунках повинен бути **співрозмірним** (!) тексту статті. **Фотографії можна використовувати лише за їх значної наукової цінності.**

Фон графіків, діаграм – лише білий. Колір елементів рисунку (лінії, сітка, текст) – чорний (не сірий).

Рисунки та графіки EXCEL з графіками додатково подаються в окремих файлах.

Скорочені назви фізичних величин в тексті та на графіках позначаються латинськими літерами відповідно до системи СІ.

У списку літератури повинні переважати сучасні англомовні статті та монографії.

Оформлення цитат у тексті статті

Кількість авторів статті	Приклад цитування у тексті
1 автор	(Arych, 2026)
2 автора	(Kuievda and Bront, 2026)
3 і більше авторів	(Bazopol et al., 2023)

Цитати у дужках розміщуються за алфавітом.

Приклад тексту із цитуванням: It is known (Arych, 2026; Bazopol et al., 2023), the product yield depends on temperature, but, there are some exceptions (Kuievda and Bront, 2026).

Правила оформлення списку літератури

Список літератури сортується за алфавітом, літературні джерела не нумеруються.

Стаття в журналі.

Автори: прізвище та ініціали; автори відокремлюються комами; перед останнім автором ставиться знак &. Рік публікації подається в круглих дужках. Назва статті оформлюється малими літерами (з великої літери пишеться лише перше слово назви, перше слово після двокрапки та власні назви), без курсиву. Назва журналу подається повністю та курсивом, всі основні слова у назві журналу вишуться з великої літери. Номер тому виділяється курсивом. Номер випуску подається в круглих дужках без курсиву. Після цього наводиться діапазон сторінок (наприклад, 7–36). DOI (за наявності) подається у форматі URL.

Приклад:

Ivanov, V., Shevchenko, O., Marynin, A., Stabnikov, V., Gubenia, O., Stabnikova, O., Shevchenko, A., Gavva, O., & Saliuk, A. (2021). Trends and expected benefits of the breaking edge food technologies in 2021–2030. *Ukrainian Food Journal*, *10*(1), 7–36. https://doi.org/10.24263/2304-974X-2021-10-1-3

Книга.

Автори оформлюються так само, як і для журнальних статей: прізвище та ініціали; автори відокремлюються комами; перед останнім автором ставиться знак **&**. Рік видання подається в круглих дужках. Назва книги виділяється **курсивом** та оформлюється у **sentence case**. Номер видання зазначається лише у випадку, якщо це не перше видання (наприклад, *2nd ed.*, *4th ed.*). Обов'язково зазначаються **місце видання** (місто, країна або штат/провінція відповідно до APA 6) та назва видавництва.

Формат:

Author, A. A. (Year). *Title of the book* (Edition). Place of publication: Publisher.

Приклади:

Fellows, P. J. (2017). *Food processing technology: Principles and practice* (4th ed.). Cambridge, England: Woodhead Publishing.

Damodaran, S., & Parkin, K. L. (2017). *Fennema's food chemistry* (5th ed.). Boca Raton, FL: CRC Press.

Книга під редакцією.

Прізвище та ініціали редактора(ів) оформлюються аналогічно до авторів. Після прізвищ зазначається **(Ed.)** для одного редактора або **(Eds.)** для кількох редакторів.

Формат:

Editor, A. A. (Ed.). (Year). *Title of the book*. Place: Publisher.

Editor, A. A., & Editor, B. B. (Eds.). (Year). *Title of the book*. Place: Publisher.

Приклад:

Stabnikova, O., Shevchenko, O., Stabnikov, V., & Paredes-López, O. (Eds.). (2023). *Bioconversion of waste to value-added products.* Boca Raton, London, New York: CRC Press. https://doi.org/10.1201/9781003329671

Розділ книги.

Автор(и) розділу оформлюються за загальними правилами APA. Після назви розділу подається слово **In**, прізвища та ініціали редакторів із позначкою **(Ed.)** або **(Eds.)**, назва книги курсивом, сторінки розділу в дужках, місце видання та видавництво.

Формат:

Author, A. A., & Author, B. B. (Year). Title of chapter. In Editor A. A. & Editor B. B. (Eds.), *Book title* (pp. xx–xx). Place: Publisher.

Приклад:

Topchii, O., Pasichniy, V., Marynin, A., & Stabnikova, O. (2023). Biotransformation of collagen-containing meat materials into valuable product. In Stabnikova, O., Shevchenko, O., Stabnikov, V., & Paredes-López, O. (Eds.), *Bioconversion of waste to value-added products* (pp. 37–68). Boca Raton, London, New York: CRC Press. https://doi.org/10.1201/9781003329671-2

Електронний документ.

За наявності URL використовується фраза **Retrieved from**. Якщо документ має DOI, він подається у форматі URL.

Формат:

Author, A. A. (Year). *Title of document*. Retrieved from https://xxxxx

або

Author, A. A. (Year). *Title of document*. https://doi.org/xxxxx

Приклади:

Food and Agriculture Organization of the United Nations. (2019). *Food loss and waste reduction*. Retrieved from http://www.fao.org/food-loss-and-food-waste/en/

World Health Organization. (2020). *Food safety*. https://www.who.int/news-room/fact-sheets/detail/food-safety

Опублікована доповідь у матеріалах конференції.

Автори оформлюються за правилами APA. Назва доповіді подається без курсиву. Після слова **In** зазначаються редактори (за наявності), назва збірника матеріалів конференції курсивом, сторінки, місце видання та видавництво.

Формат:

Author, A. A., & Author, B. B. (Year). Title of paper. In Editor E. E. (Ed.), *Title of proceedings* (pp. xx–xx). Place: Publisher.

Приклад:

Marynin, A., & Pasychnyi, V. (2026). Biotechnological approaches in food packaging. In A. Brown & M. Smith (Eds.), *Proceedings of the International Food Engineering Conference* (pp. 120–128). London, England: Springer.

Доповідь у матеріалах онлайн-конференції (Conference paper in online proceedings)

Формат:

Author, A. A. (Year). Title of paper. In *Title of conference proceedings*. Retrieved from URL

Приклад:

Marynin, A., & Pasychnyi, V. (2026). Biotechnological approaches in food packaging. In *Proceedings of the International Food Engineering Conference*. Retrieved from https://www.ifec2026.org/proceedings

Дисертація з інституційного репозитарію (Dissertation retrieved from an institutional repository)

Після назви дисертації в круглих дужках зазначається тип роботи (*Doctoral dissertation* або *Master's thesis*), далі — назва установи та URL.

Формат:

Author, A. A. (Year). *Title of dissertation* (Doctoral dissertation or Master's thesis). Name of Institution. Retrieved from URL

Приклад:

Smith, J. A. (2020). *Development of biodegradable edible coatings for fresh produce preservation* (Doctoral dissertation). University of California, Davis. Retrieved from https://escholarship.org/uc/item/xxxxx

Зверніть увагу:

- у назві статті всі слова, крім першого, пишуться з малої літери;
- у назві журналу всі основні слова пишуться з великої літери;
- у назві книги або збірника матеріалів конференції всі слова пишуться з малої літери.

Список літератури оформлюється лише латиницею.

Елементи списку українською мовою потрібно транслітерувати. Для транслітерації з українською мови використовується паспортний стандарт.

Стаття надсилається за електронною адресою:

ufj_nuft@meta.ua

УДК 663/664

Ukrainian Food Journal публікує оригінальні наукові статті, короткі повідомлення, оглядові статті, новини та огляди літератури.

Тематика публікацій в Ukrainian Food Journal:

Харчова інженерія	Процеси та обладнання
Харчова хімія	Нанотехнології
Мікробіологія	Економіка та управління
Фізичні властивості харчових продуктів	Автоматизація процесів
Якість та безпека харчових продуктів	Упаковка для харчових продуктів

Періодичність виходу журналу 4 номери на рік.

Результати досліджень, представлені в журналі, повинні бути новими, мати чіткий зв'язок з харчовою наукою і представляти інтерес для міжнародного наукового співтовариства.

Ukrainian Food Journal індексується наукометричними базами:

- Index Copernicus (2012)
- EBSCO (2013)
- Google Scholar (2013)
- UlrichsWeb (2013)
- CABI full text (2014)
- Online Library of University of Southern Denmark (2014)
- Directory of Open Access scholarly Resources (ROAD) (2014)
- European Reference Index for the Humanities and the Social Sciences (ERIH PLUS) (2014)
- Directory of Open Access Journals (DOAJ) (2015)
- InfoBase Index (2015)
- Chemical Abstracts Service Source Index (CASSI) (2016)
- FSTA (Food Science and Technology Abstracts) (2018)
- Web of Science (Emerging Sourses Citaton Index) (2018)
- Scopus (2022)

Рецензія рукопису статті. Матеріали, представлені для публікування в «Ukrainian Food Journal», проходять «Подвійне сліпе рецензування» двома вченими, призначеними редакційною колегією: один є членом редколегії і один незалежний науковець.

Авторське право. Автори статей гарантують, що робота не є порушенням будь-яких авторських прав, та відшкодовують видавцю порушення даної гарантії. Опубліковані матеріали є правовою власністю видавця «**Ukrainian Food Journal**», якщо не узгоджено інше.

Детальна інформація про Журнал, інструкції авторам, приклади оформлення статті та анотацій розміщені на сайті:

http://ufj.nuft.edu.ua

Редакційна колегія

Головний редактор:

Олена Стабнікова, д-р., *Національний університет харчових технологій, Україна*

Члени міжнародної редакційної колегії:

Агота Гедре Райшене, д-р., *Литовський інститут аграрної економіки, Литва*
В. І. Вернадського НАН України
Бао Тхи Вуронг, д-р., *Університет Меконгу, В'єтнам*
Годвін Д. Ндоссі, професор, *Меморіальний університет Хуберта Кайрукі, Дар-ес-Салам, Танзанія*
Дора Марінова, професор, *Університет Кертіна, Австралія*
Егон Шніцлер, д-р, професор, *Державний університет Понта Гросси, Бразилія*
Ейрін Марі Скйондал Бар, д-р., професор, *Норвезький університет науки і техніки, Тронхейм, Норвегія*
Йорданка Стефанова, д-р, *Пловдівський університет "Паісій Хілендарскі", Болгарія*
Кірстен Брандт, професорр, *Університет Ньюкасла, Великобританія*
Крістіна Луїза Міранда Сілва, д-р., професор, *Португальський католицький університет – Біотехнологічний коледж, Португалія*
Крістіна Попович, д-р., доцент, *Технічний університет Молдови*
Лелівельд Хуб, *асоціація «Міжнародна гармонізаційна ініціатива», Нідерланди*
Марія С. Тапіа, професор, *Центральний університет Венесуели, Каракас, Венесуела*
Мойзес Бурачик, д-р., *Інститут сільськогосподарської біотехнології Покапіо (INDEAR), Покапіо, Аргентина*
Октавіо Паредес Лопес, д-р., проф, *Центр перспективних досліджень Національного політехнічного інституту, Мексика.*
Олександр Шевченко, д.т.н., проф., *Національний університет харчових технологій, Україна*
Рана Мустафа, д-р., *Глобальний інститут продовольчої безпеки, Університет Саскачевана, Канада*
Семіх Отлес, д-р., *проф, Університет Еге, Туреччина*
Соня Амарей, д-р., *проф, Університет «Штефан чел Маре», Сучава, Румунія*
Станка Дам'янова, д.т.н., проф., *Русенський університет «Ангел Канчев», філія Разград, Болгарія*
Стефан Стефанов, д.т.н., проф., *Університет харчових технологій, Болгарія*
Тетяна Пирог, д.б.н., проф., *Національний університет харчових технологій, Україна*
Умезуруйке Лінус Опара, професор, *Стелленбошський університет, Кейптаун, Південна Африка*
Шейла Кілонзі, *Університет Каратіна, Кенія*
Юлія Дзязько, д-р. хім. наук, с.н.с., *Інститут загальної та неорганічної хімії імені В. І. Вернадського НАН України*
Юн-Хва Пеггі Хсі, д-р, професор, *Університет Флориди, США*
Юрій Білан, д-р., проф., *Університет Томаша Баті в Зліні, Чехія*
Ясміна Лукінак, д.т.н., професор, *Університет Осієка, Хорватія*
Ясміна Лукінак, д-р, проф., *Осієкський університет, Хорватія.*

Члени редакційної колегії:

Агота Гедре Райшене, д-р., *Литовський інститут аграрної економіки, Литва*
Бао Тхи Вуронг, д-р., *Університет Меконгу, В'єтнам*
Валерій Мирончук, д-р. техн. наук, проф., *Національний університет харчових технологій, Україна*
Володимир Ковбаса, д-р. техн. наук, проф., *Національний університет харчових технологій, Україна*
Галина Сімахіна, д-р. техн. наук, проф., *Національний університет харчових технологій, Україна*
Годвін Д. Ндоссі, професор, *Меморіальний університет Хуберта Кайрукі, Дар-ес-Салам, Танзанія*
Дора Марінова, професор, *Університет Кертіна, Австралія*
Егон Шніцлер, д-р, професор, *Державний університет Понта Гросси, Бразилія*
Ейрін Марі Скйондал Бар, д-р., професор, *Норвезький університет науки і техніки, Тронхейм, Норвегія*
Йорданка Стефанова, д-р, *Пловдівський університет "Паісій Хілендарскі", Болгарія*
Кірстен Брандт, професорр, *Університет Ньюкасла, Великобританія*
Крістіна Луїза Міранда Сілва, д-р., професор, *Португальський католицький університет – Біотехнологічний коледж, Португалія*
Крістіна Попович, д-р., доцент, *Технічний університет Молдови*
Лада Шерінян, д-р. екон. наук, професор., *Національний університет харчових технологій, Україна*
Лелівельд Хуб, *асоціація «Міжнародна гармонізаційна ініціатива», Нідерланди*
Марія С. Тапіа, професор, *Центральний університет Венесуели, Каракас, Венесуела*
Мойзес Бурачик, д-р., *Інститут сільськогосподарської біотехнології Покапіо (INDEAR), Покапіо, Аргентина*
Октавіо Паредес Лопес, д-р., проф, *Центр перспективних досліджень Національного політехнічного інституту, Мексика.*
Олександр Шевченко, д.т.н., проф., *Національний університет харчових технологій, Україна*
Ольга Рибак, канд. техн. наук, доц., *Тернопільський національний технічний унівреситет імені Івана Пулюя, Україна*
Рана Мустафа, д-р., *Глобальний інститут продовольчої безпеки, Університет Саскачевана, Канада*
Семіх Отлес, д-р., *проф, Університет Еге, Туреччина*
Соня Амарей, д-р., *проф, Університет «Штефан чел Маре», Сучава, Румунія*
Станка Дам'янова, д.т.н., проф., *Русенський університет «Ангел Канчев», філія Разград, Болгарія*
Стефан Стефанов, д.т.н., проф., *Університет харчових технологій, Болгарія*
Тетяна Пирог, д-р. біол. наук, проф., *Національний університет харчових технологій, Україна*
Умезуруйке Лінус Опара, професор, *Стелленбошський університет, Кейптаун, Південна Африка*
Шейла Кілонзі, *Університет Каратіна, Кенія*
Юлія Дзязько, д-р. хім. наук, с.н.с., *Інститут загальної та неорганічної хімії імені В. І. Вернадського НАН України*
Юн-Хва Пеггі Хсі, д-р, професор, *Університет Флориди, США*
Ясміна Лукінак, д-р, проф., *Осієкський університет, Хорватія.*
Олексій Губеня (відповідальний секретар), канд. техн. наук, доц., *Національний університет харчових технологій, Україна.*

Наукове видання

Ukrainian Food Journal

Volume 15 Issue 3
2026

Том 15 № 3
2026

Підп. до друку 30.09.2026 р. Формат 70x100/16.
Обл.-вид. арк. 14.42. Ум. друк. арк. 14.54.
Гарнітура Times New Roman. Друк офсетний.
Наклад 100 прим. Вид. № 28н/26.

НУХТ. 01601 Київ–33, вул. Володимирська, 68

Свідоцтво про державну реєстрацію
друкованого засобу масової інформації
КВ 18964–7754Р
видане 26 березня 2012 року.